The Antiferromagnetic Quantum Critical Metal: A Nonperturbative Approach

The Antiferromagnetic Quantum Critical Metal: A Nonperturbative Approach

By

Andrés Schlief, M. Sc.

A Thesis
Submitted to the School of Graduate Studies
in Partial Fulfillment of the Requirements
for the Degree Doctor of Philosophy

McMaster University

Doctor of Philosophy, Department of Physics and Astronomy, McMaster University, (2019) Hamilton, Ontario.

Title: The Antiferromagnetic Quantum Critical Metal: A Nonperturbative Approach

Author: Andrés Schlief, M. Sc. (Perimeter Institute for Theoretical Physics and University of Waterloo)

Supervisor: Dr. Sung-Sik Lee

Number of Pages: xvii, 319

Lay Abstract

The superconductivity in heavy-fermion compounds, iron pnictides and cuprates has been intensively studied for over thirty years. Amongst some of these materials, the common denominator is the presence of strong antiferromagnetic fluctuations in their normal state, signaling an underlying quantum phase transition between a paramagnetic metal and a metal with antiferromagnetic long-range order. Although the quantum critical point is experimentally inaccessible due to the presence of superconducting order, it determines the physical properties of the normal state of the metal in a wide range of temperatures. In this thesis we study the low-energy theory for the critical metallic state that arises at the aforementioned quantum critical point. We present a nonperturbative study of the theory in spatial dimensions between two and three. We pay special attention to two dimensions where we show that our physical predictions are in qualitative agreement with experiments in electron-doped cuprates. We further develop a field theoretic functional renormalization group scheme that is analytically tractable. It provides a general framework to study the low-energy theory of metallic states with or without a quasiparticle description. Within this formalism we characterize the single-particle properties of the antiferromagnetic quantum critical metal. This allows one to study the superconducting instability triggered by critical antiferromagnetic quantum fluctuations quantitatively.

Abstract

This thesis is devoted to the study of the low-energy theory describing the antiferromagnetic quantum critical metal in dimensions between two and three. In the past two decades this theory has been the subject of intense theoretical efforts due to its relevance to layered materials such as high-temperature superconductors and heavy-fermion compounds. Despite such efforts, only recently the exact low-energy properties of the theory have been determined through a nonperturbative renormalization group analysis. This thesis is mainly devoted to develop this nonperturbative approach and characterize the low-energy properties of this novel state of matter in a controlled way.

In the first part of the thesis we focus on the theory in two dimensions. Despite the strong coupling nature of the theory, its low-energy properties can be determined reliably by organizing quantum fluctuations in terms of an emergent control parameter, which differs from the standard perturbative expansion in the coupling. Based on a nonperturbative renormalization group approach we predict the exact critical exponents at the fixed point into which the theory flows in the low-energy limit. We also compare our predictions with known experimental data in electron-doped cuprates. We further compare our results with previous theoretical works and point out the main qualitative differences.

In the second part of this thesis we study how the nonperturbative solution in two dimensions evolve as the dimension of space is increased from two to three. We present a generalization of the nonperturbative approach used in two dimensions, and provide expressions for the exact critical exponents and low-energy physical observables of the theory in space dimensions between two and three. We show that, on the one hand, the critical exponents are smooth functions of the dimension. On the other hand, the physical observables display subtle crossovers that make it hard to access subleading scaling behaviors in two dimensions from the low-energy solution valid above two dimensions. This is caused by a noncommutativity between the low-energy limit and the limits in which the physical dimensions are approached.

In the last part of this thesis, we study the single-particle properties of low-energy electrons in the two-dimensional antiferromagnetic quantum critical metal within a unified theory that includes gapless electronic modes away from the hot spots on the Fermi surface. The theory studied in the first part of this thesis is generalized to account for all gapless electronic excitations on the Fermi surface. Through an analytically tractable functional renormalization group scheme, we show that low-energy electrons are characterized by a universal momentum-dependent quasiparticle weight that decays to zero as the hot spots are approached along the Fermi surface. The momentum-dependent quasiparticle weight shows how quasiparticle and non-quasiparticle excitations coexist within the same metallic state. This approach also allows one to characterize how the global shape of the Fermi surface is renormalized due to the strong interaction between the electrons and the critical spin fluctuations. These predictions are testable through angle-resolved photoemission spectroscopy experiments. The work presented in this part of the thesis provides a general theoretical framework for theories of metals with or without quasiparticles whose universal low-energy properties are characterized by an infinite amount of low-energy data. Finally, we present a preliminary analysis of the superconducting instability of the metallic state. With this we determine the temperature range in which our predictions are testable and provide an upper bound for the superconducting transition temperature of the metallic state.

Table of Contents

List of Figures

List of Tables

Acknowledgments

I will like to start by expressing my gratitude to my Ph.D. advisor and nowadays collaborator, Sung-Sik Lee. Most of all, I am very grateful for his unbreakable patience, the time spent in discussing diverse topics in theoretical physics and for treating me as peer, rather than just a student. Throughout my journey as a Ph.D. student I have been truly inspired by his approach towards doing research in theoretical physics and, in my opinion, he sets an excellent role model for what a *good* physicist should be. I can confidently say that, what I am as a theoretical physicist today has been heavily influenced by his honest, thorough and fearless approach towards science. His unbreakable will and everlasting patience in studying unsolved fundamental problems in theoretical physics from first principles is truly motivating. Finally, I am grateful for his continuous use of analogies in both academic and non-academic contexts. These, not only made our discussions more enjoyable, but it also sets an example on how to convey a message in the simplest terms irrespective of the complexity behind it.

I am also very grateful to my good friend and collaborator, Peter Lunts. It was truly an amazing experience to have collaborated together in the past years. I am not only grateful for our physics discussions, but for our conversations on diverse topics that made my time as a Ph.D. student more enjoyable even when our research projects seemed to go nowhere. I also thank Anton Borissov and Vladimir Calvera for their collaboration and friendship in the last two years. I am very inspired by their courage and hard work. Last, but not least, I will like to thank Ipsita Mandal for our multiple conversations, especially about physics.

I will like to thank Davide Gaiotto and Cliff Burgess for agreeing to be part of my supervisory committee and for their unconditional support. I am especially thankful to Davide for his financial support in my first two years of Ph.D. and for being my co-advisor. Although, during my five years of Ph.D. I spent most of the time at the Perimeter Institute for Theoretical Physics, I will like to thank the faculty, students, postdocs and staff at McMaster University. I had the privilege of taking lectures and engage in physics discussions with Bruce Gaulin, Catherin Kallin, and Takashi Imai. I am very thankful for their support, patience and overall, human quality. I will like to thank Greg Kaplanek, Ryan Plestid, László Salavári and Zhiqiang Wang for their kindness and support. Finally, I will like to thank Rosemary McNiece, Cheryl Johnston, Mara Esposto and Tina Stewart for their administrative help and patience.

If there is one thing that I must highlight from Perimeter Institute beyond the undeniable excellency in the academic realm, is the continuous inflow of people with extraordinary human quality. I had the privilege of having Lucía Gómez Córdova as my flatmate for the full duration of my Ph.D. I am extremely grateful to her for her friendship, our shared feline daughter Kira, her unconditional support, our discussions about life, academia and physics. For most of my Ph.D. I had the privilege of sharing Office 480, not only with Peter Lunts, but also with Gabriel Magill. I am extremely grateful for his friendship, our conversations about diverse topics and I am truly inspired by his honest approach to science and life in general. My time in Office 480 was one of the highlights of my journey as a Ph.D. student. Amongst the large number of people I met at Perimeter Institute, I am extremely grateful to my closest friends: Natacha Altamirano, Lucía Gómez Córdova, Pablo Bosch, Nayeli Galindo, Damián Galante, Julián Rincón, Carolina Carvajal, Juan Cayuso, Juan Carrasquilla, Clément Delcamp, Néstor Ortiz, Stephen Green, Emilio Trevisani, Lauren Greenspan, Diego Gutiérrez,

and Fabián Bautista. All of you made my years at Waterloo unforgettable. Thanks for your friendship, but most of all, for your continuous support. Within the researcher community at Perimeter Institute I am also thankful to Renato Dantas-Alves, Qi Hu, Florian Hopfmüller, Nafiz Ishtiaque, Faroogh Moosavian, Bohdan Kulchytskyy, Giacomo Torlai, Matthew Beach, Vasudev Shyam, Hugo Marrochio, Heidar Moradi, Angelika Fertig, Laura Sberna, Job Feldbrugge, Fiona McCarthy, Tomas Gonda, Andrei Shieber, Tibra Ali, Farbod Kamiab, Mansour Karami, Adrián Franco, Alfredo Guevara, Seth Kurankyi Asante, Dalimil Mazáč, Miroslav Rapčak, Nima Duroud, Guifré Vidal and Roger Melko. I really enjoyed engaging into conversations that I will remember in the years to come.

From the nonacademic side of Perimeter Institute, I want to extend my thanks to Hayley Rutherford for her extraordinary human quality, our time together, and those lessons I learned from her that I will keep for a long time. Furthermore, I want to thank Daniel Lynch, Diana Gonçalves, Luis Cabo, Glen Heimbecker, Craig Hennessy, Stephanie Keating, Colin Hunter, Lenka Bojdova, Erica Goss, Brian Lasher, Matthew Lasher, Greg Dick and Marie Strickland. All of you have made my journey as a Ph.D. at Perimeter Institute very enjoyable. I especially thank Debbie Guenther for her patience, hard and heroic work on the administrative side of things regarding my Ph.D. I also want to thank the Outreach Department for allowing me to take part on couple of events in the past years. During one of such events I was fortunate to meet Rachel Maria Zimić, to whom I am very grateful for our conversations, time spent together and the multiple lessons about life that she taught me in the past months. Last, but not least, I will like to thank the whole staff of the Black Hole Bistro. They not only do an amazing job, but I have been fortunate enough to be friends with most of them. In particular, I want to thank Dante Walton-Zikić, Carleigh Nicholas, Nancy Baloescu, Belén Ponciano, Kaiti Egley, Amy Luce, Olivia Taylor, Chandy Thach, Angela Malaythong, Maria Garland, Erin McBurney and Tiffany Pryia for their everyday support and friendship.

To close this rather large acknowledgments section, I will like to express my infinite gratitude to the most important people in my life for their continuous support in the past years. To my effective mother, Carmen Fernández, I am infinitely grateful. Although it has been tough for both to be away from each other, I admire her strength and her continuous support towards my career choices. To my grandmother, Carmen Buitrago, I extend my warmest thanks for being a role model of strength and for always supporting my career choice despite the implications that it entails. To my aunt Virginia Fernández and uncle Enrique Hoyos, I have nothing but gratitude for your support, understanding and help. To my brothers Juan Guillermo Schlief and Claus Gunnar Schlief, my sister Maya Marcella Schlief and my aunt Erika Schlief: thank you for all your support and for taking care of me at a distance. Overall, thank you for encouraging me to follow my passion and for being supportive of my life choices. To my parents: death has not been an obstacle to feel your support. I am extremely grateful for the lessons you taught me in our short time together. It is because of them that I have come so far along my life. To all of my family, I have nothing but gratitude and everlasting love. I thank Alonso Botero Mejía for his continuous support in the past eight years. His lessons and friendship along my career as a physicist is something I will always cherish. Thank you for helping me believe in myself. I also want to thank my closest friends back in Colombia: Andrea Lorena Orjuela Ruiz, Juan Sebastián Baez, Juan Manuel Prado, Juan Camilo Romero, Andrea Álvarez, Jose Luis Duque, Simón

Fique, Ángela Núñez, Sonia Sutta, Naira Bonilla and Andrés Estrada. Thank you for your support in the last five years. Finally, and certainly not the least, I want to thank Lizeth Figueroa Grandas for always being there during my journey despite the distance. Thank you for taking care of me, for your support, for our conversations and for keeping our friendship as alive as it was five years ago. You are truly part of my family and I have nothing else than gratitude and love for you.

Declaration of Authorship and Academic Achievement

This is a thesis based on two publications and a forthcoming work which appear as follows

Chapter 2:

A. Schlief†, P. Lunts†, and S.-S. Lee. *Exact Critical Exponents for the Antiferromagnetic Quantum Critical Metal in Two Dimensions.* Phys. Rev. X **7,** 021010 (2017).

DOI: https://doi.org/10.1103/PhysRevX.7.021010

† : First co-authors.

Chapter 3:

A. Schlief, P. Lunts, and S.-S. Lee. *Noncommutativity between the low-energy limit and integer dimension limits in the ϵ-expansion: A case study of the antiferromagnetic quantum critical metal.* Phys. Rev. B **98,** 075140 (2018).

DOI: https://doi.org/10.1103/PhysRevB.98.075140

Chapter 4:

A. Schlief and S.-S. Lee. *Momentum-dependent single-electron properties in the antiferromagnetic quantum critical metal: From cold to lukewarm to hot electrons.* Under revision prior to submission.

In the first publication, both Andrés Schlief and Peter Lunts were responsible for a large portion of the computations and the project was completed under Sung-Sik Lee's guidance and direction. Andrés Schlief performed the computations appearing in Appendices B and D of the manuscript (Appendices C and E in this thesis), while Peter Lunts performed the computations appearing in Appendices A and C of the manuscript (Appendices A and D in this thesis). Sung-Sik Lee wrote the draft and all three authors were involved in the discussion of the work and shaping the final version of the manuscript.

In the second publication, Andrés Schlief performed all the computations shown in Appendices A to F of the manuscript (Appendices B, and F, G, H and I in this thesis). He was also responsible for writing the draft of the manuscript. Peter Lunts contributed through discussions and suggestions throughout the completion of the work and provided valuable input in developing the final version of the manuscript. Sung-Sik Lee provided guidance throughout the completion of the project and edited the draft into its final version.

In the forthcoming publication, Andrés Schlief was responsible for the entirety of the computations (Appendices J, K, L, M, N, O, P and Q in this thesis) and writing the first draft of the manuscript. Sung-Sik Lee provided guidance and edited the final version of the manuscript. Both authors were involved in the discussion and formulation of the formalism introduced in this work.

To my forebears. One day we will feast in the golden hall.

1 | Introduction

The theoretical study of universal long-distance physics of different phases of matter and their phase transitions is at the core of modern condensed matter physics. Within the vast landscape of physical phenomena that this entails, understanding the critical points associated to such phase transitions is of great importance, despite the fact that these represent only a very small set within the space of theories describing condensed matter systems. The importance of studying critical points is two-fold: First, critical points associated to continuous phase transitions separating two different phases determine the universal nature of those phases to a great extent. In this sense, the study of critical points provides a framework to organize and classify different phases of matter. Second, critical points often host novel states of matter in which there exists no well-defined single-particle excitations. Such states are often described by strongly interacting field theories.

Phase transitions are conventionally classified into two main classes: first-order (or discontinuous) and second-order (or continuous) phase transitions [1–7]. A common example of a first-order phase transition is the liquid-to-gas transition of water, which can be driven, for example, by tunning the temperature at fixed external pressure. A well-known second-order phase transition is the paramagnetic-ferromagnetic transition in which, by tunning the temperature down, a paramagnetic material spontaneously develops a nonzero magnetization at a critical temperature. Even though phase transitions are omnipresent in all materials, the theoretical description of first-order and second-order phase transitions differ tremendously and are still subject of intensive theoretical research.

First-order phase transitions are mainly characterized by a discontinuity in the entropy of the system at the transition point, giving rise to a latent heat. These transitions are highly dependent on the microscopic details of the material under consideration because, at the transition, the constituents of the system are spatially correlated on length scales that are small compared to the (linear) size of the sample. This is commonly referred to as the system having a finite correlation length [1, 4, 7]. As a consequence, a generalized theory of first order phase transitions is hard to achieve due to the lack of universal features that are material-independent. Second-order phase transitions, in contrast, do not display such a discontinuity in the entropy and there is no latent heat associated to them. Moreover, at the transition points, known as critical points, the constituents of the material are spatially correlated at length scales comparable to the (linear) size of the sample. Theoretically, this is referred to as the scale of correlations being unbounded in the thermodynamic limit [1, 4, 7]. Because of this, second-order phase transitions display universal features that are independent of the microscopic (short-distance) details of materials, which allows their description to be significantly more systematic than that of first-order phase transitions [1, 2, 4–7].

The fact that second-order phase transitions are independent of the microscopic details of materials is often referred to as *universality*. Different second-order phase transitions are characterized entirely by material-independent data such as the *critical exponents* that govern the scaling properties of long-wavelength physical observables. Such universal data is largely fixed by the dimensionality of space and the symmetries of the phases involved in the transitions. Different space dimensions and symmetries lead to different *universality classes* which are parametrized by the critical exponents [2, 4, 6, 7]. The power of this idea lies in the fact that second-order phase transitions that belong to the same universality class are described by the same physical theory irrespective of the microscopic details of the materials harboring the transition. A canonical example that illustrates this is the three-dimensional Ising universality class which describes both the the paramagnetic-ferromagnetic transition in two spatial dimensions and the liquid-vapor transition of water at the critical point [8, 9].

For the most part, the systematic understanding of second-order phase transitions has been built upon Landau's idea of symmetry and local order parameters that encode the macroscopic degrees of freedom of the system and which distinguish between the phases involved in the transition [10, 11]. In Landau's line of reasoning, second-order phase transitions are seen as occurring between a disordered (symmetric) and an ordered (broken-symmetry) phase. This naturally led to the idea that spontaneous symmetry-breaking is at the heart of second-order phase transitions. In this formalism, the way in which the expectation value of the local order parameter (in the statistical mechanics sense) transforms under a symmetry transformation encodes the broken symmetry characterizing the phase transition [2, 4, 6]. Landau's symmetry-breaking paradigm was originally conceived as a mean-field approach in which the local order parameter is treated as a static entity whose fluctuations are completely ignored. These fluctuations can either be thermal or due to quantum effects. The former are responsible for the existence of thermal (or classical) phase transitions, where the transition is driven by long-wavelength thermal fluctuations close to the transition temperature. The latter, on the other hand, are responsible for the existence of *quantum phase transitions* (QPTs) where the fluctuations arise as a consequence of the uncertainty principle that is at the core of Quantum Mechanics. The critical points of this type of transitions are known as *quantum critical points*. QPTs are driven by tunning non-thermal parameters (such as pressure, doping or magnetic fields) and only occur at zero temperature [2, 6].

Since Landau's mean-field theory ignores fluctuations of the order parameter it is expected to fail when such fluctuations become large. This is a situation that typically happens close to classical and quantum critical points that are realized in low dimensions. The reliability of Landau's mean-field theory is determined through *Ginzburg's criterion* [2, 4, 6, 12, 13], which states that a mean-field theory is valid provided that the fluctuations of the order parameter remain small compared to its expectation value arbitrarily close to the critical point in the symmetry-broken phase. Ginzburg's criterion imposes constraints on the applicability of Landau's mean-field theory as a function of the space-time dimension. In particular, this criterion gives rise to the notion of the upper critical dimension of a theory [2, 4]. That is, the dimension above which fluctuations of the order parameter can be ignored and Landau's mean-field theory is reliable. Typically, experimentally relevant second-order phase transitions are described by theories whose upper critical dimension is higher than the physical space-time dimension at which the transition occurs. Thus, a systematic understanding of these second-order phase transitions requires the inclusion of fluctuations of

the order parameter. The addition of these fluctuations to Landau's mean-field theory is commonly known as the Ginzburg-Landau paradigm and it constitutes the first stepping stone in which the work presented in this thesis is based on[1].

It is noted, however, that the Ginzburg-Landau symmetry-breaking paradigm does not provide a full characterization of all continuous phase transitions known to occur in condensed matter systems. The most prominent examples of continuous phase transitions that lie beyond this paradigm are those happening amongst topologically ordered phases of matter where no local order parameter distinguishes amongst them [3]. Even more interestingly, there are known cases of QPTs between phases that can be characterized by the Ginzburg-Landau symmetry breaking paradigm, but whose transition cannot be described within this same framework. The description of "deconfined" quantum critical points arising in two-dimensional antiferromagnets [15] is a well-known example of this. In this thesis, however, we will only focus on a QPT that falls within Ginzburg-Landau's symmetry-breaking paradigm.

Thanks to the development of *renormalization group* (RG) techniques based on the seminal works by Kadanoff [16] and Wilson [17, 18], a systematic treatment of the effects of long-wavelength fluctuations of the order parameters at critical points has been achieved in the past decades. This treatment finds no better language than that of *effective field theories* (EFTs) [2, 4, 6, 14, 19, 20]. At critical points, the physics of the system is dictated by long-wavelength fluctuations which make EFTs ideal candidates for capturing this physics without taking into account the microscopic details of the system. Furthermore, EFTs equipped with RG techniques are capable of describing the universal features of both classical and quantum phase transitions. The main reason behind using this framework to describe continuous phase transitions originates from the fact that only universal features like the space-time dimension and the symmetry of the order parameters are necessary when writing down the EFTs describing the transitions. Despite this simple starting point, many phase transitions that are found in nature occur at space-time dimensions that are below the upper critical dimension of the EFT used for their description. According to Ginzburg's criterion, the fluctuations of the order parameter become stronger as the dimension is lowered, and thus obtaining the universal data characterizing the phase transition becomes a hard problem because the description of the latter finds itself written down in terms of strongly-coupled EFTs that, in general, cannot be accessed perturbatively.

The field-theoretic description of continuous phase transitions has progressed immensely through the study of systems that are relativistic at long wavelengths and that display either conformal symmetry or supersymmetry at low energies [2, 4–6, 14, 19–24]. In the presence of these symmetries, kinematic constraints can be strong enough to fix some dynamical properties of the system. An example of this is provided by the conformal boostrap which has gained considerable attention recently and, to date, is the method that yields the most accurate results for the critical exponents characterizing the three-dimensional Ising universality class [5, 19, 23, 24]. The kinematic constraints offered by either conformal symmetry and

[1] Although the Ginzburg-Landau paradigm originated in the study of classical phase transitions, it also applicable to the study of QPTs. This is due to the *quantum to classical* mapping [2, 5, 6, 14] in which a d-dimensional quantum system that evolves in *imaginary* time can be mapped to a $(d+1)$-dimensional classical system at finite "temperature". However, it is important to note that this *does not* imply an equivalence between classical and quantum phase transitions, but rather that these are objects that can be studied within the same formalism.

supersymmetry are often supplemented with perturbative techniques such as the ϵ expansion [25, 26] and the large N expansion [27]. In this context the latter perturbative techniques have proven to be powerful tools in the study of strongly coupled field theories.

Although the study of relativistic EFTs has greatly increased our understanding of QPTs between insulating materials, it has not been as successful in furthering our understanding of QPTs of metallic systems. Metallic systems are not relativistic at long-wavelengths and many of the theoretical tools developed for relativistic EFTs do not directly apply in this setting. The main roadblock in the study of metallic QPTs is the existence of an extensive number of gapless modes present at the Fermi surface[2]. These QPTs of *itinerant electrons* are characterized by the strong coupling between the gapless electronic excitations and a bosonic local order parameter whose quantum fluctuations drive the transition [6]. The low-energy properties of conventional metallic phases are well understood thanks to *Landau's Fermi-Liquid Theory*. However, this description usually breaks down at itinerant quantum critical points due to the strong coupling between the large number of gapless electronic excitations and the order parameter fluctuations [28]. In this scenario, Landau's Fermi-Liquid theory breaks down in two main ways: Either the Fermi surface of the metal gets destroyed by the strong interaction between the gapless electrons and the order parameter, or it remains sharp, but with incoherent electronic excitations. In the former, the metallic state is destroyed while in the later the system still retains metallic properties [6, 28]. In this thesis we focus on the latter case, where the metallic state realized at the quantum critical point is commonly referred to as a "non-Fermi liquid metal" whose long-wavelength description is expressed in terms of a strongly-coupled EFT. The strongly-coupled nature of the EFT description of non-Fermi liquid metals is the reason why a systematic understanding of these exotic states of matter is still lacking.

To date there is no universal theory of non-Fermi liquid metals that is analogous to Landau's Fermi-Liquid Theory for conventional metals. To achieve a general theory of non-Fermi liquid metallic states, it is useful to scrutinize concrete examples in order to obtain some insights for the broader setting. Guided by this philosophy, in this thesis we tackle the strongly-coupled EFT describing the non-Fermi liquid metallic state arising at the *antiferromagnetic quantum critical point* in two spatial dimensions. This is motivated by experimental observations in quasi-two-dimensional layered materials such as electron-doped cuprates [29–36], heavy fermion compounds [37–40] and iron pnictides [41–47] which suggest the presence of such a quantum critical point. We not only present a nonperturbative RG approach that allows the extraction of the *exact* universal data of the transition in two spatial dimensions, but also extend this approach to spatial dimensions between two and three, where the latter is the upper critical dimension of the theory. Because the theory is exactly solvable in this dimensional range, we use it as a model theory to put to the test the extent to which perturbative RG schemes based on dimensional regularization and the ϵ expansion can be used to infer the universal data of strongly-coupled field theories. Before we delve deep into the details of the EFT description of the metallic state realized at the antiferromagnetic quantum critical point, we give a brief review of the key points behind Landau's Fermi-Liquid theory and recent theoretical progress in understanding non-Fermi liquid metals.

[2] That is, the surface in momentum space separating the occupied and unoccupied single particle electronic states.

1.1 Fermi Liquid Theory

In the simplest terms, conventional metals can be viewed as gas of electrons in the presence of a crystalline structure of ions and which interact with each other through the long-range Coulomb interaction. The metallic state is characterized by electronic single-particle wave functions that are spread around the interstitial space between the positively charged ions forming the underlying crystal [48]. Despite the fact that the Coulomb interaction is long-ranged, the electrons interact with each other through an effective short-range potential because the Coulomb potential gets screened. The screening arises as a consequence of the electrons being in a positively charged background and the fact that the electronic density of states is nonzero at the Fermi energy [48, 49]. Even with the short-range interaction, understanding the properties of conventional metals involves solving the many-body Schrödinger's equation in the presence of the screened Coulomb potential. This is, in general, a hard endeavor. However, it was first due to Landau's phenomenological *Fermi-Liquid Theory* [50, 51] that the low-energy properties of conventional metals could be understood. We devote this section to review the key properties of Landau's Fermi-liquid theory as an EFT and show that all low-temperature features of conventional metals that were originally postulated by Landau from a phenomenological point of view, arise as low-energy emergent phenomena of a system with a large number of electrons at finite density in the presence of short-range interactions.

1.1-(*a*) Landau's Phenomenological Fermi-Liquid Theory

In the absence of interactions, a metal is an ideal Fermi gas that can be described in terms of single-particle electronic wave functions parametrized by the electron's momentum and spin. At zero temperature, the ground state is constructed by filling the energy levels with the electrons under the constraint imposed by Pauli's exclusion principle. This gives rise to a ball of occupied states in the momentum space whose radius is the Fermi momentum $k_{\rm F} \equiv |\vec{k}_{\rm F}|$, and whose boundary is a constant energy surface known as the *Fermi surface* (FS). All energy levels below the FS are filled (commonly known as the Fermi sea) and all energy levels above the FS are empty. This is expressed in terms of the single-particle occupation number distribution as a function of momentum:

$$n_{\rm G.S}(\vec{k}) = \Theta\left(k_{\rm F} - |\vec{k}\,|\right). \tag{1.1}$$

At nonzero temperature, Eq. (1.1) is replaced by the Fermi-Dirac distribution:

$$n_{\rm F.D.}(\vec{k}) = \frac{1}{1 + e^{\frac{[E(\vec{k})-\mu]}{T}}}, \tag{1.2}$$

where we have chosen the convention in which the Boltzmann constant is $k_B = 1$. Here, $E(\vec{k}) = \vec{k}^2/(2m)$ denotes the energy of the electron, with m being its mass and μ the chemical potential which at zero temperature is nothing but the Fermi energy: $E_{\rm F} = E(\vec{k}_{\rm F})$. Excitations over the ground state of the ideal Fermi gas arise by creating electrons (holes) above (below) the FS. For example, electron-like excitations are created when electrons in the Fermi sea acquire momentum $\vec{k}$ such that $E(\vec{k}) > E_{\rm F}$, or equivalently, $|\vec{k}| > k_{\rm F}$.

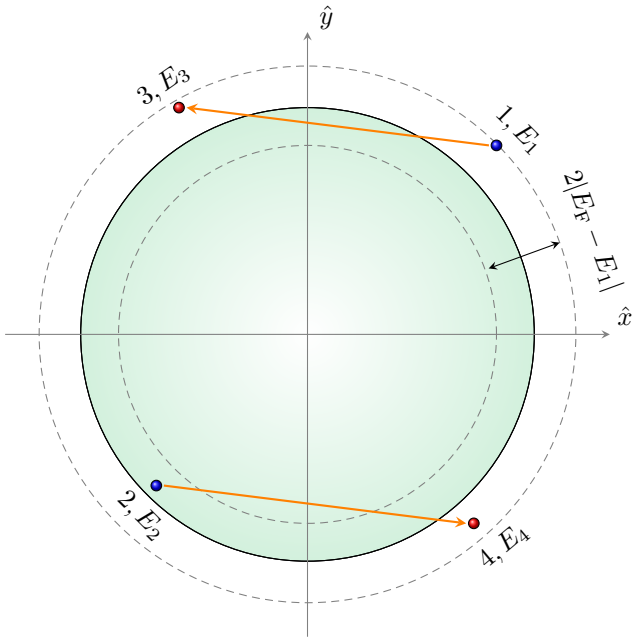

Figure 1.1: Scattering processes around a one-dimensional Fermi surface (black circle) in two-dimensional momentum space. The shaded region corresponds to the occupied states. An electron (1) with energy E_1 over the Fermi energy E_F interacts with an electron (2) with energy $E_2 < E_F$ and get scattered into states with energy $E_3 > E_F$ (3) and $E_4 > E_F$ (4), respectively, as a consequence of Pauli's exclusion principle. Energy conservation requires that E_2, E_3 and E_4 lie within a shell of thickness $2|E_F - E_1|$ around the Fermi surface (region bounded by the dashed circles).

The key question is whether the ideal Fermi gas picture remains valid once short-range electron-electron interactions are turned on. Landau postulated that some of these features are preserved in the low-energy sector of the interacting theory provided that the interactions are turned on adiabatically[3]. This is commonly known as *Landau's Fermi-Liquid Theory* (FLT) [50, 51]. The starting point of this phenomenological theory is the assumption that the ground state of the interacting system is in one-to-one correspondence with that of the ideal Fermi gas. Landau's key idea is to describe the low energy excitations of the interacting system in terms of fermionic *quasiparticles* which have a similar spectrum as that of free electrons, but renormalized due to the effect of the short-range interactions [50, 51]. In Landau's picture, the energy levels of the quasiparticles are labeled by the same quantum numbers as those for the ideal Fermi gas (i.e., spin and momentum). The low-lying excitations of the interacting system are labeled by the occupation number of quasiparticles whose energy E (or equivalently, momentum $\vec{k}$) satisfy the condition: $|E - E_F| \ll E_F$ ($|\vec{k} - \vec{k}_F| \ll k_F$).

It is legitimate to question the validity of Landau's idea since, even in the presence of a screened Coulomb potential, the electron-electron scattering rates can be quite high and therefore the quasiparticle picture may be invalidated due to the absence of stable (long-lived) low-energy excitations. However, Pauli's exclusion principle dramatically reduces the possible electronic non-forward scatterings at temperatures $T \ll E_F$ [48]. To see how this comes about, consider the system at zero temperature and suppose that there is a *single* quasiparticle excitation with energy $E_1 > E_F$ in the system. For this quasiparticle to get scattered, it necessarily has to interact with a quasiparticle within the Fermi sea with energy $E_2 < E_F$. Pauli's exclusion principle requires these two electrons to be scattered into *unoccupied* states, i.e., into states with energies $E_3 > E_F$ and $E_4 > E_F$. This is shown in Fig.

[3]By this it is meant that the noninteracting states evolve smoothly into the interacting ones without encountering any singular behavior as a consequence of a phase transition.

1.1 for the simple case of a circular FS in two dimensions. In addition to these conditions, energy conservation requires that

$$E_1 + E_2 = E_3 + E_4. \tag{1.3}$$

Since $E_1 > E_\mathrm{F}$, all $E_2 < E_\mathrm{F}, E_3 > E_\mathrm{F}$ and $E_4 > E_\mathrm{F}$ should be chosen to lie between a shell of thickness $2|E_\mathrm{F} - E_1|$ around the FS. Therefore, there is a nonvanishing phase space for the scattering process and thus a non vanishing cross section. Consequently, the quasiparticle with energy $E_1 > E_\mathrm{F}$ will have a finite lifetime, and thus can become incoherent. However, the energy conservation in Eq. (1.3) imposes a strong constraint in the choice of energies E_2, E_3 and E_4 for $|E_1 - E_\mathrm{F}| \ll E_\mathrm{F}$. Such a constraint implies that the scattering rate of the electrons scales as $(E_1 - E_\mathrm{F})^2$, and the lifetime of the quasiparticle excitation at zero temperature scales with energy as

$$\tau \sim \frac{E_\mathrm{F}}{(E_1 - E_\mathrm{F})^2}. \tag{1.4}$$

Hence, at zero temperature, the quasiparticle excitations above the FS become more stable as their energy approaches the Fermi energy. This is one of the key features of Landau's FLT and this argument shows that the low-energy sector of the theory of interacting electrons is well described by the quasiparticle picture.

At a given nonzero temperature T, Eq. (1.1) is smeared into the Fermi-Dirac distribution in Eq. (1.2) and the single-particle levels are partially occupied on a shell of thickness of order T. This provides an extra range for the energies E_2, E_3 and E_4 in the previous discussion and thus the scattering rate receives a thermal correction of order T^2. In this case, Eq. (1.4) is modified to

$$\tau \sim \frac{E_\mathrm{F}}{(E - E_\mathrm{F})^2 + T^2}. \tag{1.5}$$

At nonzero temperature, quasiparticles on the FS have a finite lifetime $\tau \sim E_\mathrm{F} T^{-2}$. Eq. (1.5) shows that Landau's quasiparticle picture becomes well-defined at sufficiently low energies and temperature.

Now we turn our attention to the main physical signatures of Fermi-liquid metals. In the low-temperature limit, Eq. (1.5) implies, according to Drude's theory of metals [48], that the resistivity of a Fermi-liquid metal scales with temperature as

$$\rho(T) \sim \rho_0 + \rho_1 T^2, \tag{1.6}$$

where ρ_0 and ρ_1 are temperature-independent constants that are not universal (i.e., material-dependent). Apart from the scaling of the resistivity with temperature, the most important experimental signatures of Fermi-liquid metals are the temperature dependences of thermodynamic observables. Since Landau's FLT is reliable when the quasiparticle occupation number deviates slightly from the thermal equilibrium one, the total energy of the system is well approximated by [50]:

$$\begin{aligned} \mathscr{E}[\delta n(\vec{k})] = \mathscr{E}_0 &+ \sum_{\sigma=\uparrow,\downarrow} \int \mathrm{d}\vec{k}\; E_0(\vec{k}) \delta n_{\sigma\sigma}(\vec{k}) \\ &+ \frac{1}{2} \sum_{\alpha,\beta,\gamma,\delta=\uparrow,\downarrow} \int \mathrm{d}\vec{k} \int \mathrm{d}\vec{k}'\; f^{\alpha\beta}_{\gamma\delta}(\vec{k},\vec{k}') \delta n_{\alpha\beta}(\vec{k}) n_{\gamma\delta}(\vec{k}') + \mathcal{O}[\delta n(\vec{k})^3], \end{aligned} \tag{1.7}$$

where $\mathscr{E}_0$ is the ground state energy at zero temperature, $E_0(\vec{k})$ is the energy of quasiparticles at zero temperature measured with respect to the Fermi energy, and $\delta n_{\sigma\sigma'}(\vec{k}) = n_{\sigma\sigma'}(\vec{k}) - 2\delta_{\sigma\sigma'} n_{\mathrm{F.D}}(\vec{k})$ is the deviation from the thermal equilibrium quasiparticle distribution. The quasiparticle density and magnetization at momentum $\vec{k}$ are given by $\mathfrak{N} \equiv \mathrm{Tr}[n_{\sigma\sigma'}(\vec{k})]$ and $\vec{\mathfrak{M}} \equiv \mathrm{Tr}[n(\vec{k})\vec{\sigma}]$, where $\vec{\sigma} = (\sigma_x, \sigma_y, \sigma_z)$ denotes the vector of Pauli matrices and the trace is taken over the spin indices. The function $f^{\alpha\beta}_{\gamma\delta}(\vec{k}, \vec{k}')$, known as Landau's interaction function, captures the forward scattering between quasiparticles and it satisfies the symmetry property: $f^{\alpha\beta}_{\gamma\delta}(\vec{k}, \vec{k}') = f^{\gamma\delta}_{\alpha\beta}(\vec{k}', \vec{k})$. In Eq. (1.7), $\mathrm{d}\vec{k} = \mathrm{d}^d\vec{k}/(2\pi)^d$ denotes the integration measure in d spatial dimensions. In the following discussion we keep the dimensionality general and only fix it when needed.

Eq. (1.7) postulates that the main features of Fermi-liquid metals are captured by the quasiparticle energy spectrum and Landau's interaction function. Since Landau's FLT is valid only when the quasiparticle momentum is such that $|\vec{k} - \vec{k}_{\mathrm{F}}| \ll k_F$, the quasiparticle energy can be written as

$$E_0(\vec{k}) \approx \frac{1}{m^*}(\vec{k} - \vec{k}_{\mathrm{F}}) \cdot \vec{k}_{\mathrm{F}}, \tag{1.8}$$

where, m^* is the *effective mass* of the quasiparticle which differs from the bare electronic mass m. The quasiparticle effective mass determines the specific heat in the low-temperature limit [48]:

$$c_V = \frac{1}{3} m^* k_{\mathrm{F}} T. \tag{1.9}$$

The specific heat has the same temperature-dependence as that of free electrons, but with a renormalized mass as a consequence of the electron-electron interactions. As we shall see below, m^* is related to the mass of the free electron through Landau's interaction function in the presence of Galilean invariance.

Since the deviation of the quasiparticle occupation number from the ground state distribution is significant only in the proximity of the FS at low temperatures, the momenta in the Landau function in Eq. (1.7) can be evaluated at the Fermi momentum. Therefore, the interaction function will depend only on the direction of the momenta $\vec{k}$ and $\vec{k}'$. To build some intuition about this function we assume that the system is in two spatial dimensions with a circular FS and that it has SU(2)-spin symmetry[4]. In this case, Landau's interaction function depends only on the relative angle φ between $\vec{k}$ and $\vec{k}'$ and one can write it in the most general form as [51]

$$\mathcal{N}_{\mathrm{F}}(0) f^{\alpha\beta}_{\gamma\delta}(\vec{k}, \vec{k}') \approx \mathsf{F}(\varphi)\delta_{\alpha\beta}\delta_{\gamma\delta} + \mathsf{G}(\varphi)\left(\vec{\sigma}_{\alpha\beta} \cdot \vec{\sigma}_{\gamma\delta}\right), \tag{1.10}$$

where $\mathcal{N}_{\mathrm{F}}(0)$ is the quasiparticle density of states at the Fermi energy. The functions $\mathsf{F}(\varphi)$ and $\mathsf{G}(\varphi)$ encode the effect of the electron-electron interaction through their expansion coefficients when written in the Legendre polynomial basis:

$$\mathsf{R}(\varphi) = \sum_{l=0}^{\infty} (2l+1) R_l P_l(\cos\varphi), \quad \mathsf{R}_l = \frac{1}{2}\int_0^{\pi} \mathrm{d}\varphi \ \sin\varphi \ \mathsf{R}(\varphi) P_l(\cos\varphi), \tag{1.11}$$

[4] A similar treatment holds for any dimensionality and for arbitrary shapes of the FS. Here we assume that the FS has spherical symmetry for simplicity and this corresponds to the physical situation in which there is a low density of electrons.

where $\mathsf{R} = \mathsf{F}, \mathsf{G}$, and F_l and G_l are expansion coefficients with l denoting the angular momentum quantum number, and $P_l(x)$ is the lth Legendre polynomial. These coefficients encapsulate the electron-electron interactions in the different angular momentum channels and are known as the *Landau parameters*. For Galilean-invariant systems, the effective mass of the quasiparticles is related to the mass of the free electron through the Landau parameters as [50, 51]:

$$\frac{m^*}{m} = 1 + \mathsf{F}_1. \tag{1.12}$$

Similarly, the compressibility (κ) and spin-susceptibility (χ) of the Fermi liquid are given, in terms of the Landau parameters by

$$\kappa = \frac{1}{n^2}\frac{\mathcal{N}_{\mathrm{F}}(0)}{1+\mathsf{F}_0}, \qquad \& \qquad \chi = \frac{g^2}{4}\frac{\mathcal{N}_{\mathrm{F}}(0)}{1+\mathsf{G}_0}, \tag{1.13}$$

where n is the quasiparticle density and g is the gyromagnetic ratio. We note that these are exactly the same expressions as in the ideal Fermi gas up to the factors of the form $(1+\mathsf{F}_0)^{-1}$ and $(1+\mathsf{G}_0)^{-1}$ which encapsulate the renormalization effects generated by the interaction amongst the quasiparticles [50, 51]. To end this section we note that Pomeranchuk developed a criterion for the stability of the Fermi-liquid metallic phase against the formation of any type of order [52]. For the simple case under consideration, Pomeranchuk's stability criterion asserts that if the Landau parameters satisfy the condition

$$\mathsf{F}_l > -1, \qquad \& \qquad \mathsf{G}_l > -1, \quad \forall l \in \mathbb{N}, \tag{1.14}$$

the Fermi-liquid metallic phase is stable.

1.1-(*b*) The Fermi-Liquid as a Renormalization Group Fixed Point

We now proceed on describing Landau's FLT in the language of EFTs. Although successful in the description of the low-energy properties of conventional metals, Landau's FLT was originally conceived as a phenomenological theory. It was not until the problem of interacting electrons at finite density was studied under the framework of EFTs, and analyzed through the lens of the RG, that Landau's FLT found a solid theoretical ground. Through the use of zero and nonzero temperature RG techniques, Landau's FLT is understood as a stable *low-energy fixed point* of metals with short-range electron-electron interactions [53–58].

The EFT describing electrons at finite density with short-range electron-electron interactions in the $(d+1)$-dimensional Euclidean space is written as [54–58]

$$\begin{aligned} S_{\mathrm{FL}} = \sum_{\sigma=\uparrow,\downarrow}\int \mathrm{d}k\ \psi^\dagger_\sigma(k)[ik_0 + \varepsilon(\vec{k}) - E_{\mathrm{F}}]\psi_\sigma(k) + \sum_{\sigma_i=\uparrow,\downarrow}\left[\prod_{i=1}^{4}\int \mathrm{d}k_i\right]\lambda^{\sigma_1\sigma_2}_{\sigma_3\sigma_4}(\vec{k}_1,\vec{k}_2,\vec{k}_3,\vec{k}_4) \\ \times\ \psi^\dagger_{\sigma_1}(k_1)\psi^\dagger_{\sigma_2}(k_2)\psi_{\sigma_3}(k_3)\psi_{\sigma_4}(k_4)(2\pi)^{d+1}\delta^{(d+1)}(k_1+k_2-k_3-k_4). \end{aligned} \tag{1.15}$$

Here, $k = (k_0, \vec{k})$ denotes fermionic Matsubara frequency (k_0) and d-dimensional spatial momentum ($\vec{k}$). We use the notation $\mathrm{d}k = [\mathrm{d}k_0/(2\pi)][\mathrm{d}^d\vec{k}/(2\pi)^d]$ for the integration measure. The field $\psi_\sigma(k)$ is a Grassmann field representing an electron with frequency and momentum

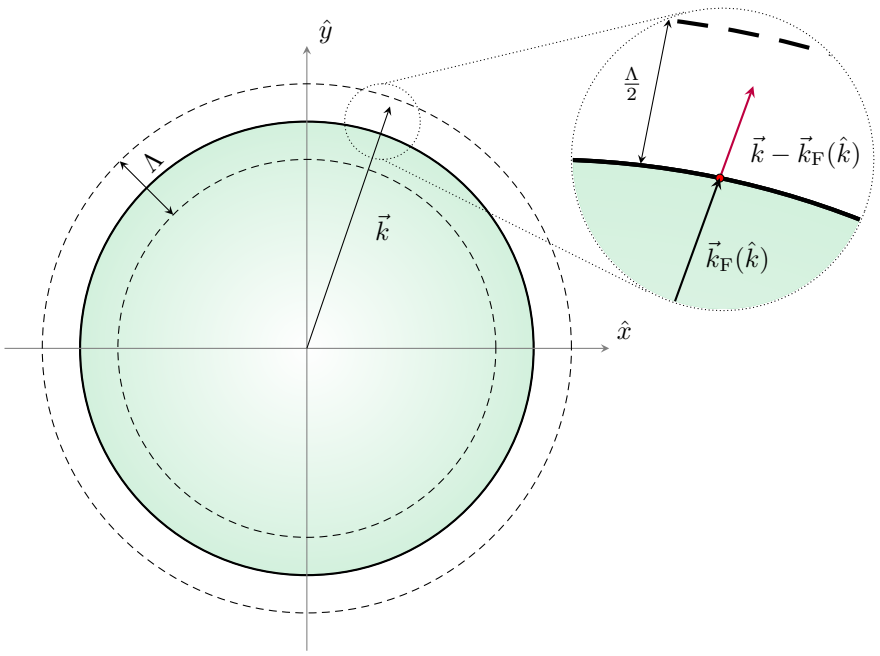

Figure 1.2: One-dimensional circular Fermi surface (solid circle) in two-dimensional momentum space. The dashed circles bound the shell of thickness $\Lambda \ll k_{\rm F}$ which enclose the low-energy degrees of freedom of the metallic phase.

k and spin $\sigma = \uparrow, \downarrow$. The energy dispersion of the electron is denoted by $\varepsilon(\vec{k})$ and $E_{\rm F} = \varepsilon(\vec{k}_{\rm F})$ is the Fermi energy. The four-fermion interaction sources the scattering of electron pairs where momentum is conserved. The strength of the interactions is encoded in the momentum-dependent coupling function $\lambda^{\sigma_1\sigma_2}_{\sigma_3\sigma_4}(\vec{k}_1, \vec{k}_2, \vec{k}_3, \vec{k}_4)$. The local interaction term in Eq. (1.15) can be thought of arising from a short-range interaction encompassing a combination of the screened Coulomb potential and the phonon-induced electron-electron interaction that the electrons are subjected to in a conventional metal. Finally, $\delta^{(d+1)}(k)$ is the $(d+1)$-dimensional Dirac distribution. We note the similarity between Eqs. (1.15) and (1.7). Indeed, the Landau interaction function is related to the four-fermion coupling function and as we shall see, the latter corresponds to the low-energy fixed point of the four-fermion coupling under the RG. The latter resemblance becomes more apparent when it is noted that the most general four-fermion interaction that is invariant under SU(2)-spin rotations can be decomposed as [see Eq.(1.10) for a comparison] [56]

$$\lambda^{\sigma_1\sigma_2}_{\sigma_3\sigma_4}(\vec{k}_1, \vec{k}_2, \vec{k}_3, \vec{k}_4) = F(\vec{k}_1, \vec{k}_2, \vec{k}_3, \vec{k}_4)\delta_{\sigma_1\sigma_3}\delta_{\sigma_2\sigma_4} + G(\vec{k}_1, \vec{k}_2, \vec{k}_3, \vec{k}_4)\left(\vec{\sigma}_{\sigma_1\sigma_3} \cdot \vec{\sigma}_{\sigma_2\sigma_4}\right), \quad (1.16)$$

with F and G some analytic functions of the momenta. The analyticity condition comes from the fact that the four-fermion interaction is local and short-ranged.

The RG analysis of Eq. (1.15) starts by noting that the low-energy excitations of the system are electrons whose energy is close to the Fermi energy. In the spirit of the Wilsonian RG [54, 55], we consider a shell of thickness $\Lambda \ll k_{\rm F}$ around the Fermi surface (as shown in Fig. 1.2 for the case of a circular FS in two spatial dimensions) and write down the EFT

by integrating out electronic modes that have energies outside the shell. This renders an effective theory with ultraviolet (UV) cutoff Λ:

$$\begin{aligned} S_{\rm FL}^{\Lambda} = & \sum_{\sigma=\uparrow,\downarrow} \int_{\Lambda} \mathrm{d}k \; \psi_{\sigma}^{\dagger}(k) \left\{ ik_0 + \vec{v}_{\rm F}(\widehat{k}) \cdot [\vec{k} - \vec{k}_{\rm F}(\widehat{k})] \right\} \psi_{\sigma}(k) \\ & + \sum_{\sigma_i=\uparrow,\downarrow} \left[\prod_{i=1}^{4} \int_{\Lambda} \mathrm{d}k_i \right] \lambda_{\sigma_3\sigma_4}^{\sigma_1\sigma_2}(\vec{k}_1, \vec{k}_2, \vec{k}_3, \vec{k}_4) \psi_{\sigma_1}^{\dagger}(k_1) \psi_{\sigma_2}^{\dagger}(k_2) \psi_{\sigma_3}(k_3) \widetilde{\psi}_{\sigma_4}(k_4) \\ & \times (2\pi)^{d+1} \delta^{(d+1)}(k_1 + k_2 - k_3 - k_4), \end{aligned} \tag{1.17}$$

where $\vec{k}_{\rm F}(\widehat{k})$ is the Fermi momentum closest to $\vec{k}$ which depends on the orientation of the momentum $\widehat{k} \equiv \vec{k}/|\vec{k}|$. In Eq. (1.17), the dispersion of the electron has been linearized close to the FS with $\vec{v}_{\rm F}(\widehat{k})$ denoting the Fermi velocity which also depends on orientation of the electronic momentum. The subscript in the integration symbol is used to denote that the integration is done over momenta such that $\left| \vec{v}_{\rm F}(\widehat{k}) \cdot [\vec{k} - \vec{k}_{\rm F}(\widehat{k})] \right| \ll \Lambda \ll k_{\rm F}$. At low-energies, and in the spirit of the RG [54–58], we expand the four-fermion coupling function in powers of $[\vec{k} - \vec{k}_{\rm F}(\widehat{k})]$ and keep only the first term in the expansion because the momentum-dependent terms are irrelevant in the RG sense. Therefore, to leading order in this expansion the four-fermion coupling function in Eq. (1.17) depends only on the orientation of the electronic momenta: $\lambda_{\sigma_3\sigma_4}^{\sigma_1\sigma_2}(\vec{k}_1, \vec{k}_2, \vec{k}_3, \vec{k}_4) \approx \lambda_{\sigma_3\sigma_4}^{\sigma_1\sigma_2}(\hat{k}_1, \hat{k}_2, \hat{k}_3, \hat{k}_4; k_{\rm F})$. From now on we focus on the zero temperature case and we note that the results we are about to present hold for temperatures such that $T \ll E_{\rm F}$ [54–58]. We further consider the case of a spherically symmetric FS, in which case the Fermi velocity is uniform and normal to every point on the zero energy manifold. In this concrete case, one can further manipulate Eq. (1.17) in order to write it in terms of the momentum *along* and *normal* to the FS. Using generalized spherical coordinates Eq. (1.17) takes the form

$$\begin{aligned} S_{\rm FL}^{\Lambda} = & \sum_{\sigma=\uparrow,\downarrow} \int_{S^{d-1}} \frac{\mathrm{d}\Omega_{d-1}}{(2\pi)^{d-1}} \int_{\mathbb{R}} \frac{\mathrm{d}k_0}{(2\pi)} \int_{-\Lambda}^{\Lambda} \frac{\mathrm{d}k}{(2\pi)} \; \widehat{\psi}_{\sigma}^{\dagger}(k_0, k; \Omega_{d-1}) [ik_0 + v_{\rm F}k] \widehat{\psi}_{\sigma}(k_0, k; \Omega_{d-1}) \\ & + \sum_{\sigma_i=\uparrow,\downarrow} \left[\prod_{i=1}^{4} \int_{S^{d-1}} \frac{\mathrm{d}\Omega_{d-1}^{(i)}}{(2\pi)^{d-1}} \int_{\mathbb{R}} \frac{\mathrm{d}k_{0;i}}{(2\pi)} \int_{-\Lambda}^{\Lambda} \frac{\mathrm{d}k_i}{(2\pi)} \right] \widehat{\lambda}_{\sigma_3\sigma_4}^{\sigma_1\sigma_2}(\Omega_{d-1}^{(1)}, \Omega_{d-1}^{(2)}, \Omega_{d-1}^{(3)}, \Omega_{d-1}^{(4)}) \\ & \times \widehat{\psi}_{\sigma_1}^{\dagger}(k_{0;1}, k_1, \Omega_{d-1}^{(1)}) \widehat{\psi}_{\sigma_2}^{\dagger}(k_{0;2}, k_2, \Omega_{d-1}^{(2)}) \widehat{\psi}_{\sigma_3}(k_{0;3}, k_3, \Omega_{d-1}^{(3)}) \widehat{\psi}_{\sigma_4}(k_{0;4}, k_4, \Omega_{d-1}^{(4)}) \\ & (2\pi)^{d+1} \delta(k_{0;1} + k_{0;2} - k_{0;3} - k_{0;4}) \delta^{(d)} \left[\widehat{k}_1(\Omega_{d-1}^{(1)}) + \widehat{k}_2(\Omega_{d-1}^{(2)}) - \widehat{k}_3(\Omega_{d-1}^{(3)}) - \widehat{k}_4(\Omega_{d-1}^{(4)}) \right]. \end{aligned} \tag{1.18}$$

where Ω_{d-1} denotes the angle of $\vec{k}$ on the FS and which parametrizes the $(d-1)$-dimensional sphere. In this action, the fields and four-fermion couplings are given, in terms of the original ones by $\widehat{\psi}_{\sigma}(k_0, k, \Omega_{d-1}) = k_{\rm F}^{\frac{(d-1)}{2}} \psi(k_0, [k+k_{\rm F}]\Omega_{d-1})$ and $\widehat{\lambda}_{\sigma_3\sigma_4}^{\sigma_1\sigma_2}(\Omega_{d-1}^{(1)}, \Omega_{d-1}^{(2)}, \Omega_{d-1}^{(3)}, \Omega_{d-1}^{(4)}) = k_{\rm F}^{(d-1)} \lambda(\widehat{k}_1', \widehat{k}_2', \widehat{k}_3', \widehat{k}_4'; k_{\rm F})$, respectively, with, k_i' denoting the momentum written in generalized spherical coordinates. It is noted that this action is valid in the limit in which $|k_i| \ll k_{\rm F}$ for all $i = 1, 2, 3, 4$, which justifies dropping the magnitude of the fermionic momenta compared to $k_{\rm F}$ inside the momentum-conserving Dirac distribution and approximating the

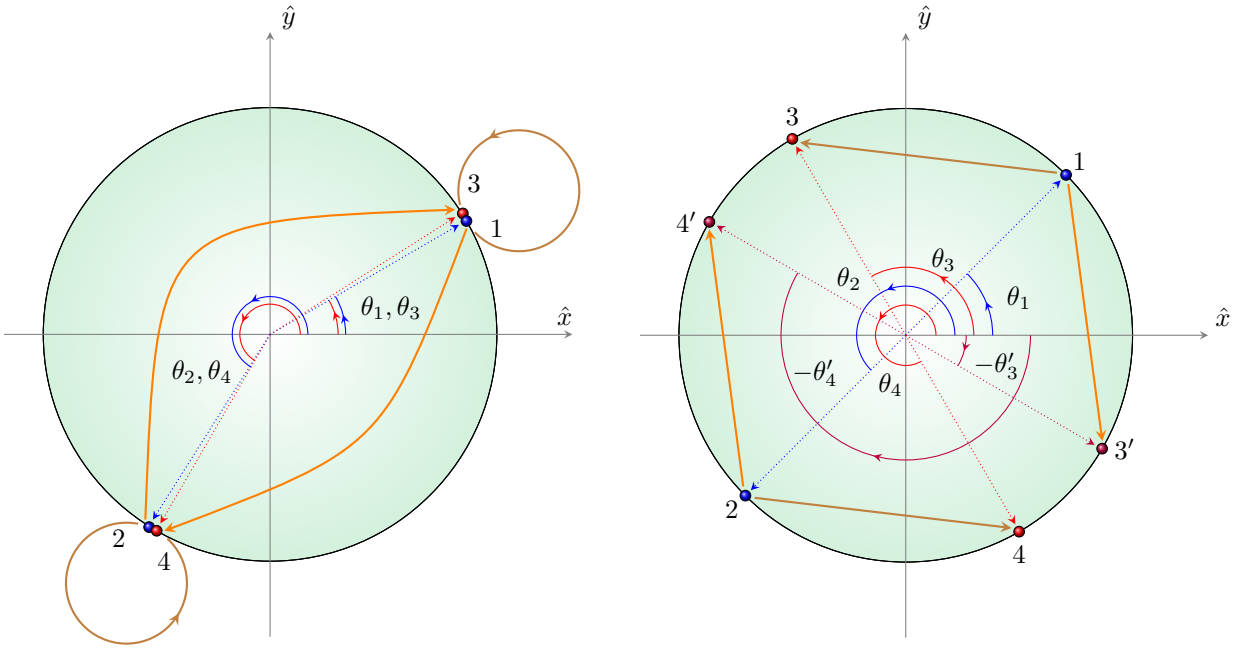

(a) (b)

Figure 1.3: (a) The forward scattering and (b) BCS scattering channels. For a circular Fermi surface in two-dimensional momentum space, the orientation of the electronic momenta of the ith electron is parametrized by the angles $0 \leq \theta_i \leq 2\pi$. In ($a$) the initial and final states of the scattering have been displaced for clarity.

integration measure over the spatial momentum as $\mathrm{d}^d\vec{k} \approx k_{\mathrm{F}}^{(d-1)}\mathrm{d}k\ \mathrm{d}\Omega_{d-1}$. As it can be seen from Eq. (1.18), the angle along the FS becomes merely a dimensionless flavor. These coordinates label the low-energy gapless electronic modes of the metal. In contrast, the momentum normal to the FS is dimensionful in the conventional RG scaling analysis[5]. Writing the action as in Eq. (1.18) effectively maps the $(d+1)$-dimensional theory into a $(1+1)$-dimensional theory of electrons with a continuous flavor parametrized by the momentum along the FS [54, 55].

The action in Eq. (1.18) depends implicitly on the UV scale Λ and the size of the FS, which is parametrized by k_{F}. The low-energy sector of the theory is characterized by the hierarchy of scales: $\Lambda \ll k_{\mathrm{F}}$. In the Wilsonian RG picture for interacting fermions, the process of lowering the UV scale Λ is tantamount to gradually approach the FS, and thus

[5] We note that the decomposition of the spatial momenta in terms of momentum along and normal to the FS does not require the FS to have any particular symmetry. In fact, for any smooth surface a decomposition into the tangent and normal directions is always possible. Furthermore, when the electrons are in the presence of short-range interactions (a fundamental assumption behind Landau's FLT), the momentum along the FS is parametrized by dimensionless quantities and only the momentum normal to the surface is important in the scaling analysis. In Chapter 4 we show an example where this picture breaks down due to the presence of long-range interactions. In there, the momentum along the FS not only acts as a continuous flavor parametrizing the low-energy fermionic degrees of freedom, but it also enters in the scaling analysis of the low-energy theory.

the dimensionless ratio $\Lambda/k_{\rm F}$ becomes a small parameter in the theory. Therefore, under successive mode elimination, $\Lambda/k_{\rm F} \to 0$ [54, 55]. The fact that $\Lambda/k_{\rm F}$ is a small parameter at low-energies has striking consequences on the allowed electron-electron scatterings of the theory. These arise from momentum conservation, which enforces the condition on the orientation of the fermionic momenta:

$$\widehat{k}_1(\Omega_{d-1}^{(1)}) + \widehat{k}_2(\Omega_{d-1}^{(2)}) - \widehat{k}_3(\Omega_{d-1}^{(3)}) - \widehat{k}_4(\Omega_{d-1}^{(4)}) = 0, \tag{1.19}$$

where $\widehat{k}_i \equiv \widehat{k}_i(\Omega_{d-1}^{(i)})$ with $\widehat{k}_i^2 = 1$. As $\Lambda/k_{\rm F} \to 0$, the phase space of most scatterings channels shrinks and therefore, Eq. (1.19) has only a few possible solutions. In this limit, the only significant scattering channels at low energies are the *forward scattering* and the *Bardeen-Cooper-Schrieffer* (BCS) [59, 60] channels [54–58]. These are depicted in Fig. 1.3 for the case of a circular FS in two dimensions.

The forward scattering channel is characterized by the scattering with $\widehat{k}_3 = \widehat{k}_1$ and $\widehat{k}_4 = \widehat{k}_2$ or $\widehat{k}_3 = \widehat{k}_2$ and $\widehat{k}_4 = \widehat{k}_1$ arbitrarily close to the FS. These two possibilities are depicted in Fig. 1.3(*a*). The BCS channel, on the other hand, corresponds to the case in which the orientation of the initial and final momenta are given by $\widehat{k}_1 = -\widehat{k}_2$ and $\widehat{k}_3 = -\widehat{k}_4$, respectively. This allows two electrons on antipodal points arbitrarily close to the FS to be scattered to any other two antipodal points close to the FS. In Fig. 1.3(*b*) we exemplify the BCS processes. It follows that the four-fermion coupling functions that survive at low energies effectively depend only on two independent momenta, and in the case of spherical symmetry, it depends only on the relative angle between these momenta. The forward scattering channel is precisely what Landau's FLT postulates in Eqs. (1.7) and (1.10) from a phenomenological perspective [50, 51]. Here, we view this as emerging from a tree-level scaling analysis of the action in Eq. (1.18) [54–58].

A straightforward scaling analysis of Eq. (1.18) in which frequency and momentum have scaling dimensions $[k_0] = [k] = 1$, reveals that the scaling dimension of the fermion field is given by $[\widehat{\psi}_\sigma(k)] = -3/2$ which implies hat both the forward scattering and BCS channels are marginal at the tree-level ($[\widehat{\lambda}^{\sigma_1\sigma_2}_{\sigma_3\sigma_4}(\Omega_{d-1}^{(1)}, \Omega_{d-1}^{(2)}, \Omega_{d-1}^{(3)}, \Omega_{d-1}^{(4)})] = 0$). This remains to be true for the forward scattering channel upon including loop corrections. However, the BCS channel becomes either marginally relevant or irrelevant depending on the sign of the value of the bare four-fermion coupling. This comes as a solution to the one-loop flow equations for the four-fermion coupling functions. In the case of spherical symmetry, this translates into computing the beta function for the Landau parameters [54–58]. Therefore, the Landau parameters introduced earlier from a phenomenological perspective correspond to the marginal couplings at the fixed point.

In the EFT and RG languages, Pomeranchuk's stability criterion [52] in Eq. (1.14) is nothing else than the condition for the low-energy fixed point of the theory to be stable. However, we point out that even if Pomeranchuk's stability criterion is met, the Fermi-liquid metallic phase becomes unstable at sufficiently low energies. The RG analysis for the BCS channel shows that, if at the bare level there is a nonzero attractive interaction (i.e., the value of the bare coupling is negative), the system becomes unstable and eventually transitions into a superconducting phase. This is commonly known as the BCS instability and happens at a finite energy scale which is associated to the superconducting temperature of the underlying material [54–58]. Provided that Pomeranchuk's conditions are satisfied, the Fermi-liquid metallic phase is stable and only the forward scattering channel governs

the low-energy physics of the metallic phase at temperatures above the superconducting transition temperature [52, 56–58].

Although the four-fermion coupling in the forward scattering channel is marginal, it offers corrections to the free electron picture without modifying its scaling properties. Such corrections are also manifest themselves in the two-point function for the electron. From Eq. (1.17), this one reads,

$$G(k_0,\vec{k}) = \frac{1}{ik_0 + \vec{v}_{\rm F}(\widehat{k})\cdot[\vec{k}-\vec{k}_{\rm F}(\widehat{k})] + \Sigma(k_0,\vec{k};\lambda)}, \tag{1.20}$$

where $\Sigma(k_0,\vec{k};\lambda)$ is the fermion self-energy and λ is a short-hand notation for the four-fermion couplings. Analytic continuation of this expression to real frequency ($-ik_0 \to \omega + i0^+$) yields the retarded Green's function [61]

$$G^{\rm R}(k_0,\vec{k}) = \frac{1}{\omega - i0^+ - \vec{v}_{\rm F}(\widehat{k})\cdot[\vec{k}-\vec{k}_{\rm F}(\widehat{k})] - \Sigma^{\rm R}(\omega,\vec{k};\lambda)}, \tag{1.21}$$

where $\Sigma^{\rm R}(\omega,\vec{k};\lambda) = \Sigma(i\omega - 0^+,\vec{k};\lambda)$. The spectroscopic properties are encoded in the *electronic spectral function*, $\mathcal{A}(\omega,\vec{k}) \equiv 2{\rm Im}\left[G^{\rm R}(\omega,\vec{k})\right]$, which takes the generic form

$$\mathcal{A}(\omega,\vec{k}) = \frac{2{\rm Im}\left[\Sigma^{\rm R}(\omega,\vec{k};\lambda)\right]}{\left\{\omega - \vec{v}_{\rm F}(\widehat{k})\cdot[\vec{k}-\vec{k}_{\rm F}(\widehat{k})] - {\rm Re}\left[\Sigma^{\rm R}(\omega,\vec{k};\lambda)\right]\right\}^2 + {\rm Im}\left[\Sigma^{\rm R}(\omega,\vec{k};\lambda)\right]^2}. \tag{1.22}$$

The spectral function has a peak at the *renormalized energy* $\omega(\vec{k})$ satisfying the equation

$$\omega(\vec{k}) - \vec{v}_{\rm F}(\widehat{k})\cdot[\vec{k}-\vec{k}_{\rm F}(\widehat{k})] - {\rm Re}\left\{\Sigma^{\rm R}\left[\omega(\vec{k}),\vec{k};\lambda\right]\right\} = 0, \tag{1.23}$$

provided that ${\rm Im}\left[\Sigma^{\rm R}(\omega,\vec{k};\lambda)\right]$ varies slowly in ω near $\omega \approx \omega(\vec{k})$. The width of the peak is controlled by ${\rm Im}\left\{\Sigma^{\rm R}\left[\omega(\vec{k}),\vec{k};\lambda\right]\right\}$. If the imaginary part of the fermion-self energy is small, the peak is sharp and this is interpreted as a particle-like excitation with energy $\omega(\vec{k})$ and life time $\tau(\vec{k}) \sim 1/{\rm Im}\left\{\Sigma^{\rm R}\left[\omega(\vec{k}),\vec{k};\lambda\right]\right\}$ [61]. The condition $\omega(\vec{k}) = 0$ defines the *renormalized* FS. Although the interactions may deform the FS from that of the free electrons, the volume of the Fermi ball does not change. This is commonly known as *Luttinger's theorem* [53].

If the spectral function is highly peaked around $\omega(\vec{k})$ given in Eq. (1.23), one can approximate the spectral function by expanding it around $\omega \approx \omega(\vec{k})$:

$$\mathcal{A}(\omega,\vec{k}) = \frac{Z(\vec{k})}{\tau(\vec{k})}\frac{1}{[\omega-\omega(\vec{k})]^2 + \tau(\vec{k})^{-2}} + \mathcal{A}_{\rm Inc.}(\omega,\vec{k}), \tag{1.24}$$

where the *quasiparticle weight* $Z(\vec{k})$ and *quasiparticle lifetime* $\tau(\vec{k})$ are obtained from the fermion self-energy through the expressions [53, 61]

$$Z(\vec{k}) = \left\{1 - \frac{\partial}{\partial\omega}{\rm Re}\left[\Sigma^{\rm R}(\omega,\vec{k};\lambda)\right]\Big|_{\omega=\omega(\vec{k})}\right\}^{-1}, \tag{1.25}$$

$$\frac{1}{\tau(\vec{k})} = Z(\vec{k})\mathrm{Im}\left\{\Sigma^{\mathrm{R}}\left[\omega(\vec{k}),\vec{k};\lambda\right]\right\}, \tag{1.26}$$

and $\mathcal{A}_{\mathrm{inc.}}(\omega,\vec{k})$ denotes the incoherent part of the spectral function which corresponds to a broad excitation spectrum with no particle-like features. We note at this point that Eq. (1.23) shows that the electron-electron interaction renormalizes the spectrum of the free electrons. This provides a renormalization of the electron mass which is expressed in terms of the renormalization of the Fermi velocity $\vec{v}_{\mathrm{F}}(\widehat{k})$. The quasiparticle weight $Z(\vec{k})$ encodes the overlap between the single-particle wave function of a free electron and the single-particle wave function of the quasiparticle excitation at a given momentum $\vec{k}$. Notice that in the limit of no interaction it reduces to one. Finally, an explicit computation of the self-energy shows that the quasiparticle lifetime diverges at the FS [i.e., at $\omega(\vec{k}) = \vec{0}$] and it decays as the energy of the electron strays away from the Fermi energy in accordance with Eq. (1.5). Very close to the FS, the lifetime of the quasiparticle excitation can be taken as infinite, in which case the spectral function in Eq. (1.24) is given by:

$$\mathcal{A}(\omega,\vec{k}) = Z(\vec{k})\delta\left[\omega - \omega(\vec{k})\right] + \mathcal{A}_{\mathrm{Inc.}}(\omega,\vec{k}). \tag{1.27}$$

It is important to note that the quasiparticle weight, quasiparticle lifetime and spectrum of the excitations are physical observables of the theory that can be accessed experimentally through angle-resolved photoemission spectroscopy (ARPES) experiments.

Not surprisingly, the above discussion shows that Landau's FLT is recovered as an emergent effective theory in the RG treatment of the EFT for electrons at finite density in the presence of short range interactions. In particular, the quantum corrections are not strong enough to modify the scaling properties of the theory. This is expressed in the fact that the Fermi liquid has a dynamical critical exponent $z = 1$, where, z quantifies the scaling dimension of frequency relative to that of the spatial momentum. Although Landau's FLT theory has been successful in determining the low-energy and low-temperature properties of conventional metals, it is far from being a general theory of all metallic states. To date there are several known metallic materials that display spectroscopic and thermodynamic properties that deviate from the predictions of Landau's FLT and in which there is no low-energy quasiparticle excitations. Such metallic states of matter are dubbed *non-Fermi-liquid metals*.

1.2 Non-Fermi Liquid Metals

The most prominent example that lies beyond the framework of Landau's FLT is the *Tomonaga-Luttinger liquid* which arises as the low-energy description of interacting fermions in one dimension [62–66]. The low-energy excitations of this metallic phase are charge and spin waves that propagate independently. Their single-particle spectral function exhibits no sharply defined peaks. The existence of metallic states beyond Landau's FLT is not endemic to one-dimensional electron systems. There are numerous examples of higher-dimensional *non-Fermi-liquid* (n-FL) metals. Amongst these, quantum hall systems [67–71] and layered materials such as high-temperature superconductors [29–36], heavy fermion compounds [37–40] and iron pnictides [41–47], excel as experimental examples in which spectral, transport

and thermodynamic observables display features that are inconsistent with Landau's FLT [72] and whose origin is still a matter of intensive research.

Strictly speaking, conventional metals also exhibit non-Fermi-liquid metallic behavior at sufficiently low energies due to electromagnetic fields. In the presence of an electromagnetic field, the Amperean (current-current) interaction between electrons is always present in conventional metals [73]. The Amperean interaction is induced by the transverse component of the electromagnetic field which is not screened, and therefore remains long-ranged. The effect of the Amperean interaction manifest itself through a vanishing quasiparticle weight on the FS and a logarithmic correction in temperature to the specific heat of free electrons [73]. However, such effects are significant only at temperatures way below the superconducting transition temperature due to the small value of the hyperfine coupling, and thus the normal state of the metal is still described by Landau's FLT[6]. Although the effect of the Amperean interaction will probably never see an experimental confirmation, it brings up the main ingredient that causes the demise of Landau's FLT: *long-range interactions between electrons*.

To develop a theory of n-FL metallic states that is analogous to Landau's FLT, it is of prime importance to study the effect of long-range interactions in systems with a finite density of electrons. Long-range interactions between electrons can be induced by their interaction with a massless collective bosonic mode. The bosonic degree of freedom can arise either as an emergent *gauge* field which remains gapless within a phase[7] or a *critical mode* which appears at critical points associated to a spontaneously broken symmetry [2, 4, 6, 7, 14, 20]. In the rest of the discussion we focus on the latter and restrict our discussion to those phase transitions that are driven by quantum fluctuations of the bosonic mode and whose description conforms to the Ginzburg-Landau symmetry-breaking paradigm[8]. Our goal is to understand the n-FL metallic states that arise in these quantum critical points (QCPs) of itinerant electrons. Although reaching a QCP requires fine tuning, the universal scaling properties of the QCP have the potential of dictating the finite temperature scaling behavior of thermodynamic and transport properties of the n-FL metal [85].

Although the study of itinerant QCPs is well motivated from a theoretical perspective, it has received more attention due to a large amount of experimental evidence that suggests the presence of one or more QCPs in high-temperature superconductors [29–36, 86–93], heavy fermion compounds [37–40] and iron pnictides [41–47, 94, 95]. In these materials, the temperature scaling of the resistivity signals the break down of Landau's FLT as a description of their normal state above the superconducting transition temperature [28]. This is commonly attributed to the physical properties of the n-FL metallic state realized at the QCP even if it is inaccessible in an experimental setting due to the onset of superconductivity. Therefore, a full understanding of n-FL metals arising in QCPs of itinerant electrons is crucial in explaining the anomalous properties of layered compounds.

The experimentally relevant itinerant QCPs can be roughly classified into two categories

[6] We further note that the effects of the interaction between vector-photons and electrons has also been studied and it constitutes another instance where Landau's FLT breaks down [74].

[7] Examples of these are the phases realized by the interaction between electrons at finite density and a gauge field [68, 73–82], and systems of itinerant electrons with a broken symmetry, where the momentum operator (which gives a well-defined quantum number for the free electrons) does not commute with the generators of the broken symmetry group [83].

[8] However, we note that there are known phase transitions that do not conform to this description and can, in principle, lead to novel n-FL metallic states [15, 84].

depending on whether the bosonic order parameter that drives the transition is spatially modulated or not [6, 96]. The spatial modulation of the order parameter determines the ordering wave vector $\vec{Q}_{\text{Order.}}$. Examples of QCPs where the order parameter is not spatially modulated ($\vec{Q}_{\text{Order.}} = \vec{0}$) arise at the *nematic* [89, 90, 93–95, 97–120] and *ferromagnetic* [87, 121–129] metallic transitions. Itinerant QCPs that involve the transition between a Fermi-liquid metal with no order and a metal with long-range *charge-density wave order* or *spin-density wave order* are examples of QCPs where the order parameter is spatially modulated ($\vec{Q}_{\text{Order.}} \neq \vec{0}$) [86, 88, 91, 92, 129–149]. The transition between a paramagnetic metal and a metal with long-range antiferromagnetic order constitutes an example of the latter. The QCP separating these two phases is commonly known as the *antiferromagnetic quantum critical point* (AFM QCP) [129, 131–135, 137–151] and the n-FL metal realized at the QCP is dubbed the *antiferromagnetic quantum critical metal*. In this thesis we focus, from a theoretical perspective, on the study of the critical properties of the AFM QCP and the low-energy properties of the AFM quantum critical metal. Before we delve into the study of this transition, we introduce the main strategy behind the study n-FL metals and recent theoretical developments in the field that are pertinent to this thesis.

1.2-(a) Effective Field Theories for Non-Fermi Liquid Metals

The low-energy properties of n-FL metallic states emerging at QCPs are best described through the language of EFTs. The reason for this is two-fold. On the one hand, the n-FL metallic states arise as a consequence of long-range interactions between electrons that are mediated by critical bosonic modes. On the other hand, as shown in Sec. 1.1-(b) , these states arise in QPTs of Fermi-liquid metallic states for which their EFT description is well understood. The RG machinery provides a powerful tool in the study of the universal low-energy properties of n-FL metals. Hence, the study of n-FL metals follows a similar strategy as the one introduce in Sec. 1.1-(b) : We seek for a description of these novel metallic states as a RG fixed point of the flow triggered by the interaction between the electrons and the gapless collective mode.

From an analytic point of view, the starting point is an EFT of a Fermi-liquid metal interacting with a critical order parameter. In Sec. 1.1-(b) we showed that, at the field theory level, a Fermi-liquid metal in $(d+1)$ dimensions can be understood in terms of a $(1+1)$-dimensional EFT that remains weakly coupled at low energies irrespective of the space dimension[9]. In the EFTs of n-FL metals such a mapping is generally unfeasible due to the interplay between the long-range interaction between electrons mediated by the collective mode. It is not surprising that the dimension of space plays an important role in their description when n-FL metals arising at QCPs are thought of as belonging to different universality classes. In one spatial dimension, for example, the absence of an extended zero-energy manifold for the electrons allows the low-energy EFT to be cast in terms of a relativistic field theory that usually has an emergent conformal symmetry. This is exemplified in the description of the one-dimensional Tomonaga-Luttinger liquid [62–66]. In higher

[9]Notice that this *does not* imply that the temperature scaling of thermodynamic and transport observables is independent of the space dimension. What this merely states is the fact that the low-energy scaling properties of Fermi liquid are governed by the scaling of a (1+1)-dimensional field theory of interacting electrons which *does not* modify the temperature scaling of observables obtained from the free electron picture.

dimensions, in contrast, the FS provides a large amount of particle-hole excitations that interact with the order parameter and the EFT has very low symmetry. Usually n-FL metallic states arise in dimensions below the upper critical dimension of the EFT used for their description, and in which fluctuations of the order parameter are expected to be strong [98–100, 102–114, 120–123, 129, 131–135, 137–139, 141–144, 146, 148]. In two spatial dimensions, quantum fluctuations of the order parameter are strong and their interaction with the gapless electronic modes close to the FS remains strong at low energies. Therefore, a wide class of n-FL metallic states are described by strongly-coupled field theories in two dimensions[10]. In what follows we focus on n-FL metals in two spatial dimensions.

The strong-coupling nature of the field theory renders perturbative approaches unfeasible. At a first glance one can think on borrowing nonperturbative methods engineered for strongly-coupled field theories of bosons and electrons at zero density. However, these usually rely on the presence of Lorentz symmetry, conformal symmetry [5, 19, 22–24, 155] or supersymmetry [21, 24, 156–159], which are absent in n-FL metals due to the presence of a FS. The absence of these symmetries makes the number of systematic nonperturbative tools that can be used in the treatment of n-FL metals very limited. Despite this roadblock, in the last decades there has been a vast progress in understanding the strongly-coupled theories of two-dimensional n-FL metals. Let us briefly review those advancements that are pertinent to the contents of this thesis.

In the quest of understanding the universal properties of two-dimensional n-FL metals, two main approaches were adopted in the first place. These approaches aimed to treat the underlying EFT as one that involves only electronic or critical bosonic degrees of freedom. In the first case this is achieved by integrating out the bosonic mode (in the path integral sense). However, this yields a long-range effective interaction between the fermions that becomes rapidly uncontrolled due to the proliferation of non-forward scatterings between the electrons [54, 55]. In the second approach, the electrons are integrated out with the goal of obtaining an EFT for the critical order parameter [160, 161]. However, due to the presence of an infinite number of fermionic gapless excitations close to the FS, the remaining effective action becomes nonlocal and includes an infinite number of marginal interactions [133], deeming the resulting EFT intractable. The failure of these two approaches evidenced the need of treating the electronic modes and the order parameter on an equal footing in the EFT.

In those theories that keep both the order parameter and the gapless fermionic excitations, the common problem is the loss of control of the perturbative expansion due to the strong coupling between the electrons and the collective mode. To gain control over the theory, the large N expansion used in relativistic field theories [27] has been imported to the realm of metallic quantum criticality. In the latter, an expansion in powers of $1/N$ (where N denotes either the number of electronic or bosonic flavors) has been continuously used to study n-FL metals from a perturbative perspective [76, 110, 131, 132, 162]. Although at a first glance this approach seemed to be controlled, it was later shown to fail. In the EFTs

[10] It is important to point out that a strong-coupling EFT is not necessary for the deviation from Landau's FLT to occur. In fact, there are weakly-coupled field theories from which a marginal deviation from Landau's FLT is evidenced. These are known as *marginal Fermi-liquids* (mFLs) and are mainly characterized by an incoherent spectral function which, at the FS, behaves as $\mathcal{A}_{\rm mFL}(\omega) \sim [\omega \log(\mu_0/\omega)]^{-1}$, where μ_0 is some reference energy scale [142, 152–154]. We shall see an example of this in Chapter 3.

for n-FL metallic states known to date, the $1/N$ expansion is not enough to control the perturbative expansion because, even to the leading order in the $N \to \infty$ limit, there are an infinite number of quantum corrections that need to be taken into account to capture correctly the low-energy physics of the system [81, 113, 134]. A completely opposite approach has also been used in order to gain perturbative control. This approach takes the number of electronic flavors to be small: $N \ll 1$. In this line of thought, a small N expansion is performed while keeping the product $Nk_{\rm F} \sim \mathcal{O}(1)$ fixed [78, 163–165]. In this limit, the effects of the underlying FS is neglected because keeping $Nk_{\rm F} \sim \mathcal{O}(1)$ fixed in the $N \to 0$ limit implies keeping only a finite number of gapless excitations in the low-energy limit. Although a controlled approach, it is unclear if it can be connected to physical systems where N is an order one number and $k_{\rm F}$ is large in the low-energy limit.

Although the large N expansion fails to capture the low-energy physics of all known n-FL metals by itself, there has been progress in combining this approach with additional small parameters in the theory. An example of this is provided by tunning the dynamics of the bosonic order parameter. In this approach, the dispersion of the boson is tunned to have a momentum dependence of the form $|\vec{q}|^{1+\delta}$, where $\vec{q}$ is the spatial two-dimensional momentum and δ is a small parameter [77, 166]. When $\delta = 1$, the boson dispersion coincides with that of an ordinary boson. Tunning δ to smaller values reduces the bosonic density of states and, in combination with a large N expansion, the theory is controlled provided that, in the $N \to \infty$ and $\delta \to 0$ limits, the product $N\delta \sim \mathcal{O}(1)$ is kept fixed [82]. Although this procedure yields controlled results and preserves the symmetries of the physical theory, it introduces nonlocalities for $\delta < 1$ and it is questionable whether this approach correctly captures the low-energy features of the physical theory.

Finally, in the past years there have been successful approaches to n-FL metals based on ϵ expansions. These are motivated by the success of the *dimensional regularization* scheme in relativistic field theories [2, 8, 25, 26]. In this approach, the strength of quantum fluctuations is tamed by promoting the theory to general space dimensions and then performing a controlled expansion in the deviation from the the upper critical dimension ot the theory (ϵ expansion). However, we point out that, even in the case of relativistic theories, the extrapolation of results to the physical dimension of interest is subtle and there is nothing that guarantees that such extrapolation yields correct results [159, 167–171]. Besides this caveat, the standard dimensional regularization approach applied to theories of n-FL metals conveys further subtleties due to the presence of a FS. In these cases, enlarging the spatial dimension bifurcates into two possible scenarios: one can either keep the co-dimension or the dimension of the FS fixed.

In the dimensional regularization approach that tunes the dimension of space but keeps the co-dimension of the FS fixed [172, 173], it is hard to access the low-energy physics of two-dimensional n-FLs from a perturbative expansion close to the upper critical dimension. This is because when the dimension of the FS is greater than one, the system suffers from ultraviolet (UV)/infrared (IR) mixing caused by the size of the FS [174]. Such an UV/IR mixing is spurious because it is absent in two dimensions and extrapolating results to two dimensions yields unphysical predictions [175]. In contrast, the dimensional regularization approach that tunes the co-dimension of the FS while keeping its dimension fixed to one [114, 142, 148, 176] avoids such an UV/IR mixing. To date, it has been, arguably, the most successful perturbative approach in the the study of n-FL metals. Although this approach

keeps the theory local, and therefore suitable for the use of conventional RG techniques, one has to break some symmetries of the two-dimensional theory in order to keep the dimension of the FS fixed to one in arbitrary space dimensions. It is therefore legitimate to question the validity of the extrapolation quantities sensitive to such broken symmetries from the upper critical dimension to two dimensions.

The vast majority of approaches in the study of n-FL metals have been guided by controlled perturbative methods. This is due to the scarcity of nonperturbative methods in the study of these novel phases of matter. Nevertheless, there has been only few n-FL metals that can be understood in a controlled way without relying on a perturbative treatment. Amongst these, the *chiral* n-FL metal in two dimensions stands out as an exceptional example in which the low-energy properties of the state can be accessed nonperturbatively due to the hard constraints that are imposed by the chiral nature of the state [177]. Even though there exist examples of n-FL metallic states that can be understood nonperturbatively, a systematic understanding of two-dimensional n-FL metals is still far from reach. For a brief review on recent progress on controlled descriptions of n-FL metals, see Ref. [96]. Because of the lack of controlled understanding over a large variety of n-FL metallic states, it is still a matter of debate whether the enhancement of the superconducting transition temperature and the anomalous temperature dependences of transport quantities in the strange metallic phase of layered compounds find their roots in the low-energy properties of the n-FL state realized at the QCPs present in these materials. Moreover, it is still theoretically unknown if there are n-FL metals whose universal properties can be seen in the normal state of these materials before superconductivity sets in. In principle, the n-FL effects can be only appreciable at temperatures lower than the superconducting transition temperature [114, 146, 177]. Motivated by this debate, we present in this thesis a nonperturbative study of one specific n-FL metal in two-dimensions: *the antiferromagnetic quantum critical metal.*

In the following sections of this chapter we introduce the EFT for the AFM quantum critical metal and review previous works on the matter. In the rest of the thesis we devise a nonperturbative approach that allows the determination of the exact low-energy properties of the state in two dimensions. We further study the system in dimensions between two and three using the aforementioned co-dimensional regularization. Because the theory admits an exact solution in dimensions between two and three, we use it as a model theory to test the extent to which (co-) dimensional regularization schemes can be used to capture the correct universal data of strongly-coupled field theories. Finally, we study the low-energy single-particle properties of the two-dimensional AFM quantum critical metal by including into the theory all gapless electronic excitations on the FS. Through a field theoretical functional RG scheme that admits an analytic treatment, we show that this metallic state hosts both quasiparticle and non-quasiparticle excitations. We further comment on the superconducting instability of the state and determine to what extent our experimental predictions are applicable to the normal state of electron-doped cuprate superconductors, heavy-fermion compounds and iron pnictides. The formalism developed in this thesis provides a general theoretical framework for the study of low-energy properties of metallic states whose low-energy properties are characterized by an infinite amount of low-energy universal data.

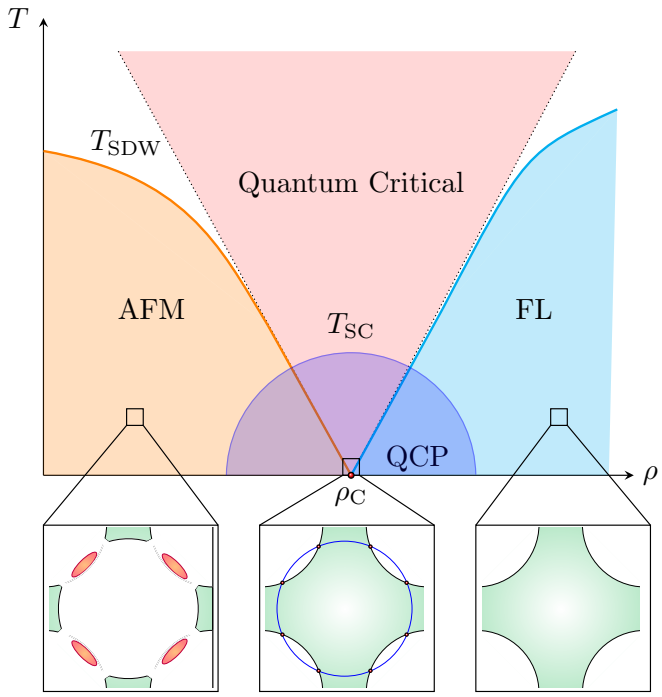

Figure 1.4: A schematic phase diagram for metals that undergo AFM QPTs. T denotes temperature and ρ denotes a tunning parameter that drives the transition from a paramagnetic Fermi-liquid metal (FL) to an antiferromagnetically ordered metallic phase (AFM). The physics in the quantum critical regime above the superconducting dome is dictated by the underlying quantum critical point QCP. The lower panel schematically shows the FS reconstruction characteristic of AFM QPTs.

1.3 Antiferromagnetic Quantum Criticality: Effective Field Theory

Some quasi-two-dimensional materials such as high-temperature superconductors [29–36], heavy fermion compounds [37–40] and iron pnictides [41–47] exhibit strong AFM fluctuations. These fluctuations are usually associated to the existence of a QCP that separates a paramagnetic metallic phase from a metallic phase with long-range AFM order. A schematic phase diagram for these materials is shown in Fig. 1.4. Due to the strong fluctuations present at the QCP, it is reasonable to think that many of the physical properties of the normal state of the system that are seen in the the quantum critical regime are tied to the universal properties of the QCP. This is the reason why this transition has been extensively addressed through both analytical and numerical methods [129, 131–135, 137–143, 143–150, 178, 179]. In this section we introduce the EFT describing the universal features of this transition in two spatial dimensions.

Following the notation of Fig. 1.4, the AFM QPT can be described as follows. For $\rho > \rho_C$, the system is well described by a parmagnetic Fermi-liquid metal with a FS that is determined by the band structure of the material. As the tunning parameter crosses the critical value $\rho = \rho_C$, the SU(2) symmetry of the paramagnetic metal is spontaneously broken, giving rise to a collective spin-density wave with spatial modulation dictated by the ordering wave vector $\vec{Q}_{AFM} \neq \vec{0}$. The spatial modulation of the order parameter, in combination with the conservation of energy and momentum, implies that only electrons close to certain regions on the FS interact with the order parameter at low-energies. These regions can be either points on the FS or extended regions of the FS that are *nested*, that is, parallel to each other, and which are connected by the ordering wave vector. Typically, finding nested regions of the FS connected by the ordering wave vector requires fine tunning

the band structure, and thus, in the most general situation, only electrons close to a discrete set of points on the FS can interact strongly with the order parameter. The points on the FS that are connected by the ordering wave vector are known as *hot spots*. When the tunning parameter is such that $\rho < \rho_C$, the electrons at the hot spots become gapped and the system enters into a metallic phase with a long-range AFM order which supports disconnected electron and hole pockets. The change in the topology of the FS along the transition is known as *Fermi surface reconstruction* and it is characteristic of AFM QPTs [6].

Different AFM QCPs are characterized by different ordering wave vectors $\vec{Q}_{\mathrm{AFM}}$. The ordering wave vector can either be *incommensurable* or *commensurable* with the lattice[11]. In the class of incommensurate AFM QCPs, the special case in which $|\vec{Q}_{\mathrm{AFM}}| = 2k_{\mathrm{F}}$ stands out due to its relevance to cuprate superconductors [150, 178, 179]. Recently, the original claim that such a transition is discontinuous [150] (first-order) has been contested [179] and whether the onset of incommensurate AFM order is described by a first-order or second-order phase transition is still a matter of debate. Nevertheless, there is consensus in the fact that a n-FL metallic state is realized at the QCP. In the case of commensurate AFM QCPs, the are two possibilities. The first one arises when $\vec{Q}_{\mathrm{AFM}} = 2\vec{k}_{\mathrm{F}}$. In this case (as in the incommensurate case), the hot spots on the Fermi surface are locally nested since $2\vec{k}_{\mathrm{F}}$ vector connects antipodal points on the FS. Originally, the transition was thought to be a weakly first-order and to realize a marginal Fermi-liquid metallic state at the QCP [150]. It was later shown, however, that umklapp scatterings play an important role at low energies. Once these are taken into account, the low-energy description of the AFM transition is consistent with a continuous second-order phase transition, and the metallic state realized at the QCP is a n-FL metal [151]. The second scenario is the one in which the commensurate wave vector is such that $\vec{Q}_{\mathrm{AFM}} \neq 2\vec{k}_{\mathrm{F}}$ and it is, arguably, the most interesting case [129, 131–135, 137–143, 143–149]. In this case the FS is generically not nested since the wave vector $\vec{Q}_{\mathrm{AFM}}$ connects points on the FS that are not antipodal to each other. The rest of this thesis is devoted to the study the low-energy properties of the n-FL metallic state arising in this scenario.

Commensurate AFM QCPs in which the hot spots are generally not nested, are believed to be present in electron-doped cuprates, iron pnictides and heavy-fermion compounds [29–47]. Amongst these materials, electron-doped cuprates [29–36] are the simplest because these materials have a simple band structure with no more degrees of freedom than the conduction electrons, and the AFM transition is driven by electron doping which maintains inversion and time-reversal symmetries. A large class of the cuprate superconductors have the tetrahedral crystal structure and the Bravais lattice of the two-dimensional superconducting layers is a square lattice [31–34, 36]. Therefore we focus on a system whose FS has a C_4 symmetry (i.e., 90°-rotational and reflection symmetry). In this case, there are eight hot spots on the FS. For a square lattice, the commensurate wave vector is given by $\vec{Q}_{\mathrm{AFM}} = (\pi, \pi)$, in units of the inverse lattice spacing, and thus the long-wavelength spin-density wave fluctuations with small momentum on top of $\vec{Q}_{\mathrm{AFM}}$ correspond to the low-energy excitations [6, 14, 20]. Finally we note that inelastic neutron scattering measurements in the electron-doped cuprates show the existence of spin fluctuations peaked at momenta $\vec{Q} = (\pi, \pi)$, signaling the existence of

[11] A wave vector is said to be commensurable with the lattice if the real space periodicity of the order parameter is a rational multiple of the lattice constant. This sometimes is phrased as the fact that, if $\vec{Q}_{\mathrm{AFM}} = \vec{G}/2$, with $\vec{G}$ a reciprocal lattice vector, then $\vec{Q}_{\mathrm{AFM}}$ is commensurate.

strong AFM fluctuations [32, 33].

Having discussed the main assumptions under which we will analyze the AFM quantum critical metal in two dimensions, we proceed on writing down the EFT that describes this transition. The low-energy degrees of freedom of the theory are clearly the electrons close to the FS and the low-energy spin-density excitations whose momentum deviates slightly from $\vec{Q}_{\rm AFM} = (\pi, \pi)$. Since the zero energy fluctuations of the order parameter already carry nonzero momentum, only electrons close to the hot spots on the FS interact strongly with the collective mode. Electrons that are far away from the hot spots, but close to the FS, require high-energy spin fluctuations to be scattered into other points close to the FS. Although those electrons that do not interact with the spin-density wave fluctuations still affect the low-energy physics of the metallic state, its long-wavelength physics, apart from the superconducting instability of the state, is dominated by the interaction of the collective mode with electrons close to the hot spots. The description of those electrons residing far away from the hot spots are expected to be described by Landau's FLT. This will become manifest in Chapter 4 once we include electrons away from the hot spots into the low-energy description of the AFM quantum critical metal. For now, we focus only on the low-energy theory that includes electrons close to the hot spots.

Having identified the low-energy degrees of freedom involved in the commensurate AFM transition, we can write down the EFT for the AFM QCP by following the Wilsonian RG picture used in Sec. 1.1-(*b*) and integrating out high-energy electronic modes away from the FS and high-energy bosonic modes whose momentum deviates largely from the ordering wave vector. This is tantamount to expand the dispersion of the electrons locally at each of the eight hot spots on the FS and expanding the dispersion of the spin fluctuations close to the ordering wave vector. The low-energy theory for the AFM quantum critical metal in two dimensions reads [131, 132, 134, 142, 148]:

$$\begin{aligned} S_{d=2} = & \sum_{N=1}^{8} \sum_{\sigma=\uparrow,\downarrow} \int \mathrm{d}k \; \psi^{\dagger}_{N,\sigma}(k) \left[ik_0 + e_N(\vec{k}; v) \right] \psi_{N,\sigma}(k) \\ & + \frac{1}{4} \int \mathrm{d}q \; \left[q_0^2 + \mathsf{c}_0^2 |\vec{q}|^2 \right] \mathrm{Tr}[\Phi(q)\Phi(-q)] \\ & + g \sum_{N=1}^{8} \sum_{\sigma,\sigma'=\uparrow,\downarrow} \int \mathrm{d}k \int \mathrm{d}q \; \left[\psi^{\dagger}_{\overline{N},\sigma}(k+q) \Phi_{\sigma\sigma'}(q) \psi_{N,\sigma'}(k) \right] \\ & + \frac{u}{4} \int \mathrm{d}q_1 \int \mathrm{d}q_2 \int \mathrm{d}q_3 \; \mathrm{Tr}\left[\Phi(q_1+q_3)\Phi(q_2-q_3)\right] \mathrm{Tr}\left[\Phi(-q_1)\Phi(-q_2)\right]. \end{aligned} \tag{1.28}$$

Here, $k = (k_0, \vec{k})$ [$q = (q_0, \vec{q})$] denotes fermionic (bosonic) Matsubara frequency and two-dimensional momentum $\vec{k} = (k_x, k_y)$ [$\vec{q} = (q_x, q_y)$], with $\mathrm{d}k \equiv \mathrm{d}^3k/(2\pi)^3$ [$\mathrm{d}q \equiv \mathrm{d}^3q/(2\pi)^3$]. The coordinate system in which the two-dimensional momenta is written is shown in Fig. 1.5(*a*). In this choice of coordinates, the commensurate wave vector is written as $\vec{Q}_{\rm AFM} = \pm\sqrt{2}(\pi, 0)$ or $\vec{Q}_{\rm AFM} = \pm\sqrt{2}(0, \pi)$ up to reciprocal lattice vectors. The Grassman field $\psi_{N,\sigma}(k)$ represents an electron near hot spot N that carries momentum $\vec{k}$ measured with respect to the hot spot and SU(2)-spin flavor $\sigma = \uparrow, \downarrow$. At low energies, the dispersion of the electrons is linearized close to the hot spots as shown in Fig. 1.5(*b*). At each hot spot the dispersion is written as $e_1(\vec{k}; v) = -e_5(\vec{k}; v) = vk_x + k_y$, $e_2(\vec{k}; v) = -e_6(\vec{k}; v) = -k_x - vk_y$,

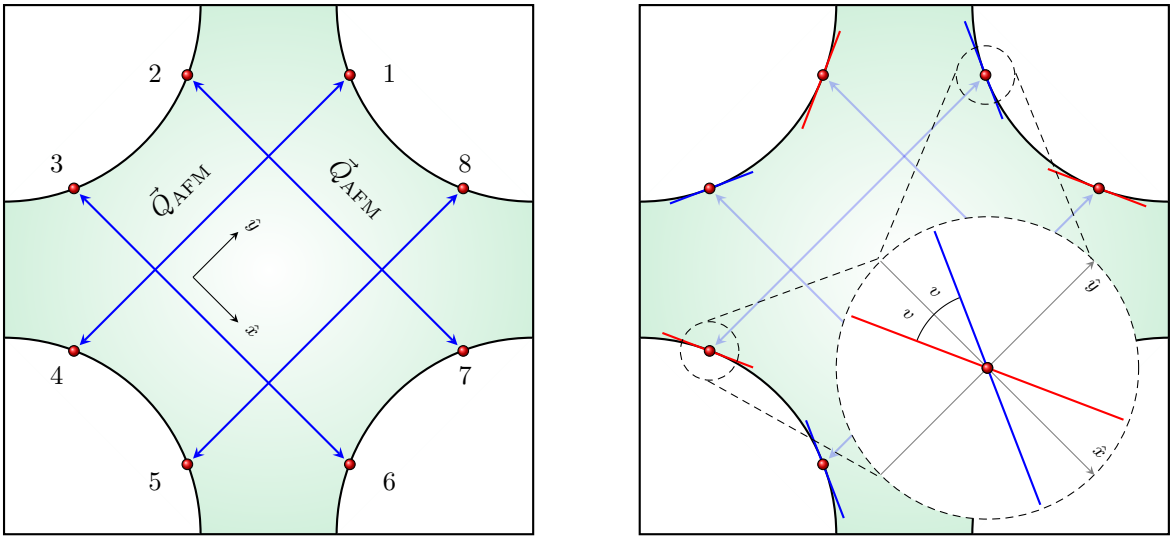

(*a*) (*b*)

Figure 1.5: (*a*) A one-dimensional FS (solid lines) with fourfold rotational symmetry. The (red) dots represent the hot spots connected by the AFM wave vector $\vec{Q}_{\rm AFM}$, where $\vec{Q}_{\rm AFM} = \pm\sqrt{2}\pi\hat{x}$ or $\vec{Q}_{\rm AFM} = \pm\sqrt{2}\pi\hat{y}$ up to reciprocal lattice vectors. (*b*) Linearized FS at each of the hot spots where the angle between FS's connected by the same $\vec{Q}_{\rm AFM}$ vectors is $2v$ in the $v \ll 1$ limit.

$e_3(\vec{k}; v) = -e_7(\vec{k}; v) = -k_x + vk_y$ and $e_4(\vec{k}; v) = -e_8(\vec{k}; v) = vk_x - k_y$. The component of the Fermi velocity along the ordering wave vector $\vec{Q}_{\rm AFM}$ is set to one while v denotes the component perpendicular to it. We note that v also corresponds to the local slope of the FS at the hot spots. Thus, in the rest of this thesis, we will refer to v as the "fermion velocity" or "slope", interchangeably. The patches of the FS that are connected by $\vec{Q}_{\rm AFM}$ have a relative angle of $2\tan^{-1}(v)$ which becomes $2v$ in the $v \ll 1$ limit as shown in Fig. 1.5(*b*). When $v = 0$, we say that the FS becomes locally nested.

The collective AFM spin fluctuations are represented by the matrix field

$$\Phi(q) = \sum_{a=1}^{3} \tau^a \phi^a(q), \tag{1.29}$$

where τ^a are the generators of SU(2) subject to the normalization $\mathrm{Tr}[\tau^a \tau^b] = 2\delta_{ab}$, and $\phi^a(q)$ are bosonic fields satisfying $\phi^a(q) = \phi^a(-q)^*$. In the kinetic term of the boson, c_0 denotes the velocity of the AFM spin fluctuations and $\vec{q}$ denotes the bosonic momentum relative to $\vec{Q}_{\rm AFM}$: $\phi^a(q)$ carries total momentum $\vec{Q}_{\rm AFM} + \vec{q}$. The Yukawa coupling g denotes the strength of the interaction between the collective mode and the electrons near hot spots connected by $\vec{Q}_{\rm AFM}$. Physically, it describes the processes where an electron is scattered from hot spot N to hot spot $\overline{N}$ by absorbing or emitting a spin fluctuation, where $\overline{1} = 4$, $\overline{2} = 7$, $\overline{3} = 6$, $\overline{4} = 1$, $\overline{5} = 8$, $\overline{6} = 3$, $\overline{7} = 2$ and $\overline{8} = 5$. The quartic coupling between the collective modes is denoted by u.

Understanding the universal low-energy properties of Eq. (1.28) is the central goal of

this thesis. As it will be proven to be useful for Chapters 2 and 3, it is convenient to rewrite Eq. (1.28) in terms spinor fields that pair electrons at antipodal hot spots on the FS. As we will see in Chapter 3, this allows a straightforward locality-preserving generalization of the theory to space dimensions higher than two [142, 148]. Defining the two-component spinor fields,

$$\begin{aligned} \Psi_{1,\sigma}(k) &\equiv \begin{pmatrix} \psi_{1,\sigma}(k) \\ \psi_{5,\sigma}(k) \end{pmatrix}, \qquad \Psi_{2,\sigma}(k) \equiv \begin{pmatrix} \psi_{3,\sigma}(k) \\ \psi_{7,\sigma}(k) \end{pmatrix}, \\ \Psi_{3,\sigma}(k) &\equiv \begin{pmatrix} \psi_{4,\sigma}(k) \\ -\psi_{8,\sigma}(k) \end{pmatrix}, \quad \Psi_{4,\sigma}(k) \equiv \begin{pmatrix} \psi_{6,\sigma}(k) \\ -\psi_{2,\sigma}(k) \end{pmatrix}, \end{aligned} \tag{1.30}$$

Eq. (1.28) is written as

$$\begin{aligned} S_{d=2} = &\sum_{n=1}^{4} \sum_{\sigma=\uparrow,\downarrow} \int \mathrm{d}k \; \overline{\Psi}_{n,\sigma}(k) \left[i\gamma_0 k_0 + i\gamma_1 \varepsilon(\vec{k}; v) \right] \Psi_{n,\sigma}(k) \\ &+ \frac{1}{4} \int \mathrm{d}q \; \left[q_0^2 + \mathsf{c}_0^2 |\vec{q}|^2 \right] \mathrm{Tr}\left[\Phi(q)\Phi(-q) \right] \\ &+ ig \sum_{n=1}^{4} \sum_{\sigma,\sigma'=\uparrow,\downarrow} \int \mathrm{d}k \int \mathrm{d}q \; \left[\overline{\Psi}_{\overline{n},\sigma}(k+q) \Phi_{\sigma\sigma'}(q) \gamma_1 \Psi_{n,\sigma'}(k) \right] \\ &+ \frac{u}{4} \int \mathrm{d}q_1 \int \mathrm{d}q_2 \int \mathrm{d}q_3 \; \mathrm{Tr}\left[\Phi(q_1+q_3)\Phi(q_2-q_3) \right] \mathrm{Tr}\left[\Phi(-q_1)\Phi(-q_2) \right], \end{aligned} \tag{1.31}$$

where $n = 1, 2, 3, 4$ will now be referred to as the hot spot index and $\overline{n}$ denotes the hot spot connected to n by the ordering wave vector. In this notation $\overline{1} = 3$, $\overline{2} = 4$, $\overline{3} = 1$ and $\overline{4} = 2$. The energy dispersion of the two-component spinor fields are given, in terms of the original dispersion of the electrons near the hot spots, by $\varepsilon_1(\vec{k}; v) = e_1(\vec{k}; v)$, $\varepsilon_2(\vec{k}; v) = e_3(\vec{k}; v)$, $\varepsilon_3(\vec{k}; v) = e_4(\vec{k}; v)$ and $\varepsilon_4(\vec{k}; v) = e_6(\vec{k}; v)$. Furthermore, $\gamma_0 = \sigma_y$, $\gamma_1 = \sigma_x$ and $\overline{\Psi}_{n,\sigma}(k) \equiv \Psi^{\dagger}_{n,\sigma}(k)\gamma_0$, with σ_x and σ_y denoting the first two Pauli matrices.

To make the discussion as general as possible, we promote the spin symmetry of the fermions from SU(2) to SU(N_c) and endow the fermions with an extra SU(N_f) flavor. This generalizes Eq. (1.31) to:

$$\begin{aligned} S_{d=2} = &\sum_{n=1}^{4} \sum_{\sigma=1}^{N_c} \sum_{j=1}^{N_f} \int \mathrm{d}k \; \overline{\Psi}_{n,\sigma,j}(k) \left[i\gamma_0 k_0 + i\gamma_1 \varepsilon(\vec{k}; v) \right] \Psi_{n,\sigma,j}(k) \\ &+ \frac{1}{4} \int \mathrm{d}q \; \left[q_0^2 + \mathsf{c}_0^2 |\vec{q}|^2 \right] \mathrm{Tr}\left[\Phi(q)\Phi(-q) \right] \\ &+ \frac{ig}{\sqrt{N_f}} \sum_{n=1}^{4} \sum_{\sigma,\sigma'=1}^{N_c} \sum_{j=1}^{N_f} \int \mathrm{d}k \int \mathrm{d}q \; \left[\overline{\Psi}_{\overline{n},\sigma,j}(k+q) \Phi_{\sigma\sigma'}(q) \gamma_1 \Psi_{n,\sigma',j}(k) \right] \\ &+ \frac{u_1}{4} \int \mathrm{d}q_1 \int \mathrm{d}q_2 \int \mathrm{d}q_3 \; \mathrm{Tr}\left[\Phi(q_1+q_3)\Phi(q_2-q_3) \right] \mathrm{Tr}\left[\Phi(-q_1)\Phi(-q_2) \right], \\ &+ \frac{u_2}{4} \int \mathrm{d}q_1 \int \mathrm{d}q_2 \int \mathrm{d}q_3 \; \mathrm{Tr}\left[\Phi(q_1+q_3)\Phi(q_2-q_3)\Phi(-q_1)\Phi(-q_2) \right]. \end{aligned} \tag{1.32}$$

In this generalization, the spinor fields $\Psi_{n,\sigma,j}(k)$ transform under the fundamental representations of SU(N_c) and SU(N_f). The collective mode in Eq. (1.29) is now promoted to an SU(N_c) matrix field

$$\Phi(q) = \sum_{a=1}^{N_c^2-1} \tau^a \phi^a(q), \tag{1.33}$$

where τ^a are the $(N_c^2 - 1)$ generators of SU(N_c) with the normalization $\mathrm{Tr}[\tau^a \tau^b] = 2\delta_{ab}$. The quartic interaction between the AFM spin fluctuations is promoted to two independent interactions for $N_c \geq 4$. For $N_c < 4$, these are not independent as a consequence of the identity $\mathrm{Tr}[\Phi^4] = \frac{1}{2}(\mathrm{Tr}[\Phi^2])^2$ and either u_1 and u_2 can be set to zero. Although we are considering the AFM quantum critical metal for general values of N_c and N_f, none of the results presented in the remaining of this thesis rely on any of these being large parameters in the theory.

The action in Eq. (1.32) is the starting point for the bulk of this thesis. In Sec. 1.5 we outline the path we will follow in this thesis. Before getting into the details of this nonperturbative approach, we briefly discuss earlier analytical works done on the AFM quantum critical metal in two dimensions.

1.4 Summary of Past Progress

There have been intensive theoretical works on the AFM quantum critical metal in the numerical [129, 137, 140, 145, 147, 149] and analytical fronts in the past two decades [131–135, 138, 139, 141–143, 143, 144, 146, 148]. In this section we briefly summarize earlier analytical works on the EFT for the AFM quantum critical metal.

Due to the strong-coupling nature of the EFT in two dimensions, most of the previous works have been done through perturbative methods that rely on the introduction of small parameters. The theory was first studied through a large N expansion, where N is the number of hot spots on the FS [131, 132]. At the one-loop order, this predicted an asymptotic nesting of the FS at the hot spots and a dynamical critical exponent[12] $z > 2$ which signifies the breakdown of Landau's FLT near the hot spots. It was later shown that this $1/N$ expansion fails to control the perturbative expansion [134] in analogy to the breakdown of the $1/N$ expansion in the case in which electrons on a FS interact with a U(1) gauge field [81]. The perturbative expansion has been extended beyond the one-loop order in which the collective mode dynamics has dynamical critical exponent $z = 2$. This approach also predicted a local nesting of the FS at the hot spots, but in contrast to the one-loop result, it predicts a dynamical critical exponent $z < 2$ [134]. Although higher-order quantum corrections are only logarithmically divergent, the low-energy fixed point found therein is not under control because such divergences can introduce $\mathcal{O}(1)$ corrections as a consequence of the strong-coupling nature of the theory.

The failure of the $1/N$ expansion motivated the study of the AFM quantum critical metal through the more systematic perturbative approach offered by the co-dimensional regularization scheme [142, 146, 148]. The one-loop analysis based on this scheme and an

[12] We recall that the dynamical critical exponent sets the scaling dimension of the frequency relative to that of the spatial momentum.

ϵ expansion close to three spatial dimensions (the upper critical dimension of the theory) predicts a dynamical critical exponent $z > 1$ and an asymptotic nesting of the FS at the hot spots [142]. However, the one-loop fixed point of the theory is uncontrolled due to an infrared singularity at the two-loop order associated with the emergent quasi-locality characterizing the metallic state [142, 148]. The study of the onset of commensurate spin-density wave order in anisotropic Fermi-liquid metals evidenced the necessity of extending the one-loop analysis to higher loops in order to cure the emergent infrared singularity even if the deviation from the upper critical dimension of the theory is small [146]. Indeed, once a two-loop correction is introduced into the analysis and all quantum corrections are captured to the leading order in the deviation from the upper critical dimension, the perturbative expansion is controlled. This controlled expansion predicts a dynamical critical exponent $z = 1$ and an asymptotic nesting of the FS at the hot spots [148].

We point out that the two-dimensional AFM quantum critical metal has been also studied nonperturbatively based on the Polchinski-Wetterich functional renormalization group (FRG) [180, 181] supplemented with numerical methods. This approach predicts a local nesting of the FS at the the hot spots with signatures of n-FL metallic physics characterized by a common dynamical critical exponent $z > 1$ for the electrons and the collective mode [138, 144]. However, these approaches miss some of the important higher-loop effects mentioned earlier [146, 148].

Prior to the controlled treatment of the theory based on the ϵ expansion, earlier works concluded invariably that $z > 1$. The results from the controlled ϵ expansion puts these results into question. However, most of the works predict some common qualitative features. Amongst them are the enhacement of d-wave superconducting order in the proximity of the QCP, the local nesting of the FS close to the hot spots and a vanishing quasiparticle weight at the hot spots on the FS [131, 132, 134, 137, 142, 182–185]. In this thesis we study the two-dimensional theory through a nonperturbative approach that provides a controlled understanding of the AFM quantum critical metal and which opens the gate to the study of its equilibrium and out-equilibrium properties.

1.5 Outline of the thesis

This thesis revolves around the nonperturbative approach to the n-FL metallic state realized at the AFM QCP in two dimensions. Motivated by the controlled results from the ϵ expansion close to three spatial dimensions, we engineer the nonperturbative approach by building an ansatz for the critical exponents of the transition. In Chapter 2 we introduce such a scaling ansatz and the nonperturbative approach to show that it is self-consistent. We determine the exact critical exponents characterizing the transition, the low-energy scaling form of spectroscopic and thermodynamic observables, and compare our predictions with known experimental data in the electron-doped cuprates.

In Chapter 3 we generalize the nonperturbative approach used in two dimensions to dimensions between two and three, building a bridge between the nonperturbative results in two space dimensions and the controlled perturbative results close to three dimensions. We extract the exact critical exponents and scaling form of physical observables that characterize the AFM quantum critical metal that supports a one-dimensional FS in this dimensional range. We show that the critical exponents obtained from the controlled ϵ expansion

are smoothly connected to those in the two-dimensional theory, but also point out subtle crossovers that obscure the extrapolation of the scaling form of physical observables. Being an exactly solvable theory in a wide dimensional range we use the field theory for the AFM quantum critical metal as a model theory to test, for the first time, to what extent the RG schemes based on (co-) dimensional regularization are reliable in extracting low-energy universal data of strongly-coupled field theories.

In Chapter 4 we generalize the theory that describes critical spin fluctuations and electrons near the hot spots on the FS by including electrons far away from the hot spots. We devise an analytically tractable field theoretical functional renormalization group scheme that keeps track of the momentum-dependent universal low-energy properties of electrons across the FS. In there we study, within a unified theory, the single-particle properties of cold, lukewarm and hot electrons that coexist in the two-dimensional AFM quantum critical metal. We characterize the quasiparticle weight of the electronic excitations and the global shape of the FS, which are both testable through ARPES experiments. Finally, we present a preliminary analysis on the superconducting instability of the state and determine the temperature range in which our predictions are testable. We further provide an upper bound for the superconducting transition temperature of the AFM quantum critical metal. This chapter provides a general theoretical framework for metallic states with or without quasiparticles which are characterized at low-energies by an infinite amount of low-energy data.

We end this thesis with some concluding remarks and an outlook for future work.

2 | Exact Critical Exponents for the Antiferromagnetic Quantum Critical Metal in Two Dimensions

2.1 Introduction

So far, the intense theoretical work dedicated to the study of the two-dimensional EFT for the AFM QCP has yielded inconclusive results on the nature of the n-FL metallic state realized at the QCP. Due to the failure of perturbative schemes, the strong coupling nature of the theory in two spatial dimensions, and the lack of small parameters that can be used in taming the rapid growth of the interaction at low energies, this EFT has been deemed unsolvable for several years. However, the controlled perturbative approach close to three spatial dimensions based on the ϵ expansion devised recently [148] has provided a new hope in addressing the two-dimensional theory.

The results of the controlled ϵ expansion challenge those of previous works by predicting a dynamical critical exponent $z = 1$ that is independent of the dimension. A key feature of the theory close to the upper critical dimension is the emergence of a *dynamical* small parameter that allows further control in the strength of higher-order quantum corrections. This parameter is the ratio of the fermion velocity to that of the collective mode, which becomes smaller as the long-wavelength limit is approached. Furthermore, this work predicts that the scaling dimension of the fields receive only linear in ϵ corrections for any $0 < \epsilon \leq 1$, *provided that* the ratio of the velocities becomes smaller in the low-energy limit for any given ϵ [148]. Of course, this statement can only be checked perturbatively in ϵ due to the nature of the expansion and whether such a small parameter is present in two dimensions or not is a legitimate concern. Nevertheless, due to the controlled nature of the expansion and the knowledge of the nonperturbative effects that must be taken into account below three dimensions, one can use these results as a guiding intuition in order to tackle the theory in two dimensions.

In this chapter, we present a nonperturbative field theoretic study of the EFT describing the AFM quantum critical metal in two dimensions. Although the theory in two dimensions is strongly coupled at the lowest energies, we show that, similarly as in the controlled ϵ expansion of the theory close to the upper critical dimension [148], a small parameter that differs from the conventional coupling emerges dynamically. This parameter allows for a reliable extraction of the universal low-energy data of the theory. We show that our results in two dimensions are consistent with the extrapolation of those results obtained from the controlled ϵ expansion. Our work is not only relevant from an experimental perspective, but also from a theoretical one. On the one hand, our work gives a controlled understanding of a specific n-FL metallic state which opens the door to the study of its equilbirum and out-of-equilibrium properties. This has the potential of shedding light on general aspects

of n-FL metallic phases and it is a first step in answering long standing questions such as the origin of the superconducting transition temperature enhancement and the anomalous transport properties of the strange metallic phase arising in layered materials. On the other hand, examples of exactly solvable strongly-coupled field theories in more than one spatial dimension that lack conformal symmetry or supersymmetry are scarce. Although the nonperturabtive method designed in this chapter may seem to be tailor made for the EFT under consideration, it provides insights on nonperturbative effects that may be general in a wide class of strongly-coupled EFTs. This may be the first push in opening the door towards the development of more systematic nonperturbative approaches for EFTs in condensed matter physics.

This chapter is organized as follows. In Sec. 2.2 we introduce the scaling ansatz and the nonperturbative approach used to analyze the low-energy properties of the EFT and show in Sec. 2.3 that our approach is self-consistent. In Sec. 2.4 we show the scaling form of spectral and thermodynamic observables that are accessible in experiments. We finish this chapter by comparing our results to known experimental data in electron-doped cuprates and comparing our results to the previous works on the matter that were mentioned in Sec. 1.4.

2.2 Low-Energy Theory and Interaction-Driven Scaling

The low-energy properties of the AFM quantum critical metal in two dimensions are encoded in the action given in Eq. (1.31):

$$\begin{aligned} S_{d=2} = & \sum_{n=1}^{4} \sum_{\sigma=\uparrow,\downarrow} \int \mathrm{d}k \; \overline{\Psi}_{n,\sigma}(k) \left[i\gamma_0 k_0 + i\gamma_1 \varepsilon(\vec{k}; v) \right] \Psi_{n,\sigma}(k) \\ & + \frac{1}{4} \int \mathrm{d}q \; \left[q_0^2 + \mathsf{c}_0^2 |\vec{q}|^2 \right] \mathrm{Tr}\left[\Phi(q)\Phi(-q) \right] \\ & + ig \sum_{n=1}^{4} \sum_{\sigma,\sigma'=\uparrow,\downarrow} \int \mathrm{d}k \int \mathrm{d}q \; \left[\overline{\Psi}_{\bar{n},\sigma}(k+q) \Phi_{\sigma\sigma'}(q) \gamma_1 \Psi_{n,\sigma'}(k) \right] \\ & + \frac{u}{4} \int \mathrm{d}k_1 \int \mathrm{d}k_2 \int \mathrm{d}q \; \mathrm{Tr}\left[\Phi(k_1+q)\Phi(k_2-q) \right] \mathrm{Tr}\left[\Phi(-k_1)\Phi(-k_2) \right]. \end{aligned} \tag{2.1}$$

In two dimensions, the conventional perturbative expansion becomes unreliable because both the Yukawa and quartic couplings grow rapidly as the low-energy limit is approached. Since the interaction plays a dominant role, we need to include the interaction up front rather than treating it as a perturbation to the kinetic energy. Therefore, we start with an interaction-driven scaling [177] in which the Yukawa coupling is deemed marginal, i.e., $[g] = 0$. Under such a scaling, one cannot keep all the kinetic terms as marginal operators. Here we choose a scaling that keeps the fermion kinetic term marginal at the expense of making the boson kinetic term irrelevant. This is a choice that will be justified through explicit calculations. It reflects the fact that the dynamics of the boson is dominated by particle-hole excitations near the FS in the low-energy limit, unless the number of bosons per fermion is infinite [173]. Requiring the fermion kinetic term and the fermion-boson interaction term to be simultaneously marginal uniquely fixes the dimensions of momentum

and the fields under the interaction-driven tree-level scaling:

$$[k_0] = [k_x] = [k_y] = 1, \quad \text{and} \quad [\Psi_{n,\sigma}(k)] = [\Phi(q)] = -2. \tag{2.2}$$

Under this scaling, the electron keeps the classical scaling dimension, while the boson has an $\mathcal{O}(1)$ anomalous dimension compared to the Gaussian scaling (under which both the couplings and the boson field have scaling dimensions: $[g] = 1/2, [u] = 1$ and $[\Phi(q)] = -5/2$, respectively). At this point, Eq. (2.2) is merely an ansatz. In this chapter we show that these exponents are indeed exact.

Under the interaction driven scaling in Eq. (2.2), the entire boson kinetic term and the quartic coupling are irrelevant. The minimal action which includes only marginal terms is written as

$$\begin{aligned} S_{d=2} = &\sum_{n=1}^{4} \sum_{\sigma=\uparrow,\downarrow} \int \mathrm{d}k \; \overline{\Psi}_{n,\sigma}(k) \left[i\gamma_0 k_0 + i\gamma_1 \varepsilon_n(\vec{k}; v) \right] \Psi_{n,\sigma}(k) \\ &+ i\sqrt{\frac{\pi v}{2}} \sum_{n=1}^{4} \sum_{\sigma,\sigma'=\uparrow,\downarrow} \int \mathrm{d}k \int \mathrm{d}q \; \left[\bar{\Psi}_{\bar{n},\sigma}(k+q) \Phi_{\sigma,\sigma'}(q) \gamma_1 \Psi_{n,\sigma'}(k) \right]. \end{aligned} \tag{2.3}$$

An alternative way of arriving to Eq. (2.3) from Eq. (2.1) is through the field redefinition $\widetilde{\Phi}(q) = g\Phi(q)$. Under the Gaussian tree-level scaling, $[g] = 1/2$ and $[\Phi(q)] = -5/2$ and thus, under this same scaling, the redefined field has scaling dimension $[\widetilde{\Phi}(q)] = -2$, which accounts for the $\mathcal{O}(1)$ difference between the Gaussian scaling dimension of the boson and that obtained from the interaction-driven scaling. Under this field redefinition Eq. (2.1) can be cast as

$$\begin{aligned} S_{d=2} = &\sum_{n=1}^{4} \sum_{\sigma=\uparrow,\downarrow} \int \mathrm{d}k \; \overline{\Psi}_{n,\sigma}(k) \left[i\gamma_0 k_0 + i\gamma_1 \varepsilon(\vec{k}; v) \right] \Psi_{n,\sigma}(k) \\ &+ \frac{1}{4g^2} \int \mathrm{d}q \; \left[q_0^2 + \mathsf{c}_0^2 |\vec{q}|^2 \right] \mathrm{Tr} \left[\widetilde{\Phi}(q) \widetilde{\Phi}(-q) \right] \\ &+ i \sum_{n=1}^{4} \sum_{\sigma,\sigma'=\uparrow,\downarrow} \int \mathrm{d}k \int \mathrm{d}q \; \left[\overline{\Psi}_{\bar{n},\sigma}(k+q) \widetilde{\Phi}_{\sigma\sigma'}(q) \gamma_1 \Psi_{n,\sigma'}(k) \right] \\ &+ \frac{u}{4g^4} \int \mathrm{d}k_1 \int \mathrm{d}k_2 \int \mathrm{d}q \; \mathrm{Tr} \left[\widetilde{\Phi}(k_1+q) \widetilde{\Phi}(k_2-q) \right] \mathrm{Tr} \left[\widetilde{\Phi}(-k_1) \widetilde{\Phi}(-k_2) \right]. \end{aligned} \tag{2.4}$$

Since the Yukawa coupling is dimensionful and relevant under the Gaussian tree-level scaling, the kinetic term of the boson becomes irrelevant because, at low-energies, $g^2 \sim \widetilde{\Lambda}$, with $\widetilde{\Lambda}$ a large energy scale. Furthermore, the effective coupling in front of the quartic coupling is now $\widetilde{u} = u/g^4$ which has a Gaussian tree-level scaling dimension $[\widetilde{u}] = -1$ and therefore is also irrelevant. Thus, both the kinetic term of the boson and the quartic interaction become unimportant in the low-energy limit and the low-energy theory for the AFM quantum critical metal in two dimensions is dominated by the minimal local action in Eq. (2.3).

In Eq. (2.3), and under the interaction-driven scaling, the fermion-boson coupling is set to be proportional to $\sqrt{v}$ by rescaling the boson field. The Yukawa coupling is replaced with $\sqrt{v}$ because the interaction is screened such that g^2 becomes of $\mathcal{O}(v)$ in the low-energy

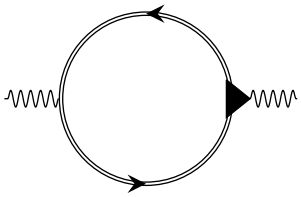

Figure 2.1: The exact boson self-energy. The double line is the fully dressed fermion propagator. The triangle represents the fully dressed interaction vertex.

limit [142]. Although g and v can be independently tuned in the microscopic theory, they rapidly flow to a universal line defined by $g^2 \sim v$ at low energies [148]. Eq. (2.3) should be understood as the minimal theory that captures the universal physics at low energies, where the dynamics of the collective mode is dominated by particle-hole excitations rather than the bare kinetic term, and v is the only dimensionless parameter of the theory. In the small v limit, g also vanishes because the FS becomes nested, which provides a large phase space for low-energy particle-hole excitations with momentum $\vec{Q}_{\rm AFM}$ that screen the interaction. Even when g and v are small, this is a strongly interacting theory because $g^2/v \sim 1$ is the expansion parameter in the conventional perturbative series. With $g^2/v \sim 1$, the leading boson kinetic term, which is generated from particle-hole excitations, is of $\mathcal{O}(1)$, as we show in the following section.

2.3 Self-Consistent Solution

The absence of a boson kinetic term in the action suggests that the theory is ill-defined. However, particle-hole excitations generate a self-energy (shown in Fig. 2.1) which provides nontrivial dynamics for the collective mode through the Schwinger-Dyson equation:

$$D(q)^{-1} = m_{\rm C.T.} - \pi v \sum_{n=1}^{4} \int \mathrm{d}k \ \mathrm{Tr}\left[\gamma_1 G_{\overline{n}}(k+q;v)\Gamma_n^{(2,1)}(k,q)G_n(k;v)\right]. \tag{2.5}$$

Here $D(k)$, $G_n(k;v)$ and $\Gamma_n^{(2,1)}(k,q)$ represent the fully dressed propagators of the boson and the fermion, and the interaction vertex function, respectively. $m_{\rm C.T.}$ is a mass counterterm that is added to tune the renormalized mass to zero. The trace in Eq. (2.5) is over the spinor indices. Solving the full self-consistent Schwinger-Dyson equation is a hard task because $G_n(k;v)$ and $\Gamma_n^{(2,1)}(k,q)$ depend on the unknown $D(q)$. One may use v as a small parameter to solve the equation. A one-loop RG analysis of the theory shows that v flows to zero due to the emergent nesting of the FS near the hot spots [131, 132, 137, 186]. This has been also confirmed in the ϵ expansion based on the co-dimensional regularization scheme [142, 148]. Of course, the perturbative result valid close to three dimensions does not necessarily extend to two dimensions. Nonetheless, we show that this is indeed the case. Here we proceed with the following steps: (*i*) we solve the Schwinger-Dyson equation for the boson propagator in the small v limit and (*ii*) we show that v flows to zero at low energies by using the boson propagator obtained under the assumption that $v \ll 1$.

We emphasize that the expansion in v is different from the conventional perturbative expansion in the coupling. Rather, it involves a nonperturbative summation over an infinite series of diagrams as will be shown below.

Let us discuss step (*i*) first. In the small v limit, the solution to the Schwinger-Dyson equation is given by

$$D(q)^{-1} = |q_0| + c(v)\left[|q_x| + |q_y|\right], \tag{2.6}$$

where the 'velocity' of the strongly damped collective mode is given by

$$c(v) = \frac{1}{4}\sqrt{v \log\left(\frac{1}{v}\right)}. \tag{2.7}$$

Solving the Schwinger-Dyson equation consists of two parts. First, we assume Eq. (2.6) with a hierarchy of the velocities $v \ll c(v) \ll 1$ as an ansatz to show that only the one-loop vertex correction is important in Eq. (2.5). Then we show that Eqs. (2.6) and (2.7) actually satisfy Eq. (2.5) with the one-loop dressed interaction vertex.

To accomplish the aforementioned steps, we begin by estimating the magnitude of general diagrams, assuming that the fully dressed boson propagator is given by Eq. (2.6) with Eq. (2.7) in the small v limit. The first thing to notice is that the magnitude of a general diagram is not only determined by the number of vertices, V, because both the bare fermion propagator and fully dressed boson propagator depend on v and $c(v)$, respectively. In general, the integrations over loop momenta diverge in the small v limit as fermions and bosons lose their dispersion in some directions. In each fermion loop, the component of the internal momentum tangential to the FS is unbounded in the small v limit due to the nesting of the FS. For a small but nonzero v, the divergence is cut off at a scale proportional to $1/v$, and each fermion loop contributes a factor of $1/v$. Each of the remaining loops necessarily has at least one boson propagator. For those loops, the momentum along the FS is cut off by the energy of the boson which provides a lower cutoff momentum proportional to $1/c(v)$ for $c(v) \gg v$. Therefore, the magnitude of a general L-loop diagram with L_f fermion loops and E external legs is at most

$$\mathcal{G}(L, L_f, E) \sim v^{V/2-L_f} c(v)^{-(L-L_f)} = v^{\frac{1}{2}(E-2)} \left(\frac{v}{c(v)}\right)^{(L-L_f)}, \tag{2.8}$$

where we have used the fact that for the present theory $V = 2L + E - 2$. Higher-loop diagrams are systematically suppressed with increasing $(L - L_f)$ provided that $v \ll c(v)$. This is analogous to the situation where a ratio between velocities is used as a control parameter in a Dirac semi-metal[1] [110]. If Eq. (2.7) holds, the upper bound becomes $\mathcal{G}(L, L_f, E) \sim v^{\frac{1}{2}(E-2+L-L_f)}$ up to a logarithmic correction in v. It is noted that Eq. (2.8) is only an upper bound because some loop integrals which involve unnested fermions remain finite even in the small v limit. Some diagrams can also be smaller than the upper bound because their dependences on external momentum are suppressed in the small v and $c(v)$ limit. As we shall see below, this is the case for the one-loop fermion self-energy. A systematic proof of the upper bound in Eq. (2.8) is available in Appendix A.

Provided that $v \ll c(v)$, the Schwinger-Dyson equation in Eq. (2.5) takes the diagrammatic form depicted in Fig. 2.2(*a*) to leading order in v: The leading order contribution

[1] There has been an attempt to use a different ratio of velocities as a control parameter in non-Fermi-liquid metals with critical bosons centered at zero momentum [187].

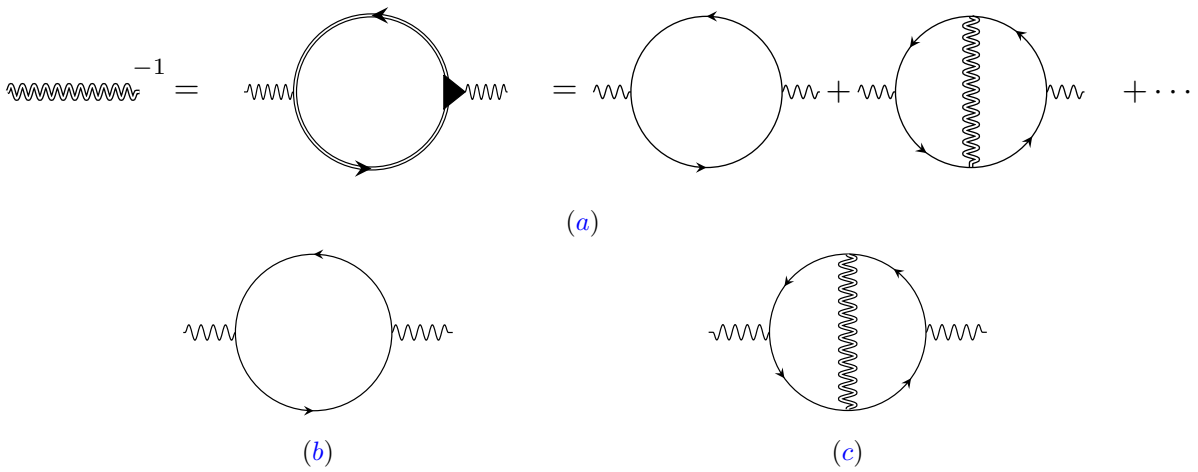

Figure 2.2: (*a*) The Schwinger-Dyson equation to the leading order in the small v limit. The ellipsis denote subleading contributions in v. Solid lines represent the bare fermion propagators. The wiggly double line represents the boson propagator consistently dressed with the self-energy in (*b*) and (*c*). The dressed boson propagator includes an infinite series of nested self-energies with a fractal structure.

to the boson self-energy ($E = 2$) is generated from Fig. 2.2(*b*), which is the only diagram that satisfies $L = L_f$. All other diagrams are subleading in v. However, this is not enough because the one-loop diagram gives $D(q)^{-1} = |q_0|$, which is independent of the spatial momentum. One has to include the next order diagram [Fig. 2.2(*c*)] which generates a dispersion. Therefore, Eq. (2.5) is reduced to

$$D(q)^{-1} = m'_{\text{C.T.}} + |q_0| - \frac{\pi^2 v^2}{2} \sum_{n=1}^{4} \int \mathrm{d}p \int \mathrm{d}k \mathrm{Tr} \Big[\gamma_1 G_n^{(0)}(k+p;v) \gamma_1 G_{\overline{n}}^{(0)}(p+q+k;v) \times \gamma_1 G_n^{(0)}(q+k;v) \gamma_1 G_{\overline{n}}^{(0)}(k;v) \Big] D(p). \tag{2.9}$$

Here $m'_{\text{C.T.}}$ is a two-loop mass counterterm. We can use the free fermion propagator $G_n^{(0)}(k;v)$,

$$G_n^{(0)}(k;v) = \frac{1}{i} \left[\frac{\gamma_0 k_0 + \gamma_1 \varepsilon(\vec{k};v)}{k_0^2 + \varepsilon_n(\vec{k};v)^2} \right] \tag{2.10}$$

because the fermion self-energy correction is subleading in v. An explicit calculation of Eq. (2.9) confirms that the self-consistent boson propagator takes the form given in Eq. (2.6). The boson velocity satisfies the self-consistent equation

$$c(v) = \frac{v}{8c(v)} \log \left(\frac{c(v)}{v} \right), \tag{2.11}$$

which is solved by Eq. (2.7) in the small v limit. It is noted that $c(v)$ is much larger than v in the small v limit because of the enhancement factor $1/c(v)$ in the two-loop diagram: the

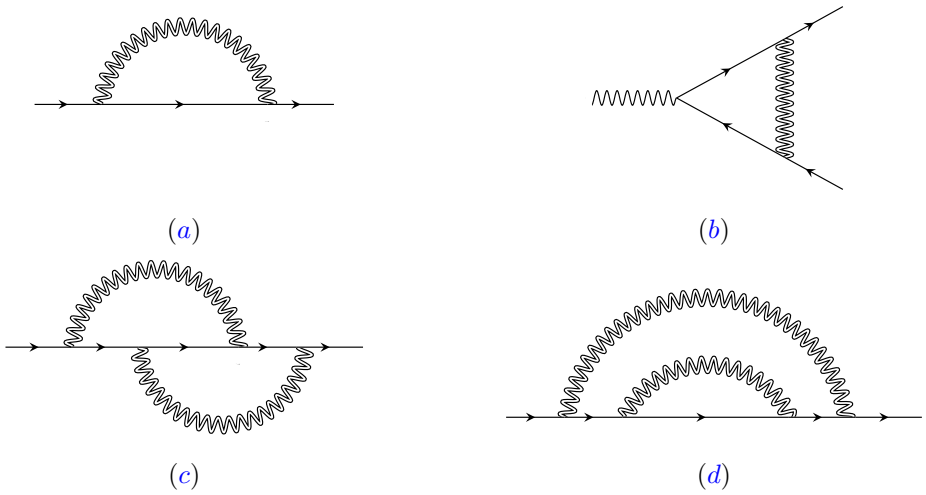

Figure 2.3: Leading order quantum corrections to the minimal local action. Two-loop fermion self-energies. As explained in the text, the two-loop diagram in (*c*) is of the same order as the one-loop diagram in (*a*). The diagram in (*d*) is subleading due to an additional suppression by $c(v)$.

collective mode speeds up itself through enhanced quantum fluctuations if it gets too slow. We further note that the antiscreening nature of the vertex correction associated with the non-Abelian SU(2) vertex,

$$\sum_{a=1}^{3} \tau^a \tau^b \tau^a = -\tau^b, \tag{2.12}$$

is crucial to generate the right sign for the boson kinetic term [146]. This does not hold for Ising-like or XY-like spin fluctuations [188]. The details on the computation of Eq. (2.9) are available in Appendix C. Notice that Eq. (2.9) constitutes a nonperturbative sum over an infinite series of diagrams beyond the random phase approximation. The dynamics of the boson generated from the fermionic sector dominates over the bare bosonic kinetic term at low energies. Therefore, the choice to drop the bare kinetic term of the collective mode in Eq. (2.3) is rather natural.

So far, we have assumed that v is small to obtain the self-consistent dynamics of the AFM collective mode. Now we turn to step (*ii*) and show that v indeed flows to zero in the low-energy limit. According to Eq. (2.8), the leading quantum corrections to the local action in Eq. (2.3) are the one-loop diagrams for the fermion self-energy and the interaction vertex function depicted in Figs. 2.3(*a*) and 2.3(*b*).

However, the momentum-dependent one-loop fermion self-energy happens to be smaller than what is expected from Eq. (2.8) by an additional power of $c(v) \sim \sqrt{v}$. This is because the dependence on the external momentum is suppressed in the small $c(v)$ limit for the one-loop self-energy. Therefore, the one-loop correction can become of the same order as higher-loop corrections. As a result, we must include the two-loop fermion self-energy corrections depicted in Figs. 2.3(*c*) and 2.3(*d*) in order to capture all quantum corrections to the leading order in v. All other higher-loop diagrams are negligible in the small v limit. Amongst the

two corrections at the two-loop order, only the momentum-dependent part of the correction depicted in Fig. 2.3(c) becomes of the same order as the momentum-dependent one-loop fermion self-energy. The momentum-dependent part of the correction depicted in Fig. 2.3(d) receives an additional suppression in $c(v)$ by the same reason that the one-loop fermion self-energy has an extra power of $c(v)$ compared to the expectation set by Eq. (2.8).

The self-energy and vertex corrections are logarithmically divergent in the UV. Therefore, the theory must be regularized and counterterms must be added to the minimal local action in Eq. (2.3) such that the renormalized quantum effective action becomes independent of the UV scales set by the microscopic details of the theory. Following the steps of the regularization and RG scheme that is detailed in Appendix B, we find that, as a function of the running energy scale μ, the fermion velocity obeys the flow equation

$$\mu \frac{\mathrm{d}v}{\mathrm{d}\mu} = \frac{6}{\pi^2} v^2 \log\left(\frac{1}{c(v)}\right). \tag{2.13}$$

If the bare value of v is small, Eq. (2.13) is reliable. In fact it predicts that v becomes even smaller and flows to zero as

$$v(\mu) = \frac{\pi^2}{3} \frac{1}{\log\left(\frac{\Lambda}{\mu}\right) \log\left[\log\left(\frac{\Lambda}{\mu}\right)\right]} \tag{2.14}$$

for $\mu/\Lambda \ll 1$, where Λ is the UV scale at which the bare theory is defined. Notice that the way v flows to zero in the low-energy limit does not depend on the bare value of v [$v_0 \equiv v(\Lambda)$]. This completes the cycle of self-consistency. It follows from this that, Eq. (2.6), which is obtained in the small v limit, becomes asymptotically exact in the low-energy limit within a nonzero basin of attraction in the space of v whose fixed point is $v = 0$. As it is shown in full detail in Appendix D, the dynamical critical exponent (z) and the anomalous dimensions of the boson (η_Φ) and fermion (η_Ψ) fields are given by

$$\begin{aligned} z &= 1 + \frac{3}{4\pi} \frac{v}{c(v)}, \\ \eta_\Phi &= \frac{1}{4\pi} \frac{v}{c(v)} \log\left(\frac{c(v)}{v}\right), \\ \eta_\Psi &= -\frac{3}{8\pi} \frac{v}{c(v)}, \end{aligned} \tag{2.15}$$

to the leading order in v. Here z sets the dimension of frequency relative to momentum. Moreover, η_Φ and η_Ψ are the corrections to the interaction-driven tree-level scaling dimensions of the boson and fermion fields, respectively. It is clear that the critical exponents are controlled by $w(v) \equiv v/c(v)$, which, according to Eqs. (2.7) and (2.14), flow to zero as

$$w(\mu) = \frac{4\pi}{\sqrt{3}} \frac{1}{\sqrt{\log\left(\frac{\Lambda}{\mu}\right)} \log\left[\log\left(\frac{\Lambda}{\mu}\right)\right]} \tag{2.16}$$

for $\mu/\Lambda \ll 1$. This confirms that the scaling dimensions in Eq. (2.2) become asymptotically exact in the low-energy limit. This is compatible with the fact that an inclusion of higher-loop corrections in the ϵ expansion reproduces $z = 1$, irrespective of ϵ, provided that $w(v)$

flows to zero for any $0 < \epsilon \leq 1$ [148]. As we will show in Chapter 3 this is a feature of the low-energy theory in dimensions $2 \leq d < 3$, where the nonperturbative solution is characterized by the interaction-driven scaling with a $z = 1$ exponent.

2.4 Physical Observables

The critical exponents $z - 1$, η_Ψ and η_Φ vanish in the low-energy limit. However, the sublogarithmic decay of $w(v)$ with energy introduces corrections to the correlation functions at intermediate energy scales, which are weaker than power-law but stronger than logarithmic corrections [153]. The retarded Green's function for electrons near the hot spot $N = 1$ takes the form,

$$G_1^{\mathrm{R}}(\omega, \vec{k}) = \frac{1}{F_\Psi(\omega)\left\{\omega F_z(\omega)\left[1 + i\frac{\sqrt{3}\pi}{2}\frac{1}{\sqrt{\log\left(\frac{\Lambda}{\omega}\right)}\log\left[\log\left(\frac{\Lambda}{\omega}\right)\right]}\right] - \left[\frac{\pi^2}{3}\frac{k_x}{\log\left(\frac{\Lambda}{\omega}\right)\log\left[\log\left(\frac{\Lambda}{\omega}\right)\right]} + k_y\right]\right\}} \tag{2.17}$$

for $\omega/\Lambda \ll 1$, with $\omega > 0$ and with the ratio $\vec{k}/[\omega F_z(\omega)]$ been fixed. Here ω is the real frequency and Λ is the UV scale at which the bare theory is defined. The scaling form of the retarded electronic Green's function at different hot spots can be obtained by applying a sequence of 90° rotations and a space inversion to Eq. (2.17). Details on the derivation of this expression are given in Appendix E. $F_\Psi(\omega)$ and $F_z(\omega)$ are functions which capture the contributions from η_Ψ and z at intermediate energy scales. For $\omega \ll \Lambda$, these are given by

$$F_\Psi(\omega) = \left[\log\left(\frac{\Lambda}{\omega}\right)\right]^{\frac{3}{8}}, \tag{2.18}$$

$$F_z(\omega) = \exp\left\{2\sqrt{3}\frac{\left[\log\left(\frac{\Lambda}{\omega}\right)\right]^{\frac{1}{2}}}{\log\left[\log\left(\frac{\Lambda}{\omega}\right)\right]}\right\}. \tag{2.19}$$

$F_\Psi(\omega)$ and $F_z(\omega)$ only contribute as subleading corrections instead of modifying the exponents. However, they still constitute part of the low-energy universal data that characterizes the critical point [134]. The additional logarithmic suppression in the dependence of k_x is due to v which flows to zero in the low-energy limit. Close to the hot spot $N = 1$, the local shape of the FS is deformed as

$$k_y \sim \frac{k_x}{\log\left(\frac{\Lambda}{|k_x|}\right)\log\left[\log\left(\frac{\Lambda}{|k_x|}\right)\right]}. \tag{2.20}$$

The spectral function at the hot spots, $\mathcal{A}_N(\omega) \equiv 2\mathrm{Im}\left[G_N^{\mathrm{R}}(\omega, \vec{0})\right]$, exhibits a power-law decay with a superlogarithmic correction as a function of frequency,

$$A_N(\omega) \sim \frac{1}{\omega F_z(\omega) F_\Psi(\omega)\left[\log\left(\frac{\Lambda}{\omega}\right)\right]^{1/2}\log\left[\log\left(\frac{\Lambda}{\omega}\right)\right]}. \tag{2.21}$$

We note that the spectral function displays no Dirac-delta peak characteristic of quasiparticle excitations. Instead, the Dirac-delta peak is replaced by a weaker singularity at $\omega = 0$ which

is a signature of incoherent electronic excitations [See Sec. 1.1-(*b*)]. This implies that the quasiparticle weight for the electronic excitations [as defined in Landau's FLT through Eq. (1.24) or Eq. (1.27)] vanishes at the hot spots.

The retarded spin-spin correlation function is given by

$$D^R(\omega,\vec{q}) = \frac{1}{F_\Phi(\omega)\left(-i\omega F_z(\omega) + \frac{\pi}{4\sqrt{3}}\frac{|q_x|+|q_y|}{\left[\log\left(\frac{\Lambda}{\omega}\right)\right]^{1/2}}\right)} \tag{2.22}$$

for $\omega/\Lambda \ll 1$, with fixed $\vec{q}/[\omega\ F_z(\omega)]$. $F_\Phi(\omega)$ is another universal function that describes the superlogarithmic correction of η_Φ,

$$F_\Phi(\omega) = \exp\left\{\frac{2}{\sqrt{3}}\left[\log\left(\frac{\Lambda}{\omega}\right)\right]^{\frac{1}{2}}\right\} \tag{2.23}$$

in the ω/Λ limit. The factor of $[\log(\Lambda/\omega)]^{-\frac{1}{2}}$ in the momentum-dependent term is due to the boson velocity which flows to zero in the low-energy limit. Details on the derivation of Eq. (2.22) are given in Appendix E.

Due to the strong Landau damping generated by the decay of the collective mode's fluctuations into particle-hole pairs, the spin fluctuation is highly incoherent. It will be of great interest to test precisely the scaling forms in Eqs. (2.17) and (2.22) from ARPES and neutron scattering experiments, respectively. In the next section we compare our theoretical predictions to known experimental results on materials that are believed to harbor the AFM QCP.

Now we turn our attention to the thermodynamic properties of the theory. The total free energy density can be written as

$$f = \frac{1}{2}\ \mathrm{Tr}\left[\log \mathsf{D}^{-1} - \mathsf{\Pi}\cdot\mathsf{D}\right] - \mathrm{Tr}\left[\log \mathsf{G}^{-1} - \mathsf{\Sigma}\cdot\mathsf{G}\right] + \Phi_2, \tag{2.24}$$

where $\mathsf{\Pi}$, $\mathsf{\Sigma}$ are the self-energies of the boson and fermion respectively, and Φ_2 includes the two-particle irreducible diagrams [63]. Here, the traces sum over the frequency, two-dimensional momenta and flavors, and $\mathsf{\Pi}$, $\mathsf{\Sigma}$, D and G are used to denote the self-energies and propagators, respectively, as operators in the frequency, two-dimensional momenta and flavor space. To the leading order in v, the dominant contributions are $f_{\text{Bos.}} = \frac{1}{2}\ \mathrm{Tr}[\log \mathsf{D}^{-1}]$ and $f_{\text{Fer.}} = \mathrm{Tr}[\log \mathsf{G}^{(0)}]$, with $\mathsf{G}^{(0)}$ denoting the bare fermion propagator. The dominant fermionic contribution comes from electrons away from the hot spots, $f_{\text{Fer.}} \sim k_{\text{F}}T^2$, where k_{F} is the magnitude of the Fermi momentum which parametrizes the size of the FS. Naively, the bosonic contribution is expected to obey hyperscaling, because low-energy excitations are confined near the ordering vector. However, the free energy density of the mode with momentum $\vec{p}$ is suppressed only algebraically as $T^2/[c(v)(|p_x| + |p_y|)]$ at large momenta, in contrast to the exponential suppression exhibited by free bosons. The slow decay of the free energy density per mode originates in the incoherent nature of the damped AFM spin fluctuations, which have a significant spectral weight at low energies even at large momenta. As a result,

$$f_{\text{Bos.}} \sim \int_{\mathbb{R}^2} \frac{\mathrm{d}\vec{p}}{(2\pi)}\ \frac{T^2}{c(v)(|p_x| + |p_y|)} \tag{2.25}$$

is unbounded. In the presence of the irrelevant local kinetic term in the boson action, $(\mathsf{c}_0^2/\widetilde{\Lambda})|\vec{p}|^2$ with $\mathsf{c}_0 \sim 1$, the momentum integration is cut off at $p_{\max} \sim c(v)\widetilde{\Lambda}$, and $f_{\text{Bos.}}$ is proportional to $\widetilde{\Lambda}$. From the scaling equation for $f_{\text{Bos.}}$,

$$\left[zT\frac{\partial}{\partial T} + \widetilde{\Lambda}\frac{\partial}{\partial \widetilde{\Lambda}} - \beta_c(v)\frac{\partial}{\partial c(v)} - (2+z)\right] f_{\text{Bos.}}[T, c(v), \widetilde{\Lambda}] = 0, \tag{2.26}$$

where, $\beta_c(v) \equiv \mathrm{d}c(v)/\mathrm{d}\log\mu$, we obtain

$$f_{\text{Bos.}} \sim \widetilde{\Lambda} T^2 F_z(T) \tag{2.27}$$

in the low temperature limit, where $F_z(T)$ is defined in Eq. (2.19). Remarkably, the bosonic contribution violates the hyperscaling, and it is larger than the fermionic contribution at low temperatures. In this case, the power-law violation of the hyperscaling is a consequence of the $z = 1$ scaling rather than the fact that v and $c(v)$ flow to zero [143]. The free energy density gives rise to the specific heat which exhibits the T-linear behavior with the superlogarithmic correction:

$$c_V \sim \widetilde{\Lambda} T F_z(T). \tag{2.28}$$

It is noted the deviation from the T-linear behavior is stronger than a simple logarithmic correction because $F_z(T)$ includes all powers of $\sqrt{\log(\Lambda/T)}$. Details on the derivation of the free energy density are given in Appendix E.

If the system is tuned away from the critical point, the boson acquires a mass term

$$\delta S_{d=2}^{\text{Mass.}} \sim (\lambda - \lambda^*) \int \mathrm{d}q \ \mathrm{Tr}\left[\Phi(q)\Phi(-q)\right], \tag{2.29}$$

where λ is a tuning parameter and λ^* its critical value. Due to the suppression of higher-loop diagrams, the scaling dimension of $\Phi(q)^2$ is -4 in momentum space. This implies a critical exponent $\nu = 1$ in the low-energy limit, which is different from the mean-field exponent ($\nu = 1/2$). The power-law scaling of the correlation length ξ with λ is modified by a superlogarithmic correction,

$$\xi \sim (\lambda - \lambda^*)^{-1} F_\xi(\lambda - \lambda^*), \tag{2.30}$$

where $F_\xi(\delta\lambda)$, with $\delta\lambda = \lambda - \lambda^*$, is a universal function which embodies both the anomalous dimension of the boson and the vertex correction to the mass insertion. The former dominates close to the critical point, and $F_\xi(\delta\lambda) = F_\Phi(\delta\lambda)$ to the leading order in small $\delta\lambda$.

The scaling forms of the physical observables discussed above are valid in the low-energy limit. At high energies, there will be crossovers to different behaviors. The first crossover is set by the scale below which the dynamics of the collective mode is dominated by particle-hole excitations, and therefore Eqs. (2.22) and (2.28) hold. It is determined by the competition between Eq. (2.6) and the irrelevant local kinetic term for the collective mode in Eq. (2.1). For $\omega < (c(v)^2/\mathsf{c}_0^2)\widetilde{\Lambda}$, the terms linear in frequency and momentum dominate, where $\widetilde{\Lambda}$ is an energy scale associated with the irrelevant kinetic term. The details on the crossover are described in Appendix C and summarized in Tables C.1(a) and C.1(b) therein. In the small v limit with $\mathsf{c}_0 \sim 1$, this crossover scale for the boson goes as

$$E_{\text{Bos.}}^* \sim c(v_0)^2 \widetilde{\Lambda}, \tag{2.31}$$

where $v_0 \ll 1$ is the bare value of the fermion velocity. The second crossover scale, denoted as $E^*_{\text{Fer.}}$, is the one below which the behavior of the fermions at the hot spots deviates from the Fermi-liquid one. For a small but non-zero v, the leading order self-energy correction to the fermion propagator is $(3/4\pi)[v/c(v)]\omega \log(\Lambda/\omega)$, which becomes larger than the bare term for $\omega < E^*_{\text{Fer.}}$ with

$$E^*_{\text{Fer.}} \sim \Lambda \exp\left(-\frac{\pi}{3}\sqrt{\frac{\log(1/v_0)}{v_0}}\right). \tag{2.32}$$

Since v flows to zero only logarithmically, the deviation of v away from it's bare value can be ignored for the estimation of both $E^*_{\text{Fer.}}$ and $E^*_{\text{Bos.}}$. As is shown in Appendix D, the value of v changes appreciably below the scale $\Lambda e^{-\ell_0}$, where $\ell_0 \sim (1/v_0)\log(1/v_0)$.

At sufficiently low temperatures, the system eventually becomes unstable against pairing. An important question is how the crossover scales compare with the superconducting transition temperature T_c. The spin fluctuations renormalize pairing interactions between electrons near the hot spots, and enhance d-wave superconductivity [137, 182–185]. In the small v limit, however, the renormalization of the pairing interaction by the AFM spin fluctuations is suppressed by $v/c(v)$ for the same reason that the vertex correction is suppressed. Because the Yukawa coupling is marginal at the fixed point, it adds an additional logarithmic divergence to the usual logarithmic divergence caused by the BCS instability [189–191]. The pairing vertex is enhanced by $\alpha[v/c(v)]\log(\Lambda/\omega)\log(E^*_{\text{Bos.}}/\omega)$ with $\alpha \sim 1$ at frequency ω. The first logarithm is from the usual BCS mechanism. The second logarithm is from the gapless spin fluctuations, where $E^*_{\text{Bos.}}$ given in Eq. (2.31) is the energy cutoff for the spin fluctuations in the small $c(v)$ limit as is shown in Appendix C. This gives rise to

$$T_c \sim c(v_0)\sqrt{\Lambda\widetilde{\Lambda}}\exp\left(-\sqrt{\frac{c(v_0)}{\alpha v_0}}\right). \tag{2.33}$$

Although T_c is enhanced by the critical spin fluctuations, it remains exponentially small in $\sqrt{c(v_0)/v_0} \sim v_0^{-\frac{1}{4}}$ in the small v_0 limit. There is a hierarchy among the energy scales, $E^*_{\text{Fer.}} \ll T_c \ll E^*_{\text{Bos.}}$ in the small v_0 limit. This suggests that the system undergoes a superconducting transition before the fermions at the hot spots lose coherence. On the one hand, this is similar to the nematic quantum critical point in two dimensions where the system is prone to develop a superconducting instability before the coherence of quasiparticles breaks down [115, 192]. On the other hand, even without superconductivity, the fermions are only weakly perturbed by the spin fluctuations in the present case. It is the collective mode that is heavily dressed by quantum effects. For the collective mode, there is a large window between T_c and $E^*_{\text{Bos.}}$ within which the universal scaling given by Eq. (2.6) is obeyed. The size of the energy window for the critical scaling is non-universal due to the slow flow of v, and it depends on v_0, the bare value of v. Our prediction is that there is a better chance to observe the $z = 1$ critical scaling above T_c, and the enhancement of T_c by AFM spin fluctuations is rather minimal [193] in materials whose bare FS's are closer to perfect nesting near the hot spots.

2.5 Summary and Discussion

In this chapter we have presented a controlled nonperturbative approach that allows the extraction of the exact universal data characterizing the low-energy field theory describing the AFM quantum critical metal in two spatial dimensions. We not only have determined the exact critical exponents of the transition, but also the universal scaling form of physical observables at low temperatures. To end our discussion we comment on how our work compares to earlier theoretical approaches that where mentioned in Sec. 1.4 and provide a comparison between our predictions and existing experiments on materials that are believed to host the AFM QCP in question.

Putting our results into context with the discussion in Sec. 1.4 it is clear that there are qualitative differences with previous theoretical works. Earlier theoretical works [131–134, 186] have invariably predicted the dynamical critical exponent z to be larger than one. In particular, if one uses the one-loop dressed propagators that respect the $z = 2$ scaling, individual higher-loop corrections are, at most, logarithmically divergent. However, this does not imply that the higher-loop corrections are small. The logarithmic corrections remain important in two dimensions due to the strong coupling nature of the theory, and they can introduce $\mathcal{O}(1)$ anomalous dimensions to the fields. The one-loop analysis based on the dimensional regularization scheme also predicts that the dynamical critical exponent is $z = 1 + \mathcal{O}(\epsilon)$ in $3 - \epsilon$ space dimensions [142]. It turns out that it is not enough to include only the one-loop corrections even to the leading order in ϵ due to an infrared singularity associated with the emergent quasi-locality of the metallic state [146]. Once all quantum corrections are taken into account to the leading order in ϵ consistently, the dynamical critical exponent becomes $z = 1$ again [148] in agreement with the current result. The key that makes the present theory solvable is the emergent hierarchy of the velocities $v \ll c(v)$, which becomes manifest only after quantum fluctuations are included consistently. The results from the ϵ expansion not only show that the hierarchy of velocities $v \ll c(v)$ is maintained perturbatively close to three dimensions, but that, if it is maintained for any $2 \leq d < 3$, the critical exponents are given by the ones predicted from this controlled perturbative treatment [148]. Even though the hierarchy of velocities is also maintained in two dimensions and the extrapolation to $\epsilon = 1$ of the critical exponents obtained from the ϵ expansion coincide with the ones found in this chapter, there is no guarantee that such a hierarchy is maintained for any $2 < d < 3$ or that the universal data of the theory close to three dimensions smoothly interpolates with the results for the two-dimensional theory. We address this missing link in Chapter 3 where we also expose the strengths and weaknesses of the dimensional regularization scheme applied to strongly coupled field theories.

Now we make an attempt to compare our predictions with experiments. Electron doped cuprates are probably the simplest examples of quasi-two-dimensional compounds that exhibit AFM phase transitions in the presence of itinerant electrons, without having extra degrees of freedom such as local moments or extra bands. In the normal state of the optimally doped $Pr_{0.88}LaCe_{0.12}CuO_{4-\delta}$ (PLCCO), inelastic neutron scattering shows an overdamped AFM spin fluctuation peaked at (π, π) whose width in momentum space exhibits a weak growth with increasing energy [32]. The theoretical prediction from Eq. (2.22) is that the width of the incoherent peak scales linearly with energy upto a superlogarithmic correction in the low-energy limit. However, it is hard to make a quantitative comparison

due to the limited momentum resolution in the experiment. In $Nd_{2-x}Ce_xCuO_{4\pm\delta}$ (NCCO), inelastic neutron scattering suggests that the magnetic correlation length ξ scales inversely with temperature near the critical doping [33]. Furthermore, ξ measured at the pseudogap temperature diverges as $(x - x_c)^{-1}$. If interpreted in terms of the clean AFM quantum critical scenario, which may be questionable due to the presence of disorder, this is consistent with a $z = 1$ and $\nu = 1$ scaling at the transition. ARPES experiments for NCCO show a reduced quasiparticle weight at the hot spots [31, 34]. This is in qualitative agreement with the prediction of Eqs. (2.17) and (2.21), which imply that the quasiparticle weight vanishes at the hot spots, as compared to the region away from the hot spots where quasiparticles are well defined. Although the spectroscopic measurements are in qualitative agreement with the theoretical predictions, we believe that more experiments are needed to make quantitative comparisons. On the theoretical side, the instabilities of the model towards different types of ordering and the transport properties of the theory need to be better understood, for which electrons away from hot spots are expected to play an important role. This calls for a theoretical study of the theory that includes electrons away from the hot spots and determine how the AFM spin fluctuations affect their Fermi-liquid-like properties. In Chapter 4 we focus on this, where we provide a full characterization of the non-Fermi liquid and Fermi-liquid-like electronic excitations of the AFM quantum critical metal in two dimensions in a controlled manner.

3 | Noncommutativity between the low-energy limit and integer dimension limits in the ϵ expansion: A case study of the antiferromagnetic quantum critical metal

3.1 Introduction

In the previous chapter we obtained the universal low-energy data for the commensurate AFM quantum critical metal supporting a C_4-symmetric FS in two dimensions. Remarkably, the critical exponents governing the transition coincide with the extrapolation of the results found through the controlled ϵ expansion close to the upper critical dimension of the theory [148]. However, this could be just a coincidence. Although the analysis provided by the ϵ expansion indicates the emergence of nonperturbative physics below three dimensions that is correctly captured in the two-dimensional theory, the connection between the perturbative results close to three dimensions and the nonperturbative results obtained in two dimensions is still lacking. The availability of both the perturbative solution near the upper critical dimension of the theory and the nonperturbative one in two dimensions provides a *rare* opportunity to test the extent to which RG schemes based on dimensional regularization and the ϵ expansion are applicable to strongly coupled theories in which $\epsilon \sim 1$.

In this chapter we test this methodology using the EFT for the commensurate AFM quantum critical metal as a model theory. Generalizing the nonperturbative approach presented in Chapter 2 to higher dimensions, we obtain the low-energy universal data of the theory in dimensions between two and three. In doing so, we provide an understanding on how the perturbative results from the ϵ expansion near the upper critical dimension evolve as nonperturbative effects become stronger with decreasing dimension. From this we expose both strengths and weaknesses of RG schemes based on dimensional regularization. On the one hand, the exact critical exponents are smooth functions of the space dimension, and the ϵ expansion can provide an useful ansatz for the critical exponents in two dimensions. On the other hand, it is difficult to capture the full scaling behaviors in two dimensions from the low-energy solution above two dimensions because the low-energy limit and the $d \to 2^+$ limit do no commute.

The results of this chapter are of great theoretical importance and they constitute a word of caution when addressing strongly-coupled field theories from a perturbative perspective. The EFT for the commensurate AFM QCP provides the first example of a non-relativistic field theory where the low-energy data is known exactly in a wide dimensional range. Our work allows to address the subtleties of extrapolating results to lower integer dimensions from those obtained close to the upper critical dimension of the theory. We note that the

	$d=2$	$2<d<3$	$d=3$
$F_z(\mu)$	$\exp\left(2\sqrt{N_c^2-1}\frac{\ell^{\frac{1}{2}}}{\log(\ell)}\right)$	$\exp\left[(d-2)\mathfrak{F}_z(d)(N_c^2-1)^{\frac{1}{d}}\ell^{\frac{1}{d}}\right]$	$\frac{(N_c^2+N_cN_f-1)}{\ell^{2(N_c^2+N_cN_f-3)}}$
$F_\Psi(\mu)$	$\ell^{\frac{3}{8}}$	$\sqrt{\ell}$	$\sqrt{\log(\ell)}$
$F_\Phi(\mu)$	$\exp\left(\frac{2\ell^{\frac{1}{2}}}{\sqrt{N_c^2-1}}\right)$	$\exp\left(-\frac{\mathfrak{F}_\Phi(d)}{2}\frac{[(d-2)N_c^2-d]}{(N_c^2-1)^{\frac{d-1}{d}}}\ell^{\frac{1}{d}}\right)$	$\log(\ell)$
$v(\mu)$	$\frac{\pi^2 N_cN_f}{2(N_c^2-1)\ell\log(\ell)}$	$\frac{\pi N_cN_f(d-2)}{4(N_c^2-1)\zeta(d)(d-1)\ell}$	$\frac{\pi N_cN_f(N_c^2-N_cN_f-3)}{4(N_c^2-1)(N_c^2+N_cN_f-1)\log(\ell)}$
$c(\mu)$	$\frac{\pi}{4\sqrt{N_c^2-1}}\frac{1}{\sqrt{\ell}}$	$\left[\frac{\pi\beta_d^4\mathfrak{B}(d)}{(3-d)(d-1)\zeta(d)(N_c^2-1)}\right]^{\frac{1}{d}}\frac{1}{\ell^{\frac{1}{d}}}$	$\frac{\pi(N_c^2-N_cN_f-3)}{4(N_c^2-1+N_cN_f)}\frac{1}{\log(\ell)}$

Table 3.1: Scale-dependent universal crossover functions and renormalized velocities in the low-energy limit for each fixed d. Here $\ell \equiv \log(\Lambda/\mu)$ is a logarithmic length scale associated with a running energy scale μ, and a UV cutoff Λ. $\beta_d, \zeta(d), \mathfrak{F}_z(d), \mathfrak{F}_\Phi(d)$ and $\mathfrak{B}(d)$ are smooth and positive functions defined in Eqs. (3.19), (3.31), (3.40), (3.42), and (G.21) respectively. It is noted that $\beta_2 = \sqrt{\pi/2}, \zeta(2) = (2\pi)^{-1}, \mathfrak{F}_z(2) = \sqrt{2}, \mathfrak{F}_\Phi(2) = 2\sqrt{2}$ and $\mathfrak{B}(2) = (4\pi^2)^{-1}$ in $d = 2$, and $\beta_{3-\epsilon} = \sqrt{4\pi\epsilon}$, $\zeta(3-\epsilon) = \epsilon/2$, $\mathfrak{F}_z(3) = 3/(2^{14}h_5^*)^{\frac{1}{3}}$, $\mathfrak{F}_\Phi(3) = 3/(2^8 h_5^*)^{\frac{1}{3}}$ and $\mathfrak{B}(3) = 2h_5^*$ with $h_5^* \approx 5.7\times10^{-4}$ in $d = 3-\epsilon$ to leading order in $\epsilon \ll 1$.

ϵ expansion in relativistic field theories [25, 26] also display similar subtleties [169–171]. Therefore, our work constitutes a step forward in the understanding of such subtle issues that cloud the connection between controlled perturbative and nonperturbative results in strongly-coupled field theories.

This chapter is organized as follows. In Sec. 3.2 we review the field theory that describes the AFM quantum critical metal in dimensions between two and three [142, 148]. In Sec. 3.3 we summarize the scaling forms of the low-energy Green's functions. Table 3.1 encapsulates the main result of this chapter: *physical observables exhibit noncommutativities in the sense that the low-energy limit and the limit in which the physical dimensions are approached do not commute*. After the summary, we provide details that lead to such scaling forms. We first review the one-loop solution valid in $d = 3$ [142], and discuss how the solution fails to capture the low-energy physics in $d = 3-\epsilon$ for any nonzero ϵ. This is caused by a noncommutativity between the low-energy limit and the $d \to 3^-$ limit. We then move on to the general solution valid in any $2 < d < 3$, which shows how nonperturbative effects become important as the space dimension is lowered. Finally, we compare this solution to the nonperturbative solution presented in Chapter 2 for the two-dimensional theory. While critical exponents vary smoothly in d, the full low-energy Green's function in $d = 2$ *cannot* be obtained from the $d \to 2^+$ limit of the low-energy Green's function obtained in $d > 2$ due to a noncommutativity between the $d \to 2^+$ limit and the low-energy limit. We finish this chapter with some concluding remarks in Sec. 3.4.

3.2 Field Theory in $2 \leq d \leq 3$

We start by promoting the action in Eq. (1.32) to d-spatial dimensions by increasing the co-dimension of the FS [176] while keeping its dimension fixed to one. In this choice of dimensional regularization, not only locality is maintained [114, 142, 148, 177], but the spurious UV/IR mixing that arises through couplings between different patches of the FS when its dimension is greater than one [174], is avoided. Following Refs. [142, 148], we write the action for the theory in $2 \leq d \leq 3$ as

$$\begin{aligned} S_d = & \sum_{n=1}^{4} \sum_{\sigma=1}^{N_c} \sum_{j=1}^{N_f} \int \mathrm{d}k \; \overline{\Psi}_{n,\sigma,j}(k) \left[i\mathbf{\Gamma} \cdot \mathbf{K} + i\gamma_{d-1} \varepsilon(\vec{k}; v) \right] \Psi_{n,\sigma,j}(k) \\ & + \frac{1}{4} \int \mathrm{d}q \; \left[|\mathbf{Q}|^2 + \mathsf{c}_0^2 |\vec{q}|^2 \right] \mathrm{Tr} \left[\Phi(q) \Phi(-q) \right] \\ & + \frac{ig}{\sqrt{N_f}} \sum_{n=1}^{4} \sum_{\sigma,\sigma'=1}^{N_c} \sum_{j=1}^{N_f} \int \mathrm{d}k \int \mathrm{d}q \; \left[\overline{\Psi}_{\overline{n},\sigma,j}(k+q) \Phi_{\sigma\sigma'}(q) \gamma_{d-1} \Psi_{n,\sigma',j}(k) \right] \\ & + \frac{u_1}{4} \int \mathrm{d}q_1 \int \mathrm{d}q_2 \int \mathrm{d}q_3 \; \mathrm{Tr} \left[\Phi(q_1+q_3) \Phi(q_2-q_3) \right] \mathrm{Tr} \left[\Phi(-q_1) \Phi(-q_2) \right], \\ & + \frac{u_2}{4} \int \mathrm{d}q_1 \int \mathrm{d}q_2 \int \mathrm{d}q_3 \; \mathrm{Tr} \left[\Phi(q_1+q_3) \Phi(q_2-q_3) \Phi(-q_1) \Phi(-q_2) \right]. \end{aligned} \tag{3.1}$$

Here, $k = (\mathbf{K}, \vec{k})$ [$q = (\mathbf{Q}, \vec{q})$] where $\mathbf{K}$ ($\mathbf{Q}$) denotes the $(d-1)$-dimensional vector composed of fermionic (bosonic) Matsubara frequency and $(d-2)$ co-dimensional momentum components. $\vec{k}$ ($\vec{q}$) still denotes the original fermionic (bosonic) two-dimensional spatial momentum measured relative to the hot spots (commensurate wavevector $\vec{Q}_{\mathrm{AFM}}$). The integration measure is now denoted by $\mathrm{d}k = \mathrm{d}^{d-1}\mathbf{K}\mathrm{d}^2\vec{k}/(2\pi)^{d+1}$. In $2 \leq d \leq 3$ the spinors are kept two-dimensional and $(\mathbf{\Gamma}, \gamma_{d-1}) = (\gamma_0, \gamma_1, \ldots, \gamma_{d-2}, \gamma_{d-1})$ denote 2×2 matrices satisfying the Clifford algebra: $\{\gamma_\mu, \gamma_\nu\} = 2\delta_{\mu\nu}\mathbb{I}_{2\times 2}$ with $\mathbb{I}_{2\times 2}$ denoting the 2×2 identity matrix. In what follows we choose $\gamma_0 = \sigma_y$ and $\gamma_{d-1} = \sigma_x$, where σ_x and σ_y are the two first Pauli matrices. Keeping the spinors two-dimensional is justified by the fact that, for each hot spot, the fermionic kinetic term in Eq. (3.1) is identical to that of a $[(d-1)+1]$-dimensional Dirac fermion where the location of the Dirac point is parametrized by the momentum along the locally linear FS [114].

The fermionic kinetic term in Eq. (3.1) describes a metal with a one-dimensional FS embedded in d-dimensional momentum space and such that the FS is locally linear near each of the hot spots. This is seen from the fact that the energy of a fermion close to hot spot n is given by [142]:

$$E_n(k_1, \ldots, k_{d-2}, \vec{k}) = \pm \sqrt{\sum_{j=1}^{d-2} k_j^2 + [\varepsilon_n(\vec{k}; v)]^2}. \tag{3.2}$$

Therefore, at the Fermi level $[E_n(k_1, \ldots, k_{d-2}, \vec{k}) = 0]$ the system supports line nodes defined by $k_j = 0$ for $j = 1, \ldots, d-2$ and $\varepsilon_n(\vec{k}; v) = 0$. We further note that Eq. (3.2) implies that the electrons disperse linearly in the $(d-1)$-dimensional space perpendicular to the

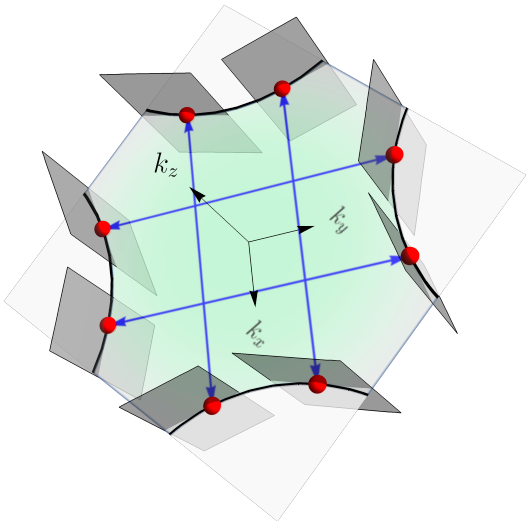

Figure 3.1: A one-dimensional FS embedded in the three-dimensional momentum space. The (gray) planes correspond to locally flat patches that include line nodes (solid lines) where the hot spots are located.

aforementioned line node. This is shown in Fig. 3.1 for $d = 3$. The action in Eq. (3.1) is not just a mathematical construction and there is physical content behind it. In $d = 3$, we can choose $(\gamma_0, \gamma_1, \gamma_2) = (\sigma_y, \sigma_z, \sigma_x)$ and $k_1 = k_z$. In this dimension, the action in Eq. (3.1) describes the low-energy theory of the line-nodal AFM quantum critical metal in the presence of p_z-charge density wave (CDW) carrying momentum $2\vec{k}_{\rm F}$ and where the AFM transition is driven by electrons near the hot spots on the line nodes [142]. This becomes manifest when we use Eq. (1.30) to write the free fermion action in terms of the spinor components as

$$S^{\rm F.F.}_{d=3} = \sum_{N=1}^{8}\sum_{\sigma=1}^{N_c}\sum_{j=1}^{N_f}\int {\rm d}k \left\{\psi^\dagger_{N,\sigma,j}(k)\left[ik_0 + e_N(\vec{k};v)\right]\psi_{N,\sigma,j} + (-1)^N k_z \psi^\dagger_{N,\sigma,j}(k)\psi_{[N+4]_8,\sigma,j}(k)\right\}, \tag{3.3}$$

where $[x]_8$ denotes the reminder of x divided by 8. The first term in this action is the one that gives rise to a locally flat two-dimensional FS in three dimensions. The second term, which represents the $2\vec{k}_F$-p_z-CDW, is responsible for gapping out the two-dimensional FS except at $k_z = 0$, where the line nodes are located.

Taking into account the above observations, it follows that the action in Eq. (3.1) continuously interpolates the low-energy theory of the AFM quantum critical metals in $d = 2$ and $d = 3$. In the rest of this chapter we proceed on extracting the low-energy universal data of the theory in $2 \leq d \leq 3$.

3.3 Noncommutativity between the low-energy limit and the physical dimension limits

In this section, we first summarize the main results of this chapter without derivation. The scaling form of the electronic and bosonic Green's functions of the theory in $2 \leq d \leq 3$ is

given by

$$G_1(k;d) = \frac{1}{iF_\Psi(|\mathbf{K}|)} \frac{1}{F_z(|\mathbf{K}|)\mathbf{\Gamma}\cdot\mathbf{K} + \gamma_{d-1}[v(|\mathbf{K}|)k_x + k_y]}, \tag{3.4}$$

$$D(k;d) = \frac{1}{F_\Phi(|\mathbf{K}|)} \frac{1}{F_z(|\mathbf{K}|)^{d-1}|\mathbf{K}|^{d-1} + c(|\mathbf{K}|)^{d-1}(|k_x|^{d-1} + |k_y|^{d-1})}, \tag{3.5}$$

for $\vec{k}/[|\mathbf{K}|F_z(|\mathbf{K}|)] \sim 1$. $G_1(k;d)$ denotes the fermion Green's function at hot spot $n = 1$ in d space dimensions. The Green's functions at other hot spots are related to $G_1(k;d)$ through the C_4 symmetry of the theory. $D(k;d)$ denotes the Green's function for the AFM collective mode. Here, the condition $\vec{k}/[|\mathbf{K}|F_z(|\mathbf{K}|)] \sim 1$ is chosen so that the forms of the Green's functions are invariant (up to the weak scale dependence of the velocities) under scale transformations in which momentum and frequency are simultaneously taken to zero. If the dynamical critical exponent was fixed, the scale invariance of the Green's function would be manifest under the rescaling in which $\vec{k}/|\mathbf{K}|^{1/z}$ is fixed, where z is the dynamical critical exponent. In the present case, the dynamical critical exponent depends weakly on the scale, and it flows to $z = 1$ in the low-energy limit, as will be shown in the following sections. At finite energy scales, the Green's functions are invariant under the scale transformation in which $\vec{k}/[|\mathbf{K}|F_z(|\mathbf{K}|)]$ is fixed, where $F_z(|\mathbf{K}|)$ is a function that encodes the scale dependence of the dynamical critical exponent. The leading power-law dependences of the Green's functions in energy and momentum reflect the dynamical critical exponent ($z = 1$), and the scaling dimensions of the fermion ($[\Psi_{n,\sigma,j}(k)] = -(d+2)/2$) and the collective mode ($[\Phi(k)] = -d$) fields at the fixed point. The full Green's functions deviate from the perfect power-law behaviors due to a scale dependence of marginally irrelevant operators.

In $d < 3$, the ratio between velocities,

$$w(\mu) \equiv \frac{v(\mu)}{c(\mu)} \tag{3.6}$$

controls quantum corrections, where $v(\mu)$ and $c(\mu)$ are the renormalized velocities that depend on the energy scale μ. As it will be shown later, a slow flow of $w(\mu)$ generates super-logarithmic corrections captured by $F_z(\mu), F_\Psi(\mu)$ and $F_\Phi(\mu)$, that is, corrections that are smaller than a power-law but larger than any fixed power of a logarithm in energy. $F_\Psi(\mu)$ $[F_\Phi(\mu)]$ represents the correction to the scaling dimension of the fermion (boson) field. In $d = 3$, quantum corrections are controlled by g^2/v, which yield logarithmic corrections to the power-law scalings. The scale dependences of $v(\mu), c(\mu), F_z(\mu), F_\Psi(\mu)$ and $F_\Phi(\mu)$ in each dimension are summarized in Table 3.1.

Although the critical exponents that characterize the fixed point are smooth functions of d, the functions $v(\mu), c(\mu), F_z(\mu), F_\Psi(\mu)$ and $F_\Phi(\mu)$, evaluated in the low-energy limit (i.e., for $\mu \ll \Lambda$ with Λ denoting the UV scale at which the bare theory is defined), are not, as it is can be seen from Table 3.1. This leads to discontinuities of $\lim_{k\to 0} G_1(k;d)$ and $\lim_{k\to 0} D(k;d)$ as functions of d. The discontinuities are caused by a lack of commutativity between the low-energy limit and the limits in which d approaches the physical dimensions:

$$\begin{aligned} \lim_{k\to 0}\lim_{d\to 2^+,3^-} G_1(k;d) &\neq \lim_{d\to 2^+,3^-}\lim_{k\to 0} G_1(k;d), \\ \lim_{k\to 0}\lim_{d\to 2^+,3^-} D(k;d) &\neq \lim_{d\to 2^+,3^-}\lim_{k\to 0} D(k;d). \end{aligned} \tag{3.7}$$

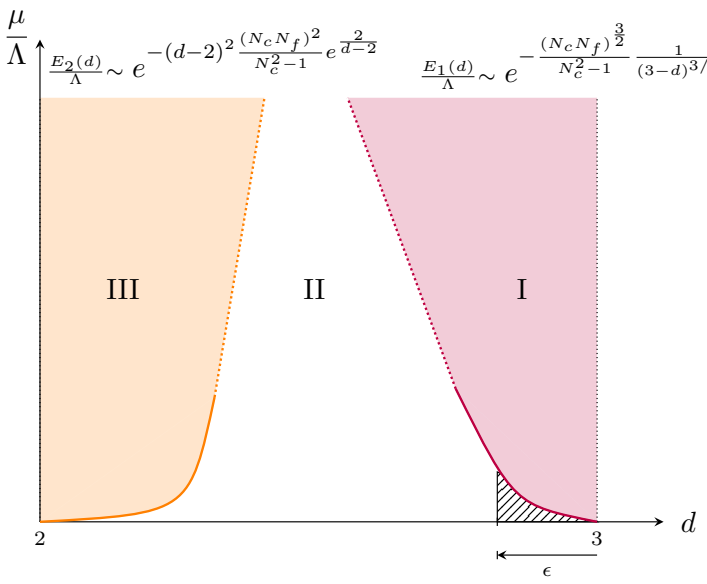

Figure 3.2: Two crossover energy scales that divide the plane of spatial dimension (d) and relative energy scale (μ/Λ) into three regions. At low energies, $w(\mu)$ flows to an order one number in region I, while it flows to zero in regions II and III. Region III is distinguished from region II by the fact that physical observables receive additional logarithmic corrections.

Since the Green's functions diverge at $k = 0$, Eq. (3.7) makes sense only if the small k limit is viewed as the asymptotic limit of the Green's functions. In other words, for the electronic Green's function, $\lim_{k\to 0} G_1(k;d)$ should be understood as the k-dependent function that $G_1(k;d)$ asymptotically approaches in the small k limit at a fixed d, rather than $G_1(0;d)$. With this, Eq. (3.7) implies that the low-energy asymptote of $G_1(k;d)$ at $d = 2$ ($d = 3$) can not be reproduced by taking the $d \to 2^+$ ($d \to 3^-$) limit of the low-energy asymptote of $G_1(k;d)$ obtained in $2 < d < 3$. This same discussion applies for the bosonic Green's function.

The expressions in Table 3.1 are obtained by taking the low-energy limit at a fixed dimension. Because of the noncommutativity in Eq. (3.7), $\lim_{k\to 0} G_1(k;d)$ is not a continuous function of d at $d = 2$ and $d = 3$. The noncommutativity arises because of the existence of crossover energy scales that vanish in the $d \to 2^+$ and $d \to 3^-$ limits. In the plane of spatial dimension and (relative) energy scale, there are three distinct regions divided by these crossover energy scales as is shown in Fig. 3.2. The first crossover energy scale is given by

$$E_1(d) \sim \Lambda \exp\left(-\frac{(N_c N_f)^{\frac{3}{2}}}{(N_c^2-1)}\frac{1}{(3-d)^{\frac{3}{2}}}\right), \tag{3.8}$$

which vanishes exponentially as d approaches three, where Λ is a UV energy scale. The second scale,

$$E_2(d) \sim \Lambda \exp\left(-(d-2)^2\frac{(N_c N_f)^2}{(N_c^2-1)}e^{\frac{2}{d-2}}\right) \tag{3.9}$$

vanishes in a doubly exponential fashion as d approaches two. The three regions divided by $E_1(d)$ and $E_2(d)$ are governed by different physics as we discuss in the following sections.

In region I of Fig. 3.2, i.e., for $\mu > E_1(d)$, the low-energy physics is described at the one-loop order by a quasi-local marginal Fermi-liquid metal, where v and c flow to zero as

$1/\log[\log(\Lambda/\mu)]$ with $w \sim \mathcal{O}(1)$ [142]. Because the velocities flow to zero, the magnitude of higher-loop diagrams is not only determined by the number of vertices, but also by enhancement factors of $1/v$ and $1/c$ that originate from the fact that modes become dispersionless at low energies. In particular, the one-loop fixed point is controlled only when g^2 flows to zero faster than v and c. In $d = 3$, the one-loop results become asymptotically exact at low energies because $\lambda \equiv g^2/v$ flows to zero much faster than any power of the velocities. While the quasi-local marginal Fermi-liquid behavior persists down to the zero energy limit in $d = 3$, the low-energy physics becomes qualitatively different below three dimensions. In $d = 3 - \epsilon$ with $\epsilon > 0$, λ becomes order of ϵ, while v and c still flow to zero logarithmically at the one-loop order. Due to the enhanced quantum fluctuations associated with the vanishing velocities and non-vanishing λ, higher-loop effects become qualitatively important at energies below the crossover energy scale $E_1(d)$ in Eq. (3.8) [142, 148]. For any $0 < \epsilon < 1$, the theory flows into a new region (region II) in which leading order quantum fluctuations are no longer contained within the one-loop order. The noncommutativity between the $d \to 3^-$ and $\mu \to 0$ limits arises because $E_1(d)$ vanishes as $d \to 3^-$.

It turns out that it is sufficient to include a two-loop quantum correction in addition to the one-loop quantum corrections to the leading order in $\epsilon \ll 1$ because all other higher-loop corrections are suppressed by ϵ in the shaded area of region II shown in Fig. 3.2 [146, 148]. The physics below $E_1(d)$ is qualitatively different from that of region I. In particular, w flows to zero in the low-energy limit in $d = 3 - \epsilon$ due to the two-loop effect that modifies the flow of the velocities. The fact that quantum corrections are not organized by the number of loops even close to the upper critical dimension is a feature caused by the emergent quasi-locality of the metallic state where velocities flow to zero in the low-energy limit.

As d decreases further away from three, an infinite set of diagrams, which are suppressed by higher powers of ϵ near three dimensions, becomes important. Although it is usually hopeless to include all higher-order quantum corrections, in the present case one can use w as a control parameter since w dynamically flows to zero in the low-energy limit. In the small w limit, only the diagrams in Figs. 3.5(a), 3.5(b), 2.3(a) and 2.3(b) remain important even when $\epsilon \sim 1$ [148]. In there, the double wiggly line represents the renormalized boson propagator which is self-consistently dressed with the diagrams in Figs. 3.5(a) and 3.5(b). The propagator of the collective mode becomes:

$$D(q) = \frac{1}{|\mathbf{Q}|^{d-1} + c(v)^{d-1}(|q_x|^{d-1} + |q_y|^{d-1})}, \tag{3.10}$$

where $c(v)$ is the velocity of the incoherent collective mode given by $c(v)^d \sim v/(d-2)$.

The behavior in region II does not extend smoothly to $d = 2$ because of the existence of another crossover set by the energy scale $E_2(d)$ in Eq. (3.9) and which vanishes in the $d \to 2^+$ limit. The existence of the crossover is expected from the fact that the relation, $c(v)^d \sim v/(d-2)$, which is valid in region II, becomes ill-defined in $d = 2$. The divergence in the $d \to 2^+$ limit is caused by the incoherent nature of the AFM collective mode which has significant low-energy spectral weight even at large momenta. At $d = 2$, the divergence gives rise to a logarithmic enhancement of $c(v)$ as $c(v)^2 \sim v \log[1/w(v)]$. As shown in Chapter 2, the extra logarithmic correction causes the additional set of diagrams in Figs. 2.3(c) and 2.3(d) to become important in region III. This gives rise to a lack of commutativity between the $d \to 2^+$ limit and the low-energy limit.

In the remaining of this chapter, we elaborate on the points summarized in this section starting from $d = 3$. Subsection 3.3-(a) is devoted to the discussion of region I and the shaded part of region II in Fig. 3.2 and it constitutes mostly a self-contained summary of Refs. [142, 148]. Subsection 3.3-(b) is devoted to region II, which is the main purpose of this chapter. Finally, Subsection 3.3-(c) is concerned with region III and it presents a straightforward generalization of the results presented in Chapter 2 to the case in which N_c and N_f take arbitrary values.

3.3-(a) Region I: From $d = 3$ to $d = 3 - \epsilon$

In three dimensions, the Yukawa coupling is marginal under the Gaussian tree-level scaling. The one-loop quantum corrections shown in Figs. 3.3(a) to 3.3(e) drive all parameters of the theory (g, v, c, u_1, and u_2) to flow to zero in such a way that the ratios defined by $\lambda = g^2/v$, $w = v/c$ and $\kappa_i = u_i/c^2$, with $i = 1, 2$, become [142]

$$\lambda^* = 0, \quad c^* = 0, \quad w^* = \frac{N_c N_f}{N_c^2 - 1}, \quad \& \quad \kappa_i^* = 0, \quad i = 1, 2, \tag{3.11}$$

in the low-energy limit. As it is shown in Table 3.1, the velocities flow to zero as $v(\ell) \sim 1/\log(\ell)$ and $c(\ell) \sim 1/\log(\ell)$ in the logarithmic length scale $\ell \equiv \log(\Lambda/\mu)$, while the rescaled coupling flows to zero as $\lambda(\ell) \sim 1/\ell$. Because λ flows to zero faster than both v and c, the ratios of the form g^{2n}/c^m and g^{2n}/v^m, which control the perturbative expansion, flow to zero for any $n, m > 1$. This implies that all higher-order corrections are suppressed at low energies. The physical observables receive only logarithmic quantum corrections compared to the Gaussian scaling. The fermionic and bosonic Green's functions are given by Eqs. (3.4) and (3.5), respectively, where the crossover functions that capture the aforementioned corrections are given by

$$F_z(|\mathbf{K}|) = \left[\log\left(\frac{\Lambda}{|\mathbf{K}|}\right)\right]^{\frac{(N_c^2+N_cN_f-1)}{2(N_c^2+N_cN_f-3)}}, \tag{3.12}$$

$$F_\Psi(|\mathbf{K}|) = \sqrt{\log\left[\log\left(\frac{\Lambda}{|\mathbf{K}|}\right)\right]}, \tag{3.13}$$

$$F_\Phi(|\mathbf{K}|) = \log\left[\log\left(\frac{\Lambda}{|\mathbf{K}|}\right)\right], \tag{3.14}$$

in the small $|\mathbf{K}|$ limit with $\vec{k}/[|\mathbf{K}|F_z(|\mathbf{K}|)] \sim 1$ fixed. The details leading to these results are throughly given in Appendix F.

For $d < 3$, $\lambda = g^2/v$ no longer flows to zero, although v and c still do under the one-loop RG flow. This puts the control of the one-loop analysis in peril even close to three dimensions. Due to the enhanced infrared quantum fluctuations caused by the modes that become increasingly dispersionless at low energies, some higher-loop diagrams, albeit suppressed by powers of ϵ, diverge at the one-loop fixed point. The divergence is cured only after the two-loop correction in Fig. 3.3(f) is included. The energy scale below which the two-loop effect becomes qualitatively important marks the crossover energy scale:

$$E_1(d) \sim \Lambda \exp\left(-\frac{(N_cN_f)^{\frac{3}{2}}}{(N_c^2-1)}\frac{1}{\epsilon^{\frac{3}{2}}}\right). \tag{3.15}$$

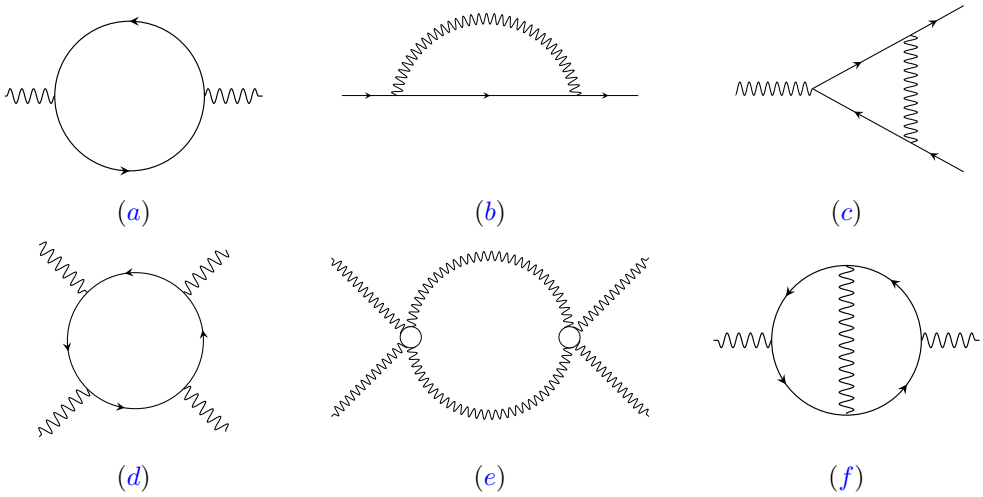

Figure 3.3: Quantum corrections at the modified one-loop order.

At energies below $E_1(d)$, the two-loop self-energy speeds up the collective mode such that v and c flow to zero with a hierarchy, $c \gg v$, with $c^3 \sim \epsilon v/(N_c N_f)$ [148]. The low-energy fixed point is characterized by

$$\lambda^* = 4\pi\epsilon, \quad x^* = \frac{N_c N_f}{16\pi \mathfrak{B}(3)}, \quad w^* = 0, \quad \& \quad \kappa_i^* = 0, \quad i = 1, 2, \tag{3.16}$$

where $x \equiv g^2/c^3$ and $\mathfrak{B}(3) \approx 0.0012434$ (See Appendix G for details). It can be shown that all other higher-loop corrections remain finite and they are suppressed by ϵ at the modified one-loop (M1L) fixed point where the two-loop effect is taken into account in addition to the one-loop corrections [148]. The shaded area of region II in Fig. 3.2 is where the M1L description is valid at low energies.

Comparing these results with those obtained in three dimensions shows a qualitative change in the low energy physics. Especially, the fixed point value of w is not a continuous function of d. In region I, the one-loop effect causes w to flow to the $\mathcal{O}(1)$ value given in Eq. (3.11). Below the crossover energy scale in Eq. (3.15), w flows to zero as [148]

$$w(\ell) = \frac{N_c N_f}{2^{\frac{10}{3}} \mathfrak{B}(3)^{\frac{1}{3}} (N_c^2 - 1)^{\frac{2}{3}}} \frac{1}{\epsilon} \frac{1}{\ell^{\frac{2}{3}}}. \tag{3.17}$$

For small but nonzero ϵ, the M1L description is controlled, and w flows to zero at sufficiently low energies. Thus, the low-energy fixed point below three dimensions is qualitatively different from the fixed point that the theory flows into in three dimensions. This discrepancy shows that the low-energy limit does not commute with the $d \to 3^-$ limit. The change in the flow of w is responsible for the disparity between the low-energy physical observables in $d = 3 - \epsilon$ in the $\epsilon \to 0^+$ limit and those in $d = 3$.

There are two relatively well separated stages of the RG flow in the space of λ, x, w, κ_1 and κ_2 for $\epsilon > 0$ and $\mu < E_1(d)$. In the first stage, the RG flow converges towards a one-dimensional manifold, where deviations away from the manifold die out as a power-law in the energy scale. The one-dimensional manifold can be parameterized by one of the parameters,

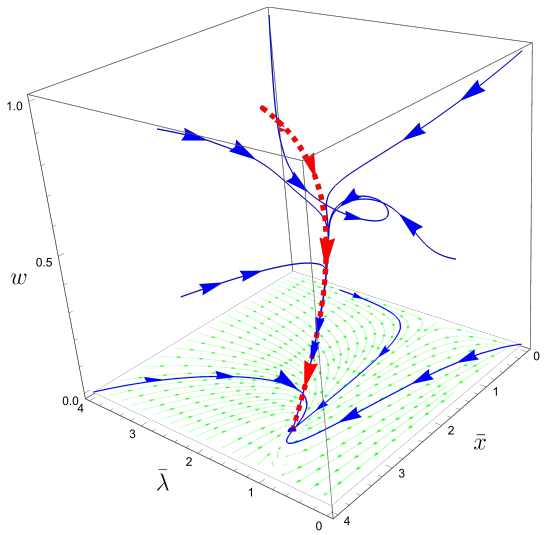

Figure 3.4: The RG flow projected in the space of $(\overline{\lambda}, \overline{x}, w)$ for $N_c = 2$, $N_f = 1$ and $\epsilon = 0.01$ with $\kappa_i = 0$. The axes are scaled as $\overline{\lambda} = 10\lambda$ and $\overline{x} = x/10$. The dashed (red) line corresponds to the one-dimensional manifold towards which the RG flow is rapidly attracted before a slow flow along the manifold takes the couplings to the low-energy fixed point located on the $w = 0$ plane. The three trajectories that do not seem to converge to the universal one-dimensional manifold lie on the $w = 0$ plane.

say w, where λ, x, κ_1 and κ_2 take w-dependent values. Once the RG flow converges to the one-dimensional manifold, all couplings are controlled by a slow sub-logarithmic flow of w [148]. This is shown in Fig. 3.4. At low energies, we can keep only one coupling, although the microscopic theory has five independent parameters.

At the IR fixed point, the fermion keeps the Gaussian tree-level scaling dimension, $[\Psi_{n,\sigma,j}(k)] = -(d+2)/2$ while the collective mode acquires an anomalous dimension yielding $[\Phi(k)] = -d$. Interestingly, the scaling dimensions of the fields are set such that the fermion kinetic term and the Yukawa coupling are marginal while the boson kinetic term and the quartic coupling are irrelevant. A similar protection of the scaling exponents arises in the $1/N$ expansion for the nematic QCP in d-wave superconductors [110]. Physically, the collective mode is strongly dressed by particle-hole excitations, while its feedback to fermions remains small. This provides a crucial hint in constructing a nonperturbative ansatz for regions II and III.

3.3-(b) Region II: $2 < d < 3$

As the spatial dimension approaches two, quantum fluctuations become progressively stronger, and the perturbative expansion eventually breaks down. In this section we describe a non-perturbative approach that captures the universal low-energy physics for any $0 < \epsilon \leq 1$. We do this by following the same line of thought that was introduced in Chapter 2 for the theory in two dimensions.

A. Tree Level Scaling: Gaussian vs. Interaction-driven

The Gaussian tree-level scaling prioritizes the kinetic terms over the interaction terms in Eq. (3.1). Under this scaling, $[g] = \epsilon/2$ and $[u_1] = [u_2] = \epsilon$. For $\epsilon \sim 1$, quantum corrections to the Gaussian scaling are expected to be $\mathcal{O}(1)$ and the ϵ expansion is no longer reliable. For

Quantity	Gaussian	Interaction-Driven
$[\Psi_{n,\sigma,j}(k)]$	$-\left(\frac{d+2}{2}\right)$	$-\left(\frac{d+2}{2}\right)$
$[\Phi(k)]$	$-\left(\frac{d+3}{2}\right)$	$-d$
$[g]$	$\frac{3-d}{2}$	0
$[u_i]$	$3-d$	$-(3-d)$

Table 3.2: Comparison between the scaling dimensions of fields and couplings deduced from the Gaussian and interaction-driven scalings.

strongly coupled theories, it is better to start with the interaction-driven scaling in which the interaction is treated ahead of some of the kinetic terms. As we did in Chapter 2, we use the information obtained from the ϵ expansion to construct a scaling ansatz for general ϵ. We generalize the interaction-driven scaling used in two dimensions to any dimension $2 \leq d < 3$ by requiring that the fermion kinetic term and the fermion-boson interaction are marginal operators in this dimensional range. This uniquely fixes the scaling dimensions of the fields as in Table 3.2 and, as a direct consequence, the boson kinetic term and the bosonic quartic interaction term are irrelevant.

We note that the former ansatz is consistent with the results from the ϵ expansion which suggests that the collective mode is likely to acquire an $\mathcal{O}(1)$ anomalous dimension near $d = 2$ [148]. Dropping from Eq. (3.1) those terms that are irrelevant under the interaction-driven scaling, we write down the minimal action as

$$\begin{aligned} S_d = &\sum_{n=1}^{4}\sum_{\sigma=1}^{N_c}\sum_{j=1}^{N_f}\int \mathrm{d}k\overline{\Psi}_{n,\sigma,j}(k)\left[i\mathbf{\Gamma}\cdot\mathbf{K} + i\gamma_{d-1}\varepsilon_n(\vec{k};v)\right]\Psi_{n,\sigma,j}(k) \\ &+ \frac{i\beta_d\sqrt{v}}{\sqrt{N_f}}\sum_{n=1}^{4}\sum_{\sigma,\sigma'=1}^{N_c}\sum_{j=1}^{N_f}\int \mathrm{d}k\int \mathrm{d}q\ \left[\overline{\Psi}_{\overline{n},\sigma,j}(k+q)\Phi_{\sigma\sigma'}(q)\gamma_{d-1}\Psi_{n,\sigma',j}(k)\right], \end{aligned} \tag{3.18}$$

where

$$\beta_d = \frac{\pi^{\frac{d-1}{4}}}{\Gamma\left(\frac{d}{2}\right)}\sqrt{\frac{\Gamma(d)\Gamma\left(\frac{d-1}{2}\right)\cos\left(\frac{\pi(d+2)}{2}\right)}{2^{3-d}}} \tag{3.19}$$

is a positive constant in $2 \leq d < 3$. The freedom in choosing the overall scale of the boson field is used to fix the Yukawa coupling in terms of v such that $g^2/v \sim (3-d)$. The choice of β_d is such that the one-loop boson self-energy becomes of order of one. Similarly as it was done in Chapter 2, the fermion-boson coupling is replaced by $\sqrt{v}$ as the interaction is screened in such a way that g^2 and v balance with each other in the low-energy limit

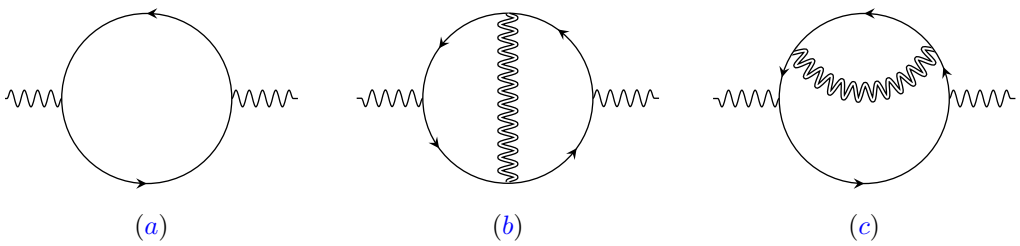

(a) (b) (c)

Figure 3.5: Leading order corrections to the boson self-energy in the small v limit and for $d > 2$. In $d = 2$ the contribution from (c) is identically zero. The solid line represents the bare fermion propagator and the double wiggly line denotes the fully dressed self-consistent propagator in Eq. (3.21).

[142, 148]. Since the ϵ expansion is organized in powers of g^2/v, the theory with $g^2/v \sim 1$ is a strongly coupled theory that cannot be accessed perturbatively in ϵ.

The five parameters in the original theory (v, c, g, u_1 and u_2) are now reduced to one (v) in the minimal theory. The velocity v specifies the low-energy EFT within the one-dimensional manifold shown in Fig. 3.4. The minimal theory is valid at energy scales low enough that the five parameters of the theory have already flown to the one-dimensional manifold, and all renormalized couplings are tied to one leading irrelevant parameter.

B. Schwinger-Dyson Equation for the Boson Dynamics

Following the same logic introduced in Chapter 2, we note that the absence of a bare kinetic term for the boson poses no obstacle since its dynamics is entirely generated through the exact boson self-energy shown in Fig. 2.1 and which solves the Schwinger-Dyson equation in $2 \leq d < 3$:

$$D(q)^{-1} = m_{\text{C.T.}} - 2\beta_d^2 v \sum_{n=1}^{4} \int \mathrm{d}k \ \mathrm{Tr}\left[\gamma_{d-1} G_{\overline{n}}(k+q;v) \Gamma_n^{(2,1)}(k,q) G_n(k;v)\right]. \tag{3.20}$$

Here $m_{\text{C.T.}}$ is a counterterm that tunes the mass to zero in order to keep the theory at criticality. $\Gamma_n^{(2,1)}(k,q)$ denotes the fully dressed vertex function. $D(q)$ and $G_n(k;v)$ denote the fully dressed boson and fermion propagators, respectively.

We proceed following the same two-step logic introduced in Sec. 2.3 of Chapter 2: (*i*) we first solve Eq. (3.20) for the boson propagator in the small v limit and then (*ii*) proceed to show that, with the obtained boson propagator, v indeed flows to zero. To accomplish the first step of this program, we propose the following ansatz for the fully dressed boson propagator in the small v limit:

$$D(q)^{-1} = |\mathbf{Q}|^{d-1} + c(v)^{d-1}(|q_x|^{d-1} + |q_y|^{d-1}), \tag{3.21}$$

where $c(v)$ is the (dimension-dependent) "velocity" of the damped AFM collective mode that is to be determined as a function of v from Eq. (3.20). This ansatz is consistent with the interaction-driven scaling and the symmetries of the theory. However, the ultimate justification for the ansatz comes from the fact that Eq. (3.21) satisfies Eq. (3.20) as will be

shown below. We further supplement this ansatz by assuming that the fermion and boson velocities satisfy the hierarchy $v \ll c(v) \ll 1$. Under this assumption we shown in Appendix A that a general L-loop diagram with L_f fermion loops and E external legs scales at most as the upper bound given in Eq. (2.8):

$$\mathcal{G}(L, L_f, E) \sim v^{\frac{1}{2}(E-2)} \left(\frac{v}{c(v)}\right)^{L-L_f}. \tag{3.22}$$

Because for the theory in dimensions $2 \leq d < 3$ we have set to one the velocities along the extra co-dimensions, and the boson propagator in Eq. (3.21) depends on the spatial momentum only through $c(v)\vec{q}$, the magnitude of general diagrams is determined in the same way as in the two-dimensional theory and thus the upper bound, as a function of v and $c(v)$, is the same as the one introduced in Chapter 2. We note, however, that the information regarding the space dimension is encoded in $c(v)$ as we shall see below. It is clear from Eq. (3.22) that, in the presence of the assumed hierarchy between velocities there is a systematic suppression of diagrams with $L > L_f$.

According to the upper bound, the zeroth order contribution in v is given by the one-loop diagram in Fig. 3.5(a). However, this graph is independent of the spatial momentum. To determine such a dependence of the boson propagator, one has to go to the next order in v shown in Figs. 3.5(b) and 3.5(c). Fig. 3.5(c) is again independent of the spatial momentum, and in contrast with the two-dimensional theory, it is not identically zero. Thus, only Fig. 3.5(b) remains important to the next leading order in v. This is shown in Appendix G. To the leading order in v, Eq. (3.20) is simplified to:

$$\begin{aligned} D(q)^{-1} = m'_{\text{C.T.}} + |\mathbf{Q}|^{d-1} - \frac{4\beta_d^4 v^2}{N_c N_f} \sum_{n=1}^{4} \int \mathrm{d}p \int \mathrm{d}k \ \mathrm{Tr} \Big[\gamma_{d-1} G_{\overline{n}}^{(0)}(k+p;v) \gamma_{d-1} \\ \times G_n^{(0)}(k+q+p;v) \gamma_{d-1} G_{\overline{n}}^{(0)}(k+q;v) \gamma_{d-1} G_n^{(0)}(k;v) \Big] D(p), \end{aligned} \tag{3.23}$$

where the bare fermion propagator is given by

$$G_n^{(0)}(k;v) = \frac{1}{i} \left(\frac{\mathbf{\Gamma} \cdot \mathbf{K} + \gamma_{d-1} \varepsilon_n(\vec{k};v)}{\mathbf{K}^2 + \varepsilon_n(\vec{k};v)^2} \right) \tag{3.24}$$

and $m'_{\text{C.T.}}$ is a two-loop mass counterterm. The term $|\mathbf{Q}|^{d-1}$ in Eq. (3.23) is the contribution from the one-loop boson self-energy. Explicit computation of the two-loop boson self-energy with Eq. (3.21) in the small v limit indeed yields the boson propagator of the form in Eq. (3.21) with a self-consistent equation for $c(v)$ (see Appendix G for details),

$$c(v)^{d-1} = \frac{4\beta_d^4 \mathfrak{B}(d)}{(3-d) N_c N_f} \frac{v}{c(v)} \mathfrak{S}\left(d-2; \frac{v}{c(v)}\right), \tag{3.25}$$

where $\mathfrak{S}[d-2; w(v)]$ is defined in Eq. (G.13). It has the following limiting behaviors:

$$\lim_{w(v)\to 0} \mathfrak{S}[d-2; w(v)] = \frac{1}{d-2}, \tag{3.26}$$

$$\lim_{d\to 2^+} \mathfrak{S}[d-2; w(v)] = \log\left(\frac{1}{w(v)}\right). \tag{3.27}$$

The function $\mathfrak{B}(d)$, defined in Eq. (G.21), is positive and finite in $2 \leq d \leq 3$. Here we consider the low-energy limit at a fixed $d > 2$. If $w(v) \ll 1$, an assumption that needs to be checked later, we can use Eq.(3.26) to solve Eq. (3.25) and obtain

$$c(v) = \left(\frac{4\beta_d^4 \mathfrak{B}(d)}{(3-d)(d-2)N_c N_f} \right)^{\frac{1}{d}} v^{\frac{1}{d}}. \tag{3.28}$$

This general expression reduces to $c(v)^3/v = 64\pi^2 \mathfrak{B}(3)\epsilon/N_c N_f$ near three dimensions, which matches the result from the ϵ expansion [148]. Finally we note that in any $2 < d < 3$, $v \ll c(v) \ll 1$, and thus the assumed hierarchy of velocities is satisfied if $v \ll 1$. This gives the first consistency check of the scaling ansatz.

C. *Low-energy fixed point*

We now execute the second step in our program and show that v flows to zero in the low-energy limit. The beta function for v is determined by the fermion self-energy, and the vertex correction determines the $\mathcal{O}[w(v)]$ correction to the scaling dimension of the collective mode. Because the Yukawa coupling remains marginal in any $2 \leq d \leq 3$ according to the interaction-driven scaling, the quantum corrections are logarithmically divergent in all $2 \leq d \leq 3$. This is in contrast to conventional perturbative approaches where logarithmic divergences arise only at the critical dimensions. Therefore, the theory needs to be regularized to tame these divergences and counterterms must be added to the minimal local action in Eq. (3.18) in order to make physical observables independent of the UV regulators. In Appendix B we describe thoroughly the regularization and RG scheme we use in the analysis of Eq. (3.18).

According to Eq. (3.22), the contribution that the diagram in Fig. 2.3(a) gives to the beta function of v is at most $\mathcal{O}[w(v)]\, v$. An explicit computation in Appendix G shows that the contribution is actually suppressed further by $c(v)$. As mentioned in Chapter 2, the reason for the additional suppression by $c(v)$ is that the external momentum can be directed to flow only through the boson propagator and thus, the self-energy depends on the external spatial momentum through $c(v)\vec{k}$. According to Eq. (3.22), higher order diagrams are suppressed by at least one more power of $w(v)$. Because for $d > 2$

$$w(v) \sim v^{(d-1)/d} \ll c(v) \sim v^{1/d}, \tag{3.29}$$

higher order diagrams remain strictly smaller than Fig. 2.3(a) despite its additional suppression by $c(v)$. This is in contrast to the findings of Chapter 2 where it was shown that in $d = 2$, the two-loop diagram in Fig. 2.3(c) becomes as important as the one-loop graph. In the following section we discuss this difference in detail. In the small v limit, Fig. 2.3(a) determines the beta function for v (See Appendix H for a derivation),

$$\beta_v \equiv \frac{\mathrm{d}v}{\mathrm{d}\log\mu} = \frac{4(N_c^2-1)}{\pi N_c N_f} \frac{(d-1)\zeta(d)}{d-2} v^2 \tag{3.30}$$

to the leading order in v in $2 < d < 3$, where

$$\zeta(d) = -\frac{\cos\left(\frac{\pi d}{2}\right)\Gamma\left(\frac{2d-3}{d-1}\right)\Gamma\left(\frac{1}{d-1}\right)\Gamma\left(\frac{d-1}{2}\right)}{2^{3-d}\pi^{3/2}\Gamma\left(\frac{d}{2}\right)} \tag{3.31}$$

is positive in $2 \leq d < 3$. The beta function indeed shows that if the bare value of v is small, v flows to zero at low energies in any $2 < d < 3$. This completes the proof that the theory flows to the fixed point described by the ansatz introduced in the previous section.

At the low-energy fixed point with $v = 0$, the dynamical critical exponent (z) and the corrections to the interaction-driven scaling dimensions of the fields (η_Ψ and η_Φ) in Table 3.2 are given by:

$$z = 1, \qquad \eta_\Psi = 0, \qquad \eta_\Phi = 0. \tag{3.32}$$

It is noted that $\eta_\Psi = \eta_\Phi = 0$ does not mean that the fixed point is the Gaussian fixed point because both η_Ψ and η_Φ denote the corrections to the interaction-driven scaling, which already includes the $\mathcal{O}(1)$ anomalous dimension for the collective mode compared to the noninteracting theory.

D. Green's Functions

Having identified the low-energy fixed-point of the theory in $2 < d < 3$ we proceed on characterizing the deviations of the critical exponents from their exact value at intermediate energy scales and the consequences these have on the physical observables of the theory.

Defining the logarithmic length scale $\ell \equiv \log(\Lambda/\mu)$, Eqs. (3.28) and (3.30) imply that $w(v)$ flows to zero as

$$w(\ell) = \frac{\pi^{\frac{d-1}{d}} N_c N_f (d-2)}{4[(d-1)\zeta(d)(N_c^2-1)]^{\frac{d-1}{d}}} \left[\frac{(3-d)}{\beta_d^4 \mathfrak{B}(d)}\right]^{\frac{1}{d}} \frac{1}{\ell^{\frac{d-1}{d}}} \tag{3.33}$$

for $\ell \gg \ell_0$ with

$$\ell_0 \equiv \frac{\pi^2}{4}\frac{1}{v_0}\frac{N_c N_f}{N_c^2-1}\mathfrak{S}\left(d-2; v_0^{\frac{d-1}{d}}\right)^{-1} \sim \frac{\pi^2}{4}\frac{(d-2)}{v_0}\frac{N_c N_f}{N_c^2-1}, \tag{3.34}$$

and $v_0 \ll 1$ denoting the bare value of v (See Appendix H for details). Here we have used the limiting form of $\mathfrak{S}\left[d-2; v_0^{(d-1)/d}\right]$ given in Eq. (3.26). Even though $w(\ell) = 0$ is a stable low-energy fixed point, $w(\ell)$ is nonzero at intermediate energy scales unless one starts with a fine tuned theory with a perfectly nested FS. This gives rise to corrections to the scaling form of physical observables. While critical exponents are well defined only at fixed points, it is useful to introduce "scale-dependent critical exponents" that determine the scaling forms of physical observables in the presence of a slowly running irrelevant coupling. The scale-dependent dynamical critical exponent and anomalous scaling dimension of the fields are given, to the leading order in $w(\ell)$, by

$$z(\ell) = 1 + \frac{(N_c^2-1)\zeta(d)}{N_c N_f} w(\ell), \tag{3.35}$$

$$\eta_\Psi(\ell) = -\frac{(N_c^2-1)(d-1)\zeta(d)}{2N_c N_f} w(\ell), \tag{3.36}$$

$$\eta_\Phi(\ell) = -\frac{\left[(d-2)N_c^2 - d + 1\right](d-1)\zeta(d)}{N_c N_f (d-2)} w(\ell). \tag{3.37}$$

Their derivation can be found in Appendix I. Had $w(\ell)$ flown to a nonzero value at the fixed point, the $\mathcal{O}[w(\ell)]$ corrections would have modified the critical exponents in Eq. (3.32). Since $w(\ell)$ flows to zero, the exponents predicted by the interaction-driven scaling are exact, and the corrections introduce only subleading scalings in the physical observables.

The scaling form of the fermion Green's function is given by Eq. (3.4) with

$$F_z(|\mathbf{K}|) = \exp\left\{(d-2)\mathfrak{F}_z(d)(N_c^2-1)^{\frac{1}{d}}\left[\log\left(\frac{\Lambda}{|\mathbf{K}|}\right)\right]^{\frac{1}{d}}\right\}, \tag{3.38}$$

$$F_\Psi(|\mathbf{K}|) = \sqrt{\log\left(\frac{\Lambda}{|\mathbf{K}|}\right)}, \tag{3.39}$$

where

$$\mathfrak{F}_z(d) = \frac{\pi d}{4(d-1)}\left[\frac{(3-d)(d-1)\zeta(d)}{\pi\beta_d^4\mathfrak{B}(d)}\right]^{\frac{1}{d}} \tag{3.40}$$

is a positive smooth function in $2 \leq d \leq 3$. It is noted that $F_z(|\mathbf{K}|)$ and $F_\Psi(|\mathbf{K}|)$ introduce corrections that are not strong enough to modify the exponents in the power-law behavior, yet $F_z(|\mathbf{K}|)$ is stronger than logarithmic corrections of marginal Fermi liquids [153, 154]. Similarly, the crossover function for the bosonic Green's function in Eq. (3.5) is given by

$$F_\Phi(|\mathbf{Q}|) = \exp\left\{\frac{\mathfrak{F}_\Phi(d)\left[d-(d-2)N_c^2\right]}{2(N_c^2-1)^{\frac{d-1}{d}}}\left[\log\left(\frac{\Lambda}{|\mathbf{Q}|}\right)\right]^{\frac{1}{d}}\right\}, \tag{3.41}$$

where

$$\mathfrak{F}_\Phi(d) = \frac{d\pi^{\frac{d-1}{d}}}{2}\left[\frac{(d-1)(3-d)\zeta(d)}{\beta_d^4\mathfrak{B}(d)}\right]^{\frac{1}{d}} \tag{3.42}$$

is a smooth and positive function in $2 \leq d \leq 3$. In Appendix I we provide the derivation of these results. Compared to the bare (and irrelevant) boson propagator, the physical propagator describing the low-energy dynamics of the AFM collective mode is highly damped and incoherent. We note that the deviation of the fermion Green's function from that of Fermi liquids as well as the incoherent nature of the AFM collective mode become stronger as the dimension approaches to $d = 2$. This is expected because the effect of interactions is stronger in lower dimensions.

3.3-(*c*) Region III: From $d > 2$ to $d = 2$

In this section, we discuss how the results obtained in $2 < d < 3$ are connected to the solution in $d = 2$ presented in Chapter 2. In here we also present a straightforward generalization of the latter results to the case in which N_c and N_f take arbitrary values. We emphasize that the results presented in this section do not rely on any of these parameters being large.

The first thing to notice is that the expression in Eq. (3.28), which is divergent in $d = 2$, is valid only for $d > 2$. This is because the $d \to 2^+$ limit and the $w(v) \to 0$ limit do not commute in Eq. (3.25). In order to access the physics in $d = 2$, we have to take the $d \to 2^+$

limit before the low-energy limit is taken. In $d = 2$, the $1/(d-2)$ divergence in Eq. (3.28) is replaced by $\log[1/w(v)]$, and the solution to Eq. (3.25) is given by

$$c(v) = \sqrt{\frac{1}{8N_cN_f} v \log\left(\frac{1}{v}\right)} \tag{3.43}$$

to the leading order in v. Notice that the hierarchy $v \ll c(v) \ll 1$ still holds if $v \ll 1$, and general diagrams still obey Eq. (3.22) up to emergent logarithmic corrections in v.

Another complication that arises in $d = 2$ is that the inequality in Eq. (3.29) no longer holds. As pointed out in Chapter 2, this means that the two-loop fermion self-energies shown in Figs. 2.3(c) and 2.3(d) can be as important as the one-loop graph in Fig. 2.3(a) due to the suppression of the latter by a power of $c(v)$. However, Fig. 2.3(d) is also additionally suppressed by $c(v)$ and therefore only the diagram in Fig. 2.3(c) is of the same order as the one-loop fermion self-energy in $d = 2$. Taking into account the contributions from Fig. 2.3(a) and Fig. 2.3(c), we obtain the beta function for v in $d = 2$,

$$\beta_v = \frac{2}{\pi^2}\frac{(N_c^2-1)}{N_cN_f} v^2 \log\left(\frac{1}{v}\right). \tag{3.44}$$

It again predicts that v flows to zero in the low-energy limit if v is small to begin with. We note that, compared to the beta function in $d > 2$ given in Eq. (3.30), the apparent divergence in the $d \to 2^+$ is replaced by $\log(1/v)$.

In $d = 2$, the scale-dependent critical exponents are given by

$$z(\ell) = 1 + \frac{(N_c^2-1)}{2\pi N_cN_f} w(\ell), \tag{3.45}$$

$$\eta_\Psi(\ell) = -\frac{(N_c^2-1)}{4\pi N_cN_f} w(\ell), \tag{3.46}$$

$$\eta_\Phi(\ell) = \frac{1}{2\pi N_cN_f} w(\ell) \log\left(\frac{1}{w(\ell)}\right), \tag{3.47}$$

where $w(\ell)$ flows to zero as

$$w(\ell) = \frac{2\pi N_cN_f}{\sqrt{N_c^2-1}} \frac{1}{\sqrt{\ell}\log(\ell)} \tag{3.48}$$

for $\ell \gg \ell_0$ with

$$\ell_0 \equiv \lim_{d\to 2^+} \frac{\pi^2}{4}\frac{1}{v_0}\frac{N_cN_f}{N_c^2-1} \mathfrak{S}\left(d-2; v_0^{\frac{d-1}{d}}\right)^{-1} \sim \frac{\pi^2}{2}\frac{1}{v_0\log(1/v_0)}\frac{N_cN_f}{N_c^2-1}, \tag{3.49}$$

and $v_0 \ll 1$ denoting the bare value of v (See Appendix H for details). Here we have used the limiting form of $\mathfrak{S}\left[d-2; v_0^{(d-1)/d}\right]$ given in Eq. (3.27).

Comparing Eq. (3.48) with the $d \to 2^+$ limit of Eq. (3.33) shows that the flow of $w(\ell)$ in $d > 2$ does not smoothly extend to $d = 2$. This is due to the existence of the crossover energy scale $E_2(d)$ given in Eq. (3.9) and which vanishes in the $d \to 2^+$ limit. As the energy

scale is lowered, the crossover from region III to region II in Fig. 3.2 occurs at a scale such that

$$\lim_{w(v)\to 0} \mathfrak{S}[d-2; w(v)] = \frac{1}{d-2} \sim \lim_{d\to 2^+} \mathfrak{S}[d-2; w(v)] = \log\left(\frac{1}{w(v)}\right). \tag{3.50}$$

From Eq. (3.48), this crossover energy scale is given by Eq. (3.9):

$$E_2(d) \sim \Lambda \exp\left[-(d-2)^2 \frac{(N_c N_f)^2}{(N_c^2-1)} e^{\frac{2}{(d-2)}}\right]. \tag{3.51}$$

The double exponential dependence originates from the fact that $w(v)$ needs to be exponentially small in $-(d-2)^{-1}$ for the crossover to happen, and, up to sublogarithmic corrections, $w(v)^2$ itself flows to zero logarithmically in two dimensions. The sublogarithmic correction to the flow of $w(\ell)$ is responsible for the extra factor of $(d-2)^2$ in the exponential. For $\mu > E_2(d)$ (region III of Fig. 3.2), $w(\ell)$ flows to zero according to Eq. (3.48), while for $\mu < E_2(d)$ (region II of Fig. 3.2), the flow is dictated by Eq. (3.33). Thus, unless $d = 2$, the theory will always flow into region II at sufficiently low energies.

Finally, the corrections to the exponents predicted by the interaction-driven scaling go to zero in the long distance limit because $w(\ell)$ flows to zero. The Green's functions at intermediate energy scales receive superlogarithmic corrections given by the crossover functions,

$$F_\Psi(k_0) = \left[\log\left(\frac{\Lambda}{|k_0|}\right)\right]^{\frac{3}{8}}, \tag{3.52}$$

$$F_z(k_0) = \exp\left\{2\sqrt{N_c^2-1}\frac{\left[\log\left(\frac{\Lambda}{|k_0|}\right)\right]^{\frac{1}{2}}}{\log\left[\log\left(\frac{\Lambda}{|k_0|}\right)\right]}\right\}, \tag{3.53}$$

$$F_\Phi(k_0) = \exp\left\{\frac{2}{\sqrt{N_c^2-1}}\left[\log\left(\frac{\Lambda}{|k_0|}\right)\right]^{\frac{1}{2}}\right\}, \tag{3.54}$$

which reduce to Eqs. (2.18), (2.19) and (2.23), respectively for $N_c = 2$, $N_f = 1$ and for $-ik_0 \to \omega + i0^+$ with $\Lambda \gg \omega > 0$.

The crossover functions in $d = 2$ are different from the $d \to 2^+$ limit of the crossover functions obtained in $d > 2$ as seen from Table 3.1. This is due to the fact that the low-energy limit and the $d \to 2^+$ limit do not commute.

3.4 Summary and Discussion

In this chapter we have extracted the low-energy universal data for for the commensurate AFM quantum critical metal with a C_4-symmetric one-dimensional FS embedded in space dimensions between two and three. The exact critical exponents and the subleading corrections generated from the leading irrelevant perturbation are obtained by extending the nonperturbative approach based on an interaction-driven scaling introduced in Chapter 2 and motivated by the controlled ϵ expansion close to three dimensions [148]. The solution in $2 \leq d \leq 3$ provides an interpolation between the perturbative solution obtained through the

ϵ expansion near the upper critical dimension of the theory and the nonperturbative solution for the two-dimensional theory. Being an exactly solvable theory in dimensions between two and three, the EFT for the AFM quantum critical metal exposes both merits and subtle issues of RG schemes based on dimensional regularization. On the one hand, the critical exponents that characterize the low-energy fixed point are smooth functions of the space dimension. This allows one to make an educated guess on the critical exponents in two dimensions from the solution obtained in higher dimensions through a controlled ϵ expansion. On the other hand, the full scaling behaviors in two dimensions are not correctly captured by the low-energy solutions obtained above two dimensions. A crossover scale that vanishes in the $d \to 2^+$ limit makes it difficult to access the full scaling forms of physical observables in $d = 2$ from solutions obtained in the low-energy limit in $d > 2$. These crossovers give rise to emergent noncommutativities, where the low-energy limit and the limits in which physical dimensions are approached do not commute.

4 | Momentum-Dependent Single-Electron Properties in the Antiferromagnetic Quantum Critical Metal: From hot to lukewarm to cold electrons

4.1 Introduction

In Chapters 2 and 3, we described the physics of spin fluctuations and electrons close to the hot spots within the framework of the hot spot theory for the AFM quantum critical metal. With four-fermion interactions ignored, the low-energy fixed point of the theory is characterized by the dynamical critical exponent $z = 1$ and an emergent nesting of the FS near the hot spots. Once short-ranged interactions amongst electrons are taken into account, the fixed point may be unstable at low energies. In the presence of instabilities driven by quartic fermion couplings, the RG flow will be cut off at a finite length scale before the system flows all the way down to the low-energy fixed point characterized by the $z = 1$ dynamical critical exponent.

Therefore, it is crucial to include four-fermion interactions that can potentially drive superconducting instabilities in order to understand the ultimate fate of the system. Since superconductivity involves electrons across the FS, it is necessary to include low-energy electronic excitations away from the hot spots, whose description goes beyond the hot spot theory. Although electrons away from the hot spots are not strongly coupled with the spin fluctuations at low energies, they may still play an important role in electronic instabilities. In understanding the role of electrons away from the hot spots, it is important to keep track of the momentum-dependent character of the electrons along the FS because only electrons close to the hot spots remain strongly coupled with the spin fluctuations at low energies.

In this chapter we generalize the hot spot theory introduced in Chapter 2 to a unified theory that incorporates all low-energy electronic degrees of freedom. We devise a functional RG scheme that keeps track of momentum-dependent properties of electrons across the FS. Although functional RG schemes for strongly correlated itinerant electrons [120, 138, 144, 194–211] are generally intractable due to the infinite amount of low-energy information that needs to be kept [180, 181, 212, 213], we identify a region in the space of coupling functions in which the functional RG is analytically tractable. In this limit, we focus mainly on the single-particle electronic properties of the AFM quantum critical metal and perform a preliminary analysis of its superconducting instabilities.

This chapter is organized as follows. In Sec. 4.2 we present a generalization of the hot spot theory that includes gapless electrons away from the hot spots whose properties are encoded in momentum-dependent coupling functions. In Sec. 4.3 we lay out the theoretical framework of our functional RG scheme. In Sec. 4.3-(a) we provide sufficient conditions

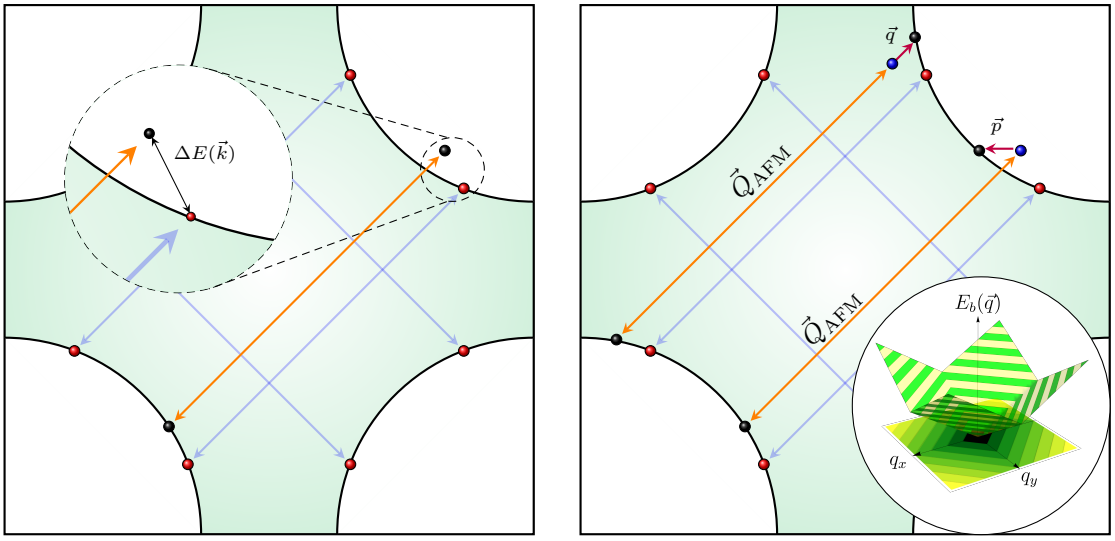

(a) (b)

Figure 4.1: (a) A zero-energy electron (black) away from the hot spots gets scattered by a zero-energy AFM spin fluctuation into a state with energy $\Delta E(\vec{k})$ where $\vec{k}$ is the momentum measured from the nearest hot spot. (b) Zero-energy electrons away from the hot spots are coupled to each other only through high-energy spin fluctuations. Zero-energy spin fluctuations scatter zero-energy electrons into higher-energy states. Inset: the energy dispersion of the collective mode $E_b(\vec{q})$ as a function of $\vec{q}$ relative to $\vec{Q}_{\rm AFM}$ according to Eq. (2.6).

for the theory with momentum-dependent couplings to be renormalizable. In Sec. 4.4 we identify the parameter region in which the RG analysis is under control. In Sec. 4.5 we address the superconducting instability of the system and provide an upper bound for the superconducting transition temperature. In Sec. 4.6, we show, within the energy window where our RG analysis is under control, that the theory is renormalizable through an explicit calculation. We extract the momentum dependent single-particle properties of the electrons across the FS. We end with some concluding remarks in Sec. 4.7.

4.2 Beyond the theory of hot spot electrons

The action in Eq. (2.3) describes the low-energy properties of critical spin fluctuations that interact strongly with electrons close to the hot spots on the FS. However, the electrons on the hot spots constitute only a small fraction of the full gapless electrons across the FS. At sufficiently low energies, electrons that lie away from the hot spots decouple from the spin fluctuations, and their low-energy properties are expected to be described by Landau's Fermi-Liquid Theory. As the hot spots are approached along the FS, the quasiparticle excitations gradually lose coherence as suggested by Eq. (2.21) which describes the spectral properties of the electrons right at the hot spots. Therefore, both non-Fermi-liquid-like and Fermi-liquid-like excitations coexist in the AFM quantum critical metal. The goal of this chapter is to understand the momentum-dependent properties of such excitations across the entire FS.

To achieve this goal, one has to understand how electrons are renormalized by the critical spin fluctuations as a function of the momentum along the FS. As it is shown in Fig. 4.1, an electron that resides far away from the hot spots on the FS decouples from the spin fluctuations below an energy scale that depends on the distance away from the closest hot spot. An electron that is closer to a hot spot remains coupled with the spin fluctuations up to a lower scale than that of an electron residing far away from the hot spot. This gives rise to a momentum-dependent lifetime for the electrons which gradually vanishes as the hot spots are approached.

In order to take into account the fact that universal properties of electrons depend on the momentum, we generalize the action in Eq. (2.3) by promoting the two components of the Fermi velocity and the Yukawa coupling to functions that depend on the momentum *along* the FS. The generalization of Eq. (2.3) reads:

$$\begin{aligned} S_{d=2} = & \sum_{N=1}^{8}\sum_{\sigma=1}^{N_c}\sum_{j=1}^{N_f}\int \mathrm{d}k\ \psi^{\dagger}_{N,\sigma,j}(k)\left\{ik_0 + V_{\mathrm{F}}^{(N)}(k_N)e_N[\vec{k};v_N(k_N)]\right\}\psi_{N,\sigma,j}(k) \\ & + \frac{1}{\sqrt{N}_f}\sum_{N=1}^{8}\sum_{\sigma\sigma'=1}^{N_c}\sum_{j=1}^{N_f}\int \mathrm{d}k\ \int \mathrm{d}k'\ g_N(k'_N,k_N)\psi^{\dagger}_{N,\sigma,j}(k')\Phi_{\sigma\sigma'}(k'-k)\psi_{\overline{N},\sigma',j}(k) \\ & + \frac{1}{4}\sum_{\{N_i=1\}}^{8}\sum_{\{\sigma_i=1\}}^{N_c}\sum_{\{j_i=1\}}^{N_f}\left[\prod_{i=1}^{4}\int \mathrm{d}k_i\right]\left\{\lambda^{j_1j_2j_3j_4}_{N_1N_2N_3N_4;\sigma_1\sigma_2\sigma_3\sigma_4}(k_{1;N_1},k_{2;N_2},k_{3;N_3},k_{4;N_4})\right. \\ & \left.\times\psi^{\dagger}_{N_1,\sigma_1,j_1}(k_1)\psi^{\dagger}_{N_2,\sigma_2,j_2}(k_2)\psi_{N_3,\sigma_3,j_3}(k_3)\psi_{N_4,\sigma_4,j_4}(k_4)(2\pi)^3\delta^{(3)}(k_1+k_2-k_3-k_4)\right\}. \end{aligned} \tag{4.1}$$

Here, k_N represents the momentum component that locally parametrizes the FS near hot spot N. These are chosen to be $k_N = k_x$ for $N = 1,4$, $k_N = -k_x$ for $N = 5,8$, $k_N = k_y$ for $N = 3,6$, and $k_N = -k_y$ for $N = 2,7$. With this choice, $k_N = k_{\overline{N}}$. Although k_N coincides with the momentum parallel to the FS only in the $v \to 0$ limit, there is a one-to-one correspondence between k_N and a point on the FS for any $v < \infty$. The momentum-dependent function $v_N(k_N)$ captures how the orientation of the FS changes as a function of momentum. At hot spot $N = 1$, the Fermi velocity is written as $V_{\mathrm{F}}^{(1)}(k_x)[\widehat{y} + v_1(k_x)\widehat{x}]$ in the coordinate system set by the ordering wave vector $\vec{Q}_{\mathrm{AFM}}$ [see Fig. 1.5(*a*)] and $e_1[\vec{k};v_1(k_x)] = V_{\mathrm{F}}^{(1)}(k_x)[v_1(k_x)k_x + k_y]$. The magnitude of the Fermi velocity is given by

$$\mathcal{V}_{\mathrm{F}}^{(1)}(k_x) = \left|V_{\mathrm{F}}^{(1)}(k_x)\right|\sqrt{1+v_1(k_x)^2}. \tag{4.2}$$

The expressions for the Fermi velocity at other hot spots follow from the C_4 symmetry of the FS. The momentum-dependent Yukawa coupling is denoted as $g_N(k'_N,k_N)$. $\lambda^{\{j_i\}}_{\{N_i\};\{\sigma_i\}}(\{k_{i;N_i}\}) \equiv \lambda^{j_1j_2j_3j_4}_{N_1N_2N_3N_4;\sigma_1\sigma_2\sigma_3\sigma_4}(k_{1;N_1},k_{2;N_2},k_{3;N_3},k_{4;N_4})$ denotes the short-ranged four-fermion interactions between electrons across the FS. The coefficient of the ik_0 term in the action is set to one by absorbing all momentum dependences into the fermion fields. The Hermiticity of the Hamiltonian and the Grasmann character of the fermionic fields enforces the following

conditions on the coupling functions:

$$\begin{aligned} g_N(k'_N,k_N) &= g_{\overline{N}}(k_N,k'_N)^*, \\ \lambda^{j_1j_2j_3j_4}_{N_1N_2N_3N_4;\sigma_1\sigma_2\sigma_3\sigma_4}(k_{1;N_1},k_{2;N_2},k_{3;N_3},k_{4;N_4}) &= \lambda^{j_4j_3j_2j_1}_{N_4N_3N_2N_1;\sigma_4\sigma_3\sigma_2\sigma_1}(k_{4;N_4},k_{3;N_3},k_{2;N_2},k_{1;N_1})^* \\ &= -\lambda^{j_2j_1j_3j_4}_{N_2N_1N_3N_4;\sigma_2\sigma_1\sigma_3\sigma_4}(k_{2;N_2},k_{1;N_1},k_{3;N_3},k_{4;N_4}) \\ &= -\lambda^{j_1j_2j_4j_3}_{N_1N_2N_4N_3;\sigma_1\sigma_2\sigma_4\sigma_3}(k_{1;N_1},k_{2;N_2},k_{4;N_4},k_{3;N_3}). \end{aligned} \tag{4.3}$$

As discussed in Sec. 1.1-(*b*) , the momentum-dependent four-fermion coupling functions in the forward scattering channel encode the Landau parameters as a function of the momentum along the FS. These also include non-forward scatterings which can lead to instabilities in the particle-hole and particle-particle channels. Henceforth, we will refer to $\{v_N(k_N)$, $g_N(k'_N,k_N)$, $V_{\rm F}^{(N)}(k_N)$, $\lambda^{\{j_i\}}_{\{N_i\};\{\sigma_i\}}(\{k_{i;N_i}\})\}$ as coupling functions collectively.

The coupling functions should transform covariantly under the action of the C_4 group. Let $J^{\{j_i\};n}_{\{N_i\};\{\sigma_i\}}(\{k_{i;N_i}\})$ denote any of the coupling functions where $i=1,\dots n$ labels different couplings. Under C_4 rotations and C_4 reflections, the coupling functions transform as

$$J^{\{j_i\};n}_{\{N_i\};\{\sigma_i\}}(\{k_{i;N_i}\}) \to \sum_{\{N'_j\}=1}^{8} \mathbf{R}_{N_1N'_1}\cdots\mathbf{R}_{N_nN'_n}\; J^{\{j_i\};n}_{\{N'_j\};\{\sigma_i\}}(\{k_{i;N'_j}\}), \tag{4.4}$$

where $\mathbf{R}$ is the 8-dimensional representation of the C_4 group defined in the space of hot spot indices. For example, for the $\pi/2$ rotation we have $\mathbf{R}^{\pi/2}_{NN'}=\delta_{N',[N+2]_8}$ where $1\le[x]_8\le 8$ gives the reminder on the division of x by 8. The action in Eq. (4.1) is also invariant under the particle-hole transformation,

$$\begin{aligned} \psi_{N,\sigma,j}(k) &\longrightarrow \mathcal{U}_{\sigma\sigma'}\psi^\dagger_{N,\sigma',j}(-k), \\ \psi^\dagger_{N,\sigma,j}(k) &\longrightarrow \psi_{N,\sigma',j}(-k)[\mathcal{U}^\dagger]_{\sigma'\sigma}, \\ \Phi(q) &\longrightarrow -\mathcal{U}\Phi(q)^{\rm T}\mathcal{U}^\dagger, \quad \mathcal{U}\in {\rm SU}(N_c), \end{aligned} \tag{4.5}$$

provided that the coupling functions satisfy the conditions $v_N(-k_N)=v_N(k_N)$, $V_{\rm F}^{(N)}(-k_N)=V_{\rm F}^{(N)}(k_N)$, $g_N(-k'_N,-k_N)=g^*_N(k'_N,k_N)$[1] and

$$\begin{aligned} &\lambda^{j_1j_2j_3j_4}_{N_1N_2N_3N_4;\sigma_1\sigma_2\sigma_3\sigma_4}(k_{1;N_1},k_{2;N_2},k_{3;N_3},k_{4;N_4}) = \\ &\sum_{\{\sigma'_i=1\}}^{N_c}\Big[\mathcal{U}^\dagger\Big]_{\sigma_4\sigma'_1}\Big[\mathcal{U}^\dagger\Big]_{\sigma_3\sigma'_2}\lambda^{j_4j_3j_2j_1}_{N_4N_3N_2N_1;\sigma'_1\sigma'_2\sigma'_3\sigma'_4}(-k_{4;N_4},-k_{3;N_3},-k_{2;N_2},-k_{1;N_1})\mathcal{U}_{\sigma'_3\sigma_2}\mathcal{U}_{\sigma'_4\sigma_1}. \end{aligned} \tag{4.6}$$

In the presence of the exact particle-hole symmetry, the position of the hot spots on the FS are protected from quantum corrections. For general momentum-dependent coupling functions, the particle-hole symmetry is not an exact symmetry, and the location of the hot

[1] The theory with $N_c=2$ is a special case where we can choose $\mathcal{U}=i\sigma^y$ such that $\Phi(q)$ is invariant under the particle-hole transformation. This special property is rooted in the fact that the fundamental and anti-fundamental representations of SU(2) are the same. Whether the field for the collective mode is invariant or not under the particle-hole symmetry in Eq. (4.5) is not important for us.

spots can be renormalized from the ones determined by the bare electronic dispersion. In what follows we assume that the action in Eq. (4.1) has the exact particle-hole symmetry. We further assume that the theory preserves the SU(N_c)× SU(N_f) global symmetry by requiring that the four-fermion couplings are covariant under these transformations:

$$\lambda^{j_1j_2j_3j_4}_{N_1N_2N_3N_4;\sigma_1\sigma_2\sigma_3\sigma_4}(k_{1;N_1},k_{2;N_2},k_{3;N_3},k_{4;N_4}) = \sum_{\{\sigma_i'=1\}}^{N_c}\left[\mathcal{U}^\dagger\right]_{\sigma_1\sigma_1'}\left[\mathcal{U}^\dagger\right]_{\sigma_2\sigma_2'}\lambda^{j_1j_2j_3j_4}_{N_1N_2N_3N_4;\sigma_1'\sigma_2'\sigma_3'\sigma_4'}(k_{1;N_1},k_{2;N_2},k_{3;N_3},k_{4;N_4})\mathcal{U}_{\sigma_3'\sigma_3}\mathcal{U}_{\sigma_4'\sigma_4}, \tag{4.7}$$

$$\lambda^{j_1j_2j_3j_4}_{N_1N_2N_3N_4;\sigma_1\sigma_2\sigma_3\sigma_4}(k_{1;N_1},k_{2;N_2},k_{3;N_3},k_{4;N_4}) = \sum_{\{j_i'=1\}}^{N_c}\left[\mathcal{V}^\dagger\right]_{j_1j_1'}\left[\mathcal{V}^\dagger\right]_{j_2j_2'}\lambda^{j_1'j_2'j_3'j_4'}_{N_1N_2N_3N_4;\sigma_1\sigma_2\sigma_3\sigma_4}(k_{1;N_1},k_{2;N_2},k_{3;N_3},k_{4;N_4})\mathcal{V}_{j_3'j_3}\mathcal{V}_{j_4'j_4}, \tag{4.8}$$

for $\mathcal{U}\in$ SU(N_c) and $\mathcal{V}\in$ SU(N_f). The four-fermion coupling functions can be decomposed into the spin symmetric and spin antisymmetric channels [56–58]:

$$\lambda^{\{j_i\}}_{\{N_i\};\{\sigma_i\}}(\{k_{i;N_i}\}) = \mathsf{A}^{\sigma_1\sigma_2}_{\sigma_3\sigma_4}\lambda^{\{j_i\};\mathsf{S}}_{\{N_i\}}(\{k_{i;N_i}\}) + \mathsf{S}^{\sigma_1\sigma_2}_{\sigma_3\sigma_4}\lambda^{\{j_i\};\mathsf{A}}_{\{N_i\}}(\{k_{i;N_i}\}), \tag{4.9}$$

where A and S are tensor encoding the spin channel symmetry and are defined as

$$\mathsf{A}^{\sigma_1\sigma_2}_{\sigma_3\sigma_4} = \delta_{\sigma_1\sigma_4}\delta_{\sigma_2\sigma_3} - \delta_{\sigma_1\sigma_3}\delta_{\sigma_2\sigma_4}, \tag{4.10}$$

$$\mathsf{S}^{\sigma_1\sigma_2}_{\sigma_3\sigma_4} = \delta_{\sigma_1\sigma_4}\delta_{\sigma_2\sigma_3} + \delta_{\sigma_1\sigma_3}\delta_{\sigma_2\sigma_4}. \tag{4.11}$$

These tensors satisfy the symmetry properties $\mathsf{A}^{\sigma_1\sigma_2}_{\sigma_3\sigma_4} = -\mathsf{A}^{\sigma_2\sigma_1}_{\sigma_3\sigma_4} = -\mathsf{A}^{\sigma_1\sigma_2}_{\sigma_4\sigma_3}$ and $\mathsf{S}^{\sigma_1\sigma_2}_{\sigma_3\sigma_4} = \mathsf{S}^{\sigma_2\sigma_1}_{\sigma_3\sigma_4} = \mathsf{S}^{\sigma_1\sigma_2}_{\sigma_4\sigma_3}$. From Eq (4.3), it follows that $\lambda^{\{j_i\};\mathsf{A}}_{\{N_i\}}(\{k_{i;N_i}\})\left[\lambda^{\{j_i\};\mathsf{S}}_{\{N_i\}}(\{k_{i;N_i}\})\right]$ is a fully antisymmetric (symmetric) function with respect to the simultaneous exchange of the first two or last two hot spot, flavor and momentum indices. Therefore, $\lambda^{\{j_i\};\mathsf{A}}_{\{N_i\}}(\{k_{i;N_i}\})\left[\lambda^{\{j_i\};\mathsf{S}}_{\{N_i\}}(\{k_{i;N_i}\})\right]$ corresponds to the coupling function in the spin symmetric (antisymmetric) and orbital momentum antisymmetric (symmetric) channels. We emphasize that the products of the form $\mathsf{A}^{\sigma_1\sigma_2}_{\sigma_3\sigma_4}\lambda^{\{j_i\};\mathsf{S}}_{\{N_i\}}(\{k_{i;N_i}\})$ and $\mathsf{A}^{\sigma_1\sigma_2}_{\sigma_3\sigma_4}\lambda^{\{j_i\};\mathsf{S}}_{\{N_i\}}(\{k_{i;N_i}\})$ are effectively antisymmetric functions under the exchange of the first two or last two set of indices as required by Eq. (4.3). For $N_c = 2$, the symmetric (antisymmetric) channel corresponds to the spin triplet (singlet) channel. The choice of hot spots indices in the four-fermion couplings are restricted by the momentum conservation because hot spots are located at different points in the momentum space. For example, the coupling function $\lambda^{\{j_i\}}_{1548;\{\sigma_i\}}(\{k_{i;N_i}\})$ is allowed by momentum conservation because the electron pair whose constituents reside on hot spots $(1,5)$ carries the same total momentum as the pair made up of electrons residing on hot spots $(4,8)$. On the other hand, the coupling function $\lambda^{\{j_i\}}_{1125;\{\sigma_i\}}(\{k_{i;N_i}\})$ is not allowed because the total momentum of the electron pair whose constituents lie on hot spots $(1,1)$ is different from that of a pair made up of electrons at hot spots $(2,5)$. In Fig. 4.2 we show all possible choices of the hot spot indices that are independent under the C_4 symmetry of the theory.

Given that the action in Eq. (4.1) is local, all coupling functions can be expanded in the

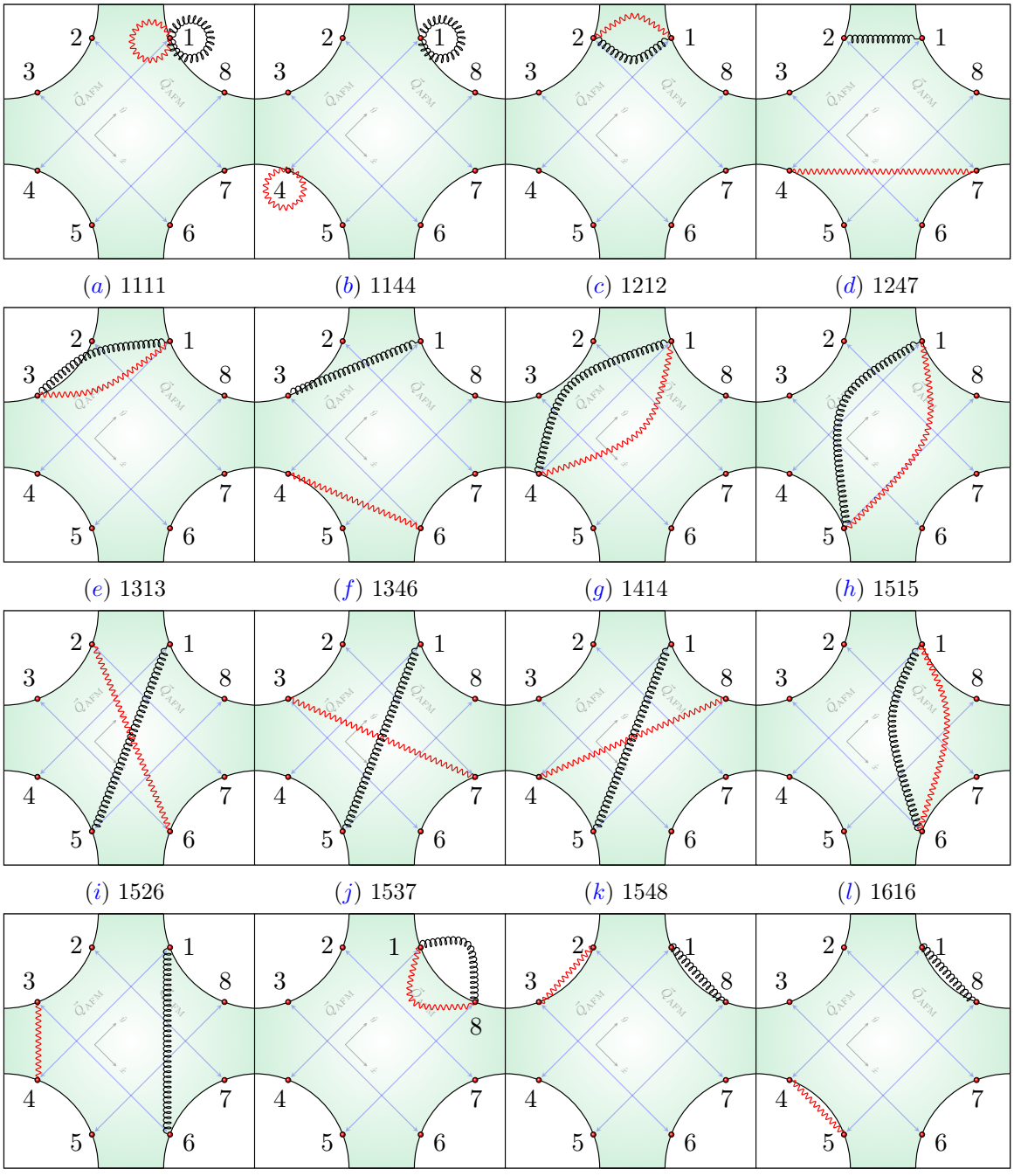

Figure 4.2: The sixteen independent choices for the hot spot indices in the four-fermion interaction that respect global momentum conservation. With the notation for the four-fermion coupling $\lambda^{\{j_i\}}_{N_1N_2N_3N_4;\{\sigma_i\}}(\{k_{i;N_i}\})$ we adopt the convention where the (red) wiggly solid line represents the incoming pair of electrons $\psi_{N_3,\sigma_3,j_4}(k_3)\psi_{N_4,\sigma_4,j_4}(k_4)$ and the (black) coil-like line represents the outgoing pair of electrons $\psi^\dagger_{N_1,\sigma_1,j_1}(k_1)\psi^\dagger_{N_2,\sigma_2,j_2}(k_2)$. In each panel we specify the choice of hot spot indices. All other allowed four-fermion interactions can be obtained through the C_4 symmetry of the theory (See Table Q.1 in Appendix Q).

Taylor series of momentum along the FS as

$$\begin{aligned} v_N(k_N) &= \sum_{n=0}^{\infty} \frac{v_N^n}{n!} k_N^n, \\ V_{\mathrm{F}}^{(N)}(k_N) &= \sum_{n=0}^{\infty} \frac{V_N^n}{n!} k_N^n, \\ g_N(k'_N, k_N) &= \sum_{m,n=0}^{\infty} \frac{g_N^{m,n}}{m!n!} k'^m_N k_N^n, \\ \lambda^{\{j_i\}}_{\{N_i\};\{\sigma_i\}}(\{k_{i;N_i}\}) &= \sum_{\{l_i\}=0}^{\infty} \frac{\lambda^{\{j_i\};\{l_i\}}_{\{N_i\};\{\sigma_i\}}}{l_1!l_2!l_3!l_4!} k_{1;N_1}^{l_1} k_{2;N_2}^{l_2} k_{3;N_3}^{l_3} k_{4;N_4}^{l_4}, \end{aligned} \tag{4.12}$$

where the zeroth order terms in these expansions are written as

$$v_N(0) = v, \quad V_{\mathrm{F}}^{(N)}(0) = 1, \quad g_N(0,0) = \sqrt{\frac{\pi v}{2}}, \quad \lambda^{\{j_i\}}_{\{N_i\};\{\sigma_i\}} \equiv \lambda^{\{j_i\}}_{\{N_i\};\{\sigma_i\}}(0,0,0,0). \tag{4.13}$$

The Fermi velocity is set to unity at the hot spots by a choice of momentum scale. Similarly, the the Yukawa coupling at $k_{N'} = k_N = 0$ is set to be related to the slope of the FS at the hot spots by choosing the normalization of the boson field.

Under the interaction-driven scaling in which frequency and momentum are scaled by a factor $\mathsf{b} > 1$, the coupling functions transform as

$$\begin{aligned} v'_N(k_N) &= v_N(\mathsf{b}^{-1} k_N), \\ V_{\mathrm{F}}^{(N)'}(k_N) &= V_{\mathrm{F}}^{(N)}(\mathsf{b}^{-1} k_N), \\ g'_N(k'_N, k_N) &= g_N(\mathsf{b}^{-1} k'_N, \mathsf{b}^{-1} k_N), \\ \lambda^{\{j_i\}}_{\{N_i\};\{\sigma_i\}}(\{k_{i;N_i}\}) &= \mathsf{b}^{-1} \lambda^{\{j_i\}}_{\{N_i\};\{\sigma_i\}}(\{\mathsf{b}^{-1} k_{i;N_i}\}). \end{aligned} \tag{4.14}$$

Although the momentum-dependent four-fermion coupling functions are irrelevant by power counting, we still keep the four-fermion interactions. This is because the effective couplings that control the perturbative expansion in the four-fermion couplings are given by a combination of the couplings themselves and a momentum scale that measures the density of states on the FS. In the case in which the four-fermion couplings are momentum independent, the effective couplings of the theory become $\widetilde{\lambda}^{\{j_i\}}_{\{N_i\};\{\sigma_i\}}(\{k_{i;N_i}\}) \sim k_{\mathrm{F}} \lambda^{\{j_i\}}_{\{N_i\};\{\sigma_i\}}(\{k_{i;N_i}\})$, where k_{F} denotes the size of the FS [see Sec. 1.1-(*b*)]. This effectively increases the scaling dimension of the couplings in channels that involve extended regions on the FS, such as the pairing channels. In the case where the couplings acquire momentum dependence, the effective couplings are given by an integration over the momentum along the FS,

$$\widetilde{\lambda}^{\{j_i\};(1)}_{\{N_i\};\{\sigma_i\}}(k_{3;N_3}, k_{4;N_4}) \equiv \int_{\mathrm{FS}} \mathrm{d}q \lambda^{\{j_i\}}_{\{N_i\};\{\sigma_i\}}(q, -q, k_{3;N_3}, k_{4;N_4}), \tag{4.15}$$

$$\widetilde{\lambda}^{\{j_i\};(2)}_{\{N_i\};\{\sigma_i\}}(k_{2;N_2}, k_{4;N_4}) \equiv \int_{\mathrm{FS}} \mathrm{d}q \lambda^{\{j_i\}}_{\{N_i\};\{\sigma_i\}}(q, k_{2;N_2}, q, k_{4;N_4}), \tag{4.16}$$

as it will be discussed later. Eq. (4.15) and (4.16) denote the effective couplings that control loop corrections associated with nested fermions in the particle-particle and particle-hole channels, respectively. It is understood that the the hot spot indices N_1 and N_2 (N_1 and N_3) in Eq. (4.15) [Eq. (4.16)] are such that the FS's are locally parametrized by the same component of momentum. Physically, the integration in Eq. (4.15) [Eq. (4.16)] is done over the relative momentum of the incoming particle-particle (particle-hole) pair. In the absence of momentum dependence this is precisely the integration that yields the $k_{\rm F}$ enhancement in the pairing channels. The symmetry properties of the momentum-dependent couplings allows us to obtain all other effective couplings of the theory. The interaction driven scaling fixes the the scaling dimensions of the coefficients in Eq. (4.12) to $[v_N^n] = [V_N^n] = -n$, $[g_N^{m,n}] = -(m+n)$ and $\left[\lambda^{\{j_i\};\{l_i\}}_{\{N_i\};\{\sigma_i\}}\right] = -(1+l_1+l_2+l_3+l_4)$. Therefore, allowing the general momentum dependence along the FS in the coupling functions amounts to introducing an infinite set of coupling constants from the point of view of the hot spot theory. While those higher order terms in the coupling functions are irrelevant to hot spot electrons, they are still part of the universal low-energy data that characterize the behavior of gapless electrons away from the hot spots. This rather unusual role of irrelevant couplings is due to the fact that the momentum along the FS not only acts as a scale but also as a label for the gapless electronic degrees of freedom.

4.2-(a) The Microscopic Theory: UV Scale Structure

Before we delve into a systematic analysis of Eq. (4.1), we describe its range of validity in the momentum space. For this we first identify the scales present in the theory. Besides the scales associated to the momentum-dependent couplings, the theory has multiple momentum scales. The first is the size of the FS, $k_{\rm F}$. It determines the size of the patch in the momentum space over which the FS can be regarded as a straight line. This is illustrated in Fig. 4.3(b). The second momentum scale is Λ_0 which sets the cutoff momentum in the direction perpendicular to the FS as shown in Fig. 4.3(a). Physically, this is the scale below which the energy of the electrons disperse linearly in the momentum perpendicular to the FS. The third momentum scale is Λ_b, below which the boson self-energy dominates over the bare kinetic term for the spin fluctuations. To understand the physical origin of Λ_b, we recall that the full dynamics of the collective mode is given by the propagator:

$$D(q)^{-1} = \frac{1}{\widetilde{\Lambda}}\left[q_0^2 + \mathsf{c}_0^2|\vec{q}|^2\right] + \Pi(q). \tag{4.17}$$

Here $\widetilde{\Lambda}$ is a scale associated with the bare kinetic term of the boson (see Sec. 2.2). $\Pi(q)$ is the self-energy of the boson generated from particle-hole excitations. It behaves as $\Pi(q) = |q_0| + c(v)(|q_x| + |q_y|)$ provided that $|q_x| \ll \Lambda_0$ and $|q_y| \ll \Lambda_0$. For $|q_x| > \Lambda_0$ and $|q_y| > \Lambda_0$, one has to take into account the nonlinear terms in the electronic dispersion in solving the Schwinger-Dyson equation in Eq. (2.5), and the self-energy that is linear in frequency and momentum no longer holds. Furthermore, we note that $D(q)^{-1} = |q_0| + c(v)(|q_x| + |q_y|)$ in Eq. (4.17) provided that $|q_x| \ll (c(v)/\mathsf{c}_0^2)\widetilde{\Lambda}$ and $|q_y| \ll (c(v)/\mathsf{c}_0^2)\widetilde{\Lambda}$. Therefore, it follows that the Schwinger-Dyson equation in Eq. (2.5) is solved by $D(q)^{-1} = |q_0| + c(v)(|q_x| + |q_y|)$ provided that, for $i = x, y$, $|q_i| \ll \min\left[(c(v)/\mathsf{c}_0^2)\widetilde{\Lambda}, \Lambda_0\right]$. With this at hand we identify the

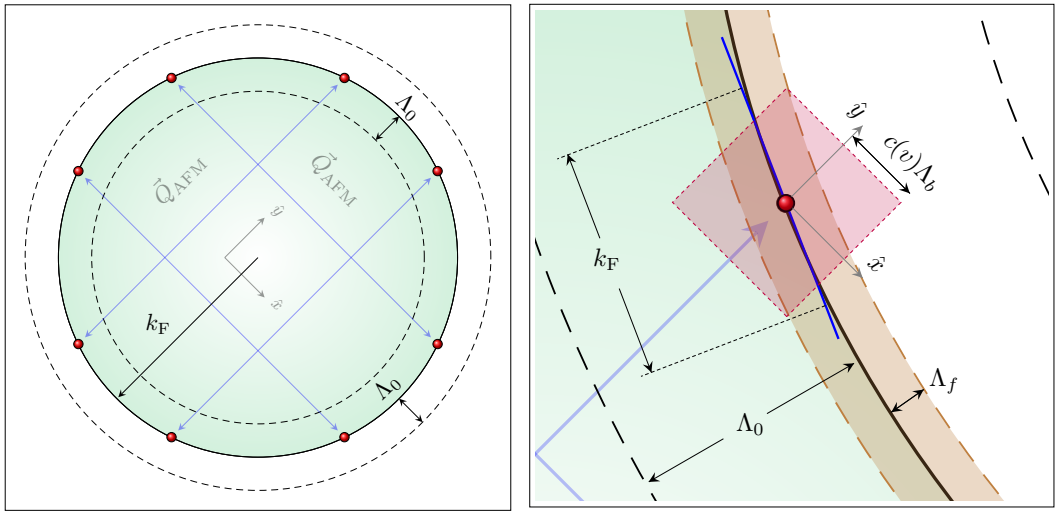

(a) (b)

Figure 4.3: UV Cutoff structure for the theory in Eq. (4.1). (a) The standard field-theoretic UV scale structure of an EFT with a FS viewed from the corners of the Brillouin zone in Fig. 1.5(a). (b) Energy UV cutoff structure for the low-energy EFT when zooming at hot spot $N = 1$ as described in the main text.

bosonic UV scale as

$$\Lambda_b \equiv \min\left[\frac{c(v)}{c_0^2}\widetilde{\Lambda}.\Lambda_0\right]. \tag{4.18}$$

While $k_{\rm F}$ is the largest momentum scale in the theory, it is *not* a UV scale. Instead it is part of the IR universal data because it encodes the number of gapless electronic modes. As a result, some physical observables are expected to depend on $k_{\rm F}$ in the low-energy limit [174, 175]. In contrast, Λ_0 is a genuine UV scale that cuts off the dispersion of high-energy electrons. As a consequence, the universal low-energy physics should be independent of this scale. With this observation, we define our EFT for electrons within an energy shell of width $\Lambda_f < \Lambda_0$ around the FS by integrating out electronic modes with energies $\Lambda_f < E < \Lambda_0$. Finally, Λ_b is the UV momentum cutoff for the boson. In the sense that $c(v)\Lambda_b$ determines the energy cutoff for the collective mode, it is similar to Λ_0. However, we will see that the low-energy physics is not completely decoupled from Λ_b, as it is the case for Λ_0 and Λ_f. The low-energy physics remains sensitive to Λ_b because it determines the phase space of low-energy states near the FS that an electron near a hot spot can scatter to due to its interaction with the spin fluctuations. In this regard, Λ_b also plays a role similar to $k_{\rm F}$.

In summary, our low-energy EFT comes with three momentum scales $k_{\rm F}$, Λ_f and Λ_b. While Λ_f is strictly a UV energy scale, $k_{\rm F}$ and Λ_b are a part of the universal data that characterize the low-energy physics. We consider a theory in which $\Lambda_f \ll c(v)\Lambda_b \ll k_{\rm F}$. We depict these three scales close to the $N = 1$ hot spot in Fig. 4.3(b).

4.3 Field-theoretic functional renormalization group

In this section we lay out the field theoretic functional RG scheme that is employed in this chapter, and discuss the issue of renormalizability of the theory with the momentum-dependent coupling functions. For other functional RG approaches to EFTs, see Refs. [120, 138, 144, 155, 180, 181, 194–213].

4.3-(a) Renormalizability of the theory

The momentum-dependent coupling functions in Eq. (4.1) include infinitely many irrelevant couplings by power counting. In relativistic quantum field theories, an inclusion of irrelevant couplings generates a proliferation of power-law UV divergences. In order to fix physical observables at a low-energy scale, one generally needs to tune infinitely many couplings in the UV by including counterterms to all operators allowed by symmetry. This is a consequence of including couplings that are irrelevant at low energies but become strong at high energies. In this case, it is hard to extract universal relations between low-energy observables without a full control over the strong coupling physics at high energies, and the theory has no predictive power. One usually bypasses this problem by choosing a specific UV theory amongst the ones that describe the same IR physics, i.e., a representative of the associated universality class. Within each university class, the renormalizable field theory, which includes only marginal and relevant couplings, is chosen. In renormalizable theories, one only fixes universal low-energy data that are insensitive to the UV physics by tuning relevant and marginal couplings that are already in the theory. All other low-energy observables are completely determined by the universal low-energy data. This is the power of renormalizable field theories, which can be tested against experiments at low energies. The renormalizability of the theory guarantees that one can make physical observables independent of UV scales in the limit in which these are large, by adding counterterms to the local operators that are already present in the theory.

In theories with a FS, the amount of universal low-energy data is infinite. This is because the FS supports an infinite number of gapless modes, and the low-energy data is encoded in the coupling functions that depend on the momentum along the FS. However, the goal of low-energy EFTs in this situation is still the same: *identifying the minimal set of low-energy data (finite or infinite), in terms of which all low-energy observables can be determined.* Theories with an infinite amount of low-energy data can still have predictive power if one can identify universal relations amongst a finite subset of low-energy observables that can be experimentally tested.

In the present theory, there are three large momentum scales, $k_{\rm F}$, Λ_b and Λ_f, not just one. In the limit in which these are large, quantum corrections can diverge in any of these scales. In identifying different types of divergences in the large momentum scales, it is useful to consider two types of quantum corrections separately. In the first type of diagrams, electrons in the loops are not nested. In this case, both components of the internal momenta are cut off by momentum scales that are proportional to Λ_f in the limit that $k_{\rm F} \gg c(v)\Lambda_b \gg \Lambda_f$ for a fixed $v \neq 0$. Figs. 4.4(a) and 4.4(b) illustrate the allowed range of momentum in a loop that describes an electron at hot spot N scattered into hot spot $N' \neq [N+4]_8$. Since the two patches of the FS are not parallel to each other, both components of the loop momenta should be bounded by the scale proportional to Λ_f in order for electrons to stay near the

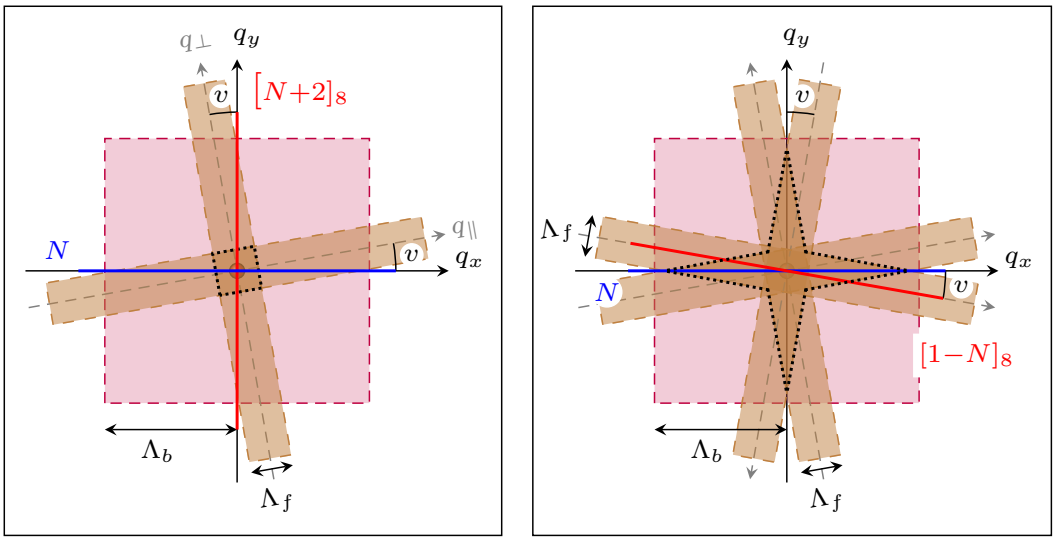

(a) (b)

Figure 4.4: The momentum space available for a low-energy spin fluctuation to scatter an electron at hot spot N to hot spot (a) $[N+2]_8$ whose FS is perpendicular to that of N, and (b) $[1-N]_8$ whose FS is becomes nested with that of N when $v=0$. The overlap between the effective momentum ranges set by the scales Λ_f and Λ_b determines the effective range of momenta for the collective mode (region bounded by dotted lines). In both cases the dashed axes correspond to the directions perpendicular and along the FS at each hot spot. In (a) the decomposition into momentum along ($q_\parallel$) and away ($q_\perp$) from the FS is done with respect to the hot spot N. In (b) we show both directions locally at each of the hot spots.

FS. As a result, quantum corrections of the first type do not depend on either $k_{\rm F}$, nor Λ_b. The second type of diagrams include electrons that are nested in the loops. For example, these include particle-particle and particle-hole diagrams for electrons that are located at antipodal points on the FS. In these nested diagrams, the components of the loop momenta along the FS are not cut off by Λ_f because electrons near nested parts of the FS can exchange a large momentum along the FS while staying close to the FS. The momentum along the FS is cutoff either by Λ_b or $k_{\rm F}$ depending on whether the relevant scattering process is mediated by the spin fluctuations or the short-ranged four-fermion interactions, respectively. The phase space for nested electrons whose scattering is mediated by spin fluctuations, is depicted in Fig. 4.5.

Naively one might require that divergences in all of those large momentum scales are removed by adding local counterterms in renormalizable theories. However, this is impossible. While dependences on Λ_f can be removed by adding local counterterms, one cannot make all low-energy physical observables independent of Λ_b and $k_{\rm F}$. This peculiar property follows from the fact that the momentum along the FS is a label for different gapless electronic degrees of freedom. As such, a momentum along the FS can be regarded as a continuous 'flavor'. In nested diagrams, for instance, $k_{\rm F}$ or Λ_b set the range of flavor an electron can have in virtual states. Therefore, these two scales must be a part of the universal low-energy

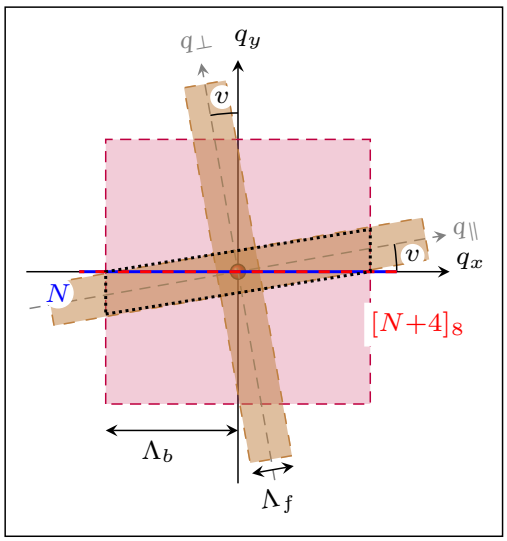

Figure 4.5: The momentum space available for a low-energy spin fluctuation to scatter an electron at hot spot N to hot spot $[N+4]_8$ whose FS is always nested with that of N. The overlap between the effective momentum ranges set by the scales Λ_f and Λ_b determines the effective range of momenta for the collective mode (region bounded by dotted lines). The dashed axes correspond to the directions perpendicular and along the FS at each hot spot. The same situation arises when considering electrons belonging to the same hot spot.

data. Specifically, k_{F} sets the total number of gapless electronic modes on the FS, and Λ_b determines the phase space of gapless states an electron on the FS can scatter into by emitting or absorbing a spin fluctuation. Since Λ_f is the only genuine high-energy scale, the renormalizability of the theory boils down to the question of whether one can remove the Λ_f dependence in physical observables by adding local counterterms to the action. Physical observables can still depend on Λ_b and k_{F} as these are part of the low-energy data of the theory. We have already encountered an example of this in Sec. 2.4, where the specific heat depends on these two scales.

The amount of data that can be specified on the FS, while being infinite, is still much smaller than the full information a microscopic theory carries. This is because the low-energy effective theory only keeps track of the information on gapless degrees of freedom on the FS. If the theory is renormalizable, all low-energy observables can be expressed in terms of data specified on the FS. At a first glance, the theory in Eq. (4.1) seems unrenormalizable because it includes infinitely many irrelevant couplings by power counting. If one computes quantum corrections as a power series in v_N^n, V_N^n, $g_N^{m,n}$ and $\lambda^{\{j_i\};\{l_i\}}_{\{N_i\};\{\sigma_i\}}$ in Eq. (4.12), one generally encounters increasingly stronger power-law UV divergences at higher orders in the expansion. If one is forced to introduce coupling functions that depend on momentum perpendicular to the FS to remove divergences in Λ_f, one eventually needs infinitely many counterterms beyond the coupling functions defined along the FS to cure such divergences. A proliferation of counterterms with unbounded degrees of divergence in Λ_f would spoil renormalizability. However, the presence of power-law UV divergences in the Taylor expansion of the coupling functions does not necessarily mean that the theory is not renormalizable. Instead, this can merely be a failure of the Taylor expansion of the coupling functions in Eq. (4.12). If the full momentum dependences of the coupling functions are included, it is possible that the UV divergences can be removed by *local* counterterms that are

already in Eq. (4.1). A simple example that illustrates this is the integral $\int_0^{\Lambda_f/\mu} \mathrm{d}k \, \frac{\cos^2 k}{\sqrt{k^2+1}}$, where k represents momentum along the FS. If one computes this order by order using the Taylor expansion $\cos^2 k = 1 - k^2 + \frac{k^4}{3} - ...$, one encounters increasingly stronger power-law divergences in $\Lambda_f/\mu \gg 1$ at higher orders in the expansion. However, the full expression is only logarithmically divergent in Λ_f/μ. This example reveals that the degree of divergence of a given quantum correction does not increase even if the couplings of the theory become momentum dependent, provided these are integrable in an appropriate sense. A theory can be renormalizable if full momentum dependences of the coupling functions are included. Even tough it is not renormalizable order by order in the expansion in the momentum along the FS.

Now we spell out the sufficient conditions for the theory defined by Eq. (4.1) to be renormalizable *perturbatively*. The first set of conditions is that, for all momentum, hot spot, spin and flavor indices,

$$g_N(k'_N, k_N) \leq 1, \tag{4.19}$$

$$V_{\mathrm{F}}^{(N)}(k_N) \geq 1, \tag{4.20}$$

$$\left|\widetilde{\lambda}^{\{j_i\}}_{\{N_i\};\{\sigma_i\}}(\{k_{i;N_i}\})\right| \leq 1, \qquad n = 1, 2. \tag{4.21}$$

Eq. (4.19) implies that the Yukawa coupling is bounded from above everywhere on the FS. On the other hand, Eq. (4.20) implies that the Fermi velocity away from the hot spots remains greater than the Fermi velocity at the hot spots, which is set to one. Finally, the condition in Eq. (4.21) requires that the effective dimensionless four-fermion couplings defined in Eqs. (4.15) and (4.16) are bounded from above. In Appendix J, we show that Eqs. (4.19) to (4.21) guarantee that the degree of divergence of general Feynman diagrams in Λ_f does not increase compared to the same diagrams with momentum-independent coupling functions. In particular, those quantum corrections that have negative degrees of divergence remain UV finite in the limit that Λ_f is large in the presence of momentum-dependent coupling functions and to leading order in $\widetilde{\lambda}^{\{j_i\}}_{\{N_i\};\{\sigma_i\}}(\{k_{i;N_i}\})$. Therefore, the unified theory with momentum-dependent couplings for gapless excitations across the entire FS remains renormalizable as far as the hot spot theory is renormalizable, provided Eqs. (4.19) to (4.21) are satisfied. We have shown in Chapter 2 that the latter is the case at the two-loop order by an explicit computation. As we shall see in the remaining of this chapter, this is also the case for the theory that includes the momentum-dependent couplings. As we we will show by explicit computation, the theory is renormalizable to leading order in both v and $\widetilde{\lambda}^{\{j_i\}}_{\{N_i\};\{\sigma_i\}}(\{k_{i;N_i}\})$.

The above discussion suggests that divergences in the UV scale Λ_f can be removed from the electronic two-point function, the cubic vertex function and the electronic four-point vertex function by introducing local counterterms to the operators already present in Eq. (4.1),

$$S_{\mathrm{C.T}} = \sum_{N=1}^{8}\sum_{\sigma=1}^{N_c}\sum_{j=1}^{N_f}\int \mathrm{d}k \; \psi^\dagger_{N,\sigma,j}(k)\left\{ik_0 A_N^{(1)}(k_N) + A_N^{(3)}(k_N)V_{\mathrm{F}}^{(N)}(k_N)e_N\left[\vec{k}; \frac{A_N^{(2)}(k_N)}{A_N^{(3)}(k_N)}v_N(k_N)\right]\right\}\psi_{N,\sigma,j}(k)$$

$$+ \frac{1}{\sqrt{N_f}}\sum_{N=1}^{8}\sum_{\sigma\sigma'=1}^{N_c}\sum_{j=1}^{N_f}\int \mathrm{d}k' \int \mathrm{d}k \; A_N^{(4)}(k'_N, k_N)g_N(k'_N, k_N)\psi^\dagger_{N,\sigma,j}(k')\Phi_{\sigma\sigma'}(k'-k)\psi_{\overline{N},\sigma',j}(k)$$

$$+\frac{1}{4\mu}\sum_{\{N_i=1\}}^{8}\sum_{\{\sigma_i=1\}}^{N_c}\sum_{\{j_i=1\}}^{N_f}\left[\prod_{i=1}^{4}\int \mathrm{d}k_i\right]\Big\{A^{\{j_i\}}_{\{N_i\};\{\sigma_i\}}(\{k_{i;N_i}\})\lambda^{\{j_i\}}_{\{N_i\};\{\sigma_i\}}(\{k_{i;N_i}\}) \times\psi^{\dagger}_{N_1,\sigma_1,j_1}(k_1)\psi^{\dagger}_{N_2,\sigma_2,j_2}(k_2)\psi_{N_3,\sigma_3,j_3}(k_3)\psi_{N_4,\sigma_4,j_4}(k_4)(2\pi)^3\delta^{(3)}(k_1+k_2-k_3-k_4)\Big\}. \tag{4.22}$$

Here, $A^{(i)}_N(k_N)$ with $i=1,2,3$, $A^{(4)}_N(k'_N,k_N)$ and $A^{\{j_i\}}_{\{N_i\};\{\sigma_i\}}(\{k_{i;N_i}\})$ are momentum-dependent dimensionless functions which are functionals of the coupling functions of the theory. Since the four-fermion coupling functions are irrelevant under the interaction-driven scaling, we have introduced an inverse power of the running energy scale μ in front of the four-fermion interaction to make the coupling function dimensionless. Henceforth, we will use $\lambda^{\{j_i\}}_{\{N_i\};\{\sigma_i\}}(\{k_{i;N_i}\})$ to denote the dimensionless four-fermion coupling functions.

With the counterterms added to the action, one also needs to consider loop corrections generated by the momentum-dependent counterterms. In order for the theory to be renormalizable, those corrections should not have power-law divergences in Λ_f either. Therefore, the second condition that the theory should satisfy for renormalizability is that the counterterm functions do not grow faster than powers of a logarithm at large momentum. That is, we require that the lth order counterterm functions satisfy the condition

$$\begin{aligned}|A^{(i);(l)}_N(k_N)| &\lessapprox |\log(|k_N|)|^{\alpha_l}, \quad i=1,2,3,\\ |A^{(4);(l)}_N(k'_N,k_N)| &\lessapprox \left|\log[\max(|k'_N|,|k_N|)]\right|^{\alpha_l},\\ |A^{\{j_i\};(l)}_{\{N_i\};\{\sigma_i\}}(\{k_{i;N_i}\})| &\lessapprox |\log[\max(\{k_{i;N_i}\})]|^{\alpha_l},\end{aligned} \tag{4.23}$$

in the large momentum limit for given $\alpha_l>0$. By these conditions, we require that counterterms do not introduce a positive degree of divergence in the quantum corrections. Eq. (4.23) represents the condition that the quantum corrections themselves can not grow too fast at large momentum along the FS.

Later, we will show through an explicit computation that Eqs. (4.19) to (4.21) and Eq. (4.23) are satisfied in the present theory. Here, we give a physical argument why this is the case. First, electrons that are far away from the hot spots decouple from the spin fluctuations at sufficiently low energies, and therefore we expect the renormalized Yukawa coupling to become smaller far away from the hot spots. Second, the momentum-dependent Fermi velocity normalized with respect to the Fermi velocity at the hot spots is expected to grow at large momentum because the spin fluctuations renormalize the Fermi velocity at the hot spots to zero relative to the Fermi velocity far away from them. Third, four-fermion couplings acquire momentum dependences along the FS as well. If one starts with a theory in which the bare four-fermion couplings are tunned to zero at the scale Λ_f, the spin fluctuations generate four-fermion couplings at lower energies near the hot spots. Because the four-fermion couplings are nonzero only near the hot spots, there exists a window of energy scales within which the effective couplings in Eqs. (4.15) and (4.16) remain small. If the system becomes unstable against pairing at low energies, Eq. (4.21) can be violated as some four-fermion couplings become large at low energies. This signifies a breakdown of the perturbative expansion in the coupling, but not necessarily a breakdown of the renormalizability of the theory. For this reason, Eqs. (4.19) to (4.21) and Eq. (4.23) are *sufficient* conditions for the theory to be *perturbatively* renormalizable.

With Eqs. (4.19) to (4.21) and Eq. (4.23), the electronic two-point function, the three-point function and the electronic four-point function can be made independent of the UV cutoff Λ_f by including local counterterms with momentum-dependent coupling functions. We consider a subtraction scheme in which the physical observables satisfy the RG conditions

$$\frac{\partial}{\partial k_0}\Gamma_1^{(2,0)}(k)\Big|_{k=k^*} = i + \mathscr{F}_1(k_x;[v_N, g_N, V_{\rm F}^{(N)}, \lambda^{\{j_i\}}_{\{N_i\};\{\sigma_i\}}];\widehat{k}_{\rm F};\widehat{\Lambda}_b;\mu;\Lambda_f), \tag{4.24}$$

$$\Gamma_1^{(2,0)}(k)\Big|_{k=k^*} = i\mu + \mathscr{F}_2(k_x;[v_N, g_N, V_{\rm F}^{(N)}, \lambda^{\{j_i\}}_{\{N_i\};\{\sigma_i\}}];\widehat{k}_{\rm F};\widehat{\Lambda}_b;\mu;\Lambda_f), \tag{4.25}$$

$$\frac{\partial}{\partial k_y}\Gamma_1^{(2,0)}(k)\Big|_{k=k^*} = V_{\rm F}^{(1)}(k_x) + \mathscr{F}_3(k_x;[v_N, g_N, V_{\rm F}^{(N)}, \lambda^{\{j_i\}}_{\{N_i\};\{\sigma_i\}}];\widehat{k}_{\rm F};\widehat{\Lambda}_b;\mu;\Lambda_f), \tag{4.26}$$

$$\Gamma_1^{(2,1)}(k',k)\Big|_{k'=q,k=p^*} = \frac{g_1(q_x,p_x)}{\sqrt{N_f}} + \mathscr{F}_4(q_x,p_x;[v_N, g_N, V_{\rm F}^{(N)}, \lambda^{\{j_i\}}_{\{N_i\};\{\sigma_i\}}];\widehat{k}_{\rm F};\widehat{\Lambda}_b;\mu;\Lambda_f), \tag{4.27}$$

$$\Gamma^{(4,0);\{j_i\}}_{\{N_i\};\{\sigma_i\}}(\{k_i\})\Big|_{k_i=k_i^*} = \mu^{-1}\lambda^{j_1j_2j_3j_4}_{N_1N_2N_3N_4;\sigma_1\sigma_2\sigma_3\sigma_4}(k_{1;N_1},k_{2;N_2},k_{3;N_3},k_{4;N_4}). \tag{4.28}$$

Here, $\Gamma_N^{(2,0)}(k)$ denotes the two-point function of electrons near hot spot N and $\Gamma_N^{(2,1)}(k',k)$ denotes the cubic vertex function at hot spot N. Furthermore, $k^* = (\mu, k_x, -v_1(k_x)k_x)$ represents the frequency and momentum vector at which the renormalized two-point function for electrons close to hot spot $N = 1$ is defined through Eqs. (4.24) to (4.26). The momentum vector $(k_x, -v_1(k_x)k_x)$ lies on the renormalized FS, with $v_1(k_x)$ denoting the local orientation of the latter and the function $\mathscr{F}_2$ vanishes in the $\mu \to 0$ limit. In defining the renormalized cubic vertex function in Eq. (4.27), we use $q = (\mu, q_x, -v_1(q_x)q_x)$ and $p^* = (\mu, p_x, v_4(p_x)p_x)$. The latter represents the frequency and momentum vector on the renormalized FS for electrons near the $N = 4$ hot spot. In Eq. (4.28), $\Gamma^{(4,0);\{j_i\}}_{\{N_i\};\{\sigma_i\}}(\{k_i\})$ denotes the electronic four-point function and $k_1^* = (3\mu/2, \vec{k}^*_{1;N_1})$, $k_2^* = (-\mu/2, \vec{k}^*_{2;N_2})$, $k_3^* = (\mu/2, \vec{k}^*_{3;N_3})$ and $k_4^* = (\mu/2, \vec{k}^*_{4;N_4})$ denote the four frequency and momentum vectors at which the renormalization condition is imposed for the four-fermion coupling functions. For example, for $N_i = 1$, $\vec{k}^*_{N_i} = (k_x, -v_1(k_x)k_x)$ and similarly for all other choices of hot spots. Finally, $\widehat{k}_{\rm F} = \mu^{-1}k_{\rm F}$ and $\widehat{\Lambda}_b = \mu^{-1}\Lambda_b$ are the dimensionless IR scales of the theory. The two-point function and the vertex functions at other hot spots are related to $\Gamma_1^{(2,0)}(k)$ and $\Gamma_1^{(2,1)}(k',k)$ through the C_4 symmetry. The $\mathscr{F}_i$'s are functions that are finite in the $\Lambda_f/\mu \gg 1$ limit. Furthermore these vanish in the $g_N(k'_N, k_N) \to 0$ and $\lambda^{\{j_i\}}_{\{N_i\};\{\sigma_i\}}(\{k_{i;N_i}\}) \to 0$ limits. It is noted that $\lambda^{\{j_i\}}_{\{N_i\};\{\sigma_i\}}(\{k_{i;N_i}\})$ is defined to be the four-point vertex function itself without any finite part in Eq. (4.27). We choose this condition for convenience. Other renormalization conditions could have been employed as well.

Adding Eqs. (4.22) and (4.1) yields the renormalized action

$$S_{\rm Ren} = \sum_{N=1}^{8}\sum_{\sigma=1}^{N_c}\sum_{j=1}^{N_f}\int {\rm d}k_{\mathsf{B}}\ \psi^\dagger_{\mathsf{B};N,\sigma,j}(k_{\mathsf{B}})\left\{ik_0^{\mathsf{B}} + V^{(N)}_{\mathsf{B};\mathsf{F}}(k_N^{\mathsf{B}})e_N\left[\vec{k}^{\mathsf{B}};v_N^{\mathsf{B}}(k_N^{\mathsf{B}})\right]\right\}\psi_{\mathsf{B};N,\sigma,j}(k_{\mathsf{B}})$$

$$+\frac{1}{\sqrt{N_f}}\sum_{N=1}^{8}\sum_{\sigma\sigma'=1}^{N_c}\sum_{j=1}^{N_f}\int \mathrm{d}k'_{\mathsf{B}}\int \mathrm{d}k_{\mathsf{B}}\; g_N^{\mathsf{B}}(k'^{\mathsf{B}}_N,k_N^{\mathsf{B}})\psi^{\dagger}_{\mathsf{B};N,\sigma,j}(k'_{\mathsf{B}})\Phi^{\mathsf{B}}_{\sigma\sigma'}(k'_{\mathsf{B}}-k_{\mathsf{B}})\psi_{\mathsf{B};\overline{N},\sigma',j}(k_{\mathsf{B}})$$
$$+\frac{1}{4}\sum_{\{N_i=1\}}^{8}\sum_{\{\sigma_i=1\}}^{N_c}\sum_{\{j_i=1\}}^{N_f}\left[\prod_{i=1}^{4}\int \mathrm{d}k_i^{\mathsf{B}}\right]\Big\{{}^{\mathsf{B}}\lambda^{j_1j_2j_3j_4}_{N_1N_2N_3N_4;\sigma_1\sigma_2\sigma_3\sigma_4}(k^{\mathsf{B}}_{1;N_1},k^{\mathsf{B}}_{2;N_2},k^{\mathsf{B}}_{3;N_3},k^{\mathsf{B}}_{4;N_4}) \tag{4.29}$$
$$\times\psi^{\dagger}_{\mathsf{B};N_1,\sigma_1,j_1}(k_1^{\mathsf{B}})\psi^{\dagger}_{\mathsf{B};N_2,\sigma_2,j_2}(k_2^{\mathsf{B}})\psi_{\mathsf{B};N_3,\sigma_3,j_3}(k_3^{\mathsf{B}})\psi_{\mathsf{B};N_4,\sigma_4,j_4}(k_4^{\mathsf{B}})(2\pi)^3\delta^{(3)}(k_1^{\mathsf{B}}+k_2^{\mathsf{B}}-k_3^{\mathsf{B}}-k_4^{\mathsf{B}})\Big\},$$

where the subscript B stands for 'bare'. Eq. (4.13) determines the relations between the bare and renormalized quantities as

$$\begin{aligned}
&k_0^{\mathsf{B}}=Z_\tau k_0,\quad \vec{k}_{\mathsf{B}}=\vec{k},\quad v_N^{\mathsf{B}}(k_N^{\mathsf{B}})=\frac{Z_N^{(2)}(k_N)}{Z_N^{(3)}(k_N)}v_N(k_N),\quad \Phi^{\mathsf{B}}_{\sigma\sigma'}(q_{\mathsf{B}})=\sqrt{Z^{(\Phi)}}\Phi_{\sigma\sigma'}(q),\\
&V^{(N)}_{\mathsf{B};\mathrm{F}}(k_N^{\mathsf{B}})=Z_\tau\frac{Z_N^{(3)}(k_N)}{Z_N^{(1)}(k_N)}V^{(N)}_{\mathrm{F}}(k_N),\quad \psi_{\mathsf{B};N,\sigma,j}(k_{\mathsf{B}})=\sqrt{Z_N^{(\psi)}(k_N)}\psi_{N,\sigma,j}(k),\\
&g_N^{\mathsf{B}}(k'^{\mathsf{B}}_N,k_N^{\mathsf{B}})=\frac{Z_1}{Z_4}\sqrt{\frac{Z_2}{Z_3}}\frac{Z_N^{(4)}(k'_N,k_N)}{\sqrt{Z_{\overline{N}}^{(1)}(k_N)Z_N^{(1)}(k'_N)}}g_N(k'_N,k_N),
\end{aligned}\tag{4.30}$$
$${}^{\mathsf{B}}\lambda^{\{j_i\}}_{\{N_i\};\{\sigma_i\}}(\{k^{\mathsf{B}}_{i;N_i}\})=\mu^{-1}Z_\tau^{-3}\left[\prod_{i=1}^{4}Z_{N_i}^{(\psi)}(k_{i;N_i})\right]^{-\frac{1}{2}}Z^{\{j_i\}}_{\{N_i\};\{\sigma_i\}}(\{k_{i;N_i}\})\lambda^{\{j_i\}}_{\{N_i\};\{\sigma_i\}}(\{k_{i;N_i}\}).$$

Here, $Z_N^{(i)}(k_N)\equiv 1+A_N^{(i)}(k_N)$ with $i=1,2,3$, $Z_N^{(4)}(k'_N,k_N)\equiv 1+A_N^{(4)}(k'_N,k_N)$ and $Z^{\{j_i\}}_{\{N_i\};\{\sigma_i\}}(\{k_{i;N_i}\})\equiv 1+A^{\{j_i\}}_{\{N_i\};\{\sigma_i\}}(\{k_{i;N_i}\})$ are momentum-dependent scaling factors. Moreover, $Z_\tau\equiv Z_1/Z_3$ is the momentum-independent scaling factor for the frequency with $Z_i\equiv Z_N^{(i)}(0)$. For the obvious reason, frequency is rescaled independently of the spatial momentum to keep energy conservation manifest under scaling. Finally, $Z_N^{(\psi)}(k_N)\equiv Z_N^{(1)}(k_N)/Z_\tau^2$ and $Z^{(\Phi)}\equiv Z_4^2Z_3/Z_1^2Z_2$ are the field renormalizations, where $Z_4\equiv Z_N^{(4)}(0,0)$. The field renormalization of the electron depends on momentum because gapless electronic modes are labeled by the momentum along the FS, and quantum corrections depend on this momentum. On the contrary, the bosonic field is rescaled in a momentum-independent way because the only gapless point for the collective mode is $\vec{q}=\vec{0}$. It is noted that these expressions reduce to those for the hot spot theory discussed in Chapters 2 and 3 in the absence of momentum dependence in the coupling functions (see Appendix B for comparison). The main goal of this chapter is to determine the single-particle low-energy features of electrons as a function of the momentum along the FS. Therefore, we focus on the RG equation governing the scaling properties of the electronic two-point vertex function. For completeness, we provide details regarding the RG equation governing the scaling properties of general vertex functions of the theory in Appendix K.

4.3-(*b*) The functional renormalization group equation

Under the interaction-driven scaling, the electronic two-point vertex function has engineering scaling dimension $\left[\Gamma_N^{(2,0)}\left(k;\left[v_M,g_M,V_{\mathrm{F}}^{(M)},\lambda^{\{j_i\}}_{\{M_i\};\{\sigma_i\}}\right];\widehat{k}_{\mathrm{F}};\widehat{\Lambda}_b;\mu\right)\right]=1$. According to Eq.

(4.30), the bare vertex function is related to the renormalized one through the multiplicative relation,

$$\Gamma^{(2,0)}_{\mathsf{B};N}\left(k_{\mathsf{B}};k^{\mathsf{B}}_{\mathrm{F}};\Lambda^{\mathsf{B}}_b;\Lambda_f\right)=\frac{Z^{(\psi)}_N(k_N)}{Z_\tau}\Gamma^{(2,0)}_N\left(k;\widehat{k}_{\mathrm{F}};\widehat{\Lambda}_b;\mu\right), \tag{4.31}$$

where, for simplicity, we use the simplified notation for the renormalized two-point function $\Gamma^{(2,0)}_N\left(k;\widehat{k}_{\mathrm{F}};\widehat{\Lambda}_b;\mu\right)\equiv\Gamma^{(2,0)}_N\left(k;\left[v_M,g_M,V^{(M)}_{\mathrm{F}};\lambda^{\{j_i\}}_{\{M_i\};\{\sigma_i\}}\right];\widehat{k}_{\mathrm{F}};\widehat{\Lambda}_b;\mu\right)$, and similarly for the bare one. Here, $k^{\mathsf{B}}_{\mathrm{F}}=\mu\widehat{k}_{\mathrm{F}}$ and $\Lambda^{\mathsf{B}}_b=\mu\widehat{\Lambda}_b$. As shown in Appendix K, the electronic two-point function satisfies the RG equation,

$$\begin{aligned}
&\Bigg\{(2\widetilde{\eta}^{(\psi)}_N(k_N)-z)+zk_0\frac{\partial}{\partial k_0}+\vec{k}\cdot\frac{\partial}{\partial\vec{k}}-\beta_{\widehat{k}_{\mathrm{F}}}\frac{\partial}{\partial\widehat{k}_{\mathrm{F}}}-\beta_{\widehat{\Lambda}_b}\frac{\partial}{\partial\widehat{\Lambda}_b}\\
&-\sum_{M_1=1}^{8}\int\mathrm{d}x_1\left(\left[x_1\frac{\partial v_{M_1}(x_1)}{\partial x_1}+\beta^{(v)}_{M_1}(x_1)\right]\frac{\delta}{\delta v_{M_1}(x)}+\left[x_1\frac{\partial V^{(M_1)}_{\mathrm{F}}}{\partial x_1}+\beta^{(V_{\mathrm{F}})}_{M_1}(x_1)\right]\frac{\delta}{\delta V^{(M_1)}_{\mathrm{F}}(x)}\right.\\
&+\int\mathrm{d}x_2\left[\left\{x_1\frac{\partial g_{M_1}(x_1,x_2)}{\partial x_1}+x_2\frac{\partial g_{M_1}(x_1,x_2)}{\partial x_2}+\beta^{(g)}_{M_1}(x_1,x_2)\right\}\frac{\delta}{\delta g_{M_1}(x_1,x_2)}\right.\\
&+\sum_{M_2,M_3,M_4=1}^{8}\sum_{\{\sigma_i=1\}}^{N_c}\sum_{\{j_i=1\}}^{N_f}\int\mathrm{d}x_3\int\mathrm{d}x_4\left\{\beta^{(\lambda);\{j_i\}}_{\{M_i\};\{\sigma_i\}}(\{x_i\})\right.\\
&\left.\left.\left.+\sum_{\{x_i=1\}}^{4}x_i\frac{\partial\lambda^{\{j_i\}}_{\{M_i\};\{\sigma_i\}}(\{x_i\})}{\partial x_i}\right\}\frac{\delta}{\delta\lambda^{\{j_i\}}_{\{N_i\};\{\sigma_i\}}(\{x_i\})}\right]\right)\Bigg\}\Gamma^{(2,0)}_N\left(k;\widehat{k}_{\mathrm{F}};\widehat{\Lambda}_b;\mu\right)=0,
\end{aligned} \tag{4.32}$$

for *any* fixed μ. Here, $\delta/\delta\mathsf{A}$ denotes a functional derivative with respect to A, with A denoting the momentum-dependent coupling functions. The integrations over x_i are done over the momenta along the FS in the patch that includes hot spot M_i with $i=1,2,3,4$. Since the bare theory is defined at the scale Λ_f, we set $\mu=\Lambda_f$ in Eq. (4.32). The dynamical critical exponent, the anomalous scaling dimension of the fermionic field, the beta functions of the coupling functions, and the beta functions of $\widehat{k}_{\mathrm{F}}$ and $\widehat{\Lambda}_b$ are defined by

$$\begin{aligned}
&z=1+\left.\frac{\mathrm{d}\log Z_\tau}{\mathrm{d}\log\mu}\right|_{\mu=\Lambda_f},\quad \widetilde{\eta}^{(\psi)}_N(k_N)=\frac{1}{2}\left.\frac{\mathrm{d}\log Z^{(1)}_N(k_N)}{\mathrm{d}\log\mu}\right|_{\mu=\Lambda_f},\\
&\beta^{(v)}_L(x)=\left.\frac{\mathrm{d}v_L(x)}{\mathrm{d}\log\mu}\right|_{\mu=\Lambda_f},\quad \beta^{(V_{\mathrm{F}})}_L(x)=\left.\frac{\mathrm{d}V^{(L)}_{\mathrm{F}}(x)}{\mathrm{d}\log\mu}\right|_{\mu=\Lambda_f},\\
&\beta^{(g)}_L(x_1,x_2)=\left.\frac{\mathrm{d}g_L(x_1,x_2)}{\mathrm{d}\log\mu}\right|_{\mu=\Lambda_f},\quad \beta^{(\lambda);\{j_i\}}_{\{L_i\};\{\sigma_i\}}(\{x_i\})=\left.\frac{\mathrm{d}\lambda^{\{j_i\}}_{\{L_i\};\{\sigma_i\}}(\{x_i\})}{\mathrm{d}\log\mu}\right|_{\mu=\Lambda_f},\\
&\beta_{\widehat{k}_{\mathrm{F}}}=\left.\frac{\mathrm{d}\widehat{k}_{\mathrm{F}}}{\mathrm{d}\log\mu}\right|_{\mu=\Lambda_f},\quad \beta_{\widehat{\Lambda}_b}=\left.\frac{\mathrm{d}\widehat{\Lambda}_b}{\mathrm{d}\log\mu}\right|_{\mu=\Lambda_f},
\end{aligned} \tag{4.33}$$

respectively. The beta functions describe the flow of the momentum-dependent coupling functions with increasing energy scale μ at a fixed momentum. Here, it becomes manifest

that the momentum along the FS plays a dual role [177]. On the one hand, it labels the gapless modes on the FS. The momentum-dependent coupling functions encode how quantum corrections vary along the FS. On the other hand, this momentum acts as a scale. This is manifest in the fact that the momentum along the FS should be rescaled in order to have scale invariance in Eq. (4.32). Unlike Landau's Fermi-liquid theory, the momentum along the FS cannot be viewed purely as a dimensionless flavor [6, 54, 56–58, 214] because of the non-forward scatterings mediated by the spin fluctuations. For this dual role of the momentum along the FS, $\widehat{k}_{\rm F}$ and $\widehat{\Lambda}_b$ are also treated as couplings that run under the RG flow. Physically, this means that the momentum scales $k_{\rm F}$ and Λ_b grow relative to an energy scale μ which is taken to zero in the low-energy limits.

In Appendix L we show that the solutions to Eq. (4.32) satisfy the scaling equation

$$\begin{aligned}\Gamma_N^{(2,0)}\left(k;\left[\mathsf{v}_M,\mathsf{g}_M,\mathsf{V}_{\rm F}^{(M)},\boldsymbol{\lambda}^{\{j_i\}}_{\{N_i\};\{\sigma_i\}}\right];\widehat{k}_{\rm F}^{(0)};\widehat{\Lambda}_b^{(0)}\right)&=\exp\left\{\int_0^l {\rm d}\ell\,\frac{[2\widetilde{\eta}_N^{(\psi)}(k_N(\ell);\ell)-z(\ell)]}{z(\ell)}\right\}\\&\times\Gamma_N^{(2,0)}\left(k_0(l),\vec{k}(l);\left[v_M(l),g_M(l),V_{\rm F}^{(M)}(l),\lambda^{\{j_i\}}_{\{N_i\};\{\sigma_i\}}(l)\right];\widehat{k}_{\rm F}(l);\widehat{\Lambda}_b(l)\right).\end{aligned}\tag{4.34}$$

Here, l is the logarithmic length scale. The scale-dependent coupling functions and energy scales are determined by solving the set of functional differential equations:

$$\frac{\partial v_M(k_M;l)}{\partial l}=-\frac{1}{z(l)}\left[\beta_M^{(v)}(k_M;l)+k_M\frac{\partial v_M(k_M;l)}{\partial k_M}\right],\tag{4.35}$$

$$\frac{\partial V_{\rm F}^{(M)}(k_M;l)}{\partial l}=-\frac{1}{z(l)}\left[\beta_M^{(V_{\rm F})}(k_M;l)+k_M\frac{\partial V_{\rm F}^{(M)}(k_M;l)}{\partial k_M}\right],\tag{4.36}$$

$$\frac{\partial g_M(k'_M,k_M;l)}{\partial l}=-\frac{1}{z(l)}\left[\beta_M^{(g)}(k'_M,k_M;l)+k'_M\frac{\partial g_M(k'_M,k_M;l)}{\partial k'_M}+k_M\frac{\partial g_M(k'_M,k_M;l)}{\partial k_M}\right],\tag{4.37}$$

$$\frac{\partial \lambda^{\{j_i\}}_{\{N_i\};\{\sigma_i\}}(\{k_{i;N_i}\};l)}{\partial l}=-\frac{1}{z(l)}\left[\beta^{(\lambda);\{j_i\}}_{\{N_i\};\{\sigma_i\}}(\{k_{i;N_i}\};l)+\sum_{j=1}^{4}k_{j;N_j}\frac{\partial \lambda^{\{j_i\}}_{\{N_i\};\{\sigma_i\}}(\{k_{i;N_i}\};l)}{\partial k_{j;N_j}}\right],\tag{4.38}$$

$$\frac{\partial\widehat{k}_{\rm F}(l)}{\partial l}=-\frac{1}{z(l)}\beta_{\widehat{k}_{\rm F}}=\frac{1}{z(l)}\widehat{k}_{\rm F}(l),\tag{4.39}$$

$$\frac{\partial\widehat{\Lambda}_b(l)}{\partial l}=-\frac{1}{z(l)}\beta_{\widehat{\Lambda}_b}=\frac{1}{z(l)}\widehat{\Lambda}_b(l),\tag{4.40}$$

with the initial conditions, $v_M(k_M;0)=\mathsf{v}_M(k_M)$, $V_{\rm F}^{(M)}(k_M;0)=\mathsf{V}_{\rm F}^{(M)}(k_M)$, $g_M(k'_M,k_M;0)=\mathsf{g}_M(k'_M,k_M)$, $\boldsymbol{\lambda}^{\{j_i\}}_{\{j_i\};\{\sigma_i\}}(\{k_{i;N_i}\})=\lambda^{\{j_i\}}_{\{N_i\};\{\sigma_i\}}(\{k_{i;N_i}\};0)$, $\widehat{k}_{\rm F}^{(0)}=\widehat{k}_{\rm F}(0)$ and $\widehat{\Lambda}_b^{(0)}=\widehat{\Lambda}_b(0)$. On the right-hand side of Eq. (4.34), the scale-dependent frequency and momentum are given by

$$k_0(l)\equiv e^l k_0,\qquad\&\qquad\vec{k}(l)\equiv e^{\int_0^l\frac{{\rm d}\ell}{z(\ell)}}\vec{k}.\tag{4.41}$$

The effect of the momentum dilations in Eqs. (4.35) to (4.37) can be singled out by writing

the coupling functions as

$$v_N(k_N;l) = \widehat{v}_N\left(e^{-\int_0^l \frac{\mathrm{d}\ell}{z(\ell)}} k_N; l\right), \tag{4.42}$$

$$V_{\mathrm{F}}^{(N)}(k_N;l) = \widehat{V}_{\mathrm{F}}^{(N)}\left(e^{-\int_0^l \frac{\mathrm{d}\ell}{z(\ell)}} k_N; l\right), \tag{4.43}$$

$$g_N(k'_N,k_N;l) = \widehat{g}_N\left(e^{-\int_0^l \frac{\mathrm{d}\ell}{z(\ell)}} k'_N, e^{-\int_0^l \frac{\mathrm{d}\ell}{z(\ell)}} k_N; l\right), \tag{4.44}$$

$$\lambda^{\{j_i\}}_{\{N_i\};\{\sigma_i\}}(\{k_{i;N_i}\};l) = \widehat{\lambda}^{\{j_i\}}_{\{N_i\};\{\sigma_i\}}\left(\left\{e^{-\int_0^\ell \frac{\mathrm{d}\ell}{z(\ell)}} k_{i;N_i}\right\}; l\right), \tag{4.45}$$

where $\widehat{v}_N(k_N;l)$, $\widehat{V}_{\mathrm{F}}^{(N)}(k_N;l)$, $\widehat{g}_N(k'_N,k_N;l)$ and $\widehat{\lambda}^{\{j_i\}}_{\{N_i\};\{\sigma_i\}}(\{k_{i;N_i}\};l)$ satisfy

$$\frac{\partial}{\partial l}\widehat{v}_N(k_N;l) = -\frac{1}{z(l)}\frac{\partial \widehat{v}_N(k_N;l)}{\partial \log \mu}\bigg|_{\mu=\Lambda_f}, \tag{4.46}$$

$$\frac{\partial}{\partial l}\widehat{V}_{\mathrm{F}}^{(N)}(k_N;l) = -\frac{1}{z(l)}\frac{\partial \widehat{V}_{\mathrm{F}}^{(N)}(k_N;l)}{\partial \log \mu}\bigg|_{\mu=\Lambda_f}, \tag{4.47}$$

$$\frac{\partial}{\partial l}\widehat{g}_N(k'_N,k_N;l) = -\frac{1}{z(l)}\frac{\partial \widehat{g}_N(k'_N,k_N;l)}{\partial \log \mu}\bigg|_{\mu=\Lambda_f}, \tag{4.48}$$

$$\frac{\partial}{\partial l}\widehat{\lambda}^{\{j_i\}}_{\{N_i\};\{\sigma_i\}}(\{k_{i;N_i}\};l) = -\frac{1}{z(l)}\frac{\partial \widehat{\lambda}^{\{j_i\}}_{\{N_i\};\{\sigma_i\}}(\{k_{i;N_i}\};l)}{\partial \log \mu}\bigg|_{\mu=\Lambda_f}. \tag{4.49}$$

Eqs. (4.46) to (4.49) track the renormalization of the coupling functions with increasing logarithmic length scale l for a fixed physical momenta along the FS. In other words, these only track the renormalization as the energy is scaled without scaling the momenta along the FS.

4.4 The weak momentum dependence limit

Once the counterterm functions in Eq. (4.22) are determined according to the RG conditions in Eqs. (4.24) to (4.28), the scaling form of the momentum dependent electron two-point function is determined from Eq. (4.32). However, it is difficult to compute the quantum corrections in the presence of coupling functions with arbitrary momentum dependence. In order to achieve the control in our calculation, we consider the limit in which

$$v \ll 1, \tag{4.50}$$

$$\left|\widetilde{\lambda}^{\{j_i\};(n)}_{\{N_i\};\{\sigma_i\}}(\{k_{i;N_i}\})\right| \ll 1, \tag{4.51}$$

$$\left|\frac{\partial \log J^{\{j_i\};n}_{\{N_i\};\{\sigma_i\}}(\{k_{i;N_i}\})}{\partial \log k_{l;N_l}}\right| \ll 1, \tag{4.52}$$

where $J^{\{j_i\};n}_{\{N_i\};\{\sigma_i\}}(\{k_{i;N_i}\})$ with $i = 1 \dots n$, represents any of the coupling functions, $\{V_{\rm F}^{(N)}(k_N)$, $\mathsf{v}_N(k_N), g_N(k'_N, k_N), \lambda^{\{j_i\}}_{\{N_i\};\{\sigma_i\}}(\{k_{i;N_i}\})\}$, and we have used the notation defined in Eq. (4.13). Eq. (4.50) is the limit in which the nonperturbative solution is under control for the hot spot electrons and the critical spin fluctuations. Eq. (4.51) is the condition that the dimensionless four-fermion couplings are small. Eq. (4.52) is the condition that requires all coupling functions vary slowly in momentum along the FS. We refer to this limit as the weak momentum dependence limit (WMDL). If the system is unstable against superconductivity, Eq. (4.51) will be violated in the low-energy limit. Here we focus on an intermediate energy scale window in which Eqs. (4.50) to (4.52) are satisfied. We will show that (*i*) v flows to zero, and (*ii*) only weak momentum-dependent quantum corrections are generated for the coupling functions at low energies if one starts with a bare theory in which the coupling functions satisfy Eqs. (4.50) to (4.51). Physically, this is due to the fact that, in the WMDL, the FS is close to nesting at the hot spots, and low-energy electrons are dressed in a way that depends weakly on the momentum along the FS. Furthermore, we will show through an explicit calculation that, in this limit, the theory is renormalizable to the leading order in v and $\widetilde{\lambda}^{\{j_i\}}_{\{N_i\}\{\sigma_i\}}(\{k_{i;N_i}\})$. The WMDL provides a window in which the leading momentum dependence of the coupling functions can be understood in a controlled manner. The size of this window is determined by the scale below which a superconducting instability kicks in. Obviously, the superconducting transition temperature is not universal and it depends on the bare value of the four-fermion couplings.

To understand how the superconducting temperature is affected by the universal long-range four-fermion interaction mediated by the spin fluctuations, we consider a specific microscopic theory whose coupling functions at the scale $\mu = \Lambda_f$ are given by

$$\mathsf{v}_N(k_N) = v_0 \ll 1, \tag{4.53}$$

$$\mathsf{V}_{\rm F}^{(N)}(k_N) = 1, \tag{4.54}$$

$$\mathsf{g}_N(k'_N, k_N) = \sqrt{\frac{\pi}{2} v_0}, \tag{4.55}$$

$$\boldsymbol{\lambda}^{\{j_i\}}_{\{N_i\};\{\sigma_i\}}(\{k_{i;N_i}\}) = 0, \tag{4.56}$$

for all $N, k_N, k'_N, j_i, N_i, \sigma_i$ and $k_{i;N_i}$. This corresponds to a UV theory in which the four-fermion couplings are tuned to zero at the bare level. At low-energies, spin fluctuations generate four-fermion interactions which eventually drive the system into a superconducting state. This allows us to isolate the role of the spin fluctuations from the bare four-fermion couplings in driving the superconducting instability. In the small v_0 and $\widetilde{\lambda}^{\{j_i\},(n)}_{\{N_i\};\{\sigma_i\}}(\{k_{i;N_i}\})$ limits, quantum corrections can be computed order by order in these parameters. In the WMDL, the RG conditions given in Eqs. (4.24) to (4.28) boil down to

$$\begin{aligned}
\Gamma_1^{(2,0)}(k)\Big|_{k=\widetilde{k}} &= i + \mathscr{E}_1\left(k_x; v; \lambda^{\{j_i\}}_{\{N_i\};\{\sigma_i\}}; \widehat{k}_{\rm F}; \widehat{\Lambda}_b; \mu, \Lambda_f\right), \\
\Gamma_1^{(2,0)}(k)\Big|_{k=\widetilde{k}} &= i\mu + \mathscr{E}_2\left(k_x; v; \lambda^{\{j_i\}}_{\{N_i\};\{\sigma_i\}}; \widehat{k}_{\rm F}; \widehat{\Lambda}_b; \mu, \Lambda_f\right), \\
\frac{\partial}{\partial k_y}\Gamma_1^{(2,0)}(k)\Big|_{k=\widetilde{k}} &= 1 + \mathscr{E}_3\left(k_x; v; \lambda^{\{j_i\}}_{\{N_i\};\{\sigma_i\}}; \widehat{k}_{\rm F}; \widehat{\Lambda}_b; \mu, \Lambda_f\right),
\end{aligned} \tag{4.57}$$

$$\Gamma_1^{(2,1)}(k',k)\Big|_{k=\widetilde{q},k'=\widetilde{p}} = \sqrt{\frac{\pi v}{2}} + \mathscr{E}_4\left(k_x; v; \lambda^{\{j_i\}}_{\{N_i\};\{\sigma_i\}}; \widehat{k}_{\rm F}; \widehat{\Lambda}_b; \mu, \Lambda_f\right),$$
$$\Gamma^{(4,0);\{j_i\}}_{\{N_i\};\{\sigma_i\}}(\{k_i\})\Big|_{k_i=k_i^*} = \mu^{-1}\lambda^{j_1 j_2 j_3 j_4}_{N_1 N_2 N_3 N_4;\sigma_1\sigma_2\sigma_3\sigma_4},$$

where $\widetilde{k} = (\mu, k_x, -vk_x)$, $\widetilde{q} = (\mu, q_x, -vq_x)$ and $\widetilde{p} = (\mu, p_x, vp_x)$. The functions denoted by $\mathscr{E}_i$ are independent of Λ_f in the $\Lambda_f/\mu \gg 1$ limit. These functions vanish in the small v and $\lambda^{\{j_i\}}_{\{N_i\};\{\sigma_i\}}$ limits. These are obtained from the $v_0 \ll 1$ limit of the functions $\mathscr{F}_i$ appearing in Eqs. (4.24) to (4.28). To the leading order in $v_0 \ll 1$, the spatial components of the momenta $\vec{k}_i^*$ can be set to be on the FS with a momentum-independent slope.

In the WMDL, the electronic two-point function in Eq. (4.34) takes the form

$$\Gamma_N^{(2,0)}(k) = ik_0 F_z^{(N)}(k_N; k_0) + F_{V_{\rm F}}^{(N)}(k_N; k_0) e_N[\vec{k}; \widehat{v}_N(k_N; \ell_\omega)], \tag{4.58}$$

where

$$\widehat{v}_N(k_N;\ell_\omega) = v_0 e^{\int_0^{\ell_\omega} \frac{d\ell}{z(l)}\left[Z_N^{(2)}(k_N(\ell);\ell)' - Z_N^{(3)}(k_N(\ell);\ell)'\right]}, \tag{4.59}$$

$$F_z^{(N)}(k_N;k_0) = \exp\left(\int_0^{\ell_\omega} \frac{d\ell}{z(\ell)}[Z_N^{(1)}(k_N(\ell);\ell)']\right), \tag{4.60}$$

$$F_{V_{\rm F}}^{(N)}(k_N;k_0) = \exp\left(\int_0^{\ell_\omega} \frac{d\ell}{z(\ell)}[Z_N^{(3)}(k_N(\ell);\ell)']\right), \tag{4.61}$$

with $\ell_\omega \equiv \log(\Lambda_f/k_0)$ with $k_0 > 0$, $Z_N^{(i)}(k_N(\ell);\ell)' \equiv \frac{\partial}{\partial \log \mu} Z_N^{(i)}(k_N(\ell);\ell)\big|_{\mu=\Lambda_f}$, and $z(\ell)$ is the scale-dependent dynamical critical exponent given in Eq. (3.45). The functions $F_z^{(N)}(k_N;k_0)$ and $F_{V_{\rm F}}^{(N)}(k_N;k_0)$ describe the momentum-dependent field renormalization and Fermi velocity, respectively. Similarly, $\widehat{v}_N(k_N;\ell_\omega)$ describes the flow of the momentum-dependent shape of the FS with decreasing energy. These expressions fully determine the single-particle properties of low-energy electrons at arbitrary momentum along the FS. We note that all $z(\ell)$, $\widehat{v}_N(k_N;\ell_\omega)$, $F_z^{(N)}(k_N;k_0)$ and $F_{V_{\rm F}}^{(N)}(k_N;k_0)$ are, in general, functions of the four-fermion couplings. In the following, we will consider the case in which the four-fermion couplings are small so that their contribution to the electron two-point function can be ignored.

4.4-(*a*) Range of Validity: How far along the FS?

Here we discuss the range of momentum in which the description based on the WMDL is valid. The full propagator that includes the bare kinetic term of the spin fluctuations is given by Eq. (4.17). The singular part of the propagator that is dominant at low energies is generated by electrons near the hot spots. One can ignore the irrelevant quadratic kinetic term provided that $|q_j| < \Lambda_b$ for $j = x, y$. This translates to an energy scale $\mu \sim c(v)(|q_x| + |q_y|) \sim c(v)\Lambda_b$. Below this frequency, one can also ignore q_0^2 in the full propagator for $c(v) \ll 1$. In order for an electron on the FS at a distance k_N away from hot spot N to

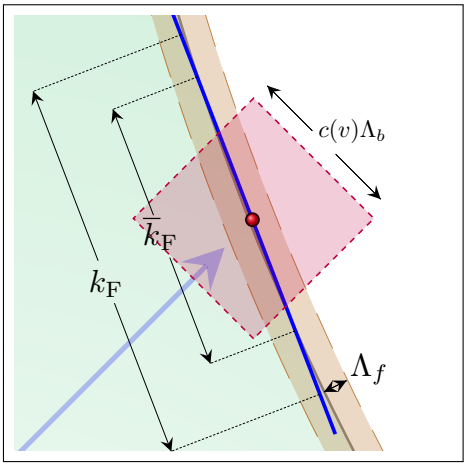

Figure 4.6: A closer look to Fig. 4.3(*b*) near hot spot $N = 1$. The region of the FS where electrons are described by the action in Eq. (4.1) corresponds $|k_x| < \overline{k}_{\rm F} \ll k_{\rm F}$, where $k_{\rm F}$ is the momentum scale above which the curvature of the FS becomes important.

scatter to a point on the FS near hot spot $\overline{N}$, the electron should emit or absorb a boson with momentum $|q_N| \sim v k_N$. Those scattering processes are governed by the universal boson dynamics in Eq. (2.6) as far as $v|k_N| < \Lambda_b$, with Λ_b given in Eq. (4.18). Similarly, scatterings of electrons with energy smaller than $\mu \sim c(v)\Lambda_b$ are described by Eq. (2.6). Therefore, scatterings of electrons within the range of momentum $|k_N| < \overline{k}_F$ with

$$\overline{k}_F \sim \frac{1}{v_0}\Lambda_b \tag{4.62}$$

in the direction parallel to the FS around each hot spot and with energy less than

$$\mu \sim c(v_0)\Lambda_b, \tag{4.63}$$

are described by the universal low-energy theory. Here Λ_b in Eq. (4.18) is evaluated at $v = v_0$. In the estimation of $\overline{k}_{\rm F}$ and μ we have ignored the flow of v because, as we will show, the renormalized FS deviates only slightly from the bare one away from the hot spots and it becomes nested only at the hot spots. We note that $\overline{k}_{\rm F} \ll k_{\rm F}$, where $k_{\rm F}$ is the size of the patch of the FS where it can be regarded as a straight line. In the small v_0 limit that we consider here, $\overline{k}_F \gg c(v_0)\Lambda_b$, and a region of the FS larger than the effective energy cutoff for the boson dynamics is described by the universal low-energy physics governed by Eq. (2.6). This is depicted in Fig. 4.6.

4.5 Superconducting Instability

Now, we discuss the RG flow of the four-fermion couplings in the limit that the latter are weak. In this section we specialize in the physical case with $N_c = 2$ and $N_f = 1$, where we suppress the flavor index and adopt the notation $\lambda^{\{\sigma_i\}}_{\{N_i\}}(\{k_{i;N_i}\}) \equiv \lambda^{\sigma_1\sigma_2\sigma_3\sigma_4}_{N_1N_2N_3N_4}(\{k_{i;N_i}\})$ for the dimensionless four-fermion coupling functions. The main purpose of this section is to provide a conservative estimate of the size of the energy window within which our calculation that ignores the four-fermion couplings remains under control prior to the onset of superconducting order. To perform the estimation, we first focus on the four-fermion couplings at the hot spots. As it will become evident in the remaining of this chapter, the momentum acquired by the coupling functions is directly tied to the flow of the zero momentum couplings in the WMDL.

Group 1	Group 2	Group 3	Group 4
$\lambda_{1515}^{\sigma_1\sigma_2\sigma_3\sigma_4}$	$\lambda_{1526}^{\sigma_1\sigma_2\sigma_3\sigma_4}$	$\lambda_{1111}^{\sigma_1\sigma_2\sigma_3\sigma_4}$	$\lambda_{1212}^{\sigma_1\sigma_2\sigma_3\sigma_4}$
$\lambda_{1818}^{\sigma_1\sigma_2\sigma_3\sigma_4}$	$\lambda_{1823}^{\sigma_1\sigma_2\sigma_3\sigma_4}$	$\lambda_{1144}^{\sigma_1\sigma_2\sigma_3\sigma_4}$	$\lambda_{1313}^{\sigma_1\sigma_2\sigma_3\sigma_4}$
$\lambda_{1845}^{\sigma_1\sigma_2\sigma_3\sigma_4}$	$\lambda_{1537}^{\sigma_1\sigma_2\sigma_3\sigma_4}$	$\lambda_{1414}^{\sigma_1\sigma_2\sigma_3\sigma_4}$	$\lambda_{1616}^{\sigma_1\sigma_2\sigma_3\sigma_4}$
$\lambda_{1548}^{\sigma_1\sigma_2\sigma_3\sigma_4}$			$\lambda_{1346}^{\sigma_1\sigma_2\sigma_3\sigma_4}$
			$\lambda_{1634}^{\sigma_1\sigma_2\sigma_3\sigma_4}$
			$\lambda_{1247}^{\sigma_1\sigma_2\sigma_3\sigma_4}$

Table 4.1: Closed sets of four-fermion couplings under the RG to linear order in $\lambda_{\{N_i\}}^{\{\sigma_i\}}$.

4.5-(a) Leading Order Beta Functions

We start by considering the beta function for the four-fermion couplings at the hot spots to linear order in $\lambda_{\{N_i\}}^{\{\sigma_i\}}$. The sixteen couplings in Fig. 4.2 can be divided into four groups as shown in Table 4.1. To linear order in the four-fermion couplings, the couplings in each group are closed under the RG flow. Amongst these groups, only the couplings in the first group are sourced by the spin fluctuations. Therefore, we focus on this group to the leading order in $\lambda_{\{N_i\}}^{\{\sigma_i\}}$. The diagrams in Fig. 4.7 contribute to the beta functions of the couplings in the first group. In the $\lambda_{\{N_i\}}^{\{\sigma_i\}} \ll 1$, $w(v) \ll 1$ and $\ell \gg 1$ limits, with ℓ denoting the logarithmic length scale, the beta functions for the four-fermion couplings at the hot spots are given by:

$$\frac{\mathrm{d}\lambda_{1515}^{\mathsf{S}}}{\mathrm{d}\ell} = -\lambda_{1515}^{\mathsf{S}} - \frac{3w(v)\ell}{8\pi}\lambda_{1845}^{\mathsf{A}} - \frac{3w(v)\ell}{8\pi}\lambda_{1548}^{\mathsf{S}} - \mathscr{J}_1\frac{v^2}{c(v)}, \tag{4.64}$$

$$\frac{\mathrm{d}\lambda_{1515}^{\mathsf{A}}}{\mathrm{d}\ell} = -\lambda_{1515}^{\mathsf{A}} - \frac{w(v)\ell}{8\pi}\lambda_{1845}^{\mathsf{S}} - \frac{w(v)\ell}{4\pi}\lambda_{1845}^{\mathsf{A}} + \frac{w(v)}{8\pi}\lambda_{1548}^{\mathsf{A}} - \frac{\mathscr{J}_1}{3}\frac{v^2}{c(v)}, \tag{4.65}$$

$$\frac{\mathrm{d}\lambda_{1548}^{\mathsf{S}}}{\mathrm{d}\ell} = -\lambda_{1548}^{\mathsf{S}} - \frac{w(v)\ell}{8\pi}\lambda_{1515}^{\mathsf{S}}, \tag{4.66}$$

$$\frac{\mathrm{d}\lambda_{1548}^{\mathsf{A}}}{\mathrm{d}\ell} = -\lambda_{1548}^{\mathsf{A}} + \frac{w(v)\ell}{8\pi}\lambda_{1515}^{\mathsf{A}}, \tag{4.67}$$

$$\frac{\mathrm{d}\lambda_{1845}^{\mathsf{S}}}{\mathrm{d}\ell} = -\lambda_{1845}^{\mathsf{S}} - \frac{3w(v)\ell}{8\pi}\lambda_{1515}^{\mathsf{A}}, \tag{4.68}$$

$$\frac{\mathrm{d}\lambda_{1845}^{\mathsf{A}}}{\mathrm{d}\ell} = -\lambda_{1845}^{\mathsf{A}} + \frac{w(v)}{8\pi}\lambda_{1515}^{\mathsf{S}} - \frac{w(v)}{4\pi}\lambda_{1515}^{\mathsf{A}}, \tag{4.69}$$

$$\frac{\mathrm{d}\lambda_{1818}^{\mathsf{S}}}{\mathrm{d}\ell} = -\lambda_{1818}^{\mathsf{S}} - \frac{3w(v)\ell}{16\pi}\lambda_{1515}^{\mathsf{A}} - \mathscr{J}_2\frac{v^2}{c(v)}, \tag{4.70}$$

$$\frac{\mathrm{d}\lambda_{1818}^{\mathsf{A}}}{\mathrm{d}\ell} = -\lambda_{1818}^{\mathsf{A}} + \frac{w(v)\ell}{8\pi}\lambda_{1515}^{\mathsf{A}} - \frac{w(v)\ell}{16\pi}\lambda_{1515}^{\mathsf{S}} - \frac{\mathscr{J}_2}{3}\frac{v^2}{c(v)}, \tag{4.71}$$

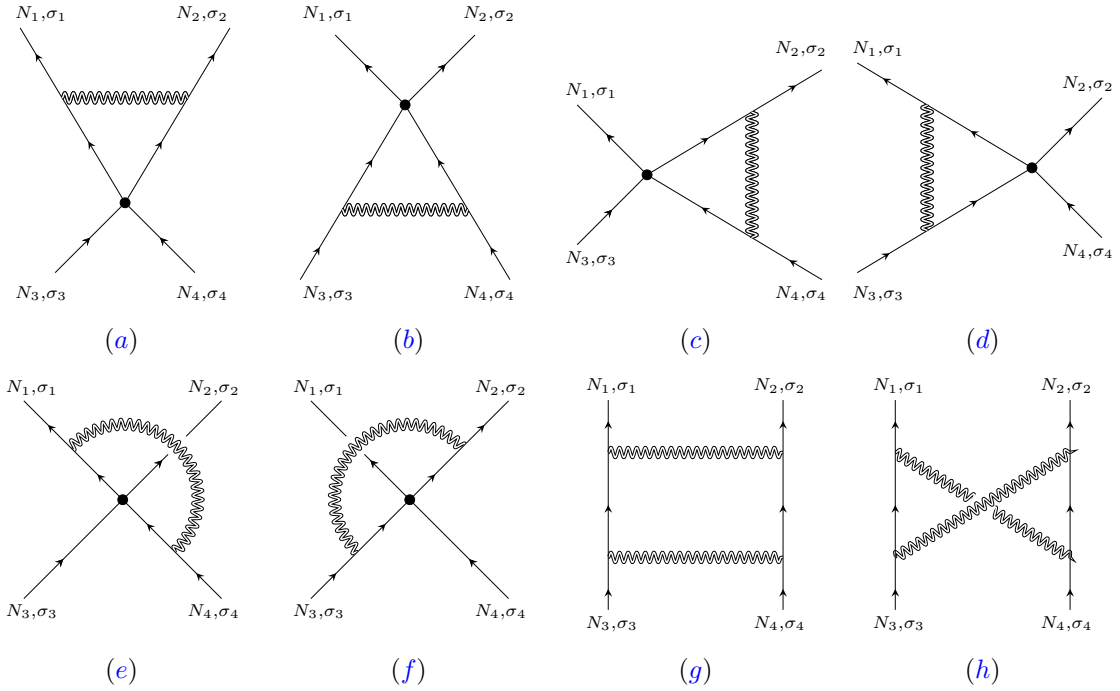

Figure 4.7: Contributions to the beta function of the four-fermion couplings to linear order in $\lambda^{\{\sigma_i\}}_{\{N_i\}}$. The black dot denotes the four-fermion interaction vertex.

where,

$$\mathscr{J}_1 = \frac{1}{8}\left[\pi^2 + \log(2)^2 + 2\mathrm{Li}_2\left(-\frac{1}{2}\right)\right], \tag{4.72}$$

$$\mathscr{J}_2 = \frac{1}{16}\left[\pi^2 + \log\left(\frac{27}{4}\right)\right], \tag{4.73}$$

with $\mathrm{Li}_2(x)$ denoting the dilogarithm function. Here, we have decomposed the couplings into the singlet (S) and triplet (A) spin channels as in Eq. (4.9). We recall that $\lambda^{\mathsf{S}}_{\{N_i\}}$ ($\lambda^{\mathsf{A}}_{\{N_i\}}$) is a symmetric (antisymmetric) function in the exchange of the first or last two hot spot indices. The derivations of these expressions are given in Appendices P and Q. In these expressions, we have kept only terms to leading order in $\ell \gg 1$. In Eqs. (4.64) to (4.71), the singlet and triplet spin channels are mixed because spin fluctuations scatter individual electrons, rather than pairs and different spin channels are mixed. For example, consider a quantum correction to the four-fermion interaction in the singlet channel. In the intermediate state, one of the two electrons of the pair with total momentum $S = 0$, can emit a spin fluctuation, which changes the total spin of the pair to $S = 1$. This generates the mixing between the singlet and triplet channels.

Let us consider the physical origin of each term in the beta functions. We focus on Eq. (4.64), which determines the flow of $\lambda^{\sigma_1\sigma_2\sigma_3\sigma_4}_{1515}$ in the singlet channel. Other channels can be understood in a similar manner. The first term on the right-hand side of Eq. (4.64) reflects the fact that the four-fermion coupling has scaling dimension $[\lambda^{\sigma_1\sigma_2\sigma_3\sigma_4}_{1515}] = -1$ under

the interaction driven scaling. The last term arises from the diagrams in Figs. 4.7(g) and 4.7(h). It represents the process where four-fermion interactions are generated by the high-energy spin fluctuations. This source term is present in channels that involve electrons near hot spots connected by the commensurate wave vector $\vec{Q}_{\rm AFM}$. The remaining terms correspond to the vertex corrections: the second term is from the particle-hole diagrams in Figs. 4.7(e) and 4.7(f), and the third term is from the particle-particle diagrams in Figs. 4.7(a) and 4.7(b). It is remarkable that the vertex corrections explicitly depend on the logarithmic length scale ℓ. This implies that the quartic vertex functions at an energy scale $\Lambda_f e^{-(\ell+{\rm d}\ell)}$ cannot be entirely expressed in terms of the vertex functions at the scale $\Lambda_f e^{-\ell}$ and the beta functions explicitly depend on the scale itself. This is due to the fact that the vertex functions depend on the scale, not only through the scale-dependent couplings, but also explicitly. In the vertex corrections that involve a pair of fermions in antipodal patches of the FS, the component of the loop momentum along the FS is cut off by a scale proportional to Λ_b, where Λ_b is the momentum cutoff for the spin fluctuations given in Eq. (4.18) [See discussion in Sec. 4.2-(a)]. While Λ_b is a UV cutoff for the collective mode, it sets the size of the phase space that can be reached by gapless electronic modes through the absorption or emission of spin fluctuations. As a result, the vertex corrections associated with antipodal patches diverge, not only in the energy cutoff of the electrons, but also in Λ_b. This can be understood as a 'UV/IR' mixing, where the IR physics remains sensitive to large momentum scales. As shown in Appendix Q, the UV/IR mixing gives rise to double logarithmic divergences in the four-point vertex functions evaluated at the hot spots:

$$\delta\Gamma^{(4,0);1{\rm L}}_{1515}(\mu) \sim w(v)\left[\log\left(\frac{c(v)\Lambda_b}{\mu}\right)-\frac{1}{2}\log\left(\frac{\Lambda_f}{\mu}\right)\right]\log\left(\frac{\Lambda_f}{\mu}\right), \tag{4.74}$$

in the $\Lambda_f/\mu \gg 1$ and $c(v)\Lambda_b/\mu \gg 1$ limits, with $\Lambda_f \ll c(v)\Lambda_b$, where μ is an external frequency of the quartic vertex. Usually, double logarithmic divergences ruin the renormalizability of the EFT as UV divergences cannot be removed by local counterterms. However, the present theory remains renormalizable. This is due to the fact that we only need to remove divergences in Λ_f, but not in Λ_b. Only Λ_f is a genuine UV scale associated with high-energy electronic modes. While Λ_b is a UV scale for the collective mode, it is an IR scale for eletronic degrees of freedom because it characterizes the volume of the phase space for gapless electrons that contribute to the vertex corrections. Therefore, Λ_b is part of the IR data which low-energy physical observables and beta functions depend on. The divergences in Λ_f can be removed by local counterterms that depend on $\log(c(v)\Lambda_b/\mu)$ and the beta function is proportional to $w(v)\log(c(v)\Lambda_b/\mu) \sim w(v)\log(c(v)\widehat{\Lambda}_b(\ell)) \sim w(v)\ell$. This can be viewed as a scale-dependent anomalous dimension. Interestingly, both the particle-particle diagrams in Figs. 4.7(a) and 4.7(b), and the particle-hole diagrams in Figs. 4.7(e) and 4.7(f) yield the logarithmic UV/IR mixing in the $k_{\rm F} \gg c(v)\Lambda_b$ limit. This is due to the fact that segments of the FS near the antipodal points on the FS can be regarded as being nested within a scale of order Λ_b in the $k_{\rm F} \gg c(v)\Lambda_b$ limit. This is in contrast to Landau's Fermi-liquid theory where the particle-hole channel yields a finite contribution due to the curvature of the FS (See Appendix Q). The unusual enhancement arising in the particle-hole channel also has significant effects on the forward-scattering channels. The study of this effect, however, lies beyond the scope of this thesis and it is left as the subject of future research. We note that the UV/IR mixing does not arise in quantum corrections that involve

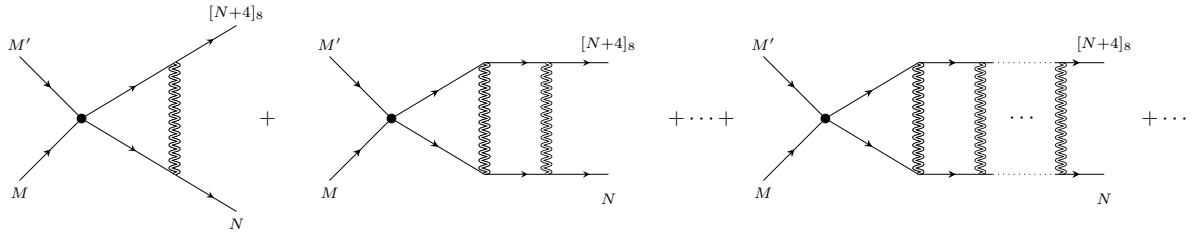

Figure 4.8: Infinite set of particle-particle ladder diagrams to linear order in the four-fermion coupling (solid dot) that involve the collective mode.

fermions that are not nested. Quantum corrections for the latter case are not enhanced by $\log(c(v)\Lambda_b)$ and are negligible compared to contributions from the nested channels.

In higher-loop diagrams that contribute to the anomalous dimension of the four-fermion coupling, the largest contributions to the four-fermion couplings are generated from a series of particle-particle and particle-hole ladder diagrams that involve nested electrons. Fig. 4.8 shows an example of a particle-particle ladder series. As shown in Appendix J, a L-loop nested ladder diagram scales, at most, as $w(v)^L \log(c(v)\Lambda_b)^L \log(\Lambda_f)^L$ in the $w(v) \ll 1$, $c(v)\Lambda_b \gg \Lambda_f \gg \mu$ limits. Here, $\log(c(v)\Lambda_b)$ measures the phase space of gapless electrons in each of the L internal loops. The factor $\log(\Lambda_f)^L$ corresponds to the usual higher-loop UV divergences. Locality of the field theory guarantees that the divergences in $\log(\Lambda_f)^n$ with $n > 1$ are canceled by diagrams that involve counterterms added at lower orders in the number of loops, and the remaining divergence in Λ_f can be removed by adding a local counterterm. The L-loop counterterms are therefore of order $w(v)^L \log(c(v)\Lambda_b)^L \log(\Lambda_f)$. This discussion implies that $w(v)\ell$ controls the perturbative series of the beta functions in Eqs. (4.64) to (4.71) to the linear order in the four-fermion couplings. Therefore, the leading order beta functions are under control provided that

$$\ell < \ell_{\text{con.}} \equiv \frac{1}{w(v_0)}. \tag{4.75}$$

We recall that $w(\ell) = w[v(\ell)]$ depends in the scale as

$$w(\ell) = \frac{4\pi}{\sqrt{3}} \frac{1}{\sqrt{\ell + \ell_0}\log(\ell + \ell_0)}, \tag{4.76}$$

where ℓ_0 is the length scale below which the flow of $w(v)$ becomes important [See Eq. (3.49)]. In terms of the bare value of v, ℓ_0 is is given by

$$\ell_0 = \frac{\pi^2}{3} \frac{1}{v_0 \log(1/v_0)}. \tag{4.77}$$

In the small v_0 limit, $\ell_0 \gg w(v_0)^{-1}$ and therefore, the flow of $w(v)$ can be ignored within the energy scale in which the perturbative series for the beta functions of the four-fermion couplings is under control.

Now, we examine the RG flow of the four-fermion couplings. The precise nature of the RG flow depends on the microscopic details which are encoded in their initial conditions. If a large attractive four-fermion interaction is turned on, the system will develop a

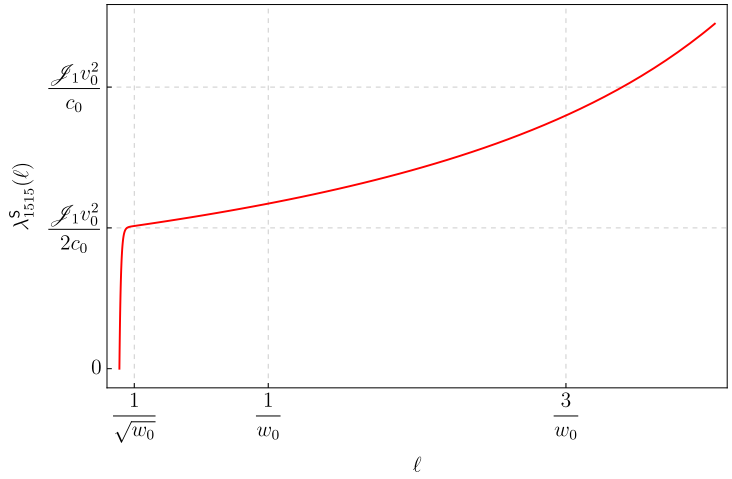

Figure 4.9: The four-fermion coupling $\lambda^{\mathsf{S}}_{1515}(\ell)$.

superconducting instability at relatively high energies before the theory flows into the universal scaling regime. On the other hand, one can tune the four-fermion couplings to reduce the superconducting transition temperature. However, one cannot ignore the four-fermion couplings even if one chooses a microscopic Hamiltonian with vanishing bare four-fermion couplings. This is because the gapless spin fluctuations generate four-fermion interactions at low energies. Here, our goal is to understand the role of the spin fluctuations in the flow of the four-fermion couplings. We therefore make our discussion concrete by considering the natural UV theory in which the bare four-fermion interactions are set to zero at the scale Λ_f.

We first note that only the first six beta functions are coupled to each other and receive no feedback from the couplings $\lambda^{\mathsf{S}}_{1818}$ and $\lambda^{\mathsf{A}}_{1818}$. This allows us to focus on Eqs. (4.64) to (4.69). In Appendix P we solve the system of equations and show that $\lambda^{\mathsf{S}}_{1515}$ is the fastest growing coupling. In what follows we focus on this coupling only. The scale-dependence of this coupling reads

$$\lambda^{\mathsf{S}}_{1515}(\ell) = \frac{\mathscr{J}_1\sqrt{\pi}}{4}\frac{v_0^2}{c_0}\frac{e^{\frac{1}{4w_0 a}}}{\sqrt{aw_0}}\exp\left(-\ell + aw_0\ell^2\right)\left[\mathrm{Erf}\left(\frac{1-2aw_0\ell}{2\sqrt{aw_0}}\right) - \mathrm{Erf}\left(\frac{1}{2\sqrt{aw_0}}\right)\right], \quad (4.78)$$

where $a = \sqrt{14}/16\pi < 1$. Here $\mathrm{Erf}(x)$ denotes the error function and in arriving to this expression we have neglected the flow of $w(v)$ (see Appendix P for details). A plot of the coupling is shown in Fig. 4.9. At the length scale $\ell \sim 1/w_0$ it becomes

$$\lambda^{\mathsf{S}}_{1515}(\ell_{\mathrm{con.}}) = \frac{\mathscr{J}_1}{2(1-2a)}\frac{v_0^2}{c_0}\left[1-(1-2a)e^{-\frac{(1-a)}{w_0}}\right] \sim \mathcal{O}(v_0^{\frac{3}{2}}) \quad (4.79)$$

to leading order in $v_0 \ll 1$. Since $a < 1$, the exponential factor is negligible and the coupling remains small and of order $v_0^{\frac{3}{2}}$ in the $v_0 \ll 1$ limit. For $\ell \gg 1/w_0$, Eq. (4.78) suggests that the coupling grows rapidly as $\lambda^{\mathsf{S}}_{1515}(\ell) \sim e^{aw_0\ell^2}$ due to the scale dependence of the anomalous scaling dimension of the four-fermion coupling which makes it relevant at low energies. We note that, at a parametrically larger scale $\ell' \sim 1/(aw_0)$, the coupling becomes large and of order $\lambda^{\mathsf{S}}_{1515}(\ell') \sim v_0^{\frac{5}{4}} e^{\frac{1}{aw_0}}$, signaling that the perturbative expansion in the four-fermion

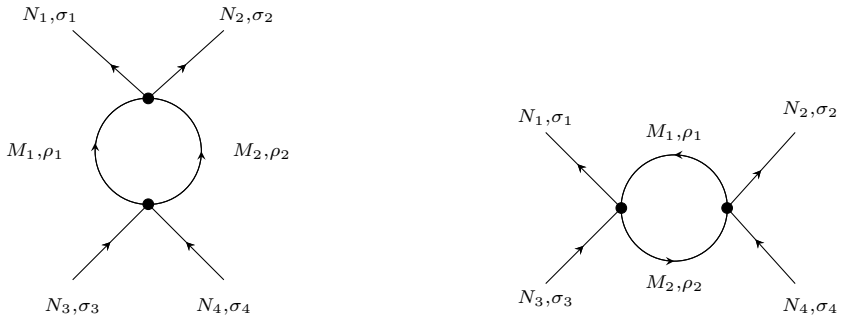

(a) (b)

Figure 4.10: Quadratic order corrections to the four-fermion interaction.

couplings breaks down at energy scales below

$$\mu_{\rm SC}^{(1)} \sim \Lambda_f e^{-\frac{1}{w_0}}. \tag{4.80}$$

So far we have analyzed the effect of the spin fluctuations on the anomalous scaling dimension of the four-fermion couplings. As we showed, the four-fermion couplings that pair electrons at antipodal hot spots on the FS grow rapidly and, in principle, we have to include higher order terms in the beta functions within the window of control set by Eq. (4.80). This could, in principle, reduce the window of energy scales in which we can trust our results. We now address this issue by estimating the quadratic order contribution to the beta functions arising from the fastest growing coupling.

4.5-(b) Beta Functions at Quadratic Order

At quadratic order in the four-fermion couplings, the contributions to the beta function come from the particle-particle and particle-hole diagrams shown in Figs. 4.10(a) and 4.10(b). When including the full momentum dependence of the coupling functions, the contributions from these diagrams to the four-point vertex function have the form

$$\delta\Gamma^{\{\sigma_i\};\mathrm{P.P}}_{\{N_i\}}(\{k_i\}) = \frac{1}{2\mu^2}\sum_{\rho_1,\rho_2=\uparrow,\downarrow}^{N_c}\sum_{M_1,M_2=1}^{8}\int \mathrm{d}q\,\lambda^{\sigma_1\sigma_2\rho_1\rho_2}_{N_1N_2M_1M_2}(k_{1;N_1},k_{2;N_2},[k_1+q]_{M_1},[k_2-q]_{M_2})$$
$$\times\,\lambda^{\rho_1\rho_2\sigma_3\sigma_4}_{M_1M_2N_3N_4}([k_1+q]_{M_1},[k_2-q]_{M_2},k_{3;N_3},k_{4;N_4})G_{M_1}(q+k_1)G_{M_2}(k_2-q), \tag{4.81}$$

$$\delta\Gamma^{\{\sigma_i\};\mathrm{P.H}}_{\{N_i\}}(\{k_i\}) = -\frac{1}{2\mu^2}\sum_{\rho_1,\rho_2=\uparrow,\downarrow}^{N_c}\sum_{M_1,M_2=1}^{8}\int \mathrm{d}q\,\lambda^{\sigma_1\rho_1\sigma_3\rho_2}_{N_1M_1N_3M_2}(k_{1;N_1},[q-k_1]_{M_1},k_{3;N_3},[q-k_3]_{M_2})$$
$$\times\,\lambda^{\rho_2\sigma_2\rho_1\sigma_4}_{M_2N_2M_1N_4}([q-k_3]_{M_2},k_{2;N_2},[q-k_1]_{M_1},k_{4;N_4})G_{M_1}(q-k_1)G_{M_2}(q-k_3). \tag{4.82}$$

Let us analyze the contribution of each of these expressions to the beta function of the four-fermion couplings. In a first approximation, one can invoke the WMDL and ignore the momentum dependence in the coupling functions. This amounts to assume that the four-fermion couplings are nonzero and uniform along the FS. In this case, and as we show in full detail in Appendix Q, the largest contribution to the beta function comes from those quantum

corrections in the pairing channel in which the internal electrons belong to antipodal patches on the FS. This is because in these channels, the electron pair carries zero momentum and both electrons are free to move around the FS without any energy cost. Therefore, these contributions scale with the size of the FS as a consequence of a nonzero density of states at the Fermi level. For electrons that belong to patches that are not antipodal, this is no longer the case as it is energetically unfavorable for them to move along extended regions of the FS. This originates in the fact that the electron pair carries nonzero momentum. In these cases, the diagrams give contributions to the beta functions that are negligible compared to the zero momentum pairing channels that are enhanced by k_{F}.

In the absence of curvature of the FS, the particle-particle and particle-hole contributions are identical due to the particle-hole symmetry of the theory. Therefore, the particle-hole contribution that involves electrons on antipodal points on the FS also scales with the size of the FS. However, if we include a small, but nonzero curvature, this degeneracy is lifted and the contributions from the particle-hole channel to the beta functions are absent (See Appendix Q). Therefore, the largest contribution arising at quadratic order comes from the zero momentum particle-particle channel. This contribution to the beta function of the four-fermion coupling functions at the hot spots is given by (See Appendices P and Q for further details):

$$\delta_2\beta^{\{\sigma_i\}}_{\{N_i\};\{\sigma_i\}} \sim -\frac{k_{\mathrm{F}}}{4\pi\Lambda_f}\sum_{\rho_1,\rho_2=\uparrow,\downarrow}\sum_{M_1=1}^{8}\lambda^{\sigma_1\sigma_2\rho_1\rho_2}_{N_1N_2M_1[M_1+4]_8}\lambda^{\rho_1\rho_2\sigma_3\sigma_4}_{M_1[M_1+4]_8N_3N_4}, \tag{4.83}$$

where k_{F} is the dimensionful Fermi momentum, $\delta_2\beta^{\{\sigma_i\}}_{\{N_i\};\{\sigma_i\}}$ denotes the contribution to the beta functions at second order in the four-fermion couplings and $[x]_8$ denotes the remainder of the division of x by 8. Notice that the enhancement by k_{F} is analogous to the situation arising in the analysis of the BCS instability in Fermi-liquids [See Sec. 1.1-(*b*)]. Therefore, in a first approximation, and following the same logic as Fermi-Liquid theory, we define the control parameters of the perturbative expansion in the four-fermion couplings as

$$\widetilde{\lambda}^{\sigma_1\sigma_2\rho_1\rho_2}_{N_1N_2N_3N_4}(l) \equiv \frac{k_{\mathrm{F}}}{\Lambda_f}\lambda^{\sigma_1\sigma_2\rho_1\rho_2}_{N_1N_2N_3N_4}(l) = \widehat{k}^{(0)}_{\mathrm{F}}e^{l}\lambda^{\sigma_1\sigma_2\rho_1\rho_2}_{N_1N_2N_3N_4}(l), \tag{4.84}$$

where $\widehat{k}^{(0)}_{\mathrm{F}}$ is the bare value of the (dimensionless) Fermi momentum and we have used the fact that, at the scale $\mu = \Lambda_f$, $k_{\mathrm{F}} = \Lambda_f\widehat{k}_{\mathrm{F}}$, with the dimensionless scale-dependent Fermi momentum $\widehat{k}_{\mathrm{F}} = \widehat{k}^{(0)}_{\mathrm{F}}e^{l}$. We can now use this definition in order to determine the length scales below which the solution obtained from the leading order beta function is reliable in the case that we tune all the four-fermion couplings to zero at the bare level. For this we focus only on the control parameter associated to the fastest growing coupling. Following the discussion from the previous section, this one is given by combining Eq. (4.84) and (4.78):

$$\widetilde{\lambda}^{\mathsf{S}}_{1515}(\ell) = \frac{\mathscr{J}_1\sqrt{\pi}\widehat{k}^{(0)}_{\mathrm{F}}}{4}\frac{v_0^2}{c_0}\frac{e^{\frac{1}{4w_0a}}}{\sqrt{aw_0}}\exp\left(aw_0\ell^2\right)\left[\mathrm{Erf}\left(\frac{1-2aw_0\ell}{2\sqrt{aw_0}}\right)-\mathrm{Erf}\left(\frac{1}{2\sqrt{aw_0}}\right)\right]. \tag{4.85}$$

The perturbative expansion in the effective couplings $\widetilde{\lambda}^{\sigma_1\sigma_2\rho_1\rho_2}_{N_1N_2N_3N_4}$ breaks down whenever $\widetilde{\lambda}^{\mathsf{S}}_{1515}(\ell)$ becomes of order one. In this case, the quadratic (and higher order) terms become

important in determining the flow of the couplings at the hot spots. The condition $\widetilde{\lambda}^{\mathsf{S}}_{1515}(\ell) \sim 1$ yields the length scale

$$\ell'_{\text{con.}} \sim \sqrt{\frac{1}{w_0} \log\left(\frac{c_0}{v_0^2}\frac{1}{\widehat{k}_{\text{F}}^{(0)}}\right)}. \tag{4.86}$$

This scale is parametrically larger than $1/\sqrt{w_0}$ due to the large value of the (dimensionless) bare Fermi momentum and the fact that $v_0 \ll 1$. Furthermore, we note that $\ell'_{\text{con.}} \ll \ell_{\text{con.}}$ in Eq. (4.75). This suggests that the perturbative expansion in the four-fermion coupling breaks down before we lose control over the leading order contributions to the beta functions. In particular the expression in Eq. (4.85) is controlled and remains small at energies above

$$\mu^{(2)}_{\text{SC}} \sim \Lambda_f e^{-\frac{1}{\sqrt{w_0}}\sqrt{\log(c_0/v_0^2\widehat{k}_{\text{F}}^{(0)})}}. \tag{4.87}$$

Below this scale, the perturbative expansion in the effective four-fermion couplings breaks down.

The estimation of the control scale obtained from Eq. (4.86) is very conservative as we now explain. The reason for this is that we have implicitly assumed, by using the WMDL, that the four-fermion couplings are nonzero everywhere on the FS. However, for a theory where the couplings are tuned to zero at the UV scale Λ_f, the four-fermion couplings are sourced by the spin fluctuations. Since electrons far away from the hot spots effectively decouple from the collective mode, the four-fermion interactions generated by the spin fluctuations are nonzero only in a region of the FS close to the hot spots that is small compared to k_{F}. To be more accurate in the determination of the control scale, and therefore, the superconducting transition temperature T_c, one needs to consider the inherent momentum dependence of the four-fermion couplings.

In Eqs. (4.81) and (4.82), the largest contribution arises when electrons in the loop are on antipodal points on the FS, that is, $M_2 = [M_1 + 4]_8$. In this case, the loop momentum along the FS runs over the entire region of the FS in which the four-fermion coupling functions are nonzero. This is because a particle-particle pair with zero total momentum can stay close to the FS while having a large momentum exchange. Similarly, a particle-hole pair with momentum $2\vec{k}_{\text{F}}$ can have a large momentum exchange while staying close to the FS. Therefore, the dimensionless parameters that control the magnitude of the quantum corrections are given by

$$\widetilde{\lambda}^{\{\sigma_i\};(1)}_{\{N_i\}}(k_{3;N_3}, k_{4;N_4}) \equiv \frac{1}{\mu}\int_{-k_{\text{F}}}^{k_{\text{F}}} \mathrm{d}q \lambda^{\{\sigma_i\}}_{\{N_i\}}(q, -q, k_{3;N_3}, k_{4;N_4}), \tag{4.88}$$

$$\widetilde{\lambda}^{\{\sigma_i\};(2)}_{\{N_i\}}(k_{2;N_2}, k_{4;N_4}) \equiv \frac{1}{\mu}\int_{-k_{\text{F}}}^{k_{\text{F}}} \mathrm{d}q \lambda^{\{\sigma_i\}}_{\{N_i\}}(q, k_{2;N_2}, q, k_{4;N_4}), \tag{4.89}$$

where it is understood that $N_2 = [N_1 + 4]_8$ in Eq. (4.88) and $N_3 = [N_1 + 4]_8$ in Eq. (4.89). Here, the integration is done over the relative momentum of the electron-electron (electron-hole) pair. The perturbative expansion in the four-fermion couplings is under control as

far the coupling functions in Eqs. (4.88) and (4.89) remain small. The energy scale below which the perturbative expansion breaks down can be identified as the upper bound for the superconducting transition temperature $T_c \sim \Lambda_f e^{-\ell_{\rm SC}}$. The precise determination of the control parameter of the four-fermion coupling expansion requires the solution to the full momentum-dependent beta function for the four-fermion couplings. This is beyond the scope of this thesis and therefore we content ourselves with the fact that the length scale at which the perturbative control in the four-fermion couplings is lost, denoted by $\ell_{\rm SC}$, is bounded from above and below by Eqs. (4.75) and (4.86), respectively:

$$\sqrt{\frac{1}{w_0}\log\left(\frac{c_0}{v_0^2}\frac{1}{\widehat{k}_{\rm F}^{(0)}}\right)} < \ell_{\rm SC} < \frac{1}{w_0}. \tag{4.90}$$

According to Eqs. (4.80) and (4.87), this predicts that the superconducting transition temperature is still exponentially small in the $v_0 \ll 1$ limit and therefore, at sufficiently low energies, the theory still enters into the universal scaling regime that is governed by a dynamical critical exponent $z \approx 1$. We note that, up to logarithmic accuracy, the lower bound in Eq. (4.90) is consistent with the analysis done in Chapter 2 and the estimation of the superconducting transition temperature given in Eq. (2.33). With this at hand, we proceed on determining the single-particle properties of the AFM quantum critical metal within the window of control implied by Eq. (4.90).

4.6 Single-particle properties of the antiferromagnetic quantum critical metal

In the rest of this chapter, we focus on the single-particle properties of the electronic excitations of the AFM quantum critical metal. We ignore the effects of the four-fermion interactions while keeping in mind that our results are valid at energy scales above $T_c \sim \Lambda_f e^{-\ell_{\rm SC}}$. We divide this section into two parts. In the first part we consider the electronic single-particle properties in the ideal case where there is no superconducting instabilities. In the second part we show how these results are modified once we incorporate the fact that superconductivity enters at some finite length scale $\ell_{\rm SC}$ satisfying Eq. (4.90).

4.6-(a) Electronic Spectral Function in the Absence of Superconducting Instabilities

In this section we focus on the single-particle spectral function of the electrons in the WMDL and in the ideal case where it has no superconducting instabilities.

In the WMDL we consider a microscopic theory in which the coupling functions are momentum-independent at the scale $\mu = \Lambda_f$. At lower energies, the coupling functions acquire momentum dependences through the fermion self-energy and vertex corrections. This is because the IR cutoff scales of quantum corrections depend on the momentum of the external electrons. For example, an electron on the FS at momentum k_N away from hot spot N should excite a virtual bosonic excitation with a minimum energy of $c(v)vk_N$ in order to scatter to a point on the FS near hot spot $\overline{N}$. At energies less than $c(v)vk_N$, those processes are suppressed, and electrons with momentum k_N effectively decouple from

critical spin fluctuations. Since electrons at different locations on the FS decouple from spin fluctuations at different energy scales, they acquire a self-energy that depends on the momentum along the FS. In particular, the lifetime of quasiparticles gradually goes to zero as one approaches the hot spots because electrons closer to the hot spots remain coupled with the spin fluctuations to lower energy scales than those electrons away from the hot spots.

For $v_0 \ll 1$, quantum corrections in Eqs. (4.59), (4.60) and (4.61) are dominated by the one-loop and two-loop self-energy diagrams depicted in Figs. 2.3(a) and 2.3(c), respectively. An explicit computation of these diagrams, combined with the renormalization conditions in Eq. (4.57), gives rise to the following momentum-dependent counterterm functions in the WMDL (see Appendix M for details):

$$Z_N^{(1)}(k_N) = 1 - \frac{2(N_c^2-1)}{\sqrt{2\pi^2 N_c N_f}} \sqrt{\frac{v}{\log(1/v)}} \log\left(\frac{\Lambda_f}{\mathscr{G}_1(\mu, 2vc(v)|k_N|)}\right), \tag{4.91}$$

$$Z_N^{(2)}(k_N) = 1 + \frac{(N_c^2-1)}{2\pi^2 N_c N_f} v \log\left(\frac{1}{v}\right)\left[\log\left(\frac{\Lambda_f}{\mathscr{G}_2(\mu, 2vc(v)|k_N|)}\right) + \frac{3}{2}\log\left(\frac{\Lambda_f}{\mathscr{G}_3(\mu, 2v|k_N|)}\right)\right], \tag{4.92}$$

$$Z_N^{(3)}(k_N) = 1 - \frac{(N_c^2-1)}{2\pi^2 N_c N_f} v \log\left(\frac{1}{v}\right)\left[\log\left(\frac{\Lambda_f}{\mathscr{G}_2(\mu, 2vc(v)|k_N|)}\right) + \frac{1}{2}\log\left(\frac{\Lambda_f}{\mathscr{G}_3(\mu, 2v|k_N|)}\right)\right]. \tag{4.93}$$

Here, $\mathscr{G}_j(x,y)$ with $j = 1,2,3$ are crossover functions which approach $\mathscr{G}_j(x,y) \sim \max(x,y)$ for $x \gg y$ or $y \gg x$. Since it is difficult to determine the precise functional form of these functions, we will approximate the crossover functions as $\mathscr{G}_j(x,y) = \max(x,y)$ for $j = 1,2,3$. In this approximation, the quantum corrections sharply turn on and off as the energy (μ) crosses the momentum-dependent crossover scales. Mathematically, this is attributed to

$$\frac{\partial}{\partial x}\mathscr{G}_j(x,y) \approx \Theta(x-y), \quad j = 1,2,3, \tag{4.94}$$

where $\Theta(x)$ is the Heaviside function. It is noted that the counterterm functions $A_N^{(i)}(k_N)$ satisfy the condition in Eq. (4.23) to leading order in $v_0 \ll 1$. In Appendix M we show explicitly that this is also the case for $A_N^{(4)}(k_N', k_N)$. Therefore, the theory is renormalizable. From Eqs. (4.59), (4.60) and (4.61), we obtain (see Appendix L for details)

$$\widehat{v}_N(k_N;\ell_\omega) = v_0 \exp\left\{-\frac{(N_c^2-1)}{\pi^2 N_c N_f}\int_0^{\ell_\omega} \mathrm{d}\ell v(\ell) \log\left(\frac{1}{v(\ell)}\right)\left[\Theta\left(\Lambda_f e^{-\ell} - 2v(\ell)c(\ell)\,|k_N|\right) + \Theta\left(\Lambda_f e^{-\ell} - 2v(\ell)\,|k_N|\right)\right]\right\}, \tag{4.95}$$

$$F_z^{(N)}(k_N;k_0) = \exp\left\{\frac{2(N_c^2-1)}{\sqrt{2\pi^2 N_c N_f}}\int_0^{\ell_\omega} \mathrm{d}\ell \sqrt{\frac{v(\ell)}{\log(1/v(\ell))}}\Theta\left(\Lambda_f e^{-\ell} - 2v(\ell)c(\ell)\,|k_N|\right)\right\}, \tag{4.96}$$

$$F_{V_F}^{(N)}(k_N;k_0) = \exp\left\{\frac{(N_c^2-1)}{2\pi^2 N_c N_f}\int_0^{\ell_\omega} \mathrm{d}\ell v(\ell) \log\left(\frac{1}{v(\ell)}\right)\left[\Theta\left(\Lambda_f e^{-\ell} - 2v(\ell)c(\ell)\,|k_N|\right) + \frac{1}{2}\Theta\left(\Lambda_f e^{-\ell} - 2v(\ell)\,|k_N|\right)\right]\right\}, \tag{4.97}$$

where $c(\ell) \equiv c(v(\ell))$. These expressions show that the momentum-dependent slope and universal functions are tied to $v(\ell)$ which determines the flow of the slope of the FS at the hot spots. The scale-dependent slope $v(\ell)$ is given by

$$v(\ell) = \frac{\pi^2 N_c N_f}{2(N_c^2-1)} \frac{1}{(\ell+\ell_0)\log(\ell+\ell_0)}, \tag{4.98}$$

where ℓ_0 given in Eq. (3.49) marks the scale below which the slope at the hot spots on the FS flows to zero in a way that is independent of its bare value. In Appendix L we show that this expression is self-consistently reproduced from Eq. (4.95).

The theta functions in Eqs. (4.95) to (4.97) encode the fact that quantum corrections are suppressed below specific momentum-dependent energy scales. The threshold energy scales for the one-loop and two-loop quantum corrections are determined by the transcendental equations

$$\Lambda_f e^{-\ell_N^{(1)}} = 2v(\ell_N^{(1)})c(\ell_N^{(1)})|k_N|, \tag{4.99}$$

$$\Lambda_f e^{-\ell_N^{(2)}} = 2v(\ell_N^{(2)})|k_N|, \tag{4.100}$$

respectively. Because $\Lambda_f e^{-\ell_N^{(1)}} \ll \Lambda_f e^{-\ell_N^{(2)}}$ in the small v limit, the one-loop correction survives up to a lower energy scale than the two-loop quantum correction. This is due to the fact that the minimum energy of the virtual excitations that need to be excited in the one-loop process is smaller than that in the two-loop process. For an external electron on the FS with momentum k_N away from a hot spot, one can always find a loop momentum in the diagram in Fig. 2.3(a) such that the electron in the intermediate state stays on the FS at the expense of the boson carrying a non-zero momentum vk_N and therefore carrying minimum energy $vc(v)|k_N|$. Because $v \ll c(v)$, this configuration that puts the virtual electron on the FS is energetically favorable compared to the one in which the boson carries zero momentum at the expense of creating a virtual electron away from the FS that carries minimum energy vk_N. This is the origin of $\Theta\left(\Lambda_f e^{-\ell} - 2v(\ell)c(\ell)\,|k_N|\right)$ in Eq. (4.95). As a result, the one-loop quantum correction for an electron with momentum k_N turns off at an energy scale below $\mu \sim \Lambda_f e^{-\ell_N^{(1)}}$ defined through Eq. (4.99). In contrast, one cannot find loop momenta at which all internal fermions stay on the FS in the two-loop process shown in Fig. 2.3(c). As a result, one necessarily has to go through intermediate states in which a virtual electron is created away from the FS with minimum energy vk_N. This gives rise to the threshold behavior given by $\Theta\left(\Lambda_f e^{-\ell} - 2v(\ell)\,|k_N|\right)$ for the two-loop contribution.

A. *Electronic Single-Particle Spectral Function*

In this section, we compute the spectral function of electrons near the renormalized FS as a function of momentum along it. For this, we consider the $\ell_\omega \gg 1$ limit with a fixed $k_N \neq 0$ in Eq. (4.58). This is the limit that is complimentary to the dynamical range covered by the hot spot theory presented in Chapter 2. In the hot spot theory, the form of the spectral function is obtained by taking the $\ell_\omega \to \infty$ and $k_N \to 0$ limits simultaneously. For nonzero frequency, $\ell_\omega < \infty$, the momentum-dependent slope and universal functions in Eqs. (4.95)

to (4.97) are piecewise continuous functions as a consequence of the integration identity:

$$\int_0^{\ell_\omega} \mathrm{d}\ell f(\ell)\Theta[\Lambda_f e^{-\ell} - \Delta(\ell)] = \Theta(\ell_\omega - \ell_\Delta)\Theta(\ell_\Delta)\int_0^{\ell_\Delta} \mathrm{d}\ell f(\ell) + \Theta(\ell_\Delta - \ell_\omega)\int_0^{\ell_\omega} \mathrm{d}\ell f(\ell), \quad (4.101)$$

where $f(\ell)$ is a function of the scale and ℓ_Δ solves the transcendental equation $\Lambda_f e^{-\ell_\Delta} = \Delta(\ell)$. For a given real frequency $\omega > 0$, the spectral function is sharply peaked at the renormalized electronic energy $\omega(\vec{k})$. The shape of the constant energy contour in the momentum space is renormalized with respect to the bare one as a consequence of the interaction of the electrons with the collective mode. For $\omega \approx \omega(\vec{k})$, the spectral function is well approximated by

$$\mathcal{A}_N(\vec{k},\omega) = \frac{\mathcal{Z}_N[k_N;\omega(\vec{k})]}{\tau_N[k_N;\omega(\vec{k})]}\frac{1}{[\omega-\omega(\vec{k})]^2 + \tau_N[k_N,\omega(\vec{k})]^{-2}}. \quad (4.102)$$

In Appendix L we justify this in full detail through an explicit computation. This spectral function is characteristic of particle-like excitations. Here, $\mathcal{Z}_N[k_N;\omega(\vec{k})]$ ($\tau_N[k_N;\omega(\vec{k})]$) denotes the quasiparticle weight (lifetime). In principle, the quasiparticle weight and lifetime depend on the momentum along the FS and the renormalized energies independently. Here we examine how the spectral function evolves as a function of k_N in the limit that $\omega \to \omega(\vec{k})$ for a fixed $\omega(\vec{k})$.

In order to quantify the degree of incoherence of the single-particle electronic excitations, we consider the dimensionless parameter

$$\mathscr{W}_N(k_N;\vec{k}) \equiv \frac{1}{\tau_N[k_N,\omega(\vec{k})]\omega(\vec{k})}, \quad (4.103)$$

which measures the ratio of the scattering rate to the energy of a single-particle excitation. If $|\mathscr{W}_N(k_N;\vec{k})| \ll 1$, the scattering rate is much smaller than the energy, and the quasiparticle is coherent. In the standard Fermi-liquid metal, the quasiparticle lifetime scales as $\tau_N[k_N;\omega(\vec{k})] \sim E_{\mathrm{F}}/\omega(\vec{k})^2$, where E_{F} is the Fermi energy and $\omega(\vec{k})$ is measured with respect to the Fermi level. Therefore, $|\mathscr{W}_N(k_N;\vec{k})| \sim |\omega(\vec{k})|/E_{\mathrm{F}} \ll 1$, which becomes smaller as the electronic energy approaches the Fermi level. In the following discussion we will use this parameter to characterize the nature of the particle-like excitations in the AFM quantum critical metal and show that the latter deviate strongly from those in Fermi-liquid metals.

As a consequence of Eq. (4.101), the spectral function in Eq. (4.102) displays several crossovers as a function of the frequency and the momentum along the FS. In the remaining of this section we focus on the zero frequency limit of Eq. (4.102). This corresponds to the ideal case in which the system has no superconducting instabilities down to zero temperature. While this is unphysical, it serves as a useful starting point in understanding physical cases with nonzero superconducting transition temperatures. In Sec. 4.6-(*b*) we analyze the spectral function at nonzero frequencies $\omega \gtrapprox T_c$, with T_c denoting the superconducting transition temperature.

For $\omega = 0$ and $k_N \neq 0$, $\tau_N[k_N,\omega(\vec{k})] = \infty$ in Eq. (4.102). In this limit, the spectral function is given by

$$\mathcal{A}_N(\vec{k},\omega) = \mathcal{Z}_N(k_N)\delta\left(\omega - \mathfrak{V}_{\mathrm{F}}^{(N)} e_N[\vec{k};\widehat{v}_N(k_N)]\right), \quad (4.104)$$

where, $\widehat{v}_N(k_N) \equiv \widehat{v}_N(k_N;\infty)$. Here, the momentum-dependent quasiparticle weight and renormalized Fermi velocity are given by

$$\mathcal{Z}_N(k_N) = \frac{1}{F_z^{(N)}(k_N)}, \tag{4.105}$$

$$\mathfrak{V}_{\rm F}(k_N) = \frac{F_{V_{\rm F}}^{(N)}(k_N)}{F_z^{(N)}(k_N)}, \tag{4.106}$$

with $F_z^{(N)}(k_N) = F_z^{(N)}(k_N;0)$ and $F_{V_{\rm F}}^{(N)}(k_N) = F_{V_{\rm F}}^{(N)}(k_N;0)$. This spectral function is characteristic of coherent quasiparticle excitations with infinite lifetime. At zero frequency, the spectral function diverges at the *renormalized* FS defined by

$$e_N[\vec{k}, \widehat{v}_N(k_N)] = 0. \tag{4.107}$$

In the zero frequency limit the quasiparticle weight depends only on the momentum along the renormalized FS. Therefore, it acquires a momentum profile that depends on the location of the quasiparticle on the renormalized FS. Similarly, Eq. (4.106) represents the magnitude of the Fermi velocity at each point on the renormalized FS. The infinite quasiparticle lifetime is due to the fact that spin fluctuations decouple from electrons away from the hot spots at sufficiently low energies.

The momentum-dependent profile of the slope and universal functions that fully determine the quasiparticle weight, renormalized Fermi velocity and renormalized FS are given by

$$\widehat{v}_N(k_N) = v_0 \exp\left\{-\frac{1}{2}\sum_{j=1}^{2}\Theta(\ell_N^{(j)})\log\left[\frac{(\ell_0+\ell_N^{(j)})\log(\ell_N^{(j)}+\ell_0)}{\ell_0\log(\ell_0)}\right]\right\}, \tag{4.108}$$

$$F_z^{(N)}(k_N) = \exp\left\{\sqrt{N_c^2-1}\Theta(\ell_N^{(1)})\left[\mathrm{Ei}\left(\frac{\log(\ell_N^{(1)}+\ell_0)}{2}\right) - \mathrm{Ei}\left(\frac{\log(\ell_0)}{2}\right)\right]\right\}, \tag{4.109}$$

$$F_{V_{\rm F}}^{(N)}(k_N) = \exp\left\{\frac{1}{2}\sum_{j=1}^{2}\frac{\Theta(\ell_N^{(j)})}{2^j}\log\left[\frac{(\ell_0+\ell_N^{(j)})\log(\ell_N^{(j)}+\ell_0)}{\ell_0\log(\ell_0)}\right]\right\}, \tag{4.110}$$

where ℓ_0 is given in Eq. (3.49). The details leading to these results are given in Appendix L. The appearance of the Heaviside functions in these expressions give rise to momentum-dependent crossovers. Before we discuss the shape of the renormalized FS, momentum-dependent Fermi velocity and the momentum-dependent quasiparticle weight in detail, we first provide an intuitive explanation for these momentum crossovers.

B. Momentum-dependent crossovers

The momentum dependence of low-energy electronic properties is determined by the interplay between multiple energy scales that we now address. The first energy scale is the UV scale Λ_f at which the bare coupling functions are momentum independent. At energies below Λ_f, spin fluctuations are governed by the propagator given in Eq. (2.6) to the leading

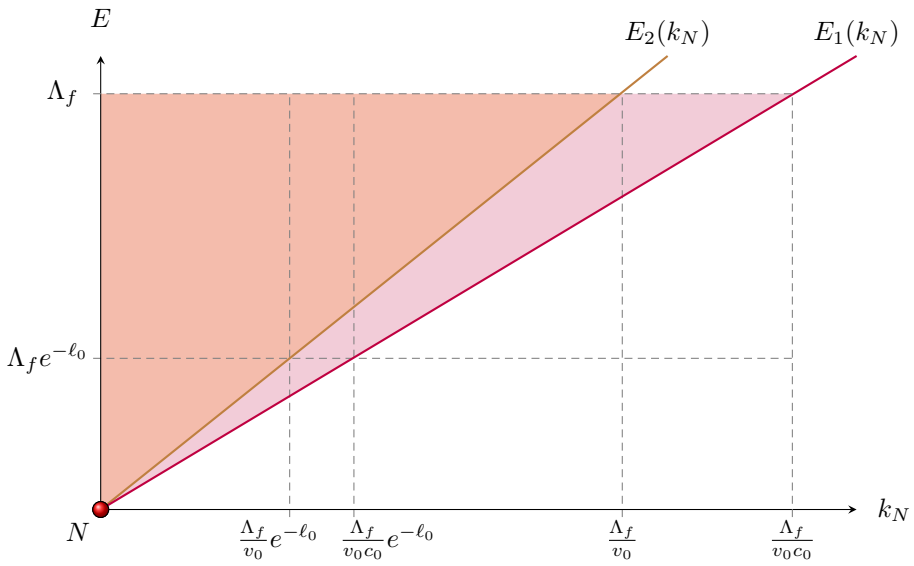

Figure 4.11: Crossover energy scales in the case in which $\ell_{\rm SC} = \infty$. The shaded regions are where the quantum corrections have nonzero support as a function of energy and momentum.

order in v. In particular, the FS defined at this energy scale is straight with a constant slope $v_0 \ll 1$ away from the perfect nesting. The velocity of the spin fluctuations is given by $c_0 \equiv c(v_0)$ at this scale. The second energy scale is that below which the flow of v, the slope of the FS at the hot spots, kicks in. In the small v_0 limit, this energy scale is $\Lambda_f e^{-\ell_0}$, with ℓ_0 given in Eq. (3.49). At energy scales above $\Lambda_f e^{-\ell_0}$, the flow of v can be ignored. At lower energies, v flows to zero logarithmically. This energy scale is exponentially smaller in $1/v_0$ compared to Λ_f because of the logarithmic flow of v. The third energy scale is given by $E_1(k_N) \sim \Lambda_f e^{-\ell_N^{(1)}}$ in Eq. (4.99). It is the minimum energy of the virtual state in the one-loop self-energy of the electron on the FS at momentum k_N away from hot spot N. The last energy scale is given by $E_2(k_N) \sim \Lambda_f e^{-\ell_N^{(2)}}$ in Eq. (4.100). It corresponds to the minimum energy of the virtual state in the two-loop self-energy of an electron with momentum k_N on the FS near hot spot N. $E_1(k_N)$ and $E_2(k_N)$ represent the IR cutoff scales for the one and two-loop quantum corrections for the zero energy electron with momentum k_N, respectively.

Now we describe the crossovers that arise as a function of k_N in terms of these four energy scales. We focus, without loss of generality, in the $k_N > 0$ case. The crossovers occur at momenta at which $E_1(k_N)$ or $E_2(k_N)$ coincide either with Λ_f or $\Lambda_f e^{-\ell_0}$. We denote those four momenta as k_1^*, k_2^*, k_3^* and k_4^*. These are given by

$$E_1(k_1^*) = \Lambda_f, \qquad \Rightarrow \qquad k_1^* \sim \frac{\Lambda_f}{v_0 c_0}, \tag{4.111}$$

$$E_2(k_2^*) = \Lambda_f, \qquad \Rightarrow \qquad k_2^* \sim \frac{\Lambda_f}{v_0}, \tag{4.112}$$

$$E_1(k_3^*) = \Lambda_f e^{-\ell_0}, \qquad \Rightarrow \qquad k_3^* \sim \frac{\Lambda_f e^{-\ell_0}}{v_0 c_0}, \tag{4.113}$$

$$E_2(k_4^*) = \Lambda_f e^{-\ell_0}, \qquad \Rightarrow \qquad k_4^* \sim \frac{\Lambda_f}{v_0} e^{-\ell_0}. \tag{4.114}$$

In the small v_0 limit, the four crossover momenta are well separated: $k_1^* \gg k_2^* \gg k_3^* \gg k_4^*$. The crossover scales are illustrated in Fig. 4.11. First we note that $k_1^* \ll \overline{k}_F$ with $\overline{k}_\mathrm{F}$ defined in Eq. (4.62). The renormalization of the electrons in this range of momentum is governed by the universal low-energy spin fluctuations whose dynamics is governed by the propagator in Eq. (2.6). Let us illustrate the physics behind the different momentum crossovers.

Region 1: $k_1^* \ll k_N \ll \overline{k}_\mathrm{F}$:

Electrons in this range of momentum are completely decoupled from the spin fluctuations. This is because quantum corrections in this region exist only at energy scales $E \gg \Lambda_f$. Therefore, quantum corrections are negligible.

Region 2: $k_2^* \ll k_N \ll k_1^*$:

Electrons in this range of momentum are renormalized only by the one-loop quantum correction to the leading order in v_0. The flow of v can be ignored in this region because quantum corrections exist only at energy scales $E \gg \Lambda_f e^{-\ell_0}$. Because the flow of v can be ignored, the quantum correction gives rise to power-law momentum-dependences to physical observables, where the power is controlled by $v_0 \ll 1$.

Region 3: $k_3^* \ll k_N \ll k_2^*$:

As k_N becomes smaller than k_2^*, there exists an energy window in which the two-loop quantum correction turns on. The flow of v is still negligible within this range, and both the one-loop and two-loop quantum corrections give rise to power-law momentum-dependences in the physical observable with exponents that differ from those in Region 2.

Region 4: $k_4^* \ll k_N \ll k_3^*$:

For $k_N \ll k_3^*$, electrons are close enough to the hot spots so that quantum corrections persist down to energy scales in which the flow of v can not be ignored. In this region on the FS, there exists an energy window below $\Lambda_f e^{-\ell_0}$ in which only the one-loop correction survives, but not the two-loop correction. In this window, the one-loop correction gives rise to a logarithmic or superlogarithmic momentum dependences because of the flow of v while the two-loop correction gives rise only to power-law momentum dependences.

Region 5: $k_N \ll k_4^*$:

If the electron is close enough to the hot spots, there exists an energy window in which the flow of v becomes important for both the one and two-loop quantum corrections. In this regime, all power-law momentum dependences in the physical observables are replaced by either logarithmic or superlogarithmic momentum dependences.

In the following, we show the explicit momentum dependences of the renormalized Fermi velocity and the quasiparticle weight along the renormalized FS.

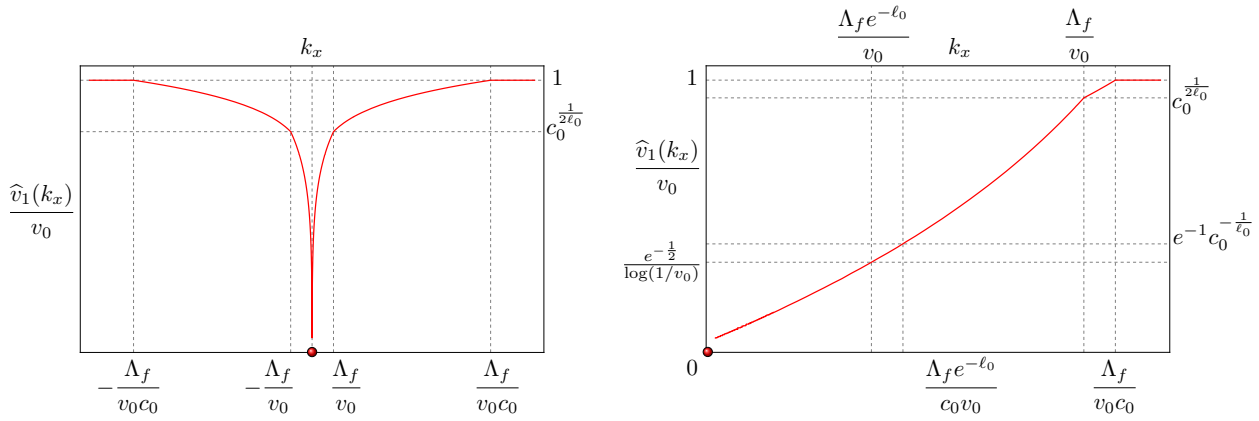

Figure 4.12: Momentum profile of the slope along the renormalized FS. The plot in the right panel is in logarithmic scale.

C. *The renormalized FS and quasiparticle weight*

Without loss of generality we consider the hot spot with $N = 1$. All other hot spots follow the same logic due to the C_4 symmetry of the theory. From Eq. (4.107), the renormalized FS is given by

$$k_y \sim -v_0 k_x \begin{cases} 1 & \frac{\Lambda_f}{c_0 v_0} \ll k_x \ll \overline{k}_{\rm F}, \\ \left(\frac{v_0 c_0 k_x}{\Lambda_f}\right)^{\frac{(N_c^2-1)}{\pi^2 N_c N_f} v_0 \log(1/v_0)} & \frac{\Lambda_f}{v_0} \ll k_x \ll \frac{\Lambda_f}{c_0 v_0}, \\ \left(\frac{v_0 \sqrt{c_0} k_x}{\Lambda_f}\right)^{\frac{2(N_c^2-1)}{\pi^2 N_c N_f} v_0 \log(1/v_0)} & \frac{\Lambda_f}{v_0 c_0} e^{-\ell_0} \ll k_x \ll \frac{\Lambda_f}{v_0}, \\ \left(\frac{v_0 k_x}{\Lambda_f}\right)^{\frac{(N_c^2-1)}{\pi^2 N_c N_f} v_0 \log(1/v_0)} \sqrt{\frac{\ell_0 \log(\ell_0)}{\log\left(\frac{\Lambda_f}{k_x}\right) \log\log\left(\frac{\Lambda_f}{k_x}\right)}} & \frac{\Lambda_f}{v_0} e^{-\ell_0} \ll k_x \ll \frac{\Lambda_f}{v_0 c_0} e^{-\ell_0}, \\ \frac{\pi^2 N_c N_f}{2 v_0 (N_c^2-1)} \frac{1}{\log\left(\frac{\Lambda_f}{k_x}\right) \log\log\left(\frac{\Lambda_f}{k_x}\right)} & k_x \ll \frac{\Lambda_f}{v_0} e^{-\ell_0}. \end{cases} \tag{4.115}$$

where $c_0 = c(v_0)$ with $c(v)$ given by Eq. (3.43) and ℓ_0 defined in Eq. (3.49). In Appendix L we show the derivation of Eq. (4.115) from Eq. (4.108). It is noted that the shape of the renormalized FS depends weakly on k_x in the small v_0 limit.

The shape of the renormalized FS is determined from the local slope of the renormalized FS which is plotted in Fig. 4.12. As one approaches the hot spots, the FS becomes more nested because spin fluctuations remain coupled to electrons down to lower energy scales. Far away from the hot spots, the FS gets deformed in a power-law fashion which crosses over to a logarithmic deformation close to the hot spots.

Now we proceed to describe the profile of the quasiparticle weight and renormalized Fermi velocity along the FS. For the hot spot $N = 1$, Eqs. (4.105) and (4.106) are given by

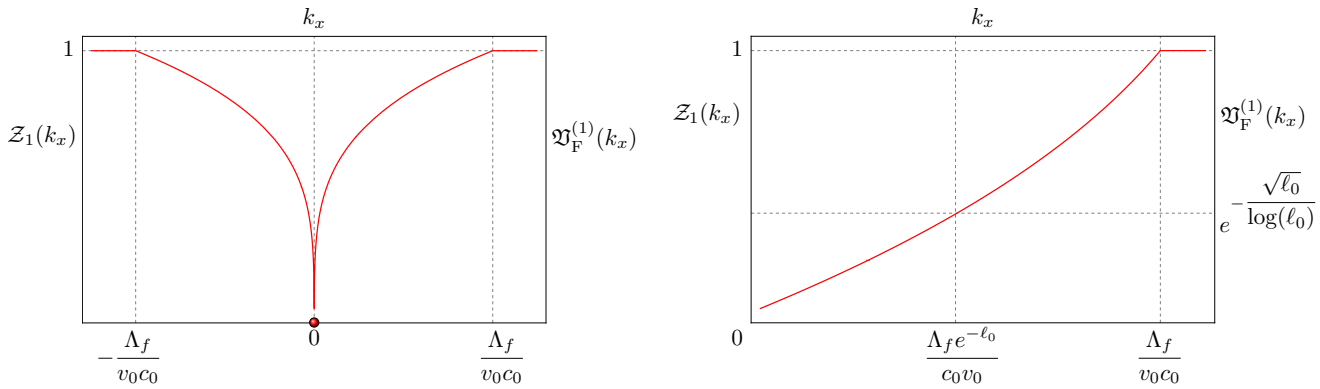

Figure 4.13: Momentum profile of the quasiparticle weight and renormalized Fermi velocity. The plot in the right panel is in logarithmic scale.

(see Appendix L for details)

$$\mathcal{Z}_1(k_x)=\mathfrak{V}_{\rm F}^{(1)}(k_x)=\begin{cases}1 & \frac{\Lambda_f}{v_0c_0}\ll k_x\ll \overline{k}_{\rm F},\\ \left(\frac{v_0c_0k_x}{\Lambda_f}\right)^{\frac{\sqrt{2}(N_c^2-1)}{\pi\sqrt{N_cN_f}}\sqrt{\frac{v_0}{\log(1/v_0)}}} & \frac{\Lambda_f e^{-\ell_0}}{v_0c_0}\ll k_x\ll \frac{\Lambda_f}{v_0c_0},\\ \exp\left(-\frac{2\sqrt{N_c^2-1}\sqrt{\log\left(\frac{\Lambda_f}{k_x}\right)}}{\log\log\left(\frac{\Lambda_f}{k_x}\right)}\right) & k_x\ll \frac{\Lambda_f e^{-\ell_0}}{v_0c_0}.\end{cases}\tag{4.116}$$

The quasiparticle weight and the renormalized Fermi velocity have the same momentum profile to the leading order in v_0 because both $F_z^{(N)}(k_N)$ and $F_{V_{\rm F}}^{(N)}(k_N)$ are dominated by the counterterm function $Z_N^{(1)}(k_N)$ in Eq. (4.91). Since these are determined only by the one-loop self-energy correction at low energies, there are only two crossover momenta $k_1^*\sim\Lambda_f/(v_0c_0)$ and $k_3^*\sim\Lambda_f e^{-\ell_0}/(v_0c_0)$. For $k_1^*\ll k_N\ll\overline{k}_{\rm F}$, the quasiparticle weight is equal to one because in this momentum regime the electrons are completely decoupled from the spin fluctuations. We refer to this range of momentum as the *cold* region. For $k_N\gg k_3^*$, the flow of v can be ignored over the window of energy scales in which the one-loop quantum correction is present. In this region, the quasiparticle weight decays algebraically from unity until it reaches an exponentially small value at $k_N\sim k_3^*$. This owes to the fact that the electrons remain coupled with the critical spin fluctuations down to lower energy scales at momenta closer to the hot spots[2]. However, the interaction effect is cut off before the flow of v becomes important. We call this range of momentum on the FS the *lukewarm* region.

For $k_N\ll k_3^*$, the flow of v becomes important. Since v itself flows to zero logarithmically at low energies, the power-law momentum dependence crosses over into a superlogarithmic momentum dependence in this region. In this region, the quasiparticle weight is exponentially small in $1/v_0$. We call this range of momentum on the FS the *hot* region. The momentum-dependent quasiparticle weight and renormalized Fermi velocity are plotted in Fig. 4.13.

[2]In Appendix N we provide a quantitative analysis of the momentum dependence of the interaction vertex function that evidences this feature.

Eq. (4.116) characterizes the way that the electrons along the FS lose their coherence due to the strong interaction with the collective mode as the hot spots are approached. The *hot, lukewarm and cold* regions can be probed by ARPES experiments. Here, the cold electrons reside at momentum $\frac{\Lambda_f}{v_0 c_0} \ll k_N \ll \overline{k}_{\rm F}$ and have unit quasiparticle weights since these decouple completely from the spin fluctuations at energies below Λ_f. The lukewarm region: $\Lambda_f e^{-\ell_0}/(v_0 c_0) \ll k_N \ll \Lambda_f/(v_0 c_0)$ is characterized by a universal power-law momentum-dependent quasiparticle weight. Finally, the hot electrons with momentum $k_N \ll \Lambda_f e^{-\ell_0}/(v_0 c_0)$ are characterized by a superlogarithmic decay in momentum of the quasiparticle weight close to the hot spots.

We now proceed on showing how the results presented in this section change in the realistic case where the superconducting instability of the system develops at nonzero energy scales.

4.6-(*b*) Electronic Spectral Function in the Presence of Superconducting Instabilities

In the presence of superconducting instabilities the single-particle spectral function in Eq. (4.102) can be trusted only up to energy scales $\mu \sim \Lambda_f e^{-\ell_{\rm SC}}$, where $\ell_{\rm SC}$ denotes the length scale above which superconductivity develops. In superconducting states, the single-particle excitations are gapped out. However, the effects of the critical spin fluctuations are still present in the spectral function of the electrons whose energies are larger than the superconducting gap. In what follows we consider the theory in which all four-fermion couplings are set to zero in the UV. In this case, we have shown that the scale at which superconductivity develops is such that $\ell_{\rm SC} \ll \ell_0$ and is bounded as in Eq. (4.90). Although the precise form the scale is unknown, the only relevant information we need is the fact that $\ell_{\rm SC}$ is much smaller than the length scale at which the flow of v becomes appreciable. In what follows we analyze the spectral function in Eq. (4.102) as a function of momentum at a fixed frequency $\omega \gtrsim \omega_{\rm SC}$, with $\omega_{\rm SC} = T_c \sim \Lambda_f e^{-\ell_{\rm SC}}$.

At a fixed nonzero frequency, the spectral function displays further crossovers apart from those that arise at the momentum scales in Eqs. (4.111) to (4.114). These crossovers arise at a frequency that coincides with the momentum-dependent IR scales of the one-loop and two-loop fermion self-energies. The momentum scales for the new crossovers are given by

$$E_1(k_5^*) = \Lambda_f e^{-\ell_{\rm SC}}, \qquad \Rightarrow \qquad k_5^* \sim \frac{\Lambda_f e^{-\ell_{\rm SC}}}{v_0 c_0}, \tag{4.117}$$

$$E_2(k_6^*) = \Lambda_f e^{-\ell_{\rm SC}}, \qquad \Rightarrow \qquad k_6^* \sim \frac{\Lambda_f e^{-\ell_{\rm SC}}}{v_0}. \tag{4.118}$$

The interplay of these two momentum scales and those in Eq. (4.114) to (4.111) gives rise to different frequency and momentum dependences that we now discuss in detail. For the theory under consideration, the momentum scales in Eqs. (4.111) to (4.114), (4.117) and (4.118) are organized as $k_1^* \gg k_2^* \gg k_5^* \gg k_6^* \gg k_3^* \gg k_4^*$. This is a consequence of the fact that $\ell_{\rm SC} \ll \ell_0$. These are depicted in Fig. 4.14. In this case, Region 4 and Region 5 illustrated in the ideal case are absent. In Region 1, Region 2 and Region 3 physical observables acquire power-law momentum dependences because the logarithmic flow of v can be ignored.

Let us analyze the crossovers displayed by Eq. (4.102) as a function of the momentum along the FS for the $N = 1$ with $k_x > 0$.

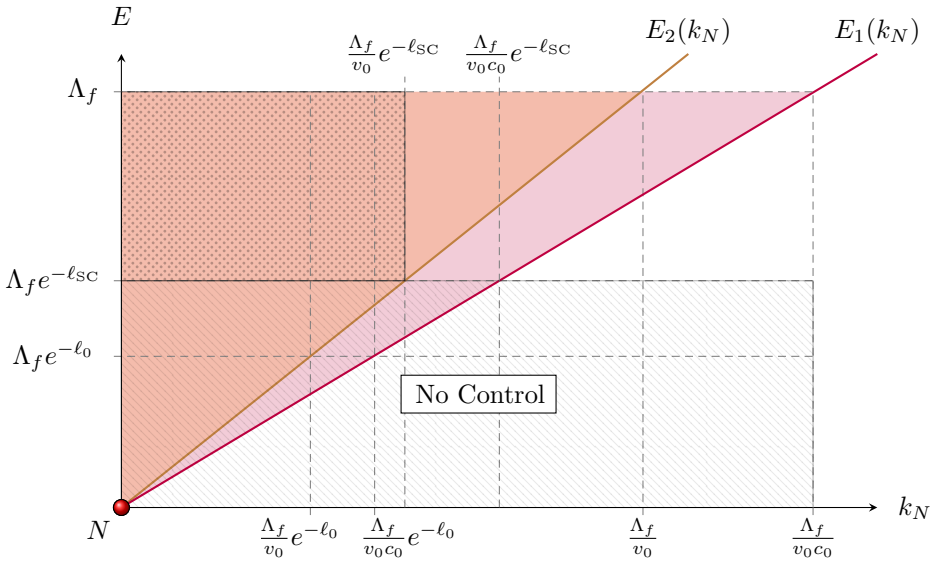

Figure 4.14: Crossover energy scales in the case in which the onset of superconductivity occurs at $\mu_{SC} \sim \Lambda_f e^{-\ell_{SC}}$ with ℓ_{SC} bounded as in Eq. (4.90). The hatched region is where we loose control in our computation. The dotted region is where we cannot resolve the momentum-dependent properties of the electronic excitations.

(*i*) For momentum $k_x \gg \frac{\Lambda}{v_0 c_0} e^{-\ell_{SC}}$, the quasiparticle lifetime in Eq. (4.102) becomes infinite and the the spectral function takes the form:

$$\mathcal{A}_1(\vec{k},\omega) = \mathcal{Z}_1(k_x)\delta\left(\omega - \mathfrak{V}_F^{(1)}(k_x) e_1\left[\vec{k};\widehat{v}_1(k_x)\right]\right), \tag{4.119}$$

where the quasiparticle weight is given by

$$\mathcal{Z}_1(k_x) = \begin{cases} 1 & \frac{\Lambda_f}{v_0 c_0} \ll k_x \ll \overline{k}_F, \\ \left(\frac{v_0 c_0 k_x}{\Lambda_f}\right)^{\frac{\sqrt{2}(N_c^2-1)}{\pi\sqrt{N_c N_f}}\sqrt{\frac{v_0}{\log(1/v_0)}}} & \frac{\Lambda_F}{v_0 c_0} e^{-\ell_{SC}} \ll k_x \ll \frac{\Lambda_f}{v_0 c_0}. \end{cases} \tag{4.120}$$

The spectral function has a well-defined quasiparticle peak at energy,

$$\omega(\vec{k}) = \mathfrak{V}_F^{(1)}(k_x)\left[\widehat{v}_1(k_x)k_x + k_y\right]. \tag{4.121}$$

This provides the information regarding how the electronic energy levels get renormalized by the interaction of the electrons with the critical spin fluctuations for $k_x \gg \frac{\Lambda_f}{v_0 c_0} e^{-\ell_{SC}}$. With $\omega \gtrapprox \omega_{SC}$, the superconducting gap is ignored in Eq. (4.121) because the spectral function is well approximated by the one in the normal state at intermediate energy scales. We note that the equal energy contours approach the renormalized FS in the zero energy limit. These contours are determined by the Fermi

velocity given by Eq. (4.120) and the renormalized momentum dependent slope:

$$\widehat{v}_1(k_x) = v_0 \begin{cases} 1 & \frac{\Lambda_f}{v_0 c_0} \ll k_x \ll \overline{k}_{\rm F}, \\ \left(\frac{v_0 c_0 k_x}{\Lambda_f}\right)^{\frac{(N_c^2-1)}{\pi^2 N_c N_f} v_0 \log(1/v_0)} & \frac{\Lambda_f}{v_0} \ll k_x \ll \frac{\Lambda_f}{v_0 c_0}, \\ \left(\frac{v_0 \sqrt{c_0} k_x}{\Lambda_f}\right)^{\frac{2(N_c^2-1)}{\pi^2 N_c N_f} v_0 \log(1/v_0)} & \frac{\Lambda_f}{v_0 c_0} e^{-\ell_{\rm SC}} \ll k_x \ll \frac{\Lambda_f}{v_0}. \end{cases} \tag{4.122}$$

For $k_x \gg \frac{\Lambda}{v_0 c_0} e^{-\ell_{\rm SC}}$, the shape of the momentum-dependent slope coincides with that of the renormalized FS found in the ideal case without a superconducting instability. This is because in this region of the momentum space, the interaction between the electrons and the spin fluctuations is either weak or absent. Therefore resolving the momentum-dependent profile of the spectral weight and lifetime of the quasiparticles can be achieved at intermediate frequencies. Furthermore, the infinite quasiparticle lifetime for electrons is a consequence of the decoupling of the electrons from the spin fluctuations in this region.

(*ii*) If the momentum of the electron lies within the window $\frac{\Lambda_f}{v_0} e^{-\ell_{\rm SC}} \ll k_x \ll \frac{\Lambda_f}{v_0 c_0} e^{-\ell_{\rm SC}}$, the single-particle excitations acquire a finite quasiparticle lifetime. This is a consequence of the frequency dependent self-energy. The frequency dependence arises because spin fluctuations remain strongly coupled with electrons down to the frequency scale at which the electrons are probed. The spectral function in Eq. (4.102) is characterized by the quasiparticle lifetime and spectral weight in the $\omega(\vec{k})/\Lambda_f \ll 1$ and $\ell_0 \gg 1$ limits:

$$\tau_1(\vec{k})^{-1} = \frac{\pi}{2} \frac{\sqrt{N_c^2 - 1}}{\sqrt{\ell_0} \log(\ell_0)} \omega(\vec{k}), \tag{4.123}$$

$$\mathcal{Z}_1(\vec{k}) = \left(\frac{\omega(\vec{k})}{\Lambda_f}\right)^{\frac{\sqrt{2}(N_c^2-1)}{\pi\sqrt{N_c N_f}} \sqrt{\frac{v_0}{\log(1/v_0)}}}, \tag{4.124}$$

respectively. The renormalized electronic dispersion is given by

$$\omega(\vec{k}) \approx \mathfrak{V}_{\rm F}^{(1)}(k_x) \left[\widehat{v}_1(k_x) k_x + k_y\right], \tag{4.125}$$

with the renormalized Fermi velocity and slope,

$$\mathfrak{V}_{\rm F}^{(1)}(k_x) = \left(\frac{v_0 k_x}{\Lambda_f}\right)^{-\frac{(N_c^2-1)}{4\pi^2 N_c N_f} v_0 \log(1/v_0)}, \tag{4.126}$$

$$\widehat{v}_1(k_x) = v_0 \left(\frac{v_0 k_x}{\Lambda_f}\right)^{\frac{(N_c^2-1)}{\pi^2 N_c N_f} v_0 \log(1/v_0)}. \tag{4.127}$$

The scattering rate $1/\tau_1(\vec{k})$ in Eq. (4.123) is proportional to the renormalized energy $\omega(\vec{k})$. This non-Fermi liquid behavior is in stark contrast with the one expected from Fermi-liquid theory, in which the scattering rate decreases much faster than the energy

in the low-energy limit. As a result, the incoherence parameter introduced in Eq. (4.103) saturates to a nonzero value,

$$\mathscr{W}_1(k_x, \omega(\vec{k})) \sim \frac{\pi}{2} \frac{\sqrt{N_c^2 - 1}}{\sqrt{\ell_0} \log(\ell_0)}, \tag{4.128}$$

in the $\omega(\vec{k}) \to 0$ limit. The incoherence parameter decreases with increasing ℓ_0. The influence of the spin fluctuations on the electrons becomes weaker for systems with smaller $v_0 \sim 1/\ell_0$ because the Landau damping is stronger in systems with FS's closer to the perfect nesting. The fact that Eq. (4.128) is independent of the energy implies a qualitative deviation from Fermi-liquids despite the fact that in the $v_0 \ll 1$, the quasiparticle excitations with momentum $\frac{\Lambda_f}{v_0} e^{-\ell_{\rm SC}} \ll k_x \ll \frac{\Lambda_f}{v_0 c_0} e^{-\ell_{\rm SC}}$ have parametrically large lifetimes. This deviation from Fermi-liquid theory is attributed to the strong interaction between the electrons in this region of the momentum space and the spin fluctuations. The linear scaling of the scattering rate with the energy is analogous to that of marginal Fermi liquids [152–154].

(*iii*) For momentum $k_x \ll \frac{\Lambda_f}{v_0} e^{-\ell_{\rm SC}}$, the situation is similar to the previous case. The scattering rate and the spectral weight are still given by Eqs. (4.123) and (4.124), respectively. The only difference is the renormalized energy dispersion: $\omega(\vec{k})$ is determined by the self-consistent equation

$$\omega(\vec{k}) \left(\frac{\Lambda_f}{\omega(\vec{k})} \right)^{\frac{\sqrt{N_c^2-1}}{\sqrt{\ell_0}\log(\ell_0)}} = \left(\frac{\omega(\vec{k})}{\Lambda_f} \right)^{-\frac{3}{8\ell_0}} \left\{ v_0 \left(\frac{\omega(\vec{k})}{\Lambda_f} \right)^{\frac{1}{\ell_0}} k_x + k_y \right\}. \tag{4.129}$$

The dispersion is modified because in this momentum region, $\omega \gtrapprox \omega_{\rm SC}$ is sufficiently large compared to the momentum-dependent IR cutoffs of the one-loop and two-loop fermion self-energy corrections and these depend only on frequency.

The discussions in (*i*), (*ii*) and (*iii*) summarize how the electronic spectral function evolves as one approaches the hot spots parallel to the FS at a nonzero energy above the superconducting gap. Probing electrons above the superconducting transition temperature allows one to find signatures of a non-Fermi liquid normal state even though the ground state is a superconducting state. Far away from the hot spots in the momentum space region described in (*i*), the spin fluctuations decouple from the electrons at energies larger than the probing energy $\omega \gtrapprox \omega_{\rm SC}$, and the spectral function exhibits a well-defined quasiparticle peak. The energy scale at which the spin fluctuations decouple from the electrons depends on the momentum of the electron. This gives rise to a momentum-dependent spectral weight, which decays algebraically as the hot spots are approached. In the intermediate region of momentum discussed in (*ii*), the spin fluctuations remain coupled to the electrons down to the probing energy $\omega \gtrapprox \omega_{\rm SC}$ through the one-loop process. This gives rise to a frequency-dependent self-energy with a scattering rate that is linearly proportional to the energy. The two-loop process is suppressed at energy scales higher than the probing energy. In the region of momentum closest to the hot spots that is analyzed in (*iii*) , all quantum corrections survive down to the probing energy, and the self-energy acquires non-trivial

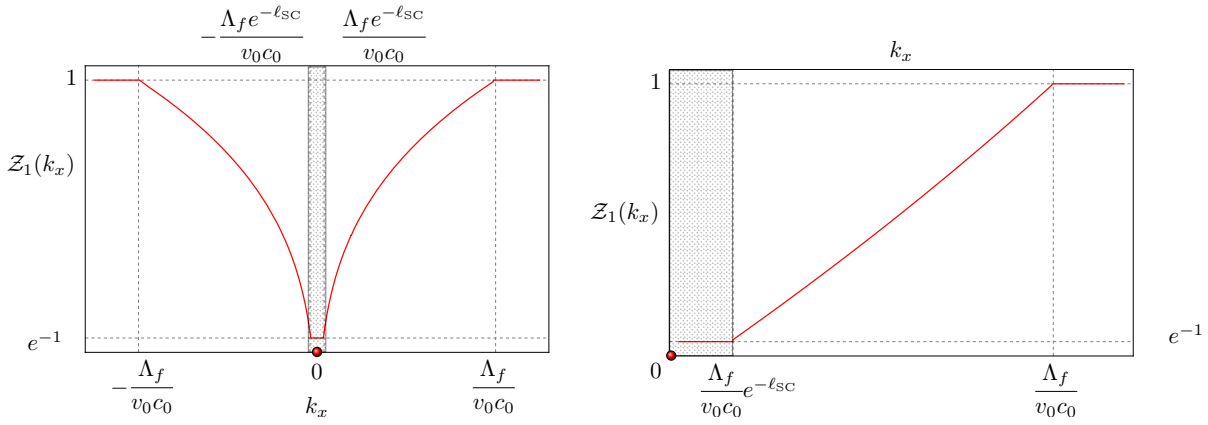

Figure 4.15: Momentum profile of the quasiparticle weight. The plot in the right panel is in logarithmic scale. The dotted regions is where we lose resolution on the momentum dependence of the quasiparticle weight.

frequency dependences from both one-loop and two-loop corrections. The non-Fermi liquid nature of the normal state manifests itself as the linear scattering rate of 'high-energy' electrons in regions (*ii*) and (*iii*).

4.7 Summary

In this chapter we have considered the low-energy theory of the AFM quantum critical metal that incorporates all gapless electronic modes. We devised a functional RG scheme that allows us to keep track of the momentum-dependent universal low-energy data of the electrons across the FS. We have shown that the functional RG scheme is analytically tractable if the bare coupling functions defined in the UV depend on momentum weakly.

We determined the shape of the renormalized FS, Fermi velocity and quasiparticle weight as a function of the momentum along the renormalized FS. Our results shed light on how the electrons on the FS lose their coherence as the interaction between the collective mode and the electrons becomes stronger as the hot spots are approached. Our results reveal qualitatively different behaviors exhibited by the electrons that depend on their momentum along the FS. Electrons far away from the hot spots (cold electrons) are not significantly renormalized by spin fluctuations. Electrons in an intermediate region (lukewarm electrons) are renormalized by spin fluctuations up to energy scales that depend on the momenta of the electrons. This gives rise to the quasiparticle weight that decays in a power-law fashion as the hot spots are approached along the FS. Electrons in the region closest to the hot spot (hot electrons) remain coupled with spin fluctuations down to the low energy scale at which the dynamical nesting of the FS at the hot spots becomes significant. This gives rise to a superlogarithmic decay in the quasiparticle weight.

The energy window in which these features are testable through ARPES experiments depends on the superconducting transition temperature. Even if the ground state is a superconducting state, the non-Fermi liquid nature of the normal state can be extracted from the electronic spectral function at energy scales larger than the superconducting gap. At nonzero

energy, the electrons near the hot spots acquire a finite lifetime that scales inversely with energy. This is a stark deviation from conventional Fermi-liquids, where the quasiparticle lifetime is inversely proportional to the square of the quasiparticle energy measured from the Fermi level. Therefore, there are no well-defined quasiparticles near the hot spots. Our predictions can be tested in ARPES experiments on materials whose FS are close to nesting. In particular, our results are in qualitative agreement with ARPES experiments done in the electron-doped cuprate superconductor $Nd_{2-x}Ce_xCuO_{4\pm\delta}$, which show a reduced quasiparticle weight close to the hot spots and a scattering rate that scales almost linearly in energy [31, 34].

5 | Conclusion and Outlook

In this thesis we have considered the effective field theory describing the universal low-energy physics of the commensurate antiferromagnetic quantum critical metal that is relevant to layered materials such as electron-doped cuprates, heavy-fermion compounds and iron pnictides.

The nonperturbative approach devised in this thesis consists of a scaling ansatz motivated from the controlled perturbative analysis of the theory close to its upper critical dimension [148] and a resummation of an infinite number of quantum corrections which cannot be captured by perturbative approaches. The nonperturbative solution is asymptotically exact in two dimensions due to a dynamically generated small parameter associated with the quasi-local nature of the non-Fermi-liquid metallic state realized at the transition [142, 148]. In two dimensions, our results deviate from those obtained by previous theoretical works [131–134, 186, 215]. In particular we predict the dynamical critical exponent $z = 1$ at the low-energy fixed point, which differs from previous approaches that invariably predicted $z \neq 1$. Some qualitative features, however, are shared with those approaches. Amongst these are the prediction of an emergent nesting of the Fermi surface at the hot spots on the Fermi surface and a vanishing quasiparticle weight at these points. Comparing our predictions with known experiments on electron-doped cuprates [31–34], we find qualitative agreement, although experiments with higher precision are required for a more quantitative comparison.

The nonperturbative approach used in two dimensions has been extended to dimensions between two and three. We have explicitly shown that critical exponents vary smoothly with dimension. However, the perturbative analysis valid near the upper critical dimension fails to capture the full scaling form of the physical observables. This is attributed to an emergent noncommutativity between the low energy limit and the limit in which the physical dimensions are approached. Using the effective field theory for the antiferromagnetic quantum critical metal as a model theory, we have exposed the merits and subtleties of renormalization group schemes based on dimensional regularization. It reveals the subtleties that arise in extrapolating results obtained from ϵ expansions to physical dimensions.

The nonperturbative approach we constructed in this thesis is applicable to the antiferromagnetic quantum critical metal. However, it is plausible that there is a class of effective field theories relevant to condensed matter systems that can be addressed with a similar nonperturbative approach. The results of this thesis adds to the small number of well-understood non-Fermi liquid metallic states and opens the door to the study of their equilibrium and out-of-equilibrium properties. Our work also provides a platform to study instabilities of the non-Fermi liquid metal towards a superconducting state.

Understanding the interplay between superconductivity the critical spin fluctuations calls for a low-energy theory that incorporates electrons that reside away from the hot spots on

the Fermi surface. In this thesis we have constructed a functional renormalization group scheme that incorporates the intrinsic momentum dependence of the interaction between the collective mode and the electrons. This scheme provides a theoretical framework for metallic states with or without quasiparticles that are characterized by an infinite amount of data in the low-energy limit. In this approach it is found that the antiferromagnetic quantum critical metal in two dimensions host both non-Fermi-liquid-like and Fermi-liquid-like excitations along the Fermi surface. The quasiparticle excitations of the metal are characterized by a quasiparticle weight that decays as the hot spots are approached along the Fermi surface. The momentum-dependence of the quasiparticle weight allows for a sharp distinction between the different physics displayed by low-energy electrons. In particular, a momentum independent quasiparticle weight close to unity distinguishes cold electrons from lukewarm ones, whose quasiparticle weight decays as a power-law in momentum. As the electrons go closer to the hot spots, the power-law decay in momentum of the quasiparticle weight crosses over to a superlogarithmic decay. We find qualitative agreement with measurements in electron-doped cuprates which show a decaying quasiparticle weight close to the hot spots on the Fermi surface [31, 34].

The formalism developed in this thesis opens the gate for a more quantitative study of the superconducting instability in the antiferromagnetic quantum critical. It also opens the gate for the future understanding of transport properties of the metal and its interaction with magnetic and non-magnetic impurities where all electrons on the Fermi surface become active in the long wavelength limit.

Appendix A | Proof of the upper bound for general diagrams

In this appendix, we prove the upper bound in Eq. (2.8) for general diagrams arising as quantum corrections to the action in Eq. (3.18) in $2 \leq d < 3$. We do so by assuming that the fully dressed boson propagator is given by Eq. (3.21) with the collective mode's velocity given by Eq. (3.28) and that the latter satisfies the hierarchy of velocities $v \ll c(v) \ll 1$ in the small v limit.

Since the boson propagator is already fully dressed, we do not need to consider boson self-energy corrections within diagrams. The magnitude of a diagram is not simply determined by the number of vertices because in the small v limit patches of the FS become locally nested, and the collective mode loses its dispersion. When a loop is formed out of dispersionless bosons and nested fermions, the loop momentum along the FS becomes unbounded. For small but nonzero v and $c(v)$, the divergent integral is cut off by a scale which is proportional to $1/v$ or $1/c(v)$. This gives rise to enhancement factors of $1/v$ or $1/c(v)$. Since the velocity along the co-dimensional directions of the FS are set to one, these enhancements come *only* from integrations over the two-dimensional spatial momentum, and therefore these are independent of the space dimensionality. Our goal is to compute the upper bound of the enhancement factors for general diagrams in dimensions $2 \leq d < 3$. A diagram is maximally enhanced when all the patches of the FS involved in the diagram are nested. Since the patches are nested pairwise (1 and 3, and 2 and 4) in the small v limit, it is enough to consider diagrams that are made of patches 1 and 3 to compute the upper bound without loss of generality. Diagrams which involve all four patches are generally smaller in magnitude than those that involve only 1 and 3 or 2 and 4 for fixed L, L_f, E, where L is the total number of loops, L_f is the number of fermion loops and E is the number of external legs. We first show that Eq. (2.8) holds for an example. Then we provide a general proof in the following section. In what follows we use the fact that, for the theory under consideration, $V = 2L + E - 2$, where V is the number of vertices in the diagram. We further denote by $\mathcal{G}(L, L_f, E)$ a diagram with L loops, L_f fermion loops and E external lines.

A.1 An Example

The diagram in A.1(a) is a fermion self-energy with one fermion loop and three other loops, which we call "mixed loops". For simplicity, we set the external momentum to zero. This does not affect the enhancement factors of $1/c(v)$ and $1/v$ which originate from large internal momenta. We label the loop momenta as shown in A.1(b). With this choice, each mixed loop momentum p_i with $i = 1, 2, 3$ has a boson line that carries only p_i, and the fermion loop momentum p_4 has a fermion line that carries only p_4. These four propagators, denoted

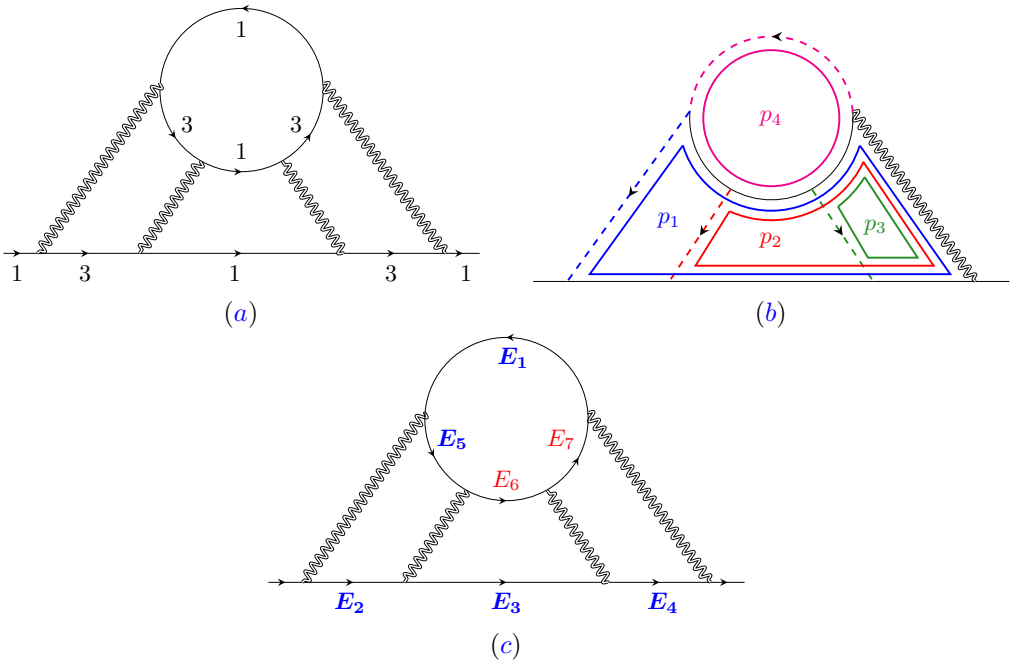

Figure A.1: (a) A four-loop diagram with one fermion loop. The numbers next to the fermion lines represent the patch indices. (b) The four exclusive propagators are denoted as dashed lines. The remaining propagators represent the connected tree diagram. Loops (closed solid lines) are chosen such that each loop momentum goes through only one of the exclusive propagators. (c) The seven internal fermion propagators whose energies are denoted as E_l with $1 \leq l \leq 7$. $E_1, E_2, .., E_5$ are used as new integration variables along with $p_i^{'} = c(v)p_{i,x}$ with $i = 1, 2, 3$, as discussed in the text.

in A.1(b) by dashed lines, are called "exclusive propagators". In the next section, we show that it is always possible to find such exclusive propagators for every loop momentum in a general diagram. The diagram in A.1(a) is written as

$$\begin{aligned}\mathcal{G}(4,1,2) \sim v^4 \int \prod_{r=1}^{4} \mathrm{d}p_r \left[\prod_{j=1}^{3} \frac{1}{|\mathbf{P}_j|^{d-1} + c(v)^{d-1}(|p_{j,x}|^{d-1} + |p_{j,y}|^{d-1})}\right] \left[\frac{1}{\boldsymbol{\Gamma}\cdot\mathbf{P}_4 + \gamma_{d-1}E_1}\right] \\ \times \left[\frac{1}{\boldsymbol{\Gamma}\cdot\mathbf{P}_1 + \gamma_{d-1}E_2}\right] \left[\frac{1}{\boldsymbol{\Gamma}\cdot(\mathbf{P}_1+\mathbf{P}_2) + \gamma_{d-1}E_3}\right] \left[\frac{1}{\boldsymbol{\Gamma}\cdot(\mathbf{P}_1+\mathbf{P}_2+\mathbf{P}_3) + \gamma_{d-1}E_4}\right] \qquad \text{(A.1)} \\ \times \left[\frac{1}{\boldsymbol{\Gamma}\cdot(\mathbf{P}_4-\mathbf{P}_1) + \gamma_{d-1}E_5}\right] \left[\frac{1}{\boldsymbol{\Gamma}\cdot(\mathbf{P}_4-\mathbf{P}_1-\mathbf{P}_2) + \gamma_{d-1}E_6}\right] \left[\frac{1}{\boldsymbol{\Gamma}\cdot(\mathbf{P}_4-\mathbf{P}_1-\mathbf{P}_2-\mathbf{P}_3) + \gamma_{d-1}E_7}\right] \\ \times \frac{1}{|\mathbf{P}_1+\mathbf{P}_2+\mathbf{P}_3|^{d-1} + c(v)^{d-1}(|p_{1,x}+p_{2,x}+p_{3,x}|^{d-1} + |p_{1,y}+p_{2,y}+p_{3,y}|^{d-1})},\end{aligned}$$

where we have used the notation $1/\mathbb{A} \equiv \mathbb{A}^{-1}$ to denote the inverse of the matrix $\mathbb{A}$, $p_r = (\mathbf{P}_r, \vec{p}_r)$ is the set of internal frequency and momenta, and E_i represents the energy of the

fermion in the ith fermion propagator as denoted in A.1(c),

$$\begin{aligned}
E_1 &= vp_{4,x} + p_{4,y},\\
E_2 &= vp_{1,x} - p_{1,y},\\
E_3 &= v(p_{1,x} + p_{2,x}) + (p_{1,y} + p_{2,y}),\\
E_4 &= v(p_{1,x} + p_{2,x} + p_{3,x}) - (p_{1,y} + p_{2,y} + p_{3,y}),\\
E_5 &= v(p_{4,x} - p_{1,x}) + (p_{1,y} - p_{4,y}),\\
E_6 &= v(p_{4,x} - p_{1,x} - p_{2,x}) - (p_{1,y} + p_{2,y} - p_{4,y}),\\
E_7 &= v(p_{4,x} - p_{1,x} - p_{2,x} - p_{3,x}) + (p_{1,y} + p_{2,y} + p_{3,y} - p_{4,y}).
\end{aligned} \tag{A.2}$$

Since frequency and co-dimensional momenta integrations are not affected by v and $c(v)$, we focus on the two-dimensional spatial components of momenta from now on. Our aim is to change the variables for the internal momenta so that the enhancement factors of $1/v$ and $1/c(v)$ become manifest. As our first three new variables we choose $p_j^{'} \equiv c(v)p_{j,x}$ with $1 \leq j \leq 3$. The last five variables are chosen to be $p_{l+3}^{'} \equiv E_l$ with $1 \leq l \leq 5$. We write the transformation between the new variables and the old ones as

$$\begin{pmatrix} p_1^{'} \\ p_2^{'} \\ \vdots \\ p_8^{'} \end{pmatrix} = \begin{pmatrix} \frac{c(v)}{v}\mathbb{I}_{3\times 3} & 0 \\ \widetilde{\mathbb{A}} & \widetilde{\mathbb{V}} \end{pmatrix} \begin{pmatrix} vp_{1,x} \\ vp_{2,x} \\ vp_{3,x} \\ vp_{4,x} \\ p_{1,y} \\ p_{2,y} \\ p_{3,y} \\ p_{4,y} \end{pmatrix}, \tag{A.3}$$

where the matrices $\widetilde{\mathbb{A}}$ and $\widetilde{\mathbb{V}}$ are written as

$$\widetilde{\mathbb{A}} = \begin{pmatrix} 0 & 0 & 0 \\ 1 & 0 & 0 \\ 1 & 1 & 0 \\ 1 & 1 & 1 \\ -1 & 0 & 0 \end{pmatrix}, \quad \widetilde{\mathbb{V}} = \begin{pmatrix} 1 & 0 & 0 & 0 & 1 \\ 0 & -1 & 0 & 0 & 0 \\ 0 & 1 & 1 & 0 & 0 \\ 0 & -1 & -1 & -1 & 0 \\ 1 & 1 & 0 & 0 & -1 \end{pmatrix}, \tag{A.4}$$

and $\mathbb{I}_{3\times 3}$ is the 3×3 identity matrix. For non-zero v and $c(v)$, the change of variables is nondegenerate, and the Jacobian of the transformation is $[2c(v)^3 v]^{-1}$. We show in the following section that such a nondegenerate choice is always possible for general diagrams. A simple mnemonic is that each fermion loop contributes a factor of $1/v$ because of the nesting of the FS at the hot spots in the small v limit, while each mixed loop contributes a factor of $1/c(v)$ because of the vanishing boson velocity.

In the new coordinates, the momentum integration in Eq. (A.1) becomes

$$\mathcal{G}(4,1,2) \sim \frac{v^3}{c(v)^3} \int \prod_{i=1}^{8} \mathrm{d}p_i^{'} \left[\prod_{j=1}^{3} \frac{1}{\cdots + |p_j^{'}|^{d-1} + \mathcal{O}[c(v)^{d-1}]}\right] \left[\prod_{l=4}^{8} \frac{1}{\cdots + \gamma_{d-1} p_l^{'}}\right] \widetilde{R}[p^{'}], \tag{A.5}$$

where $\widetilde{R}[p']$ includes the propagators that are not explicitly shown and the ellipsis denote the frequency terms that are unimportant in the determination of the diagram's upper bound. Now, we can safely take the small $c(v)$ limit inside the integrand, because every momentum component has at least one propagator which guarantees that the integrand decays at least as $1/p'_j$ in the large momentum limit. Therefore, the integrations are UV convergent up to potential logarithmic divergences. To leading order in small v, the diagram scales, at most, as

$$\mathcal{G}(4,1,2) \sim \left(\frac{v}{c(v)}\right)^3, \tag{A.6}$$

up to potential logarithmic corrections in v. It is noted that the upper bound as a function of v and $c(v)$ is independent of the space dimension.

A.2 General upper bound

Here we provide a general proof for the upper bound, by generalizing the example discussed in the previous section. We consider a general L-loop diagram that includes only fermions from patches 1 and 3:

$$\begin{aligned}\mathcal{G}(L,L_f,E) \sim v^{\frac{2L+E-2}{2}} \int \prod_{r=1}^{L} \mathrm{d}p_r \left[\prod_{l=1}^{I_f} \frac{1}{\mathbf{\Gamma}\cdot\mathbf{K}_l + \gamma_{d-1}\left[v k_{l,x} + (-1)^{\frac{n_l-1}{2}} k_{l,y}\right]}\right] \\ \times \left[\prod_{m=1}^{I_b} \frac{1}{|\mathbf{Q}_m|^{d-1} + c(v)^{d-1}(|q_{m,x}|^{d-1} + |q_{m,y}|^{d-1})}\right].\end{aligned} \tag{A.7}$$

Here, I_f (I_b) is the numbers of internal fermion (boson) propagators. $p_r = (\mathbf{P}_r, \vec{p}_r)$ is the set of internal momenta. $k_l = (\mathbf{K}_l, \vec{k}_l)$ [$q_m = (\mathbf{Q}_m, \vec{q}_m)$] represents the momentum that flows through the lth fermion (mth boson) propagator. These are linear combinations of the internal momenta and external momenta. The way k_l and q_m depend on p_r is determined by how we choose internal loops within a diagram. $n_l = 1, 3$ is the patch index for the lth fermion propagator. Since the frequency and co-dimensional momentum integrations are not affected by v and $c(v)$, we focus on the spatial components of momenta from now on.

It is convenient to choose loops in such a way that there exists a propagator exclusively assigned to each internal momentum. For this, we follow the procedure given in Sec. VI of Ref. [177]. For a given diagram, we cut internal propagators one by one. We continue cutting until all loops disappear while the diagram remains connected. First, we cut one fermion propagator in every fermion loop, which requires cutting L_f fermion lines. The remaining $L_m \equiv L - L_f$ loops, which we call mixed loops, can be removed by cutting boson propagators. After cutting L lines in total, we are left with a connected tree diagram. Now we glue the propagators back one by one to restore the original L-loop diagram. Every time we glue one propagator, we assign one internal momentum such that it goes through the propagator that is just glued back and the connected tree diagram only. This guarantees that the propagator depends only on the internal momentum which is associated with the loop that is just formed by gluing. In gluing L_f fermion propagators, the associated internal momenta go through the fermion loops. The L_m mixed loops necessarily include both fermion and

boson propagators. After all propagators are glued back, L internal momenta are assigned in such a way that for every loop momentum there is one exclusive propagator.

With this choice of loops, Eq. (A.7) is written as

$$\mathcal{G}(L, L_f, E) \sim v^{\frac{2L+E-2}{2}} \int \prod_{r=1}^{L} \mathrm{d}p_{r,x} \mathrm{d}p_{r,y} \left[\prod_{j=1}^{L_m} \frac{1}{\cdots + c(v)^{d-1}|p_{j,x}|^{d-1} + c(v)^{d-1}|p_{j,y}|^{d-1}} \right] \times \left[\prod_{l=1}^{I_f} \frac{1}{\cdots + \gamma_{d-1} E_l(p)} \right] R[p]. \tag{A.8}$$

Here, the ellipsis denote the frequency and co-dimensional momentum parts of the propagators that play the role of cutting any IR divergence in the integrations over the spatial momenta. Our focus is on the UV divergence that arises in the spatial momentum integrations in the limit of small v and $c(v)$. The first group in the integrand represents the exclusive boson propagators assigned to the L_m mixed loops. Each of the L_m boson propagators depends on only one internal momentum due to the exclusive nature of our choice of loops. The second group represents all fermion propagators. $E_l(p)$ is the energy of the fermion in the lth fermion propagator which is given by a linear superposition of $p_{r,x}$ and $p_{r,y}$. $R[p]$ represents the rest of the boson propagators that are not assigned as exclusive propagators.

Our strategy is to find a new basis for the loop momenta such that the divergences in the small v and $c(v)$ limit become manifest. The first L_m variables are chosen to be $c(v)p_{j,x}$ with $j = 1, 2, .., L_m$ while the remaining $2L - L_m$ variables are chosen among the $E_l(p)$. This is possible because $I_f \geq (2L - L_m)$ for diagrams with $E > 0$. We express $p_j^{'} \equiv c(v)p_{j,x}$ and $E_l(p)$ in terms of $vp_{r,x}$ and $p_{r,y}$ as

$$\begin{pmatrix} p_1^{'} \\ p_2^{'} \\ \vdots \\ p_{L_m}^{'} \\ E_1 \\ E_2 \\ \vdots \\ E_{I_f} \end{pmatrix} = \begin{pmatrix} \frac{c(v)}{v}\mathbb{I}_{L_m \times L_m} & 0 \\ \mathbb{A} & \mathbb{V} \end{pmatrix} \begin{pmatrix} vp_{1,x} \\ vp_{2,x} \\ \vdots \\ vp_{L_m,x} \\ vp_{L_m+1,x} \\ \vdots \\ vp_{L,x} \\ p_{1,y} \\ p_{2,y} \\ \vdots \\ p_{L,y} \end{pmatrix}. \tag{A.9}$$

Here $\mathbb{I}_{L_m \times L_m}$ is the $L_m \times L_m$ identity matrix. $A_{l,j} = (1/v)(\partial E_l/\partial p_{j,x})$ with $1 \leq l \leq I_f$ and $1 \leq j \leq L_m$. $\mathbb{V}$ is an $I_f \times (2L - L_m)$ matrix whose first $L - L_m$ columns are given by $V_{l,i-L_m} = (1/v)(\partial E_l/\partial p_{i,x})$ with $L_m + 1 \leq i \leq L$ and the remaining L columns are given

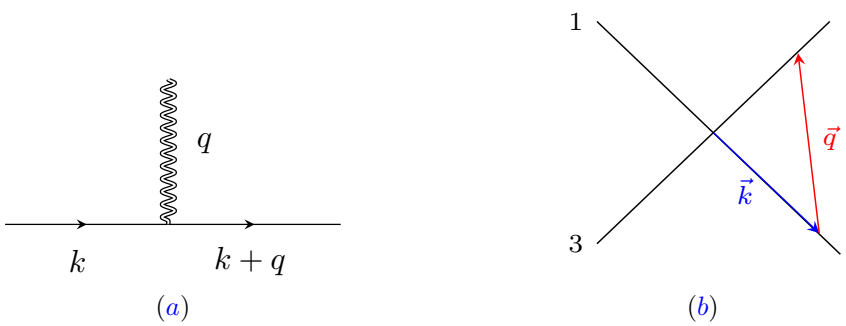

Figure A.2: (*a*) The vertex that describes the process where a boson is absorbed by a fermion. (*b*) For a boson momentum $\vec{q}$, there exists a unique $\vec{k}$ such that $\varepsilon_1(\vec{k}; v) = \varepsilon_3(\vec{k} + \vec{q}; v) = 0$ for $v \neq 0$. The solid lines depict the local FS at hot spots $n = 1$ and $n = 3$.

by $V_{l,i+(L-L_m)} = (\partial E_l / \partial p_{i,y})$ with $1 \leq i \leq L$. Now we focus on the lower right-hand corner of the transformation matrix which governs the relation between $\vec{E}^T \equiv (E_1, E_2, .., E_{I_f})$ and $\vec{P}^T \equiv (vp_{L_m+1,x}, .., vp_{L,x}, p_{1,y}, .., p_{L,y})$ when $p_{j,x} = 0$ for $1 \leq j \leq L_m$,

$$\vec{E} = \mathbb{V}\vec{P}. \tag{A.10}$$

The matrix $\mathbb{V}$ can be viewed as a collection of $2L - L_m$ column vectors, each of which have I_f components. We first show that the $2L - L_m$ column vectors are linearly independent.

If the column vectors were not linearly independent, there would exist a nonzero $\vec{P}$ such that $\mathbb{V}\vec{P} = 0$. This implies that there exists at least a one-parameter family of x and y momenta in the L_f fermion loops and y momenta in the L_m mixed loops such that all internal fermions lie on the FS (i.e., $\vec{E} = \vec{0}$). However, this is impossible for the following reason. For $v \neq 0$, a momentum on an external boson leg uniquely fixes the internal momenta on the two fermion lines attached to the boson line if both fermions are required to have zero energy. This is illustrated in Fig. A.2. Similarly, a momentum on an external fermion leg fixes the momenta on the adjacent internal fermion and boson lines if the internal fermion is required to have zero energy and only the y component of momentum is allowed to vary in the mixed loops. Once the momenta on the internal lines attached to the external lines are fixed, those internal lines in turn fix the momenta of other adjoining internal lines. As a result, all internal momenta are successively fixed by external momenta if we require that $E_l = 0$ for all l. Therefore, there cannot be a nontrivial $\vec{P}$ that satisfies $\mathbb{V}\vec{P} = 0$. This implies that the column vectors in $\mathbb{V}$ must be linearly independent.

Since $\mathbb{V}$ is made of $(2L - L_m)$ independent column vectors, it necessarily includes $(2L - L_m)$ independent row vectors. Let the l_kth rows with $k = 1, 2, .., (2L - L_m)$ be the set of rows that are linearly independent, and $\widetilde{\mathbb{V}}$ be a $(2L - L_m) \times (2L - L_m)$ invertible matrix made of these rows. We choose $p'_{L_m+k} \equiv E_{l_k}$ with $k = 1, 2, .., (2L - L_m)$ as the remaining $(2L - L_m)$ integration variables. The transformation between the original $2L$ momentum

variables and the new variables is given by

$$\begin{pmatrix} p_1^{'} \\ p_2^{'} \\ \vdots \\ p_{2L}^{'} \end{pmatrix} = \begin{pmatrix} \frac{c(v)}{v}\mathbb{I}_{L_m\times L_m} & 0 \\ \widetilde{\mathbb{A}} & \widetilde{\mathbb{V}} \end{pmatrix} \begin{pmatrix} vp_{1,x} \\ vp_{2,x} \\ \vdots \\ vp_{L,x} \\ p_{1,y} \\ p_{2,y} \\ \vdots \\ p_{L,y} \end{pmatrix}, \tag{A.11}$$

where $\widetilde{\mathbb{A}}$ is a $(2L - L_m) \times L_m$ matrix made of the collection of the l_kth rows of $\mathbb{A}$ with $k = 1, 2, .., (2L - L_m)$. The Jacobian of the transformation is given by $Y^{-1}c(v)^{-L_m}v^{-L_f}$. Here, $Y = |\det \widetilde{\mathbb{V}}|$ is a constant independent of v and $c(v)$, which is nonzero because $\widetilde{\mathbb{V}}$ is invertible.

In the new variables, Eq. (A.8) becomes

$$\begin{aligned} \mathcal{G}(L, L_f, E) \sim v^{\frac{E-2}{2}+L-L_f} c(v)^{-L_m} \int \prod_{i=1}^{2L} \mathrm{d}p_i^{'} \left[\prod_{j=1}^{L_m} \frac{1}{\cdots + |p_j^{'}|^{d-1} + \mathcal{O}[c(v)^{d-1}]}\right] \\ \times \left[\prod_{l=L_m+1}^{2L} \frac{1}{\cdots + \gamma_{d-1} p_l^{'}}\right] \widetilde{R}[p^{'}]. \end{aligned} \tag{A.12}$$

Every component of the loop momenta has at least one propagator which guarantees that the integrand decays at least as $1/p_l^{'}$ in the large momentum limit. $\widetilde{R}[p^{'}]$ is the product of all remaining propagators. Therefore, the integrations over the new variables are convergent up to potentially logarithmic divergences. As a consequence, a general diagram is bounded from above by

$$I \sim v^{\frac{E-2}{2}} \left(\frac{v}{c(v)}\right)^{L-L_f}, \tag{A.13}$$

up to logarithmic corrections in v. Diagrams with large $(L - L_f)$ are systematically suppressed for $v \ll c(v)$. This bound can be checked explicitly for individual diagrams. We end by stressing the fact that Eq. (A.13) is independent of the space dimension because the boson propagator in Eq. (3.21) depends on q_x and q_y only through $c(v)\vec{q}$ and the velocities along the extra co-dimensions are fixed to one.

Appendix B | Regularization and RG Scheme

In this appendix we introduce the RG scheme used to analyze the low-energy universal features stemming from the minimal local action in Eq. (3.18) in dimensions $2 \leq d < 3$. In particular, the results presented in Chapter 2 follow from the $d = 2, N_c = 2$ and $N_f = 1$ case of the scheme we introduce in this appendix. Quantum corrections are computed with the self-consistent boson propagator in Eq. (3.21). Under the interaction-driven scaling, the Yukawa vertex is marginal in any dimension between two and three. As a result, we expect logarithmic divergences in this dimensional range. We regularize the theory by introducing two UV cutoffs: Λ in the frequency and co-dimensional momentum space that is $\mathrm{SO}(d-1)$ symmetric, and $\widetilde{\Lambda}$ in the original two-dimensional momentum subspace. We assume that these are comparable in magnitude. Notice that for $d = 2$, Λ acts as a cutoff on the frequency domain only. We add the following local counterterm to the action in Eq. (3.18) to make low-energy physical observables independent of the UV cutoff scales:

$$\begin{aligned} S_d^{\text{C.T.}} = &\sum_{n=1}^{4}\sum_{\sigma=1}^{N_c}\sum_{j=1}^{N_f}\int \mathrm{d}k\ \overline{\Psi}_{n,\sigma,j}(k)\left[iA_1\boldsymbol{\Gamma}\cdot\mathbf{K} + i\gamma_{d-1}\widetilde{\varepsilon}_n(\vec{k};v)\right]\Psi_{n,\sigma,j}(k) \\ &+ A_6\frac{i\beta_d\sqrt{v}}{\sqrt{N_f}}\sum_{n=1}^{4}\sum_{\sigma,\sigma'=1}^{N_c}\sum_{j=1}^{N_f}\int \mathrm{d}k\int \mathrm{d}q\ \overline{\Psi}_{\overline{n},\sigma,j}(k+q)\Phi_{\sigma\sigma'}(q)\gamma_{d-1}\Psi_{n,\sigma',j}(k). \end{aligned} \tag{B.1}$$

Here, $\widetilde{\varepsilon}_1(\vec{k};v) = A_2vk_x + A_3k_y$, $\widetilde{\varepsilon}_2(\vec{k};v) = -A_3k_x + A_2vk_y$, $\widetilde{\varepsilon}_3(\vec{k};v) = A_2vk_x - A_3k_y$, and $\widetilde{\varepsilon}_4(\vec{k};v) = A_3k_x + A_2vk_y$. The $A_i's$ are momentum-independent counterterm coefficients. Adding this counterterm action to Eq. (3.18) yields the renormalized action,

$$\begin{aligned} S_d^{\text{Ren}} = &\sum_{n=1}^{4}\sum_{\sigma=1}^{N_c}\sum_{j=1}^{N_f}\int \mathrm{d}k_B\ \overline{\Psi}_{n,\sigma,j;B}(k_B)\left[i\boldsymbol{\Gamma}\cdot\mathbf{K}_B + i\gamma_{d-1}\varepsilon_n(\vec{k}_B;v_B)\right]\Psi_{n,\sigma,j,B}(k_B) \\ &+ \frac{i\beta_d\sqrt{v_B}}{\sqrt{N_f}}\sum_{n=1}^{4}\sum_{\sigma,\sigma'=1}^{N_c}\sum_{j=1}^{N_f}\int \mathrm{d}k_B\int \mathrm{d}q_B\ \overline{\Psi}_{\overline{n},\sigma,j;B}(k_B+q_B)\Phi_{B;\sigma\sigma'}(q_B)\gamma_{d-1}\Psi_{n,\sigma',j;B}(k_B). \end{aligned} \tag{B.2}$$

The renormalized frequency, momenta, fields and velocity are related to the bare ones via the multiplicative relations:

$$\mathbf{K}_B = \frac{Z_1}{Z_3}\mathbf{K}, \quad \vec{k}_B = \vec{k}, \quad v_B = \frac{Z_2}{Z_3}v, \quad \Psi_B(k_B) = Z_\Psi^{\frac{1}{2}}\Psi(k), \quad \& \quad \Phi_B(k_B) = Z_\Phi^{\frac{1}{2}}\Phi(k), \tag{B.3}$$

where $Z_i = 1 + A_i$, $Z_\Psi = Z_3(Z_3/Z_1)^{d-1}$, $Z_\Phi = (Z_3/Z_1)^{2(d-1)}\left[Z_6^2/(Z_3Z_2)\right]$, and the field indices have been suppressed. The renormalized action gives rise to the quantum effective

action that can be expanded as

$$\mathbf{\Gamma}[\{\overline{\Psi},\Psi,\Phi\},v;\mu]=\sum_{m=0}^{\infty}\sum_{n=0}^{\infty}\mathbf{\Gamma}^{(2m,n)}[\{\overline{\Psi},\Psi,\Phi\},v;\mu], \tag{B.4}$$

where

$$\mathbf{\Gamma}^{(2m,n)}[\{\overline{\Psi},\Psi,\Phi\},v;\mu]=\left[\prod_{j=1}^{2m+n}\int \mathrm{d}k_j\right](2\pi)^{d+1}\delta\left(\sum_{j=1}^{m}k_j-\sum_{j=1+m}^{2m+n}k_j\right) \tag{B.5}$$
$$\times\,\mathit{\Gamma}^{(2m,n)}\left(k_1,\ldots,k_{2m+n-1},v;\mu\right)\overline{\Psi}(k_1)\cdots\overline{\Psi}(k_m)\Psi(k_{1+m})\cdots\Psi(k_{2m})\Phi(k_{1+2m})\cdots\Phi(k_{n+2m}).$$

Here, $\mathit{\Gamma}^{(2m,n)}\left(k_1,\ldots,k_{2m+n-1},v;\mu\right)$ denote the one-particle irreducible (1PI) vertex functions that implicitly depend on all discrete indices. The summation over these indices has been left implicit. The counterterm coefficients in Eq. (B.1) are fixed by the renormalization conditions imposed over the vertex functions:

$$\frac{1}{2i}\frac{\partial}{\partial\mathbf{K}^2}\mathrm{Tr}\left[(\mathbf{K}\cdot\mathbf{\Gamma})\mathit{\Gamma}^{(2,0)}_n(k)\right]\Big|_{|\mathbf{K}|=\mu,\vec{k}=0}=1+F_1(v;\widetilde{\Lambda};\Lambda;\mu),\qquad n=1,2,3,4, \tag{B.6}$$

$$\frac{1}{2i}\frac{\partial}{\partial k_x}\mathrm{Tr}\left[\gamma_{d-1}\mathit{\Gamma}^{(2,0)}_{n=1}(k)\right]\Big|_{|\mathbf{K}|=0,k_x=\mu,k_y=0}=v\left[1+F_2(v;\widetilde{\Lambda};\Lambda;\mu)\right], \tag{B.7}$$

$$\frac{1}{2i}\frac{\partial}{\partial k_y}\mathrm{Tr}\left[\gamma_{d-1}\mathit{\Gamma}^{(2,0)}_{n=1}(k)\right]\Big|_{|\mathbf{K}|=0,k_x=0,k_y=\mu}=1+F_3(v;\widetilde{\Lambda};\Lambda;\mu), \tag{B.8}$$

$$\frac{1}{2}\mathrm{Tr}\left[\gamma_{d-1}\mathit{\Gamma}^{(2,1)}_{n}(k,q)\right]\Big|_{q=0,|\mathbf{K}|=\mu,\vec{k}=0}=1+F_4(v;\widetilde{\Lambda};\Lambda;\mu),\qquad n=1,2,3,4, \tag{B.9}$$

which follow from a minimal subtraction scheme. Here, we have left implicit the dependence of the vertex function on v. μ is an energy scale at which the physical observables are measured and the $F_i(v;\widetilde{\Lambda};\Lambda;\mu)$ are functions that vanish in the small v limit and are, in principle, dimension-dependent. These functions become independent of the UV scales $\widetilde{\Lambda}$ and Λ in the $\widetilde{\Lambda}/\mu\gg 1$ and $\Lambda/\mu\gg 1$ limits. The conditions in Eqs. (B.6) to (B.8) fix the fermion two-point function at the $n=1$ hot spot. These also fix the two-point function of fermions at the other three hot spots by the C_4 symmetry of the theory. Finally, Eq. (B.9) fixes the interaction vertex at each hot spot.

Since the bare quantities are independent of the running energy scale μ, the 1PI vertex functions obey the RG equation for any fixed μ:

$$\left[\sum_{i=1}^{2m+n-1}\left(z\mathbf{K}_i\cdot\nabla_{\mathbf{K}_i}+\vec{k}_i\cdot\nabla_{\vec{k}_i}\right)-\beta_v\frac{\partial}{\partial v}+m\left(2\eta_\Psi-(d+2)\right)+n\left(\eta_\Phi-d\right)\right.$$
$$\left.+(2m+n-1)(2+z(d-1))\right]\mathit{\Gamma}^{(2m,n)}(\{k_i\},v;\mu)=0, \tag{B.10}$$

which is obtained by combining the fact that, under the interaction-driven scaling, the vertex functions have engineering scaling dimension

$$[\mathit{\Gamma}^{(2m,n)}(\{k_i\},v;\mu)]=-md-n+d+1 \tag{B.11}$$

and that the bare vertex functions are related to the renormalized ones via

$$\Gamma_B^{(2m,n)}[\{k_{i,B}, v_B; \Lambda, \widetilde{\Lambda}\}] = \left(\frac{Z_3}{Z_1}\right)^{(d-1)(2m+n-1)} Z_\Psi^{-m} Z_\Phi^{-\frac{n}{2}} \Gamma^{(2m,n)}(\{k_i\}, v; \mu). \tag{B.12}$$

The dynamical critical exponent, the beta function for v, and the anomalous scaling dimensions of the fields appearing in Eq. (B.10) are given by

$$z = 1 - \frac{\mathrm{d}}{\mathrm{d}\log\mu} \log\left(\frac{Z_3}{Z_1}\right), \tag{B.13}$$

$$\beta_v = \frac{\mathrm{d}v}{\mathrm{d}\log\mu}, \tag{B.14}$$

$$\eta_{\Psi(\Phi)} = \frac{1}{2}\frac{\mathrm{d}\log Z_{\Psi(\Phi)}}{\mathrm{d}\log\mu}, \tag{B.15}$$

respectively. Here η_Ψ and η_Φ denote the deviations of the scaling dimensions of the fields from the ones predicted by the interaction-driven scaling (not the Gaussian scaling).

Appendix C | Derivation of the Self-Consistent Boson Self-Energy in $d = 2$

In this appendix, we present the derivation of the self-consistent boson self-energy for the theory in two dimensions with $N_c = 2$ and $N_f = 1$. In particular we derive Eqs. (2.6) and (2.7) from Eq. (2.9).

The one-loop quantum effective action of the boson generated from Fig. 2.2(*b*) is written as

$$\delta\mathbf{\Gamma}^{(0,2)}_{1\mathrm{L}} = \frac{1}{4}\int \mathrm{d}q\ \Pi^{1\mathrm{L}}(q)\ \mathrm{Tr}\left[\Phi(-q)\Phi(q)\right], \tag{C.1}$$

where the one-loop boson self-energy is defined as

$$\Pi^{1\mathrm{L}}(q_0,\vec{q}) = -\pi v\sum_{n=1}^{4}\int \mathrm{d}k\ \mathrm{Tr}\left[\gamma_1 G^{(0)}_n(k;v)\gamma_1 G^{(0)}_{\overline{n}}(k+q;v)\right], \tag{C.2}$$

with the bare fermion propagator $G^{(0)}_n(k;v)$ given by Eq. (2.10). The integration of the spatial momentum gives

$$\Pi^{1\mathrm{L}}(q_0,\vec{q}) = -\pi\int_{\mathbb{R}}\frac{\mathrm{d}k_0}{(2\pi)}\frac{(k_0+q_0)k_0}{|k_0+q_0||k_0|}. \tag{C.3}$$

The k_0 integration generates a linearly divergent mass renormalization which is removed by a counterterm, and a finite self-energy:

$$\Pi^{1\mathrm{L}}(q_0,\vec{q}) = |q_0|. \tag{C.4}$$

Since the one-loop self-energy depends only on frequency, we have to include higher-loop diagrams to generate a momentum-dependent quantum effective action, even though they are suppressed by powers of v compared to the one-loop self-energy. According to Eq. (2.8), the next leading diagrams are the ones with $L-L_f = 1$. Amongst the diagrams with $L-L_f = 1$, the only one that contributes to the momentum-dependent boson self-energy is shown in Fig. 2.2(*c*). In particular, the two-loop diagram that includes a fermion self-energy insertion does not contribute (See Appendix G for a proof). Since the two-loop diagram itself depends on the unknown dressed boson propagator, we need to solve the self-consistent equation for $D(q)$ in Eq. (2.9). Here, we first assume that the solution takes the form of Eq. (2.6) with

$v \ll c(v) \ll 1$ to compute the two-loop contribution, and show that the resulting boson propagator agrees with the assumed one. The two-loop self-energy reads

$$\Pi^{2\mathrm{L}}(q_0,\vec{q}) = -\frac{\pi^2 v^2}{2}\sum_{n=1}^{4}\int \mathrm{d}k \int \mathrm{d}p \left\{ \frac{1}{\Big[k_0+p_0-i\varepsilon_n(\vec{k}+\vec{p};v)\Big]\Big[k_0-i\varepsilon_{\overline{n}}(\vec{k};v)\Big]} \right. \\ \left. \times \frac{1}{\Big[k_0+q_0-i\varepsilon_n(\vec{k}+\vec{q};v)\Big]\Big[k_0+p_0+q_0-i\varepsilon_{\overline{n}}(\vec{k}+\vec{p}+\vec{q};v)\Big]} \right\} D(p) + \text{c.c.}. \tag{C.5}$$

Here, "c.c." denotes the complex conjugate. Straightforward integrations over $\vec{k}$ and k_0 give

$$\Pi^{2\mathrm{L}}(q_0,\vec{q}) = -\frac{\pi v}{8}\sum_{n=1}^{4}\int \mathrm{d}p \\ \times \left\{ \frac{|q_0|-|p_0|}{[(p_0+q_0)-i\varepsilon_{\overline{n}}(\vec{p}+\vec{q};v)][(q_0-p_0)-i\varepsilon_n(\vec{q}-\vec{p};v)]} \right\} D(p) + \text{c.c.}. \tag{C.6}$$

Since the frequency-dependent self-energy is already generated from the lower order one-loop graph in Fig. 2.2(*c*), we focus on the momentum-dependent part. This allows us to set the external frequency to zero to rewrite Eq. (C.6) as

$$\Pi^{2\mathrm{L}}(0,\vec{q}) = \frac{\pi v}{4}\sum_{n=1}^{4}\int \mathrm{d}p \left\{ \frac{|p_0|}{[ip_0+\varepsilon_{\overline{n}}(\vec{p}+\vec{q};v)][ip_0+\varepsilon_n(\vec{p}-\vec{q};v)]} \right\} D(p). \tag{C.7}$$

After subtracting the linearly divergent mass renormalization, $\Delta\Pi^{2\mathrm{L}}(\vec{q}) \equiv \Pi^{2\mathrm{L}}(0,\vec{q}) - \Pi^{2\mathrm{L}}(0,0)$ is UV finite, and given by

$$\Delta\Pi^{2\mathrm{L}}(\vec{q}) = \frac{\pi v}{4}\sum_{n=1}^{4}\int \mathrm{d}p \\ \times \left\{ \frac{|p_0|\mathcal{F}^{1\mathrm{L}(n)}(p_0,\vec{p},\vec{q};v)}{[p_0^2+\varepsilon_{\overline{n}}(\vec{p}+\vec{q};v)^2][p_0^2+\varepsilon_n(\vec{p}-\vec{q};v)^2][p_0^2+\varepsilon_{\overline{n}}(\vec{p};v)^2][p_0^2+\varepsilon_n(\vec{p};v)^2]} \right\} D(p), \tag{C.8}$$

where

$$\mathcal{F}^{1\mathrm{L}(n)}(p_0,\vec{p},\vec{q};v) = [p_0^2+\varepsilon_n(\vec{p};v)^2][p_0^2+\varepsilon_{\overline{n}}(\vec{p};v)^2][ip_0-\varepsilon_{\overline{n}}(\vec{p}+\vec{q};v)][ip_0-\varepsilon_n(\vec{p}-\vec{q};v)] \\ - [p_0^2+\varepsilon_{\overline{n}}(\vec{p}+\vec{q};v)^2][p_0^2+\varepsilon_n(\vec{p}-\vec{q};v)^2][ip_0-\varepsilon_{\overline{n}}(\vec{p};v)][ip_0-\varepsilon_n(\vec{p};v)]. \tag{C.9}$$

Now we consider the contribution of each hot spot separately. For $n=1$, the dependence on q_x is suppressed by v compared to the q_y-dependent self-energy. Therefore, we set $q_x = 0$ for small v. Furthermore, the p_y dependence in $D(p)$ can be safely dropped in the small $c(v)$ limit because $\varepsilon_1(\vec{p};v)$ and $\varepsilon_3(\vec{p};v)$ suppress the contributions from large p_y. Rescaling the momentum as $(p_0,p_x,p_y) \to |q_y|(p_0,p_x/c(v),p_y)$ followed by the integration over p_y, we obtain the contribution from the hot spot $n=1$,

$$\Delta\Pi^{2\mathrm{L}(1)}(\vec{q}) = \frac{v\pi}{8c(v)}|q_y|\int_{\mathbb{R}}\frac{\mathrm{d}p_0}{(2\pi)}\int_{\mathbb{R}}\frac{\mathrm{d}p_x}{(2\pi)} \\ \times \left\{ \frac{[1+p_0^2-3p_x^2w(v)^2]p_0^2}{[p_0^2+w(v)^2p_x^2][p_0^2+[w(v)p_x-1]^2]\{p_0^2+[w(v)p_x+1]^2\}} \frac{1}{|p_0|+|p_x|} \right\}, \tag{C.10}$$

Energy	Scaling	Dynamical Critical Exponent
$\lvert q_0\rvert \gg \widetilde{\Lambda}$	$\lvert q_0\rvert \sim \mathsf{c}_0\lvert\vec{q}\rvert$	$z=1$
$\frac{c(v)^2}{\mathsf{c}_0^2}\widetilde{\Lambda} \ll \lvert q_0\rvert \ll \widetilde{\Lambda}$	$\lvert q_0\rvert \sim \mathsf{c}_0^2\lvert\vec{q}\rvert^2/\widetilde{\Lambda}$	$z=2$
$\lvert q_0\rvert \ll \frac{c(v)^2}{\mathsf{c}_0^2}\widetilde{\Lambda}$	$\lvert q_0\rvert \sim c(v)(\lvert q_x\rvert + \lvert q_y\rvert)$	$z=1$

(*a*)

Energy	Scaling	Dynamical Critical Exponent
$\lvert q_0\rvert \gg \frac{c(v)}{\mathsf{c}_0}\widetilde{\Lambda}$	$\lvert q_0\rvert \sim \mathsf{c}_0\lvert\vec{q}\rvert$	$z=1$
$\widetilde{\Lambda} \ll \lvert q_0\rvert \ll \frac{c(v)}{\mathsf{c}_0}\widetilde{\Lambda}$	$\lvert q_0\rvert \sim \sqrt{c(v)\widetilde{\Lambda}(\lvert q_x\rvert + \lvert q_y\rvert)}$	$z=\frac{1}{2}$
$\lvert q_0\rvert \ll \widetilde{\Lambda}$	$\lvert q_0\rvert \sim c(v)(\lvert q_x\rvert + \lvert q_y\rvert)$	$z=1$

(*b*)

Table C.1: (*a*) The energy-dependent dynamical critical exponent for $\mathsf{c}_0 \gg c(v)$. (*b*) The energy-dependent dynamical critical exponent for $\mathsf{c}_0 \ll c(v)$.

where $w(v) \equiv v/c(v)$. In the integrand, we can not set $w(v) = 0$ because the integration over p_x is logarithmically divergent in the small $w(v)$ limit:

$$\begin{aligned}\Delta\Pi^{2\mathrm{L}(1)}(\vec{q}) = \frac{v}{16c(v)}|q_y| \int\limits_{\mathbb{R}} \frac{\mathrm{d}p_0}{(2\pi)} \frac{1}{1+p_0^2} \\ \times \left[2\log\left(\frac{1}{w(v)}\right) - 2p_0\cot^{-1}(p_0) + p_0^2\log\left(\frac{p_0^2}{1+p_0^2}\right) + \mathcal{O}[w(v)]\right].\end{aligned} \tag{C.11}$$

Finally, the integration over p_0 gives

$$\Delta\Pi^{2\mathrm{L}(1)}(\vec{q}) = \frac{|q_y|v}{16c}\left[\log\left(\frac{1}{w(v)}\right) - 1 + \mathcal{O}[w(v)]\right]. \tag{C.12}$$

In the small $w(v)$ limit, the first term dominates. Hot spot 3 generates the same term, and the contribution from hot spots 2 and 4 is obtained by replacing q_y with q_x. Summing over contributions from all the hot spots, we obtain

$$\Delta\Pi^{2\mathrm{L}}(\vec{q}) = \frac{v}{8c(v)}\log\left(\frac{c(v)}{v}\right)(|q_x| + |q_y|) + \mathcal{O}\left(\frac{v}{c(v)}\right). \tag{C.13}$$

The two-loop diagram indeed reproduces the assumed form of the self-energy, which is proportional to $|q_x| + |q_y|$ to the leading order in v. The full Schwinger-Dyson equation now boils down to a self-consistent equation for the boson velocity,

$$c(v) = \frac{v}{8c(v)}\log\left(\frac{c(v)}{v}\right). \tag{C.14}$$

From here $c(v)$ is solved in terms of v as

$$c(v) = \frac{1}{4}\sqrt{v \log\left(\frac{1}{v}\right)}\left[1 + \mathcal{O}\left(\frac{\log\left[\log(1/v)\right]}{\log(1/v)}\right)\right]. \tag{C.15}$$

This is consistent with the assumption that $v \ll c(v) \ll 1$ in the small v limit.

The full propagator of the boson which includes the bare kinetic term in Eq. (2.1) is given by

$$D(q)^{-1} = |q_0| + c(v)(|q_x| + |q_y|) + \frac{1}{\widetilde{\Lambda}}\left[q_0^2 + \mathsf{c}_0^2|\vec{q}\,|^2\right], \tag{C.16}$$

where $\widetilde{\Lambda}$ is a UV scale associated with the coupling (See discussion in Sec. 2.2). Depending on the ratio between $c(v)$ and c_0, which is determined by the microscopic details of the theory, one can have different sets of crossovers.

For $\mathsf{c}_0 \gg c(v)$, one has a series of crossovers from the Gaussian scaling with $z = 1$ at high energies, to the scaling with $z = 2$ at intermediate energies and to the non-Fermi liquid scaling with $z = 1$ at low energies. In the low-energy limit, the system eventually becomes superconducting. For $\mathsf{c}_0 \ll c(v)$, on the other hand, the $z = 2$ scaling is replaced with a scaling with $z = 1/2$ at intermediate energies. These crossovers are summarized in Tables C.1(a) and C.1(b).

Appendix D | Derivation of the Beta function for v in $d = 2$

In this appendix we derive the beta function of v given in Eq. (2.13) for the two-dimensional theory with $N_c = 2$ and $N_f = 1$. We first compute the counterterms that need to be added to the minimal local action such that the quantum effective action is independent of the UV cutoff scales to the lowest order in v. We proceed by making use of the $d = 2$ case of the RG scheme introduced in Appendix B and by setting $N_c = 2$ and $N_f = 1$. We further derive the beta function of v and its solution, which confirms that v flows to zero in the low-energy limit.

D.1 Frequency-dependent fermion self-energy

According to Eq. (2.8), the leading order fermion self-energy is generated from Fig. 2.3(a) in the small v limit. The one-loop fermion self-energy for the electrons on patch n is given by

$$\Sigma^{1\mathrm{L}(n)}(k_0, \vec{k}) = \frac{3\pi v}{2} \int \mathrm{d}p \; \gamma_1 G_{\overline{n}}^{(0)}(p + k; v) \gamma_1 D(p), \tag{D.1}$$

where the dressed boson propagator $D(q)$ is given in Eq. (2.6) and the bare fermion propagator $G_n^{(0)}(k; v)$ is given in Eq. (2.10). We first compute Eq. (D.1) for $n = 1$. The quantum correction is logarithmically divergent, and a UV cutoff $\widetilde{\Lambda}$ is imposed on p_y, which is the momentum perpendicular to the FS for $n = 1$ in the small v limit. However, the logarithmically divergent term is independent of how the UV cutoff is implemented. To extract the frequency-dependent self-energy, we set $\vec{k} = \vec{0}$ and rescale $(p_0, p_x, p_y) \to |k_0|(p_0, p_x/c(v), p_y)$ to rewrite

$$\Sigma^{1\mathrm{L}(1)}(k_0, \vec{0}) = i\gamma_0 k_0 \frac{3\pi v}{2c(v)} \int \mathrm{d}p \; \left\{ \frac{p_0 + 1}{\{(p_0 + 1)^2 + [w(v)p_x - p_y]^2\} \left[|p_0| + |p_x| + c(v)|p_y|\right]} \right\}, \tag{D.2}$$

where $w(v) \equiv v/c(v)$. Under this rescaling, the UV cutoff for p_y is also rescaled to $\Lambda_0 \equiv \widetilde{\Lambda}/|k_0|$. The p_0 integration gives

$$\Sigma^{1\mathrm{L}(1)}(k_0, \vec{0}) = i\gamma_0 k_0 \frac{3v}{4c(v)} \int_{-\Lambda_0}^{\Lambda_0} \frac{\mathrm{d}p_y}{(2\pi)} \int_{\mathbb{R}} \frac{\mathrm{d}p_x}{(2\pi)} \tag{D.3}$$
$$\left\{ \frac{\pi}{2} \left[\frac{|p_y - w(v)p_x|}{[p_y - w(v)p_x]^2 + [1 - |p_x| - c(v)|p_y|]^2} - \frac{|p_y - w(v)p_x|}{[p_y - w(v)p_x]^2 + [1 + |p_x| + c(v)|p_y|]^2} \right] \right.$$

$$- \left[\frac{[p_y - w(v)p_x]\text{arccot}[p_y - w(v)p_x]}{[p_y - w(v)p_x]^2 + [1 - |p_x| - c(v)|p_y|]^2} + \frac{[p_y - w(v)p_x]\text{arccot}[p_y - w(v)p_x]}{[p_y - w(v)p_x]^2 + [1 + |p_x| + c(v)|p_y|]^2} \right]$$
$$+ \frac{1}{2} \log \left(\frac{1 + [p_y - w(v)p_x]^2}{[|p_x| + c(v)|p_y|]^2} \right) \left[\frac{1 + |p_x| + c(v)|p_y|}{[p_y - w(v)p_x]^2 + [1 + |p_x| + c(v)|p_y|]^2} \right.$$
$$\left. - \frac{|p_x| + c(v)|p_y| - 1}{[p_y - w(v)p_x]^2 + [1 - |p_x| - c(v)|p_y|]^2} \right] \Bigg\}.$$

The logarithmically divergent contribution is obtained to be

$$\Sigma^{1\text{L}(1)}(k_0, \vec{0}) = \frac{3}{4\pi} \frac{v}{c(v)} \log \left(\frac{\widetilde{\Lambda}}{|k_0|} \right) i\gamma_0 k_0 \tag{D.4}$$

in the small v limit. The self-energy for other patches is obtained from a series of 90° rotations, and the frequency-dependent part is identical for all patches. In order to remove the cutoff dependence in the quantum effective action, we add the counterterm,

$$\sum_{n=1}^{4} \sum_{\sigma=\uparrow,\downarrow} \int \mathrm{d}k \; \overline{\Psi}_{n,\sigma}(k) \left(Z_1 \, i\gamma_0 k_0 \right) \Psi_{n,\sigma}(k) \tag{D.5}$$

with

$$Z_1 = -\frac{3}{4\pi} \frac{v}{c(v)} \log \left(\frac{\widetilde{\Lambda}}{\mu} \right), \tag{D.6}$$

where μ is the scale at which the quantum effective action is defined in terms of the renormalized velocity v (i.e., the scale at which the renormalization condition given in Eq. (B.6) is imposed in $d = 2$). The counterterm guarantees that the renormalized propagator at the scale μ is expressed solely in terms of v in the $\widetilde{\Lambda}/\mu \to \infty$ limit.

D.2 Momentum-dependent fermion self-energy

To compute the momentum-dependent fermion self-energy, we start with Eq. (D.1) for $n = 1$ and set $k_0 = 0$. Rescaling $p_x \to p_x/c(v)$ gives

$$\Sigma^{1\text{L}(1)}(0, \vec{k}) = -\frac{3\pi v}{2c(v)} i\gamma_1 \int \mathrm{d}p \; \frac{w(v)p_x - p_y + \varepsilon_3(\vec{k}; v)}{\left\{ p_0^2 + [w(v)p_x - p_y + \varepsilon_3(\vec{k}; v)]^2 \right\} [|p_0| + |p_x| + c(v)|p_y|]}. \tag{D.7}$$

The integration over p_0 results in two terms

$$\Sigma^{1\text{L}(1)}(0, \vec{k}) = \Sigma_1^{1\text{L}(1)}(\vec{k}) + \Sigma_2^{1\text{L}(1)}(\vec{k}), \tag{D.8}$$

where

$$\Sigma_1^{1\text{L}(1)}(\vec{k}) = -\, i\gamma_1 \frac{3\pi v}{4c(v)} \int_{\mathbb{R}} \frac{\mathrm{d}p_y}{(2\pi)} \int_{\mathbb{R}} \frac{\mathrm{d}p_x}{(2\pi)} \frac{\text{sgn}[w(v)p_x - p_y + \varepsilon_3(\vec{k}; v)][|p_x| + c(v)|p_y|]}{[p_y - \varepsilon_3(\vec{k}; v) - w(v)p_x]^2 + [|p_x| + c(v)|p_y|]^2}, \tag{D.9}$$

$$\Sigma_2^{1\mathrm{L}(1)}(\vec{k}) = -i\gamma_1 \frac{3v}{4c(v)} \int_{\mathbb{R}} \frac{\mathrm{d}p_y}{(2\pi)} \int_{\mathbb{R}} \frac{\mathrm{d}p_x}{(2\pi)} \frac{[p_y - \varepsilon_3(\vec{k};v) - w(v)p_x] \log\left(\frac{[|p_x|+c(v)|p_y|]^2}{[p_y-\varepsilon_3(\vec{k};v)-w(v)p_x]^2}\right)}{[p_y - \varepsilon_3(\vec{k};v) - w(v)p_x]^2 + [|p_x| + c(v)|p_y|]^2}. \quad \text{(D.10)}$$

We first compute the remaining integrations in Eq. (D.9). After performing the p_x integration, we rescale $p_y \to |\varepsilon_3(\vec{k};v)|p_y$ to obtain

$$\begin{aligned}
\Sigma_1^{1\mathrm{L}(1)}(\vec{k}) &= -\frac{3v}{8c(v)} i\gamma_1 \varepsilon_3(\vec{k};v) \int_{-\Lambda_3}^{\Lambda_3} \frac{\mathrm{d}p_y}{(2\pi)} \\
&\times \left[\frac{\pi w(v)}{2[1+w(v)^2]} \left\{ \mathrm{sgn}\left[p_y - 1 + c(v)w(v)|p_y|\right] + \mathrm{sgn}\left[p_y - 1 - c(v)w(v)|p_y|\right] \right\} \right. \quad \text{(D.11)} \\
&+ \frac{w(v)\mathrm{sgn}\,(p_y-1)}{1+w(v)^2} \left\{ \arctan\left[\frac{w(v)\,(1-p_y) + c(v)|p_y|}{p_y - 1 + c(v)w(v)|p_y|}\right] + \arctan\left[\frac{w(v)\,(p_y-1) + c(v)|p_y|}{1 - p_y + c(v)w(v)|p_y|}\right] \right. \\
&\left. \left. - \, 2\arctan\left(\frac{1}{w(v)}\right) - \frac{1}{w(v)} \log\left(\frac{c(v)^2 w(v)^2 p_y^2 + (p_y-1)^2 + 2c(v)w(v)\,|p_y-1|\,|p_y|}{w(v)^2\left[c(v)^2 p_y^2 + (p_y-1)^2\right]} \right) \right\} \right],
\end{aligned}$$

where $\Lambda_3 \equiv \widetilde{\Lambda}/|\varepsilon_3(\vec{k};v)|$ is the ratio that cuts off the divergence of the integral in the large p_y regime. The remaining p_y integration gives

$$\Sigma_1^{1\mathrm{L}(1)}(\vec{k}) = \frac{3v[w(v)-c(v)]}{4\pi} \log\left(\frac{\widetilde{\Lambda}}{|\varepsilon_3(\vec{k};v)|}\right) i\gamma_1 \varepsilon_3(\vec{k};v), \quad \text{(D.12)}$$

to the leading order in v up to terms that are finite in the $\widetilde{\Lambda} \gg |\varepsilon_3(\vec{k};v)|$ limit.

The integrations in Eq. (D.10) can be computed in a similar way and, in the small v limit, we obtain

$$\Sigma_2^{1\mathrm{L}(1)}(\vec{k}) = -\frac{3}{2\pi^2}\, v \log\left(\frac{1}{c(v)}\right) \log\left(\frac{\widetilde{\Lambda}}{|\varepsilon_3(\vec{k};v)|}\right) i\gamma_1 \varepsilon_3(\vec{k};v), \quad \text{(D.13)}$$

up to UV-finite terms. It is noted that Eq. (D.13) is dominant with respect to Eq. (D.12) in the small v limit.

According to Eq. (2.8), the upper bound for the one-loop fermion self-energy is $v/c(v)$. However, Eq. (D.13) is strictly smaller than the upper bound. The extra suppression by $c(v)$ arises due to the fact that the external momentum in Fig. 2.3(a) can be directed to flow only through the boson propagator, and the diagram becomes independent of the external momentum in the small $c(v)$ limit. Since this suppression does not happen for higher-loop diagrams in general, the one-loop diagram becomes comparable to some two-loop diagrams with $L - L_f = 2$. Therefore, we have to include the two-loop diagrams for the self-energy in order to capture all leading order corrections. The rainbow diagram in Fig. 2.3(d) is smaller for the same reason as the one-loop diagram. Three and higher-loop diagrams remain negligible, and only the diagram in Fig. 2.3(c) contributes to the leading order. The two-loop self-energy for electrons in patch n is given by

$$\begin{aligned}
\Sigma^{2\mathrm{L}(n)}(k_0,\vec{k}) = \frac{3\pi^2 v^2}{4} \int \mathrm{d}p \int \mathrm{d}q \\
\times \left[\gamma_1 G_{\overline{n}}(k+q;v)\gamma_1 G_n(k+q+p;v)\gamma_1 G_{\overline{n}}(k+p;v)\gamma_1\right] D(q)D(p).
\end{aligned} \quad \text{(D.14)}$$

It is noted that $\Sigma^{2\mathrm{L}(n)}(k_0,\vec{0})$ is strictly smaller than $\Sigma^{1\mathrm{L}(n)}(k_0,\vec{0})$, and only $\Sigma^{2\mathrm{L}(n)}(0,\vec{k})$ is of the same order as $\Sigma^{1\mathrm{L}(n)}(0,\vec{k})$. Therefore, we only compute $\Sigma^{2\mathrm{L}(n)}(0,\vec{k})$. After performing the integrations over p_y and q_y, the self-energy for patch $n=1$ becomes

$$\Sigma^{2\mathrm{L}(1)}(0,\vec{k}) = -\frac{3\pi^2 v^2}{16c(v)^2} i\gamma_1 \int_{\mathbb{R}} \frac{\mathrm{d}p_0}{(2\pi)} \int_{\mathbb{R}} \frac{\mathrm{d}q_0}{(2\pi)} \int_{\mathbb{R}} \frac{\mathrm{d}p_x}{(2\pi)} \int_{\mathbb{R}} \frac{\mathrm{d}q_x}{(2\pi)} \Bigg\{ \times [\mathrm{sgn}(p_0)+\mathrm{sgn}(p_0+q_0)][\mathrm{sgn}(q_0)+\mathrm{sgn}(2p_0+q_0)] \times \frac{2w(v)(p_x+q_x)+\delta(\vec{k};v)}{4(p_0+q_0)^2+[2w(v)(p_x+q_x)+\delta(\vec{k};v)]^2} \frac{1}{|p_0|+|p_x|} \frac{1}{|q_0|+|q_x|} \Bigg\}. \tag{D.15}$$

Where $\delta(\vec{k};v) \equiv (3vk_x - k_y)$. We single this factor out by rescaling $(p_0,p_x,q_0,q_x) \to |\delta(\vec{k};v)|(p_0,p_x,q_0,q_x)$. To perform the p_x and q_x integrals, we introduce variables $a = \frac{1}{2}(p_x+q_x)$ and $b = \frac{1}{2}(p_x-q_x)$. After the straightforward integration over b, we rescale $a \to a/w(v)$ to obtain

$$\Sigma^{2\mathrm{L}(1)}(0,\vec{k}) = -\frac{3v^2}{32c^2} i\gamma_1 \delta(\vec{k};v) \int_{\mathbb{R}} \frac{\mathrm{d}p_0}{(2\pi)} \int_{\mathbb{R}} \frac{\mathrm{d}q_0}{(2\pi)} \int_{\mathbb{R}} \mathrm{d}a \Bigg\{ \frac{4a+1}{4(p_0+q_0)^2+(4a+1)^2} \times [\mathrm{sgn}(p_0)+\mathrm{sgn}(p_0+q_0)][\mathrm{sgn}(q_0)+\mathrm{sgn}(2p_0+q_0)] \Bigg[\frac{\log\left[\frac{[2|a|+w(v)|p_0|][2|a|+w(v)|q_0|]}{w(v)^2|p_0||q_0|}\right]}{2|a|+w(v)(|p_0|+|q_0|)} - \frac{\log\left[\frac{w(v)|q_0|}{2|a|+w|p_0|}\right]}{2|a|+w(v)(|p_0|-|q_0|)} - \frac{\log\left[\frac{w(v)|p_0|}{2|a|+w|q_0|}\right]}{2|a|-w(v)(|p_0|-|q_0|)} \Bigg] \Bigg\}. \tag{D.16}$$

The frequency integrations are divergent in the UV and therefore we introduce a UV cutoff, $\Lambda_3' \equiv \Lambda/|\delta(\vec{k};v)|$ in the rescaled variables. In the small $w(v)$ limit, the a integration diverges as $\log[w(v)]^2$. The subleading terms are suppressed compared to the one-loop diagram, and we drop them in the small $w(v)$ limit. The remaining frequency integrations are logarithmically divergent in the UV cutoff,

$$\Sigma^{2L(1)}(0,\vec{k}) = -i\gamma_1 \frac{3}{32\pi^2} \left[\frac{v}{c(v)} \log\left(\frac{c}{v(v)}\right)\right]^2 \log\left(\frac{\Lambda}{|\delta(\vec{k};v)|}\right) \delta(\vec{k};v). \tag{D.17}$$

This is of the same order as Eq. (D.13) because of $\{[v/c(v)]\log[v/c(v)]\}^2 = 8v\log[1/c(v)]$ to the leading order in v.

The vertex correction in Fig. 2.3(*c*) strengthens the bare vertex, and the two-loop self-energy has the same sign as the one-loop self-energy. In particular, both the one-loop and two-loop quantum corrections enhance the nesting of the FS at the hot spots, and drive v to a smaller value at low energies. To remove the cutoff dependences of the electronic two-point vertex function in the quantum effective action, we add, according to the renormalization conditions in Eqs. (B.7) and (B.8), the counterterm

$$\sum_{\sigma=\uparrow,\downarrow} \int \mathrm{d}k\ \overline{\Psi}_{1,\sigma}(k)\left[i\gamma_1(Z_2 v k_x + Z_3 k_y)\right]\Psi_{1,\sigma}(k), \tag{D.18}$$

with

$$Z_2 = \frac{15}{4\pi^2} v \, \log\left(\frac{1}{c(v)}\right) \log\left(\frac{\Lambda}{\mu}\right), \tag{D.19}$$

$$Z_3 = -\frac{9}{4\pi^2} v \, \log\left(\frac{1}{c(v)}\right) \log\left(\frac{\Lambda}{\mu}\right). \tag{D.20}$$

In arriving to these equations, we have chosen $\widetilde{\Lambda} \approx \Lambda$ since the two UV cutoffs used to regularize the theory are comparable in magnitude and the universal features stemming from these counterterm coefficients are insensitive to the way the UV cutoffs are implemented. The counterterms for $n = 2, 3, 4$ are determined from these by the fourfold rotational symmetry of the theory.

D.3 Vertex correction

The one-loop vertex correction in Fig. 2.3(*b*) is given by

$$\Gamma_n^{(2,1)1\mathrm{L}}(k,q) = \frac{\pi v}{2} \int \mathrm{d}p \, \left[\gamma_1 G_{\overline{n}}^{(0)}(p+k+q;v)\gamma_1 G_n^{(0)}(p+k;v)\gamma_1\right] D(p). \tag{D.21}$$

Following the RG condition for the vertex function in Eq. (B.9), we set all external momenta to zero and keep $k_0 = \mu$, which plays the role of an IR regulator. For $n = 1$, it is convenient to rescale $(p_0, p_x, p_y) \to \mu(p_0, p_x/c(v), p_y)$. The p_0 integration gives

$$\begin{aligned}
\Gamma_1^{(2,1)1\mathrm{L}}(\mu) = \frac{v}{4c(v)}\gamma_1 \int_{-\Lambda_0}^{\Lambda_0} \frac{\mathrm{d}p_y}{(2\pi)} \int_{\mathbb{R}} \frac{\mathrm{d}p_x}{(2\pi)} \qquad\qquad (D.22)\\
\left\{ \begin{array}{l} \big[\big((p_y - wp_x)(p_y + wp_x)^3 + (-1 + (|p_x| + c|p_y|)^2)^2\big)\big(1 + (p_y - wp_x)^2 + (|p_x| + c|p_y|)^2\big) + \\ (p_y - wp_x)(p_y + wp_x)\big(1 + 6(|p_x| + c|p_y|)^2 + (|p_x| + c|p_y|)^4 + (p_y - wp_x)^2(1 + (|p_x| + c|p_y|)^2)\big) \\ +(p_y + wp_x)^2\big((-1 + (|p_x| + c|p_y|)^2)^2 + (p_y - wp_x)^2(1 + (|p_x| + c|p_y|)^2)\big)\big] \log(|p_x| + c|p_y|) \end{array} \right\} \\
\Big/ \\
-\tfrac{1}{2}\left\{ \begin{array}{l} \big((p_y - wp_x)^2 + (-1 + |p_x| + c|p_y|)^2\big)\big((p_y + wp_x)^2 + (-1 + |p_x| + c|p_y|)^2\big) \\ \times \big((p_y - wp_x)^2 + (1 + |p_x| + c|p_y|)^2\big)\big((p_y + wp_x)^2 + (1 + |p_x| + c|p_y|)^2\big) \end{array} \right\} \\
+ \frac{\left\{ \begin{array}{l} 2\mathrm{arccot}(p_y + wp_x)\big(1 + (p_y + wp_x)^2 - (|p_x| + c|p_y|)^2\big) \\ +(p_y + wp_x)\log(1 + (p_y + wp_x)^2)(1 + (p_y + wp_x)^2 + (|p_x| + c|p_y|)^2) \\ +\ \pi\ \mathrm{sgn}(p_y + wp_x)(|p_x| + c|p_y|)(-1 + (p_y + wp_x)^2 + (|p_x| + c|p_y|)^2) \end{array} \right\}}{2p_y\big((p_y + wp_x)^2 + (-1 + |p_x| + c|p_y|)^2\big)\big((p_y + wp_x)^2 + (1 + |p_x| + c|p_y|)^2\big)} \\
+ \frac{\left\{ \begin{array}{l} 2\mathrm{arccot}(p_y - p_x w)\big(1 + (p_y - wp_x)^2 - (|p_x| + c|p_y|)^2\big) \\ +(p_y - wp_x)\log(1 + (p_y - wp_x)^2)(1 + (p_y - wp_x)^2 + (|p_x| + c|p_y|)^2) \\ +\ \pi\ \mathrm{sgn}(p_y - wp_x)(|p_x| + c|p_y|)(-1 + (p_y - wp_x)^2 + (|p_x| + c|p_y|)^2) \end{array} \right\}}{2p_y\big((p_y - wp_x)^2 + (-1 + |p_x| + c|p_y|)^2\big)\big((p_y - wp_x)^2 + (1 + |p_x| + c|p_y|)^2\big)},
\end{aligned}$$

where the rescaled cutoff for p_y is $\Lambda_0 \equiv \widetilde{\Lambda}/\mu$ and in the integrand we have used the lighter notation $w \equiv w(v)$ and $c \equiv c(v)$. After the integration over $\vec{p}$, the logarithmically divergent

contribution is obtained to be

$$\Gamma_1^{(2,1)1\mathrm{L}}(\mu) = \frac{1}{4\pi}\frac{v}{c(v)}\log\left(\frac{c(v)}{v}\right)\log\left(\frac{\Lambda}{\mu}\right)\gamma_1, \tag{D.23}$$

in the small v limit. The vertex corrections for different $n = 2, 3, 4$ are the same by virtue of the C_4 symmetry of the theory. The counterterm for the vertex becomes

$$iZ_6\sqrt{\frac{\pi v}{2}}\sum_{n=1}^{4}\sum_{\sigma,\sigma'=\uparrow,\downarrow}\int \mathrm{d}k\int \mathrm{d}q\ \overline{\Psi}_{n,\sigma}(k+q)\Phi_{\sigma,\sigma'}(q)\gamma_1\Psi_{\overline{n},\sigma'}(k), \tag{D.24}$$

with

$$Z_6 = -\frac{1}{4\pi}\frac{v}{c(v)}\log\left(\frac{c(v)}{v}\right)\log\left(\frac{\widetilde{\Lambda}}{\mu}\right). \tag{D.25}$$

D.4 The beta function for v

In this section we use the above results to derive the beta function for v. This one is obtained by requiring that the bare slope v_B does not depend on the running energy scale μ, where the former is related to the renormalized one, v, through the multiplicative relation given in Eq. (B.3):

$$v_B = \frac{Z_2}{Z_3}v. \tag{D.26}$$

Using the latter information it follows that

$$\left[Z_2Z_3 + v\left(\frac{\partial Z_2}{\partial v}Z_3 - Z_2\frac{\partial Z_3}{\partial v}\right)\right]\beta_v + v\left[\frac{\partial Z_2}{\partial\log\mu}Z_3 - Z_2\frac{\partial Z_3}{\partial\log\mu}\right] = 0, \tag{D.27}$$

with Z_2 and Z_3 given in Eqs. (D.19) and (D.20), respectively. This gives the beta function which describes the flow of v under the change of the scale μ,

$$\frac{\mathrm{d}v}{\mathrm{d}\log\mu} = \frac{6}{\pi^2}v^2\log\left[4\left(\frac{1}{v\log 1/v}\right)^{\frac{1}{2}}\right], \tag{D.28}$$

to the leading order in v. We introduce the logarithmic scale $\ell = -\log(\mu_0/\mu)$, where μ_0 is a reference scale at which the RG flow is triggered. In what follows we take $\mu_0 = \Lambda$, where Λ is a UV scale at which the bare theory is defined and which is determined by the microscopic details of the theory. In terms of this logarithmic length scale, the beta function can be rewritten as

$$\frac{\mathrm{d}v}{\mathrm{d}\ell} = \frac{3}{\pi^2}v^2\log v + \mathcal{O}(\log[\log(v)]). \tag{D.29}$$

The solution is given by

$$\mathrm{Ei}[\log 1/v(\ell)] = \mathrm{Ei}[\log 1/v_0] + \frac{3}{\pi^2}\ell, \tag{D.30}$$

where $v_0 = v(0)$ and $\mathrm{Ei}(x)$ is the exponential integral function, which goes as $\mathrm{Ei}(x) = e^x\left[\frac{1}{x} + \mathcal{O}(1/x^2)\right]$ in the large x limit. Therefore, v flows to zero as

$$v(\ell) = \frac{\pi^2}{3}\frac{1}{\ell\,\log\ell}, \tag{D.31}$$

for $\ell \gg 1/[v_0\log(1/v_0)]$. For sufficiently large ℓ, $v(\ell)$ decays to zero in a manner which is independent of its bare value. The velocity of the collective mode flows to zero at a slower rate,

$$c(\ell) = \frac{\pi}{4\sqrt{3}}\frac{1}{\sqrt{\ell}}, \tag{D.32}$$

and the ratio $w(v) = v/c(v)$ flows to zero as

$$w(\ell) = \frac{4\pi}{\sqrt{3}}\frac{1}{\sqrt{\ell}\log\ell}. \tag{D.33}$$

Similarly, the multiplicative renormalization for the frequency and fields in Eq. (B.3) generates the deviation of the dynamical critical exponent from one and the anomalous dimensions for the fields. In terms of the counterterm coefficients in Eqs. (D.6),(D.19),(D.20) and (D.25), these are given, according to Eqs. (B.13) and (B.15), by

$$\eta_\Phi = \frac{\mathrm{d}}{\mathrm{d}\log\mu}\log\left[\frac{Z_3^{\frac{1}{2}}Z_6}{Z_1 Z_2^{\frac{1}{2}}}\right], \tag{D.34}$$

$$\eta_\Psi = \frac{\mathrm{d}}{\mathrm{d}\log\mu}\log\left[\frac{Z_3}{Z_1^{\frac{1}{2}}}\right], \tag{D.35}$$

$$z = 1 + \frac{\mathrm{d}}{\mathrm{d}\log\mu}\log\left[\frac{Z_1}{Z_3}\right], \tag{D.36}$$

which reduce to the expressions in Eqs. (2.15) to the leading order in v.

Appendix E | Scaling forms for physical observables in $d = 2$

In this section, we derive the expressions for the Green's functions and the specific heat in Eqs. (2.17), (2.22) and (2.28), respectively, and which characterize the low-energy theory for the AFM quantum critical metal in $d = 2$ with $N_c = 2$ and $N_f = 1$.

E.1 Green's functions

We start by deriving the form of the electronic Green's function near hot spot $N = 1$. The Green's function for all other hot spots are determined from that of $N = 1$ by the C_4 symmetry of the theory. From Eq. (B.10) and the fact that the electronic Green's function is the inverse of the two-point electronic vertex function, it follows that the former satisfies the renormalization group equation,

$$\left[\frac{1-2\eta_\Psi-(z-1)}{z}+k_0\frac{\partial}{\partial k_0}+\frac{1}{z}\vec{k}\cdot\frac{\partial}{\partial\vec{k}}-\frac{\beta_v}{z}\frac{\partial}{\partial v}\right]G_1(k_0,\vec{k};v)=0. \tag{E.1}$$

The solution to this equation is given by

$$G_1(k_0,\vec{k};v_0)=e^{\int_0^l\frac{d\ell}{z(\ell)}\{1-2\eta_\Psi(\ell)-[z(\ell)-1]\}}G_1\left(e^l k_0, e^{\int_0^l\frac{d\ell}{z(\ell)}}\vec{k};v(l)\right), \tag{E.2}$$

where $v(l)$ satisfies the equation

$$\frac{dv(l)}{dl}=-\frac{\beta_v}{z(l)}, \tag{E.3}$$

with the initial condition $v(0) = v_0$, and $z(l)$ and $\eta_\Psi(l)$ depend on l only through $v(l)$. We write $[1-2\eta_\Psi-(z-1)]/z = 1/z-2\widetilde{\eta}_\Psi$, where $\widetilde{\eta}_\Psi=\frac{1}{2}(\partial\log Z_3/\partial\log\mu)$ to the leading order in v. Although $\widetilde{\eta}_\Psi$ is subleading compared to $1/z$, we keep it because only $\widetilde{\eta}_\Psi$ contributes to the net anomalous dimension of the fermion propagator. From Eqs. (D.31)-(D.33), one obtains the solution to the scaling equation,

$$G_1(k_0,\vec{k};v_0)=\exp\left[l-2\sqrt{3}\frac{\sqrt{l}}{\log(l)}-\frac{3}{8}\log l\right]G_1\left[e^l k_0,\exp\left(l-2\sqrt{3}\frac{\sqrt{l}}{\log(l)}\right)\vec{k},\frac{\pi^2}{3}\frac{1}{l\log(l)}\right] \tag{E.4}$$

in the large l limit. We choose $l=\log(\mu_0/|k_0|)$, with $\mu_0=\Lambda$, and take the $|k_0|/\Lambda\ll 1$ limit with $\exp\left(l-2\sqrt{3}[\sqrt{l}/\log(l)]\right)\vec{k}\sim\Lambda$ fixed. By using the fact that the Green's function is

given by $G_1(k_0,\vec{k};v)=(ik_0+vk_x+k_y)^{-1}$ in the small v limit, we readily obtain

$$G_1(k_0,\vec{k})=\frac{1}{F_\Psi(k_0)\left[ik_0\ F_z(k_0)+\left(\frac{\pi^2}{3}\frac{k_x}{\log\left(\frac{\Lambda}{|k_0|}\right)\log\left[\log\left(\frac{\Lambda}{|k_0|}\right)\right]}+k_y\right)\right]} \tag{E.5}$$

in the low-energy limit with fixed $\vec{k}/[k_0F_z(k_0)]$, where

$$F_\Psi(k_0)\equiv\left[\log\left(\frac{\Lambda}{|k_0|}\right)\right]^{\frac{3}{8}}, \tag{E.6}$$

$$F_z(k_0)\equiv\exp\left\{2\sqrt{3}\frac{\left[\log\left(\frac{\Lambda}{|k_0|}\right)\right]^{1/2}}{\log\left[\log\left(\frac{\Lambda}{|k_0|}\right)\right]}\right\}. \tag{E.7}$$

The analytic continuation of Eq. (E.5) to the real and positive frequency gives rise to Eq. (2.17).

Similarly, Eq. (B.10) also implies that the Green's function of the boson satisfies the scaling equation

$$\left[\frac{1-2\eta_\Phi-(z-1)}{z}+q_0\frac{\partial}{\partial q_0}+\frac{1}{z}\vec{q}\cdot\frac{\partial}{\partial\vec{q}}-\frac{\beta_c(v)}{z}\frac{\partial}{\partial c(v)}\right]D[q_0,\vec{q};c(v)]=0, \tag{E.8}$$

where $\beta_c(v)=\mathrm{d}c(v)/\mathrm{d}\log\mu$. We view the boson propagator as a function of $c(v)$ instead of v because it depends on v only through $c(v)$ in the low-energy limit. However, this does not affect any physical observable since in the end there is only one independent parameter in the theory. The solution to the scaling equation takes the form,

$$D(q_0,\vec{q},c_0)=\exp\left[l-\frac{2\sqrt{l}}{\sqrt{3}}-2\sqrt{3}\frac{\sqrt{l}}{\log l}\right]D\left[e^l q_0,\exp\left(l-2\sqrt{3}\frac{\sqrt{l}}{\log(l)}\right)\vec{q};\frac{\pi}{4\sqrt{3}}\frac{1}{\sqrt{l}}\right], \tag{E.9}$$

with $c_0=c(0)$. By choosing $l=\log(\mu_0/|q_0|)$, with $\mu_0=\Lambda$, and using the fact that the boson propagator is given by Eq. (2.6) in the limit of small v and $c(v)$, we obtain

$$D(q_0,\vec{q})=\frac{1}{F_\Phi(q_0)\left[|q_0|F_z(q_0)+\frac{\pi}{4\sqrt{3}}\frac{|q_x|+|q_y|}{\left[\log\left(\frac{\Lambda}{|q_0|}\right)\right]^{1/2}}\right]} \tag{E.10}$$

in the low-energy limit with fixed $\vec{q}/[q_0F_z(q_0)]\sim 1$. Here,

$$F_\Phi(q_0)\equiv\exp\left\{\frac{2}{\sqrt{3}}\left[\log\left(\frac{\Lambda}{|q_0|}\right)\right]^{1/2}\right\} \tag{E.11}$$

is a universal function which describes the contribution from the boson anomalous dimension. The analytic continuation of Eq. (E.10) to real and positive frequency gives the retarded correlation function in Eq. (2.22).

E.2 Free energy density

We turn our attention to the computation of the leading contribution to the free energy density which is generated from the quadratic action of the dressed boson,

$$f_{\text{Bos.}}(T) = \int_{\mathbb{R}^2} \frac{\mathrm{d}\vec{k}}{(2\pi)^2} f_{\text{Bos.}}(\vec{k}, T), \tag{E.12}$$

where $f_{\text{Bos.}}(\vec{k}, T)$ is the contribution from the mode with momentum $\vec{k}$,

$$f_{\text{Bos.}}(\vec{k}, T) = \frac{3}{2}\left[T \sum_{\omega_m \in 2\pi T\mathbb{Z}} - \int_{\mathbb{R}} \frac{\mathrm{d}\omega_m}{2\pi}\right] \log\Big[|\omega_m| + \mathscr{B}(\vec{k})\Big], \tag{E.13}$$

with $\mathscr{B}(\vec{k}) = c(v)(|k_x| + |k_y|)$ and $\omega_m = 2\pi T m$ with $m \in \mathbb{Z}$. In this expression, the thermal mass is ignored because it is higher order in v, and the temperature-independent ground state energy has been subtracted.

Using the identity

$$\log a = -\int_0^\infty \frac{\mathrm{d}x}{x}\left(e^{-xa} - e^{-x}\right), \qquad a \in \mathbb{R}^+, \tag{E.14}$$

we write the free energy density per mode as

$$f_{\text{Bos.}}(\vec{k}, T) = -\frac{3}{2}\left[T \sum_{\omega_m \in 2\pi T\mathbb{Z}} - \int \frac{\mathrm{d}\omega_m}{2\pi}\right] \int_0^\infty \frac{\mathrm{d}x}{x}\left[e^{-x[|\omega_m| + \mathscr{B}(\vec{k})]} - e^{-x}\right]. \tag{E.15}$$

The summation over the Matsubara frequency results in

$$f_{\text{Bos.}}(\vec{k}, T) = -\frac{3T}{2}\int_0^\infty \frac{\mathrm{d}x}{x}\left[\coth(\pi T x) - \frac{1}{\pi T x}\right] e^{-x\mathscr{B}(\vec{k})}. \tag{E.16}$$

For $\mathscr{B}(\vec{k}) \gg T$, the free energy density is suppressed only algebraically,

$$f_{\text{Bos.}}(\vec{k}, T) = -\frac{\pi}{2}\frac{T^2}{\mathscr{B}(\vec{k})}\left[1 + \mathcal{O}\left(\frac{T}{\mathscr{B}(\vec{k})}\right)\right]. \tag{E.17}$$

This is in contrast to the noninteracting boson, whose contribution is exponentially suppressed at large momenta. Because of the relatively large contribution from high momentum modes, the bosonic free energy density becomes unbounded without a UV cutoff. This leads to a violation of hyperscaling:

$$f_{\text{Bos.}}(T) \sim -T^2\widetilde{\Lambda}, \tag{E.18}$$

where $\widetilde{\Lambda}$ is a UV cutoff associated with irrelevant terms as is discussed in the Appendix C.

Eq. (E.18) is obtained without including the renormalization of the velocity and anomalous dimensions in Eq. (2.15), which alter the scaling of the free energy density at intermediate energy scales. In order to take those into account, we consider the scaling equation for $f_{\text{Bos.}}$:

$$\left[\left(1+\frac{2}{z}\right)-T\frac{\partial}{\partial T}+\frac{\beta_c(v)}{z}\frac{\partial}{\partial c(v)}-\frac{\widetilde{\Lambda}}{z}\frac{\partial}{\partial\widetilde{\Lambda}}\right]f_{\text{Bos.}}[T,c(v),\widetilde{\Lambda}]=0. \tag{E.19}$$

This arises from the fact that the free energy density has engineering scaling dimension of 3 and that the renormalized free energy density is related to the bare one through the multiplicative relation:

$$f_{\text{Bos.}}[T,c(v),\widetilde{\Lambda};\mu]=\frac{Z_3}{Z_1}f^B_{\text{Bos.}}[T_B,c(v_B),\widetilde{\Lambda}_B], \tag{E.20}$$

with $\widetilde{\Lambda}_B=\widetilde{\Lambda}$, $T_B=(Z_1/Z_3)T$, and the renormalized fermion velocity is related to the bare one through Eq. (D.26).

The solution to Eq. (E.19) takes the form,

$$f_{\text{Bos.}}(T,c_0,\widetilde{\Lambda})=\exp\left(-\int_0^l \mathrm{d}\ell\left[1+\frac{2}{z(\ell)}\right]\right)f_B\left(e^l T,c(l),e^{\int_0^l\frac{\mathrm{d}\ell}{z(\ell)}}\widetilde{\Lambda}\right), \tag{E.21}$$

where $c(l)$ satisfies the equation

$$\frac{\mathrm{d}c(l)}{\mathrm{d}l}=-\frac{\beta_c(v)}{z(l)}, \tag{E.22}$$

with the initial condition $c(0)=c_0$. In the large l limit, $z(l)\approx 1$ and $c(l)$ is given by Eq. (D.32). By choosing $l=\log(\mu_0/T)$ with $\mu_0=\Lambda$, and using the fact that $f_{\text{Bos.}}$ is linearly proportional to $\widetilde{\Lambda}$, we obtain

$$f_{\text{Bos.}}\sim\widetilde{\Lambda}T^2F_z(T). \tag{E.23}$$

This is the dominant term at low temperatures because the contribution of free electrons away from the hot spots only goes as T^2. The contributions from vertex corrections are subleading in v. Therefore, the specific heat in the low temperature limit is given by Eq. (2.28).

Appendix F | Physical Observables in $d = 3$

In this appendix we derive the scaling form of the Green's functions in $d = 3$. We first summarize the regularization and RG prescription [142] used in this dimension, highlight the main differences with the RG prescription introduced in Appendix B, and then proceed to compute the scaling form of the low-energy Green's functions.

F.1 Regularization and RG Scheme in $d = 3$

Since $d = 3$ is the upper critical dimension of the theory, every term in Eq. (3.1) is marginal under the Gaussian scaling, and quantum corrections are expected to be logarithmically divergent. We implement the same regularization introduced in Appendix B to tame these divergences. To make sure that physical observables are independent of the UV energy scales, we add the following counterterms to the action

$$\begin{aligned} S^{\text{C.T}}_{d=3} = &\sum_{n=1}^{4}\sum_{\sigma=1}^{N_c}\sum_{j=1}^{N_f}\int \mathrm{d}k\ \overline{\Psi}_{n,\sigma,j}(k)\left[i\mathcal{A}_1\boldsymbol{\Gamma}\cdot\mathbf{K} + i\gamma_2\widehat{\varepsilon}_n(\vec{k};v)\right]\Psi_{n,\sigma,j}(k) \\ &+\frac{1}{4}\int \mathrm{d}q\left[\mathcal{A}_4|\mathbf{Q}|^2+\mathcal{A}_5c^2|\vec{q}|^2\right]\mathrm{Tr}\left[\Phi(-q)\Phi(q)\right] \\ &+\frac{ig\mathcal{A}_6}{\sqrt{N_f}}\sum_{n=1}^{4}\sum_{\sigma,\sigma'=1}^{N_c}\sum_{j=1}^{N_f}\int \mathrm{d}k\int \mathrm{d}q\ \overline{\Psi}_{\overline{n},\sigma,j}(k+q)\Phi_{\sigma\sigma'}(q)\gamma_2\Psi_{n,\sigma',j}(k) \\ &+\frac{1}{4}\left[\prod_{i=1}^{3}\int \mathrm{d}q_i\right]\{\mathcal{A}_7u_1\mathrm{Tr}\left[\Phi(q_1+q_3)\Phi(q_2-q_3)\right]\mathrm{Tr}\left[\Phi(-q_1)\Phi(-q_2)\right] \\ &\qquad +\mathcal{A}_8u_2\mathrm{Tr}\left[\Phi(q_1+q_3)\Phi(q_2-q_3)\Phi(-q_1)\Phi(-q_2)\right]\}\,. \end{aligned} \tag{F.1}$$

Here, $\gamma_2=\sigma_x$ is the first Pauli matrix, $\widehat{\varepsilon}_1(\vec{k};v)=\mathcal{A}_2vk_x+\mathcal{A}_3k_y$, $\widehat{\varepsilon}_2(\vec{k};v)=-\mathcal{A}_3k_x+\mathcal{A}_2vk_y$, $\widehat{\varepsilon}_3(\vec{k};v)=\mathcal{A}_2vk_x-\mathcal{A}_3k_y$, and $\widehat{\varepsilon}_4(\vec{k};v)=\mathcal{A}_3k_x+\mathcal{A}_2vk_y$. The $\mathcal{A}_i$'s are momentum-independent counterterm coefficients. Adding this counterterm action to Eq. (3.1) in $d = 3$ yields the renormalized action,

$$\begin{aligned} S^{\text{Ren}}_{d=3} = &\sum_{n=1}^{4}\sum_{\sigma=1}^{N_c}\sum_{j=1}^{N_f}\int \mathrm{d}k_B\ \overline{\Psi}_{n,\sigma,j;B}(k_B)\left[i\boldsymbol{\Gamma}\cdot\mathbf{K}_B + i\gamma_2\varepsilon_n(\vec{k}_B;v_B)\right]\Psi_{n,\sigma,j;B}(k_B). \\ &+\frac{1}{4}\int \mathrm{d}q_B\left[|\mathbf{Q}_B|^2+c_B^2|\vec{q}_B|^2\right]\mathrm{Tr}\left[\Phi_B(-q_B)\Phi_B(q_B)\right] \end{aligned}$$

$$+\frac{ig_B}{\sqrt{N_f}}\sum_{n=1}^{4}\sum_{\sigma,\sigma'=1}^{N_c}\sum_{j=1}^{N_f}\int \mathrm{d}k_B\int \mathrm{d}q_B\overline{\Psi}_{\overline{n},\sigma,j;B}(k_B+q_B)\Phi_{B;\sigma\sigma'}(q_B)\gamma_2\Psi_{n,\sigma',j;B}(k_B) \tag{F.2}$$

$$+\frac{1}{4}\left[\prod_{i=1}^{3}\int \mathrm{d}q_{i;B}\right]\{u_{1;B}\mathrm{Tr}\left[\Phi_B(q_{1;B}+q_{3;B})\Phi_B(q_{2;B}-q_{3;B})\right]\mathrm{Tr}\left[\Phi_B(-q_{1;B})\Phi_B(-q_{2;B})\right]$$
$$+u_{2;B}\mathrm{Tr}\left[\Phi(q_{1;B}+q_{3;B})\Phi_B(q_{2;B}-q_{3;B})\Phi_B(-q_{1;B})\Phi_B(-q_{2;B})\right]\}.$$

The renormalized frequency, momenta, fields, velocities and couplings are related to the bare ones through

$$\mathbf{K}_B=\frac{\mathcal{Z}_1}{\mathcal{Z}_3}\mathbf{K},\qquad \vec{k}_B=\vec{k},\qquad v_B=\frac{\mathcal{Z}_2}{\mathcal{Z}_3}v,\qquad c_B=\sqrt{\frac{\mathcal{Z}_5}{\mathcal{Z}_4}}\left(\frac{\mathcal{Z}_1}{\mathcal{Z}_3}\right)c, \tag{F.3}$$

$$g_B=\frac{\mathcal{Z}_6}{\mathcal{Z}_3\sqrt{\mathcal{Z}_4}}g,\qquad u_{1;B}=\frac{\mathcal{Z}_7}{\mathcal{Z}_4^2}\left(\frac{\mathcal{Z}_1}{\mathcal{Z}_3}\right)^2u_1,\qquad u_{2;B}=\frac{\mathcal{Z}_8}{\mathcal{Z}_4^2}\left(\frac{\mathcal{Z}_1}{\mathcal{Z}_3}\right)^2u_2, \tag{F.4}$$

$$\Psi_B(k_B)=\mathcal{Z}_\Psi^{\frac{1}{2}}\Psi(k),\qquad \text{and}\qquad \Phi_B(k_B)=\mathcal{Z}_\Phi^{\frac{1}{2}}\Phi(k), \tag{F.5}$$

where $\mathcal{Z}_i=1+\mathcal{A}_i$, $\mathcal{Z}_\Psi=\mathcal{Z}_3(\mathcal{Z}_3/\mathcal{Z}_1)^2$, $\mathcal{Z}_\Phi=\mathcal{Z}_4(\mathcal{Z}_3/\mathcal{Z}_1)^4$, and the field indices have been suppressed. It is noted that the expression for $\mathcal{Z}_\Phi$ is different from the one obtained in $2\leq d<3$ (See Appendix B) because here we are using the Gaussian scaling rather than the interaction-driven scaling. The renormalized action gives rise to the quantum effective action in Eq. (B.5). In contrast to the theory in $2\leq d<3$, the quantum effective action and 1PI vertex functions for the three-dimensional theory depend on v,c,g,u_1 and u_2 rather than a single parameter (v). The counterterm coefficients in Eq. (F.1) are determined according to a minimal subtraction scheme which imposes the following renormalization conditions on the vertex functions:

$$\frac{1}{2i}\frac{\partial}{\partial\mathbf{K}^2}\mathrm{Tr}\left[(\mathbf{K}\cdot\mathbf{\Gamma})\Gamma_n^{(2,0)}(k)\right]\Big|_{|\mathbf{K}|=\mu,\vec{k}=0}=1+E_1(v,c,g,u_i;\widetilde{\Lambda};\Lambda;\mu),\qquad n=1,2,3,4, \tag{F.6}$$

$$\frac{1}{2i}\frac{\partial}{\partial k_x}\mathrm{Tr}\left[\gamma_2\Gamma_{n=1}^{(2,0)}(k)\right]\Big|_{|\mathbf{K}|=0,k_x=\mu,k_y=0}=v\left[1+E_2(v,c,g,u_i;\widetilde{\Lambda};\Lambda;\mu)\right], \tag{F.7}$$

$$\frac{1}{2i}\frac{\partial}{\partial k_y}\mathrm{Tr}\left[\gamma_2\Gamma_{n=1}^{(2,0)}(k)\right]\Big|_{|\mathbf{K}|=0,k_x=0,k_y=\mu}=1+E_3(v,c,g,u_i;\widetilde{\Lambda};\Lambda;\mu), \tag{F.8}$$

$$\frac{\partial}{\partial\mathbf{Q}^2}\left[\Gamma^{(0,2)}(q)\right]\Big|_{|\mathbf{Q}|=\mu,\vec{q}=0}=1+E_4(v,c,g,u_i;\widetilde{\Lambda};\Lambda;\mu), \tag{F.9}$$

$$\frac{\partial}{\partial q_j^2}\left[\Gamma^{(0,2)}(q)\right]\Big|_{|\mathbf{Q}|=0,\vec{q}=(\mu,\mu)}=c^2\left[1+E_5(v,c,g,u_i;\widetilde{\Lambda};\Lambda;\mu)\right],\qquad j=x,y, \tag{F.10}$$

$$\frac{1}{2}\mathrm{Tr}\left[\gamma_2\Gamma_n^{(2,1)}(k,q)\right]\Big|_{q=0,|\mathbf{K}|=\mu,\vec{k}=0}=1+E_6(v,c,g,u_i;\widetilde{\Lambda};\Lambda;\mu),\qquad n=1,2,3,4, \tag{F.11}$$

$$\Gamma_{abcd}^{(0,4)}(k_1,k_2,k_3)\Big|_{|\mathbf{K}_i|=\mu,\vec{k}_i=\vec{0}}=\frac{1}{4}(u_1\mathrm{Tr}[\tau^a\tau^b]\mathrm{Tr}[\tau^c\tau^d]+u_2\mathrm{Tr}[\tau^a\tau^b\tau^c\tau^d])$$
$$+E_7(v,c,g,u_i;\widetilde{\Lambda};\Lambda;\mu). \tag{F.12}$$

Here, μ is an energy scale at which the physical observables are measured. The functions $E_i(v, c, g, u_i; \widetilde{\Lambda}; \Lambda; \mu)$ are finite functions of the renormalized couplings that become independent of the UV scales $\widetilde{\Lambda}$ and Λ in the $\widetilde{\Lambda} \gg \mu$ and $\Lambda \gg \mu$ limits. They vanish in the $u_i \to 0$ and $g \to 0$ limits. τ^a denotes the generators of SU(N_c) with $a = 1, 2, \ldots, N_c^2 - 1$. The conditions in Eqs. (F.6) to (F.8) fix the fermion two-point function at the $n = 1$ hot spot and, by virtue of the C_4 symmetry of the theory, they also fix the two-point function at the other three hot spots. The renormalization conditions in Eqs. (F.9) and (F.10) fix the bosonic two-point function. Eqs. (F.11) and (F.12) fix the Yukawa vertex and the bosonic four-point function, respectively.

Under the tree-level Gaussian scaling, the 1PI vertex functions have scaling dimension

$$[\Gamma^{(2m,n)}(\{k_i\}; v, c, g, u_i; \mu)] = 4 - n - 3m, \tag{F.13}$$

and the renormalized vertex functions are related to the bare ones via,

$$\Gamma_B^{(2m,n)}(\{k_{i;B}\}; v_B, c_B, g_B, u_{i;B}; \Lambda, \widetilde{\Lambda}) = \left(\frac{\mathcal{Z}_3}{\mathcal{Z}_1}\right)^{2(2m+n-1)} \frac{\Gamma^{(2m,n)}(\{k_i\}; v, c, g, u_i; \mu)}{\mathcal{Z}_\Psi^m \mathcal{Z}_\Phi^{\frac{n}{2}}}. \tag{F.14}$$

Since the bare vertex functions are independent of the running energy scale μ, the renormalized vertex functions satisfy the RG equation for a fixed μ:

$$\begin{aligned}\Bigg[&\sum_{i=1}^{2m+n-1} \left(z\mathbf{K}_i \cdot \nabla_{\mathbf{K}_i} + \vec{k}_i \cdot \nabla_{\vec{k}_i}\right) - \beta_v \frac{\partial}{\partial v} - \beta_c \frac{\partial}{\partial c} - \beta_g \frac{\partial}{\partial g} - \beta_{u_1} \frac{\partial}{\partial u_1} - \beta_{u_2} \frac{\partial}{\partial u_2} \\ &+2m\left(\eta_\Psi - \frac{5}{2}\right) + n(\eta_\Phi - 3) + 2(2m + n - 1)(z + 1)\Bigg] \Gamma^{(2m,n)}(\{k_i\}, v, c, g, u_i; \mu) = 0,\end{aligned} \tag{F.15}$$

where the critical exponents and beta functions of the velocities and couplings are given by

$$z = 1 - \frac{\mathrm{d}}{\mathrm{d}\log\mu} \log\left(\frac{\mathcal{Z}_3}{\mathcal{Z}_1}\right), \tag{F.16}$$

$$\eta_{\Psi(\Phi)} = \frac{1}{2} \frac{\mathrm{d}}{\mathrm{d}\log\mu} \log \mathcal{Z}_{\Psi(\Phi)}, \tag{F.17}$$

$$\beta_{\mathsf{A}} = \frac{\mathrm{d}\mathsf{A}}{\mathrm{d}\log\mu}, \qquad \mathsf{A} = v, c, g, u_1, u_2. \tag{F.18}$$

Here, z denotes the dynamical critical exponent and η_Ψ (η_Φ) denotes the anomalous scaling dimension of the fermion (boson) field with respect to the Gaussian tree-level scaling.

The one-loop counterterm coefficients in $d = 3$ are given by [142]

$$\mathcal{Z}_1 = 1 - \frac{(N_c^2 - 1)}{4\pi^2 N_c N_f} \frac{g^2}{c} h_1(v, c) \log\left(\frac{\Lambda}{\mu}\right), \tag{F.19}$$

$$\mathcal{Z}_2 = 1 + \frac{(N_c^2 - 1)}{4\pi^2 N_c N_f} \frac{g^2}{c} h_2(v, c) \log\left(\frac{\Lambda}{\mu}\right), \tag{F.20}$$

$$\mathcal{Z}_3 = 1 - \frac{(N_c^2 - 1)}{4\pi^2 N_c N_f} \frac{g^2}{c} h_2(v, c) \log\left(\frac{\Lambda}{\mu}\right), \tag{F.21}$$

$$\mathcal{Z}_4 = 1 - \frac{1}{4\pi}\frac{g^2}{v}\log\left(\frac{\Lambda}{\mu}\right), \tag{F.22}$$

$$\mathcal{Z}_5 = 0, \tag{F.23}$$

$$\mathcal{Z}_6 = 1 - \frac{1}{8\pi^3 N_c N_f}\frac{g^2}{c}h_3(v,c)\log\left(\frac{\Lambda}{\mu}\right), \tag{F.24}$$

$$\mathcal{Z}_7 = 1 + \frac{1}{2\pi^2 c^2}\left[(N_c^2+7)u_1 + 2\left(\frac{2N_c^2-3}{N_c}\right)u_2 + 3\left(\frac{N_c^2+3}{N_c^2}\right)\frac{u_2^2}{u_1}\right]\log\left(\frac{\Lambda}{\mu}\right), \tag{F.25}$$

$$\mathcal{Z}_8 = 1 + \frac{1}{2\pi^2 c^2}\left[12u_1 + 2\left(\frac{N_c^2-9}{N_c}\right)u_2\right]\log\left(\frac{\Lambda}{\mu}\right). \tag{F.26}$$

Here, the $h_i(v,c)$ are finite functions of v and c defined in Ref. [142]. They have the following limiting behaviors:

$$\lim_{c\to 0} h_1(wc,c) = \frac{\pi}{2}, \quad \lim_{c\to 0} h_2(wc,c) = 2c, \quad \text{and} \quad \lim_{c\to 0} h_3(wc,c) = \frac{2\pi^2}{1+w}, \tag{F.27}$$

with $w = v/c$ fixed. In the low-energy limit, all g, v, c, u_1 and u_2 flow to zero such that $\lambda \equiv g^2/v \sim 1/l$, $\kappa_i \equiv u_i/c^2 \sim 1/l$, for $i = 1, 2$, and $v \sim c \sim 1/\log(l)$, where l is the logarithmic length scale [142]. The quasi-local marginal Fermi-liquid fixed point is stable. While the leading scaling behaviors are characterized by the Gaussian critical exponents, there exist logarithmic corrections generated from the marginally irrelevant couplings. Below, we discuss those corrections in the two-point functions. For simplicity, we set $u_1 = u_2 = 0$, and focus on the corrections from the Yukawa coupling.

F.2 Fermionic and Bosonic Green's Functions

According to Eq. (F.15), the scaling form of the two-point functions is governed by

$$\left[z\mathbf{K}\cdot\nabla_{\mathbf{K}} + \vec{k}\cdot\nabla_{\vec{k}} - \beta_w\frac{\partial}{\partial w} - \beta_\lambda\frac{\partial}{\partial\lambda} - \beta_c\frac{\partial}{\partial c} + \widetilde{D}_{\mathsf{a}}\right]\Gamma^{(2)}_{\mathsf{a}}(k,\lambda,w,c;\mu) = 0. \tag{F.28}$$

Here, $\mathsf{a} = \mathsf{b}, \mathsf{f}$ labels the bosonic and fermionic two-point functions, respectively. We write the RG equation in terms of c, $\lambda \equiv g^2/v$ and $w \equiv v/c$. In particular, λ controls the perturbative expansion in three dimensions [142]. $\widetilde{D}_{\mathsf{a}}$ denotes the total scaling dimension of the two-point vertex functions,

$$\widetilde{D}_{\mathsf{f}} = 2(\eta_\Psi + z) - 3, \tag{F.29}$$

$$\widetilde{D}_{\mathsf{b}} = 2(\eta_\Phi + z - 2), \tag{F.30}$$

where the dynamical critical exponent and the anomalous dimensions of the fields are defined in Eq. (F.16) and (F.17), respectively. Eq. (F.28) can be rewritten as

$$\left[\mathbf{K}\cdot\nabla_{\mathbf{K}} + \frac{\vec{k}}{z(l)}\cdot\nabla_{\vec{k}} + \frac{\mathrm{d}}{\mathrm{d}l} + \frac{\widetilde{D}_{\mathsf{a}}(l)}{z(l)}\right]\Gamma^{(2)}_{\mathsf{a}}[k,\lambda(l),w(l),c(l)] = 0, \tag{F.31}$$

where the scale-dependent couplings obey

$$\frac{\mathrm{d}w(l)}{\mathrm{d}l} = -\frac{\beta_w}{z(l)}, \quad \frac{\mathrm{d}\lambda(l)}{\mathrm{d}l} = -\frac{\beta_\lambda}{z(l)}, \qquad \frac{\mathrm{d}c(l)}{\mathrm{d}l} = -\frac{\beta_c}{z(l)}, \tag{F.32}$$

with $[w(0), \lambda(0), c(0)] = (w_0, \lambda_0, c_0)$ and l is the logarithmic length scale. The solution to Eq. (F.31) is given by

$$\Gamma^{(2)}_{\mathsf{a}}(\mathbf{K}, \vec{k}, \lambda_0, w_0, c_0) = \exp\left[\int_0^l \mathrm{d}\ell \frac{\widetilde{D}_{\mathsf{a}}(\ell)}{z(\ell)}\right] \Gamma^{(2)}_{\mathsf{a}}\left[e^l \mathbf{K}, \exp\left\{\int_0^l \frac{\mathrm{d}\ell}{z(\ell)}\right\} \vec{k}, \lambda(l), w(l), c(l)\right]. \tag{F.33}$$

The boundary problems in Eq. (F.32) are solved by following the results of Ref. [142],

$$\lambda(l) = \frac{4\pi(N_c^2 - 1 + N_c N_f)}{N_c^2 + N_c N_f - 3} \frac{1}{l}, \tag{F.34}$$

$$w(l) = \frac{N_c N_f}{N_c^2 - 1} + \mathcal{O}\left(\frac{1}{\log(l)}\right), \tag{F.35}$$

$$c(l) = \frac{\pi(N_c^2 + N_c N_f - 3)}{4(N_c^2 - 1 + N_c N_f)} \frac{1}{\log l}, \tag{F.36}$$

in the large l limit.

The integrations over the length scale in Eq. (F.33) are straightforward to perform in both the bosonic and fermionic cases after separating the contributions from the dynamical critical exponent and the net anomalous dimension of the fields. Choosing $l = \log(\mu_0/|\mathbf{K}|)$ with $\mu_0 = \Lambda$ being the UV scale at which the bare theory is defined, Eq. (F.33) takes the scaling form:

$$\Gamma^{(2,0)}_n(\mathbf{K}, \vec{k}) = \Gamma^{(2)}_f(\mathbf{K}, \vec{k}) = F_\Psi(|\mathbf{K}|) \left[i F_z(|\mathbf{K}|) \mathbf{\Gamma} \cdot \mathbf{K} + i\gamma_2 \varepsilon_n(\vec{k}; v_{|\mathbf{K}|})\right], \tag{F.37}$$

where

$$F_z(|\mathbf{K}|) = \exp\left\{\frac{(N_c^2 + N_c N_f - 1)}{2(N_c^2 + N_c N_f - 3)} \log\left[\log\left(\frac{\Lambda}{|\mathbf{K}|}\right)\right]\right\}, \tag{F.38}$$

$$F_\Psi(|\mathbf{K}|) = \sqrt{\log\left[\log\left(\frac{\Lambda}{|\mathbf{K}|}\right)\right]}. \tag{F.39}$$

Moreover, $v_{|\mathbf{K}|} = v\left[\log(\Lambda/|\mathbf{K}|)\right]$ with

$$v(l) = w(l)c(l) \approx \frac{\pi N_c N_f (N_c^2 + N_c N_f - 3)}{4(N_c^2 - 1)(N_c^2 + N_c N_f - 1)} \frac{1}{\log l}, \tag{F.40}$$

in the low-energy limit and Eq. (F.37) is obtained by keeping $\vec{k}/[|\mathbf{K}| F_z(|\mathbf{K}|)] \sim 1$ fixed.

Similarly, the boson two-point function takes the form,

$$\Gamma^{(0,2)}(\mathbf{Q}, \vec{q}) = \Gamma^{(2)}_b(\mathbf{Q}, \vec{q}) = F_\Phi(|\mathbf{Q}|) \left[F_z(|\mathbf{Q}|)^2 |\mathbf{Q}|^2 + c^2_{|\mathbf{Q}|} |\vec{q}|^2\right], \tag{F.41}$$

where

$$F_\Phi(|\mathbf{Q}|) = \log\left[\log\left(\frac{\Lambda}{|\mathbf{Q}|}\right)\right], \tag{F.42}$$

and $c_{|\mathbf{Q}|} = c\left[\log(\Lambda/|\mathbf{Q}|)\right]$. Eq. (F.41) is obtained by setting $l = \log(\Lambda/|\mathbf{Q}|)$ while keeping $\vec{q}/[|\mathbf{Q}|F_z(|\mathbf{Q}|)] \sim 1$ fixed and $c(l)$ is given by Eq. (F.36).

Appendix G | Quantum Corrections in $2 \leq d < 3$

In this appendix we provide details on the computations of the quantum corrections to the minimal local action depicted in Figs. 2.2(b), 2.2(c), 3.5(c), 2.3(a), 2.3(b) and 2.3(c) for the theory in dimensions $2 \leq d < 3$.

G.1 One-loop boson self-energy

The one-loop correction that generates dynamics of the boson is shown in Fig. 2.2(b). Its contribution to the quantum effective action reads

$$\delta\mathbf{\Gamma}^{(0,2)}_{1\mathrm{L}} = \frac{1}{4}\int \mathrm{d}q \Pi^{1\mathrm{L}}(q)\mathrm{Tr}\left[\Phi(-q)\Phi(q)\right], \tag{G.1}$$

where the one-loop boson self-energy is given by

$$\Pi^{1\mathrm{L}}(q) = -2v\beta_d^2 \sum_{n=1}^{4}\int \mathrm{d}k \mathrm{Tr}\left[\gamma_{d-1}G^{(0)}_{\overline{n}}(k+q;v)\gamma_{d-1}G^{(0)}_{n}(k;v)\right]. \tag{G.2}$$

Here $G^{(0)}_n(k;v)$ is the bare fermion propagator given in Eq. (3.24) and β_d is defined in Eq. (3.19). Taking the trace over the spinor indices and integrating over the spatial momenta $\vec{k}$, yields

$$\Pi^{1\mathrm{L}}(q) = -2\beta_d^2 \int\limits_{\mathbb{R}^{d-1}} \frac{\mathrm{d}\mathbf{K}}{(2\pi)^{d-1}} \frac{\mathbf{K}\cdot(\mathbf{K}+\mathbf{Q})}{|\mathbf{K}||\mathbf{K}+\mathbf{Q}|}. \tag{G.3}$$

Subtracting the mass renormalization, we focus on the momentum dependent self-energy: $\Delta\Pi^{1\mathrm{L}}(q) = \Pi^{1\mathrm{L}}(q) - \Pi^{1\mathrm{L}}(0)$. Integration over $\mathbf{K}$ is done after imposing a cutoff Λ in the UV. In the $\Lambda/|\mathbf{Q}| \gg 1$ limit this becomes

$$\Delta\Pi^{1\mathrm{L}}(q) = \frac{\beta_d^2\Gamma\left(\frac{5-d}{2}\right)\Gamma\left(\frac{d}{2}\right)}{2^{2d-5}\pi^{\frac{d}{2}}\Gamma\left(\frac{d+1}{2}\right)}|\mathbf{Q}|^{d-1}\left(\frac{1}{3-d} - \frac{1}{3-d}\left[\frac{2\cos\left(\frac{\pi d}{2}\right)}{\pi(d-3)}\right]\left(\frac{\Lambda}{|\mathbf{Q}|}\right)^{d-3}\right). \tag{G.4}$$

While the expression is logarithmically divergent in $d = 3$, it is UV finite for $d < 3$. In $d < 3$, the one-loop boson self-energy is given by

$$\Delta\Pi^{1\mathrm{L}}(q) = |\mathbf{Q}|^{d-1}. \tag{G.5}$$

Notice that this reduces to Eq. (C.4) when $d = 2$.

G.2 Two-loop boson self-energy

We first compute the two-loop boson self-energy shown in Fig. 2.2(c), and then comment on the contribution arising from Fig. 3.5(c). The contribution of Fig. 2.2(c) to the quantum effective action is given by

$$\delta\mathbf{\Gamma}^{(0,2)}_{\rm 2L} = \frac{1}{4}\int \mathrm{d}q \Pi^{\rm 2L}(q) \mathrm{Tr}\left[\Phi(q)\Phi(-q)\right] \tag{G.6}$$

with

$$\begin{aligned}\Pi^{\rm 2L}(q) = -\frac{4\beta_d^4 v^2}{N_c N_f}\sum_{n=1}^{4}\int \mathrm{d}k \int \mathrm{d}p \mathrm{Tr}\Big[&\gamma_{d-1} G^{(0)}_{\overline{n}}(k+p;v) \\ &\times \gamma_{d-1} G^{(0)}_{n}(k+q+p;v)\gamma_{d-1} G^{(0)}_{\overline{n}}(k+q;v)\gamma_{d-1} G^{(0)}_{n}(k;v)\Big] D(p).\end{aligned} \tag{G.7}$$

Here β_d is defined in Eq. (3.19), $D(p)$ is given by the self-consistent propagator in Eq. (3.21) and $G^{(0)}_n(k;v)$ is the bare fermion propagator given in Eq. (3.24). The frequency-dependent part of the two-loop self-energy is subleading with respect to the one-loop boson self-energy by a factor of $w(v) = v/c(v)$. Therefore, we focus on the momentum-dependent part by setting $\mathbf{Q} = \mathbf{0}$. Taking the trace over the spinor indices, changing variables to $k_+ = \varepsilon_n(\vec{k};v)$ and $k_- = \varepsilon_{\overline{n}}(\vec{k}+\vec{q};v)$, and noting that the latter has a Jacobian of $1/(2v)$, allows the spatial part of the two-loop boson self-energy to be written as

$$\begin{aligned}\Pi^{\rm 2L}(\mathbf{0},\vec{q}) = -\frac{4v\beta_d^4}{N_c N_f}\sum_{n=1}^{4}\int \mathrm{d}k \int \mathrm{d}p \Bigg(&\frac{1}{(\mathbf{K}^2+k_+^2)(\mathbf{K}^2+k_-^2)} \\ &\times \frac{1}{\{(\mathbf{K}+\mathbf{P})^2 + [k_- + \varepsilon_{\overline{n}}(\vec{p}-\vec{q};v)]^2\}\{(\mathbf{K}+\mathbf{P})^2 + [k_+ + \varepsilon_n(\vec{p}+\vec{q};v)]^2\}} \\ &\times \Big\{\big[(\mathbf{K}^2 - k_+k_-)\left\{(\mathbf{K}+\mathbf{P})^2 - [k_+ + \varepsilon_n(\vec{p}+\vec{q};v)][k_- + \varepsilon_{\overline{n}}(\vec{p}-\vec{q};v)]\right\} \\ &-\mathbf{K}\cdot(\mathbf{K}+\mathbf{P})[k_+ + k_- + \varepsilon_n(\vec{p}+\vec{q};v) + \varepsilon_{\overline{n}}(\vec{p}-\vec{q};v)](k_+ + k_-)]\Big\}\Bigg) D(p).\end{aligned} \tag{G.8}$$

This expression can be written as a sum of the contributions from the four hot spots,

$$\Pi^{\rm 2L}(\mathbf{0},\vec{q}) = \sum_{n=1}^{4}\Pi^{\rm 2L}_n(\vec{q}). \tag{G.9}$$

Let us first consider the contribution from the $n=1$ hot spot. Since the self-energy depends on the external momentum component q_x only through vq_x, the first hot spot gives rise to the self-energy that depends on q_y to the leading order in the small v limit. After setting $q_x = 0$, we perform a change of variables $p_x \to p_x/v$ to write the the two-loop boson self-energy as

$$\begin{aligned}\Pi^{\rm 2L}_1(\vec{q}) = -\frac{4w(v)^{d-1}\beta_d^4}{N_c N_f}\int \mathrm{d}k \int \mathrm{d}p \Bigg\{&\frac{1}{w(v)^{d-1}|\mathbf{P}|^{d-1} + |p_x|^{d-1} + v^{d-1}|p_y|^{d-1}} \\ &\times \frac{1}{(\mathbf{K}^2+k_-^2)[(\mathbf{K}+\mathbf{P})^2 + (k_- + p_x - p_y + q_y)^2][(\mathbf{K}+\mathbf{P})^2 + (k_+ + p_x + p_y + q_y)^2]}\end{aligned} \tag{G.10}$$

$$\times \frac{1}{(\mathbf{K}^2+k_+^2)}\left[(\mathbf{K}^2-k_+k_-)\left[(\mathbf{K}+\mathbf{P})^2-(k_++p_x+p_y+q_y)(k_-+p_x-p_y+q_y)\right]\right.$$
$$\left.-\mathbf{K}\cdot(\mathbf{K}+\mathbf{P})(k_++k_-+2p_x+2q_y)(k_++k_-)]\right\}.$$

We can neglect $|vp_y|^{d-1}$ in the boson propagator in the small v limit. The integration over p_x is divided into two regimes: $p_x \in (-\lambda,\lambda)$ and $p_x \in \mathbb{R}\setminus(-\lambda,\lambda)$ where $\lambda \sim \min(k_+,k_-,\mathbf{P},\mathbf{K},p_y)$ is a momentum scale below which the p_x dependence in the fermion propagators can be ignored. The exact form of λ is unimportant in the small $w(v)$ limit. The integration over the first regime is divergent in the small $w(v)$ limit due to the infrared singularity that is cut off by $w(v)|\mathbf{P}|$. On the other hand, the contribution from the second regime is regular. To the leading order in $w(v)\ll 1$, we can keep only the first contribution to write the p_x integration as

$$\overline{\mathfrak{S}}\left(d-2;w(v);\frac{\lambda}{|\mathbf{P}|}\right)\equiv\frac{\pi(d-2)^{-1}|\mathbf{P}|^{d-2}}{\Gamma\left(\frac{d-2}{d-1}\right)\Gamma\left(\frac{d}{d-1}\right)}\int_{-\lambda}^{\lambda}\frac{\mathrm{d}p_x}{(2\pi)}\left[\frac{w(v)^{d-2}}{w(v)^{d-1}|\mathbf{P}|^{d-1}+|p_x|^{d-1}}\right]. \tag{G.11}$$

In the $w(v)\to 0$ and in the $d\to 2^+$ limits, $\overline{\mathfrak{S}}[d-2;w(v);\lambda/|\mathbf{P}|]$ becomes independent of $\lambda/|\mathbf{P}|$ because it has the following limiting behaviors:

$$\lim_{d\to 2^+}\overline{\mathfrak{S}}\left(d-2;w(v);\frac{\lambda}{|\mathbf{P}|}\right)=-\log\left[w(v)\right],\quad \lim_{w(v)\to 0}\overline{\mathfrak{S}}\left(d-2;w(v);\frac{\lambda}{|\mathbf{P}|}\right)=\frac{1}{d-2}. \tag{G.12}$$

Since we are mainly interested in these limits, we can replace $\overline{\mathfrak{S}}[d-2;w(v);\lambda/|\mathbf{P}|]$ with

$$\mathfrak{S}[d-2;w(v)]\equiv\overline{\mathfrak{S}}[d-2;w(v);1]=\frac{1}{d-2}\left[1-w(v)^{d-2}\right], \tag{G.13}$$

where the last equality comes from explicitly computing Eq. (G.11) at $\lambda/|\mathbf{P}|=1$ in the small $w(v)$ limit. The p_x, p_y and k_+ integrations in Eq. (G.10) result in

$$\Pi_1^{2\mathrm{L}}(\vec{q})=-\frac{4(d-2)\beta_d^4 w(v)}{\pi N_c N_f}\Gamma\left(\frac{d-2}{d-1}\right)\Gamma\left(\frac{d}{d-1}\right)\mathfrak{S}[d-2;w(v)]\int_{\mathbb{R}^{d-1}}\frac{\mathrm{d}\mathbf{K}}{(2\pi)^{d-1}}\int_{\mathbb{R}}\frac{\mathrm{d}k_-}{(2\pi)}$$
$$\times\int_{\mathbb{R}^{d-1}}\frac{\mathrm{d}\mathbf{P}}{(2\pi)^{d-1}}\frac{|\mathbf{P}|^{2-d}}{|\mathbf{K}||\mathbf{K}+\mathbf{P}|}\left[\frac{4\mathbf{K}^2(\mathbf{K}+\mathbf{P})^2-2q_yk_-\mathbf{K}\cdot(\mathbf{K}+\mathbf{P})-\mathbf{K}\cdot(\mathbf{K}+\mathbf{P})k_-^2}{(4\mathbf{K}^2+k_-^2)[4(\mathbf{K}+\mathbf{P})^2+(k_-+2q_y)^2]}\right], \tag{G.14}$$

to leading order in $v\ll 1$. Subtracting the mass renormalization, the momentum dependent self-energy [defined as $\Delta\Pi_1^{2\mathrm{L}}(\vec{q})\equiv\Pi_1^{2\mathrm{L}}(\vec{q})-\Pi_1^{2\mathrm{L}}(\vec{0})$] is obtained to be

$$\Delta\Pi_1^{2\mathrm{L}}(\vec{q})=-\frac{4(d-2)\beta_d^4 w(v)}{\pi N_c N_f}\Gamma\left(\frac{d-2}{d-1}\right)\Gamma\left(\frac{d}{d-1}\right)\mathfrak{S}[d-2;w(v)]\int_{\mathbb{R}^{d-1}}\frac{\mathrm{d}\mathbf{K}}{(2\pi)^{d-1}}\int_{\mathbb{R}}\frac{\mathrm{d}k_-}{(2\pi)}$$
$$\times\int_{\mathbb{R}^{d-1}}\frac{\mathrm{d}\mathbf{P}}{(2\pi)^{d-1}}\frac{|\mathbf{P}|^{2-d}}{|\mathbf{K}||\mathbf{K}+\mathbf{P}|}\left[\frac{\mathcal{F}(\mathbf{P},\mathbf{K},k_-,q_y)}{(4\mathbf{K}^2+k_-^2)[4(\mathbf{K}+\mathbf{P})^2+(k_-+2q_y)^2][4(\mathbf{K}+\mathbf{P})^2+k_-^2]}\right], \tag{G.15}$$

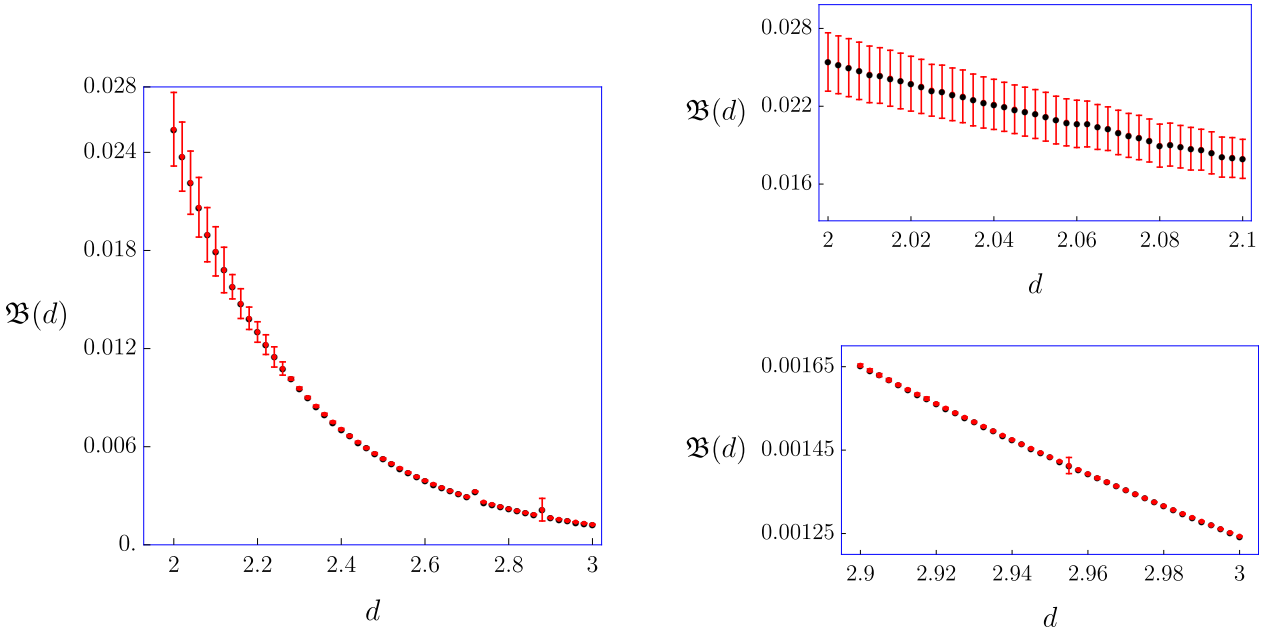

(a) $\mathfrak{B}(d)$ for $2 \leq d \leq 3$.

(b) $\mathfrak{B}(d)$ near $d = 2$ (top panel) and $d = 3$ (bottom panel).

Figure G.1: (a) The function $\mathfrak{B}(d)$. The (black) dots correspond to the value of the numerical integration and the (red) error bars represent the numerical error in the computation. (b) Numerical evaluation near $d = 2$ (top) and $d = 3$ (bottom).

where

$$\begin{aligned}\mathcal{F}(\mathbf{P},\mathbf{K},k_-,q_y) = &\left[4\mathbf{K}^2(\mathbf{K}+\mathbf{P})^2 - 2q_y k_- \mathbf{K}\cdot(\mathbf{K}+\mathbf{P}) - \mathbf{K}\cdot(\mathbf{K}+\mathbf{P})k_-^2\right]\left(4(\mathbf{K}+\mathbf{P})^2 + k_-^2\right)\\ &- \left[4\mathbf{K}^2(\mathbf{K}+\mathbf{P})^2 - \mathbf{K}\cdot(\mathbf{K}+\mathbf{P})k_-^2\right]\left[4(\mathbf{K}+\mathbf{P})^2 + (k_- + 2q_y)^2\right]. \qquad \text{(G.16)}\end{aligned}$$

We proceed by scaling out q_y from the above integral and introduce a two-variable Feynman parametrization that allows the explicit computation of the k_- integration. Performing this integration yields

$$\begin{aligned}\Delta\Pi_1^{2\mathrm{L}}(\vec{q}) = &-\frac{\beta_d^4(d-2)|q_y|^{d-1}w(v)}{64\pi N_c N_f}\Gamma\left(\frac{d-2}{d-1}\right)\Gamma\left(\frac{d}{d-1}\right)\mathfrak{S}[d-2;w(v)]\\ &\times\int\limits_{\mathbb{R}^{d-1}}\frac{\mathrm{d}\mathbf{K}}{(2\pi)^{d-1}}\int\limits_{\mathbb{R}^{d-1}}\frac{\mathrm{d}\mathbf{P}}{(2\pi)^{d-1}}\int\limits_0^1\mathrm{d}x_1\int\limits_0^{1-x_1}\mathrm{d}x_2\,\frac{|\mathbf{P}|^{2-d}}{|\mathbf{K}||\mathbf{K}+\mathbf{P}|} \qquad \text{(G.17)}\\ &\times\left\{\frac{3A+4B\left[\mathbf{K}\cdot(\mathbf{K}+\mathbf{P})(3x_1+3x_2-2)\right]}{\left[\mathbf{K}^2-2\mathbf{K}\cdot\mathbf{P}(x_1-1)-\mathbf{P}^2(x_1-1)-(x_1+x_2)^2+x_1+x_2\right]^{\frac{5}{2}}}\right\},\end{aligned}$$

where

$$\begin{aligned}A = -16\big\{&\mathbf{K}^2(2x_1+2x_2-1)(\mathbf{K}+\mathbf{P})^2\\ &+(x_1+x_2-1)\mathbf{K}\cdot(\mathbf{K}+\mathbf{P})\left[(\mathbf{K}+\mathbf{P})^2-(x_1+x_2-1)(x_1+x_2)\right]\big\},\end{aligned} \qquad \text{(G.18)}$$

$$B = 4\left[\mathbf{K}^2 - 2\mathbf{K}\cdot\mathbf{P}\,(x_1-1) - \mathbf{P}^2\,(x_1-1) - (x_1+x_2)^{\,2} + x_1 + x_2\right]. \tag{G.19}$$

Integrations over the remaining frequency and co-dimensional momentum components are done by introducing another two-variable Feynman parametrization. This yields the contribution from the $n=1$ hot spot to the two-loop boson self energy

$$\Delta\Pi_1^{2\mathrm{L}}(\vec{q}) = \frac{2\beta_d^4|q_y|^{d-1}}{N_c N_f} w(v)\mathfrak{B}(d)\mathfrak{S}[d-2;w(v)]\widetilde{\mathfrak{S}}\left(3-d;\frac{|q_y|}{\Lambda}\right), \tag{G.20}$$

where $\mathfrak{B}(d)$ is a smooth function of d (see Fig. G.1) defined by

$$\begin{aligned}\mathfrak{B}(d) = {}& \frac{(d-2)\Gamma(3-d)}{3\times 2^{d+4}\pi^{\frac{2d+3}{2}}}\frac{\cos\left(\frac{\pi d}{2}\right)\Gamma\left(\frac{d-2}{d-1}\right)\Gamma\left(\frac{d}{d-1}\right)\Gamma\left(\frac{5-d}{2}\right)}{\Gamma\left(\frac{8-d}{2}\right)}\int_0^1 \mathrm{d}x_1\int_0^{1-x_1}\mathrm{d}x_2\int_0^1\mathrm{d}y_1 \\ &\times\int_0^{1-y_1}\mathrm{d}y_2\left[\frac{(1-y_1-y_2)^{\frac{3}{2}}}{\sqrt{y_1}\sqrt{y_2}}\frac{(d-5)(d-3)C_3D_1^2 + D_2\left((3-d)C_2D_1+3C_1D_2\right)}{D_1^{\frac{5}{2}}D_2^{\frac{7-d}{2}}}\right],\end{aligned} \tag{G.21}$$

with

$$D_1 = -\left(x_1\left(y_1+y_2-1\right)-y_1\right)\left(x_1\left(y_1+y_2-1\right)-y_1+1\right), \tag{G.22}$$

$$D_2 = \left(x_1+x_2-1\right)\left(x_1+x_2\right)\left(y_1+y_2-1\right), \tag{G.23}$$

$$\begin{aligned}C_1 = {}& \left[-x_1^2\left(y_1+y_2-1\right)^{\,2} + x_1\left(2y_1-1\right)\left(y_1+y_2-1\right) - \left(y_1-1\right)y_1\right]\left\{\left(d^2-1\right)\left(-6x_1-6x_2+4\right)\right. \\ &\times\left(-x_1^2\left(y_1+y_2-1\right)^{\,2} + x_1\left(2y_1-1\right)\left(y_1+y_2-1\right) - \left(y_1-1\right)y_1\right) + (4-d)\left[(d-1)\left(-6x_1^3\left(y_1+y_2-1\right)\right.\right. \\ &\times\left.\left(2y_1+2y_2-3\right) + x_1^2\left(2\left(4\left(y_1+y_2\right)\left(4y_1+y_2\right) - 3x_2\left(y_1+y_2-1\right)\left(2y_1+2y_2-3\right)\right) - 62y_1 - 32y_2\right.\right. \\ &+\left.\left. 27\right) + x_1\left(3x_2\left(2y_1-1\right)\left(4y_1+4y_2-5\right) + y_1\left(-28y_1-16y_2+39\right) + 7y_2 - 15\right) - 6x_2\left(2\left(y_1-1\right)y_1+1\right) \\ &+\left. y_1\left(8y_1-7\right)+3\right) - 2\left(6x_1^3\left(y_1+y_2-1\right)\left(2y_1+2y_2-3\right) + x_1^2\left(2\left(3x_2\left(y_1+y_2-1\right)\left(2y_1+2y_2-3\right)\right.\right.\right. \\ &-\left.\left.\left. 4\left(y_1+y_2\right)\left(4y_1+y_2\right)\right) + 62y_1 + 32y_2 - 27\right) + x_1\left(-3x_2\left(2y_1-1\right)\left(4y_1+4y_2-5\right) - 7y_2\right.\right. \\ &+\left.\left. y_1\left(28y_1+16y_2-39\right)+9\right) + y_1\left(12x_2\left(y_1-1\right) - 8y_1 + 7\right)\right)]\left.\right\} - (d-6)(d-4)\left(x_1\left(y_1+y_2-1\right)-y_1\right) \\ &\times\left(x_1\left(y_1+y_2-1\right)-y_1+1\right)\left\{6x_1^3\left(y_1+y_2-2\right)\left(y_1+y_2-1\right) + x_1^2\left(2\left(3x_2\left(y_1+y_2-2\right)\left(y_1+y_2-1\right)\right.\right.\right. \\ &-\left.\left.\left. 2\left(y_1+y_2\right)\left(4y_1+y_2\right)\right) + 36y_1 + 18y_2 - 17\right) + x_1\left(-3x_2\left(2y_1-1\right)\left(2y_1+2y_2-3\right) - 3y_2\right.\right. \\ &+\left.\left. y_1\left(14y_1+8y_2-21\right)+5\right) + 6x_2\left(y_1-1\right)y_1 + \left(3-4y_1\right)y_1\right\},\end{aligned} \tag{G.24}$$

$$\begin{aligned}C_2 = {}& \left(-x_1^2\left(y_1+y_2-1\right)^{\,2} + x_1\left(2y_1-1\right)\left(y_1+y_2-1\right) - \left(y_1-1\right)y_1\right)\left[\left(d^2-1\right)\left(-6x_1-6x_2+4\right)\right. \\ &\times\left.\left(x_1^2 + \left(2x_2-1\right)x_1 + \left(x_2-1\right)x_2\right)\left(y_1+y_2-1\right) + (4-d)(d-1)\left(-\left(x_1+x_2\right)^{\,2} + x_1 + x_2\right)\right] \\ &+\left(x_1^2 + \left(2x_2-1\right)x_1 + \left(x_2-1\right)x_2\right)\left(y_1+y_2-1\right)\left\{\left(d^2-1\right)\left(-6x_1-6x_2+4\right)\left(-x_1^2\left(y_1+y_2-1\right)^{\,2}\right.\right. \\ &+\left. x_1\left(2y_1-1\right)\left(y_1+y_2-1\right) - \left(y_1-1\right)y_1\right) + (4-d)\left[(d-1)\left(-6x_1^3\left(y_1+y_2-1\right)\left(2y_1+2y_2-3\right)\right.\right. \\ &+\left. x_1^2\left(2\left(4\left(y_1+y_2\right)\left(4y_1+y_2\right) - 3x_2\left(y_1+y_2-1\right)\left(2y_1+2y_2-3\right)\right) - 62y_1 - 32y_2 + 27\right) \\ &+\left. x_1\left(3x_2\left(2y_1-1\right)\left(4y_1+4y_2-5\right) + y_1\left(-28y_1-16y_2+39\right) + 7y_2 - 15\right) - 6x_2\left(2\left(y_1-1\right)y_1+1\right)\right. \\ &+\left. y_1\left(8y_1-7\right)+3\right) - 2\left\{6x_1^3\left(y_1+y_2-1\right)\left(2y_1+2y_2-3\right) + x_1^2\left(2\left(3x_2\left(y_1+y_2-1\right)\left(2y_1+2y_2-3\right)\right.\right.\right. \\ &-\left.\left.\left. 4\left(y_1+y_2\right)\left(4y_1+y_2\right)\right) + 62y_1 + 32y_2 - 27\right) + x_1\left(-3x_2\left(2y_1-1\right)\left(4y_1+4y_2-5\right) - 7y_2\right.\right. \\ &+\left.\left. y_1\left(28y_1+16y_2-39\right)+9\right) + y_1\left(12x_2\left(y_1-1\right) - 8y_1 + 7\right)\right\}]\left.\right\} - (d-6)(d-4)\left(x_1^2 + \left(2x_2-1\right)x_1\right. \\ &+\left.\left(x_2-1\right)x_2\right)\left(x_1\left(y_1+y_2-1\right)-y_1\right)\left(x_1\left(y_1+y_2-1\right)-y_1+1\right),\end{aligned} \tag{G.25}$$

$$C_3 = \left(x_1^2 + (2x_2-1)\,x_1 + (x_2-1)\,x_2\right)(y_1+y_2-1)\left\{\left(d^2-1\right)(-6x_1-6x_2+4)\left(x_1^2+(2x_2-1)\,x_1 + (x_2-1)\,x_2\right)(y_1+y_2-1) + (4-d)(d-1)\left(-(x_1+x_2)^2 + x_1 + x_2\right)\right\}, \tag{G.26}$$

and

$$\widetilde{\mathfrak{S}}\left(3-d;\frac{|q_y|}{\Lambda}\right) \equiv -\frac{(d-2)\Gamma(3-d)\sin(\pi d)\csc\left(\frac{\pi d}{2}\right)}{6(2\pi)^{d+2}\mathfrak{B}(d)}\Gamma\left(\frac{d-2}{d-1}\right)\Gamma\left(\frac{d}{d-1}\right) \times \int_0^1 \mathrm{d}x_1 \int_0^{1-x_1}\mathrm{d}x_2 \int_0^1 \mathrm{d}y_1 \int_0^{1-y_1}\mathrm{d}y_2 \frac{(1-y_1-y_2)^{\frac{3}{2}}}{\sqrt{y_1}\sqrt{y_2}} \int_0^{\frac{\Lambda}{|q_y|}} \mathrm{d}P \left[\frac{C_1P^4+C_2P^2+C_3}{\left(D_1P^2+D_2\right)^{\frac{8-d}{2}}}\right]. \tag{G.27}$$

The function $\widetilde{\mathfrak{S}}\left(3-d;\frac{|q_y|}{\Lambda}\right)$ singles out the contribution that is divergent in the $d\to 3^-$ limit. In the large $\Lambda/|q_y|$ limit, it satisfies the limits

$$\lim_{d\to 3^-}\widetilde{\mathfrak{S}}\left(3-d;\frac{|q_y|}{\Lambda}\right) = -\log\left(\frac{|q_y|}{\Lambda}\right), \qquad \lim_{\frac{|q_y|}{\Lambda}\to 0}\widetilde{\mathfrak{S}}\left(3-d;\frac{|q_y|}{\Lambda}\right) = \frac{1}{3-d}. \tag{G.28}$$

The contribution from the remaining hot spots are obtained by performing a C_4 transformation on the $n=1$ hot spot contribution. Taking the contributions from all hot spots into account, Eq. (G.9) leads to

$$\Delta\Pi^{\mathrm{2L}}(\mathbf{0},\vec{q}) = \frac{4\beta_d^4}{N_cN_f}w(v)\mathfrak{B}(d)\mathfrak{S}[d-2;w(v)] \times\left[|q_y|^{d-1}\widetilde{\mathfrak{S}}\left(3-d;\frac{|q_y|}{\Lambda}\right)+|q_x|^{d-1}\widetilde{\mathfrak{S}}\left(3-d;\frac{|q_x|}{\Lambda}\right)\right]. \tag{G.29}$$

According to Eq. (G.28), the UV cutoff drops out in $d<3$ and we have

$$\Delta\Pi^{\mathrm{2L}}(\mathbf{0},\vec{q}) = \frac{4\beta_d^4}{(3-d)N_cN_f}w(v)\mathfrak{B}(d)\mathfrak{S}[d-2;w(v)]\left[|q_y|^{d-1}+|q_x|^{d-1}\right]. \tag{G.30}$$

We note that Eq. (G.21) in combination with Eq. (G.20) reproduce the result obtained in Appendix C in the $d\to 2^+$ limit and it is consistent with the findings of Ref. [148] close to three dimensions.

Now we show that Fig. 3.5(c) does not contribute to the momentum dependent self-energy. Fig. 3.5(c) is proportional to

$$\Upsilon^{\mathrm{2L}}(q) = \frac{4(N_c^2-1)\beta_d^4v^2}{N_cN_f}\sum_{n=1}^4\int\mathrm{d}k\int\mathrm{d}p\ \mathrm{Tr}\left[G^{(0)}_{\overline{n}}(k+q;v)\gamma_{d-1}G^{(0)}_n(k;v) \times\gamma_{d-1}G^{(0)}_{\overline{n}}(k+p;v)\gamma_{d-1}G^{(0)}_n(k;v)\gamma_{d-1}\right]D(p). \tag{G.31}$$

Taking the trace over the spinor indices, making the change of variables $k_+=\varepsilon_n(\vec{k};v)$, and $k_-=\varepsilon_{\overline{n}}(\vec{k}+\vec{p};v)$ and integrating over k_+ results in

$$\Upsilon^{\mathrm{2L}}(q) = \frac{2(N_c^2-1)\beta_d^4v}{N_cN_f}\sum_{n=1}^4\int\mathrm{d}p\int_{\mathbb{R}^{d-1}}\frac{\mathrm{d}\mathbf{K}}{(2\pi)^{d-1}}\int_{\mathbb{R}}\frac{\mathrm{d}k_-}{(2\pi)} \times\left[\frac{((\mathbf{K}\cdot\mathbf{P})(\mathbf{K}\cdot\mathbf{Q})-\mathbf{K}^2(\mathbf{P}\cdot\mathbf{Q}))D(p)}{|\mathbf{K}|^3[(\mathbf{K}+\mathbf{P})^2+k_-^2]\{(\mathbf{K}+\mathbf{Q})^2+[k_--\varepsilon_{\overline{n}}(\vec{p}-\vec{q};v)]^2\}}\right]. \tag{G.32}$$

This expression vanishes when $\mathbf{Q}=\mathbf{0}$ for any v, and there is no spatial momentum dependent contribution in $d>2$. We note that this diagram is exactly zero in $d=2$ [131, 133, 134] as pointed out in Sec. 2.3.

G.3 One-loop fermion self-energy

The quantum correction in Fig. 2.3(a) reads

$$\delta\mathbf{\Gamma}^{(2,0)}_{1\mathrm{L}}=\sum_{n=1}^{4}\sum_{\sigma=1}^{N_c}\sum_{j=1}^{N_f}\int \mathrm{d}q\overline{\Psi}_{n,\sigma,j}(q)\Sigma^{1\mathrm{L}}_{n}(q)\Psi_{n,\sigma,j}(q), \tag{G.33}$$

where the one-loop fermion self-energy is given by

$$\Sigma^{1\mathrm{L}}_{n}(q)=\frac{2\beta_d^2(N_c^2-1)v}{N_cN_f}\int \mathrm{d}k\ \left[\gamma_{d-1}G^{(0)}_{\overline{n}}(k+q;v)\gamma_{d-1}\right]D(k). \tag{G.34}$$

Here $G^{(0)}_n(k;v)$, β_d and $D(k)$ are defined in Eqs. (3.24), (3.19) and (3.21), respectively. We will consider the part of the self-energy that depends on the spatial momentum and the one that depends on the frequency and co-dimensional momentum, separately. For this purpose we write

$$\Sigma_n(\mathbf{Q},\vec{q})=(\mathbf{\Gamma}\cdot\mathbf{Q})\overline{\Sigma}_{n,\mathrm{f}}(\mathbf{Q})+\gamma_{d-1}\Sigma_{n,\mathrm{s}}(\vec{q}), \tag{G.35}$$

with

$$\overline{\Sigma}_{n,\mathrm{f}}(\mathbf{Q})=\frac{1}{2}\mathrm{Tr}\left[\frac{(\mathbf{\Gamma}\cdot\mathbf{Q})}{\mathbf{Q}^2}\Sigma_n(\mathbf{Q},\vec{0})\right],\qquad \Sigma_{n,\mathrm{s}}(\vec{q})=\frac{1}{2}\mathrm{Tr}\left[\gamma_{d-1}\Sigma_n(\mathbf{0},\vec{q})\right]. \tag{G.36}$$

G.3-(a) $\overline{\Sigma}_{n,\mathrm{f}}(\mathbf{Q})$

We focus on the frequency and co-dimensional momentum component first,

$$\overline{\Sigma}^{1\mathrm{L}}_{n,\mathrm{f}}(\mathbf{Q})=\frac{2i\beta_d^2(N_c^2-1)v}{N_cN_f}\frac{1}{\mathbf{Q}^2}\int \mathrm{d}k\left(\frac{\mathbf{Q}\cdot(\mathbf{K}+\mathbf{Q})}{(\mathbf{K}+\mathbf{Q})^2+\varepsilon_{\overline{n}}(\vec{k};v)^2}\right)D(k). \tag{G.37}$$

For concreteness we consider the $n=1$ hot spot in the small v limit. Performing the scaling $k_x\to k_x/c(v)$ yields

$$\begin{aligned}\overline{\Sigma}^{1\mathrm{L}}_{1,\mathrm{f}}(\mathbf{Q})=\frac{2i\beta_d^2(N_c^2-1)w(v)}{N_cN_f}\frac{1}{\mathbf{Q}^2}\int \mathrm{d}k\Bigg\{&\left(\frac{\mathbf{Q}\cdot(\mathbf{K}+\mathbf{Q})}{(\mathbf{K}+\mathbf{Q})^2+[w(v)k_x-k_y]^2}\right)\\ &\times\frac{1}{|\mathbf{K}|^{d-1}+|k_x|^{d-1}+c(v)^{d-1}|k_y|^{d-1}}\Bigg\},\end{aligned} \tag{G.38}$$

where $w(v)=v/c(v)$. The integration over $\vec{k}$ gives

$$\begin{aligned}\overline{\Sigma}^{1\mathrm{L}}_{1,\mathrm{f}}(\mathbf{Q})=\frac{i\beta_d^2(N_c^2-1)w(v)}{N_cN_f\pi\mathbf{Q}^2}\Gamma\left(\frac{d}{d-1}\right)\int\limits_{\mathbb{R}^{d-1}}\frac{\mathrm{d}\mathbf{K}}{(2\pi)^{d-1}}\left(\frac{\mathbf{Q}\cdot(\mathbf{K}+\mathbf{Q})}{|\mathbf{K}+\mathbf{Q}|}\right)\\ \times\left[|\mathbf{K}|^{2-d}\Gamma\left(\frac{d-2}{d-1}\right)-\frac{[c(v)\widetilde{\Lambda}]^{2-d}(d-1)}{(d-2)\Gamma\left(\frac{1}{d-1}\right)}\right]\end{aligned} \tag{G.39}$$

in the small $c(v)$ limit.

In $d > 2$, the second term in the square brackets of Eq. (G.39) can be dropped, and the first term gives rise to a logarithmically divergent contribution. In $d = 2$, the two terms in the square brackets combine to become a logarithm, and the integration over $\mathbf{K}$ is finite. The latter can be seen explicitly in the computation of the one-loop fermion self-energy that is presented in Appendix D.

In all cases, the logarithmically divergent contribution can be written as

$$\overline{\Sigma}^{\text{1L}}_{1,\text{f}}(\mathbf{Q}) = -\frac{(N_c^2-1)\cos\left(\frac{\pi d}{2}\right)\Gamma\left(\frac{2d-3}{d-1}\right)\Gamma\left(\frac{1}{d-1}\right)\Gamma\left(\frac{d-1}{2}\right)}{2^{3-d}N_cN_f\pi^{3/2}\Gamma\left(\frac{d}{2}\right)} iw(v)\log\left(\frac{\Lambda}{|\mathbf{Q}|}\right). \tag{G.40}$$

Here we have used the fact that $\Lambda \approx \widetilde{\Lambda}$ and the definition of β_d in Eq. (3.19). Combining this result with the renormalization condition in Eq. (B.6) and the fact that the other three hot spots give the same contribution, fixes Z_1 to

$$Z_1 = 1 - \frac{(N_c^2-1)\zeta(d)}{N_cN_f} w(v)\log\left(\frac{\Lambda}{\mu}\right), \tag{G.41}$$

with $\zeta(d)$ defined in Eq. (3.31).

G.3-(b) $\quad \Sigma_{n,\text{s}}(\vec{q})$

Now we turn our attention to the spatial part of the self-energy defined in Eq. (G.36):

$$\Sigma^{\text{1L}}_{n,\text{s}}(\vec{q}) = -\frac{2(N_c^2-1)i\beta_d^2 v}{N_cN_f}\int \mathrm{d}k \left(\frac{\varepsilon_{\overline{n}}(\vec{k}+\vec{q};v)}{\varepsilon_{\overline{n}}(\vec{k}+\vec{q};v)^2+\mathbf{K}^2}\right) D(k). \tag{G.42}$$

Without loss of generality we consider the contribution from the $n = 1$ hot spot,

$$\Sigma^{\text{1L}}_{1,\text{s}}(\vec{q}) = -\frac{2i(N_c^2-1)\beta_d^2 v}{N_cN_f}\int \mathrm{d}k \left\{\left(\frac{[vk_x - k_y + \varepsilon_3(\vec{q};v)]}{[vk_x - k_y + \varepsilon_3(\vec{q};v)]^2+\mathbf{K}^2}\right) \times \frac{1}{|\mathbf{K}|^{d-1} + c(v)^{d-1}(|k_x|^{d-1}+|k_y|^{d-1})}\right\}. \tag{G.43}$$

When v and $c(v)$ are small, the integration over k_x yields

$$\Sigma^{\text{1L}}_{1,\text{s}}(\vec{q}) = -\frac{2i(N_c^2-1)\beta_d^2}{(d-1)\pi N_cN_f} w(v) \int_{\mathbb{R}^{d-1}} \frac{\mathrm{d}\mathbf{K}}{(2\pi)^{d-1}} \int_{\mathbb{R}} \frac{\mathrm{d}k_y}{(2\pi)} \left[\left(\frac{[\varepsilon_3(\vec{q};v)-k_y]}{[\varepsilon_3(\vec{q};v)-k_y]^2+\mathbf{K}^2}\right) \times \left[\Gamma\left(\frac{d-2}{d-1}\right)\Gamma\left(\frac{1}{d-1}\right)\frac{1}{[|\mathbf{K}|^{d-1}+c(v)^{d-1}|k_y|^{d-1}]^{\frac{d-2}{d-1}}} - \frac{c(v)^{2-d}\widetilde{\Lambda}^{2-d}(d-1)}{(d-2)}\right]. \tag{G.44}$$

We drop the second term in the square brackets because the integrand is odd in $[\varepsilon_3(\vec{q};v)-k_y]$. Focusing only on the first term, the remaining integrations are done by writing the expression

as an antiderivative with respect to $c(v)$:

$$\Sigma^{1L}_{1,s}(\vec{q}) = \frac{2(d-2)i(N_c^2-1)\beta_d^2}{(d-1)\pi N_c N_f}\Gamma\left(\frac{d-2}{d-1}\right)\Gamma\left(\frac{1}{d-1}\right)w(v)\int_0^{c(v)} \mathrm{d}\mathsf{c}\mathsf{c}^{d-2}\int_{\mathbb{R}^{d-1}}\frac{\mathrm{d}\mathbf{K}}{(2\pi)^{d-1}} \times \int_{\mathbb{R}}\frac{\mathrm{d}k_y}{(2\pi)}\left[\left(\frac{[\varepsilon_3(\vec{q};v)-k_y]}{[\varepsilon_3(\vec{q};v)-k_y]^2+\mathbf{K}^2}\right)\frac{|k_y|^{d-1}}{(|\mathbf{K}|^{d-1}+\mathsf{c}^{d-1}|k_y|^{d-1})^{\frac{2d-3}{d-1}}}\right]. \tag{G.45}$$

The lower limit of the integration over c is determined from the fact that the integration over k_y in Eq. (G.44) vanishes in the small $c(v)$ limit. The radial integration for $\mathbf{K}$ is divided into two regions: $K \equiv |\mathbf{K}| \in (0, |\varepsilon_3(\vec{q};v)-k_y|)$ and $K \in (|\varepsilon_3(\vec{q};v)-k_y|, \infty)$. In the first region, the fermionic contribution to the integrand varies slowly in $\mathbf{K}$ and can be Taylor expanded around the origin. Only the zeroth order term in the expansion becomes IR divergent when $\mathsf{c}=0$, and thus, provides the leading order contribution to the integration in the small $c(v)$ limit. The contribution from the second region is regular at $\mathsf{c}=0$ and therefore it is subleading in the small $c(v)$ limit. Keeping only the leading contribution in the small $c(v)$ limit, we obtain

$$\Sigma^{1L}_{1,s}(\vec{q}) = \frac{(d-2)i(N_c^2-1)\beta_d^2 w(v)}{2^{d-2}\pi^{\frac{d+1}{2}}N_c N_f}\frac{\Gamma\left(\frac{d-2}{d-1}\right)\Gamma\left(\frac{1}{d-1}\right)}{\Gamma\left(\frac{d+1}{2}\right)} \times \int_0^{c(v)}\mathrm{d}\mathsf{c}\int_{\mathbb{R}}\frac{\mathrm{d}k_y}{(2\pi)}\frac{[\varepsilon_3(\vec{q};v)-k_y]}{[\varepsilon_3(\vec{q};v)-k_y]^2}|k_y|\overline{\mathfrak{S}}'\left(d-2;\mathsf{c};\frac{|\varepsilon_3(\vec{q};v)-k_y|}{|k_y|}\right), \tag{G.46}$$

where

$$\overline{\mathfrak{S}}'\left(d-2;\mathsf{c};\frac{|\varepsilon_3(\vec{q};v)-k_y|}{|k_y|}\right) \equiv \frac{1}{|k_y|}\int_0^{|\varepsilon_3(\vec{q};v)-k_y|}\mathrm{d}K\frac{\mathsf{c}^{d-2}|k_y|^{d-1}K^{d-2}}{(K^{d-1}+\mathsf{c}^{d-1}|k_y|^{d-1})^{\frac{2d-3}{d-1}}}. \tag{G.47}$$

While $\overline{\mathfrak{S}}'(d-2;\mathsf{c};|\varepsilon_3(\vec{q};v)-k_y|/|k_y|)$ depends on k_y and $\varepsilon_3(\vec{q};v)$, these dependences are suppressed in the $d\to 2^+$ or $\mathsf{c}\to 0$ limits. In either of these limits, $\overline{\mathfrak{S}}'(d-2;\mathsf{c};|\varepsilon_3(\vec{q};v)-k_y|/|k_y|)$ reduces to $\mathfrak{S}(d-2;\mathsf{c})$ defined in Eq. (G.13). From now on, we replace $\overline{\mathfrak{S}}'(d-2;\mathsf{c};|\varepsilon_3(\vec{q};v)-k_y|/|k_y|)$ with $\mathfrak{S}(d-2;\mathsf{c})$ in Eq. (G.46). Integration over c can be done by using the following limits:

$$\lim_{\xi\to 0^+}\int \mathrm{d}a\mathfrak{S}(\xi;a) = a - a\log(a) \overset{a\ll 1}{=} \lim_{\xi\to 0^+} a\mathfrak{S}(\xi;a), \tag{G.48}$$

$$\lim_{b\to 0}\int \mathrm{d}a\mathfrak{S}(\xi;ba) = \frac{a}{\xi} = a\lim_{a\to 0^+}\mathfrak{S}(\xi;a). \tag{G.49}$$

This allows us to write Eq. (G.46) as

$$\Sigma^{1L}_{1,s}(\vec{q}) = \frac{(d-2)i(N_c^2-1)\beta_d^2}{2^{d-2}\pi^{\frac{d+1}{2}}N_c N_f}\frac{\Gamma\left(\frac{d-2}{d-1}\right)\Gamma\left(\frac{1}{d-1}\right)}{\Gamma\left(\frac{d+1}{2}\right)}v\mathfrak{S}\left[d-2;c(v)\right]\varepsilon_3(\vec{q};v) \times \int_{\mathbb{R}}\frac{\mathrm{d}k_y}{(2\pi)}\left[\frac{(1-k_y)}{(1-k_y)^2}\right]|k_y|. \tag{G.50}$$

Here, we have scaled out the external momentum through the change of variables $k_y \to |\varepsilon_3(\vec{q};v)|k_y$. The integration over k_y is UV divergent and we cut it off by $\widetilde{\Lambda}/|\varepsilon_3(\vec{q};v)|$. In the large $\widetilde{\Lambda}/|\varepsilon_3(\vec{q};v)|$ limit,

$$\begin{aligned}\int_{-\frac{\widetilde{\Lambda}}{|\varepsilon_3(\vec{q};v)|}}^{\frac{\widetilde{\Lambda}}{|\varepsilon_3(\vec{q};v)|}} \frac{\mathrm{d}k_y}{(2\pi)}\left[\frac{1-k_y}{(1-k_y)^2}\right]|k_y| &= \lim_{\delta\to 0}\left[\int_{-\frac{\widetilde{\Lambda}}{|\varepsilon_3(\vec{q};v)|}}^{1-\delta}\frac{\mathrm{d}k_y}{(2\pi)} + \int_{1+\delta}^{\frac{\widetilde{\Lambda}}{|\varepsilon_3(\vec{q};v)|}}\frac{\mathrm{d}k_y}{(2\pi)}\right]\left[\frac{1-k_y}{(1-k_y)^2}\right]|k_y| \\ &= \frac{1}{\pi}\log\left(\frac{|\varepsilon_3(\vec{q};v)|}{\widetilde{\Lambda}}\right).\end{aligned} \tag{G.51}$$

Hence, the divergent contribution to the spatial part of the one-loop fermion self-energy for the fermions at the $n=1$ hot spot is given by

$$\Sigma^{1\mathrm{L}}_{1,\mathrm{s}}(\vec{q}) = -\frac{(d-2)i(N_c^2-1)\beta_d^2}{2^{d-2}\pi^{\frac{d+3}{2}}N_cN_f}\frac{\Gamma\left(\frac{d-2}{d-1}\right)\Gamma\left(\frac{1}{d-1}\right)}{\Gamma\left(\frac{d+1}{2}\right)}v\mathfrak{S}\left[d-2;c(v)\right]\varepsilon_3(\vec{q};v)\log\left(\frac{\widetilde{\Lambda}}{|\varepsilon_3(\vec{q};v)|}\right), \tag{G.52}$$

in the small v and large $\widetilde{\Lambda}/|\varepsilon_3(\vec{q};v)|$ limits. Introducing the value of β_d defined in Eq. (3.19) and combining this expression with the renormalization conditions in Eqs. (B.7) and (B.8) fixes the counterterm coefficients A_2 and A_3 to the one-loop order,

$$A_2^{1\mathrm{L}} = \frac{2(d-1)(N_c^2-1)\zeta(d)}{\pi N_cN_f}v\mathfrak{S}\left[d-2;c(v)\right]\log\left(\frac{\widetilde{\Lambda}}{\mu}\right), \tag{G.53}$$

$$A_3^{1\mathrm{L}} = -\frac{2(d-1)(N_c^2-1)\zeta(d)}{\pi N_cN_f}v\mathfrak{S}\left[d-2;c(v)\right]\log\left(\frac{\widetilde{\Lambda}}{\mu}\right), \tag{G.54}$$

with $\zeta(d)$ defined in Eq. (3.31). These expressions reduce to the ones found in Appendix D in the $d\to 2^+$ limit.

G.4 Two-loop fermion self-energy

We consider the two-loop fermion self-energy depicted in Fig. 2.3(c),

$$\delta\mathbf{\Gamma}^{(2,0)}_{2\mathrm{L}} = \sum_{n=1}^{4}\sum_{\sigma=1}^{N_c}\sum_{j=1}^{N_f}\int \mathrm{d}q\,\overline{\Psi}_{n,\sigma,j}(q)\Sigma^{2\mathrm{L}}_n(q)\Psi_{n,\sigma,j}(q), \tag{G.55}$$

where the two-loop fermion self-energy is given by

$$\begin{aligned}\Sigma^{2\mathrm{L}}_n(k) = \frac{4(N_c^2-1)\beta_d^4v^2}{N_c^2N_f^2}\int\mathrm{d}q\int\mathrm{d}p\,\Big[&\gamma_{d-1}G^{(0)}_{\overline{n}}(k+q;v) \\ &\times\gamma_{d-1}G^{(0)}_{n}(k+q+p;v)\gamma_{d-1}G^{(0)}_{\overline{n}}(k+p;v)\gamma_{d-1}\Big]D(p)D(q).\end{aligned} \tag{G.56}$$

Without loss of generality, we consider the $n=1$ hot spot contribution to the spatial piece of this quantum correction since its frequency part is strictly subleading with respect

to the one-loop correction due to an additional factor of $w(v) = v/c(v)$. The self-energy at $\mathbf{K} = \mathbf{0}$ becomes

$$\begin{aligned}\Sigma^{\mathrm{2L}}_{1,\mathrm{s}}(\vec{k}) = &-\frac{4i(N_c^2-1)\beta_d^4 v^2}{N_c^2 N_f^2}\int \mathrm{d}q \int \mathrm{d}p \\ &\times \Bigg\{ \frac{D(p)D(q)}{[\mathbf{P}^2+\varepsilon_3(\vec{k}+\vec{p};v)^2][\mathbf{Q}^2+\varepsilon_3(\vec{k}+\vec{q};v)^2][(\mathbf{P}+\mathbf{Q})^2+\varepsilon_1(\vec{k}+\vec{q}+\vec{p};v)^2]} \\ &\times \Big[(\mathbf{P}\cdot\mathbf{Q})\varepsilon_1(\vec{k}+\vec{p}+\vec{q};v) + \mathbf{Q}\cdot(\mathbf{P}+\mathbf{Q})\varepsilon_3(\vec{k}+\vec{p};v) \\ &\qquad + \Big[\mathbf{P}\cdot(\mathbf{P}+\mathbf{Q}) - \varepsilon_1(\vec{k}+\vec{p}+\vec{q};v)\varepsilon_3(\vec{k}+\vec{p};v)\Big]\varepsilon_3(\vec{k}+\vec{q};v)\Big]\Bigg\}.\end{aligned} \tag{G.57}$$

We proceed by performing the scaling $p_x \to p_x/v$ and $q_x \to q_x/v$ and dropping the dependences on p_y and q_y inside the boson propagators in the small v limit. In the small $c(v)$ limit, the integrations over p_x and q_x give

$$\begin{aligned}\Sigma^{\mathrm{2L}}_{1,\mathrm{s}}(\vec{k}) = &-\frac{4(d-2)^2 i(N_c^2-1)\beta_d^4 w(v)^2}{\pi^2 N_c^2 N_f^2}\Gamma\left(\frac{d-2}{d-1}\right)^2\Gamma\left(\frac{d}{d-1}\right)^2 \mathfrak{S}\left[d-2;w(v)\right]^2 \int\limits_{\mathbb{R}^{d-1}} \frac{\mathrm{d}\mathbf{Q}}{(2\pi)^{d-1}} \\ &\times \int\limits_{\mathbb{R}^{d-1}} \frac{\mathrm{d}\mathbf{P}}{(2\pi)^{d-1}} \int\limits_{\mathbb{R}} \frac{\mathrm{d}q_y}{(2\pi)} \int\limits_{\mathbb{R}} \frac{\mathrm{d}p_y}{(2\pi)} \Bigg\{ \frac{|\mathbf{P}|^{2-d}|\mathbf{Q}|^{2-d}}{[\mathbf{Q}^2+(\varepsilon_3(\vec{k};v)-q_y)^2]\{(\mathbf{P}+\mathbf{Q})^2+[\varepsilon_1(\vec{k};v)+p_y+q_y]^2\}} \\ &\times \frac{1}{(\mathbf{P}^2+(\varepsilon_3(\vec{k};v)-p_y)^2)}\Big[(\mathbf{P}\cdot\mathbf{Q})[\varepsilon_1(\vec{k};v)+p_y+q_y] + \mathbf{Q}\cdot(\mathbf{P}+\mathbf{Q})[\varepsilon_3(\vec{k};v)-p_y] \\ &+\{\mathbf{P}\cdot(\mathbf{P}+\mathbf{Q}) - [\varepsilon_1(\vec{k};v)+p_y+q_y][\varepsilon_3(\vec{k};v)-p_y]\}[\varepsilon_3(\vec{k};v)-q_y]\Big]\Bigg\},\end{aligned} \tag{G.58}$$

where $\mathfrak{S}[d-2;w(v)]$ is defined in Eq. (G.13). Here we ignore terms that are subleading in $c(v)$. We continue by making the change of variables $p_y \to p_y + \varepsilon_3(\vec{k};v)$ and $q_y \to q_y + \varepsilon_3(\vec{k};v)$ which makes the two-loop fermion self-energy depend on the external spatial momentum only through $\delta(\vec{k};v) \equiv \varepsilon_1(\vec{k};v) + 2\varepsilon_3(\vec{k};v) = 3vk_x - k_y$. After an introduction of a single-variable Feynman parametrization, the integration over p_y yields

$$\begin{aligned}\Sigma^{\mathrm{2L}}_{1,\mathrm{s}}(\vec{k}) = &-\frac{i(d-2)^2(N_c^2-1)\beta_d^4 w(v)^2}{\pi^2 N_c^2 N_f^2}\Gamma\left(\frac{d-2}{d-1}\right)^2\Gamma\left(\frac{d}{d-1}\right)^2 \mathfrak{S}[d-2;w(v)]^2 \\ &\times \int\limits_{\mathbb{R}^{d-1}} \frac{\mathrm{d}\mathbf{Q}}{(2\pi)^{d-1}} \int\limits_{\mathbb{R}^{d-1}} \frac{\mathrm{d}\mathbf{P}}{(2\pi)^{d-1}} \int\limits_{\mathbb{R}} \frac{\mathrm{d}q_y}{(2\pi)} |\mathbf{P}|^{2-d}|\mathbf{Q}|^{2-d} \int\limits_0^1 \mathrm{d}x \\ &\times \left[\frac{\mathcal{A} - q_y\{\mathbf{P}^2 + 2(1-x)\mathbf{P}\cdot\mathbf{Q} + (1-x)(\mathbf{Q}^2 + x[q_y+\delta(\vec{k};v)]^2)\}}{\{\mathbf{P}^2 + 2(1-x)\mathbf{P}\cdot\mathbf{Q} + (1-x)(\mathbf{Q}^2 + x[q_y+\delta(\vec{k};v)]^2)\}^{\frac{3}{2}}(q_y^2+\mathbf{Q}^2)}\right]\end{aligned} \tag{G.59}$$

with

$$\begin{aligned}\mathcal{A} = &-q_y[\mathbf{P}\cdot(\mathbf{P}+\mathbf{Q})] + x(\mathbf{P}\cdot\mathbf{Q})[q_y+\delta(\vec{k};v)] \\ &+ (1-x)[q_y+\delta(\vec{k};v)]\{\mathbf{Q}\cdot(\mathbf{Q}+\mathbf{P}) + xq_y[q_y+\delta(\vec{k};v)]\}.\end{aligned} \tag{G.60}$$

By introducing a second single-variable Feynman parametrization, the integration over q_y yields

$$\Sigma^{\mathrm{2L}}_{1,\mathrm{s}}(\vec{k}) = -\frac{i(d-2)^2(N_c^2-1)\delta(\vec{k};v)\beta_d^4 w(v)^2}{\pi^3 N_c^2 N_f^2}\Gamma\left(\frac{d-2}{d-1}\right)^2\Gamma\left(\frac{d}{d-1}\right)^2\mathfrak{S}[d-2;w(v)]^2 \\ \times\int\limits_{\mathbb{R}^{d-1}}\frac{\mathrm{d}\mathbf{Q}}{(2\pi)^{d-1}}\int\limits_{\mathbb{R}^{d-1}}\frac{\mathrm{d}\mathbf{P}}{(2\pi)^{d-1}}\int\limits_0^1\mathrm{d}x\int\limits_0^1\mathrm{d}y\frac{|\mathbf{P}|^{2-d}|\mathbf{Q}|^{2-d}}{\sqrt{y+x(1-x)(1-y)}}\left(\frac{\mathcal{C}_1}{\mathcal{D}_1^2}\right), \tag{G.61}$$

where

$$\mathcal{C}_1 = \frac{\sqrt{1-y}}{x+x^2(y-1)+y-xy}\left[xy(\mathbf{P}\cdot\mathbf{Q})+(1-x)\left\{x(1-y)\mathbf{P}\cdot(\mathbf{P}+\mathbf{Q})\right.\right. \\ \left.\left.+y\mathbf{Q}\cdot(\mathbf{P}+\mathbf{Q})+x(1-y)\left[\mathbf{P}^2+2(1-x)(\mathbf{P}\cdot\mathbf{Q})+(1-x)\mathbf{Q}^2\right]\right\}\right], \tag{G.62}$$

$$\mathcal{D}_1 = (1-y)\mathbf{P}^2+2(1-x)(1-y)(\mathbf{P}\cdot\mathbf{Q})+[1-x(1-y)]\mathbf{Q}^2 \\ +\frac{(1-x)(1-y)xy}{y+(1-x)(1-y)x}\delta(\vec{k};v)^2. \tag{G.63}$$

Integration over $\mathbf{P}$ is done by introducing a third single-variable Feynman parametrization. This process yields a $\mathbf{Q}$-dependent integrand that can be cast in the rotationally invariant way,

$$\Sigma^{\mathrm{2L}}_{1,\mathrm{s}}(\vec{k}) = \frac{i(d-2)^2(N_c^2-1)\delta(\vec{k};v)\beta_d^4 w(v)^2}{2^{2d-2}\pi^{\frac{2d+3}{2}}N_c^2N_f^2}\frac{\Gamma\left(\frac{d-2}{d-1}\right)^2\Gamma\left(\frac{d}{d-1}\right)^2}{\Gamma\left(\frac{d-2}{2}\right)\Gamma\left(\frac{d-1}{2}\right)}\mathfrak{S}[d-2;w(v)]^2\int\limits_0^1\mathrm{d}x \\ \times\int\limits_0^1\mathrm{d}y\int\limits_0^1\mathrm{d}z\frac{(1-z)z^{\frac{d-4}{2}}\sqrt{1-y}}{[y+x(1-x)(1-y)]^{\frac{3}{2}}[1-y(1-z)]^{\frac{d+1}{2}}}\int\limits_0^{\frac{\Lambda}{|\delta(\vec{k};v)|}}\mathrm{d}Q\left[\frac{(\mathcal{E}_1Q^2+\mathcal{E}_2)}{(\mathcal{H}_1Q^2+\mathcal{H}_2)^{\frac{3}{2}}}\right], \tag{G.64}$$

where the integration over the angular components has been done, and the integration over $Q\equiv|\mathbf{Q}|$ has been cut off in the UV since it is logarithmically divergent. The coefficients $\mathcal{E}_i$ and $\mathcal{H}_i$ are defined as follows:

$$\mathcal{E}_1 = \frac{1}{1-y(1-z)}\left\{(x-1)\left[2x^3(y-1)^2(z-1)(d(y-1)(z-1)-yz+y+2z-1)\right.\right. \\ +x^2(y-1)\left(-2d(y-1)(z-1)(y(z-1)-2z+1)+2y^2(z-1)^2\right. \\ -y(9z-4)(z-1)+z(8z-9)+2)+x(y-1)\left(2(d-1)y^2(z-1)^2\right. \\ \left.\left.\left.-y(z-1)(2d(z-1)-3z+2)+z(2d(z-1)-4z+3))+yz(y(z-1)+1)\right]\right\}, \tag{G.65}$$

$$\mathcal{E}_2 = \frac{2(d-1)(x-1)^2x^2(y-1)^2y(z-1)}{(x-1)x(y-1)+y}, \tag{G.66}$$

$$\mathcal{H}_1 = -\frac{(z-1)}{1-y(1-z)}\left[x^2(y-1)^2(z-1)-x(y-1)(y(z-1)-2z+1)\right. \\ \left.+y(y-1)(z-1)+z\right], \tag{G.67}$$

$$\mathcal{H}_2 = -\frac{(1-x)x(1-y)y(1-z)}{((x-1)x(y-1)+y)}. \tag{G.68}$$

For $\Lambda/|\delta(\vec{k};v)| \gg 1$, the divergent contribution to the two-loop fermion self-energy is given by

$$\Sigma^{2\mathrm{L}}_{1,\mathrm{s}}(\vec{k}) = -\frac{2i\beta_d^4(N_c^2-1)}{N_c^2N_f^2}\mathfrak{F}(d)w(v)^2\mathfrak{S}[d-2;w(v)]^2\delta(\vec{k};v)\log\left(\frac{\Lambda}{|\delta(\vec{k};v)|}\right), \tag{G.69}$$

where the positive function $\mathfrak{F}(d)$ is defined as

$$\begin{aligned}\mathfrak{F}(d) = {}& \frac{(d-2)^2}{(2\pi)^{d+2}}\frac{\Gamma\left(\frac{d-2}{d-1}\right)^2\Gamma\left(\frac{d}{d-1}\right)^2}{\Gamma(d-2)}\int_0^1 \mathrm{d}x\int_0^1 \mathrm{d}y\int_0^1 \mathrm{d}z\frac{(1-x)(1-y(1-z))^{\frac{-d}{2}}\sqrt{1-y}z^{\frac{d-4}{2}}}{[y+(1-x)x(1-y)]^{\frac{3}{2}}\sqrt{1-z}}\\
&\times\left\{\frac{\left(2x^3(y-1)^2(z-1)(d(y-1)(z-1)-yz+y+2z-1)+\right.}{((x(1-y)(1+y(-1+z)-2z)+x^2(-1+y)^2(-1+z)+(-1+y)y(-1+z)+z))^{\frac{3}{2}}}\right.\\
&+\frac{x^2(y-1)\left[-2d(y-1)(z-1)(y(z-1)-2z+1)+2y^2(z-1)^2-y(9z-4)(z-1)\right.}{((x(1-y)(1+y(-1+z)-2z)+x^2(-1+y)^2(-1+z)+(-1+y)y(-1+z)+z))^{\frac{3}{2}}}\\
&+\frac{\left.z(8z-9)+2]+x(y-1)\left(2(d-1)y^2(z-1)^2-y(z-1)(2d(z-1)-3z+2)+\right.\right.}{((x(1-y)(1+y(-1+z)-2z)+x^2(-1+y)^2(-1+z)+(-1+y)y(-1+z)+z))^{\frac{3}{2}}}\\
&\left.+\frac{\left.z(2d(z-1)-4z+3))+yz(y(z-1)+1))\right.}{((x(1-y)(1+y(-1+z)-2z)+x^2(-1+y)^2(-1+z)+(-1+y)y(-1+z)+z))^{\frac{3}{2}}}\right\}.\end{aligned} \tag{G.70}$$

Despite the multiplicative factor that vanishes in $d=2$, Eq. (G.70) does not vanish because the integration over z is divergent in $d=2$. In this dimension, an explicit integration over the Feynman parameters gives rise to

$$\mathfrak{F}(2) = \frac{1}{4\pi^4}\int_0^1 \mathrm{d}x\int_0^1 \mathrm{d}y\frac{(1-x)x}{(y+(1-y)(1-x)x)^2} = \frac{1}{4\pi^4}. \tag{G.71}$$

This agrees with the result obtained form the computation shown in Appendix D. For $d>2$, the expression is computed numerically as shown in Fig. G.2. From Eq. (G.69) and the renormalization conditions in Eqs. (B.7) and (B.8), the two-loop counterterm coefficients are determined to be

$$A_2^{2\mathrm{L}} = \frac{6(N_c^2-1)\beta_d^4}{N_c^2N_f^2}\mathfrak{F}(d)w(v)^2\mathfrak{S}\left[d-2;w(v)\right]^2\log\left(\frac{\Lambda}{\mu}\right), \tag{G.72}$$

$$A_3^{2\mathrm{L}} = -\frac{2(N_c^2-1)\beta_d^4}{N_c^2N_f^2}\mathfrak{F}(d)w(v)^2\mathfrak{S}\left[d-2;w(v)\right]^2\log\left(\frac{\Lambda}{\mu}\right). \tag{G.73}$$

Combining this result with Eqs. (G.53) and (G.54), and by assuming that $\Lambda \approx \widetilde{\Lambda}$, it follows that the counterterm coefficients Z_2 and Z_3 are given, to the leading order in v, by

$$\begin{aligned}Z_2 = {}& 1+\frac{(N_c^2-1)}{N_cN_f}\\
&\times\left\{\frac{2(d-1)}{\pi}\zeta(d)v\mathfrak{S}[d-2;c(v)]+\frac{6\beta_d^4}{N_cN_f}\mathfrak{F}(d)w(v)^2\mathfrak{S}\left[d-2;w(v)\right]^2\right\}\log\left(\frac{\Lambda}{\mu}\right),\end{aligned} \tag{G.74}$$

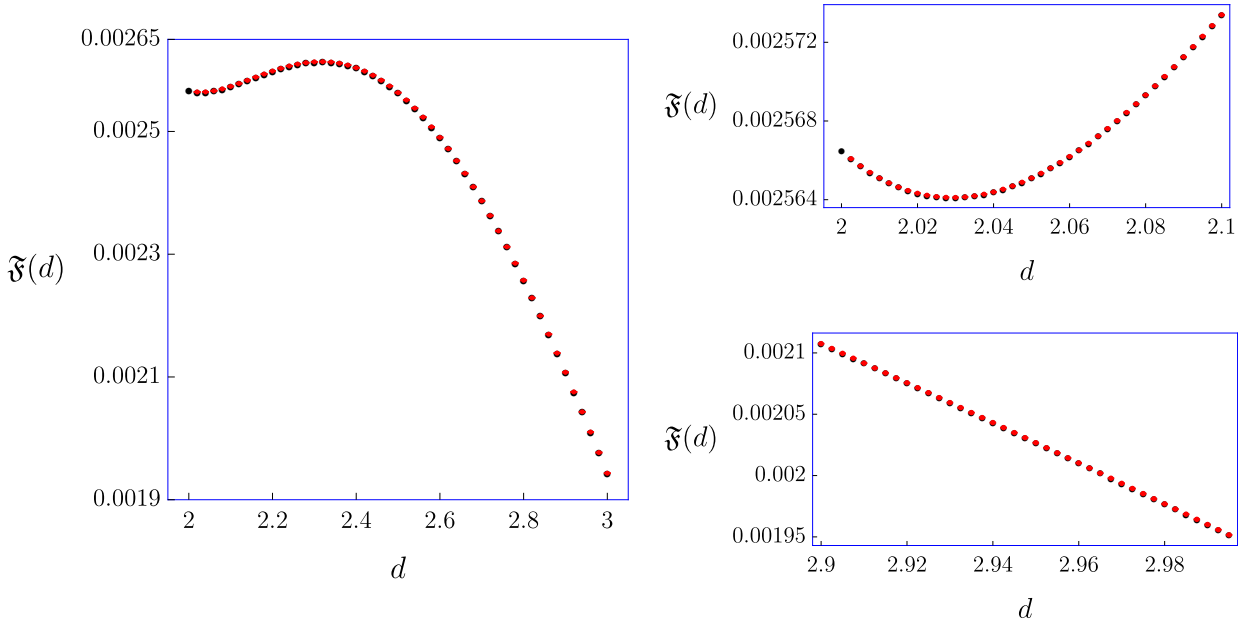

(*a*) $\mathfrak{F}(d)$ for $2 \leq d \leq 3$.

(*b*) $\mathfrak{F}(d)$ near $d = 2$ (top) and $d = 3$ (bottom).

Figure G.2: (*a*) The function $\mathfrak{F}(d)$. Each point is computed numerically except for the one in $d = 2$ where it can be determined analytically. The (black) dots correspond the value of the numerical integration and the (red) error bars represent the numerical error in the computation. (*b*) Numerical evaluation near $d = 2$ (top) and $d = 3$ (bottom).

$$Z_3 = 1 - \frac{(N_c^2-1)}{N_c N_f} \times \left\{ \frac{2(d-1)}{\pi} \zeta(d) v \mathfrak{S}[d-2; c(v)] + \frac{2\beta_d^4}{N_c N_f} \mathfrak{F}(d) w(v)^2 \mathfrak{S}\left[d-2; w(v)\right]^2 \right\} \log\left(\frac{\Lambda}{\mu}\right). \tag{G.75}$$

We finally note that these two expressions reduce to Eqs. (D.19) and (D.20) for $N_c = 2$, $N_f = 1$ and in the $d \to 2^+$ limit.

G.5 One-loop vertex correction

We consider the one-loop vertex correction in Fig. 2.3(*b*),

$$\delta\mathbf{\Gamma}^{(2,1)}_{1\mathrm{L}} = \frac{i\beta_d\sqrt{v}}{\sqrt{N_f}} \sum_{n=1}^{4} \sum_{\sigma,\sigma'=1}^{N_c} \sum_{j=1}^{N_f} \int \mathrm{d}k \int \mathrm{d}q \overline{\Psi}_{\overline{n},\sigma,j}(k+q) \Phi_{\sigma\sigma'}(q) \Gamma_n^{(2,1),1\mathrm{L}}(k,q) \Psi_{n,\sigma',j}(k), \tag{G.76}$$

where the one-loop vertex function is given by

$$\Gamma_n^{(2,1),1\mathrm{L}}(k,q) = \frac{2\beta_d^2 v}{N_c N_f} \int \mathrm{d}p \left[\gamma_{d-1} G^{(0)}_{\overline{n}}(p+k+q; v) \gamma_{d-1} G^{(0)}_n(p+k; v) \gamma_{d-1} \right] D(p). \tag{G.77}$$

In view of the renormalization condition in Eq. (B.9), we consider the vertex function at $k=0$ and $\vec{q}=\vec{0}$,

$$\Upsilon_n^{1\mathrm{L}}(\mathbf{Q})=\frac{1}{2}\mathrm{Tr}\left[\gamma_{d-1}\Gamma_n^{(2,1),1\mathrm{L}}(k,q)\right]\Big|_{k=0,\vec{q}=\vec{0}}. \tag{G.78}$$

For $n=1$, Eq. (G.78) becomes

$$\Upsilon_1^{1\mathrm{L}}(\mathbf{Q})=\frac{2\beta_d^2 v}{N_cN_f}\int \mathrm{d}p\left(\frac{\mathbf{P}\cdot(\mathbf{P}+\mathbf{Q})-(v^2p_x^2-p_y^2)}{[\mathbf{P}^2+(vp_x+p_y)^2][(\mathbf{P}+\mathbf{Q})^2+(vp_x-p_y)^2]}\right)D(p). \tag{G.79}$$

Following the same steps used in Secs. G.2 and G.4 of this appendix, we obtain

$$\begin{aligned}\Upsilon_1^{1\mathrm{L}}(\mathbf{Q})=&\frac{2(d-2)\beta_d^2 w(v)}{\pi N_cN_f}\Gamma\left(\frac{d-2}{d-1}\right)\Gamma\left(\frac{d}{d-1}\right)\mathfrak{S}[d-2;w(v)]\\&\times\int\limits_{\mathbb{R}^{d-1}}\frac{\mathrm{d}\mathbf{P}}{(2\pi)^{d-1}}\int\limits_{\mathbb{R}}\frac{\mathrm{d}p_y}{(2\pi)}|\mathbf{P}|^{2-d}\left(\frac{\mathbf{P}\cdot(\mathbf{P}+\mathbf{Q})+p_y^2}{(\mathbf{P}^2+p_y^2)[(\mathbf{P}+\mathbf{Q})^2+p_y^2]}\right)\end{aligned} \tag{G.80}$$

to leading order in the small v limit. Here $\mathfrak{S}[d-2;w(v)]$ is defined in Eq. (G.13). We introduce a two-variable Feynman parametrization that allows a straightforward integration over p_y,

$$\begin{aligned}\Upsilon_1^{1\mathrm{L}}(\mathbf{Q})=&\frac{(d-2)\beta_d^2 w(v)}{d\pi^{\frac{3}{2}}N_cN_f}\frac{\Gamma\left(\frac{d-2}{d-1}\right)\Gamma\left(\frac{d}{d-1}\right)\Gamma\left(\frac{d+2}{2}\right)\Gamma\left(\frac{d-1}{2}\right)}{\Gamma\left(\frac{d}{2}\right)\Gamma\left(\frac{d-2}{2}\right)}\mathfrak{S}[d-2;w(v)]\int\limits_0^1\mathrm{d}x_1\int\limits_0^{1-x_1}\mathrm{d}x_2\\&\times\int\limits_{\mathbb{R}^{d-1}}\frac{\mathrm{d}\mathbf{P}}{(2\pi)^{d-1}}\frac{(1-x_1-x_2)^{\frac{d-4}{2}}}{(x_1+x_2)^{\frac{3}{2}}}\frac{[\mathbf{P}^2-(d-1)(x_1+x_2)\mathbf{P}\cdot(\mathbf{P}+\mathbf{Q})+x_2\mathbf{Q}\cdot(\mathbf{Q}+2\mathbf{P})]}{(\mathbf{P}^2+2x_2\mathbf{P}\cdot\mathbf{Q}+x_2\mathbf{Q}^2)^{\frac{d+1}{2}}}.\end{aligned} \tag{G.81}$$

The integration over $\mathbf{P}$ is logarithmically divergent, and in the large $\Lambda/|\mathbf{Q}|$ limit one obtains

$$\Upsilon_1^{1\mathrm{L}}(\mathbf{Q})=\frac{(2-d)\beta_d^2 w(v)}{2^{d-2}N_cN_f\pi^{\frac{d+1}{2}}}\frac{\Gamma\left(\frac{d-2}{d-1}\right)\Gamma\left(\frac{d}{d-1}\right)}{\Gamma\left(\frac{d-1}{2}\right)}\mathfrak{S}[d-2;w(v)]\log\left(\frac{\Lambda}{|\mathbf{Q}|}\right). \tag{G.82}$$

From Eq. (3.19) and the renormalization condition in Eq. (B.9), we obtain a counterterm for the vertex with

$$Z_6=1-\frac{(d-1)\zeta(d)}{N_cN_f}w(v)\mathfrak{S}\left[d-2;w(v)\right]\log\left(\frac{\Lambda}{\mu}\right), \tag{G.83}$$

with $\zeta(d)$ defined in Eq. (3.31). This expression reduces to that in Eq. (D.25) in the $d=2$ limit for $N_c=2$ and $N_f=1$.

Appendix H | Derivation of the Low-Energy Fixed Point in $2 \leq d < 3$

In this appendix we show the explicit derivation of the low-energy fixed point for the theory in dimensions $2 \leq d < 3$. In doing so we follow a similar logic as the one presented in Appendix D. The self-consistent equation for the dynamically generated boson velocity reads

$$c(v)^{d-1} = \frac{4\beta_d^4 \mathfrak{B}(d)}{(3-d)N_c N_f} \frac{v}{c(v)} \mathfrak{S}\left(d-2; \frac{v}{c(v)}\right), \tag{H.1}$$

where $\mathfrak{S}[d-2; v/c(v)]$ its given in Eq. (G.13). It is easy to see that

$$c(v) = \left(\frac{4\beta_d^4 \mathfrak{B}(d)}{(3-d)N_c N_f}\right)^{\frac{1}{d}} v^{\frac{1}{d}} \mathfrak{S}\left(d-2; v^{\frac{(d-1)}{d}}\right)^{\frac{1}{d}} \tag{H.2}$$

solves Eq. (H.1) to the leading order in $v/c(v)$ both in the $v/c(v) \to 0$ limit with $d > 2$ and in the $d \to 2^+$ limit. This follows from the two limiting forms of Eq. (G.13) given in Eqs. (3.26) and (3.27).

Now we compute the beta function for v in $2 \leq d < 3$. Eqs. (B.3) and (B.14), and the fact that the bare velocity is independent of the running energy scale μ, yield the beta function for v as a solution to the equation

$$\beta_v = v\left(\frac{1}{Z_3}\frac{\partial Z_3}{\partial \log \mu} - \frac{1}{Z_2}\frac{\partial Z_2}{\partial \log \mu}\right) + v\beta_v\left(\frac{1}{Z_3}\frac{\partial Z_3}{\partial v} - \frac{1}{Z_2}\frac{\partial Z_2}{\partial v}\right). \tag{H.3}$$

From the counterterm coefficients Z_2 and Z_3 given in Eqs. (G.74) and (G.75), the beta function ($\beta_v \equiv \partial v/\partial \ln \mu$) becomes

$$\beta_v = \frac{4(N_c^2-1)}{N_c N_f} v\left\{\frac{(d-1)}{\pi}\zeta(d) v \mathfrak{S}[d-2; c(v)] + \frac{2\beta_d^4}{N_c N_f}\mathfrak{F}(d) w(v)^2 \mathfrak{S}\left[d-2; w(v)\right]^2\right\}. \tag{H.4}$$

In any $2 \leq d < 3$, $\beta_v > 0$ for $v \ll 1$. This implies that v decreases as energy is lowered once the bare value of v is small. Since our calculation is controlled in the small v limit, we conclude that $v \to 0$ limit is a stable fixed point with a finite basin of attraction.

Factoring out the first term in the curly brackets of Eq. (H.4) we can use the identity

$$\frac{2\pi\beta_d^4 \mathfrak{F}(d)}{N_c N_f (d-1)\zeta(d)} \frac{w(v)^2}{v} \frac{\mathfrak{S}\left[d-2; w(v)\right]^2}{\mathfrak{S}\left[d-2; c(v)\right]} \approx v^{\frac{(d-2)}{d}} \mathfrak{S}\left(d-2; v^{\frac{d-1}{d}}\right)^{\frac{(d-2)}{d}} \tag{H.5}$$

close to $d = 2$, to rewrite the beta function as

$$\beta_v = \frac{4(d-1)(N_c^2-1)}{\pi N_c N_f}\zeta(d) v^2 \mathfrak{S}\left(d-2; v^{\frac{d-1}{d}}\right)\left[1 + v^{\frac{(d-2)}{d}} \mathfrak{S}\left(d-2; v^{\frac{d-1}{d}}\right)^{\frac{(d-2)}{d}}\right]. \tag{H.6}$$

The property in Eq. (H.5) follows from Eq. (H.1) and the fact that $\mathfrak{S}[d-2;c(v)] \approx \mathfrak{S}[d-2;w(v)] \approx \mathfrak{S}\left(d-2;v^{\frac{d-1}{d}}\right)$ close to $d=2$. In Eq. (H.5), we use the numerical coefficient evaluated at $d=2$ because the second term in the square brackets of Eq. (H.4) is only important in the low-energy limit in $d=2$.

We define the logarithmic length scale $l=\log(\Lambda/\mu)$, where Λ is a UV energy scale at which the bare theory is defined. The beta function that describes the flow of v with increasing length scale can be rewritten as

$$\begin{aligned}\frac{\mathrm{d}v(l)}{\mathrm{d}l} = -\frac{4(d-1)(N_c^2-1)}{\pi N_c N_f}\zeta(d)v(l)^2\mathfrak{S}\left(d-2;v(l)^{\frac{d-1}{d}}\right) \\ \times\left[1+v(l)^{\frac{(d-2)}{d}}\mathfrak{S}\left(d-2;v(l)^{\frac{d-1}{d}}\right)^{\frac{(d-2)}{d}}\right],\end{aligned} \tag{H.7}$$

with a boundary condition $v(0)=v_0$. We note that the term in square brackets is merely a constant in the small v limit in $d\geq 2$. On the other hand, $\mathfrak{S}\left(d-2;v(l)^{\frac{d-1}{d}}\right)$ provides, at most, a logarithmic correction in $d=2$. With the l-dependence of $v(l)$ ignored inside logarithms, the solution to Eq. (H.7) can be cast in the following implicit form:

$$\begin{aligned}v(l) &= \frac{1}{\frac{1}{v_0}+\mathbb{F}[v(l)]l}, \\ \mathbb{F}[v(l)] &= \frac{4(d-1)(N_c^2-1)\zeta(d)}{\pi N_c N_f}\mathfrak{S}\left(d-2;v(l)^{\frac{d-1}{d}}\right) \\ &\quad\times\left[1+v(l)^{\frac{(d-2)}{d}}\mathfrak{S}\left(d-2;v(l)^{\frac{d-1}{d}}\right)^{\frac{(d-2)}{d}}\right].\end{aligned} \tag{H.8}$$

This equation for $v(l)$ can be solved iteratively in the low-energy limit. The initial condition naturally provides the logarithmic length scale $l_0^{-1}=v_0\mathbb{F}(v_0)\sim\frac{\pi^2}{4}\frac{(N_c^2-1)}{N_cN_f}v_0\mathfrak{S}\left(d-2;v_0^{\frac{d-1}{d}}\right)$ below which the solution in Eq. (O.8) becomes independent of v_0 and reduces to the universal form:

$$v(l)=\frac{\pi N_cN_f}{4(d-1)(N_c^2-1)}\frac{1}{\zeta(d)}\frac{1}{l}\frac{1}{\mathfrak{S}\left(d-2;l^{-\frac{(d-1)}{d}}\right)}\left[\frac{1}{1+l^{-\frac{(d-2)}{d}}}\right]. \tag{H.9}$$

Eq. (H.9) continuously interpolates the form of $v(l)$ found in two and close to three dimensions [148] and the two-dimensional form given in Eq. (D.31) for $N_c=2$ and $N_f=1$. In obtaining Eq. (H.9) we used the limiting forms of Eq. (G.13) repeatedly to discard subleading terms in the $l\gg l_0$ limit.

Appendix I | Critical Exponents and Physical Observables in $2 \leq d < 3$

In this appendix we provide details in the derivation of the critical exponents and scaling form of the physical observables for the theory in $2 \leq d < 3$. From Eqs. (B.13) and (B.15), the dynamical critical exponent and the anomalous dimensions of the fields, defined as the deviations from the interaction-driven scaling, are given by

$$z = 1 - \frac{\mathrm{d}}{\mathrm{d}\log\mu}\left(\log Z_3 - \log Z_1\right), \tag{I.1}$$

$$\eta_\Psi = \frac{1}{2}\frac{\mathrm{d}}{\mathrm{d}\log\mu}\left(d\log Z_3 - (d-1)\log Z_1\right), \tag{I.2}$$

$$\eta_\Phi = \frac{1}{2}\frac{\mathrm{d}}{\mathrm{d}\log\mu}\left(2\log Z_6 - 2(d-1)\log Z_1 - \log Z_2 + (2d-3)\log Z_3\right), \tag{I.3}$$

where the counterterm coefficients Z_1, Z_2, Z_3 and Z_6 are given in Eqs. (G.41), (G.74), (G.75) and (G.83), respectively. At low energies, v flows to zero faster than the ratio $w(v) = v/c(v)$. The dominant contributions to z and η_Ψ come from Z_1 in the small v limit, while η_Φ is dominated by Z_6 and Z_1. To the leading order in v, the dynamical critical exponent and the anomalous scaling dimensions are given by

$$z = 1 + \frac{(N_c^2-1)}{N_c N_f}\zeta(d) w(v), \tag{I.4}$$

$$\eta_\Psi = -\frac{(N_c^2-1)}{N_c N_f}\frac{(d-1)\zeta(d)}{2} w(v), \tag{I.5}$$

$$\eta_\Phi = \frac{(d-1)\zeta(d)}{N_c N_f}\left\{\mathfrak{S}\left[d-2; w(v)\right] - (N_c^2-1)\right\} w(v). \tag{I.6}$$

The scaling forms of the two-point functions are dictated by the RG equation,

$$\left[\left(z\mathbf{K}\cdot\nabla_{\mathbf{K}} + \vec{k}\cdot\nabla_{\vec{k}}\right) - \beta_v\frac{\partial}{\partial v} + D_{\mathsf{a}}\right]\Gamma^{(2)}_{\mathsf{a}}(k, v; \mu) = 0. \tag{I.7}$$

Here $\mathsf{a} = \mathsf{b}, \mathsf{f}$ labels the bosonic and fermionic cases, respectively. D_{a} denotes the total scaling dimension of the operator given by

$$D_{\mathsf{f}} = 2\eta_\Psi + z(d-1) - d, \tag{I.8}$$

$$D_{\mathsf{b}} = 2\eta_\Phi + z(d-1) - 2(d-1). \tag{I.9}$$

Eq. (I.7) can be written as

$$\left[\mathbf{K}\cdot\nabla_{\mathbf{K}}+\frac{\vec{k}}{z(l)}\cdot\nabla_{\vec{k}}+\frac{\mathrm{d}}{\mathrm{d}l}+\frac{D_{\mathsf{a}}(l)}{z(l)}\right]\Gamma_{\mathsf{a}}^{(2)}[k,v(l)]=0, \tag{I.10}$$

where $v(l)$ is the solution of

$$\frac{\mathrm{d}v(l)}{\mathrm{d}l}=-\frac{\beta_v}{z(l)},\qquad v(0)=v_0, \tag{I.11}$$

and l is the logarithmic length scale. The solution to Eq. (I.10) can be written as

$$\Gamma_{\mathsf{a}}^{(2)}(\mathbf{K},\vec{k},v_0)=\exp\left(\int_0^l \mathrm{d}\ell\frac{D_{\mathsf{a}}(\ell)}{z(\ell)}\right)\Gamma_{\mathsf{a}}^{(2)}\left(e^l\mathbf{K},\exp\left(\int_0^l\frac{\mathrm{d}\ell}{z(\ell)}\right)\vec{k},v(l)\right). \tag{I.12}$$

Here $z(\ell)$ and $D_{\mathsf{a}}(\ell)$ should be viewed as functions of the logarithmic length scale, where $w(v)$ in Eqs. (I.4), (I.5) and (I.6) are replaced by

$$\begin{aligned}w(l)=\frac{\pi N_cN_f}{4(d-1)\left[\zeta(d)(N_c^2-1)\right]^{\frac{d-1}{d}}}&\left[\frac{(3-d)(d-1)}{\pi\beta_d^4\mathfrak{B}(d)}\right]^{\frac{1}{d}}\\&\times\left[\frac{1}{1+l^{-\frac{(d-2)}{d}}}\right]^{\frac{d-1}{d}}\frac{1}{l^{\frac{d-1}{d}}}\frac{1}{\mathfrak{S}\left(d-2;l^{-\frac{d-1}{d}}\right)},\end{aligned} \tag{I.13}$$

in the large l limit. Here, $\mathfrak{S}(\xi;a)$ is defined in Eq. (G.13). Similarly, the scale-dependent velocity of the collective mode is given by

$$c(l)=\left(\frac{\pi\beta_d^4\mathfrak{B}(d)}{(3-d)(d-1)(N_c^2-1)\zeta(d)}\right)^{\frac{1}{d}}\left[\frac{1}{1+l^{-\frac{(d-2)}{d}}}\right]^{\frac{1}{d}}\frac{1}{l^{\frac{1}{d}}}. \tag{I.14}$$

In order to compute Eq. (I.12) for the fermionic two-point function, we consider

$$\frac{D_{\mathsf{f}}(l)}{z(l)}=\frac{2\eta_\Psi(l)+z(l)(d-1)-d}{z(l)}=-\frac{1}{z(l)}+\frac{2\eta_\Psi(l)+(d-1)[z(l)-1]}{z(l)}, \tag{I.15}$$

where the contribution from the dynamical critical exponent and that from the net anomalous scaling dimension of the fermion field are separated. The crossover function in Eq. (I.12) is determined by the scale-dependent functions:

$$I_z(l)=\int_0^l\frac{\mathrm{d}\ell}{z(\ell)},\qquad\text{and}\qquad I_\Psi(l)=\int_0^l\mathrm{d}\ell\left(\frac{2\eta_\Psi(\ell)+(d-1)[z(\ell)-1]}{z(\ell)}\right). \tag{I.16}$$

Since the critical exponents are controlled by $w(v)=v/c(v)\gg v$ it follows that, to the leading order in v, the contribution from the dynamical critical exponent is dominated by

the counter term coefficient Z_1 and, consequently,

$$\begin{aligned} I_z(l) &= \int_0^l \mathrm{d}\ell \ \left[1 - \frac{(N_c^2-1)}{N_c N_f}\zeta(d) w(\ell)\right] \\ &= l - \mathfrak{F}_z(d)(N_c^2-1)^{\frac{1}{d}} \left[\frac{1}{1+l^{-\frac{(d-2)}{d}}}\right]^{\frac{d-1}{d}} \frac{l^{\frac{1}{d}}}{\mathfrak{S}\left(d-2; l^{-\frac{(d-1)}{d}}\right)}, \end{aligned} \tag{I.17}$$

where $\mathfrak{F}_z(d)$ is defined in Eq. (3.40) and the last equality follows from taking the large l limit. Similarly, the contribution from the net anomalous scaling dimension is dominated by Z_3 at low energies,

$$\begin{aligned} I_\Psi(l) = \frac{(N_c^2-1)}{N_c N_f} \int_0^l \mathrm{d}\ell \Bigg\{ &\frac{2(d-1)}{\pi}\zeta(d) v(\ell) \mathfrak{S}[d-2; c(\ell)] \\ &+ \frac{2\beta_d^4}{N_c N_f} \mathfrak{F}(d) w(\ell)^2 \mathfrak{S}\left[d-2; w(\ell)\right]^2 \Bigg\}. \end{aligned} \tag{I.18}$$

From Eq. (H.9) we use

$$v(l)\mathfrak{S}\left(d-2; v(l)^{\frac{d-1}{d}}\right) \approx \frac{\pi N_c N_f}{4(d-1)(N_c^2-1)} \frac{1}{\zeta(d)} \left[\frac{1}{1+l^{-\frac{(d-2)}{d}}}\right] \frac{1}{l} \tag{I.19}$$

to write

$$I_\Psi(l) = \frac{1}{2}\left[\frac{1}{1+l^{-\frac{(d-2)}{d}}}\right]\left[\log l + \mathfrak{S}\left(d-2; l^{-\frac{1}{d}}\right)\right]. \tag{I.20}$$

in the large l limit. In obtaining Eq. (I.20) from Eq. (I.18) one has to use the expression for $v(l)$ without dropping the term depending on v_0 prior to the integration. Only after the integration is done, the terms depending on v_0 can be thrown away safely. Since the fermion two-point function reduces to the bare one in the small v limit, the two-point function for nonzero v is given by

$$\Gamma_n^{(2,0)}(\mathbf{K}, \vec{k}) = \Gamma_{\mathfrak{f}}^{(2)}(\mathbf{K}, \vec{k}) = F_\Psi(|\mathbf{K}|)\Big[iF_z(|\mathbf{K}|)\mathbf{\Gamma}\cdot\mathbf{K} + i\gamma_{d-1}\varepsilon_n(\vec{k}; v_{|\mathbf{K}|})\Big], \tag{I.21}$$

for $e^{I_z[\log(\Lambda/|\mathbf{K}|)]}\vec{k}$ fixed. Here, $v_{|\mathbf{K}|} = v\left[\log(\Lambda/|\mathbf{K}|)\right]$. The universal functions,

$$F_z(|\mathbf{K}|) = \exp\left\{\left[\frac{1}{1+[\log(\Lambda/|\mathbf{K}|)]^{-\frac{(d-2)}{d}}}\right]^{\frac{d-1}{d}} \frac{\mathfrak{F}_z(d)(N_c^2-1)^{\frac{1}{d}}[\log(\Lambda/|\mathbf{K}|)]^{\frac{1}{d}}}{\mathfrak{S}\left(d-2; [\log(\Lambda/|\mathbf{K}|)]^{-\frac{(d-1)}{d}}\right)}\right\}, \tag{I.22}$$

$$\begin{aligned} F_\Psi(|\mathbf{K}|) = \exp\Bigg\{\frac{1}{2}\left[\frac{1}{1+[\log(\Lambda/|\mathbf{K}|)]^{-\frac{(d-2)}{d}}}\right]\Big[&\log\left[\log(\Lambda/|\mathbf{K}|)\right] \\ &+\mathfrak{S}\left(d-2; [\log(\Lambda/|\mathbf{K}|)]^{-\frac{1}{d}}\right)\Big]\Bigg\}, \end{aligned} \tag{I.23}$$

capture the deviations of the dynamical critical exponent and the anomalous scaling dimension of the fermion field from their values at the low-energy fixed point, respectively.

For the bosonic two-point function in Eq. (I.12), we consider

$$\frac{D_{\mathsf{b}}(l)}{z(l)} = \frac{2\eta_\Phi(l) + z(l)(d-1) - 2(d-1)}{z(l)} = -\frac{(d-1)}{z(l)} + \frac{2\eta_\Phi(l) + [z(l)-1](d-1)}{z(l)}, \quad \text{(I.24)}$$

where we have separated the contribution from the dynamical critical exponent and the net anomalous dimension of the bosonic field. The latter contribution to the two-point function is captured by

$$I_\Phi(l) = \int_0^l \mathrm{d}\ell \frac{(2\eta_\Phi(\ell) + (d-1)[z(\ell)-1])}{z(\ell)}. \quad \text{(I.25)}$$

$I_\Phi(l)$ is dominated by the counter terms Z_6 and Z_1 in the small v limit, and we can write

$$I_\Phi(l) = \frac{\mathfrak{F}_\Phi(d)}{(N_c^2-1)^{\frac{d-1}{d}}} \left[\frac{1}{1+l^{-\frac{(d-2)}{d}}}\right]^{\frac{d-1}{d}} l^{\frac{1}{d}} \left(1 - \frac{(N_c^2-1)}{2\mathfrak{S}\left(d-2; l^{-\frac{(d-1)}{d}}\right)}\right), \quad \text{(I.26)}$$

where $\mathfrak{F}_\Phi(d)$ is defined in Eq. (3.42). Using Eqs. (I.12) and (I.17) and taking into account the fact that inverse of the bosonic two-point vertex function reduces to Eq. (3.21) for $v \ll 1$, we obtain

$$\Gamma^{(0,2)}(\mathbf{Q},\vec{q}) = \Gamma^{(2)}_{\mathsf{b}}(\mathbf{Q},\vec{q}) = F_\Phi(|\mathbf{Q}|)\Big[F_z(|\mathbf{Q}|)^{d-1}|\mathbf{Q}|^{d-1} + c_{|\mathbf{Q}|}^{d-1}(|q_x|^{d-1} + |q_y|^{d-1})\Big], \quad \text{(I.27)}$$

for $e^{I_z[\log(\Lambda/|\mathbf{Q}|)]}\vec{q}$ fixed. Here,

$$F_\Phi(|\mathbf{Q}|) = \exp\left\{\frac{\mathfrak{F}_\Phi(d)\left[\log(\Lambda/|\mathbf{Q}|)\right]^{\frac{1}{d}}}{(N_c^2-1)^{\frac{d-1}{d}}} \left[\frac{1}{1+\left[\log(\Lambda/|\mathbf{Q}|)\right]^{-\frac{(d-2)}{d}}}\right]^{\frac{d-1}{d}} \times \left[1 - \frac{(N_c^2-1)}{2\mathfrak{S}\left(d-2; \left[\log(\Lambda/|\mathbf{Q}|)\right]^{-\frac{(d-1)}{d}}\right)}\right]\right\}, \quad \text{(I.28)}$$

and $c_{|\mathbf{Q}|} = c\left[\log(\Lambda/|\mathbf{Q}|)\right]$, capture the scale-dependent anomalous dimension and the velocity of the collective mode, respectively.

Appendix J | Renormalizability of the Antiferromagnetic Quantum Critical Metal

Here we address the renormalizability of the EFT defined by the action in Eq. (4.1). We show that, if Eqs. (4.19) to (4.21) and (4.23) hold, the superficial degree divergence of a given quantum corrections is, at most, that of the quantum correction computed in the absence of momentum dependence in the coupling functions. Using this we show that, to zeroth order in the four-fermion couplings, the physical observables of the theory can me made independent of the UV scale Λ_f by adding local counterterms that depend only on the momentum along the FS. In other words, if such local counterterm functions exist, then the physical observables of the theory can me made independent of the UV scale Λ_f. In Appendices M and Q we show by an explicit computation that such local counterterms exist to leading order in v and the four-fermion couplings.

J.1 Superficial Degree of Divergence of Quantum Corrections

Let us consider a quantum correction within renormalized perturbation theory that contains L loops, L_f fermion loops, E_f (E_b) external fermionic (bosonic) legs, V_g Yukawa vertices, V_λ four-fermion vertices, $\mathcal{N}_i$ insertions of the counterterm functions with $A_N^{(i)}(k_N)$ for $i = 1, 2, 3$, $\mathcal{N}_4$ insertions of the counterterm function with $A_N^{(4)}(k'_N, k_N)$ and $\mathcal{N}_\lambda$ insertions of the counterterm function $A^{\{j_i\}}_{\{N_i\};\{\sigma_i\}}(\{k_{i;N_i}\})$. Moreover, let I_f (I_b) denote the number of internal fermion (boson) propagators. Let us denote such a quantum correction by $\mathcal{D}(\{l_j\})$, where the l_j with $j = 1, \ldots, L$ denote the external momenta. The formal expression for this quantum correction can be written as

$$\begin{aligned}
\mathcal{D}_{L_j}(\{l_j\}) \sim & \left[\prod_{i=1}^{L}\int \mathrm{d}p_i\right]\left[\prod_{i=1}^{V_g} g_{M_i}(x'_{M_i}, x_{M_i})\right]\left[\prod_{i=1}^{V_\lambda}\lambda^{\{j_k^{(i)}\}}_{\{S_k^{(i)}\};\{\sigma_k^{(i)}\}}(\{z_{i;S_k^{(i)}}\})\right] \\
& \times \left[\prod_{i=1}^{I_f} G^{(0)}_{N_i}(q_i)\right]\left[\prod_{i=1}^{\mathcal{N}_1} A^{(1)}_{O_i}(r_{O_i}) r_{i;0}\right]\left[\prod_{i=1}^{\mathcal{N}_2} A^{(2)}_{Q_i}(s_{Q_i}) V_{\mathrm{F}}^{(Q_i)}(s_{Q_i}) v_{Q_i}(s_{Q_i}) s_{Q_i}\right] \\
& \times \left[\prod_{i=1}^{I_b} D(k_i)\right]\left[\prod_{i=1}^{\mathcal{N}_3} A^{(3)}_{P_i}(t_{P_i}) V_{\mathrm{F}}^{(P_i)}(t_{P_i})\bar{t}_{P_i}\right]\left[\prod_{i=1}^{\mathcal{N}_4} A^{(4)}_{R_i}(y'_{R_i}, y_{R_i}) g_{R_i}(y'_{R_i}, y_{R_i})\right] \\
& \times \left[\prod_{i=1}^{\mathcal{N}_\lambda} A^{\{l_k^{(i)}\}}_{\{U_k^{(i)}\};\{\rho_k^{(i)}\}}(\{u_{i;U_k^{(i)}}\})\lambda^{\{l_k^{(i)}\}}_{\{U_k^{(i)}\};\{\rho_k^{(i)}\}}(\{u_{i;U_k^{(i)}}\})\right].
\end{aligned} \tag{J.1}$$

Here, p_i denotes the L frequency and momentum vectors that run through the L loops of the diagram. The frequency and momenta denoted by $q_i, k_i, x_i, x_i', r_i, s_i, t_i, y_i, y_i', z_i$ and u_i are linear combinations of both internal and external frequencies and momenta. The notation $\bar{t}_{P_i}$ is used to denote the component of the momentum stemming form hot spot P_i along the direction of $\vec{Q}_{\mathrm{AFM}}$. Summation over the hot spot indices is implied and the structure factor that depends on the hot spot, spin and flavor indices has been omitted since it will not play an important role. The bare fermion propagator for electrons close to hot spot N is given by

$$G_N^{(0)}(q) = \frac{1}{iq_0 + V_{\mathrm{F}}^{(N)}(q_N) e_N[\vec{q}; v_N(q_N)]}, \tag{J.2}$$

and the bosonic propagator, $D(q)$, solves the Schwinger-Dyson equation in the presence of the momentum-dependent coupling functions:

$$D(q)^{-1} = \mathrm{m}_{\mathrm{C.T}} + 2\sum_{N=1}^{8} \int \mathrm{d}k \; g_N(k_N + q_N, k_N) G_{\overline{N}}(k) \Gamma_{\overline{N}}^{(2,1)}(k, q) G_N(k + q), \tag{J.3}$$

where $\mathrm{m}_{\mathrm{C.T}}$ is a counterterm that tunes the mass of the collective mode to zero in order to keep the theory at criticality. In here $G_N(k)$ denotes the fully dressed fermion propagator whose dependence on the momentum-dependent couplings has been left implicit. Finally, $\Gamma_N^{(2,1)}(k, q)$ denotes the fully dressed vertex function of the theory which is also a functional of coupling functions. We note that this one involves, in principle, quantum corrections sourced by the four-fermion couplings.

Determining the boson propagator requires solving Eq. (2.5). For a generic momentum dependence in the coupling functions, this is an impossible task. However, there are two key properties that can be determined without solving the Schwinger-Dyson equation explicitly. First, the propagator for the collective mode has scaling dimension $[D(q)] = -1$ under the interaction driven scaling. Second, since $\Phi(q) = \sum_{a=1}^{N_c^2-1} \tau^a \phi^a(q)$, with $\phi^a(q) = \phi^a(-q)^*$, the boson propagator must be a real and even function of q. Finally, the low-energy dynamics of the boson is subject to frequency and momenta such that $|q| \ll \Lambda_b$ and $|q| \ll \Lambda_0$, from which Λ_0 is the only genuine UV scale. This, with the two aforementioned properties, implies that all analytic contributions to the boson propagator are irrelevant. This is because, besides the mass term that is tunned to zero, a Taylor expansion around $q = 0$ must start at quadratic order in frequency and momentum and therefore must be weighted by an inverse power of Λ_0 or Λ_b. Consequently, the only frequency and momentum dependence that the boson propagator can acquire in the low-energy limit must be non-analytic and linear in frequency and momentum.

In what follows we will use the fact that the bosonic propagator depends linearly on the frequency and momentum without specifying the solution to Eq. (2.5) provided that $|q| \ll \Lambda_b \ll \Lambda_0$. In the remaining of this appendix we focus on the effective low-energy theory defined in an energy shell of width $\Lambda_f < \Lambda_0$ around the FS. We now proceed on showing that, provided that Eqs. (4.19) to (4.21) and (4.23) hold, the superficial degree of divergence of higher-loop corrections to Eq. (4.1) is, at most, the superficial degree of divergence of the correction computed by ignoring the momentum dependence of the coupling functions.

In the absence of momentum dependence in the couplings and counterterm functions, the superficial degree of Eq. (J.1) is given by $\mathscr{D}_0 = 3L - I_f - I_b + \sum_{i=1}^{3} \mathcal{N}_i$. Let us now consider the diagram with the momentum-dependent couplings and denote by $\mathscr{D}$ its superficial degree of divergence. Using Eqs. (4.19) to (4.21) and Eq. (4.23), we can bound Eq. (J.1) from above by

$$\begin{aligned}
\left|\mathcal{D}_{L_j}(\{l_j\})\right| \lessapprox & \left[\prod_{i=1}^{L}\int \mathrm{d}p_i\right]\left[\prod_{i=1}^{I_f}\left|G_{N_i}^{(0)}(q_i)\right|\right]\left[\prod_{i=1}^{I_b}|D(k_i)|\right] \\
& \times\left[\prod_{i=1}^{\mathcal{N}_1}|\log\left(|r_{O_i}|\right)|^{\alpha_l}\,|r_{i;0}|\right]\left[\prod_{i=1}^{\mathcal{N}_2}|\log(|s_{Q_i}|)|^{\alpha_l}\left|V_{\mathrm{F}}^{(Q_i)}(s_{Q_i})\right||s_{Q_i}|\right] \\
& \times\left[\prod_{i=1}^{\mathcal{N}_3}|\log(|t_{P_i}|)|^{\alpha_l}\left|V_{\mathrm{F}}^{(P_i)}(t_{P_i})\right||\bar{t}_{P_i}|\right]\left[\prod_{i=1}^{\mathcal{N}_4}\left|\log(\max(|y'_{R_i}|,|y_{R_i}|))\right|^{\alpha_l}\right] \\
& \times\left[\prod_{i=1}^{\mathcal{N}_\lambda}\left|\log(\max(\{|u_{i;U_k^{(i)}}|\}))\right|^{\alpha_l}\right],
\end{aligned} \tag{J.4}$$

for a given $\alpha_l > 0$. To determine the superficial degree of divergence of this integral, we consider a coordinate transformation from the $3L$ frequency and momentum components to a set of generalized spherical coordinates. In doing so, any divergence coming from the large momenta regimes will arise from the integration over the radial coordinate r. In these coordinates, Eq. (J.4) can be written as

$$\begin{aligned}
\left|\mathcal{D}_{L_j}(\{l_j\})\right| \lessapprox & \int_{S^{3L-1}}\mathrm{d}\Omega_{3L-1}\int_0^\infty \mathrm{d}r\; r^{3L-1}\left[\prod_{i=1}^{I_f}\left|G_{N_i}^{(0)}(r,\{\theta_j\})\right|\right]\left[\prod_{i=1}^{I_b}|D(r,\{\theta_j\})|\right] \\
& \times\left[\prod_{i=1}^{\mathcal{N}_1}\left|\log\left(r|f_1^{(i)}(\{\theta_j\})|\right)\right|^{\alpha_l} r|f_0^{(i)}(\{\theta_j\})|\right]\left[\prod_{i=1}^{\mathcal{N}_4}\left|\log\left(r|f_6^{(i)}(\{\theta_j\})|\right)\right|^{\alpha_l}\right] \\
& \times\left[\prod_{i=1}^{\mathcal{N}_2}\left|\log\left(r|f_3^{(i)}(\{\theta_j\})|\right)\right|^{\alpha_l}\left|V_{\mathrm{F}}^{(Q_i)}(r;\{\theta_j\})\right| r|f_2^{(i)}(\{\theta_j\})|\right] \\
\times & \left[\prod_{i=1}^{\mathcal{N}_3}|\log\left(r|f_5^{(i)}(\{\theta_j\})|\right)|^{\alpha_l}\left|V_{\mathrm{F}}^{(P_i)}(r;\{\theta_j\})\right| r|f_4^{(i)}(\{\theta_j\})|\right]\left[\prod_{i=1}^{\mathcal{N}_\lambda}\left|\log\left(r|f_7^{(i)}(\{\theta_i\})|\right)\right|^{\alpha_l}\right].
\end{aligned} \tag{J.5}$$

Here $\mathrm{d}\Omega_{3L-1}$ denotes the volume element of a unit radius sphere in $3L$-dimensions and $\{\theta_j\}$ denotes the set of generalized angular coordinates. The functions $f_k^{(i)}(\{\theta_j\})$ are functions that only depend on the angular variables. In what follows we ignore the angular dependence within the integrand and consider its large r limit. For large r, $D(r,\{\theta_j\}) \sim r^{-1}$ and $G_N^{(0)}(r,\{\theta_j\}) \sim r^{-1}V_{\mathrm{F}}^{(N)}(r;\{\theta_j\})^{-1}$ as a consequence of Eqs. (4.19) to (4.21) which imply that $v_N(r,\{\theta_j\}) \lessapprox 1$ and $V_{\mathrm{F}}^{(N)}(r,\{\theta_j\}) \gtrapprox 1$. Let us denote with $\mathcal{I}$ the integrand in Eq. (J.5). Then, in the large r limit, and by ignoring the angular and hot spot dependence in the Fermi

velocity,

$$\begin{aligned}\mathcal{I} &\sim r^{3L-1-I_f-I_b+\sum_{i=1}^{3}\mathcal{N}_i}\log(r)^{\left[\mathcal{N}_\lambda+\sum_{i=1}^{4}\mathcal{N}_i\right]\alpha_l}|V_{\mathrm{F}}(r)|^{\mathcal{N}_2+\mathcal{N}_3-I_f}\\ &= r^{\mathscr{D}_0-1}\log(r)^{\left[\mathcal{N}_\lambda+\sum_{i=1}^{4}\mathcal{N}_i\right]\alpha_l}|V_{\mathrm{F}}(r)|^{\mathcal{N}_2+\mathcal{N}_3-I_f}.\end{aligned} \tag{J.6}$$

Since $I_f \geq \mathcal{N}_2+\mathcal{N}_3+1$, and $|V_{\mathrm{F}}(r)| \gtrapprox 1$ by assumption, it follows that the integrand decays faster than the same integration in the absence of momentum-dependent couplings. Moreover, the appearance of the logarithms modify the superficial degree of divergence only marginally. In other words, the superficial degree of divergence of the right-hand side of Eq. (J.5) satisfies $\mathscr{D} \leq \mathscr{D}_0$. Hence, the superficial degree of divergence of a general quantum correction is bounded from above by the superficial degree of divergence of the same quantum correction computed in the absence of momentum dependence in the coupling functions.

This conclusion has several important consequences that we now discuss. The first thing to note is that those quantum corrections to the action in Eq. (4.1) that are irrelevant in the absence of momentum-dependent couplings, remain irrelevant and independent of the UV scale of the theory. This shows that, from a nonperturbative perspective, the proliferation of UV power-law divergences discussed in Sec. 4.3-(*a*) is absent for the theory under consideration, provided that Eqs. (4.19) to (4.21) and (4.23) are satisfied. In what follows we focus only on quantum corrections whose superficial degree of divergence is $\mathscr{D}_0 = 0$ and $\mathscr{D}_0 = 1$. To zeroth order in the four-fermion couplings, the corrections with $\mathscr{D}_0 = 0$ correspond to the Yukawa vertex correction and those diagrams that contribute to the anomalous scaling dimension of the four-fermion couplings. To the same order in the four-fermion couplings, those corrections with $\mathscr{D}_0 = 1$ correspond to the boson and fermion-self energy corrections.

We note that, in the presence of four-fermion couplings, the degree of divergence of quantum corrections increases with the number of four-fermion vertices. This is a consequence of the irrelevancy of the couplings under the interaction driven scaling. This, in principle, can lead to a proliferation of power-law UV divergences that will destroy the renormalizability of the theory. However, since the coupling-functions depend only on the momentum along the FS, such divergences are expected to be cutoff by, either the size of the FS, k_{F}, or Λ_b, which measures the phases space of nested electrons that can be scattered by the spin fluctuations. This suggests that even in this case, the dependence of the physical observables on the genuine UV cutoff Λ_f can be removed by adding local counterterms that depend only on the momentum along the FS. A rigorous analysis of the renormalizability of the theory beyond zeroth order in the four-fermion couplings goes beyond the scope of this thesis. Therefore, in the remaining of this appendix we ignore the feedback of the four-fermion couplings and focus only on showing that the theory is renormalizable to zeroth order in the four-fermion couplings.

In the following section we show that the renormalized physical observables are independent of the UV scales by showing that, to zeroth order in the four-fermion coupling, the renormalized electronic two-point function, the renormalized interaction vertex function and the four-point vertex function are independent of the UV scale Λ_f after adding the counterterm action in Eq. (4.22) to Eq. (4.1). Before we delve into this, we note that, to leading order in the four-fermion couplings, the introduction of the momentum-dependent counterterms does not increase the degree of divergence of the quantum corrections. Therefore, all contributions to the Schwinger-Dyson equation remain finite. This implies that the physical bosonic two-point function is independent of Λ_f.

J.2 Yukawa Interaction Vertex Function

The renormalized interaction vertex function that stems from the action in Eq. (4.29) can be written as

$$\Gamma_N^{(2,1)}(k',k) = \left[1 + A_N^{(4)}(k'_N, k_N)\right] \frac{g_N(k'_N, k_N)}{\sqrt{N_f}} + \delta\Gamma_N^{(2,1)}(k',k), \tag{J.7}$$

where $\delta\Gamma_N^{(2,1)}(k',k)$ encodes the quantum corrections to the vertex function. According to Eq. (4.27), the counterterm function $A_N^{(4)}(k'_N, k_N)$ is fixed, in terms of the quantum corrections, by

$$A_N^{(4)}(k_N, k'_N) = -\text{div}\left[\delta\Gamma_N^{(2,1)}(k^*, \overline{k}')\right], \tag{J.8}$$

with k^* and $\overline{k}'$ being the frequency and momentum vectors evaluated at the RG conditions. For example, for $N = 1$, $k^* = (\mu, k_x, -v_1(k_x)k_x)$ and $\overline{k}' = (\mu, k'_x, v_4(k'_x)k'_x)$. div$[\cdots]$ denotes the divergent part of the expression in the $\Lambda_f \gg \mu$, where μ is the energy scale at which the RG conditions are imposed. We note that, to zeroth order in the four-fermion couplings, the corrections to the Yukawa interaction vertex function only involve virtual processes where fermions are not nested and therefore, only Λ_f is the relevant momentum scale that will cutoff the possible UV divergences in the quantum corrections.

Without loss of generality, let us consider the $N = 1$ hot spot. Around the frequencies and momenta at which the RG condition for the vertex function is imposed [see Eq. (4.27)], we can write the renormalized vertex function as follows

$$\Gamma_1^{(2,1)}(k',k) = \sum_{n,m,r,s=0}^{\infty} (\mu - k_0)^n (\mu - k'_0)^m (k_y + v_1(k_x)k_x)^r (k'_y - v_4(k'_x)k'_x)^s \varphi^{(m,n,r,s)}(k'_x, k_x; \mu), \tag{J.9}$$

where we have defined

$$\varphi^{(m,n,r,s)}(k'_x, k_x; \mu) = \frac{1}{n!m!s!r!} \frac{\partial^{n+m+r+s}}{\partial k_0^n \partial {k'_0}^m \partial k_y^r \partial {k'_y}^s} \Gamma_1^{(2,1)}(k',k)\Big|_{k=k^*, k'=\overline{k}'}, \tag{J.10}$$

Under the interaction driven scaling, the functions $\varphi^{(m,n,r,s)}(k'_x, k_x; \mu)$ have scaling dimension $[\varphi^{(m,n,r,s)}(k'_x, k_x; \mu)] = -m - n - r - s$. Now, for $n = m = r = s = 0$, Eq. (J.8) immediately guarantees that

$$\varphi^{(0,0,0,0)}(k'_x, k_x; \mu) = \frac{g_1(k'_x, k_x)}{\sqrt{N_f}}, \tag{J.11}$$

and therefore it is finite. Now, for $n + m + r + s \geq 1$, the scaling dimension of the functions $\varphi^{(m,n,r,s)}(k'_x, k_x; \mu)$ is negative. Ignoring the momentum dependence of the couplings of the theory, the superficial degree of divergence of the quantum corrections to these functions is $\mathscr{D}_0 = -m - n - r - s < 0$ and therefore, these are independent of the UV scale for $n + m + r + s \geq 1$. In the presence of the momentum-dependent coupling functions it follows from the results presented in the previous section that the degree of divergence of such corrections is $\mathscr{D} \leq \mathscr{D}_0 < 0$ and therefore all $\varphi^{(m,n,r,s)}(k'_x, k_x; \mu)$ are independent of the UV scale for $m + n + r + s \geq 0$. Hence, the renormalized interaction vertex can be made independent of the UV scale of the theory by adding the counterterm action in Eq. (4.22) to zeroth order in the four-fermion couplings.

J.3 Electronic Two-Point Function

We consider now the renormalized two-point function that stems from the action in Eq. (4.29) and which can be formally written as

$$\begin{aligned}\Gamma_N^{(2,0)}(k) = i\left[1+A_N^{(1)}(k_N)\right]k_0 \\ + \left[1+A_N^{(3)}(k_N)\right]V_{\mathrm{F}}^{(N)}(k_N)e_N\left(\vec{k};\frac{[1+A_N^{(2)}(k_N)]}{[1+A_N^{(3)}(k_N)]}v_N(k_N)\right)+\Sigma_N(k),\end{aligned} \tag{J.12}$$

where $\Sigma_N(k)$ denotes the fermion self-energy that captures all quantum corrections to the fermion dynamics and which are computed within *renormalized* perturbation theory. According to the minimal subtraction scheme enforced by the RG conditions in Eqs. (4.24) to (4.26), the counterterm functions $A_N^{(i)}(k_N)$ for $i=1,2,3$ and $N=1$ are determined from the fermion self-energy through the expressions

$$A_1^{(1)}(k_x) = i\mathrm{div}\left[\frac{\partial}{\partial k_0}\Sigma_1(k)\Big|_{k=k^*}\right], \tag{J.13}$$

$$\begin{aligned}A_1^{(2)}(k_x) = &\frac{1}{v_1(k_x)V_{\mathrm{F}}^{(1)}(k_x)k_x} \\ &\times \mathrm{div}\left[\mu\frac{\partial}{\partial k_0}\Sigma_1(k)\Big|_{k=k^*} - v_1(k_x)k_x\frac{\partial}{\partial k_y}\Sigma_1(k)\Big|_{k=k^*} - \Sigma_1(k^*)\right],\end{aligned} \tag{J.14}$$

$$A_1^{(3)}(k_x) = -\frac{1}{V_{\mathrm{F}}^{(1)}(k_x)}\mathrm{div}\left[\frac{\partial}{\partial k_y}\Sigma_1(k)\Big|_{k=k^*}\right], \tag{J.15}$$

where $\mathrm{div}[\cdots]$ denotes the divergent piece of the expression in the $\Lambda_f \gg \mu$ limit. Here $k^* = (\mu, k_x, -v_1(k_x)k_x)$. The counterterm functions at all other hot spots can be obtained from these expressions through a C_4 transformation. Let us now show that the counterterms $A_N^{(i)}(k_N)$ for $i=1,2,3$ are real for the theory under consideration. In the presence of particle-hole symmetry and time-reversal symmetry, the fermion self-energy has the properties

$$\Sigma_N(k_0,\vec{k}) = \Sigma_N^*(-k_0,\vec{k}), \quad \& \quad \Sigma_N(k_0,\vec{k}) = -\Sigma_N(-k_0,-\vec{k}), \tag{J.16}$$

which allows the fermion self-energy to be written in the general form

$$\Sigma_N(k_0,\vec{k}) = ik_0 f_{\mathrm{I}}^{(N)}(k_0,\vec{k}) + f_{\mathrm{R},2}^{(N)}(k_0,\vec{k})V_{\mathrm{F}}^{(N)}(k_N)e_N\left[\vec{k};\frac{f_{\mathrm{R},1}^{(N)}(k_0,\vec{k})}{f_{\mathrm{R},2}^{(N)}(k_0,\vec{k})}v_N(k_N)\right], \tag{J.17}$$

where the $f_{\mathrm{I}}^{(N)}$, $f_{\mathrm{R},1}^{(N)}$ and $f_{\mathrm{R},2}^{(N)}$ are real functions that are independently even in frequency and momentum. Combining Eq. (J.17) with Eqs. (J.13) to (J.15) it follows that the counterterm functions are real and given by

$$A_1^{(1)}(k_x) = -\mathrm{div}\left[f_{\mathrm{I}}^{(1)}(\mu,\vec{k}^*)\right], \tag{J.18}$$

$$A_1^{(2)}(k_x) = -\mathrm{div}\left[f_{\mathrm{R},1}^{(1)}(\mu,\vec{k}^*)\right], \tag{J.19}$$

$$A_1^{(3)}(k_x) = -\text{div}\left[f_{\text{R},2}^{(1)}(\mu, \vec{k}^*)\right]. \tag{J.20}$$

and similarly for all other hot spots.

With the counterterm functions being determined in terms of the fermion self-energy, let us show that the renormalized two-point function is independent of the UV scales of the theory. We focus on the $N = 1$ hot spot without loss of generality. For this purpose we note that the two-point function can be written as the following Taylor expansion around the frequency and momentum point at which the RG conditions are specified [see Eqs. (4.24) to (4.26)]:

$$\Gamma_1^{(2,0)}(k) = \sum_{n=0}^{\infty}\sum_{m=0}^{\infty}(k_0 - \mu)^m(k_y + v_1(k_x)k_x)^n \varrho^{(m,n)}(k_x;\mu), \tag{J.21}$$

where

$$\varrho^{(m,n)}(k_x;\mu) = \frac{1}{n!m!}\frac{\partial^{m+n}}{\partial k_0^m \partial k_y^n}\Gamma_1^{(2,0)}(k)\bigg|_{k=k^*}. \tag{J.22}$$

Under the interaction driven scaling, the functions $\varrho^{(m,n)}(k_x;\mu)$ have scaling dimension $[\varrho^{(m,n)}(k_x;\mu)] = 1 - n - m$. Let us show that each of these functions is independent of the UV scales of the theory. For $m = 0$ and $n = 0$,

$$\varrho^{(0,0)}(k_x;\mu) = i[1 + A_1^{(1)}(k_x)]\mu + V_{\text{F}}^{(1)}(k_x)v_1(k_x)k_x\left[A_1^{(2)}(k_x) - A_1^{(3)}(k_x)\right] + \Sigma_1(k^*) = i\mu, \tag{J.23}$$

where the last equality follows from Eqs. (J.13) to (J.15). Similarly, using the same expressions it follows that for $m = 1, n = 0$ and $m = 0, n = 1$ we have,

$$\varrho^{(1,0)}(k_x;\mu) = i\left[1 + A_1^{(1)}(k_x)\right] + \frac{\partial}{\partial k_0}\Sigma_1(k)\bigg|_{k=k^*} = i, \tag{J.24}$$

$$\varrho^{(0,1)}(k_x;\mu) = [1 + A_1^{(3)}(k_x)]V_{\text{F}}^{(1)}(k_x) + \frac{\partial}{\partial k_y}\Sigma_1(k)\bigg|_{k=k^*} = V_{\text{F}}^{(1)}(k_x), \tag{J.25}$$

respectively. Thus the first three terms in Eq. (J.21) are all finite. Now, we focus on Eq. (J.22) for $m + n \geq 2$ which are given by

$$\varrho^{(m,n)}(k_x;\mu) = \frac{1}{n!m!}\frac{\partial}{\partial k_0^m \partial k_y^n}\Sigma_1(k)\bigg|_{k=k^*}, \tag{J.26}$$

and therefore these depend only on the quantum corrections to the fermion dynamics. Under the interaction driven scaling, the scaling dimension of $\varrho^{(m,n)}(k_x;\mu)$ is negative for $m+n \geq 2$. In the absence of momentum dependence in the coupling functions and to zeroth order in the four-fermion coupling functions, the diagrammatic corrections to $\varrho^{(m,n)}(k_x;\mu)$ have superficial degree of divergence $\mathscr{D}_0 = 1 - m - n < 0$ and therefore are independent of the UV scale of the theory. As shown in the previous section, the introduction of the momentum dependence in the coupling functions does not increase the degree of divergence of the quantum corrections provided that Eqs. (4.19), (4.20) and Eq. (4.23) hold. Therefore, all of the functions in Eq. (J.22) have a degree of divergence $\mathscr{D} \leq \mathscr{D}_0 < 0$ for $m + n \geq 2$ and thus these are independent of the UV scale of the theory. As a consequence, the renormalized electronic two-point function is independent of the UV scale once the counterterm action in Eq. (4.22) is added to Eq. (4.1) to the leading order in four-fermion couplings.

J.4 Four-Point Vertex Function

We now focus on the four-point vertex function to zeroth order in the four-fermion couplings. That is, we consider those quantum corrections that contribute to the anomalous scaling dimension of the four-fermion coupling. These correspond to quantum corrections linear in the four-fermion couplings and arbitrary orders in the Yukawa vertex which have a superficial degree of divergence $\mathscr{D}_0 = 0$. The renormalized four-point vertex function is given by

$$\Gamma^{(4,0);\{j_i\}}_{\{N_i\};\{\sigma_i\}}(\{k_i\}) = \left[1 + A^{\{j_i\}}_{\{N_i\};\{\sigma_i\}}(\{k_{i;N_i}\})\right] \lambda^{\{j_i\}}_{\{N_i\};\{\sigma_i\}}(\{k_{i;N_i}\}) + \delta\Gamma^{(4,0);\{j_i\}}_{\{N_i\};\{\sigma_i\}}(\{k_i\}), \tag{J.27}$$

where $\delta\Gamma^{(4,0);\{j_i\}}_{\{N_i\};\{\sigma_i\}}(\{k_i\})$ encodes the quantum corrections to the four-point vertex function that are linear in the four-fermion couplings. According to the RG condition in Eq. (4.28), the counterterm function is fixed to be

$$A^{\{j_i\}}_{\{N_i\};\{\sigma_i\}}(\{k_{i;N_i}\}) = -\text{div}\left[\delta\Gamma^{(4,0);\{j_i\}}_{\{N_i\};\{\sigma_i\}}(\{k^*_i\})\right] + \text{finite terms}, \tag{J.28}$$

where k^*_i correspond to the frequency and momenta at which the RG conditions are imposed and $\text{div}[\cdots]$ denotes the divergent part of the expression in the $\Lambda_f \gg \mu$ limit, where μ is the energy scale at which the RG conditions are imposed. At this stage one can use the same argument that was used in showing that the Yukawa vertex corrections becomes independent of Λ_f once the momentum-dependent counterterm functions are added to the bare action. This guarantees that, if $A^{\{j_i\}}_{\{N_i\};\{\sigma_i\}}(\{k_{i;N_i}\})$ exists and it is local, the four-point vertex function becomes independent of Λ_f. As shown in Appendix Q by an explicit computation, such counterterms exist to the leading order in $v \ll 1$.

J.5 Scaling of Ladder Diagrams in the Particle-Particle Channel

In this section we focus on the particle-particle ladder diagrams shown in Fig. 4.8 that involve nested fermions within each loop. These diagrams are the ones that dominate the contributions to the anomalous scaling dimension of the four-fermion couplings. We estimate their magnitude in the $c(v)\Lambda_b \gg \Lambda_f$ limit and show that, a diagram in the ladder series with L loops scales, at most, as

$$\mathcal{L}(L) \sim \lambda^{\{j_i\}}_{\{N_i\};\{\sigma_i\}} w(v)^L \log(c(v)\Lambda_b)^L \log(\Lambda_f)^L, \tag{J.29}$$

in the $w(v) \ll 1$, $c(v)\Lambda_b \gg \Lambda_f \gg \Delta$ limits, where Δ denotes the IR scale of the diagram, which depends on the external frequencies and momenta.

Let us consider a L-loop diagram within the ladder series in Fig. 4.8 that involves only internal fermions at hot spots $N = 1$ and $N = 5$. For simplicity, we set the external frequencies and momenta to zero since these only play the role of IR cutoffs for the integration. To be concrete, we consider the quantum correction to the coupling $\lambda^{\{j_i\}}_{1515;\{\sigma_i\}}$ depicted in Fig. J.1. All other cases that involve nested fermions in each loop follows the same logic. The

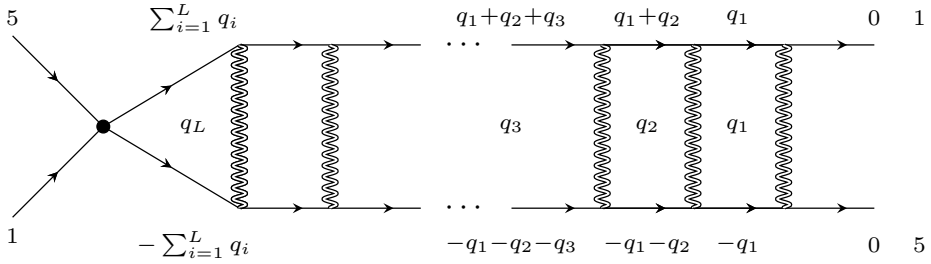

Figure J.1: L-loop contribution to $\lambda^{\{j_i\}}_{1515;\{\sigma_i\}}$ to linear order in $\lambda^{\{j_i\}}_{1515;\{\sigma_i\}}$.

expression for such a quantum correction reads, in the WMDL,

$$\begin{aligned}\mathcal{L}(L) = v^L \lambda^{\{j_i\}}_{1515;\{\sigma_i\}} \left[\prod_{j=1}^{L}\int \mathrm{d}q_j\right]\left[\prod_{j=1}^{L} D(q_j)\right] G_4(q_1;v)G_1(q_1+q_2;v)\times\cdots \\ \times G_4(q_1+\cdots+q_{L-1};v)G_1(q_1+\cdots+q_L;v)G_8(-q_1;v)G_5(-q_1-q_2;v)\times\cdots \\ \times G_5(-q_1-\cdots-q_{L-1};v)G_8(-q_1-\cdots-q_L;v).\end{aligned} \tag{J.30}$$

Here, q_j denotes the momentum flowing through the collective mode's propagator in every rung of the ladder diagram. According to the discussion in Sec. 4.2-(a) , the integration over the momenta must be done over the region:

$$|q_{j;x}| < \Lambda_b, \qquad |q_{j;y}| < \Lambda_b, \quad |e_4(\vec{q}_1;v)| < \Lambda_f, \quad |e_1(\vec{q}_1;v)+e_1(\vec{q}_2;v)| < \Lambda_f, \tag{J.31}$$

$$|e_4(\vec{q}_1;v)+e_4(\vec{q}_2;v)+e_4(\vec{q}_3;v)| < \Lambda_f, \quad \ldots \quad \& \quad \left|\sum_{j=1}^{L} e_4\left(\vec{q}_j;v\right)\right| < \Lambda_f. \tag{J.32}$$

To make the UV cutoff structure explicit in Eq. (J.30), it is convenient to change variables that make the integration over the energy of the internal electrons explicit. We consider then the nondegenerate change of variables:

$$Y_1 = e_4(\vec{q}_1;v), \qquad X_1 = q_{1,x}, \tag{J.33}$$

$$Y_2 = e_1(\vec{q}_1;v)+e_1(\vec{q}_2;v), \qquad X_2 = q_{2,x}, \tag{J.34}$$

$$Y_3 = e_4(\vec{q}_1;v)+e_4(\vec{q}_2;v)+e_4(\vec{q}_3;v), \qquad X_3 = q_{3,x}, \tag{J.35}$$

$$\vdots \tag{J.36}$$

$$Y_L = \sum_{j=1}^{L} e_4\left(\vec{q}_j;v\right), \qquad X_L = q_{L,x}. \tag{J.37}$$

Under this change of variables, the integration over Y_i are effectively performed on the regime $|Y_i| < \Lambda_f$. The integration over the X_i, on the other hand is done over $|X_i| < \Lambda_b$ in the $c(v)\Lambda_b \gg \Lambda_f$ limit. Using the fact that $e_4(\vec{q};v) = e_8(-\vec{q};v)$ and $e_1(\vec{q};v) = e_5(-\vec{q};v)$, Eq.

(J.30) takes the following form

$$\mathcal{L}(L) = v^L \lambda^{\{j_i\}}_{1515;\{\sigma_i\}} \left[\prod_{j=1}^{L} \int_{\mathbb{R}} \frac{\mathrm{d}q_0}{(2\pi)}\right] \left[\prod_{j=1}^{L} \int_{-\Lambda_b}^{\Lambda_b} \frac{\mathrm{d}X_j}{(2\pi)}\right] \left[\prod_{j=1}^{L} \int_{-\Lambda_f}^{\Lambda_f} \frac{\mathrm{d}Y_j}{(2\pi)}\right] \left[\prod_{j=1}^{L} \frac{1}{Y_j^2 + \left[\sum_{k=1}^{j} q_{k;0}\right]^2}\right] \times \left[\prod_{j=1}^{L} \frac{1}{|q_{j;0}| + c(v)|X_j| + |g^{(j)}(\{c(v)X_i, c(v)Y_i\})|}\right]. \tag{J.38}$$

Here $c(v)q_{j;y} \equiv g^{(j)}(\{c(v)X_i, c(v)Y_i\})$ are functions that depend both on Y_i and X_i at most linearly in each of the integration variables. Moreover, these depend on X_i only through vX_i. For example, for $j = 1, 2, 3$, these are given by

$$g^{(1)}(\{c(v)X_i, c(v)Y_i\}) = c(v)\left[Y_1 - vX_1\right], \tag{J.39}$$

$$g^{(2)}(\{c(v)X_i, c(v)Y_i\}) = c(v)[v(2X_1 + X_2) - Y_1 - Y_2], \tag{J.40}$$

$$g^{(3)}(\{c(v)X_i, c(v)Y_i\}) = c(v)\left[Y_2 + Y_3 - v(2X_1 + X_3 + 2X_2)\right], \tag{J.41}$$

and similarly for all $4 \leq j \leq L$. An important feature of these functions is that, for a fixed j, these depend only on X_i with $i \leq j$. We proceed by noting that, in the large Λ_f limit, the Y_i integrations are all convergent because the integrand decays faster than Y_i^{-2} in every direction. In particular, if one ignores the terms of order $c(v)Y_i$ inside the boson propagator, the integrand decays as Y_i in every direction. Therefore, one can perform the integration over the Y_i in the $v \ll 1$ limit to obtain

$$\mathcal{L}(L) \sim v^L \lambda^{\{j_i\}}_{1515;\{\sigma_i\}} \left[\prod_{j=1}^{L} \int_{\mathbb{R}} \frac{\mathrm{d}q_0}{(2\pi)}\right] \left[\prod_{j=1}^{L} \int_{-\Lambda_b}^{\Lambda_b} \frac{\mathrm{d}X_j}{(2\pi)}\right] \left[\prod_{j=1}^{L} \frac{\arctan\left(\frac{\Lambda_f}{\sum_{k=1}^{j} q_{k;0}}\right)}{\sum_{k=1}^{j} q_{k;0}}\right] \times \left[\prod_{j=1}^{L} \frac{1}{|q_{j;0}| + c(v)|X_j| + |g^{(j)}(\{c(v)X_i, 0\})|}\right]. \tag{J.42}$$

To integrate over X_i we use the fact that for a fixed j, the functions $g^{(j)}$ depend only on X_i with $i \leq j$. In the small v limit, the terms of order $vc(v)X_i$ can be ignored with respect to the terms of order $c(v)|X_i|$, *within the same bosonic propagator*. In this limit, the integration over X_L can be done straightforwardly to yield

$$\mathcal{L}(L) \sim w(v)^L \lambda^{\{j_i\}}_{1515;\{\sigma_i\}} \left[\prod_{j=1}^{L} \int_{\mathbb{R}} \frac{\mathrm{d}q_0}{(2\pi)}\right] \left[\prod_{j=1}^{L-1} \int_{-c(v)\Lambda_b}^{c(v)\Lambda_b} \frac{\mathrm{d}X_j}{(2\pi)}\right] \left[\prod_{j=1}^{L} \frac{\arctan\left(\frac{\Lambda_f}{\sum_{k=1}^{j} q_{k;0}}\right)}{\sum_{k=1}^{j} q_{k;0}}\right] \times \left[\prod_{j=1}^{L-1} \frac{1}{|q_{j;0}| + |X_j| + |\overline{g}^{(j)}(\{X_i, 0\})|}\right] \log\left[1 + \frac{c(v)\Lambda_b}{|q_{L;0}| + |\overline{g}^{(L)}(X_i, 0)|}\right]. \tag{J.43}$$

where $\overline{g}^{(j)}(X_i, 0) = g^{(j)}(X_i, 0)|_{vX_j=0}$. Since this function depends on X_{L-1} through vX_{L-1}, setting $v = 0$ makes the integration over X_{L-1} logarithmically divergent in the large $c(v)\Lambda_b$

limit. Therefore, one is tempted to say that the UV divergence is cut off by a momentum scale proportional to $1/v$. Indeed, this is the case and this scale depends on the internal frequency and momentum. This doesn't rule out the possibility of a divergence stronger than a single logarithm in the UV scale Λ_f. This is due to the logarithmic dependence on the momentum scale that cuts off the aforementioned divergence once the integration over the X_i's is performed. We can, however, bound this integral from above by

$$\mathcal{L}(L) \lessapprox w(v)^L \lambda^{\{j_i\}}_{1515;\{\sigma_i\}} \left[\prod_{j=1}^{L} \int_{\mathbb{R}} \frac{\mathrm{d}q_0}{(2\pi)}\right] \left[\prod_{j=1}^{L-1} \int_{-c(v)\Lambda_b}^{c(v)\Lambda_b} \frac{\mathrm{d}X_j}{(2\pi)}\right] \left[\prod_{j=1}^{L} \left| \frac{\arctan\left(\frac{\Lambda_f}{\sum_{k=1}^{j} q_{k;0}}\right)}{\sum_{k=1}^{j} q_{k;0}} \right|\right] \times \left[\prod_{j=1}^{L-1} \frac{1}{|q_{j;0}| + |X_j| + |\overline{g}^{(j)}(\{X_i, 0\})|}\right] \log\left[1 + \frac{c(v)\Lambda_b}{|q_{L;0}|}\right]. \tag{J.44}$$

This allows for an integration over X_{L-1} that follows the same logic as the one used in the integration over X_i. Thus, by the same token, we have that

$$\mathcal{L}(L) \lessapprox w(v)^L \lambda^{\{j_i\}}_{1515;\{\sigma_i\}} \left[\prod_{j=1}^{L} \int_{\mathbb{R}} \frac{\mathrm{d}q_0}{(2\pi)}\right] \left[\prod_{j=1}^{L-2} \int_{-c(v)\Lambda_b}^{c(v)\Lambda_b} \frac{\mathrm{d}X_j}{(2\pi)}\right] \left[\prod_{j=1}^{L} \left| \frac{\arctan\left(\frac{\Lambda_f}{\sum_{k=1}^{j} q_{k;0}}\right)}{\sum_{k=1}^{j} q_{k;0}} \right|\right] \times \left[\prod_{j=1}^{L-2} \frac{1}{|q_{j;0}| + |X_j| + |\overline{g}^{(j)}(\{X_i, 0\})|}\right] \log\left[1 + \frac{c(v)\Lambda_b}{|q_{L;0}|}\right] \log\left[1 + \frac{c(v)\Lambda_b}{|q_{L-1;0}|}\right]. \tag{J.45}$$

Iterating the same bound until all of the X_i integrations are done, we can bound the integration from above by

$$\mathcal{L}(L) \lessapprox w(v)^L \lambda^{\{j_i\}}_{1515;\{\sigma_i\}} \left[\prod_{j=1}^{L} \int_{\mathbb{R}} \frac{\mathrm{d}q_0}{(2\pi)}\right] \left[\prod_{j=1}^{L} \left| \frac{\arctan\left(\frac{\Lambda_f}{\sum_{k=1}^{j} q_{k;0}}\right)}{\sum_{k=1}^{j} q_{k;0}} \right|\right] \left[\prod_{j=1}^{L} \log\left[1 + \frac{c(v)\Lambda_b}{|q_{j;0}|}\right]\right]. \tag{J.46}$$

We now address the remaining integrations in the $\Lambda_f \ll c(v)\Lambda_b$ limit. In here, the arctangent functions play an important role. If the frequencies are large compared to Λ_f, the integration vanishes very rapidly in the large frequency limits, offering only contributions that vanish in the $\Lambda_f \to \infty$ limit. Therefore, the leading order dependence in Λ_f comes from frequencies that are, at most, of order Λ_f. This implies that the arctangent functions effectively cutoff the large frequency integrations at a scale Λ_f. In this case, $c(v)\Lambda_b/|q_0| \gg 1$ and in this limit we have

$$\mathcal{L}(L) \lessapprox w(v)^L \lambda^{\{j_i\}}_{1515;\{\sigma_i\}} \log(c(v)\Lambda_b)^L \left[\prod_{j=1}^{L} \int_{\mathbb{R}} \frac{\mathrm{d}q_0}{(2\pi)}\right] \left[\prod_{j=1}^{L} \left| \frac{\arctan\left(\frac{\Lambda_f}{\sum_{k=1}^{j} q_{k;0}}\right)}{\sum_{k=1}^{j} q_{k;0}} \right|\right]. \tag{J.47}$$

This integration can be bounded even further by

$$\mathcal{L}(L) \lessapprox w(v)^L \lambda^{\{j_i\}}_{1515;\{\sigma_i\}} \log(c(v)\Lambda_b)^L \left[\prod_{j=1}^{L} \int_{\mathbb{R}} \frac{\mathrm{d}q_0}{(2\pi)}\right] \left[\prod_{j=1}^{L} \left| \frac{\arctan\left(\frac{\Lambda_f}{|q_{j;0}|}\right)}{q_{j;0}} \right|\right]. \tag{J.48}$$

Individual integration over the frequencies yield, in the large Λ_f limit, a logarithmic divergence in Λ_f. Therefore we have that

$$\mathcal{L}(L) \lessapprox w(v)^L \lambda^{\{j_i\}}_{1515;\{\sigma_i\}} \log(c(v)\Lambda_b)^L \log(\Lambda_f)^L. \tag{J.49}$$

The same argument applies for any choice of external hot spot indices. Therefore, a diagram with L loops in the ladder series shown in Fig. 4.8 scales with $w(v), \Lambda_b$ and Λ_f, at most, as show in Eq. (J.29) in the $w(v) \ll 1$ and $c(v)\Lambda_b \gg \Lambda_f \gg \Delta$ limits, where Δ represents the IR scale of the diagram and which depends on the external frequencies and momenta.

Appendix K | Functional RG Scheme and the Functional RG Equation

In this appendix we elaborate further on the functional RG scheme introduced in Sec. 4.3 and derive the RG equation governing the scaling form of arbitrary vertex functions. This appendix constitutes a generalization of the scheme presented in Appendix B for the case in which we include the momentum dependence in the couplings of the theory.

The renormalized quantum effective action arising from the action in Eq. (4.1) can be written formally as

$$\begin{aligned}\mathbf{\Gamma}([\{\psi^\dagger,\psi,\Phi\},v_N,g_N,V_{\mathrm{F}}^{(N)},\lambda^{\{j_i\}}_{\{N_i\};\{\sigma_i\}}];\widehat{k}_{\mathrm{F}};\widehat{\Lambda}_b;\mu)=\\ \sum_{n,m=0}^{\infty}\mathbf{\Gamma}^{(2m,n)}([\{\psi^\dagger,\psi,\Phi\},v_N,g_N,V_{\mathrm{F}}^{(N)},\lambda^{\{j_i\}}_{\{N_i\};\{\sigma_i\}}];\widehat{k}_{\mathrm{F}};\widehat{\Lambda}_b;\mu),\end{aligned} \tag{K.1}$$

where $\lambda^{\{j_i\}}_{\{N_i\};\{\sigma_i\}}(\{k_{i;N_i}\})$, $\widehat{k}_{\mathrm{F}}$ and $\widehat{\Lambda}_b$ are the dimensionless four-fermion coupling functions and the dimensionless IR scales of the theory, respectively. Here, the vertex functionals are expanded as

$$\begin{aligned}\mathbf{\Gamma}^{(2m,n)}([\{\psi^\dagger,\psi,\Phi\},v_N,g_N,V_{\mathrm{F}}^{(N)},\lambda^{\{j_i\}}_{\{N_i\};\{\sigma_i\}}];\widehat{k}_{\mathrm{F}};\widehat{\Lambda}_b;\mu)=(2\pi)^3\left[\prod_{j=1}^{2m+n}\int \mathrm{d}k_j\right]\\ \times\left\{\delta\left(\sum_{j=1}^{m}k_j-\sum_{j=m+1}^{2m+n}k_j\right)\psi^\dagger(k_1)\cdots\psi^\dagger(k_m)\psi(k_{m+1})\cdots\psi(k_{2m})\right.\\ \left.\times\,\Phi(k_{1+2m})\cdots\Phi(k_{n+2m})\mathit{\Gamma}^{(2m,n)}(k_1,\ldots,k_{2m+n-1};[v_N,g_N,V_{\mathrm{F}}^{(N)},\lambda^{\{j_i\}}_{\{N_i\};\{\sigma_i\}}];\widehat{k}_{\mathrm{F}};\widehat{\Lambda}_b;\mu)\right\}.\end{aligned} \tag{K.2}$$

Here $\mathit{\Gamma}^{(2m,n)}(\{k_i\})\equiv\mathit{\Gamma}^{(2m,n)}(k_1,\ldots,k_{2m+n-1};[v_N,g_N,V_{\mathrm{F}}^{(N)},\lambda^{\{j_i\}}_{\{N_i\};\{\sigma_i\}}];\widehat{k}_{\mathrm{F}};\widehat{\Lambda}_b;\mu)$ denotes the one-particle irreducible (1PI) vertex functionals of the theory, where the square brackets are used to indicate their functional dependence on the coupling functions. In what follows we keep implicit the dependence on the coupling functions and dimensionless scales of the vertex functions. The vertex functions depend explicitly on the hot spot, spin and flavor indices and, in Eq. (K.2), the summation over these indices, as well as the dependence of the fields and vertex functions on them, have been left implicit for clarity.

Under the interaction-driven scaling, the 1PI vertex functions have engineering scaling dimension $[\mathit{\Gamma}^{(2m,n)}(\{k_i\})]=3-2m-n$. Therefore, under a scaling transformation

$$\mathit{\Gamma}^{(2m,n)}(\{k_i\})'=\mathsf{b}^{3-2m-n}\mathit{\Gamma}^{(2m,n)}(\{k_i\}), \tag{K.3}$$

where $\Gamma^{(2m,n)}(\{k_i\})' = \Gamma^{(2m,n)}(\{\mathsf{b}k_i\}; [v'_N, g'_N, V_{\rm F}^{(N)'}, \lambda^{\{j_i\}'}_{\{N_i\};\{\sigma_i\}}]; \widehat{k}_{\rm F}; \widehat{\Lambda}_b; \mathsf{b}\mu)$ for $\mathsf{b} \in \mathbb{R}$, and the primes are use to denote a scaling transformation on the coupling functions:

$$v'_N(k_N) = v_N(\mathsf{b}^{-1}k_N), \tag{K.4}$$

$$V_{\rm F}^{(N)}(k_N)' = V_{\rm F}^{(N)}(\mathsf{b}^{-1}k_N), \tag{K.5}$$

$$g'_N(q_N, k_N) = g_N(\mathsf{b}^{-1}q_N, \mathsf{b}^{-1}k_N), \tag{K.6}$$

$$\lambda^{\{j_i\}'}_{\{N_i\};\{\sigma_i\}}(\{k_{i;N_i}\}) = \lambda^{\{j_i\}'}_{\{N_i\};\{\sigma_i\}}(\{\mathsf{b}^{-1}k_{i;N_i}\}). \tag{K.7}$$

It is noted that, under the simultaneous scaling of time and space, the frequency and momentum in the coupling functions must transform with the inverse scaling transformation to preserve the domain and range of these functions.

On the support of the momentum conserving Dirac distribution in Eq. (K.2), the bare vertex functions are related to the renormalized one through the multiplicative relation

$$\Gamma^{(2m,n)}_{\mathsf{B}}(\{k_i^{\mathsf{B}}\}) = \frac{\left[Z^{(\Phi)}\right]^{-\frac{n}{2}}}{Z_\tau^{2m+n-1}} \left[\prod_{j=1}^{2m\,\prime} Z^{(\psi)}_{N_j}(k_{N_j})\right]^{-\frac{1}{2}} \Gamma^{(2m,n)}(\{k_i\}), \tag{K.8}$$

with $\Gamma^{(2m,n)}(\{k_i^{\mathsf{B}}\})'_{\mathsf{B}} = \Gamma^{(2m,n)}(\{\lambda k_i^{\mathsf{B}}\}; [v_N^{\mathsf{B}}, g_N^{\mathsf{B}}, V_{\mathsf{B};\mathrm{F}}^{(N)}, {}^{\mathsf{B}}\lambda^{\{j_i\}}_{\{N_i\};\{\sigma_i\}}]; \widehat{k}_{\rm F}^{\mathsf{B}}; \widehat{\Lambda}_b^{\mathsf{B}}; \Lambda_f)$ where $\widehat{k}_{\rm F}^{\mathsf{B}} = \mu\widehat{k}_{\rm F}$ and $\widehat{\Lambda}_b^{\mathsf{B}} = \mu\widehat{\Lambda}_b$. Here $Z^{(\Phi)} = Z_4^2 Z_3/Z_1^2 Z_2$, $Z_\tau = Z_1/Z_3$ and $Z^{(\psi)}_{N_i}(k_{N_i}) \equiv Z_N^{(1)}(k_N)/Z_\tau^2$, and the renormalized coupling functions are related to the bare ones according to Eq. (4.30). The prime in the product symbol in Eq. (K.8) is used to denote the fact that the momenta appearing in the fermion field renormalization factors must comply to the momentum conservation implied by the Dirac distribution in Eqs. (K.2). Combining Eqs. (K.3), (K.8) and (4.30), and using the fact that the bare quantities are independent of the floating energy scale μ, it follows that the scaling form of the vertex functions is governed by the *functional* RG equation

$$\begin{aligned}
&\Bigg\{ z(n-1) + 2(m-1) + n\eta^{(\Phi)} + \sum_{j=1}^{2m\,\prime} \widetilde{\eta}^{(\psi)}_{N_j}(k_{N_j}) + \sum_{j=1}^{2m+n-1} \left[z k_{j;0} \frac{\partial}{\partial k_{j;0}} + \vec{k}_j \cdot \frac{\partial}{\partial \vec{k}_j} \right] \\
&- \sum_{M_1=1}^{8} \int \mathrm{d}x_1 \left(\left[x_1 \frac{\partial v_{M_1}(x_1)}{\partial x_1} + \beta^{(v)}_{M_1}(x_1) \right] \frac{\delta}{\delta v_{M_1}(x)} + \left[x_1 \frac{\partial V_{\rm F}^{(M_1)}}{\partial x_1} + \beta^{(V_{\rm F})}_{M_1}(x_1) \right] \frac{\delta}{\delta V_{\rm F}^{(M_1)}(x)} \right. \\
&+ \int \mathrm{d}x_2 \left[\left\{ x_1 \frac{\partial g_{M_1}(x_1,x_2)}{\partial x_1} + x_2 \frac{\partial g_{M_1}(x_1,x_2)}{\partial x_2} + \beta^{(g)}_{M_1}(x_1,x_2) \right\} \frac{\delta}{\delta g_{M_1}(x_1,x_2)} \right. \\
&+ \sum_{M_2,M_3,M_4=1}^{8} \sum_{\{\sigma_i=1\}}^{N_c} \sum_{\{j_i=1\}}^{N_f} \int \mathrm{d}x_3 \int \mathrm{d}x_4 \left\{ \beta^{(\lambda);\{j_i\}}_{\{M_i\};\{\sigma_i\}}(\{x_i\}) \right. \\
&\left. \left. \left. + \sum_{\{x_i=1\}}^{4} x_i \frac{\partial \lambda^{\{j_i\}}_{\{M_i\};\{\sigma_i\}}(\{x_i\})}{\partial x_i} \right\} \frac{\delta}{\delta \lambda^{\{j_i\}}_{\{N_i\};\{\sigma_i\}}(\{x_i\})} \right] \right) - \beta_{\widehat{k}_{\rm F}} \frac{\partial}{\partial \widehat{k}_{\rm F}} - \beta_{\widehat{\Lambda}_b} \frac{\partial}{\partial \widehat{\Lambda}_b} \Bigg\} \Gamma_N^{(2m,n)}(\{k_i\}) = 0,
\end{aligned} \tag{K.9}$$

for *any fixed energy scale* μ. Here x_i with $i = 1, 2, 3, 4$, denote one-dimensional momentum and $\delta/\delta\mathsf{A}$ denotes a functional derivative with respect to $\mathsf{A} = v_M(x)$, $V_{\rm F}^{(M)}(x)$, $g_M(x_1, x_2)$

and $\lambda^{\{j_i\}}_{\{N_i\};\{\sigma_i\}}(\{x_i\})$. The dynamical critical exponent, effective anomalous dimensions of the fields and beta function of the dimensionless IR scales are defined by

$$z = 1 + \frac{\mathrm{d}\log Z_\tau}{\mathrm{d}\log\mu}, \quad \widetilde{\eta}^{(\psi)}_N(k_N) = \frac{1}{2}\frac{\mathrm{d}\log Z^{(1)}_N(k_N)}{\mathrm{d}\log\mu}, \quad \eta^{(\Phi)} = \frac{1}{2}\frac{\mathrm{d}\log Z^{(\Phi)}}{\mathrm{d}\log\mu}, \\ \beta_{\widehat{k}_\mathrm{F}} = \frac{\mathrm{d}\widehat{k}_\mathrm{F}}{\mathrm{d}\log\mu}, \quad \beta_{\widehat{\Lambda}_b} = \frac{\mathrm{d}\widehat{\Lambda}_b}{\mathrm{d}\log\mu}, \tag{K.10}$$

respectively, with $Z_\tau = Z_1/Z_3$, $Z^{(\psi)}_N(k_N) = Z^{(1)}_N(k_N)/Z^2_\tau$ and $Z^{(\Phi)} = Z^2_4 Z_3/(Z^2_1 Z_2)$. The last two terms in Eq. (K.9) encode the scaling properties of the coupling functions under simultaneous scaling of the running energy scale and momentum. There, the beta functions

$$\beta^{(v)}_M(x) = \frac{\mathrm{d}v_M(x)}{\mathrm{d}\log\mu}, \quad \beta^{(V_\mathrm{F})}_M(x) = \frac{\mathrm{d}V^{(M)}_\mathrm{F}(x)}{\mathrm{d}\log\mu}, \quad \beta^{(g)}_M(x_1,x_2) = \frac{\mathrm{d}g_M(x_1,x_2)}{\mathrm{d}\log\mu}, \tag{K.11}$$

$$\beta^{(\lambda);\{j_i\}}_{\{L_i\};\{\sigma_i\}}(\{x_i\}) = \frac{\mathrm{d}\lambda^{\{j_i\}}_{\{L_i\};\{\sigma_i\}}}{\mathrm{d}\log\mu}, \tag{K.12}$$

track the flow of the couplings with increasing energy scale μ and for a fixed momentum. Analogously, the momentum dilation operators of the form $x_i\frac{\partial}{\partial x_i}$ in Eq. (B.10) track the effect of scaling the momentum at a fixed energy scale μ. Choosing $m = 1$, $n = 0$ in Eq. (K.9) we obtain Eq. (4.32). Finally, since Eq. (K.9) is valid for any fixed μ, we choose $\mu = \Lambda_f$, from where Eq. (4.33) follows.

Appendix L | Single-Particle Electronic Spectral Function

In this appendix we solve the RG equation for the electronic two-point function in full generality and then simplify the discussion within the context of the WMDL. For simplicity in the discussion we ignore the presence of the four-fermion couplings, meaning we will analyze the electronic two-point function at energy scales above the scale at which superconducting order develops. We later compute the single-particle spectral function. Choosing $m = 1$ and $n = 0$ in Eq. (K.9), the RG equation for the electronic two-point function reads

$$\left\{ k_0 \frac{\partial}{\partial k_0} + \frac{1}{z}\vec{k}\cdot\frac{\partial}{\partial \vec{k}} - \frac{1}{z}\beta_{\widehat{k}_{\rm F}}\frac{\partial}{\partial \widehat{k}_{\rm F}} - \frac{1}{z}\beta_{\widehat{\Lambda}_b}\frac{\partial}{\partial \widehat{\Lambda}_b} - \mathsf{G}[v] - \mathsf{G}[V_{\rm F}] - \mathsf{F}[g] + \frac{[2\widetilde{\eta}_N^{(\psi)}(k_N) - z]}{z} \right\} \Gamma_N^{(2)}(k;\widehat{k}_{\rm F};\widehat{\Lambda}_b;\mu) = 0, \tag{L.1}$$

where $\Gamma_N^{(2)}(k;\widehat{k}_{\rm F};\widehat{\Lambda}_b;\mu) \equiv \Gamma_N^{(2)}(k_0,\vec{k};[v_M,g_M,V_{\rm F}^{(M)}];\widehat{k}_{\rm F};\widehat{\Lambda}_b;\mu)$ and we have defined the following functional operators

$$\mathsf{G}[\mathsf{A}] \equiv \frac{1}{z}\sum_{M=1}^{8}\int {\rm d}x \left[x\frac{\partial \mathsf{A}_M(x)}{\partial x} + \beta_M^{(\mathsf{A})}(x)\right]\frac{\delta}{\delta \mathsf{A}_M(x)}, \qquad \mathsf{A} = v, V_{\rm F},$$

$$\mathsf{F}[g] \equiv \frac{1}{z}\sum_{M=1}^{8}\int {\rm d}x \int {\rm d}y \left[x\frac{\partial g_M(x,y)}{\partial x} + y\frac{\partial g_M(x,y)}{\partial y} + \beta_M^{(g)}(x,y)\right]\frac{\delta}{\delta g_M(x,y)}.$$

Since Eq. (L.1) is valid for any μ we set $\mu = \Lambda_f$ because we are interested in the scaling properties of the two-point function as we go to energy scales lower than Λ_f. Eq. (L.1) is solved by a family of functions parametrized by a real parameter l. This becomes manifest once we write it as,

$$\left\{ k_0 \frac{\partial}{\partial k_0} + \frac{1}{z(l)}\vec{k}\cdot\frac{\partial}{\partial \vec{k}} + \frac{\partial}{\partial l} + \frac{[2\widetilde{\eta}_N^{(\psi)}(k_N;l) - z(l)]}{z(l)} \right\} \Gamma_N^{(2)}(k;\widehat{k}_{\rm F}(l);\widehat{\Lambda}_b(l);\Lambda_f) = 0, \tag{L.2}$$

provided that the following equations are satisfied

$$\frac{\partial v_M(k_M;l)}{\partial l} = -\frac{1}{z(l)}\left[k_M \frac{\partial v_M(k_M;l)}{\partial k_M} + \beta_M^{(v)}(k_M;l)\right], \tag{L.3}$$

$$\frac{\partial V_{\rm F}^{(M)}(k_M;l)}{\partial l} = -\frac{1}{z(l)}\left[k_M \frac{\partial V_{\rm F}^{(M)}(k_M;l)}{\partial k_M} + \beta_M^{(V_{\rm F})}(k_M;l)\right], \tag{L.4}$$

$$\frac{\partial g_M(k'_M,k_M;l)}{\partial l} = -\frac{1}{z(l)}\left[k'_M\frac{\partial g_M(k'_M,k_M;l)}{\partial k'_M} + k_M\frac{\partial g_M(k'_M,k_M;l)}{\partial k_M} + \beta_M^{(g)}(k'_M,k_M;l)\right], \tag{L.5}$$

$$\frac{\partial \widehat{k}_{\rm F}(l)}{\partial l} = -\frac{1}{z(l)}\beta_{\widehat{k}_{\rm F}}(l), \tag{L.6}$$

$$\frac{\partial \widehat{\Lambda}_b(l)}{\partial l} = -\frac{1}{z(l)}\beta_{\widehat{\Lambda}_b(l)}(l). \tag{L.7}$$

Here the dynamical critical exponent $[z(l)]$, anomalous scaling dimension of the fermion field $[\widetilde{\eta}_N^{(\psi)}(k_N;l)]$, beta functions for the scales $\widehat{k}_{\rm F}$ and $\widehat{\Lambda}_b$, and the beta functions that track the behavior of the momentum-dependent couplings as a function of the scale l for a fixed momenta are defined in Eq. (4.33). These equations follow directly from the definitions in Eq. (L.2). We note that the dynamical critical exponent and the effective anomalous scaling dimension of the fermion field acquire a scale dependence through the zero momentum coupling functions that solve Eqs. (L.3) to (L.6).

For the initial conditions $v_N(k_N;0) \equiv \mathsf{v}_N(k_N)$, $V_{\rm F}^{(N)}(k_N;0) \equiv \mathsf{V}_{\rm F}^{(N)}(k_N)$, $g_N(k'_N,k_N;0) = \mathsf{g}_N(k'_N,k_N)$, $k_{\rm F}(0) = k_{\rm F}^{(0)}$, and $\widehat{\Lambda}_b^{(0)} = \widehat{\Lambda}_b(0)$, where $\mathsf{v}_N, \mathsf{V}_{\rm F}^{(N)}$ and g_N are known functions of momentum, the solution to Eq. (L.1) can be written as

$$\Gamma_N^{(2,0)}(k;\widehat{k}_{\rm F}^{(0)};\widehat{\Lambda}_b^{(0)}) = \exp\left(\int_0^l {\rm d}\ell\,\frac{\{2\widetilde{\eta}_N^{(\psi)}[k_N(\ell);\ell] - z(\ell)\}}{z(\ell)}\right)\Gamma_N^{(2,0)}[k(l);\widehat{k}_{\rm F}(l),\widehat{\Lambda}_b(l)], \tag{L.8}$$

where $k(l) = [k_0(l),\vec{k}(l)]$, with the scale dependent frequency and momentum are given by Eq. (4.41), $\widehat{k}_{\rm F}(l) = \widehat{k}_{\rm F}^{(0)}e^{\int_0^l \frac{{\rm d}\ell}{z(\ell)}}$ and $\widehat{\Lambda}_b(l) = \widehat{\Lambda}_b^{(0)}e^{\int_0^l \frac{{\rm d}\ell}{z(\ell)}}$. By acting on this expression with the operator ${\rm d}/{\rm d}l$, it is straightforward to check that Eq. (L.8) solves Eq. (L.1). To fully determine the electronic two-point function, Eqs. (L.3) to (L.6) need to be solved. This is accomplished by first singling out the effect of the momentum dilation operator on the coupling functions. This is done by defining the rescaled coupling functions in Eqs. (4.42) to (4.44) which satisfy the Eqs. (4.46) to (4.48), respectively. The latter can be solved once the momentum-dependent counterterms of the theory are known and the fact that the bare quantities are independent of the energy scale μ. In what follows we determine the form of the electronic two-point function in the WMDL by using the results for the momentum-dependent counterterms obtained in Appendix M.

L.1 Electronic two-point function in the WMDL

In the WMDL and to leading order in $v_0 \ll 1$, the counterterm functions relating the renormalized and bare quantities in Eq. (4.30) are given, to leading order in $w(v) \ll 1$, by

$$Z_N^{(1)}(k_N) = 1 - \frac{(N_c^2-1)w(v)}{2\pi N_c N_f}\log\left(\frac{\Lambda_f}{\mathscr{G}_1(\mu,2vc(v)|k_N|)}\right), \tag{L.9}$$

$$Z_N^{(2)}(k_N) = 1 + \frac{(N_c^2-1)}{\pi^2 N_c N_f}\left[v\log\left(\frac{1}{c(v)}\right)\log\left(\frac{\Lambda_f}{\mathscr{G}_2(|k_0|,2vc(v)|k_N|)}\right) + \frac{3\log[w(v)]^2 w(v)^2}{8N_cN_f}\log\left(\frac{\Lambda_f}{\mathscr{G}_3(k_0,2v|k_N|)}\right)\right], \tag{L.10}$$

$$Z_N^{(3)}(k_N) = 1 - \frac{(N_c^2-1)}{\pi^2 N_c N_f}\left[v\log\left(\frac{1}{c(v)}\right)\log\left(\frac{\Lambda_f}{\mathscr{G}_2(|k_0|,2vc(v)|k_N|)}\right) + \frac{\log[w(v)]^2 w(v)^2}{8N_cN_f}\log\left(\frac{\Lambda_f}{\mathscr{G}_3(k_0,2v|k_N|)}\right)\right], \tag{L.11}$$

$$Z_N^{(4)}(k'_N,k_N) = 1 - \frac{1}{2\pi N_c N_f} w(v)\log\left(\frac{1}{w(v)}\right)\log\left(\frac{\Lambda_f}{\mathscr{H}_1(\mu,v^2|k_N|,v|k'_N+k_N|)}\right). \tag{L.12}$$

These expressions follow from Eqs. (M.17), (M.49), (M.50), (M.71), (M.87), (M.88) and (M.109). Here, $\mathscr{G}_i(x,y) \sim \max(x,y)$ for $i = 1,2,3$ and $\mathscr{H}_1(x,y,u) \sim \max(x,y,u)$. By using Eq. (3.43) the counterterm functions reduce to Eqs. (D.6) to (D.20) to leading order in $v \ll 1$. In Appendix M we provide a full fledged computation of these expressions. Since the counterterm functions only depend on the zero momentum slope and are controlled by it, Eqs. (4.46) to (4.48) can be written, to leading order in $v(l) \ll 1$, as

$$\frac{\partial}{\partial l}\widehat{v}_N(k_N;l) = \frac{\widehat{v}_N(k_N;l)}{z(l)}\left\{Z_N^{(2)}[k_N(l);l]' - Z_N^{(3)}[k_N(l);l]'\right\}, \tag{L.13}$$

$$\frac{\partial}{\partial l}\widehat{V}_{\mathrm{F}}^{(N)}(\vec{k};l) = \frac{\widehat{V}_{\mathrm{F}}^{(N)}(k_N;l)}{z(l)}\left\{Z_N^{(3)}[k_N(l);l]' - Z_N^{(1)}[k_N(l);l]' + z(l) - 1\right\}, \tag{L.14}$$

$$\frac{\partial}{\partial l}\widehat{g}(k'_N,k_N;l) = \frac{g(k'_N,k_N;l)}{z(l)}\left(\frac{1}{2}\left\{Z_2(l)' - Z_3(l)' - Z_N^{(1)}[k'_N(l);l]' - Z_{\overline{N}}^{(1)}[k_N(l);l]'\right\} + Z_N^{(4)}[k'_N(l),k_N(l);l]' - Z_4(l)' + Z_1(l)'\right), \tag{L.15}$$

where, $Z_i(l) \equiv Z_N^{(i)}(0;l)$, $Z_4(l) \equiv Z_N^{(4)}(0,0;l)$, $Z_N^{(i)}(k_N(l);l)' \equiv \frac{\partial}{\partial \log\mu} Z_N^{(i)}(k_N(l);l)\big|_{\mu=\Lambda_f}$ and $Z_N^{(4)}(k'_N(l),k_N(l);l)' \equiv \frac{\partial}{\partial\log\mu} Z_N^{(4)}(k'_N(l),k_N(l);l)\big|_{\mu=\Lambda_f}$. For the initial conditions in Eqs. (4.53) to (4.55), these expressions are solved by direct exponentiation:

$$\widehat{v}_N(k_N;l) = v_0 \exp\left(\int_0^l \frac{\mathrm{d}\ell}{z(\ell)}\left\{Z_N^{(2)}[k_N(\ell);\ell]' - Z_N^{(3)}[k_N(\ell);\ell]'\right\}\right), \tag{L.16}$$

$$\widehat{V}_{\mathrm{F}}^{(N)}(k_N;l) = \exp\left(\int_0^l \frac{\mathrm{d}\ell}{z(\ell)}\left\{Z_N^{(3)}[k_N(\ell);\ell]' - Z_N^{(1)}[k_N(\ell);\ell]' + z(\ell) - 1\right\}\right), \tag{L.17}$$

$$\widehat{g}_N(k'_N,k_N;l) = \sqrt{\frac{\pi v_0}{2}}\exp\left(\frac{1}{2}\int_0^l \frac{\mathrm{d}\ell}{z(\ell)}\left\{Z_2(\ell)' - Z_3(\ell)' - Z_N^{(1)}[k'_N(\ell);\ell]' - Z_{\overline{N}}^{(1)}[k_N(\ell);\ell]' + 2Z_N^{(4)}[k'_N(\ell),k_N(\ell);\ell]' - 2Z_4(\ell)' + 2Z_1(\ell)'\right\}\right). \tag{L.18}$$

With a formal solution for the rescaled coupling functions, the electronic two-point function in Eq. (L.8) is determined by noting that, at the length scale $\ell_\omega = \log(\Lambda_f/k_0)$ with $k_0 > 0$, the RG conditions in Eqs. (4.24) to (4.26), combined with the suppression of higher-loop quantum corrections beyond tree level, imply that the electronic two-point function is given

by

$$\Gamma_N^{(2,0)}(k_0,\vec{k}) = \exp\left(\int_0^{\ell_\omega} \frac{\mathrm{d}\ell}{z(\ell)}\{Z_N^{(1)}[k_N(\ell);\ell]' - z(\ell)\}\right) \times \left\{ i\Lambda_f + e^{\int_0^{\ell_\omega} \frac{\mathrm{d}\ell}{z(\ell)}} \widehat{V}_{\mathrm{F}}^{(N)}(k_N;\ell_\omega) e_N[\vec{k};\widehat{v}_N(k_N;\ell_\omega)] \right\}, \tag{L.19}$$

where we have used the definitions in Eq. (4.41) and Eqs. (4.42) and (4.43) for the scale-dependent momentum and the rescaled coupling functions. Upon simplification of this expression, the two-point electronic function takes the form given in Eq. (4.58). In what follows we focus on the momentum-dependent rescaled slope and the universal functions $F_z^{(N)}(\vec{k};k_0)$ and $F_{V_{\mathrm{F}}}^{(N)}(\vec{k};k_0)$ defined in Eqs. (2.19) and (4.61), respectively. We defer the discussion regarding the momentum profile of the rescaled Yukawa coupling to Appendix O and its effect on the interaction vertex function to Appendix N.

Introducing the expressions for the counterterm functions in Eqs. (D.6) to (D.20), using the properties in Eq. (4.94) and the expression for the dynamical critical exponent in Eq. (3.45), the slope and universal functions take the form displayed in Eqs (4.95), (4.96) and (4.97), respectively. The latter can be integrated by first using the fact that, in the $\ell \gg 1$ and $\ell_0 \gg 1$ limits,

$$\begin{aligned} v(\ell)\log\left(\frac{1}{v(\ell)}\right) &= \frac{\pi^2 N_c N_f}{2(N_c^2-1)}\frac{1}{(\ell+\ell_0)}\left[1+\frac{1}{\log(\ell+\ell_0)}\right], \\ c(\ell) &= \frac{\pi}{4\sqrt{N_c^2-1}}\frac{1}{\sqrt{\ell+\ell_0}}, \end{aligned} \tag{L.20}$$

where the last expression is obtained by making use of Eq. (3.43) and ℓ_0 is given in Eq. (3.49). At this stage we note that, by setting $k_N = 0$ in Eq. (4.95) followed by a straightforward integration reproduces the result found in Chapters 2 and 3 for $\ell = \ell_\omega \gg 1$. Similarly, the zero momentum limits for of Eqs. (4.96) and (4.97) reduce to the analogous expressions found in Chapter 2.

As explained in Sec. 4.5, our results are controlled only in a window of length scales $\ell \ll \ell_{\mathrm{SC}}$, where ℓ_{SC} is the length scale above which the AFM quantum critical metal becomes unstable towards the development of superconducting order. In what follows we consider the two point function at scales $\ell_\omega \lessapprox \ell_{\mathrm{SC}}$, with ℓ_{SC} satisfying Eq. (4.90). With this at hand we note that, for nonzero momentum, Eqs. (4.95) to (4.97) can be tackled by making use of Eq. (4.101) and the integration identities

$$\int \frac{\mathrm{d}x}{x}\left[1+\frac{1}{\log(x)}\right] = \log\left[x\log(x)\right], \qquad \& \qquad \int \frac{\mathrm{d}x}{\sqrt{x}\log(x)} = \mathrm{Ei}\left[\frac{\log(x)}{2}\right]. \tag{L.21}$$

In doing so, we note that Eqs. (4.95) to (4.97) acquire the following form at length scales

$\ell_\omega \lessapprox \ell_{\rm SC}$

$$\widehat{v}_N(k_N;\ell_\omega) = v_0 \left\{ -\frac{1}{2}\sum_{j=1}^{2} \Theta(\ell_\omega - \ell_N^{(j)})\Theta(\ell_N^{(j)}) \log\left[\frac{(\ell_0+\ell_N^{(j)})\log(\ell_0+\ell_N^{(j)})}{\ell_0\log(\ell_0)}\right] \right. \\ \left. -\frac{1}{2}\sum_{j=1}^{N} \Theta(\ell_N^{(j)} - \ell_\omega) \log\left[\frac{(\ell_0+\ell_\omega)\log(\ell_0+\ell_\omega)}{\ell_0\log(\ell_0)}\right] \right\}, \tag{L.22}$$

$$F_z^{(N)}(k_N;k_0) = \exp\left\{ \sqrt{N_c^2-1}\Theta(\ell_\omega - \ell_N^{(1)})\Theta(\ell_N^{(1)}) \left[{\rm Ei}\left(\frac{\log(\ell_N^{(1)}+\ell_0)}{2}\right) - {\rm Ei}\left(\frac{\log(\ell_0)}{2}\right)\right] \right. \\ \left. +\sqrt{N_c^2-1}\Theta(\ell_N^{(1)} - \ell_\omega) \left[{\rm Ei}\left(\frac{\log(\ell_\omega+\ell_0)}{2}\right) - {\rm Ei}\left(\frac{\log(\ell_0)}{2}\right)\right]\right\}, \tag{L.23}$$

$$F_{V_{\rm F}}^{(N)}(k_N;k_0) = \exp\left\{ \frac{1}{2}\sum_{j=1}^{2} \frac{\Theta(\ell_\omega - \ell_N^{(j)})\Theta(\ell_N^{(j)})}{2^j} \log\left[\frac{(\ell_0+\ell_N^{(j)})\log(\ell_N^{(j)}+\ell_0)}{\ell_0\log(\ell_0)}\right] \right. \\ \left. +\frac{1}{2}\sum_{j=1}^{2} \frac{\Theta(\ell_N^{(j)} - \ell_\omega)}{2^j} \log\left[\frac{(\ell_0+\ell_\omega)\log(\ell_\omega+\ell_0)}{\ell_0\log(\ell_0)}\right] \right\}, \tag{L.24}$$

where the scales $\ell_N^{(1)}$ and $\ell_N^{(2)}$ satisfy Eqs. (4.99) and (4.100), respectively. These are given given by

$$\ell_N^{(1)}(k_N) = \log\left(\frac{\Lambda_f}{v_0 c_0 |k_N|}\right), \quad |k_N| \ll \frac{\Lambda_f}{v_0 c_0}, \tag{L.25}$$

$$\ell_N^{(2)}(k_N) = \log\left(\frac{\Lambda_f}{v_0 |k_N|}\right), \quad |k_N| \ll \frac{\Lambda_f}{v_0}. \tag{L.26}$$

These expressions follow from analyzing Eqs. (4.99) and (4.100) in the $\ell_0 \gg 1$ limit and in the limits in which, for $i = 1, 2$, $\ell_N^{(i)}(k_N) \gg \ell_0$ and $\ell_N^{(i)}(k_N) \ll \ell_0$. These are the limits in which Eqs. (4.99) and (4.100) admit an analytic solution and therefore we can only analytically capture the asymptotic crossover behaviors of the momentum-dependent functions in Eqs. (L.23) to (L.26). Despite this, these limits provide extended regions in the momentum space that we now proceed on considering.

L.2 Retarded Electronic Green's Function and Single-particle Spectral Function

We now compute explicitly Eqs. (L.22) to (L.24) in order to determine the retarded electronic Green's function and the single-particle spectral function. For this purpose we note that the two-point electronic function in Eq. (4.58) can be written as the piecewise continuous function

$$\Gamma_N^{(2,0)}(\vec{k};k_0) = \Theta(\ell_\omega - \ell_N^{(1)})\Gamma_{N;1}(\vec{k},k_0) + \Theta(\ell_\omega - \ell_N^{(2)})\Theta(\ell_N^{(1)} - \ell_\omega)\Gamma_{N;2}(\vec{k},k_0) \\ + \Theta(\ell_N^{(2)} - \ell_\omega)\Gamma_{N;3}(\vec{k},k_0), \tag{L.27}$$

where we have used the fact that $\ell_N^{(2)} \ll \ell_N^{(1)}$. Here,

$$\Gamma_{i;N}(\vec{k};k_0) = ik_0 f_z^{(N);i}(k_N,k_0) + f_{V_F}^{(N);i}(k_N,k_0) e_N\left[\vec{k};u_N^{(i)}(k_N,k_0)\right], \quad i=1,2,3, \tag{L.28}$$

where the functions $f_z^{(N);i}(k_N,k_0)$ are given by

$$f_z^{(N);1}(k_N,k_0) = \exp\left\{\sqrt{N_c^2-1}\Theta(\ell_N^{(1)})\left[\mathrm{Ei}\left(\frac{\log(\ell_N^{(1)}+\ell_0)}{2}\right) - \mathrm{Ei}\left(\frac{\log(\ell_0)}{2}\right)\right]\right\}, \tag{L.29}$$

$$f_z^{(N);j}(k_N,k_0) = \exp\left\{\sqrt{N_c^2-1}\left[\mathrm{Ei}\left(\frac{\log(\ell_\omega+\ell_0)}{2}\right) - \mathrm{Ei}\left(\frac{\log(\ell_0)}{2}\right)\right]\right\}, \tag{L.30}$$

where $j=2,3$. Similarly, the functions $f_{V_F}^{(N);i}(k_N,k_0)$ are given by

$$f_{V_F}^{(N);1}(k_N,k_0) = \exp\left\{\frac{1}{2}\sum_{j=1}^{2}\frac{\Theta(\ell_N^{(j)})}{2^j}\log\left[\frac{(\ell_0+\ell_N^{(j)})\log(\ell_N^{(j)}+\ell_0)}{\ell_0\log(\ell_0)}\right]\right\}, \tag{L.31}$$

$$\begin{aligned} f_{V_F}^{(N);2}(k_N,k_0) = \exp\Bigg\{&\frac{1}{8}\Theta(\ell_N^{(2)})\log\left[\frac{(\ell_0+\ell_N^{(2)})\log(\ell_N^{(2)}+\ell_0)}{\ell_0\log(\ell_0)}\right] \\ &+\frac{1}{4}\log\left[\frac{(\ell_0+\ell_\omega)\log(\ell_\omega+\ell_0)}{\ell_0\log(\ell_0)}\right]\Bigg\}, \end{aligned} \tag{L.32}$$

$$f_{V_F}^{(N);3}(k_N,k_0) = \exp\left\{\frac{1}{2}\sum_{j=1}^{2}\frac{1}{2^j}\log\left[\frac{(\ell_0+\ell_\omega)\log(\ell_\omega+\ell_0)}{\ell_0\log(\ell_0)}\right]\right\}. \tag{L.33}$$

Finally, the slope of the FS is encoded in the functions:

$$u_N^{(1)}(k_N,k_0) = v_0\exp\left\{-\frac{1}{2}\sum_{j=1}^{2}\Theta(\ell_N^{(j)})\log\left[\frac{(\ell_0+\ell_N^{(j)})\log(\ell_N^{(j)}+\ell_0)}{\ell_0\log(\ell_0)}\right]\right\}, \tag{L.34}$$

$$\begin{aligned} u_N^{(2)}(k_N,k_0) = v_0\exp\Bigg\{&-\frac{1}{2}\Theta(\ell_N^{(2)})\log\left[\frac{(\ell_0+\ell_N^{(2)})\log(\ell_N^{(2)}+\ell_0)}{\ell_0\log(\ell_0)}\right] \\ &-\frac{1}{2}\log\left[\frac{(\ell_0+\ell_\omega)\log(\ell_\omega+\ell_0)}{\ell_0\log(\ell_0)}\right]\Bigg\}, \end{aligned} \tag{L.35}$$

$$u_N^{(3)}(k_N,k_0) = v_0\exp\left\{-\log\left[\frac{(\ell_0+\ell_\omega)\log(\ell_\omega+\ell_0)}{\ell_0\log(\ell_0)}\right]\right\} = \frac{v_0\ell_0\log(\ell_0)}{(\ell_\omega+\ell_0)\log(\ell_\omega+\ell_0)}. \tag{L.36}$$

The two-point function in Eq. (L.28) displays different crossovers as a function of Matsubara frequency that will carry on into the retarded Green's function and therefore into the single-particle spectral function. To analytically continue Eq. (L.28) to the real frequency domain we first note that we can write the Heaviside distributions displaying the crossovers as a function of Matsubara frequency in the following form:

$$\Theta(\ell_\omega - \ell_N^{(j)}) = \Theta\left(\Lambda_f e^{-\ell_N^{(j)}} - k_0\right), \tag{L.37}$$

$$\Theta(\ell_N^{(j)} - \ell_\omega) = \Theta\left(k_0 - \Lambda_f e^{-\ell_N^{(j)}}\right). \tag{L.38}$$

Eq. (L.28) is a piecewise continuous function of frequency. Therefore, under analytic continuation to real frequency $-ik_0 \to \omega + i0^+$ the Heaviside functions, which simply determine the domain in which each $\mathit{\Gamma}_{j;N}(\vec{k}, k_0)$ in Eq. (L.27) give a contribution, can be analytically continued as

$$\Theta\left(\Lambda_f e^{-\ell_N(j)} - k_0\right) \overset{-ik_0\to\omega+i0^+}{\longrightarrow} \Theta\left(\Lambda_f e^{-\ell_N^{(j)}} - \omega\right), \tag{L.39}$$

$$\Theta\left(k_0 - \Lambda_f e^{-\ell_N^{(j)}}\right) \overset{-ik_0\to\omega+i0^+}{\longrightarrow} \Theta\left(\omega - \Lambda_f e^{-\ell_N^{(j)}}\right). \tag{L.40}$$

Therefore, defining the retarded two-point crossover functions as $\mathit{\Gamma}^{\mathrm{R}}_{N;j}(\vec{k}, \omega) = \mathit{\Gamma}_{N;j}(\vec{k}, i\omega - 0^+)$ and their corresponding crossover retarded Green's functions $\mathsf{G}^{\mathrm{R}}_{N;j}(\vec{k}, \omega) \equiv \mathit{\Gamma}^{\mathrm{R}}_{N;j}(\vec{k}, \omega)^{-1}$, we can write the retarded Green's function for the electrons as

$$\begin{aligned} G^{\mathrm{R}}_N(\vec{k}, \omega) = \Theta\left(\Lambda_f e^{-\ell_N^{(1)}} - \omega\right) \mathsf{G}^{\mathrm{R}}_{1;N}(\vec{k}, \omega) + \Theta\left(\omega - \Lambda_f e^{-\ell_N^{(2)}}\right) \mathsf{G}^{\mathrm{R}}_{3;N}(\vec{k}, \omega) \\ + \Theta\left(\Lambda_f e^{-\ell_N^{(2)}} - \omega\right) \Theta\left(\omega - \Lambda_f e^{-\ell_N^{(1)}}\right) \mathsf{G}^{\mathrm{R}}_{2;N}(\vec{k}, \omega). \end{aligned} \tag{L.41}$$

Taking the imaginary part of the retarded Green's function we obtain the spectral function:

$$\begin{aligned} \mathcal{A}_N(\vec{k}, \omega) = \Theta\left(\Lambda_f e^{-\ell_N^{(1)}} - \omega\right) \mathcal{A}_{1;N}(\vec{k}, \omega) + \Theta\left(\omega - \Lambda_f e^{-\ell_N^{(2)}}\right) \mathcal{A}_{3;N}(\vec{k}, \omega) \\ + \Theta\left(\Lambda_f e^{-\ell_N^{(2)}} - \omega\right) \Theta\left(\omega - \Lambda_f e^{-\ell_N^{(1)}}\right) \mathcal{A}_{2;N}(\vec{k}, \omega), \end{aligned} \tag{L.42}$$

where

$$\mathcal{A}_{1;N}(\vec{k}, \omega) = \frac{1}{f_z^{(N);1}(k_N, 0)} \delta\left(\omega - \frac{f_{V_{\mathrm{F}}}^{(N);1}(k_N, 0)}{f_z^{(N);1}(k_N, 0)} e_N[\vec{k}; u_N^{(1)}(k_N, 0)]\right), \tag{L.43}$$

$$\mathcal{A}_{i;N}(\vec{k}\omega) = -\frac{2\mathrm{Im}\left[\mathit{\Gamma}^{\mathrm{R}}_{i;N}(\vec{k}, \omega)\right]}{\mathrm{Re}\left[\mathit{\Gamma}^{\mathrm{R}}_{i;N}(\vec{k}, \omega)\right]^2 + \mathrm{Im}\left[\mathit{\Gamma}^{\mathrm{R}}_{i;N}(\vec{k}, \omega)\right]^2}, \qquad i = 2, 3, \tag{L.44}$$

with

$$\begin{aligned} \mathrm{Re}\left[\mathit{\Gamma}^{\mathrm{R}}_{i;N}(\vec{k}, \omega)\right] = -\omega \mathrm{Re}\left[f^{(N);i}_{z;\mathrm{R}}(k_N, \omega)\right] + \mathrm{Re}\left[f^{(N);i}_{V_{\mathrm{F}};\mathrm{R}}(k_N, \omega)\right] \mathrm{Re}\left(e_N[\vec{k}; u^{(i)}_{N;\mathrm{R}}(k_N, \omega)]\right) \\ + \mathrm{Im}\left[f^{(N);i}_{V_{\mathrm{F}};\mathrm{R}}(k_N, \omega)\right] \mathrm{Im}\left(e_N[\vec{k}; u^{(i)}_{N;\mathrm{R}}(k_N, \omega)]\right), \end{aligned} \tag{L.45}$$

$$\begin{aligned} \mathrm{Im}\left[\mathit{\Gamma}^{\mathrm{R}}_{i;N}(\vec{k}, \omega)\right] = -\omega \mathrm{Im}\left[f^{(N);i}_{z;\mathrm{R}}(k_N, \omega)\right] + \mathrm{Re}\left[f^{(N);i}_{V_{\mathrm{F}};\mathrm{R}}(k_N, \omega)\right] \mathrm{Im}\left(e_N[\vec{k}; u^{(i)}_{N;\mathrm{R}}(k_N, \omega)]\right) \\ + \mathrm{Im}\left[f^{(N);i}_{V_{\mathrm{F}};\mathrm{R}}(k_N, \omega)\right] \mathrm{Re}\left(e_N[\vec{k}; u^{(i)}_{N;\mathrm{R}}(k_N, \omega)]\right). \end{aligned} \tag{L.46}$$

Here we have used the definitions for the retarded functions $f^{(N);i}_{z;\mathrm{R}}(k_N, \omega) \equiv f^{(N);i}_z(k_N, i\omega - 0^+)$, $f^{(N);i}_{V_{\mathrm{F}};\mathrm{R}}(k_N, \omega) \equiv f^{(N);i}_{V_{\mathrm{F}}}(k_N, i\omega - 0^+)$ and $u^{(i)}_{N;\mathrm{R}}(k_N, \omega) \equiv u^{(i)}_N(k_N, i\omega - 0^+)$. In deriving the spectral functions we used the fact that $f^{(N);1}_{z;\mathrm{R}}(k_N, \omega) = f^{(N);1}_{z;\mathrm{R}}(k_N, 0)$, $f^{(N);1}_{V_{\mathrm{F}};\mathrm{R}}(k_N, \omega) = f^{(N);1}_{V_{\mathrm{F}};\mathrm{R}}(k_N, 0)$ and $u^{(1)}_{N;\mathrm{R}}(k_N, \omega) = u^{(1)}_{N;\mathrm{R}}(k_N, 0)$ are purely real. We proceed on analyzing the electronic spectral function in the ideal scenario where there is no superconducting instability. After this we consider the effects of the imminent superconducting instability of the state.

L.3 Electronic Spectral Function in the Absence of Superconducting Instabilities

Here we fill the details that lead to the shape of the renormalized FS displayed in Eq. (4.115) and the momentum dependence of the quasiparticle weight and the renormalized Fermi velocity along this one-dimensional zero-energy manifold in the ideal scenario where the system doesn't undergo a superconducting transition. In this case we take a look at the spectral function in Eq. (L.42) in the zero frequency limit. In this limit, the spectral function takes the form

$$\mathcal{A}_N(\vec{k},\omega)=\frac{1}{f^{(N);1}_{z;\mathrm{R}}(k_N,0)}\delta\left(\omega-\frac{f^{(N);1}_{V_\mathrm{F};\mathrm{R}}(k_N,0)}{f^{(N);1}_{z;\mathrm{R}}(k_N,0)}e_N[\vec{k};u^{(1)}_{N;\mathrm{R}}(k_N,0)]\right), \tag{L.47}$$

where the quasiparticle weight and renormalized Fermi velocity are given by

$$\mathcal{Z}_N(k_N)\equiv\frac{1}{f^{(N);1}_{z;\mathrm{R}}(k_N,0)}, \tag{L.48}$$

$$\mathfrak{V}^{(N)}_\mathrm{F}(k_N)\equiv\frac{f^{(N);1}_{V_\mathrm{F};\mathrm{R}}(k_N,0)}{f^{(N);1}_{z;\mathrm{R}}(k_N,0)}\approx\frac{1}{f^{(N);1}_{z;\mathrm{R}}(k_N,0)}, \tag{L.49}$$

respectively. The last expression follows from the fact that, in the small v_0 limit, the contribution from Eq. (L.29) dominates over that in Eq. (L.31) as it can be seen from the fact that, in the small v limit, the contribution from the counterterm function $Z^{(1)}_N(k_N)$ in Eq. (4.60) dominates over the contribution from $Z^{(3)}_N(k_N)$ in Eq. (4.61). In the zero frequency limit, Eq. (L.47) has a singularity at the renormalized FS:

$$e_N[\vec{k},u^{(1)}_{N;\mathrm{R}}(k_N,0)]=0, \tag{L.50}$$

with $u^{(1)}_N(k_N)$ given in Eq. (L.34). We proceed by analyzing the momentum profile of the renormalized FS and then we consider the profile for the quasiparticle weight and renormalized Fermi velocity in Eqs. (L.48) and (L.49), respectively.

L.3-(*a*) Renormalized FS

For simplicity we restrict the discussion to the $N=1$ hot spot, for which the renormalized FS in Eq. (L.50) is given by:

$$k_y=-u^{(1)}_1(k_x)k_x, \tag{L.51}$$

where $u^{(1)}_1(k_x)$ is given by Eq. (L.34):

$$u^{(1)}_1(k_x)=v_0\exp\left\{-\frac{1}{2}\sum_{j=1}^{2}\Theta(\ell^{(j)}_1)\log\left[\frac{(\ell_0+\ell^{(j)}_1)\log(\ell^{(j)}_1+\ell_0)}{\ell_0\log(\ell_0)}\right]\right\}. \tag{L.52}$$

Here, the length scales $\ell_1^{(1)} \equiv \ell_1^{(1)}(k_x)$ and $\ell_1^{(2)} \equiv \ell_2^{(1)}(k_x)$ are given by Eqs. (L.25) and (L.26) for $N = 1$, and ℓ_0 is defined in Eq. (4.77).

We analyze Eq. (L.51) the the momentum regimes: (*i*) $\frac{\Lambda_f}{v_0 c_0} \ll |k_x| \ll \overline{k}_{\rm F}$, (*ii*) $\frac{\Lambda_f}{v_0} \ll |k_x| \ll \frac{\Lambda_f}{v_0 c_0}$, (*iii*) $\frac{\Lambda_f}{v_0 c_0} e^{-\ell_0} \ll |k_x| \ll \frac{\Lambda_f}{c_0}$, (*iv*) $\frac{\Lambda_f}{v_0} e^{-\ell_0} \ll |k_x| \ll \frac{\Lambda_f}{v_0 c_0} e^{-\ell_0}$, and (*v*) $|k_x| \ll \frac{\Lambda_f}{v_0} e^{-\ell_0}$. We note that he momentum range $|k_x| \gg \overline{k}_{\rm F}$, with $\overline{k}_{\rm F}$ give in Eq. (4.62), is out of the scope of our computation as explained in Sec. 4.4-(*a*) .

(*i*) For $\frac{\Lambda_f}{v_0 c_0} \ll |k_x| \ll \overline{k}_{\rm F}$, the electrons are completely decoupled from the spin fluctuations as evidenced by the fact that both scales in Eq. (L.25) and (L.26) become negative. Therefore, in this regime th e renormalized FS is the same as the bare one:

$$k_y = -v_0 k_x. \tag{L.53}$$

(*ii*) For $\frac{\Lambda_f}{v_0} \ll |k_x| \ll \frac{\Lambda_f}{v_0 c_0}$ only the length scale in Eq. (L.26) is negative. As a consequence, only the term depending on the length scale in $\ell_1^{(1)}(k_x)$ is responsible for introducing a momentum dependence in the rescaled slope. Eq. (L.52) therefore takes the form

$$k_y = -v_0 \exp\left(-\frac{1}{2}\log\left[\frac{[\ell_0 + \ell_1^{(1)}(k_x)]\log[\ell_1^{(1)}(k_x) + \ell_0]}{\ell_0 \log(\ell_0)}\right]\right) k_x. \tag{L.54}$$

In this momentum regime, $\ell_1^{(1)}(k_x) \ll \ell_0$, and to leading order in $\ell_1^{(1)}(k_x)/\ell_0 \ll 1$, the renormalized FS reads

$$k_y = -v_0 \left(\frac{v_0 c_0 |k_x|}{\Lambda_f}\right)^{\frac{(N_c^2-1)}{\pi^2 N_c N_f} v_0 \log(1/v_0)} k_x. \tag{L.55}$$

(*iii*) For $\frac{\Lambda_f}{v_0 c_0} e^{-\ell_0} \ll |k_x| \ll \frac{\Lambda_f}{v_0}$ both length scales in Eqs. (L.25) and (L.26) are positive. This, in combination with Eq. (L.51), yields in this regime

$$k_y = -v_0 \exp\left(-\frac{1}{2}\sum_{i=1}^{2}\log\left[\frac{[\ell_0 + \ell_1^{(i)}(k_x)]\log[\ell_1^{(i)}(k_x) + \ell_0]}{\ell_0 \log(\ell_0)}\right]\right) k_x. \tag{L.56}$$

In this regime the he length scales satisfy $\ell_1^{(1)}(k_x) \ll \ell_0$ and $\ell_1^{(2)}(k_x) \ll \ell_0$. Hence, to leading order in $\ell_1^{(1)}(k_x)/\ell_0 \ll 1$ and $\ell_1^{(2)}(k_x)/\ell_0 \ll 1$, Eq. (L.56) takes the following form

$$k_y = -v_0 \left(\frac{v_0 \sqrt{c_0} |k_x|}{\Lambda_f}\right)^{\frac{2(N_c^2-1)}{\pi^2 N_c N_f} v_0 \log(1/v_0)} k_x. \tag{L.57}$$

(*iv*) For $\frac{\Lambda_f}{v_0} e^{-\ell_0} \ll |k_x| \ll \frac{\Lambda_f}{v_0 c_0} e^{-\ell_0}$, the length scales satisfy $\ell_1^{(1)}(k_x) \gg \ell_0$ while $\ell_1^{(2)}(k_x) \ll \ell_0$. Hence, expanding Eq. (L.56) to leading order in $\ell_1^{(1)}(k_x)/\ell_0 \gg 1$ and $\ell_1^{(2)}(k_x)/\ell_0 \ll 1$ yields

$$k_y = -v_0 \left(\frac{v_0 |k_x|}{\Lambda_f}\right)^{\frac{(N_c^2-1)}{\pi^2 N_c N_f} v_0 \log(1/v_0)} \sqrt{\frac{\ell_0 \log(\ell_0)}{\ell_x^{(1)} \log(\ell_x^{(1)})}} k_x, \tag{L.58}$$

where $\ell_x^{(1)} = \log(\Lambda_f/v_0 c_0|k_x|)$. We note that in this momentum region, we can further approximate $\log(\Lambda_f/c_0 v_0|k_x|) \approx \log(\Lambda_f/|k_x|)$ to leading order in the momentum.

(*v*) For $|k_x| \ll \frac{\Lambda_f}{v_0} e^{-\ell_0}$ both length scales satisfy $\ell_1^{(1)}(k_x) \gg \ell_0$ and $\ell_1^{(2)}(k_x) \gg \ell_0$. Consequently, Eq. (L.56) is given, to leading order in $\ell_1^{(1)}(k_x)/\ell_0 \gg 1$ and $\ell_1^{(2)}(k_x)/\ell_0 \gg 1$, by

$$k_y = -v_0 \sqrt{\frac{\ell_0 \log(\ell_0)}{\ell_x^{(1)} \log(\ell_x^{(1)})}} \sqrt{\frac{\ell_0 \log(\ell_0)}{\ell_x^{(2)} \log(\ell_x^{(2)})}} k_x, \tag{L.59}$$

where $\ell_x^{(2)} = \log(\Lambda_f/v_0|k_x|)$. In this momentum region we can further approximate the logarithms as $\log(\Lambda_f/c_0 v_0|k_x|) \approx \log(\mu/|k_x|)$ and $\log(\Lambda_f/v_0|k_x|) \approx \log(\mu/|k_x|)$.

Collecting these results we obtain the expression displayed in Eq. (4.115).

L.3-(*b*) Quasiparticle Weight and Renormalized Fermi Velocity

We turn our attention to the computation of the momentum profile acquired by the quasiparticle weight and renormalized Fermi velocity given in Eqs. (L.48) and (L.49), respectively, for $N = 1$. These two quantities are given, according to Eq. (L.29), by

$$\mathcal{Z}_1(k_x) = \mathfrak{V}_{\mathrm{F}}^{(1)}(k_x) = \exp\left\{ -\sqrt{N_c^2 - 1}\,\Theta(\ell_N^{(1)}) \left[\mathrm{Ei}\left(\frac{\log(\ell_N^{(1)} + \ell_0)}{2} \right) - \mathrm{Ei}\left(\frac{\log(\ell_0)}{2} \right) \right] \right\}. \tag{L.60}$$

Here, $\ell_1^{(1)} = \ell_1^{(1)}(k_x)$ is given in Eq. (L.25) and depending on its magnitude with respect to ℓ_0, the quasiparticle weight and Fermi velocity display different momentum profiles. In the region in which $\frac{\Lambda_f}{v_0 c_0} \ll |k_x| \ll \overline{k}_{\mathrm{F}}$, $\ell_1^{(1)}(k_x) < 0$ and therefore the exponent in Eq. (L.60) vanishes yielding a unit quasiparticle weight and Fermi velocity. For momenta such that $\frac{\Lambda_f}{v_0 c_0} e^{-\ell_0} \ll |k_x| \ll \frac{\Lambda_f}{v_0 c_0}$, $\ell_1^{(1)}(k_x) \ll \ell_0$ and using the expansion for the exponential integral function, $\mathrm{Ei}(x) = e^x \left[\frac{1}{x} + \mathcal{O}\left(\frac{1}{x^2} \right) \right]$ for $x \gg 1$, we write Eq. (L.60) as

$$\mathcal{Z}_1(k_x) = \mathfrak{V}_{\mathrm{F}}^{(1)}(k_x) = \left(\frac{v_0 c_0 |k_x|}{\Lambda_f} \right)^{\frac{\sqrt{2}(N_c^2 - 1)}{\pi \sqrt{N_c N_f}} \sqrt{\frac{v_0}{\log(1/v_0)}}}, \tag{L.61}$$

in the small v_0 limit. Finally, in the regime in which $|k_x| \ll \frac{\Lambda_f}{v_0 c_0} e^{-\ell_0}$, $\ell_1^{(1)}(k_x) \gg \ell_0$ and an expansion of Eq. (L.60) yields the superlogarithmic contribution

$$\mathcal{Z}_1(k_x) = \mathfrak{V}_{\mathrm{F}}^{(1)}(k_x) = \exp\left(-\frac{2\sqrt{N_c^2 - 1} \sqrt{\log\left(\frac{\Lambda_f}{|k_x|} \right)}}{\log\log\left(\frac{\Lambda_f}{|k_x|} \right)} \right). \tag{L.62}$$

Collecting these results we obtain the expression displayed in Eq. (4.116).

L.4 Electronic Spectral Function in the Presence of Superconducting Instabilities

We now consider how the results in the previous section get modified once we consider the imminent superconducting instability of the metallic state. As described in Sec. 4.5, the superconducting instability develops at length scales above $\ell_{\rm SC}$, where the latter satisfies Eq. (4.90). In particular, we note that $\ell_{\rm SC} \ll \ell_0$ and the flow of v can be ignored in the discussion that follows. We consider the spectral function given in Eq. (L.42) at low nonzero frequencies $\omega \gtrsim \omega_{\rm SC} \sim \Lambda_f e^{-\ell_{\rm SC}}$:

$$\begin{aligned}\mathcal{A}_N(\vec{k},\omega) = \Theta\left(\Lambda_f e^{-\ell_N^{(1)}} - \omega\right)\mathcal{A}_{1;N}(\vec{k},\omega) + \Theta\left(\omega - \Lambda_f e^{-\ell_N^{(2)}}\right)\mathcal{A}_{3;N}(\vec{k},\omega) \\ + \Theta\left(\Lambda_f e^{-\ell_N^{(2)}} - \omega\right)\Theta\left(\omega - \Lambda_f e^{-\ell_N^{(1)}}\right)\mathcal{A}_{2;N}(\vec{k},\omega),\end{aligned} \tag{L.63}$$

where $\mathcal{A}_{i;N}(\vec{k},\omega)$ with $i = 2,3$ are given in Eq. (L.44) and for $i = 1$, we have

$$\mathcal{A}_{1;N}(\vec{k},\omega) = \frac{1}{f_{z;\mathrm{R}}^{(N);1}(k_N,0)}\delta\left(\omega - \frac{f_{V_\mathrm{F};\mathrm{R}}^{(N);1}(k_N,0)}{f_{z;\mathrm{R}}^{(N);1}(k_N,0)} e_N[\vec{k}; u_{N;\mathrm{R}}^{(1)}(k_N,0)]\right). \tag{L.64}$$

Let us focus on each term separately for $N = 1$. The spectral function at all other hot spots can be recovered from this one through a C_4 transformation.

(i) $\mathcal{A}_{1;1}(\vec{k},\omega)$: For momenta $|k_x| \gg \frac{\Lambda_f}{v_0 c_0} e^{-\ell_{\rm SC}} = \frac{\omega_{\rm SC}}{v_0 c_0}$ the spectral function in Eq. (L.64) takes the form

$$\mathcal{A}_{1;N}(\vec{k};\omega) = \mathcal{Z}_1(k_x)\delta\left(\omega - \mathfrak{V}_{\mathrm{F}}^{(1)}(k_x)\left[u_1^{(1)}(k_x)k_x + k_y\right]\right). \tag{L.65}$$

This spectral function shows a response of quasiparticles that are on the constant energy manifold defined by $\omega = \mathfrak{V}_{\mathrm{F}}^{(1)}(k_x)\left[u_1^{(1)}(k_x)k_x + k_y\right]$. In this region of the momentum space, the quasiparticle weight and Fermi velocity are effectively given by Eq. (L.61). Following the same steps outlined in Sec. L.3-(a) it follows that, in this momentum regime, the momentum-dependent slope takes the form

$$u_1(k_x) = v_0\begin{cases} 1 & \frac{\Lambda_f}{v_0 c_0} \ll |k_x| \ll \overline{k}_{\mathrm{F}}, \\ \left(\frac{v_0 c_0 |k_x|}{\Lambda_f}\right)^{\frac{(N_c^2-1)}{\pi^2 N_c N_f} v_0 \log(1/v_0)} & \frac{\Lambda_f}{v_0} \ll |k_x| \ll \frac{\Lambda_f}{v_0 c_0}, \\ \left(\frac{v_0\sqrt{c_0}|k_x|}{\Lambda_f}\right)^{\frac{2(N_c^2-1)}{\pi^2 N_c N_f} v_0 \log(1/v_0)} & \frac{\Lambda_f}{v_0 c_0} e^{-\ell_{\rm SC}} \ll |k_x| \ll \frac{\Lambda_f}{v_0}. \end{cases} \tag{L.66}$$

(ii) $\mathcal{A}_{2;1}(\vec{k},\omega)$: For momenta $\frac{\Lambda_f}{v_0} e^{-\ell_{\rm SC}} \ll |k_x| \ll \frac{\Lambda_f}{v_0 c_0} e^{-\ell_{\rm SC}}$ the spectral function takes the form

$$\mathcal{A}_{2;1}(\vec{k},\omega) = -\frac{2\mathrm{Im}\left[\mathit{\Gamma}_{2;1}^{\mathrm{R}}(\vec{k},\omega)\right]}{\mathrm{Re}\left[\mathit{\Gamma}_{2;1}^{\mathrm{R}}(\vec{k},\omega)\right]^2 + \mathrm{Im}\left[\mathit{\Gamma}_{2;1}^{\mathrm{R}}(\vec{k},\omega)\right]^2}, \tag{L.67}$$

where the real and imaginary parts of the retarded two-point function in this momentum regime are given in Eqs. (L.45) and (L.46), respectively. These are characterized by the functions in Eqs. (L.30), (L.32), and (L.35). Since $\ell_\omega \lessapprox \ell_{\rm SC} \ll \ell_0$, to leading order in $\ell_\omega/\ell_0 \ll 1$, we have

$$f_z^{(1);2}(k_x,k_0) = \exp\left(\frac{\sqrt{N_c^2-1}}{\sqrt{\ell_0}\log(\ell_0)}\ell_\omega\right), \tag{L.68}$$

$$f_{V_{\rm F}}^{(1);2}(k_x,k_0) = h_1(k_x)^{-1}\exp\left(\frac{\ell_\omega}{4\ell_0}\right), \tag{L.69}$$

$$u_1^{(2)}(k_x,k_0) = v_0 h_1(k_x)^4\exp\left(-\frac{\ell_\omega}{2\ell_0}\right), \tag{L.70}$$

where

$$h_1(k_x) = \exp\left(-\frac{1}{8}\Theta(\ell_N^{(2)})\log\left[\frac{(\ell_0+\ell_N^{(2)})\log(\ell_N^{(2)}+\ell_0)}{\ell_0\log(\ell_0)}\right]\right) = \exp\left(-\frac{\ell_1^{(2)}(k_x)}{8\ell_0}\right), \tag{L.71}$$

where the last follows from the leading order expansion in $\ell_1^{(2)}(k_x)/\ell_0 \ll 1$. We further note that in the regime of momentum we are considering, $\ell_1^{(2)}(k_x) \ll \ell_\omega$ and as a consequence, the momentum dependence is subleading and Eqs. (L.69) and (L.70) essentially become momentum independent. However, we keep the leading order contribution in momentum for completeness.

After analytic continuation to real frequency, the real and imaginary parts of these expressions at frequencies $\omega \gtrapprox \omega_{\rm SC}$ take the form

$$\mathrm{Re}[f_{z;\mathrm{R}}^{(1);2}(k_x,\omega)] = \left(\frac{\Lambda_f}{\omega}\right)^{\frac{\sqrt{N_c^2-1}}{\sqrt{\ell_0}\log(\ell_0)}}, \tag{L.72}$$

$$\mathrm{Im}[f_{z;\mathrm{R}}^{(1);2}(k_x,\omega)] = -\frac{\pi}{2}\frac{\sqrt{N_c^2-1}}{\sqrt{\ell_0}\log(\ell_0)}\left(\frac{\Lambda_f}{\omega}\right)^{\frac{\sqrt{N_c^2-1}}{\sqrt{\ell_0}\log(\ell_0)}}, \tag{L.73}$$

$$\mathrm{Re}[f_{V_{\rm F};\mathrm{R}}^{(1);2}(k_x,\omega)] = \left(\frac{v_0|k_x|}{\Lambda_f}\right)^{-\frac{1}{8\ell_0}}\left(\frac{\omega}{\Lambda_f}\right)^{-\frac{1}{4\ell_0}}, \tag{L.74}$$

$$\mathrm{Im}[f_{V_{\rm F};\mathrm{R}}^{(1);2}(k_x,\omega)] = -\frac{\pi}{8\ell_0}\left(\frac{v_0|k_x|}{\Lambda_f}\right)^{-\frac{1}{8\ell_0}}\left(\frac{\omega}{\Lambda_f}\right)^{-\frac{1}{4\ell_0}}, \tag{L.75}$$

$$\mathrm{Re}\left[u_{1;\mathrm{R}}^{(2)}(k_x,\omega)\right] = v_0\left(\frac{v_0|k_x|}{\Lambda_f}\right)^{\frac{1}{2\ell_0}}\left(\frac{\omega}{\Lambda_f}\right)^{\frac{1}{2\ell_0}}, \tag{L.76}$$

$$\mathrm{Im}\left[u_{1;\mathrm{R}}^{(2)}(k_x,\omega)\right] = \frac{\pi}{4\ell_0}v_0\left(\frac{v_0|k_x|}{\Lambda_f}\right)^{\frac{1}{2\ell_0}}\left(\frac{\omega}{\Lambda_f}\right)^{\frac{1}{2\ell_0}}. \tag{L.77}$$

With this at hand, the real and imaginary parts of the retarded two-point electronic

function defined in Eqs. (L.45) and (L.46) take the form

$$\begin{aligned}
\mathrm{Re}\left[\Gamma^{\mathrm{R}}_{2;1}(\vec{k},\omega)\right] &= -\omega\left(\frac{\Lambda_f}{\omega}\right)^{\frac{\sqrt{N_c^2-1}}{\sqrt{\ell_0}\log(\ell_0)}} \\
&+ \left(\frac{v_0|k_x|}{\Lambda_f}\right)^{-\frac{1}{8\ell_0}}\left(\frac{\omega}{\Lambda_f}\right)^{-\frac{1}{4\ell_0}}\left\{v_0\left(\frac{v_0|k_x|}{\Lambda_f}\right)^{\frac{1}{2\ell_0}}\left(\frac{\omega}{\Lambda_f}\right)^{\frac{1}{2\ell_0}}k_x + k_y\right\} \\
&- \frac{\pi^2 v_0}{32\ell_0^2}\left(\frac{v_0|k_x|}{\Lambda_f}\right)^{\frac{3}{8\ell_0}}\left(\frac{\omega}{\Lambda_f}\right)^{\frac{1}{4\ell_0}}k_x,
\end{aligned} \tag{L.78}$$

$$\begin{aligned}
\mathrm{Im}\left[\Gamma^{\mathrm{R}}_{2;1}(\vec{k},\omega)\right] &= \frac{\pi}{2}\frac{\sqrt{N_c^2-1}}{\sqrt{\ell_0}\log(\ell_0)}\omega\left(\frac{\Lambda_f}{\omega}\right)^{\frac{\sqrt{N_c^2-1}}{\sqrt{\ell_0}\log(\ell_0)}} \\
&+ v_0 k_x\frac{\pi}{4\ell_0}\left(\frac{v_0|k_x|}{\Lambda_f}\right)^{\frac{3}{8\ell_0}}\left(\frac{\omega}{\Lambda_f}\right)^{\frac{1}{4\ell_0}} \\
&- \frac{\pi}{8\ell_0}\left(\frac{v_0|k_x|}{\Lambda_f}\right)^{-\frac{1}{8\ell_0}}\left(\frac{\omega}{\Lambda_f}\right)^{-\frac{1}{4\ell_0}}\left\{v_0\left(\frac{v_0|k_x|}{\Lambda_f}\right)^{\frac{1}{2\ell_0}}\left(\frac{\omega}{\Lambda_f}\right)^{\frac{1}{2\ell_0}}k_x + k_y\right\}.
\end{aligned} \tag{L.79}$$

For $\ell_0 \gg 1$, we can further approximate the real part of the retarded two-point function to leading order by:

$$\begin{aligned}
\mathrm{Re}\left[\Gamma^{\mathrm{R}}_{2;1}(\vec{k},\omega)\right] &\approx -\omega\left(\frac{\Lambda_f}{\omega}\right)^{\frac{\sqrt{N_c^2-1}}{\sqrt{\ell_0}\log(\ell_0)}} \\
&+ \left(\frac{v_0|k_x|}{\Lambda_f}\right)^{-\frac{1}{8\ell_0}}\left(\frac{\omega}{\Lambda_f}\right)^{-\frac{1}{4\ell_0}}\left\{v_0\left(\frac{v_0|k_x|}{\Lambda_f}\right)^{\frac{1}{2\ell_0}}\left(\frac{\omega}{\Lambda_f}\right)^{\frac{1}{2\ell_0}}k_x + k_y\right\}.
\end{aligned} \tag{L.80}$$

Compared to the real part, the imaginary part is suppressed algebraically in $\ell_0 \gg 1$. Therefore, in the $\omega \ll \Lambda_f$ and $\ell_0 \gg 1$ limit, we see from Eq. (L.67) that the spectral function is peaked at frequencies $\omega \approx \omega(\vec{k})$ that satisfy

$$\begin{aligned}
&\omega(\vec{k})\left(\frac{\Lambda_f}{\omega(\vec{k})}\right)^{\frac{\sqrt{N_c^2-1}}{\sqrt{\ell_0}\log(\ell_0)}} = \\
&\left(\frac{v_0|k_x|}{\Lambda_f}\right)^{-\frac{1}{8\ell_0}}\left(\frac{\omega(\vec{k})}{\Lambda_f}\right)^{-\frac{1}{4\ell_0}}\left\{v_0\left(\frac{v_0|k_x|}{\Lambda_f}\right)^{\frac{1}{2\ell_0}}\left(\frac{\omega(\vec{k})}{\Lambda_f}\right)^{\frac{1}{2\ell_0}}k_x + k_y\right\}.
\end{aligned} \tag{L.81}$$

Since $\ell_{\mathrm{SC}} \ll \ell_0$, this expression is solved, in this limit, by

$$\omega(\vec{k}) \approx \left(\frac{v_0|k_x|}{\Lambda_f}\right)^{-\frac{1}{8\ell_0}}\left\{v_0\left(\frac{v_0|k_x|}{\Lambda_f}\right)^{\frac{1}{2\ell_0}}k_x + k_y\right\}, \tag{L.82}$$

which is nothing else than the expression for the renormalized energy levels of the electrons. At these frequencies, the imaginary part of the retarded two-point function in Eq. (L.79) is given, to leading order in $\ell_0 \gg 1$, by

$$\mathrm{Im}\left[\Gamma^{\mathrm{R}}_{2;1}(\vec{k},\omega)\right] \approx \frac{\pi}{2}\frac{\sqrt{N_c^2-1}}{\sqrt{\ell_0}\log(\ell_0)}\omega(\vec{k})\left(\frac{\Lambda_f}{\omega(\vec{k})}\right)^{\frac{\sqrt{N_c^2-1}}{\sqrt{\ell_0}\log(\ell_0)}}. \tag{L.83}$$

Close to the frequency $\omega(\vec{k})$, the real part of the retarded two-point function can be written, for $\ell_0 \gg 1$, as

$$\mathrm{Re}\left[\Gamma^{\mathrm{R}}_{2;1}(\vec{k},\omega)\right] \approx -[\omega-\omega(\vec{k})]\left(\frac{\Lambda}{\omega(\vec{k})}\right)^{\frac{\sqrt{N_c^2-1}}{\sqrt{\ell_0}\log(\ell_0)}}, \tag{L.84}$$

to leading order in $[\omega-\omega(\vec{k})]/\omega \ll 1$. Close to this frequency we can write the spectral function in Eq. (L.67) as:

$$\mathcal{A}_{1;2}(\vec{k}) \approx \frac{\mathcal{Z}_1[k_x;\omega(\vec{k})]}{\tau_1[k_x;\omega(\vec{k})]}\frac{1}{[\omega-\omega(\vec{k})]^2+\tau_1^{-2}[k_x;\omega(\vec{k})]}, \tag{L.85}$$

where the spectral weight and lifetime of the particle-like excitations are given by

$$\mathcal{Z}_1(\vec{k}) = \left(\frac{\omega(\vec{k})}{\Lambda_f}\right)^{\frac{\sqrt{N_c^2-1}}{\sqrt{\ell_0}\log(\ell_0)}}, \tag{L.86}$$

$$\tau^{-1}(\vec{k}) = \frac{\pi}{2}\frac{\sqrt{N_c^2-1}}{\sqrt{\ell_0}\log(\ell_0)}\omega(\vec{k}), \tag{L.87}$$

respectively. We note that at frequencies $\omega(\vec{k}) \approx \omega$ the quasiparticle lifetime is large because $\omega/\sqrt{\ell_0} \ll e^{-\ell_{\mathrm{SC}}}\Lambda_f/\sqrt{\ell_0} \ll 1$ with $1 \ll \ell_{\mathrm{SC}} \ll \ell_0$. Similarly, we note that the quasiparticle weight is suppressed compared to unity. Finally, it is noted that, in these same limits, the quasiparticle weight is small compared to unity.

(*iii*) $\mathcal{A}_{3;1}(\vec{k},\omega)$: For momenta $|k_x| \ll \frac{\Lambda_f}{v_0}e^{-\ell_{\mathrm{SC}}}$, the spectral function takes the form

$$\mathcal{A}_{3;1}(\vec{k},\omega) = -\frac{2\mathrm{Im}\left[\Gamma^{\mathrm{R}}_{3;1}(\vec{k},\omega)\right]}{\mathrm{Re}\left[\Gamma^{\mathrm{R}}_{3;1}(\vec{k},\omega)\right]^2+\mathrm{Im}\left[\Gamma^{\mathrm{R}}_{3;1}(\vec{k},\omega)\right]^2}, \tag{L.88}$$

where the real and imaginary parts of the retarded two-point function in this momentum regime are given in Eqs. (L.45) and (L.46), respectively. These are characterized by the functions in Eqs. (L.30), (L.33), and (L.36). Since $\ell_\omega \lessapprox \ell_{\mathrm{SC}} \ll \ell_0$ we have, to leading order in $\ell_\omega/\ell_0 \ll 1$,

$$f_z^{(1);3}(k_x,k_0) = \exp\left(\frac{\sqrt{N_c^2-1}}{\sqrt{\ell_0}\log(\ell_0)}\ell_\omega\right), \tag{L.89}$$

$$f_{V_F}^{(1);3}(k_x,k_0)=\exp\left(\frac{3\ell_\omega}{8\ell_0}\right), \tag{L.90}$$

$$u_1^{(3)}(k_x,k_0)=v_0\exp\left(-\frac{\ell_\omega}{\ell_0}\right). \tag{L.91}$$

All these functions are momentum independent and the computation of the spectral function follows the same steps we presented for $\mathcal{A}_{2;1}(\vec{k},\omega)$. To leading order in $\ell_0\gg 1$, the real and imaginary parts of the retarded two-point function now take the form

$$\mathrm{Re}\left[I^{\mathrm{R}}_{3;1}(\vec{k},\omega)\right]=-\omega\left(\frac{\Lambda_f}{\omega}\right)^{\frac{\sqrt{N_c^2-1}}{\sqrt{\ell_0}\log(\ell_0)}}+\left(\frac{\omega}{\Lambda_f}\right)^{-\frac{3}{8\ell_0}}\left\{v_0\left(\frac{\omega}{\Lambda_f}\right)^{\frac{1}{\ell_0}}k_x+k_y\right\}, \tag{L.92}$$

$$\begin{aligned}\mathrm{Im}\left[I^{\mathrm{R}}_{3;1}(\vec{k},\omega)\right]&=\frac{\pi}{2}\frac{\sqrt{N_c^2-1}}{\sqrt{\ell_0}\log(\ell_0)}\omega\left(\frac{\Lambda_f}{\omega}\right)^{\frac{\sqrt{N_c^2-1}}{\sqrt{\ell_0}\log(\ell_0)}}\\&+v_0k_x\frac{\pi}{2\ell_0}\left(\frac{\omega}{\Lambda_f}\right)^{-\frac{5}{8\ell_0}}-\frac{3\pi}{16\ell_0}\left(\frac{\omega}{\Lambda_f}\right)^{-\frac{3}{8\ell_0}}\left\{v_0\left(\frac{\omega}{\Lambda_f}\right)^{\frac{1}{\ell_0}}k_x+k_y\right\}.\end{aligned} \tag{L.93}$$

The real part of the retarded two-point function vanishes at frequencies $\omega(\vec{k})$ satisfying the equation

$$\omega(\vec{k})\left(\frac{\Lambda_f}{\omega(\vec{k})}\right)^{\frac{\sqrt{N_c^2-1}}{\sqrt{\ell_0}\log(\ell_0)}}=\left(\frac{\omega(\vec{k})}{\Lambda_f}\right)^{-\frac{3}{8\ell_0}}\left\{v_0\left(\frac{\omega(\vec{k})}{\Lambda_f}\right)^{\frac{1}{\ell_0}}k_x+k_y\right\}. \tag{L.94}$$

This equation has a nontrivial solution for nonzero momentum. The solution gives rise to the renormalized energy levels of the electronic excitations in the momentum range under consideration. At this frequency, the imaginary part is well approximate, in the $\ell_0\gg 1$ limit, by

$$\mathrm{Im}\left[I^{\mathrm{R}}_{3;1}(\vec{k},\omega)\right]=\frac{\pi}{2}\frac{\sqrt{N_c^2-1}}{\sqrt{\ell_0}\log(\ell_0)}\omega(\vec{k})\left(\frac{\Lambda_f}{\omega(\vec{k})}\right)^{\frac{\sqrt{N_c^2-1}}{\sqrt{\ell_0}\log(\ell_0)}}. \tag{L.95}$$

In the $\ell_0\ll 1$ limit this is a small quantity because $\omega(\vec{k})/\Lambda_f\ll 1$ and therefore the power-law contribution is at most order one. This implies that at frequencies $\omega\approx\omega(\vec{k})$ the spectral function is sharply peaked. Around the peak, the real part takes the form

$$\mathrm{Re}\left[I^{\mathrm{R}}_{3;1}(\vec{k},\omega)\right]\approx[\omega-\omega(\vec{k})]\left(\frac{\Lambda_f}{\omega(\vec{k})}\right)^{\frac{\sqrt{N_c^2-1}}{\sqrt{\ell_0}\log(\ell_0)}}, \tag{L.96}$$

to leading order in $[\omega-\omega(\vec{k})]/\omega\ll 1$. Therefore, Eq. (L.88) takes the form

$$\mathcal{A}_{3;1}(k_x)\approx\frac{\mathcal{Z}_1[k_x;\omega(\vec{k})]}{\tau_1[k_x;\omega(\vec{k})]}\frac{1}{[\omega-\omega(\vec{k})]^2+\tau_1^{-2}[k_x;\omega(\vec{k})]}, \tag{L.97}$$

where the quasiparticle weight and lifetime of the quasiparticle are given by Eqs. (L.86) and (L.87), respectively, but with the renormalized dispersion $\omega(\vec{k})$ that solves Eq. (L.94).

Appendix M | Momentum-Dependent Quantum Corrections

Here we provide details on the computation and the asymptotic approximation of the IR momentum structure of the leading order quantum corrections shown in Figs. 2.3(a) to 2.3(c). In what follows, we operate under the WMDL, where quantum corrections are computed with the zero momentum coupling functions and the physical observables are fixed by the RG conditions in Eq. (4.57). The quantum corrections to the fermion self-energy involve the scattering of fermions between patches of the FS that become nested in the small v limit. Therefore, following the discussion on Sec. 4.2-(a) , the only scale that cuts off the potential divergences in these corrections is Λ_f [see Fig. 4.3(b)]. Since we are interested in the logarithmic divergences in this UV cutoff, which are independent of the way that the cutoff is imposed, we will only cutoff the last momentum or frequency integration with this UV scale.

M.1 One-loop fermion self-energy

The quantum correction depicted in Fig. 2.3(a) yields the contribution to the quantum effective action

$$\delta\mathbf{\Gamma}^{(2,0)}_{1\text{L}} = \sum_{N=1}^{8}\sum_{\sigma=1}^{N_c}\sum_{j=1}^{N_f}\int \mathrm{d}k\ \psi^{\dagger}_{N,\sigma,j}(k)\Sigma^{1\text{L}}_{N}(k)\psi_{N,\sigma,j}(k), \tag{M.1}$$

where the one-loop fermion self-energy is given, in the WMDL and to leading order in v_0, by

$$\Sigma^{1\text{L}}_{N}(k) = -\frac{\pi(N_c^2-1)v}{N_cN_f}\int \mathrm{d}q\ G^{(0)}_{\overline{N}}(k+q;v)D(q), \tag{M.2}$$

where $D(q)$ is given in Eq. (2.6) and the bare fermionic Green's function for hot spot N is given by

$$G^{(0)}_{N}(k;v) = \frac{1}{ik_0 + e_N(\vec{k};v)}. \tag{M.3}$$

In the presence of nonzero external momentum and frequency, it is convenient to divide the discussion into the computation of the imaginary and real parts of Eq. (M.2). Upon introducing the expression for the propagators, these are given by

$$\mathrm{Im}\left[\Sigma^{1\text{L}}_{N}(k)\right] = \frac{\pi(N_c^2-1)v}{N_cN_f}\int \mathrm{d}q\left[\frac{(k_0+q_0)}{(k_0+q_0)^2+e_{\overline{N}}(\vec{k}+\vec{q};v)^2}\frac{1}{|q_0|+c(v)(|q_x|+|q_y|)}\right], \tag{M.4}$$

$$\text{Re}\left[\Sigma_N^{1\text{L}}(k)\right] = -\frac{\pi(N_c^2-1)v}{N_c N_f}\int \text{d}q \left[\frac{e_{\overline{N}}(\vec{k}+\vec{q};v)}{(k_0+q_0)^2+e_{\overline{N}}(\vec{k}+\vec{q};v)^2}\frac{1}{|q_0|+c(v)(|q_x|+|q_y|)}\right], \quad \text{(M.5)}$$

respectively.

M.1-(a) $\quad \text{Im}\left[\Sigma_N^{1\text{L}}(k)\right]$

Without loss of generality we consider Eq. (M.4) for the $N=1$ hot spot. At a first glance, the energy scale associated to the external momentum is given by $\Delta(\vec{k};v) = e_4(\vec{k};v)$ since the diagram depends on the external momentum only through the dispersion relation of the electrons close to the $N=4$ hot spot:

$$\text{Im}\left[\Sigma_1^{1\text{L}}(k)\right] = \frac{\pi(N_c^2-1)v}{N_c N_f}\int \text{d}q \left[\frac{(k_0+q_0)}{(k_0+q_0)^2+(vq_x-q_y+\Delta(\vec{k};v))^2}\frac{1}{|q_0|+c(v)(|q_x|+|q_y|)}\right]. \quad \text{(M.6)}$$

Following the logic in Sec. 4.4 we analyze this diagram in the limits in which the external frequency k_0 is either much larger or much smaller than the diagram's intrinsic energy scales associated to the external momentum. In here we have identified $\Delta(\vec{k};v)$ as one of the momentum scales associated to the diagram. However, a shift in the q_y momentum brings the external momentum into the boson propagator and thus $\overline{\Delta}(\vec{k};v) \equiv c(v)\Delta(\vec{k};v)$ is another intrinsic energy scale associated to the external momentum. Clearly, $\overline{\Delta}(\vec{k};v) \ll \Delta(\vec{k};v)$, and, in order to appropriately determine the asymptotic IR structure of the diagram we consider the following asymptotic limits: (*i*) $|k_0| \gg |\Delta(\vec{k};v)|$, (*ii*) $|\Delta(\vec{k};v)| \gg |k_0| \gg |\overline{\Delta}(\vec{k};v)|$, and (*iii*) $|\overline{\Delta}(\vec{k};v)| \gg |k_0|$.

(*i*) For $|k_0| \gg |\Delta(\vec{k};v)|$ we define the small parameter $\mathfrak{a}(k;v) \equiv |\Delta(\vec{k};v)|/|k_0|$ and assume, without loss of generality, that $k_0 > 0$ and $\Delta(\vec{k};v) > 0$ in the rest of the computation. Under the scaling $q \to k_0 q$, Eq. (M.6) manifestly depends on this parameter as

$$\text{Im}\left[\Sigma_1^{1\text{L}}(k)\right] = \frac{\pi(N_c^2-1)w(v)k_0}{N_c N_f}\int \text{d}q \left\{\left[\frac{(1+q_0)}{(1+q_0)^2+[w(v)q_x-q_y+\mathfrak{a}(k;v)]^2}\right] \times \left[\frac{1}{|q_0|+|q_x|+c(v)|q_y|}\right]\right\}. \quad \text{(M.7)}$$

Here we also performed the scaling $q_x \to q_x/c(v)$ and used the definition $w(v) = v/c(v)$. In the small $c(v)$ limit, the integration over q_y is convergent even if the term $c(v)|q_y|$ is dropped from the boson propagator. Dropping this term assumes that $c(v)\mathfrak{a}(k;v) \ll 1$ which is the case because in the regime of interest $\overline{\Delta}(\vec{k};v) \ll k_0$. Doing so, the integration over q_y yields an expression that is independent of $\mathfrak{a}(k;v)$:

$$\text{Im}\left[\Sigma_1^{1\text{L}}(k)\right] = \frac{\pi(N_c^2-1)w(v)k_0}{N_c N_f}\int_{\mathbb{R}^+}\frac{\text{d}q_0}{(2\pi)}\int_{\mathbb{R}^+}\frac{\text{d}q_x}{(2\pi)}\left[\frac{1+\text{sgn}(1-q_0)}{q_0+q_x}\right]. \quad \text{(M.8)}$$

The integration over q_0 is finite while the q_x integration is cutoff in the UV with the ratio $\Lambda_f/k_0 \gg 1$. In the $\Lambda_f/k_0 \gg 1$ and $k_0 \gg \Delta(\vec{k};v)$ limits, the logarithmically

divergent contribution to the imaginary part of the one-loop fermion self-energy is given by

$$\mathrm{Im}\left[\Sigma_1^{1\mathrm{L}}(k)\right] = \frac{(N_c^2-1)w(v)}{2\pi N_c N_f} k_0 \log\left(\frac{\Lambda_f}{|k_0|}\right). \tag{M.9}$$

In here, the absolute value in the frequency comes from the fact that an identical result is obtained for the $k_0 < 0$ case.

(*ii*) For $|\Delta(\vec{k};v)| \gg |k_0| \gg |\overline{\Delta}(\vec{k};v)|$ we define the small parameter $\mathfrak{b}(k;v) \equiv |k_0|/|\Delta(\vec{k};v)|$ and, without loss of generality, we assume $k_0 > 0$ and $\Delta(\vec{k};v) > 0$ in what follows. Under the scaling $q \to \Delta(\vec{k};v)q$, Eq. (M.6) manifestly depends on the small parameter as

$$\mathrm{Im}\left[\Sigma_1^{1\mathrm{L}}(k)\right] = \frac{\pi(N_c^2-1)w(v)\Delta(\vec{k};v)}{N_c N_f}\int \mathrm{d}q \left\{\left[\frac{(\mathfrak{b}(k;v)+q_0)}{(\mathfrak{b}(k;v)+q_0)^2+[w(v)q_x - q_y+1]^2}\right] \times \left[\frac{1}{|q_0|+|q_x|+c(v)|q_y|}\right]\right\}, \tag{M.10}$$

where the scaling $q_x \to q_x/c(v)$ was performed. If $\mathfrak{b}(k;v)$ is set to zero, this expression vanishes. However we note that the the q_y integration can be performed in the small $c(v)$ limit by dropping the term of order $c(v)|q_y|$ inside the boson propagator. Doing so we obtain

$$\mathrm{Im}\left[\Sigma_1^{1\mathrm{L}}(k)\right] = \frac{\pi(N_c^2-1)w(v)\Delta(\vec{k};v)}{N_c N_f}\int_{\mathbb{R}^+}\frac{\mathrm{d}q_0}{(2\pi)}\int_{\mathbb{R}^+}\frac{\mathrm{d}q_x}{(2\pi)}\left[\frac{1+\mathrm{sgn}(\mathfrak{b}(k;v)-q_0)}{q_0+q_x}\right]. \tag{M.11}$$

The integration over q_0 is finite and a straightforward integration over q_x with a UV cutoff $\Lambda_f/\Delta(\vec{k};v) \gg 1$ yields the same logarithmically divergent contribution as in Eq. (M.9):

$$\mathrm{Im}\left[\Sigma_1^{1\mathrm{L}}(k)\right] = \frac{(N_c^2-1)w(v)}{2\pi N_c N_f} k_0 \log\left(\frac{\Lambda_f}{|k_0|}\right). \tag{M.12}$$

Although $\Delta(\vec{k};v)$ is the largest scale in this regime, it does not play the role of an IR cutoff. As we are about to show, this is because the momentum can be shifted completely into the boson propagator and $\overline{\Delta}(\vec{k};v)$ is the only momentum scale that acts as the IR regulator in the $k_0 \to 0$ limit. This can be understood from the fact that, in this limit, the largest IR contribution to the quantum correction comes from the momentum space region where both the electrons and the collective mode have the lowest energy [see the discussion in Sec. 4.6-(*a*)]. Since $|\overline{\Delta}(\vec{k};v)| \ll |\Delta(\vec{k};v)|$, it is natural that $\overline{\Delta}(\vec{k};v)$ cuts off the IR behavior of the integral in the $k_0 \to 0$ limit. We now show this is the case by explicit computation.

(*iii*) For $|\overline{\Delta}(\vec{k};v)| \gg |k_0|$ we start by performing the shift $q_y \to q_y + \Delta(\vec{k};v)$ in Eq. (M.6)

which makes the dependence on $\overline{\Delta}(\vec{k};v)$ manifest:

$$\mathrm{Im}\left[\Sigma_1^{1\mathrm{L}}(k)\right] = \frac{\pi(N_c^2-1)w(v)}{N_cN_f}\int \mathrm{d}q \left\{\left[\frac{(k_0+q_0)}{(k_0+q_0)^2+(vq_x-q_y))^2}\right] \times \left[\frac{1}{|q_0|+|q_x|+|c(v)q_y+\overline{\Delta}(\vec{k};v)|}\right]\right\}. \tag{M.13}$$

In this expression we performed the scaling $q_x \to q_x/c(v)$. We define $\mathfrak{d}(k;v) \equiv |k_0|/|\overline{\Delta}(\vec{k};v)| \ll 1$ and assume, without loss of generality, that $k_0 > 0$ and $\overline{\Delta}(\vec{k};v) > 0$. We proceed by scaling out $\overline{\Delta}(\vec{k};v)$ from the integrand via $q \to \overline{\Delta}(\vec{k};v)q$. In the small $c(v)$ limit, the integration over q_y is convergent and it is done by dropping the term of order $c(v)q_y$ inside the boson propagator. Such an integration results in

$$\mathrm{Im}\left[\Sigma_1^{1\mathrm{L}}(k)\right] = \frac{\pi(N_c^2-1)w(v)\overline{\Delta}(\vec{k};v)}{N_cN_f}\int\limits_{\mathbb{R}^+}\mathrm{d}q_0\int\limits_{\mathbb{R}^+}\frac{\mathrm{d}q_x}{(2\pi)}\frac{[1+\mathrm{sgn}(\mathfrak{d}(k;v)-q_0)]}{q_0+q_x+1}, \tag{M.14}$$

where the integrand has been symmetrized in q_0. The integration over q_0 is finite, and cutting off the large q_x integration with the ratio $\Lambda_f/\overline{\Delta}(\vec{k};v) \gg 1$ yields the logarithmically divergent contribution in the $\Lambda_f/\overline{\Delta}(\vec{k};v) \gg 1$ limit:

$$\mathrm{Im}\left[\Sigma_1^{1\mathrm{L}}(k)\right] = \frac{(N_c^2-1)w(v)}{2\pi N_cN_f}k_0\log\left(\frac{\Lambda_f}{|\overline{\Delta}(\vec{k};v)|}\right). \tag{M.15}$$

Here we gave used the fact that the same result is obtained for $\overline{\Delta}(\vec{k};v) < 0$. As we mentioned earlier, the energy scale associated to the external momentum that acts as an IR regulator in the absence of an external frequency is $|\overline{\Delta}(\vec{k};v)|$ rather than $|\Delta(\vec{k};v)|$.

Collecting the results in Eq. (M.9), (M.12) and (M.15), and noting that the analogous expressions for all other hot spots can be obtained through a C_4 transformation, we write the general result for the imaginary part of the one-loop fermion self-energy as

$$\mathrm{Im}\left[\Sigma_N^{1\mathrm{L}}(k)\right] = \frac{(N_c^2-1)w(v)}{2\pi N_cN_f}k_0\log\left(\frac{\Lambda_f}{\mathscr{G}_1[|k_0|,c(v)|e_{\overline{N}}(\vec{k};v)|]}\right), \tag{M.16}$$

where the function $\mathscr{G}_1(x,y)$ is such that $\mathscr{G}_1(x,y) \sim \max(x,y)$ whenever $x \gg y$ or $y \gg x$. Using this result in combination with Eq. (J.18) fixes the counterterm function to the one-loop order

$$A_N^{(1);1\mathrm{L}}(k_N) = -\frac{(N_c^2-1)w(v)}{2\pi N_cN_f}\log\left(\frac{\Lambda_f}{\mathscr{G}_1[\mu,2vc(v)|k_N|]}\right). \tag{M.17}$$

M.1-(*b*) $\quad \mathrm{Re}\left[\Sigma_N^{1\mathrm{L}}(k)\right]$

We proceed by analyzing Eq. (M.5) for the $N = 1$ hot spot. In the previous section we showed that the naive energy scale $\Delta(\vec{k};v) = e_4(\vec{k};v)$ plays no role in the IR structure of the

quantum correction, while $\overline{\Delta}(\vec{k};v) = c(v)\Delta(\vec{k};v)$ emerged as the IR cutoff of the quantum correction in the $k_0 \to 0$ limit. This is also the case for the real part of the one-loop fermion self-energy and thus we focus only on the two asymptotic limits: (*i*) $|k_0| \gg |\overline{\Delta}(\vec{k};v)|$ and (*ii*) $|k_0| \ll |\overline{\Delta}(\vec{k};v)|$. We start by writing Eq. (M.5) as

$$\mathrm{Re}\left[\Sigma_1^{\mathrm{1L}}(k)\right] = -\frac{\pi(N_c^2-1)v}{N_c N_f}\int \mathrm{d}q \left\{\left[\frac{(vq_x - q_y)}{(k_0+q_0)^2+(vq_x-q_y)^2}\right] \times \left[\frac{1}{|q_0|+c(v)|q_x|+|c(v)q_y+\overline{\Delta}(\vec{k};v)|}\right]\right\}, \tag{M.18}$$

and note that the q_x integration is logarithmically divergent for any v if the q_y integration is done first. Along this path, such a divergence can be seen explicitly through the shift $q_y \to q_y + vq_x$. This makes the integrand decay as $1/|q_x|$ in the large q_x limit for any v. Therefore, in the small v limit

$$\mathrm{Re}\left[\Sigma_1^{\mathrm{1L}}(k)\right] = \frac{\pi(N_c^2-1)v}{N_c N_f}\int \mathrm{d}q \left[\frac{q_y}{(k_0+q_0)^2+q_y^2}\frac{1}{|q_0|+c(v)|q_x|+|c(v)q_y+\overline{\Delta}(\vec{k};v)|}\right]. \tag{M.19}$$

We now proceed on analyzing the two relevant asymptotic limits of this.

(*i*) For $|k_0| \gg |\overline{\Delta}(\vec{k};v)|$ we define the small parameter $\mathfrak{b}(k;v) = |\overline{\Delta}(\vec{k};v)|/|k_0|$ and assume that $k_0 > 0$ and $\overline{\Delta}(\vec{k};v) > 0$, without loss of generality. After performing the scaling $q \to k_0 q/c(v)$, Eq. (M.19) can be written as

$$\mathrm{Re}\left[\Sigma_1^{\mathrm{1L}}(k)\right] = \frac{\pi(N_c^2-1)w(v)k_0}{N_c N_f}\int \mathrm{d}q \left[\frac{q_y}{c(v)(1+q_0)^2+q_y^2}\frac{1}{|q_0|+|q_x|+|q_y+\mathfrak{b}(k;v)|}\right], \tag{M.20}$$

where $w(v) = v/c(v)$. In the small $c(v)$ and $\mathfrak{b}(k;v)$ limits this expression displays two interesting simultaneous behaviors. On the one hand, setting $\mathfrak{b}(k;v) = 0$ annihilates the contribution upon integrating over q_y. On the other hand, setting $c(v) = 0$ inside the integrand makes the integration along the q_y direction logarithmically divergent in the IR. These are symptoms of the fact that this quantum correction is proportional to $\mathfrak{b}(k;v)$ and that it diverges logarithmically in $c(v) \ll 1$. After the integration over q_y is done for general $c(v)$ and $\mathfrak{b}(k;v)$, the leading order contribution in $\mathfrak{b}(k;v) \ll 1$ is given by

$$\mathrm{Re}\left[\Sigma_1^{\mathrm{1L}}(k)\right] = \frac{(N_c^2-1)w(v)\overline{\Delta}(\vec{k};v)}{N_c N_f}\left[\mathsf{T}^{(1)}[c(v)] + \mathsf{T}^{(2)}[c(v)]\right], \tag{M.21}$$

where

$$\mathsf{T}^{(1)}[c(v)] = \int_{\mathbb{R}}\frac{\mathrm{d}q_0}{(2\pi)}\int_{\mathbb{R}}\frac{\mathrm{d}q_x}{(2\pi)}\frac{[c(v)^2(1+q_0)^2+(|q_0|+|q_x|)^2]-\pi c(v)|q_0+1|(|q_x|+|q_0|)}{[c(v)^2(1+q_0)^2+(|q_0|+|q_x|)^2]^2}, \tag{M.22}$$

$$\mathsf{T}^{(2)}[c(v)] = \frac{1}{2}\int_{\mathbb{R}}\frac{\mathrm{d}q_0}{(2\pi)}\int_{\mathbb{R}}\frac{\mathrm{d}q_x}{(2\pi)}\frac{[c(v)^2(1+q_0)^2-(|q_0|+|q_x|)^2]}{[c(v)^2(1+q_0)^2+(|q_0|+|q_x|)^2]^2}\log\left(\frac{(|q_0|+|q_x|)^2}{c(v)^2(1+q_0)^2}\right). \tag{M.23}$$

We consider each of these terms separately.

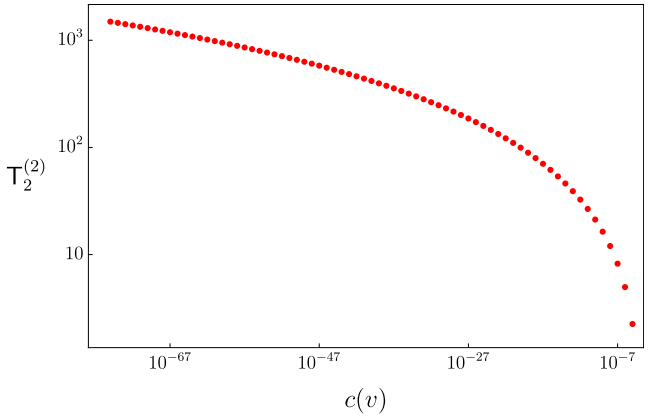

Figure M.1: Numerical integration of $\mathsf{T}_2^{(2)}$ which shows a logarithmic divergence in the $c(v) \ll 1$ limit. The error bars in the numerical integration are smaller than the size of the plot markers.

Term $\mathsf{T}^{(1)}[c(v)]$: Eq. (M.22) admits an analytic integration over q_0 which yields

$$\mathsf{T}^{(1)}[c(v)] = \frac{1}{2\pi[1+c(v)^2]} \int_{\mathbb{R}^+} \frac{\mathrm{d}q_x}{(2\pi)} \left[\frac{2(1+q_x^2)[1+c(v)^2]\left\{\arctan(q_x) - q_x c(v)\arctan[1/c(v)]\right\}}{(1+q_x^2)[1+c(v)q_x][c(v)q_x-1]} + \frac{\pi q_x\{c(v)(q_x^2+1) - [1+c(v)^2]q_x\}}{(1+q_x^2)[1+c(v)q_x][c(v)q_x-1]} \right], \tag{M.24}$$

where the scaling $q_x \to c(v)q_x$ has been performed. The q_x integration is UV divergent and it is cutoff by Λ_f/k_0. For $\Lambda_f/k_0 \gg 1$, the logarithmically divergent contribution from Eq. (M.24), to the leading order in $c(v) \ll 1$, is given by

$$\mathsf{T}^{(1)}[c(v)] = \frac{1}{\pi^2}\log\left(\frac{\Lambda_f}{k_0}\right). \tag{M.25}$$

Term $\mathsf{T}^{(2)}[c(v)]$: We separate Eq. (M.23) into two contributions:

$$\mathsf{T}_1^{(2)}[c(v)] = \log\left(\frac{1}{c(v)}\right) \int_{\mathbb{R}} \frac{\mathrm{d}q_0}{(2\pi)} \int_{\mathbb{R}} \frac{\mathrm{d}q_x}{(2\pi)} \frac{[c(v)^2(1+q_0)^2 - (|q_0|+|q_x|)^2]}{[c(v)^2(1+q_0)^2 + (|q_0|+|q_x|)^2]^2}, \tag{M.26}$$

$$\mathsf{T}_2^{(2)}[c(v)] = \frac{1}{2}\int_{\mathbb{R}} \frac{\mathrm{d}q_0}{(2\pi)} \int_{\mathbb{R}} \frac{\mathrm{d}q_x}{(2\pi)} \frac{[c(v)^2(1+q_0)^2 - (|q_0|+|q_x|)^2]}{[c(v)^2(1+q_0)^2 + (|q_0|+|q_x|)^2]^2} \log\left(\frac{(|q_0|+|q_x|)^2}{(1+q_0)^2}\right), \tag{M.27}$$

such that $\mathsf{T}^{(2)}[c(v)] = \mathsf{T}_1^{(2)}[c(v)] + \mathsf{T}_2^{(2)}[c(v)]$. The integration over q_0 in Eq. (M.26) yields, after performing the scaling $q_x \to q_x c(v)$,

$$\mathsf{T}_1^{(2)} = -\frac{1}{2\pi(1+c(v)^2)}\log\left(\frac{1}{c(v)}\right) \int_{\mathbb{R}^+} \frac{\mathrm{d}q_x}{\pi} \frac{q_x}{q_x^2+1}. \tag{M.28}$$

The integration along q_x diverges in the UV and it is cut off by Λ_f/k_0. In the $\Lambda_f/k_0 \gg 1$ limit, the logarithmically divergent contribution from Eq. (M.26) results in

$$\mathsf{T}_1^{(2)} = -\frac{1}{\pi^2}\log\left(\frac{1}{c(v)}\right)\log\left(\frac{\Lambda_f}{k_0}\right), \tag{M.29}$$

which clearly dominates over the result in Eq. (M.25) in the $c(v) \ll 1$ limit. Eq. (M.27) is finite by power-counting but it diverges logarithmically with $c(v)$ in the $c(v) \ll 1$ limit. This is confirmed numerically as shown in Fig. M.1.

Collecting the above results, and using the fact that the same result is obtained for $k_0 < 0$, it follows that, in the $|k_0| \gg |\overline{\Delta}(\vec{k}; v)|$ and $c(v) \ll 1$ limits, the logarithmically divergent contribution arising from the real part of the one-loop fermion self-energy is given by

$$\mathrm{Re}\left[\Sigma_1^{1\mathrm{L}}(k)\right] = -\frac{(N_c^2-1)w(v)}{\pi^2 N_c N_f} \log\left(\frac{1}{c(v)}\right) \overline{\Delta}(\vec{k}; v) \log\left(\frac{\Lambda_f}{|k_0|}\right). \tag{M.30}$$

(*ii*) For $|\overline{\Delta}(\vec{k}; v)| \gg |k_0|$ we use again the small parameter $\mathfrak{d}(k; v) = |k_0|/|\overline{\Delta}(\vec{k}; v)|$ and, without loss of generality we consider the case in which $k_0 > 0$ and $\overline{\Delta}(\vec{k}; v) > 0$. In terms of this parameter Eq. (M.19) reads

$$\mathrm{Re}\left[\Sigma_1^{1\mathrm{L}}(k)\right] = \frac{\pi(N_c^2-1)w(v)\overline{\Delta}(\vec{k}; v)}{N_c N_f} \int \mathrm{d}q \left\{ \left[\frac{q_y}{c(v)^2(\mathfrak{d}(k; v)+q_0)^2 + q_y^2}\right] \times \left[\frac{1}{|q_0|+|q_x|+|q_y+1|}\right]\right\}, \tag{M.31}$$

which is obtained after the rescaling $(q_0, \vec{q}) \to (q_0\overline{\Delta}(\vec{k}; v), \vec{q}[\overline{\Delta}(\vec{k}; v)/c(v)])$. Setting $\mathfrak{d}(k; v) = 0$ inside the integrand is harmless and the integration along q_0 yields

$$\mathrm{Re}\left[\Sigma_1^{1\mathrm{L}}(k)\right] = \frac{\pi(N_c^2-1)w(v)\overline{\Delta}(\vec{k}; v)}{N_c N_f} \left[\mathsf{Q}^{(1)}[c(v)] + \mathsf{Q}^{(2)}[c(v)]\right], \tag{M.32}$$

where

$$\mathsf{Q}^{(1)}[c(v)] = \frac{c(v)}{2} \int_{\mathbb{R}} \frac{\mathrm{d}q_x}{(2\pi)} \int_{\mathbb{R}} \frac{\mathrm{d}q_y}{(2\pi)} \frac{\mathrm{sgn}(q_y)(|q_x| + |1+q_y|)}{q_y^2 + c(v)^2(|q_x|+|q_y+1|)^2}, \tag{M.33}$$

$$\mathsf{Q}^{(2)}[c(v)] = \frac{1}{2\pi} \int_{\mathbb{R}} \frac{\mathrm{d}q_x}{(2\pi)} \int_{\mathbb{R}} \frac{\mathrm{d}q_y}{(2\pi)} \frac{q_y}{q_y^2 + c(v)^2(|q_x|+|q_y+1|)^2} \log\left(\frac{q_y^2}{c(v)^2(|q_x|+|q_y+1|)^2}\right). \tag{M.34}$$

We consider each of these two terms separately.

Term $\mathsf{Q}^{(1)}[c(v)]$: We symmetrize the integrand in Eq. (M.33) in q_x and q_y and write it as

$$\mathsf{Q}^{(1)}[c(v)] = \mathsf{Q}_1^{(1)}[c(v)] + \mathsf{Q}_2^{(1)}[c(v)], \tag{M.35}$$

where

$$\mathsf{Q}_1^{(1)}[c(v)] = c(v) \int_{\mathbb{R}^+} \frac{\mathrm{d}q_x}{(2\pi)} \int_1^\infty \frac{\mathrm{d}q_y}{(2\pi)} \left[\frac{q_x+q_y+1}{c(v)^2(q_x+q_y+1)^2+q_y^2} - \frac{q_x+q_y-1}{c(v)^2(q_x+q_y-1)^2+q_y^2}\right], \tag{M.36}$$

$$\mathsf{Q}_2^{(1)}[c(v)] = c(v)\int\limits_{\mathbb{R}^+}\frac{\mathrm{d}q_x}{(2\pi)}\int\limits_0^1\frac{\mathrm{d}q_y}{(2\pi)}\left[\frac{q_x+q_y+1}{c(v)^2(q_x+q_y+1)^2+q_y^2}+\frac{q_y-q_x-1}{c(v)^2(q_y-q_x-1)^2+q_y^2}\right]. \tag{M.37}$$

Integration over q_y yields

$$\begin{aligned}\mathsf{Q}_1^{(1)}[c(v)] = \frac{1}{4\pi[1+c(v)^2]}\int\limits_{\mathbb{R}^+}\frac{\mathrm{d}q_x}{(2\pi)}\Bigg\{&c(v)\log\left[\frac{c(v)^2q_x^2+1}{c(v)^2(q_x+2)^2+1}\right]+\pi[1+\mathrm{sgn}(1-q_x)]\\ &-2\arctan\left(\frac{c(v)^2q_x+1}{c(v)(1-q_x)}\right)-2\arctan\left(\frac{1+c(v)^2}{c(v)(1+q_x)}+c(v)\right)\Bigg\},\end{aligned} \tag{M.38}$$

$$\begin{aligned}\mathsf{Q}_2^{(1)}[c(v)] = \frac{1}{4\pi[1+c(v)^2]}\int\limits_{\mathbb{R}^+}\frac{\mathrm{d}q_x}{(2\pi)}\Big\{&c(v)\log\left([c(v)^2q_x^2+1][c(v)^2(q_x+2)^2+1]\right)-4\arctan[c(v)]\\ &-2\arctan\left(\frac{1-c(v)^2q_x}{c(v)(1+q_x)}\right)+2\mathrm{arccot}\left(\frac{c(v)(q_x+1)}{c(v)^2(q_x+2)+1}\right)-4c(v)\log[c(v)(q_x+1)]\Big\}.\end{aligned} \tag{M.39}$$

From these two terms, only that in Eq. (M.38) is logarithmically divergent upon the q_x integration. The term in Eq. (M.39) only offers a finite contribution that vanishes in the $c(v)\to 0$ limit. The integration along q_x in Eq. (M.38) is cutoff in the UV by the ratio $\Lambda_f/\overline{\Delta}(\vec{k};v)\gg 1$. In this limit, and for $c(v)\gg 1$, the integration over q_x yields the logarithmically divergent contribution

$$\mathsf{Q}_1^{(1)}[c(v)] = -\frac{c(v)}{2\pi^2}\log\left(\frac{\Lambda_f}{\overline{\Delta}(\vec{k};v)}\right). \tag{M.40}$$

Term $\mathsf{Q}^{(2)}[c(v)]$: We write Eq. (M.34) as

$$\mathsf{Q}^{(2)}[c(v)] = \mathsf{Q}_1^{(2)}[c(v)] + \mathsf{Q}_2^{(2)}[c(v)], \tag{M.41}$$

where

$$\mathsf{Q}_1^{(2)}[c(v)] = \frac{2}{\pi}\log\left(\frac{1}{c(v)}\right)\int\limits_{\mathbb{R}^+}\frac{\mathrm{d}q_x}{(2\pi)}\int\limits_{\mathbb{R}}\frac{\mathrm{d}q_y}{(2\pi)}\left[\frac{q_y}{q_y^2+c(v)^2(q_x+|q_y+1|)^2}\right], \tag{M.42}$$

$$\mathsf{Q}_2^{(2)}[c(v)] = \frac{1}{\pi}\int\limits_{\mathbb{R}^+}\frac{\mathrm{d}q_x}{(2\pi)}\int\limits_{\mathbb{R}}\frac{\mathrm{d}q_y}{(2\pi)}\left[\frac{q_y}{q_y^2+c(v)^2(q_x+|q_y+1|)^2}\log\left(\frac{q_y^2}{q_x+|q_y+1|)^2}\right)\right]. \tag{M.43}$$

We consider each term separately. The integration over q_y in Eq. (M.42) yields

$$\begin{aligned}\mathsf{Q}_1^{(2)}[c(v)] = -\frac{c(v)}{2\pi^2[1+c(v)^2]}\log\left(\frac{1}{c(v)}\right)\int\limits_{\mathbb{R}^+}\frac{\mathrm{d}q_x}{(2\pi)}\Bigg(&2\arctan\left(\frac{1-c(v)^2q_x}{c(v)(1+q_x)}\right)\\ &-2\arctan\left(\frac{c(v)^2q_x+1}{c(v)(1-q_x)}\right)+\pi[1+\mathrm{sgn}(1-q_x)]\Bigg).\end{aligned} \tag{M.44}$$

The integration over q_x becomes UV divergent it is cut off by $\Lambda_f/\overline{\Delta}(\vec{k};v)$. In the $\Lambda_f/\overline{\Delta}(\vec{k};v) \gg 1$ and $c(v) \ll 1$ limits, we obtain the logarithmically divergent contribution

$$\mathsf{Q}_1^{(2)}[c(v)] = -\frac{1}{\pi^3}\log\left(\frac{1}{c(v)}\right)\log\left(\frac{\Lambda_f}{\overline{\Delta}(\vec{k};v)}\right), \tag{M.45}$$

which dominates over the contribution in Eq. (M.40) in the $c(v) \ll 1$ limit. Integrating over q_x in Eq. (M.43) and taking the small $c(v)$ limit yields the finite contribution:

$$\begin{aligned}\mathsf{Q}_2^{(2)}[c(v)] = \frac{1}{4\pi^3}\int\limits_{\mathbb{R}^+}\frac{\mathrm{d}q_y}{q_y}\Bigg[&(q_y+1)\left(\log\left(\frac{q_y}{1+q_y}\right)+1\right)\\ &-|1-q_y|\left(\log\left(\frac{q_y}{|1-q_y|}\right)+1\right)\Bigg] = -\frac{1}{12}.\end{aligned} \tag{M.46}$$

Collecting the above results and noting that the $\overline{\Delta}(\vec{k};v) < 0$ case is computed in the same way, it follows that, in the $|\overline{\Delta}(\vec{k};v)| \gg |k_0|$ and $c(v) \ll 1$ limits, the logarithmically divergent contribution to the real part of the one-loop fermion self-energy is given by

$$\mathrm{Re}\left[\Sigma_1^{1\mathrm{L}}(k_0,\vec{k})\right] = -\frac{(N_c^2-1)w(v)}{\pi^2 N_c N_f}\log\left(\frac{1}{c(v)}\right)\overline{\Delta}(\vec{k};v)\log\left(\frac{\Lambda_f}{|\overline{\Delta}(\vec{k};v)|}\right). \tag{M.47}$$

Since the computations for all other hot spots follow the same logic, using Eqs. (M.30) and (M.47), we can write the real part of the one-loop fermion self-energy in the general form

$$\mathrm{Re}\left[\Sigma_N^{1\mathrm{L}}(k_0,\vec{k})\right] = -\frac{(N_c^2-1)v}{\pi^2 N_c N_f}\log\left(\frac{1}{c(v)}\right)e_{\overline{N}}(\vec{k};v)\log\left(\frac{\Lambda_f}{\mathscr{G}_2[|k_0|,c(v)|e_{\overline{N}}(\vec{k};v)|]}\right). \tag{M.48}$$

Here, $\mathscr{G}_2(x,y) \sim \max(x,y)$ whenever $x \gg y$ or $y \gg x$. Using this result in combination with the renormalization condition in Eqs. (J.19) and (J.20) fixes the momentum-dependent one-loop counterterm functions in the WMDL and to leading order in $v_0 \ll 1$:

$$A_N^{(2);1\mathrm{L}}(k_N) = \frac{(N_c^2-1)v}{\pi^2 N_c N_f}\log\left(\frac{1}{c(v)}\right)\log\left(\frac{\Lambda_f}{\mathscr{G}_2[|k_0|,2vc(v)|k_N|])}\right), \tag{M.49}$$

$$A_N^{(3);1\mathrm{L}}(k_N) = -\frac{(N_c^2-1)v}{\pi^2 N_c N_f}\log\left(\frac{1}{c(v)}\right)\log\left(\frac{\Lambda_f}{\mathscr{G}_2[|k_0|,2vc(v)|k_N|]}\right). \tag{M.50}$$

M.2 Two-loop fermion self-energy

The quantum correction depicted in Fig. 2.3(c) yields the contribution to the quantum effective action

$$\delta\mathbf{\Gamma}_{2\mathrm{L}}^{(2,0)} = \sum_{N=1}^{8}\sum_{\sigma=1}^{N_c}\sum_{j=1}^{N_f}\int \mathrm{d}k\,\psi_{N,\sigma,j}^{\dagger}(k)\Sigma_N^{2\mathrm{L}}(k)\psi_{N,\sigma,j}(k), \tag{M.51}$$

where the two-loop fermion self-energy is determined, in the WMDL and to leading order in $v_0 \ll 1$, by

$$\Sigma_N^{\rm 2L}(k) = \frac{\pi^2(N_c^2-1)v^2}{N_c^2 N_f^2}\int {\rm d}q \int {\rm d}p D(p)D(q)G_{\overline{N}}^{(0)}(k+p;v)G_N^{(0)}(k+p+q;v)G_{\overline{N}}^{(0)}(k+q;v), \quad \text{(M.52)}$$

where $D(q)$ is given in Eq. (2.6) and $G_N^{(0)}(k)$ is given in Eq. (M.3). Introducing the expressions for the propagators,

$$\begin{aligned}\Sigma_N^{\rm 2L}(k) = \frac{\pi^2(N_c^2-1)v^2}{N_c^2 N_f^2}\int {\rm d}q \int {\rm d}p \Bigg\{ &\frac{1}{|q_0|+c(v)(|q_x|+|q_y|)}\frac{1}{|p_0|+c(v)(|p_x|+|p_y|)} \\ &\times \Bigg[\frac{1}{i(k_0+p_0)+e_{\overline{N}}(\vec{k}+\vec{p};v)}\frac{1}{i(k_0+p_0+q_0)+e_N(\vec{k}+\vec{p}+\vec{q};v)} \\ &\times \frac{1}{i(k_0+q_0)+e_{\overline{N}}(\vec{k}+\vec{q};v)}\Bigg]\Bigg\}. \end{aligned} \quad \text{(M.53)}$$

Without loss of generality we consider this quantum correction for the $N=1$ hot spot. The two-loop fermion self-energy at the other hot spots can be recovered from the latter through a C_4 transformation. The q_y and p_y integrations are UV finite and thus we perform the shifts $q_y \to q_y + vq_x + e_4(\vec{k};v)$ and $p_y \to p_y + vp_x + e_4(\vec{k};v)$. Defining $\Delta(\vec{k};v) = e_4(\vec{k};v)$, $\overline{\Delta}(\vec{k};v) = c(v)\Delta(\vec{k};v)$ and $\gamma(\vec{k};v) = 2\Delta(\vec{k};v) + e_1(\vec{k};v)$, Eq. (M.53) is written as

$$\begin{aligned}\Sigma_1^{\rm 2L}(k) = \frac{\pi^2(N_c^2-1)v^2}{N_c^2 N_f^2}\int {\rm d}q \int {\rm d}p \Bigg\{ &\frac{1}{|q_0|+c(v)|q_x|+|c(v)q_y+vc(v)q_x+\overline{\Delta}(\vec{k};v)|} \\ \times \frac{1}{|p_0|+c(v)|p_x|+|c(v)p_y+vc(v)p_x+\overline{\Delta}(\vec{k};v)|}&\Bigg[\frac{1}{i(k_0+p_0)-p_y}\frac{1}{i(k_0+q_0)-q_y} \\ &\times \frac{1}{i(k_0+p_0+q_0)+(p_y+q_y+\gamma(\vec{k};v)+2v(p_x+q_x))}\Bigg]\Bigg\}. \end{aligned} \quad \text{(M.54)}$$

The integrations along the q_y and p_y directions are convergent in the absence of the terms of order $c(v)q_y$ and $c(v)p_y$ in the boson propagators. Furthermore, the convergence (or divergence) of the q_x and p_x integrations is unaffected by the terms of order $vc(v)q_x$ and $vc(v)p_x$ inside the boson propagators. Therefore, ignoring these terms the integration over p_y and q_y yields, to leading order in $v \ll 1$,

$$\begin{aligned}\Sigma_1^{\rm 2L}(k) = -\frac{\pi^2(N_c^2-1)w(v)^2}{N_c^2 N_f^2}\int_{\mathbb{R}}\frac{{\rm d}q_0}{(2\pi)}\int_{\mathbb{R}}\frac{{\rm d}p_0}{(2\pi)}\int_{\mathbb{R}}\frac{{\rm d}q_x}{(2\pi)}\int_{\mathbb{R}}\frac{{\rm d}p_x}{(2\pi)} \\ \Bigg\{\frac{[\Theta(p_0+2q_0+2k_0)-\Theta(-k_0-p_0)]}{|q_0|+|q_x|+|\overline{\Delta}(\vec{k};v)|}\frac{[\Theta(p_0+q_0+k_0)-\Theta(-k_0-q_0)]}{|p_0|+|p_x|+|\overline{\Delta}(\vec{k};v)|} \\ \times\frac{[2w(v)(p_x+q_x)+\gamma(\vec{k};v)]-i\,[2(p_0+q_0)+3k_0]}{(3k_0+2p_0+2q_0)^2+[2w(v)(p_x+q_x)+\gamma(\vec{k};v)]^2}\Bigg\}, \end{aligned} \quad \text{(M.55)}$$

where $w(v) = v/c(v)$, $\Theta(x)$ denotes the Heaviside function and we have performed the scalings $(p_x, q_x) \to (p_x/c(v), q_x/c(v))$. We divide the discussion into the real and imaginary parts of the two-loop fermion self-energy.

A. $\mathrm{Im}\left[\Sigma_1^{2\mathrm{L}}(k)\right]$

The imaginary part of the two-loop fermion self-energy reads

$$\mathrm{Im}\left[\Sigma_1^{2\mathrm{L}}(k)\right] = \frac{\pi^2(N_c^2-1)w(v)^2}{N_c^2N_f^2}\int_{\mathbb{R}}\frac{\mathrm{d}q_0}{(2\pi)}\int_{\mathbb{R}}\frac{\mathrm{d}p_0}{(2\pi)}\int_{\mathbb{R}}\frac{\mathrm{d}q_x}{(2\pi)}\int_{\mathbb{R}}\frac{\mathrm{d}p_x}{(2\pi)} \\ \left\{\frac{[\Theta(p_0+2q_0+2k_0)-\Theta(-k_0-p_0)]}{|q_0|+|q_x|+|\overline{\Delta}(\vec{k};v)|}\frac{[\Theta(p_0+q_0+k_0)-\Theta(-k_0-q_0)]}{|p_0|+|p_x|+|\overline{\Delta}(\vec{k};v)|}\right. \\ \left.\times\frac{[2(p_0+q_0)+3k_0]}{(3k_0+2p_0+2q_0)^2+[2w(v)(p_x+q_x)+\gamma(\vec{k};v)]^2}\right\}, \tag{M.56}$$

We note that the integrations over p_x and q_x are UV finite in the presence of a nonzero $w(v)$. When $w(v)=0$, these integrations become logarithmically divergent. Therefore, we expect that a scale proportional to $1/w(v)$ will cutoff such a divergence. Eq. (M.56) manifestly depends on the external frequency and momentum scales $k_0, \overline{\Delta}(\vec{k};v)$ and $\gamma(\vec{k};v)$. Therefore, we expect that the IR cutoff of this correction will be the maximum amongst these scales. However, as we will show in this section, when $k_0=0$ and $\gamma(\vec{k};v)=0$, the integration is not cutoff by $\overline{\Delta}(\vec{k};v)$ in the IR, but rather by the scale $\widetilde{\Delta}(\vec{k};v)=w(v)\overline{\Delta}(\vec{k};v)$. Motivated by this we write the imaginary part of the fermion self-energy as

$$\mathrm{Im}\left[\Sigma_1^{2\mathrm{L}}(k)\right] = \frac{\pi^2(N_c^2-1)w(v)^2}{N_c^2N_f^2}\int_{\mathbb{R}}\frac{\mathrm{d}q_0}{(2\pi)}\int_{\mathbb{R}}\frac{\mathrm{d}p_0}{(2\pi)}\int_{\mathbb{R}}\frac{\mathrm{d}q_x}{(2\pi)}\int_{\mathbb{R}}\frac{\mathrm{d}p_x}{(2\pi)} \\ \left\{\frac{[\Theta(p_0+2q_0+2k_0)-\Theta(-k_0-p_0)]}{|q_0|+|q_x|+w(v)^{-1}|\widetilde{\Delta}(\vec{k};v)|}\frac{[\Theta(p_0+q_0+k_0)-\Theta(-k_0-q_0)]}{|p_0|+|p_x|+w(v)^{-1}|\widetilde{\Delta}(\vec{k};v)|}\right. \\ \left.\times\frac{[2(p_0+q_0)+3k_0]}{(3k_0+2p_0+2q_0)^2+[2w(v)(p_x+q_x)+\gamma(\vec{k};v)]^2}\right\}. \tag{M.57}$$

We proceed on analyzing this expression in the following limits: (*i*) when $|k_0|\gg|\gamma(\vec{k};v)|$ and $|k_0|\gg|\widetilde{\Delta}(\vec{k};v)|$, (*ii*) when $|\gamma(\vec{k};v)|\gg|k_0|$ and $|\gamma(\vec{k};v)|\gg|\widetilde{\Delta}(\vec{k};v)|$, and when (*iii*) $|\widetilde{\Delta}(\vec{k};v)|\gg|k_0|$ and $|\widetilde{\Delta}(\vec{k};v)|\gg|\gamma(\vec{k};v)|$. We consider each case separately.

(*i*) For $|k_0|\gg|\gamma(\vec{k};v)|$ and $|k_0|\gg|\widetilde{\Delta}(\vec{k};v)|$ we assume, without loss of generality that $k_0>0$, $\gamma(\vec{k};v)>0$ and $\widetilde{\Delta}(\vec{k};v)>0$, and define the two small parameters $\mathfrak{C}(k;v)\equiv\gamma(\vec{k};v)/k_0$ and $\mathfrak{D}(k;v)\equiv\widetilde{\Delta}(\vec{k};v)/k_0$. Performing the scaling $(p_0,q_0,p_x,q_x)\to k_0(p_0,q_0,p_x,q_x)$, Eq. (M.56) takes the form

$$\mathrm{Im}\left[\Sigma_1^{2\mathrm{L}}(k)\right] = \frac{\pi^2(N_c^2-1)w(v)^2k_0}{N_c^2N_f^2}\int_{\mathbb{R}}\frac{\mathrm{d}q_0}{(2\pi)}\int_{\mathbb{R}}\frac{\mathrm{d}p_0}{(2\pi)}\int_{\mathbb{R}}\frac{\mathrm{d}q_x}{(2\pi)}\int_{\mathbb{R}}\frac{\mathrm{d}p_x}{(2\pi)} \\ \left\{\frac{[\Theta(p_0+2q_0+2)-\Theta(-1-p_0)]}{|q_0|+|q_x|+w(v)^{-1}\mathfrak{D}(k;v)}\frac{[\Theta(p_0+q_0+1)-\Theta(-1-q_0)]}{|p_0|+|p_x|+w(v)^{-1}\mathfrak{D}(k;v)}\right. \\ \left.\times\frac{[2(p_0+q_0)+3]}{(3+2p_0+2q_0)^2+[2w(v)(p_x+q_x)+\mathfrak{C}(k;v)]^2}\right\}. \tag{M.58}$$

For small $\mathfrak{C}(k;v)$ and $\mathfrak{D}(k;v)$, these parameters can be ignored in the integrand and a straightforward integration along the q_x and p_x directions yields, to leading order in $w(v) \ll 1$,

$$\begin{aligned}\mathrm{Im}\left[\Sigma_1^{\mathrm{2L}}(k)\right] &= \frac{(N_c^2-1)w(v)^2\log[w(v)]^2 k_0}{N_c^2 N_f^2} \\ &\times \int_{\mathbb{R}} \frac{\mathrm{d}q_0}{(2\pi)} \int_{\mathbb{R}} \frac{\mathrm{d}p_0}{(2\pi)} \frac{\left[\Theta(p_0+2q_0+2)-\Theta(-1-p_0)\right]\left[\Theta(p_0+q_0+1)-\Theta(-1-q_0)\right]}{2(p_0+q_0)+3}.\end{aligned} \tag{M.59}$$

Although this expression seems to be singular when the denominator vanishes, it is noted that the numerator vanishes faster in the same limit and thus the integration is regular. We integrate over p_0 and q_0 with a hard UV cutoff $\Lambda_f/k_0 \gg 1$. In doing so we change variables to $X = p_0+q_0$ and $Y = p_0-q_0$ and write Eq. (M.59) as

$$\begin{aligned}\mathrm{Im}\left[\Sigma_1^{\mathrm{2L}}(k)\right] &= \frac{(N_c^2-1)w(v)^2\log[w(v)]^2 k_0}{2N_c^2 N_f^2}\left[\int_0^{\frac{2\Lambda_f}{k_0}} \frac{\mathrm{d}X}{(2\pi)} \int_{X-\frac{2\Lambda_f}{k_0}}^{\frac{2\Lambda_f}{k_0}-X} \frac{\mathrm{d}Y}{(2\pi)} + \int_{-\frac{2\Lambda_f}{k_0}}^{0} \frac{\mathrm{d}X}{(2\pi)} \int_{-\frac{2\Lambda_f}{k_0}-X}^{X+\frac{2\Lambda_f}{k_0}} \frac{\mathrm{d}Y}{(2\pi)}\right] \\ &\times \frac{\left[\Theta\left(\frac{3X}{2}+\frac{Y}{2}+2\right)-\Theta\left(-1-\frac{X}{2}-\frac{Y}{2}\right)\right]\left[\Theta(X+1)-\Theta\left(-1-\frac{X}{2}+\frac{Y}{2}\right)\right]}{2X+3}.\end{aligned} \tag{M.60}$$

Integration over X and Y yields the following divergent contribution in the large Λ_f/k_0 limit

$$\mathrm{Im}\left[\Sigma_1^{\mathrm{2L}}(k)\right] = \frac{(N_c^2-1)w(v)^2\log[w(v)]^2}{8\pi^2 N_c^2 N_f^2} k_0 \log\left(\frac{\Lambda_f}{|k_0|}\right). \tag{M.61}$$

Here we have used the fact that the same result is obtained for $k_0 < 0$.

(*ii*) For $|\gamma(\vec{k};v)| \gg |k_0|$ and $|\gamma(\vec{k};v)| \gg |\widetilde{\Delta}(\vec{k};v)|$ we assume, without loss of generality that $\gamma(\vec{k};v) > 0, k_0 > 0$ and $\widetilde{\Delta}(\vec{k};v) > 0$. Performing the scaling $(p_0,q_0,p_x,q_x) \to \gamma(\vec{k};v)(p_0,q_0,p_x,q_x)$ in Eq. (M.57) and defining the small parameters $\mathfrak{K}(k;v) \equiv k_0/\gamma(\vec{k};v)$ and $\mathfrak{U}(\vec{k};v) \equiv \widetilde{\Delta}(\vec{k};v)/\gamma(\vec{k};v)$, the latter can be written as

$$\begin{aligned}\mathrm{Im}\left[\Sigma_1^{\mathrm{2L}}(k)\right] &= \frac{\pi^2(N_c^2-1)w(v)^2\gamma(\vec{k};v)}{N_c^2 N_f^2} \int_{\mathbb{R}} \frac{\mathrm{d}q_0}{(2\pi)} \int_{\mathbb{R}} \frac{\mathrm{d}p_0}{(2\pi)} \int_{\mathbb{R}} \frac{\mathrm{d}q_x}{(2\pi)} \int_{\mathbb{R}} \frac{\mathrm{d}p_x}{(2\pi)} \\ &\left\{\frac{[2(p_0+q_0)+3\mathfrak{K}(k;v)]}{|q_0|+|q_x|+w(v)^{-1}\mathfrak{U}(k;v)} \frac{[\Theta(p_0+2q_0+2\mathfrak{K}(k;v))-\Theta(-\mathfrak{K}(k;v)-p_0)]}{(3\mathfrak{K}(k;v)+2p_0+2q_0)^2+[2w(v)(p_x+q_x)+1]^2}\right. \\ &\left.\times \frac{[\Theta(p_0+q_0+\mathfrak{K}(k;v))-\Theta(-\mathfrak{K}(k;v)-q_0)]}{|p_0|+|p_x|+w(v)^{-1}\mathfrak{U}(\vec{k};v)}\right\}.\end{aligned} \tag{M.62}$$

In the small $\mathfrak{U}(\vec{k};v)$ limit, the dependence of the integral on this parameter can be ignored. On the other hand, the integrand vanishes when $\mathfrak{K}(k;v)$ vanishes, owing to

the fact that the integral is proportional to k_0 rather than to $\gamma(\vec{k};v)$. Therefore, we integrate over q_x and p_x for nonzero $\mathfrak{K}(k;v)$. This yields

$$\begin{aligned}\mathrm{Im}\left[\Sigma_1^{\mathrm{2L}}(k)\right] = \frac{\pi^2(N_c^2-1)w(v)^2\gamma(\vec{k};v)}{N_c^2N_f^2}\int\limits_{\mathbb{R}}\frac{\mathrm{d}q_0}{(2\pi)}\int\limits_{\mathbb{R}}\frac{\mathrm{d}p_0}{(2\pi)}\Bigg\{\frac{[3\mathfrak{K}(k;v)+2(p_0+q_0)]}{1+[3\mathfrak{K}(k;v)+2(p_0+q_0)]^2}\\ \times\left[\Theta(p_0+2q_0+2\mathfrak{K}(k;v))-\Theta(-\mathfrak{K}(k;v)-p_0)\right]\\ \times\left[\Theta(p_0+q_0+\mathfrak{K}(k;v))-\Theta(-\mathfrak{K}(k;v)-q_0)\right]\Bigg\}.\end{aligned} \tag{M.63}$$

We proceed on integrating over q_0 and p_0 with a UV cutoff $\Lambda_f/\gamma(\vec{k};v)\gg 1$. To perform the integrations it is convenient to change variables to $X=p_0+q_0$ and $Y=p_0-q_0$ so that Eq. (M.63) reads

$$\begin{aligned}\mathrm{Im}\left[\Sigma_1^{\mathrm{2L}}(k)\right] = \frac{\pi^2(N_c^2-1)w(v)^2\gamma(\vec{k};v)}{2N_c^2N_f^2}\times\Bigg[\int\limits_0^{\frac{2\Lambda_f}{\gamma(\vec{k};v)}}\frac{\mathrm{d}X}{(2\pi)}+\int\limits_{X-\frac{2\Lambda_f}{\gamma(\vec{k};v)}}^{\frac{2\Lambda_f}{\gamma(\vec{k};v)}-X}\frac{\mathrm{d}Y}{(2\pi)}\\ +\int\limits_{-\frac{2\Lambda_f}{\gamma(\vec{k};v)}}^{0}\frac{\mathrm{d}X}{(2\pi)}+\int\limits_{-X-\frac{2\Lambda_f}{\gamma(\vec{k};v)}}^{\frac{2\Lambda_f}{\gamma(\vec{k};v)}+X}\frac{\mathrm{d}Y}{(2\pi)}\Bigg]\Bigg\{\frac{[3\mathfrak{K}(k_0,\vec{k})+2X]}{1+[3\mathfrak{K}(k;v)+2X]^2}\\ \times\left[\Theta\left(\frac{3X}{2}+\frac{Y}{2}+2\mathfrak{K}(k;v)\right)-\Theta\left(-\mathfrak{K}(k_0,\vec{k})-\frac{X}{2}-\frac{Y}{2}\right)\right]\\ \times\left[\Theta\left[X+\mathfrak{K}(k;v)\right]-\Theta\left(-\mathfrak{K}(k;v)-\frac{X}{2}+\frac{Y}{2}\right)\right]\Bigg\}.\end{aligned} \tag{M.64}$$

Integrations over X and Y are straightforward to perform. In the small $\mathfrak{K}(k;v)$ and large $\Lambda_f/\gamma(k;v)$ limits the divergent contribution to the imaginary part of the two-loop fermion self-energy is given by

$$\mathrm{Im}\left[\Sigma_1^{\mathrm{2L}}(k)\right] = \frac{(N_c^2-1)w(v)^2\log[w(v)]^2}{8\pi^2N_c^2N_f^2}k_0\log\left(\frac{\Lambda_f}{|\gamma(\vec{k};v)|}\right), \tag{M.65}$$

where we use the fact that $\gamma(\vec{k};v)\mathfrak{K}(k;v)=k_0$ and that the $\gamma(\vec{k};v)<0$ yields the exact same result.

(*iii*) For $|\widetilde{\Delta}(\vec{k};v)|\gg|k_0|$ and $|\widetilde{\Delta}(\vec{k};v)|\gg|\gamma(\vec{k};v)|$ let us assume without loss of generality that $k_0>0$, $\gamma(\vec{k};v)>0$ and $\widetilde{\Delta}(\vec{k};v)>0$, and let us define the small parameters $\mathfrak{v}(\vec{k};v)\equiv\gamma(\vec{k};v)/\widetilde{\Delta}(\vec{k};v)$ and $\mathfrak{M}(k;v)\equiv k_0/\widetilde{\Delta}(\vec{k};v)$. To make Eq. (M.57) depend explicitly on these parameters, we perform the change of variables $(q_x,p_x)\to(p_x/w(v),q_x/w(v))$ followed by the scaling $(p_0,q_0,p_x,q_x)\to\widetilde{\Delta}(\vec{k};v)(p_0,q_0,p_x,q_x)$. Do-

ing so, Eq. (M.57) reads

$$\begin{aligned}\mathrm{Im}\left[\Sigma_1^{\mathrm{2L}}(k)\right] = \frac{\pi^2(N_c^2-1)w(v)^2\widetilde{\Delta}(\vec{k};v)}{N_c^2N_f^2}\int\limits_{\mathbb{R}}\frac{\mathrm{d}q_0}{(2\pi)}\int\limits_{\mathbb{R}}\frac{\mathrm{d}p_0}{(2\pi)}\int\limits_{\mathbb{R}}\frac{\mathrm{d}q_x}{(2\pi)}\int\limits_{\mathbb{R}}\frac{\mathrm{d}p_x}{(2\pi)}\\ \left\{\frac{[2(p_0+q_0)+3\mathfrak{M}(k;v)]}{w(v)|q_0|+|q_x|+1}\frac{[\Theta(p_0+q_0+\mathfrak{M}(k;v))-\Theta(-\mathfrak{M}(k;v)-q_0)]}{w(v)|p_0|+|p_x|+1}\right.\\ \left.\times\frac{[\Theta(p_0+2q_0+2\mathfrak{M}(k;v))-\Theta(-\mathfrak{M}(k;v)-p_0)]}{(3\mathfrak{M}(k;v)+2p_0+2q_0)^2+[2(p_x+q_x)+\mathfrak{v}(\vec{k};v)]^2}\right\}.\end{aligned} \tag{M.66}$$

In the small $\mathfrak{v}(\vec{k};v)$ limit, we can neglect this term inside the integrand. On the other hand, in the small $\mathfrak{M}(k;v)$ limit, the imaginary part of the two-loop fermion self-energy vanishes in this limit. Therefore we keep $\mathfrak{M}(k;v)$ nonzero and after performing the scaling $(p_0,q_0)\to(p_0/w(v),q_0/w(v))$ and integrating over q_x and p_x we find

$$\begin{aligned}\mathrm{Im}\left[\Sigma_1^{\mathrm{2L}}(k)\right] = \frac{\pi^2(N_c^2-1)w(v)\log[w(v)]^2\widetilde{\Delta}(\vec{k};v)}{N_c^2N_f^2}\int\limits_{\mathbb{R}}\frac{\mathrm{d}q_0}{(2\pi)}\int\limits_{\mathbb{R}}\frac{\mathrm{d}p_0}{(2\pi)}\\ \left\{\frac{[\Theta(p_0+2q_0+2\mathfrak{W}(k;v))-\Theta(-\mathfrak{W}(k;v)-p_0)]}{4w(v)^2(|p_0|-|q_0|)^2+(3\mathfrak{W}(k;v)+2(p_0+q_0))^2}\right.\\ \left.\times\frac{[\Theta(p_0+q_0+\mathfrak{W}(k;v))-\Theta(-\mathfrak{W}(k;v)-q_0)]\,[2(p_0+q_0)+3\mathfrak{W}(k;v)]^3}{(3\mathfrak{W}(k;v)+2p_0+2q_0)^2+16w(v)^2+4w(v)^2[|p_0|+|q_0|][4+|p_0|+|q_0|]}\right\},\end{aligned} \tag{M.67}$$

in the $w(v)\ll 1$ limit while keeping $\mathfrak{W}(k;v)\equiv w(v)\mathfrak{M}(k;v)$ nonzero. Proceeding with the integrations over q_0 and p_0 is not straightforward for nonzero $\mathfrak{W}(k;v)$. To leading order in $\mathfrak{W}(k;v)\ll 1$ we can cast Eq. (M.67) as

$$\begin{aligned}\mathrm{Im}\left[\Sigma_1^{\mathrm{2L}}(k)\right] = \frac{(N_c^2-1)w(v)^2\log[w(v)]^2k_0}{(1+w(v)^2)N_c^2N_f^2}\\ \left\{\int\limits_0^{\frac{\Lambda_f w(v)}{\widetilde{\Delta}(\vec{k};v)}}\frac{\mathrm{d}p_0}{(2\pi)}\left[\frac{p_0}{[(1+w(v)^2)p_0^2+4w(v)^2(1+p_0)]}\right]+\int\limits_0^{\frac{\Lambda_f w(v)}{\widetilde{\Delta}(\vec{k};v)}}\frac{\mathrm{d}p_0}{(2\pi)}\frac{3(p_0-1)^6p_0}{4\pi(1+w(v)^2)^2}\right.\\ \left.\times\left[\frac{1}{[w(v)^2(1+p_0)^2+(p_0-1)^2]^3\,[w(v)^2(2+p_0)^2+p_0^2]}\right]\right\},\end{aligned} \tag{M.68}$$

where we used the fact that $\widetilde{\Delta}(\vec{k};v)\mathfrak{W}(k;v)=w(v)k_0$. The remaining integration over p_0 is divergent in the UV and thus it is cutoff by the ratio $\Lambda_f w(v)/\widetilde{\Delta}(\vec{k};v)$. To the leading order in $w(v)\ll 1$ and $\Lambda_f/\widetilde{\Delta}(\vec{k};v)\gg 1$, the integration over p_0 yields the following divergent contribution,

$$\mathrm{Im}\left[\Sigma_1^{\mathrm{2L}}(k)\right] = \frac{(N_c^2-1)w(v)^2\log[w(v)]^2}{8\pi^2N_c^2N_f^2}k_0\log\left(\frac{\Lambda_f}{|\widetilde{\Delta}(\vec{k};v)|}\right). \tag{M.69}$$

Here, we have used the fact that the $\widetilde{\Delta}(\vec{k};v)<0$ case yields the same contribution.

The computation for all the other hot spots follows the same logic. Therefore, we can summarize Eqs. (M.61), (M.65) and (M.69) as

$$\mathrm{Im}\left[\Sigma_1^{\mathrm{2L}}(k)\right] = \frac{(N_c^2-1)w(v)^2\log[w(v)]^2}{8\pi^2 N_c^2 N_f^2} k_0 \log\left(\frac{\Lambda_f}{\mathscr{H}_0[|k_0|,|\delta_N(\vec{k};v)|,v|e_{\overline{N}}(\vec{k};v)|]}\right), \tag{M.70}$$

where $\delta_N(\vec{k};v) = e_N(\vec{k};v) + 2e_{\overline{N}}(\vec{k};v)$. Here $\mathscr{H}_0(x,y,u) \sim \max(x,y,u)$ whenever any of the three arguments is larger than the other two. Combining this result with Eq. (J.18), the two-loop contribution to the counterterm function $A_N^{(1)}(k_N)$ is given by

$$A_N^{(1);\mathrm{2L}}(k_N) = \frac{(N_c^2-1)w(v)^2\log[w(v)]^2}{8\pi^2 N_c^2 N_f^2} k_0 \log\left(\frac{\Lambda_f}{\mathscr{G}_4(|k_0|,2v|k_N|)}\right), \tag{M.71}$$

where $\mathscr{G}_4(x,y) = \mathscr{H}_0(x,y,0)$ and we have used the fact that, at the momentum at which the RG conditions are imposed, $|\delta_N(\vec{k};v)| \gg v|e_{\overline{N}}(\vec{k};v)|$.

B. $\mathrm{Re}\left[\Sigma_1^{\mathrm{2L}}(k)\right]$

From Eq. (M.55) we read off the real part of the two-loop fermion self-energy:

$$\begin{aligned}\mathrm{Re}\left[\Sigma_1^{\mathrm{2L}}(k)\right] = -\frac{\pi^2(N_c^2-1)w(v)^2}{N_c^2N_f^2}\int_{\mathbb{R}}\frac{\mathrm{d}q_0}{(2\pi)}\int_{\mathbb{R}}\frac{\mathrm{d}p_0}{(2\pi)}\int_{\mathbb{R}}\frac{\mathrm{d}q_x}{(2\pi)}\int_{\mathbb{R}}\frac{\mathrm{d}p_x}{(2\pi)}\\ \left\{\frac{[\Theta(p_0+2q_0+2k_0)-\Theta(-k_0-p_0)]}{|q_0|+|q_x|+|\overline{\Delta}(\vec{k};v)|}\frac{[\Theta(p_0+q_0+k_0)-\Theta(-k_0-q_0)]}{|p_0|+|p_x|+|\overline{\Delta}(\vec{k};v)|}\right.\\ \left.\times\frac{[2w(v)(p_x+q_x)+\gamma(\vec{k};v)]}{(3k_0+2p_0+2q_0)^2+[2w(v)(p_x+q_x)+\gamma(\vec{k};v)]^2}\right\}.\end{aligned} \tag{M.72}$$

In the small $w(v)$ limit we drop the term of order $w(v)(p_x+q_x)$ in the numerator. Furthermore, let us note that the integrations over q_x and p_x are manifestly convergent for nonzero $w(v)$. When $w(v)=0$, the integrations along these directions become logarithmically divergent at large momenta. Hence, we expect that a momentum scale proportional to $1/w(v)$ will cutoff such divergences. Following the logic used in Appendix G, we scale out $w(v)$ from the integration through $(p_x,q_x)\to(p_x/w(v),q_x/w(v))$. After such a rescaling we can write the real part of the two-loop fermions self-energy as

$$\begin{aligned}\mathrm{Re}\left[\Sigma_1^{\mathrm{2L}}(k)\right] = -\frac{\pi^2(N_c^2-1)w(v)^2\gamma(\vec{k};v)}{N_c^2N_f^2}\int_{\mathbb{R}}\frac{\mathrm{d}q_0}{(2\pi)}\int_{\mathbb{R}}\frac{\mathrm{d}p_0}{(2\pi)}\int_{\mathbb{R}}\frac{\mathrm{d}q_x}{(2\pi)}\int_{\mathbb{R}}\frac{\mathrm{d}p_x}{(2\pi)}\\ \left\{\frac{1}{w(v)|q_0|+|q_x|+|\widetilde{\Delta}(\vec{k};v)|}\frac{[\Theta(p_0+q_0+k_0)-\Theta(-k_0-q_0)]}{w(v)|p_0|+|p_x|+|\widetilde{\Delta}(\vec{k};v)|}\right.\\ \left.\times\frac{[\Theta(p_0+2q_0+2k_0)-\Theta(-k_0-p_0)]}{(3k_0+2p_0+2q_0)^2+[2(p_x+q_x)+\gamma(\vec{k};v)]^2}\right\},\end{aligned} \tag{M.73}$$

where $\widetilde{\Delta}(\vec{k};v) \equiv w(v)\overline{\Delta}(\vec{k};v) = v\Delta(\vec{k};v)$. We proceed on analyzing this expression for (*i*) $|k_0| \gg |\gamma(\vec{k};v)|$ and $|k_0| \gg |\widetilde{\Delta}(\vec{k};v)|$, (*ii*) $|\gamma(\vec{k};v)| \gg |k_0|$ and $|\gamma(\vec{k};v)| \gg |\widetilde{\Delta}(\vec{k};v)|$, and (*iii*) $|\widetilde{\Delta}(\vec{k};v)| \gg |k_0|$ and $|\widetilde{\Delta}(\vec{k};v)| \gg |\gamma(\vec{k};v)|$.

(*i*) For $|k_0| \gg |\gamma(\vec{k};v)|$ and $|k_0| \gg |\widetilde{\Delta}(\vec{k};v)|$ we assume, without loss of generality that $k_0 > 0$, $\gamma(\vec{k};v) > 0$ and $\widetilde{\Delta}(\vec{k};v) > 0$, and define the two small parameters $\mathfrak{C}(k;v) \equiv \gamma(\vec{k};v)/k_0$ and $\mathfrak{D}(k;v) \equiv \widetilde{\Delta}(\vec{k};v)/k_0$. The expression in Eq. (M.73) manifestly depends on these two parameters once we perform the scalings $(p_0, p_x) \to k_0(p_0, p_x)$ and $(q_0, q_x) \to k_0(q_0, q_x)$:

$$\begin{aligned}\mathrm{Re}\left[\Sigma_1^{\mathrm{2L}}(k)\right] = &-\frac{\pi^2(N_c^2-1)w(v)^2\gamma(\vec{k};v)}{N_c^2N_f^2}\int_{\mathbb{R}}\frac{\mathrm{d}q_0}{(2\pi)}\int_{\mathbb{R}}\frac{\mathrm{d}p_0}{(2\pi)}\int_{\mathbb{R}}\frac{\mathrm{d}q_x}{(2\pi)}\int_{\mathbb{R}}\frac{\mathrm{d}p_x}{(2\pi)}\\ &\left\{\frac{[\Theta(p_0+2q_0+2)-\Theta(-1-p_0)]}{w(v)|q_0|+|q_x|+\mathfrak{D}(k;v)}\frac{[\Theta(p_0+q_0+1)-\Theta(-1-q_0)]}{w(v)|p_0|+|p_x|+\mathfrak{D}(k;v)}\right.\\ &\left.\times\frac{1}{(3+2p_0+2q_0)^2+[2(p_x+q_x)+\mathfrak{C}(k;v)]^2}\right\}.\end{aligned} \tag{M.74}$$

For small $\mathfrak{C}(k;v)$ and $\mathfrak{D}(k;v)$ we can drop these terms inside the integrand and integrate over q_x, p_x and q_0. The leading order contribution in $w(v) \ll 1$ is given by

$$\begin{aligned}\mathrm{Re}\left[\Sigma_1^{\mathrm{2L}}(k)\right] = &-\frac{(N_c^2-1)\log[w(v)]^2w(v)^2\gamma(\vec{k};v)}{2\pi N_c^2N_f^2}\int_{\mathbb{R}}\frac{\mathrm{d}p_0}{(2\pi)}\left\{\frac{\Theta\left(-\frac{3}{2}-p_0\right)}{1+2p_0}\right.\\ &\left.+\frac{1+2p_0\Theta(p_0)-2(1+p_0)\Theta(1+p_0)}{(1+2p_0)}\Theta\left(p_0+\frac{3}{2}\right)\right\}.\end{aligned} \tag{M.75}$$

Upon symmetrizing in p_0, the integrand decays as $1/p_0$ for $p_0 \gg 1$. Therefore, we cut off the integration in the large frequency limit with the ratio Λ_f/k_0. In the $\Lambda_f/k_0 \gg 1$ limit a straightforward integration yields the logarithmically divergent contribution

$$\mathrm{Re}\left[\Sigma_1^{\mathrm{2L}}(k)\right] = -\frac{(N_c^2-1)\log[w(v)]^2w(v)^2}{8\pi^2N_c^2N_f^2}\gamma(\vec{k};v)\log\left(\frac{\Lambda_f}{|k_0|}\right), \tag{M.76}$$

where we have used the fact that the $k_0 < 0$ case yields the same result.

(*ii*) For $|\gamma(\vec{k};v)| \gg |k_0|$ and $|\gamma(\vec{k};v)| \gg |\widetilde{\Delta}(\vec{k};v)|$ we assume, without loss of generality that $k_0 > 0$, $\gamma(\vec{k};v) > 0$ and $\widetilde{\Delta}(\vec{k};v) > 0$, and define the two small parameters $\mathfrak{K}(k;v) \equiv k_0/\gamma(\vec{k};v)$ and $\mathfrak{U}(\vec{k};v) \equiv \widetilde{\Delta}(\vec{k};v)/\gamma(\vec{k};v)$. By performing the scalings $(p_0, p_x, q_0, q_x) \to \gamma(\vec{k};v)(p_0, p_x, q_0, q_x)$ in Eq. (M.73), the real part of the two-loop fermion self-energy is written in terms of these small parameters as

$$\begin{aligned}\mathrm{Re}\left[\Sigma_1^{\mathrm{2L}}(k)\right] = &-\frac{\pi^2(N_c^2-1)w(v)^2\gamma(\vec{k};v)}{N_c^2N_f^2}\int_{\mathbb{R}}\frac{\mathrm{d}q_0}{(2\pi)}\int_{\mathbb{R}}\frac{\mathrm{d}p_0}{(2\pi)}\int_{\mathbb{R}}\frac{\mathrm{d}q_x}{(2\pi)}\int_{\mathbb{R}}\frac{\mathrm{d}p_x}{(2\pi)}\\ &\left\{\frac{1}{w(v)|q_0|+|q_x|+\mathfrak{U}(\vec{k};v)}\frac{\{\Theta[p_0+q_0+\mathfrak{K}(k;v)]-\Theta[-\mathfrak{K}(k;v)-q_0]\}}{w(v)|p_0|+|p_x|+\mathfrak{U}(\vec{k};v)}\right.\\ &\left.\times\frac{\{\Theta[p_0+2q_0+2\mathfrak{K}(k;v)]-\Theta[-\mathfrak{K}(k;v)-p_0]\}}{[3\mathfrak{K}(k;v)+2p_0+2q_0]^2+[2(p_x+q_x)+1]^2}\right\}.\end{aligned} \tag{M.77}$$

In the small $\mathfrak{K}(k;v)$ and $\mathfrak{U}(\vec{k};v)$ limits, we can ignore these parameters in the integrand and integrate along the p_x, q_x and q_0 directions. In the $w(v) \ll 1$ limit, the leading order contribution is given by

$$\mathrm{Re}\left[\Sigma_1^{\mathrm{2L}}(k)\right] = -\frac{(N_c^2-1)w(v)^2\log[w(v)]^2\gamma(\vec{k};v)}{8\pi N_c^2 N_f^2}\int\limits_{\mathbb{R}^+}\frac{\mathrm{d}p_0}{\pi}\left[\pi - 2\arctan(2p_0)\right]. \quad \text{(M.78)}$$

The integration over p_0 is divergent in the UV and it is cutoff by $\Lambda_f/\gamma(\vec{k};v)$. For $\Lambda_f/\gamma(\vec{k};v) \gg 1$ we obtain the logarithmically divergent contribution

$$\mathrm{Re}\left[\Sigma_1^{\mathrm{2L}}(k)\right] = -\frac{(N_c^2-1)\log[w(v)]^2 w(v)^2}{8\pi^2 N_c^2 N_f^2}\gamma(\vec{k})\log\left(\frac{\Lambda_f}{|\gamma(\vec{k};v)|}\right), \quad \text{(M.79)}$$

where we have used the fact that the same result is obtained for $\gamma(\vec{k};v) < 0$.

(iii) For $|\widetilde{\Delta}(\vec{k};v)| \gg |\gamma(\vec{k};v)|$ and $|\widetilde{\Delta}(\vec{k};v)| \gg |k_0|$ we assume, without loss of generality that $k_0 > 0$, $\gamma(\vec{k};v) > 0$ and $\widetilde{\Delta}(\vec{k};v) > 0$, and define the two small parameters $\mathfrak{v}(\vec{k};v) \equiv \gamma(\vec{k};v)/\widetilde{\Delta}(\vec{k};v)$ and $\mathfrak{M}(k;v) \equiv k_0/\widetilde{\Delta}(\vec{k};v)$. Scaling out $\widetilde{\Delta}(\vec{k};v)$ via the transformations $(p_0,p_x,q_0,q_x) \to \widetilde{\Delta}(\vec{k};v)(p_0,p_x,q_0,q_x)$ allows us to write Eq. (M.73) as

$$\begin{aligned}\mathrm{Re}\left[\Sigma_1^{\mathrm{2L}}(k)\right] = &-\frac{\pi^2(N_c^2-1)w(v)^2\gamma(\vec{k};v)}{N_c^2N_f^2}\int\limits_{\mathbb{R}}\frac{\mathrm{d}q_0}{(2\pi)}\int\limits_{\mathbb{R}}\frac{\mathrm{d}p_0}{(2\pi)}\int\limits_{\mathbb{R}}\frac{\mathrm{d}q_x}{(2\pi)}\int\limits_{\mathbb{R}}\frac{\mathrm{d}p_x}{(2\pi)}\\ &\left\{\frac{1}{w(v)|q_0|+|q_x|+1}\times\frac{\{\Theta[p_0+q_0+\mathfrak{M}(k;v)]-\Theta[-\mathfrak{M}(k;v)-q_0]\}}{w(v)|p_0|+|p_x|+1}\right.\\ &\left.\times\frac{\{\Theta[p_0+2q_0+2\mathfrak{M}(k;v)]-\Theta[-\mathfrak{M}(k;v)-p_0]\}}{[3\mathfrak{M}(k;v)+2p_0+2q_0]^2+[2(p_x+q_x)+\mathfrak{v}(\vec{k};v)]^2}\right\}.\end{aligned} \quad \text{(M.80)}$$

In the $\mathfrak{M}(k;v) \ll 1$ and $\mathfrak{v}(\vec{k};v) \ll 1$ limits we can drop these terms in the integrand. The computation of the remaining integrals is done by first performing the scaling $(p_0,q_0) \to (p_0/w(v), q_0/w(v))$. Under this rescaling we have

$$\begin{aligned}\mathrm{Re}\left[\Sigma_1^{\mathrm{2L}}(k)\right] = &-\frac{\pi^2(N_c^2-1)w(v)^2\gamma(\vec{k};v)}{N_c^2N_f^2}\int\limits_{\mathbb{R}}\frac{\mathrm{d}q_0}{(2\pi)}\int\limits_{\mathbb{R}}\frac{\mathrm{d}p_0}{(2\pi)}\int\limits_{\mathbb{R}}\frac{\mathrm{d}q_x}{(2\pi)}\int\limits_{\mathbb{R}}\frac{\mathrm{d}p_x}{(2\pi)}\\ &\left\{\frac{1}{|q_0|+|q_x|+1}\times\frac{[\Theta(p_0+q_0)-\Theta(-q_0)]}{|p_0|+|p_x|+1}\frac{[\Theta(p_0+2q_0)-\Theta(-p_0)]}{4(p_0+q_0)^2+4w(v)^2(p_x+q_x)^2}\right\}.\end{aligned} \quad \text{(M.81)}$$

To the leading order in $w(v) \ll 1$, the integrations over q_x and p_x yield:

$$\begin{aligned}\mathrm{Re}\left[\Sigma_1^{\mathrm{2L}}(k)\right] = &-\frac{(N_c^2-1)w(v)^2\log[w(v)]^2\gamma(\vec{k};v)}{4N_c^2N_f^2}\int\limits_{\mathbb{R}}\frac{\mathrm{d}q_0}{(2\pi)}\int\limits_{\mathbb{R}}\frac{\mathrm{d}p_0}{(2\pi)}\left\{\frac{1}{4+|q_0|+|p_0|}\right.\\ &\left.\times\frac{(p_0+q_0)^2[\Theta(p_0+2q_0)-\Theta(-p_0)][\Theta(p_0+q_0)-\Theta(-q_0)]}{[(p_0+q_0)^2+w(v)^2(|q_0|-|p_0|)^2]\,[(p_0+q_0)^2+4w(v)^2+w(v)^2(|p_0|+|q_0|)]}\right\}.\end{aligned} \quad \text{(M.82)}$$

When the terms proportional to $w(v)$ are dropped in the denominator, the integrations over p_0 and q_0 become IR divergent. The integration over q_0 yields, after symmetrizing the result in p_0,

$$\begin{aligned}\mathrm{Re}\left[\Sigma_1^{\mathrm{2L}}(k)\right] = &-\frac{(N_c^2-1)w(v)\log[w(v)]^2\gamma(\vec{k};v)}{16\pi N_c^2 N_f^2}\int\limits_{\mathbb{R}^+}\frac{\mathrm{d}p_0}{(2\pi)}\\ &\left\{\frac{2p_0 w(v)\left\{\log\left[p_0^2+(p_0+2)^2w(v)^2\right]\right.}{(1+p_0)\left[w(v)^2+1\right]\left[(1+p_0)^2w(v)^2+(p_0-1)^2\right]}\right.\\ &+\frac{\left.-\log\left[p_0^2+p_0^2w(v)^2\right]\right\}+\pi\left[(p_0+1)^2w(v)^2+(p_0-1)^2\right]}{(1+p_0)\left[w(v)^2+1\right]\left[(1+p_0)^2w(v)^2+(p_0-1)^2\right]}\\ &+\frac{-2\left[(p_0+1)w(v)^2-p_0+1\right]\arctan\left(\frac{p_0\left[w(v)^2+1\right]}{2w(v)}+w(v)\right)}{(1+p_0)\left[w(v)^2+1\right]\left[(1+p_0)^2w(v)^2+(p_0-1)^2\right]}\\ &\left.+\frac{-2p_0\left[(p_0+1)w(v)^2+p_0-1\right]\operatorname{arccot}\left(\frac{2w(v)}{1-w(v)^2}\right)}{(1+p_0)\left[w(v)^2+1\right]\left[(1+p_0)^2w(v)^2+(p_0-1)^2\right]}\right\}.\end{aligned} \tag{M.83}$$

This contribution is IR finite, but UV divergent. It is noted that the $p_0\to 0$, $p_0\to\infty$ and $w(v)\to 0$ limits in the integrand do not commute. Thus, one has to integrate over p_0 and only at the final stage expand for small $w(v)$. Nevertheless, we can bypass this difficulty by performing the scaling $p_0\to p_0 w(v)$ and then expanding safely for $w(v)\ll 1$. To leading order in $w(v)\ll 1$, this yields

$$\mathrm{Re}\left[\Sigma_1^{\mathrm{2L}}(k)\right] = -\frac{(N_c^2-1)w(v)^2\log[w(v)]^2\gamma(\vec{k};v)}{16\pi N_c^2 N_f^2}\int\limits_0^{\frac{\Lambda_f}{\widetilde{\Delta}(\vec{k};v)}}\frac{\mathrm{d}p_0}{(2\pi)}\left[\pi-2\arctan\left(\frac{p_0}{2}\right)\right], \tag{M.84}$$

where the p_0 integration has been cut off in the UV by the ratio $\Lambda_f/\widetilde{\Delta}(\vec{k};v)$. For $\Lambda_f/\widetilde{\Delta}(\vec{k};v)\gg 1$, we obtain the logarithmically divergent piece

$$\mathrm{Re}\left[\Sigma_1^{\mathrm{2L}}(k)\right] = -\frac{(N_c^2-1)\log[w(v)]^2 w(v)^2}{8\pi^2 N_c^2 N_f^2}\gamma(\vec{k};v)\log\left(\frac{\Lambda_f}{|\widetilde{\Delta}(\vec{k};v)|}\right). \tag{M.85}$$

The absolute value in the IR scales arises from the fact that the same result is obtained in the case that $\widetilde{\Delta}(\vec{k};v)<0$.

Collecting the results from Eqs. (M.76), (M.79) and (M.85), and using the fact that the computations for the other seven hot spots follow the same logic, we can write the logarithmically divergent contribution to the real part of the two-loop fermion self-energy in Eq. (M.72) as

$$\mathrm{Re}\left[\Sigma_N^{\mathrm{2L}}(k)\right] = -\frac{(N_c^2-1)\log[w(v)]^2 w(v)^2}{8\pi^2 N_c^2 N_f^2}\delta_N(\vec{k})\log\left(\frac{\Lambda_f}{\mathscr{H}_0'[k_0,|\delta_N(\vec{k};v)|,v|e_{\overline{N}}(\vec{k};v)|]}\right), \tag{M.86}$$

where $\delta_N(\vec{k};v) \equiv e_N(\vec{k};v) + 2e_{\overline{N}}(\vec{k};v)$. Here $\mathscr{H}_0'(x,y,u) \sim \max(x,y,u)$ whenever any of x, y or u is much larger than the other two. Combining this result with Eqs. (J.19) and (J.20), the momentum-dependent counterterm functions $A_N^{(2)}(k_N)$ and $A_N^{(3)}(k_N)$ are given at two-loop order by

$$A_2^{(2);2\mathrm{L}}(k_N) = \frac{3(N_c^2-1)\log[w(v)]^2 w(v)^2}{8\pi^2 N_c^2 N_f^2} \log\left(\frac{\Lambda_f}{\mathscr{G}_3(k_0, 2v|k_N|)}\right), \tag{M.87}$$

$$A_2^{(2);2\mathrm{L}}(k_N) = -\frac{(N_c^2-1)\log[w(v)]^2 w(v)^2}{8\pi^2 N_c^2 N_f^2} \log\left(\frac{\Lambda_f}{\mathscr{G}_3(k_0, 2v|k_N|)}\right), \tag{M.88}$$

where we have used the fact that at the momentum at which the RG conditions are imposed, $|\delta_N(\vec{k};v)| \gg |e_{\overline{N}}(\vec{k};v)|$ and we have defined $\mathscr{G}_3(x,y) \equiv \mathscr{H}_0'(x,y,0)$.

M.3 One-loop Yukawa Vertex

The one-loop quantum correction depicted in Fig. 2.3(*b*) contributes to the quantum effective action through

$$\delta\mathbf{\Gamma}_{1\mathrm{L}}^{(2,1)} = \sum_{N=1}^{8}\sum_{\sigma,\sigma'=1}^{N_c}\sum_{j=1}^{N_f}\int \mathrm{d}k \int \mathrm{d}k' \psi^\dagger_{N,\sigma,j}(k')\Phi_{\sigma\sigma'}(k'-k)\Gamma_N^{(2,1),1\mathrm{L}}(k',k)\psi_{\overline{N},\sigma',j}(k), \tag{M.89}$$

where the one-loop vertex function is given by

$$\Gamma_N^{(2,1),1\mathrm{L}}(k',k) = -\frac{\pi^{\frac{3}{2}} v^{\frac{3}{2}}}{\sqrt{2}N_c N_f^{\frac{3}{2}}} \int \mathrm{d}p D(p) G_{\overline{N}}^{(0)}(k'+p;v) G_N(k+p;v). \tag{M.90}$$

In here $D(q)$ is given by Eq. (2.6) and $G_N^{(0)}(k;v)$ is given in Eq. (M.3). For simplicity and without any loss of generality we consider the contribution to interaction vertex for the $N=1$ hot spot. In view of the RG condition given in Eq. (4.57) it is convenient to compute this diagram with fixed external frequencies $q_0 = k_0 = \mu > 0$ and at momenta $k_y = vk_x$ and $k_y' = -vk_x'$. At these frequencies and momenta,

$$\begin{aligned}\Gamma_1^{(2,1),1\mathrm{L}}(k_x',k_x;\mu) = -\frac{\pi^{\frac{3}{2}} v^{\frac{3}{2}}}{\sqrt{2}N_c N_f^{\frac{3}{2}}} \int \mathrm{d}p \Bigg\{ &\frac{1}{|p_0| + c(v)(|p_x|+|p_y|)} \\ &\frac{1}{i(p_0+\mu) + [2vk_x' + vp_x - p_y]} \frac{1}{i(p_0+\mu) + [2vk_x + vp_x + p_y]}\Bigg\}.\end{aligned} \tag{M.91}$$

We proceed in computing this quantum correction with the same logic we have used in the case of the two-loop fermion self-energy. For this purpose we perform the shift $p_y \to p_y - vp_x - 2vk_x$, and perform the scaling $p_x \to p_x/c(v)$. After performing these transformations, Eq. (M.91) reads

$$\begin{aligned}\Gamma_1^{(2,1),1\mathrm{L}}(k_x',k_x;\mu) = -\frac{\pi^{\frac{3}{2}}\sqrt{v}w(v)}{\sqrt{2}N_c N_f^{\frac{3}{2}}} \int \mathrm{d}p \Bigg\{ &\frac{1}{|p_0| + |p_x| + c(v)|p_y - w(v)p_x - 2vk_x|} \\ &\times \frac{1}{i(p_0+\mu) + [2v(k_x'+k_x) + 2w(v)p_x - p_y]} \frac{1}{i(p_0+\mu) + p_y}\Bigg\}.\end{aligned} \tag{M.92}$$

Here we used the definition $w(v) = v/c(v)$. The convergence of the q_y and q_x integrations are not affected by the terms of order $c(v)p_y$ and $vw(v)p_x$ inside the boson propagator and thus we drop them. Using the lesson from the computation of the real part of the two-loop fermion self-energy we define the following energy scales $\rho(k'_x, k_x; v) = v(k'_x + k_x)$ and $\zeta(k_x; v) = v^2 k_x$ and perform the scaling $p_x \to p_x/w(v)$ so that Eq. (M.92) reads

$$\Gamma_1^{(2,1),1\mathrm{L}}(k'_x, k_x; \mu) = -\frac{\pi^{\frac{3}{2}}\sqrt{v}w(v)}{\sqrt{2}N_c N_f^{\frac{3}{2}}} \int \mathrm{d}p \left\{ \frac{1}{w(v)|p_0| + |p_x| + 2|\zeta(k_x; v)|} \times \frac{1}{i(p_0+\mu) + p_y} \frac{1}{i(p_0+\mu) + [2[\rho(k'_x, k_x; v) + p_x] - p_y]} \right\}. \tag{M.93}$$

Integration over q_y yields

$$\Gamma_1^{(2,1),1\mathrm{L}}(k'_x, k_x; \mu) = \frac{\pi^{\frac{3}{2}}\sqrt{v}w(v)}{2\sqrt{2}N_c N_f^{\frac{3}{2}}} \int_{\mathbb{R}} \frac{\mathrm{d}p_0}{(2\pi)} \int_{\mathbb{R}} \frac{\mathrm{d}p_x}{(2\pi)} \left\{ \frac{1}{w(v)|p_0| + |p_x| + 2|\zeta(k_x; v)|} \times \frac{i\mathrm{sign}(p_0+\mu)}{i(\mu+p_0) + p_x + \rho(k'_x, k_x; v)} \right\}. \tag{M.94}$$

In what follows it is convenient to consider the imaginary and real parts of this expression separately.

M.3-(a) $\quad \mathrm{Im}\left[\Gamma_1^{(2,1),1\mathrm{L}}(k'_x, k_x; \mu)\right]$

The imaginary part of Eq. (M.94) reads

$$\mathrm{Im}\left[\Gamma_1^{(2,1),1\mathrm{L}}(k'_x, k_x; \mu)\right] = \frac{\pi^{\frac{3}{2}}\sqrt{v}w(v)}{2\sqrt{2}N_c N_f^{\frac{3}{2}}} \int_{\mathbb{R}} \frac{\mathrm{d}p_0}{(2\pi)} \int_{\mathbb{R}} \frac{\mathrm{d}p_x}{(2\pi)} \left\{ \frac{1}{w(v)|p_0| + |p_x| + 2|\zeta(k_x; v)|} \times \frac{\mathrm{sign}(p_0+\mu)[p_x + \rho(k'_x, k_x; v)]}{(\mu+p_0)^2 + [p_x + \rho(k'_x, k_x; v)]^2} \right\}. \tag{M.95}$$

It is clear from this expression that the intrinsic energy scales of the imaginary part of the one-loop vertex function are $\zeta(k_x; v)$, μ and $\rho(k'_x, k_x; v)$. As we did with the previous quantum corrections we analyze this expression in the limits: (*i*) $\mu \gg |\zeta(k_x; v)|$ and $\mu \gg |\rho(k'_x, k_x; v)|$, (*ii*) $|\zeta(k_x; v)| \gg \mu$ and $|\zeta(k_x; v)| \gg |\rho(k'_x, k_x; v)|$, and (*iii*) $|\rho(k'_x, k_x; v)| \gg \mu$ and $|\rho(k'_x, k_x; v)| \gg |\zeta(k_x; v)|$. We note that in all of these three limits, the integration vanishes by symmetry. Therefore, the imaginary part of the quantum correction is proportional to one these energy scales and by dimensional analysis this implies that the leading order nonzero contribution in either of the aforementioned limits is UV finite.

M.3-(b) $\quad \mathrm{Re}\left[\Gamma_1^{(2,1),1\mathrm{L}}(k_x',k_x;\mu)\right]$

The real part of Eq. (M.94) reads

$$\mathrm{Re}\left[\Gamma_1^{(2,1),1\mathrm{L}}(k_x',k_x;\mu)\right] = \frac{\pi^{\frac{3}{2}}\sqrt{v}w(v)}{2\sqrt{2}N_cN_f^{\frac{3}{2}}}\int_{\mathbb{R}}\frac{\mathrm{d}p_0}{(2\pi)}\int_{\mathbb{R}}\frac{\mathrm{d}p_x}{(2\pi)} \times\left\{\frac{1}{w(v)|p_0|+|p_x|+2|\zeta(k_x;v)|}\frac{|p_0+\mu|}{(\mu+p_0)^2+[p_x+\rho(k_x',k_x;v)]^2}\right\}. \tag{M.96}$$

We separately analyze this expression in the limits: (i) $\mu \gg |\zeta(k_x;v)|$ and $\mu \gg |\rho(k_x',k_x;v)|$, ($ii$) $|\zeta(k_x;v)| \gg \mu$ and $|\zeta(k_x;v)| \gg |\rho(k_x',k_x;v)|$, and ($iii$) $|\rho(k_x',k_x;v)| \gg \mu$ and $|\rho(k_x',k_x;v)| \gg |\zeta(k_x;v)|$. In contrast with the imaginary part, this expression is non vanishing to leading order in these three limits.

(i) For $\mu \gg |\zeta(k_x;v)|$ and $\mu \gg |\rho(k_x',k_x;v)|$ we assume without loss of generality that $\zeta(k_x;v) > 0$ and $\rho(k_x',k_x;v) > 0$, and define the small parameters $\mathfrak{A}(\mu,k_x;v) = \zeta(k_x;v)/\mu$ and $\mathfrak{B}(\mu,k_x',k_x;v) = \rho(k_x',k_x;v)/\mu$. To make Eq. (M.96) manifestly dependent on these parameters we make the scaling $(p_0,p_x)\to\mu(p_0,p_x)$ and write

$$\mathrm{Re}\left[\Gamma_1^{(2,1),1\mathrm{L}}(k_x',k_x;\mu)\right] = \frac{\pi^{\frac{3}{2}}\sqrt{v}w(v)}{2\sqrt{2}N_cN_f^{\frac{3}{2}}}\int_{\mathbb{R}}\frac{\mathrm{d}p_0}{(2\pi)}\int_{\mathbb{R}}\frac{\mathrm{d}p_x}{(2\pi)} \left\{\frac{1}{w(v)|p_0|+|p_x|+2\mathfrak{A}(\mu,k_x;v)}\frac{|p_0+1|}{(1+p_0)^2+[p_x+\mathfrak{B}(\mu,k_x',k_x;v)]^2}\right\}. \tag{M.97}$$

For small $\mathfrak{A}(\mu,k_x;v)$ and $\mathfrak{B}(\mu,k_x',k_x;v)$ we can ignore these parameters in the integration. Furthermore, it is convenient to make the change of variables $p_x\to w(v)p_x$ and write Eq. (M.97) as

$$\mathrm{Re}\left[\Gamma_1^{(2,1),1\mathrm{L}}(k_x',k_x;\mu)\right] = \frac{\pi^{\frac{3}{2}}\sqrt{v}w(v)}{\sqrt{2}N_cN_f^{\frac{3}{2}}}\int_{\mathbb{R}}\frac{\mathrm{d}p_0}{(2\pi)}\int_{\mathbb{R}^+}\frac{\mathrm{d}p_x}{(2\pi)}\left\{\frac{1}{|p_0|+p_x}\frac{|p_0+1|}{(1+p_0)^2+w(v)^2p_x^2}\right\}. \tag{M.98}$$

This change of variables makes manifest the fact that the integration becomes logarithmically divergent in the $w(v)=0$ limit. Integrating over p_x and taking the small $w(v)$ limit we obtain

$$\mathrm{Re}\left[\Gamma_1^{(2,1),1\mathrm{L}}(k_x',k_x;\mu)\right] = -\frac{\pi^{\frac{1}{2}}\sqrt{v}w(v)\log[w(v)]}{4\sqrt{2}N_cN_f^{\frac{3}{2}}}\int_{\mathbb{R}}\frac{\mathrm{d}p_0}{(2\pi)} \times\left[\frac{(1+p_0)\left[\Theta(-1-p_0)-\Theta(p_0)-\Theta(-p_0)\Theta(1+p_0)\right]}{1+p_0(2+[1+w(v)]p_0)}\right]. \tag{M.99}$$

Here $\Theta(x)$ denotes the Heaviside function. The integration over p_0 is UV divergent and we cut it off with the ratio $\Lambda_f/\mu \gg 1$. After performing the integration and expanding for $w(v)\ll 1$ and $\Lambda_f/\mu \gg 1$ we obtain the logarithmically divergent contribution

$$\mathrm{Re}\left[\Gamma_1^{(2,1),1\mathrm{L}}(k_x',k_x;\mu)\right] = \frac{\pi^{\frac{1}{2}}\sqrt{v}w(v)}{2\pi\sqrt{2}N_cN_f^{\frac{3}{2}}}\log\left(\frac{1}{w(v)}\right)\log\left(\frac{\Lambda_f}{\mu}\right). \tag{M.100}$$

(*ii*) For $|\zeta(k_x;v)| \gg \mu$ and $|\zeta(k_x;v)| \gg \rho(k_x',k_x;v)$ we consider, without loss of generality the cases in which $\zeta(k_x;v) > 0$ and $\rho(k_x',k_x;v) > 0$. We further define the small parameters $\mathfrak{Z}(\mu,k_x;v) = \mu/\zeta(k_x;v)$ and $\mathfrak{R}(\mu,k_x',k_x;v) = \rho(k_x',k_x;v)/\zeta(k_x;v)$. After the scaling $(p_0,p_x) \to \zeta(k_x)(p_0,p_x)$, Eq. (M.96) depends on these parameters as

$$\mathrm{Re}\left[\Gamma_1^{(2,1),1\mathrm{L}}(k_x',k_x;\mu)\right] = \frac{\pi^{\frac{3}{2}}\sqrt{v}w(v)}{2\sqrt{2}N_cN_f^{\frac{3}{2}}}\int_{\mathbb{R}}\frac{\mathrm{d}p_0}{(2\pi)}\int_{\mathbb{R}}\frac{\mathrm{d}p_x}{(2\pi)}\left\{\frac{1}{w(v)|p_0|+|p_x|+2}\right. \times\left.\frac{|p_0+\mathfrak{Z}(\mu,k_x;v)|}{[\mathfrak{Z}(\mu,k_x;v)+p_0]^2+[p_x+\mathfrak{R}(\mu,k_x',k_x)]^2}\right\}. \tag{M.101}$$

In the small $\mathfrak{R}(\mu,k_x',k_x;v)$ and $\mathfrak{Z}(\mu,k_x;v)$ limits we can ignore these factors. Upon integration over p_x we obtain

$$\mathrm{Re}\left[\Gamma_1^{(2,1),1\mathrm{L}}(k_x',k_x;\mu)\right] = \frac{\pi^{\frac{3}{2}}\sqrt{v}w(v)}{2\pi\sqrt{2}N_cN_f^{\frac{3}{2}}}\int_{\mathbb{R}^+}\frac{\mathrm{d}p_0}{(2\pi)}\frac{\pi[2+p_0w(v)]+2p_0\log\left(\frac{p_0}{2+w(v)p_0}\right)}{4+p_0^2+4p_0w(v)+p_0^2w(v)^2}. \tag{M.102}$$

The integration over p_0 is UV divergent for nonzero $w(v)$. Cutting off the large p_0 momentum integration with the ratio $\Lambda_f/\zeta(k_x;v) \gg 1$, the integration over p_0 yields the following divergent contribution to the leading order in $w(v) \ll 1$ and $\Lambda_f/\zeta(k_x;v) \gg 1$:

$$\mathrm{Re}\left[\Gamma_1^{(2,1),1\mathrm{L}}(k_x',k_x;\mu)\right] = \frac{\pi^{\frac{1}{2}}\sqrt{v}w(v)}{2\pi\sqrt{2}N_cN_f^{\frac{3}{2}}}\log\left(\frac{1}{w(v)}\right)\log\left(\frac{\Lambda_f}{|\zeta(k_x;v)|}\right). \tag{M.103}$$

The absolute value in the IR scale originates in the fact that the case in which $\zeta(k_x,v) < 0$ yields the same result.

(*iii*) For $|\rho(k_x',k_x;v)| \gg \mu$ and $|\rho(k_x',k_x;v)| \gg |\zeta(k_x;v)|$ we define the small parameters $\mathfrak{L}(k_x',k_x;v) = |\zeta(k_x;v)|/|\rho(k_x',k_x;v)|$ and $\mathfrak{P}(\mu,k_x',k_x;v) = \mu/|\rho(k_x',k_x;v)|$ and assume, without loss of generality, that $\zeta(k_x;v) > 0$ and $\rho(k_x',k_x;v) > 0$. After performing the rescaling $(p_0,p_x) \to \rho(k_x',k_x)(p_0,p_x)$ we can write Eq. (M.96) as

$$\mathrm{Re}\left[\Gamma_1^{(2,1),1\mathrm{L}}(k_x',k_x;\mu)\right] = \frac{\pi^{\frac{3}{2}}\sqrt{v}w(v)}{2\sqrt{2}N_cN_f^{\frac{3}{2}}}\int_{\mathbb{R}}\frac{\mathrm{d}p_0}{(2\pi)}\int_{\mathbb{R}}\frac{\mathrm{d}p_x}{(2\pi)}\left\{\frac{1}{w(v)|p_0|+|p_x|+2\mathfrak{L}(k_x',k_x;v)}\right. \times\left.\frac{|p_0+\mathfrak{P}(\mu,k_x',k_x;v)|}{[\mathfrak{P}(\mu,k_x',k_x;v)+p_0]^2+(p_x+1)^2}\right\}. \tag{M.104}$$

In the small $\mathfrak{P}(\mu,k_x',k_x;v)$ and $\mathfrak{L}(k_x',k_x;v)$ these factors can be ignored inside the integrand and by performing the scaling $p_x \to w(v)p_x$ we can write this expression as

$$\mathrm{Re}\left[\Gamma_1^{(2,1),1\mathrm{L}}(k_x',k_x;\mu)\right] = \frac{\pi^{\frac{3}{2}}\sqrt{v}w(v)}{\sqrt{2}N_cN_f^{\frac{3}{2}}}\int_{\mathbb{R}^+}\frac{\mathrm{d}p_0}{(2\pi)}\int_{\mathbb{R}}\frac{\mathrm{d}p_x}{(2\pi)}\left\{\frac{1}{p_0+|p_x|}\frac{p_0}{p_0^2+[w(v)p_x+1]^2}\right\}. \tag{M.105}$$

Integration over p_x yields in the small $w(v)$ limit,

$$\mathrm{Re}\left[\Gamma_1^{(2,1),1\mathrm{L}}(k_x',k_x;\mu)\right] = -\frac{\pi^{\frac{1}{2}}\sqrt{v}w(v)\log[w(v)]}{\sqrt{2}N_cN_f^{\frac{3}{2}}}\int_{\mathbb{R}^+}\frac{\mathrm{d}p_0}{(2\pi)}\frac{p_0}{1+p_0^2}. \tag{M.106}$$

The integration over p_0 is UV divergent. Cutting it off with the scale $\Lambda_f/\rho(k'_x, k_x; v) \gg 1$, we find the divergent contribution in this limit:

$$\mathrm{Re}\left[\Gamma_1^{(2,1),1\mathrm{L}}(k'_x, k_x; \mu)\right] = \frac{\pi^{\frac{1}{2}}\sqrt{v}w(v)}{2\pi\sqrt{2}N_c N_f^{\frac{3}{2}}} \log\left(\frac{1}{w(v)}\right) \log\left(\frac{\Lambda_f}{|\rho(k'_x, k_x; v)|}\right). \quad \text{(M.107)}$$

Here we have used the fact that the case $\rho(k'_x, k_x; v) < 0$ yields the same result.

Collecting the above results, it follows that the one-loop quantum correction to the Yukawa vertex at the momenta at which the RG condition is imposed [see Eq. (4.57)] is given by

$$\Gamma_N^{(2,1),1\mathrm{L}}(k'_N, k_N; \mu) = \frac{\pi^{\frac{1}{2}}\sqrt{v}w(v)}{2\pi\sqrt{2}N_c N_f^{\frac{3}{2}}} \log\left(\frac{1}{w(v)}\right) \log\left(\frac{\Lambda_f}{\mathscr{H}_1(\mu, v^2|k_N|, v|k'_N + k_N|)}\right). \quad \text{(M.108)}$$

Here $\mathscr{H}_1(x, y, u) \sim \max(x, y, u)$ whenever any of the arguments is larger than the other two. Making use of Eq. (J.8) the counterterm function $A_N^{(4)}(k'_N, k_N)$ is fixed at the one-loop order to

$$A_N^{(4)}(k'_N, k_N) = -\frac{1}{2\pi N_c N_f} w(v) \log\left(\frac{1}{w(v)}\right) \log\left(\frac{\Lambda_f}{\mathscr{H}_1(\mu, v^2|k_N|, v|k'_N + k_N|)}\right). \quad \text{(M.109)}$$

Appendix N | The Yukawa Interaction Vertex Function

Here we consider the RG equation for the Yukawa interaction vertex function in the WMDL. To leading order we ignore the contributions from the four-fermion couplings. Choosing $m = n = 1$ in Eq. (K.9) it follows that the scaling properties of the interaction vertex function are governed by the equation:

$$\begin{aligned}\Big\{&\widetilde{\eta}^{(\Phi)} + \widetilde{\eta}_N^{(\psi)}(k'_N) + \eta_{\overline{N}}^{(\psi)}(k_N) - \beta_{\widehat{k}_{\rm F}}\frac{\partial}{\partial \widehat{k}_{\rm F}} - \widehat{\Lambda}_b\frac{\partial}{\partial \widehat{\Lambda}_b} + zk'_0\frac{\partial}{\partial k'_0} + k_0\frac{\partial}{\partial k_0} + \vec{k}'\cdot\frac{\partial}{\partial \vec{k}'} + \vec{k}\cdot\frac{\partial}{\partial \vec{k}}\\ &- \sum_{M=1}^{8}\int \mathrm{d}x\left[\left(x\frac{\partial v_M(x)}{\partial x} + \beta_M^{(v)}(x)\right)\frac{\delta}{\delta v_M(\vec{q})} + \left(x\frac{\partial V_{\rm F}^{(M)}(x)}{\partial x} + \beta_M^{(V_{\rm F})}(x)\right)\frac{\delta}{\delta V_{\rm F}^{(M)}(x)}\right.\\ &\left.\int \mathrm{d}y\left(x\frac{\partial g_M(x,y)}{\partial x} + y\frac{\partial g_M(x,y)}{\partial y} + \beta_M^{(g)}(x,y)\right)\frac{\delta}{\delta g_M(x,y)}\right]\Big\}\,\Gamma_N^{(2,1)}(k,k') = 0.\end{aligned} \tag{N.1}$$

Following the logic of Appendix L, this equation can be written as

$$\left[k_0\frac{\partial}{\partial k_0} + k'_0\frac{\partial}{\partial k'_0} + \frac{1}{z(l)}\vec{k}\cdot\frac{\partial}{\partial \vec{k}} + \frac{1}{z(l)}\vec{k}'\cdot\frac{\partial}{\partial \vec{k}'} + \frac{\partial}{\partial l} + \frac{\gamma_N(k_N,k'_N;l)}{z(l)}\right]\Gamma_N^{(2,1)}(k',k) = 0, \tag{N.2}$$

where

$$\gamma_N(k_N,k'_N;l) \equiv \eta^{(\Phi)}(l) + \widetilde{\eta}_N^{(\psi)}(k'_N;l) + \widetilde{\eta}_{\overline{N}}^{(\psi)}(k_N;l), \tag{N.3}$$

denotes the effective scaling dimension of the three-point function. Furthermore, the scale-dependent coupling functions and IR scales satisfy Eqs. (L.3) to (L.7). The solutions to this differential equation are parametrized by the logarithmic length scale l. Here, the anomalous scaling dimension of the fields and the dynamical critical exponent acquire a scale dependence through the scale dependence of the zero momentum coupling functions. For the initial conditions $v_N(k_N;0) \equiv \mathsf{v}_N(k_N)$, $V_{\rm F}^{(N)}(k_N;0) \equiv \mathsf{V}_{\rm F}^{(N)}(k_N)$, $g_N(k'_N,k_N;0) = \mathsf{g}_N(k'_N,k_N)$, $\widehat{k}_{\rm F}(0) = \widehat{k}_{\rm F}^{(0)}$, and $\widehat{\Lambda}_b(0) = \widehat{\Lambda}_b^{(0)}$, where $\mathsf{v}_N, \mathsf{V}_{\rm F}^{(N)}$ and g_N are known functions of momentum, the solution in Eq. (N.2) is given by

$$\begin{aligned}\Gamma_N^{(2,1)}(k',k;[\mathsf{v}_M,\mathsf{g}_M,\mathsf{V}_{\rm F}^{(M)}];\widehat{k}_{\rm F}^{(0)},\widehat{\Lambda}_b^{(0)}) &= \exp\left(\int_0^l \frac{\mathrm{d}\ell}{z(\ell)}\gamma_N(k_N(\ell),k'_N(\ell);\ell)\right)\\ &\times \Gamma_N^{(2,1)}\left[k'_0(l),\vec{k}'(l),k_0(l),\vec{k}(l);[v_M(l),g_M(l),V_{\rm F}^{(M)}(l)];\widehat{k}_{\rm F}(l),\widehat{\Lambda}_b(l)\right],\end{aligned} \tag{N.4}$$

which is straightforward to check by differentiating with respect to the length scale. Here, the scale-dependent momenta and frequencies are given in Eq. (4.41). Determining the full frequency and momentum dependence of this expression is not an easy task because this requires the knowledge of the leading order vertex function as a function of frequencies and the momenta away from the local FS's at hot spots N and $\overline{N}$. Nevertheless, we can fully determine the momentum profile of the interaction vertex when $k_0' = k_0$ and the electrons close to hot spots N and $\overline{N}$ lie on the FS. For hot spot $N = 1$ this corresponds to the choice of momenta $k' = (k_0, k_x', -v_1(k_x)k_x)$ and $k = (k_0, k_x, v_4(k_x)k_x)$. Thus, using the RG condition in Eq. (4.27) and the fact that, to leading order in $v_0 \ll 1$ quantum corrections beyond the tree level are suppressed, we can write the interaction vertex function at the length scale $l = \ell_\omega \equiv \log(\Lambda_f/k_0)$, with $k_0 > 0$, as

$$\Gamma_N^{(2,1)}(k_0; k_N', k_N) = \frac{\widehat{g}_N(k_N', k_N; \ell_\omega)}{\sqrt{N_f}} \exp\left(\int_0^{\ell_\omega} \frac{\mathrm{d}\ell}{z(\ell)}\, \gamma_N(k_N(\ell), k_N'(\ell); \ell) \right), \tag{N.5}$$

where $\widehat{g}(k_N', k_N; l) = g_N(k_N'(l), k_N(l); l)$ is the rescaled Yukawa coupling given in Eq. (L.18). Using this last fact in combination with Eq. (K.10) we can write the interaction vertex function in terms of the counterterm functions as follows

$$\Gamma_N^{(2,1)}(k_0; k_N', k_N) = \sqrt{\frac{\pi v_0}{2N_f}} \exp\left(\int_0^{\ell_\omega} \frac{\mathrm{d}\ell}{z(\ell)}\, Z_N^{(4)}(k_N'(\ell), k_N(\ell); \ell)' \right), \tag{N.6}$$

where $Z_N^{(4)}(k_N'(\ell), k_N(\ell); \ell)' = \frac{\partial}{\partial \log \mu} Z_N^{(4)}(k_N'(\ell), k_N(\ell); \ell)\big|_{\mu=\Lambda_f}$. From Eq. (M.109) we can write this expression as

$$\begin{aligned} \Gamma_N^{(2,1)}(k_0; k_N', k_N) = \sqrt{\frac{\pi v_0}{2N_f}} \exp\Bigg(& \frac{1}{\sqrt{2\pi^2 N_c N_f}} \int_0^{\ell_\omega} \frac{\mathrm{d}\ell}{z(\ell)} \sqrt{v(\ell) \log\left(\frac{1}{v(\ell)}\right)} \\ & \times \Theta(\Lambda_f e^{-\ell} - 2v(\ell)^2 |k_N|) \Theta(\Lambda_f e^{-\ell} - v(\ell)|k_N' + k_N|) \Bigg), \end{aligned} \tag{N.7}$$

which follows from Eq. (3.43) and the fact that the function $\mathscr{H}_1(x, y, u) \sim \max(x, y, u)$ satisfies the derivative property

$$\frac{\partial}{\partial x} \mathscr{H}_1(x, y, u) = \Theta(x - y)\Theta(x - u). \tag{N.8}$$

In the zero momentum limit, the interaction vertex describes the strength with which the electrons at the hot spots interact with each other through zero-energy spin fluctuations. In this limit, and by virtue of Eq. (L.20), Eq. (N.7) reduces to

$$\Gamma_N^{(2,1)}(k_0) = \sqrt{\frac{\pi v_0}{2N_f}} \exp\left(\frac{1}{\sqrt{N_c^2 - 1}} \left[\sqrt{\ell_0 + \ell_\omega} - \sqrt{\ell_0} \right] \right), \tag{N.9}$$

where $\Gamma^{(2,1)}(k_0) \equiv \Gamma^{(2,1)}(k_0; 0, 0)$ to leading order in $\ell_0, \ell_\omega \gg 1$ with ℓ_0 given in Eq. (3.49). In the low-energy limit ($\ell_\omega \gg \ell_0$), this becomes

$$\Gamma_N^{(2,1)}(k_0, k_0, \mu) = \sqrt{\frac{\pi v_0}{2N_f}} e^{\sqrt{\log(\Lambda_f/k_0)}}. \tag{N.10}$$

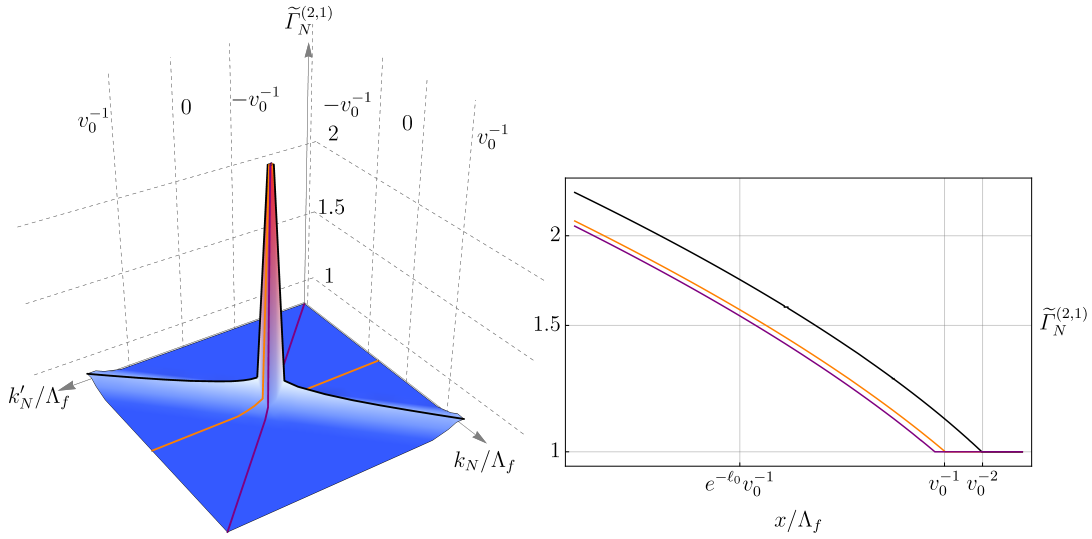

(a) (b)

Figure N.1: (a) The low-energy momentum profile of the interaction vertex function $\widetilde{\Gamma}^{(2,1)}(k'_N, k_N) \equiv \sqrt{\frac{2N_f}{\pi v_0}}\Gamma^{(2,1)}(0; k'_N, k_N)$ for $N_c = 2$, $N_f = 1$ and $v_0 = 10^{-1}$ (b) Momentum profiles along the directions $k_N = 0$ (orange), $k'_N = k_N$ (purple), $k'_N = -k_N$ (black) in the logarithmic scale. Here x represents the momentum along these directions.

This result shows the strongly coupled nature of the theory that describes the electrons at the hots pots in the low-energy limit.

For nonzero momentum, the interaction vertex describes the strength with which the electrons on the FS at hot spots N and $\overline{N}$ interact with each other through the low-energy spin fluctuations. For simplicity, let us consider the case in which either $k'_N = 0$ or $k_N = 0$. The fixed-point functional form of the vertex function for any k'_N and k_N is plotted in Fig. N.1 in the case in which there is no superconducting instabilities. At nonzero frequency, we define $\widehat{\Gamma}_N^{(2,1)}(k_N; k_0) \equiv \Gamma_N^{(2,1)}(k_0; k_N, 0; \mu) = \Gamma_N^{(2,1)}(k_0; 0; k_N; \mu)$. Then, using Eq. (4.101) we can write the interaction vertex function as

$$\widehat{\Gamma}_N^{(2,1)}(k_N) = \sqrt{\frac{\pi v_0}{2N_f}} \exp\left(\frac{1}{\sqrt{N_c^2 - 1}} \Theta(\ell_\omega - \ell_N)\Theta(\ell_N) \left[\sqrt{\ell_0 + \ell_N} - \sqrt{\ell_0}\right] + \Theta(\ell_N - \ell_\omega) \left[\sqrt{\ell_0 + \ell_\omega} - \sqrt{\ell_0}\right] \right), \tag{N.11}$$

where $\ell_N \equiv \ell_N(k_N)$ is the momentum dependent length scale that solves the transcendental equation

$$\Lambda_f e^{-\ell_N} = v(\ell)|k_N|. \tag{N.12}$$

By analyzing this expression in both the $\ell_N \gg \ell_0$ and $\ell_N \ll \ell_0$ limits, it is found that this

equation is solved by

$$\ell_N(k_N) = \log\left(\frac{\mu}{v_0|k_N|}\right), \qquad |k_N| \ll \frac{\Lambda_f}{v_0}. \tag{N.13}$$

We note that for $k_N = 0$ ($k'_N = 0$) the vertex function $\widehat{\Gamma}^{(2,1)}_N(k_N)$ quantifies the strength of the interactions between an electron at hot spot N ($\overline{N}$) that interacts with a low-energy electron near hot spot $\overline{N}$ (N). We take a look at Eq. (N.7) in two main cases: (*i*) In the absence of superconducting instabilities and (*ii*) when the superconducting instability enters at a length scale $\ell_{\rm SC} \ll \ell_0$ satisfying Eq. (4.90). Let us analyze each one of these cases separately.

(*i*) In the ideal case where there are no superconducting instabilities, we have control up to zero energy. In the low-energy limit ($\ell_\omega \gg \ell_0$) the vertex function displays the crossovers as a function of momentum:

$$\widehat{\Gamma}^{(2,1)}_N(k_N) = \begin{cases} \sqrt{\frac{\pi v_0}{2N_f}} & \frac{\Lambda_f}{v_0} \ll |k_N| \ll \overline{k}_{\rm F}, \\ \sqrt{\frac{\pi v_0}{2N_f}}\left(\frac{\Lambda_f}{v_0|k_N|}\right)^{\sqrt{\frac{v_0\log(1/v_0)}{2\pi N_c N_f}}} & \frac{\Lambda_f}{v_0}e^{-\ell_0} \ll |k_N| \ll \frac{\Lambda_f}{v_0}, \\ \sqrt{\frac{\pi v_0}{2N_f}}e^{\sqrt{\log(\Lambda_f/v_0|k_N|)}} & |k_N| \ll \frac{\Lambda_f}{v_0}e^{-\ell_0}. \end{cases} \tag{N.14}$$

This shows that as the momentum becomes smaller, the strength of the interaction becomes larger. On the other hand, as the momentum is tunned away from the hot spot, the interaction decays as a power-law in momentum where it eventually becomes constant and of order $\sqrt{v_0} \ll 1$ which implies that the electrons interact weakly with each other. We note that the momentum region $|k_N| \gg \overline{k}_{\rm F}$ is out of the scope of our analysis as explained in Sec. 4.4-(*a*) .

(*ii*) In the case where there is a superconducting instability we only have control up to lengths scales $\ell_\omega \lessapprox \ell_{\rm SC} \ll \ell_0$. In this case, the vertex function displays the crossovers as a function of momentum:

$$\widehat{\Gamma}^{(2,1)}_N(k_N) = \begin{cases} \sqrt{\frac{\pi v_0}{2N_f}} & \frac{\Lambda_f}{v_0} \ll |k_N| \ll \overline{k}_{\rm F}, \\ \sqrt{\frac{\pi v_0}{2N_f}}\left(\frac{\Lambda_f}{v_0|k_N|}\right)^{\sqrt{\frac{v_0\log(1/v_0)}{2\pi N_c N_f}}} & \frac{\Lambda_f}{v_0}e^{-\ell_{\rm SC}} \ll |k_N| \ll \frac{\Lambda_f}{v_0}, \\ \sqrt{\frac{\pi v_0}{2N_f}}\left(\frac{\Lambda_f}{\omega}\right)^{\sqrt{\frac{v_0\log(1/v_0)}{2\pi N_c N_f}}} & |k_N| \ll \frac{\Lambda_f}{v_0}e^{-\ell_{\rm SC}}, \end{cases} \tag{N.15}$$

The interaction vertex acquires only a power-law momentum dependence. This is a consequence of the superconducting transition length scale being smaller than the scale above which the flow of v is appreciable. Notice that this describes the interaction between a hot spot electron and lukewarm electrons. Below the momentum scale $|k_N| \ll \frac{\Lambda_f}{v_0}e^{-\ell_{\rm SC}}$, the interaction is effectively constant, but much larger than the bare interaction strength. Since the energy scale at which we have control is not low enough, we cannot resolve the momentum-dependent details of the interaction between a hot

spot electron and electrons lying on the hot region of the FS. Such a lack of resolution is rooted in the fact that the energy scale at which the superconducting transition enters is still larger than the momentum-dependent IR cutoff of the vertex correction in Fig. 2.3(*b*).

Appendix O | Check of renormalizability conditions

Here we focus on checking that the renormalizability conditions described in Sec. 4.3-(a) are satisfied in the WMDL and to leading order in $v_0 \ll 1$. We do this by considering the momentum-dependent slope, Fermi velocity and Yukawa coupling to leading order in $v_0 \ll 1$ and the four-fermion couplings. This is tantamount to ignoring the feedback of the four-fermion coupling functions. We leave the discussion regarding the dimensionless four-fermion coupling functions to Appendix P. Thus, we check that

$$\begin{aligned} v_N(k_N) &\leq 1, \\ V_{\mathrm{F}}^{(N)}(k_N) &\geq 1, \\ g_N(k'_N, k_N) &\leq 1. \end{aligned} \tag{O.1}$$

We that recall the renormalized momentum-dependent couplings as a function of the logarithmic length scale are given by Eqs. (4.42) to (4.43) where the rescaled momentum-dependent couplings read

$$\widehat{v}_N(k_N; l) = v_0 \exp\left(\int_0^l \frac{\mathrm{d}\ell}{z(\ell)} \left\{ Z_N^{(2)}[k_N(\ell); \ell]' - Z_N^{(3)}[k_N(\ell); \ell]' \right\} \right), \tag{O.2}$$

$$\widehat{V}_{\mathrm{F}}^{(N)}(k_N; l) = \exp\left(\int_0^l \frac{\mathrm{d}\ell}{z(\ell)} \left\{ Z_N^{(3)}[k_N(\ell); \ell]' - Z_N^{(1)}[k_N(\ell); \ell]' + z(\ell) - 1 \right\} \right), \tag{O.3}$$

$$\begin{aligned} \widehat{g}_N(k'_N, k_N; l) = \sqrt{\frac{\pi v_0}{2}} \exp\Bigg(\int_0^l \frac{\mathrm{d}\ell}{z(\ell)} \Bigg\{ \frac{1}{2} \Big(Z_2(\ell)' - Z_3(\ell)' - Z_N^{(1)}[k'_N(\ell); \ell]' - Z_{\overline{N}}^{(1)}[k_{\overline{N}}(\ell); \ell]' \Big] \\ + Z_N^{(4)}[k'_N(\ell), k_N(\ell); \ell]' - Z_4(\ell)' + Z_1(\ell)' \Bigg\} \Bigg). \end{aligned} \tag{O.4}$$

In the $v_0 \ll 1$ limit, the counterterm coefficients are given by Eqs. (L.9) to (L.12). For $w(l) \ll 1$, the momentum dependence of the rescaled momentum-dependent couplings reduces to

$$\widehat{v}_N(k_N; l) = v_0 \exp\left(\int_0^l \frac{\mathrm{d}\ell}{z(\ell)} \left\{ Z_N^{(2)}[k_N(\ell); \ell]' - Z_N^{(3)}[k_N(\ell); \ell]' \right\} \right), \tag{O.5}$$

$$\widehat{V}_{\mathrm{F}}^{(N)}(k_N; l) = \exp\left(\int_0^l \frac{\mathrm{d}\ell}{z(\ell)} \left\{ Z_1 - Z_N^{(1)}[k_N(\ell); \ell]' \right\} \right), \tag{O.6}$$

$$\widehat{g}_N(k'_N, k_N; l) = \sqrt{\frac{\pi v_0}{2}} \exp\left(\int_0^l \frac{\mathrm{d}\ell}{z(\ell)} \left\{ Z_N^{(4)}[k'_N(\ell), k_N(\ell); \ell]' - Z_4(\ell)' \right\} \right). \tag{O.7}$$

Introducing the expressions for the counterterms in Eqs. (L.9) to (L.12) and making use of Eqs. (3.43), (4.42) to (4.43), the momentum-dependent couplings are given, for large l, by

$$\begin{aligned} v(k_N; l) = v_0 \exp\Bigg(& -\frac{(N_c^2-1)}{\pi^2 N_c N_f} \int_0^l \frac{\mathrm{d}\ell}{z(\ell)} v(\ell) \log\left(\frac{1}{v(\ell)}\right) \\ & \times \left[\Theta(\Lambda_f e^{-(\ell-l)} - 2v(\ell)c(\ell)|k_N|) + \Theta(\Lambda_f e^{-(\ell-l)} - 2v(\ell)|k_N|) \right] \Bigg), \end{aligned} \tag{O.8}$$

$$V_{\mathrm{F}}^{(N)}(k_N; l) = \exp\left(\frac{2(N_c^2-1)}{\sqrt{2\pi^2 N_c N_f}} \int_0^l \frac{\mathrm{d}\ell}{z(\ell)} \sqrt{\frac{v(\ell)}{\log(1/v(\ell))}} \left[1 - \Theta(\Lambda_f e^{-(\ell-l)} - 2v(\ell)c(\ell)|k_N|) \right] \right), \tag{O.9}$$

$$\begin{aligned} g_N(k'_N, k_N; l) = \sqrt{\frac{\pi v_0}{2}} \exp\Bigg(& -\frac{1}{\sqrt{2\pi^2 N_c N_f}} \int_0^l \frac{\mathrm{d}\ell}{z(\ell)} \sqrt{v(\ell) \log\left(\frac{1}{v(\ell)}\right)} \\ & \times \left[1 - \Theta(\Lambda_f e^{-(\ell-l)} - 2v(\ell)^2|k_N|) \Theta(\Lambda_f e^{-(\ell-l)} - v(\ell)|k'_N + k_N|) \right] \Bigg), \end{aligned} \tag{O.10}$$

where we used the fact that the rescaled momentum in Eq. (4.41) is given by $\vec{k}(l) \approx e^l \vec{k}$ to leading order in $l \gg 1$, and $\Theta(x)$ denotes the Heaviside function.
At zero momentum, the conditions in Eq. (O.1) is satisfied for $l \gg 1$. This is because the slope flows to zero logarithmically, the Fermi velocity becomes one and the Yukawa coupling is simply given by its bare value. For nonzero momentum the integration over the length scale has the structure

$$\int_0^l \mathrm{d}\ell \Theta\left[\Lambda_f e^{-\ell+l} - \Delta(\ell) \right] f(\ell) = \Theta(\ell_\Delta) \int_0^l \mathrm{d}\ell f(\ell). \tag{O.11}$$

where $f(\ell)$ is some function of the length scale, $\Delta(\ell)$ is any of the momentum scales inside the Heaviside functions and ℓ_Δ is the scale that solves the transcendental equation

$$\Lambda_f e^{-\ell_\Delta + l} - \Delta(\ell_\Delta) = 0, \tag{O.12}$$

From this it follows that the coupling functions that involve the rescaled momentum are the same as the zero momentum couplings. This is to be expected because we are scaling both frequency and momentum simultaneously and therefore the support of the quantum corrections that introduce the momentum dependences into the coupling functions has no change as we lower the energy. Therefore, at a given length scale l, the IR cutoff scale of the corresponding diagram is always smaller than that associated to the logarithmic length scale l. Since the zero momentum coupling functions satisfy Eq. (O.1) for any length scale, it follows that the renormalized momentum-dependent coupling functions satisfy the sufficient conditions for the theory to be renormalizable to leading order in both v and the four-fermion couplings.

Appendix P | Beta Function for the Four-Fermion Coupling Functions in the Pairing Channel

In this appendix we determine the general form of the beta functions of the momentum-dependent four-fermion coupling functions. In particular we focus on the couplings that involve the rescaled momenta: $\widehat{\lambda}^{\{j_i\}}_{\{N_i\};\{\sigma_i\}}(\{k_{i;N_i}\};l)$. From Eq. (4.49), the beta functions of the four-fermion coupling functions are given by

$$\widehat{\beta}^{\{j_i\}}_{\{N_i;\sigma_i\}}(\{k_{i;N_i}\}) \equiv \frac{\partial \widehat{\lambda}^{\{j_i\}}_{\{N_i;\sigma_i\}}(\{k_{i;N_i}\};l)}{\partial l} = -\frac{1}{z(l)}\mu\frac{\mathrm{d}}{\mathrm{d}\mu}\widehat{\lambda}^{\{j_i\}}_{\{N_i;\sigma_i\}}(\{k_{i;N_i}\})\bigg|_{\mu=\Lambda_f}. \tag{P.1}$$

The right-hand side can be manipulated by noting that the renormalized four-fermion coupling functions are related to the bare ones through Eq. (4.30). Similarly, for the coupling functions with the rescaled momentum, we have the relation:

$${}^{\mathsf{B}}\widehat{\lambda}^{\{j_i\}}_{\{N_i\};\{\sigma_i\}}(\{k^{\mathsf{B}}_{i;N_i}\}) = \mu^{-1}Z_\tau^{-3}\left[\prod_{i=1}^{4}Z^{(\psi)}_{N_i}(k_{i;N_i}(l))\right]^{-\frac{1}{2}} Z^{\{j_i\}}_{\{N_i\};\{\sigma_i\}}(\{k_{i;N_i}(l)\})\widehat{\lambda}^{\{j_i\}}_{\{N_i\};\{\sigma_i\}}(\{k_{i;N_i}\}), \tag{P.2}$$

where the scale-dependent momenta are defined in Eq. (4.41). Using the fact that the bare coupling functions are independent of the running scale μ, we obtain the flow equation for the four-fermion couplings

$$\begin{aligned}\widehat{\beta}^{\{j_i\}}_{\{N_i;\sigma_i\}}(\{k_{i;N_i}\}) = -\frac{\widehat{\lambda}^{\{j_i\}}_{\{N_i;\sigma_i\}}(\{k_{i;N_i}\})}{z(l)}\Bigg[&2 - z(l) + \sum_{j=1}^{4}\widetilde{\eta}^{(\psi)}_{N_j}(k_{j;N_j}(l)) \\ &-\frac{1}{Z^{\{j_i\}}_{\{N_i;\sigma_i\}}(\{k_{i;N_i}(l)\})}\frac{\mathrm{d}Z^{\{j_i\}}_{\{N_i;\sigma_i\}}(\{k_{i;N_i}(l)\})}{\mathrm{d}\log\mu}\Bigg]\Bigg|_{\mu=\Lambda_f},\end{aligned} \tag{P.3}$$

where the dynamical critical exponent $z(l)$ and effective anomalous scaling dimension of the fermion field $\widetilde{\eta}^{(\psi)}_N(k_N)$ are defined in Eq. (4.33). The momentum in the counterterm function and anomalous scaling dimension of the field is rescaled according to Eq. (4.41). This expression constitutes a set of coupled equations for the beta functions of the four-fermion coupling functions. To see this we note that the coupling functions and IR scales of the theory implicitly depend on the running scale μ. Therefore, we can use the chain rule to write the μ derivative as

$$\mu\frac{\mathrm{d}}{\mathrm{d}\mu} = \mu\frac{\partial}{\partial\mu} - z(l)\sum_{M_1=1}^{8}\int \mathrm{d}x_1\left[\widehat{\beta}^{(M_1)}_{v}(x_1)\frac{\delta}{\delta v_{M_1}(x_1)} + \widehat{\beta}^{(M_1)}_{V_{\mathrm{F}}}(x_1)\frac{\delta}{\delta V^{(M_1)}_{\mathrm{F}}(x_1)}\right.$$

$$+\int \mathrm{d}x_2 \left(\widehat{\beta}_g^{(M)}(x_1,x_2)\frac{\delta}{\delta g_M(x_1,x_2)} + \sum_{M_2,M_3,M_4=1}^{8}\sum_{\{\rho_i=1\}}^{N_c}\sum_{\{l_i=1\}}^{N_f}\int \mathrm{d}x_3 \int \mathrm{d}x_4 \left\{ \right.\right. \tag{P.4}$$
$$\left.\left. \widehat{\beta}^{\{l_i\}}_{\{M_i;\rho_i\}}(\{x_i\})\frac{\delta}{\delta\widehat{\lambda}^{\{l_i\}}_{\{M_i\};\{\rho_i\}}(\{x_i\})} \right) \right] \right\} - \widehat{k}_{\mathrm{F}}\frac{\partial}{\partial \widehat{k}_{\mathrm{F}}} - \widehat{\Lambda}_b \frac{\partial}{\partial \widehat{\Lambda}_b}.$$

In here we have used explicitly the fact that the IR scales are governed by the beta functions in Eqs. (4.39) and (4.40). The beta functions for the slope, Fermi velocity and Yukawa coupling are defined as

$$\widehat{\beta}_v^{(M_1)}(x_1) \equiv -\frac{1}{z(l)}\frac{\mathrm{d}v_{M_1}[x_1(l)]}{\mathrm{d}\log\mu}, \tag{P.5}$$
$$\widehat{\beta}_{V_{\mathrm{F}}}^{(M_1)}(x_1) \equiv -\frac{1}{z(l)}\frac{\mathrm{d}v_{M_1}[x_1(l)]}{\mathrm{d}\log\mu}, \tag{P.6}$$
$$\widehat{\beta}_g^{(M_1)}(x_1,x_2) \equiv -\frac{1}{z(l)}\frac{\mathrm{d}g_{M_1}[x_1(l),x_2(l)]}{\mathrm{d}\log\mu}. \tag{P.7}$$

Introducing Eq. (P.4) into Eq. (P.3) one can solve the system of coupled equations iteratively under the assumption that $\widehat{\lambda}^{\{j_i\}}_{\{N_i;\sigma_i\}}(\{k_{i;N_i}\})$ remains small. Doing so, the perturbative beta function for the momentum-dependent four-fermion couplings adopts the form

$$\widehat{\beta}^{\{j_i\}}_{\{N_i\};\{\sigma_i\}}(\{k_{i;N_i}\}) = -\frac{1}{z(l)}\widehat{\lambda}^{\{j_i\}}_{\{N_i\};\{\sigma_i\}}(\{k_{i;N_i}\})\left[2 - z(l) + \sum_{j=1}^{4}\widetilde{\eta}^{(\psi)}_{N_j}(k_{j;N_j}(l))\right.$$
$$-\left\{\mu\frac{\partial}{\partial\mu} - \widehat{k}_{\mathrm{F}}\frac{\partial}{\partial\widehat{k}_{\mathrm{F}}} - \widehat{\Lambda}_b\frac{\partial}{\partial\widehat{\Lambda}_b} - z(l)\sum_{M_1=1}^{8}\int \mathrm{d}x_1 \left(\widehat{\beta}^{(v)}_{M_1}(x_1)\frac{\delta}{\delta\widehat{v}_{M_1}(x_1)} + \widehat{\beta}^{(V_{\mathrm{F}})}_{M_1}(x_1)\frac{\delta}{\delta\widehat{V}^{(M)}_{\mathrm{F}}(x)}\right.\right.$$
$$+\int \mathrm{d}x_2 \left\{\widehat{\beta}^{(g)}_{M_1}(x_1,x_2)\frac{\delta}{\delta\widehat{g}_{M_1}(x_1,x_2)} - \sum_{M_2,M_3,M_4=1}^{8}\sum_{\{l_i=1\}}^{N_f}\sum_{\{\rho_i\}=1}^{N_c}\int \mathrm{d}x_3\int \mathrm{d}x_4\left[\right.\right.$$
$$\left.\left.\left.\left.\left.\frac{1}{z(l)}\widehat{\lambda}^{\{l_i\}}_{\{M_i\};\{\rho_i\}}(\{x_i\})\frac{\delta}{\delta\widehat{\lambda}^{\{l_i\}}_{\{M_i\};\{\rho_i\}}(\{x_i\})}\right]\right\}\right)\right\} Z^{\{j_i\}}_{\{N_i\};\{\sigma_i\}}(k_{i;N_i}(l))\left]\right|_{\mu=\Lambda_f}. \tag{P.8}$$

In arriving to this expression we made the approximation

$$\widehat{\lambda}^{\{l_i\}}_{\{M_i\};\{\rho_i\}}(\{x_i\})\widehat{\lambda}^{\{j_i\}}_{\{N_i\};\{\sigma_i\}}(\{k_{i;N_i}\})\left[2 - z(l) + \sum_{j=1}^{4}\widetilde{\eta}^{(\psi)}_{N_j}(k_{j;N_j}(l))\right]$$
$$\approx \widehat{\lambda}^{\{l_i\}}_{\{M_i\};\{\rho_i\}}(\{x_i\})\widehat{\lambda}^{\{j_i\}}_{\{N_i\};\{\sigma_i\}}(\{k_{i;N_i}\}), \tag{P.9}$$

because corrections beyond the tree-level scaling dimension of the four-fermion include higher order terms in the coupling functions. Therefore, Eq. (P.8) must be taken as the *leading* order expression for the beta function of the momentum-dependent four-fermion coupling functions.

In the remaining of this appendix we focus on the beta function of the four-fermion couplings in the pairing channel. The generic four-fermion couplings $\lambda^{\{j_i\}}_{\{N_i\};\{\sigma_i\}}(\{k_{i;N_i}\})$ represent the scattering of a pair of electrons with momentum k_{3,N_3} and k_{4,N_4} into states with momentum k_{1,N_1} and k_{2,N_2}. In the following discussion it is convenient to choose these four momenta such that they represent the center of mass and relative momenta of the pairs involved in the process. We therefore make the following redefinition of momentum along the local FS's at hot spots N_1, N_2, N_3 and N_4:

$$k_{1;N_1} = -k + \frac{p}{2}, \quad k_{2;N_2} = k + \frac{p}{2}, \quad k_{3;N_3} = q + \frac{p}{2}, \quad k_{4;N_4} = -q + \frac{p}{2}. \tag{P.10}$$

We note that this choice of momenta is consistent with the momentum conservation constraint appearing in the four-fermion interaction term in Eq. (4.1) and, in general, each of the momenta k, q and p depend strongly on the hot spot indices. In this choice of momenta, p denotes the center of mass momentum of the electron pairs and k and q their relative momentum. It is therefore convenient to further redefine the coupling functions as

$$\alpha^{\{j_i\}}_{\{N_i\};\{\sigma_i\}}(k,q;p) \equiv \lambda^{\{j_i\}}_{\{N_i\};\{\sigma_i\}}\left(-k+\frac{p}{2}, k+\frac{p}{2}, q+\frac{p}{2}, -q+\frac{p}{2}\right), \tag{P.11}$$

and similarly for the couplings with rescaled momenta. Because the leading order superconducting instability is expected to arise in the zero momentum pairing channel, we focus only on the beta functions for the couplings in Group I shown in Table 4.1. In principle, we need to consider also the couplings in Group II because these also correspond to zero momentum pairing channels. However, these are not sourced by the spin fluctuations in the absence of bare four-fermion couplings. We consider first the beta functions to leading order in the four-fermion couplings and later analyze the contributions to quadratic order. In what follows we restrict the discussion to the physical case with $N_c = 2$ and $N_f = 1$. In this case we adopt the notation $\alpha^{\{\sigma_i\}}_{\{N_i\}}(k,q;p)$ for the coupling functions in the pairing channel. In the remaining of this appendix we further use the notation $\widehat{\alpha}^{\{\sigma_i\}}_{\{N_i\}}(k,q;p) \equiv \alpha^{\{\sigma_i\}}_{\{N_i\}}[k(l),q(l);p(l)]$ to denote the coupling functions with the momenta rescaled according to Eq. (4.41). We use the same convention for the beta functions of the four-fermion couplings.

P.1 Leading-Order Momentum-Dependent Beta Function

We construct the momentum-dependent beta functions of the couplings in Group I in Table 4.1 to linear order in the four-fermion couplings. For simplicity, and in order to get rid of the spin indices, we consider the decomposition into singlet and triplet spin channels given in Eq. (4.9):

$$\alpha^{\sigma_1\sigma_2\sigma_3\sigma_4}_{N_1N_2N_3N_4}(k,q;p) = \mathsf{A}^{\sigma_1\sigma_2}_{\sigma_3\sigma_4}\alpha^{\mathsf{S}}_{N_1N_2N_3N_4}(k,q;p) + \mathsf{S}^{\sigma_1\sigma_2}_{\sigma_3\sigma_4}\alpha^{\mathsf{A}}_{N_1N_2N_3N_4}(k,q;p), \tag{P.12}$$

where A and S are defined in Eqs. (4.10) and (4.11), respectively. These tensors satisfy the contraction identities

$$\begin{aligned}
&\sum_{\{\sigma_i=\uparrow,\downarrow\}} \mathsf{A}^{\sigma_1\sigma_2}_{\sigma_3\sigma_4}\mathsf{A}^{\sigma_1\sigma_2}_{\sigma_3\sigma_4} = 4, \qquad &&\sum_{\{\sigma_i=\uparrow,\downarrow\}} \mathsf{A}^{\sigma_1\sigma_2}_{\sigma_1\sigma_4}\mathsf{A}^{\sigma_3\sigma_2}_{\sigma_3\sigma_4} = 2,\\
&\sum_{\{\sigma_i=\uparrow,\downarrow\}} \mathsf{A}^{\sigma_1\sigma_2}_{\sigma_1\sigma_4}\mathsf{S}^{\sigma_3\sigma_2}_{\sigma_3\sigma_4} = -6, \qquad &&\sum_{\{\sigma_i=\uparrow,\downarrow\}} \mathsf{A}^{\sigma_1\sigma_2}_{\sigma_3\sigma_4}\mathsf{S}^{\sigma_1\sigma_2}_{\sigma_3\sigma_4} = 0,\\
&\sum_{\{\sigma_i=\uparrow,\downarrow\}} \mathsf{S}^{\sigma_1\sigma_2}_{\sigma_1\sigma_4}\mathsf{S}^{\sigma_3\sigma_2}_{\sigma_3\sigma_4} = 18, \qquad &&\sum_{\{\sigma_i=\uparrow,\downarrow\}} \mathsf{S}^{\sigma_1\sigma_2}_{\sigma_3\sigma_4}\mathsf{S}^{\sigma_1\sigma_2}_{\sigma_3\sigma_4} = 12.
\end{aligned} \tag{P.13}$$

From these identities it follows that the beta functions for the singlet and triplet components of the coupling functions are given by

$$\widehat{\beta}^{\mathsf{S}}_{N_1N_2N_3N_4}(k,q;p) = \frac{1}{4}\sum_{\{\sigma_i=\uparrow,\downarrow\}} \mathsf{A}^{\sigma_1\sigma_2}_{\sigma_3\sigma_4}\widehat{\beta}^{\{\sigma_i\}}_{N_1N_2N_3N_4}(k,q;p), \tag{P.14}$$

$$\widehat{\beta}^{\mathsf{A}}_{N_1N_2N_3N_4}(k,q;p) = \frac{1}{12}\sum_{\{\sigma_i=\uparrow,\downarrow\}} \mathsf{S}^{\sigma_1\sigma_2}_{\sigma_3\sigma_4}\widehat{\beta}^{\{\sigma_i\}}_{N_1N_2N_3N_4}(k,q;p). \tag{P.15}$$

We now determine the solution to the beta functions in Group I. In what follows we use the notation $\alpha^{\mathsf{S(A)}}_{N_1N_2N_3N_4} \equiv \alpha^{\mathsf{S(A)}}_{N_1N_2N_3N_4}(0,0;0)$ to denote the scale-dependent coupling functions evaluated at the hot spots.

P.1-(a) Beta functions for the four-fermion couplings in Group I

Using Eq. (P.8), the expressions for the counterterm functions in Eqs. (Q.228), (Q.238), (Q.246) and (Q.249), in combination with the derivative properties in Eqs. (Q.233), (Q.234), (Q.237), (Q.244), (Q.245) and (Q.248), we write the beta function of $\alpha^{\mathsf{S}}_{1515}(k,q;p)$ as

$$\begin{aligned}
\widehat{\beta}^{\mathsf{S}}_{1515}(k,q;p) &= -\Delta_{1515}[k(l),q(l);p(l);l]\widehat{\alpha}^{\mathsf{S}}_{1515}(k,p;q) - \frac{3w(v)}{16\pi z(l)}\alpha^{\mathsf{A}}_{1818}\\
&\times\Theta(\Lambda_f e^{-l}-v|k+q|)\Big[\Theta(\Lambda_f e^{-l}-vc(v)|p+q-k|)+\Theta(\Lambda_f e^{-l}-vc(v)|k+p-q|)\Big]\\
&-\frac{3w(v)}{16\pi z(l)}\alpha^{\mathsf{A}}_{1845}\Big\{\Theta(\Lambda_f e^{-l}-v|k-q|)\Big[\Theta(\Lambda_f e^{-l}-vc(v)|k+q+p|)\log(c(v)\widehat{\Lambda}_b)\\
&\qquad+\Theta(vc(v)|k+q+p|-\Lambda_f e^{-l})\log\left(\frac{e^{-l}\Lambda_b}{v|k+p+q|}\right)\Big]\\
&\quad+\Theta(\Lambda_f e^{-l}-v|q-k|)\Big[\Theta(\Lambda_f e^{-l}-vc(v)|q+k-p|)\log(c(v)\widehat{\Lambda}_b)\\
&\qquad+\Theta(vc(v)|q+k-p|-\Lambda_f e^{-l})\log\left(\frac{e^{-l}\Lambda_b}{v|k+q-p|}\right)\Big]\Big\}\\
&-\frac{3w(v)}{16\pi z(l)}\alpha^{\mathsf{S}}_{1548}\Theta(\Lambda_f e^{-l}-|p|)\Big\{\Big[\Theta(\Lambda e^{-l}-2vc(v)|k|)+\Theta(\Lambda_f e^{-l}-2vc(v)|q|)\Big]\log(c(v)\widehat{\Lambda}_b)\\
&+\Theta(2vc(v)|k|-\Lambda_f e^{-l})\log\left(\frac{e^{-l}\Lambda_b}{2v|k|}\right)+\Theta(2vc(v)|q|-\Lambda_f e^{-l})\log\left(\frac{e^{-l}\Lambda_b}{2v|q|}\right)\Big\},
\end{aligned} \tag{P.16}$$

$$
\begin{aligned}
&- \frac{\mathscr{J}_1}{8z(l)}\frac{v^2}{c(v)}\Theta(\Lambda_f e^{-l} - v|q-k|)\Theta(\Lambda_f e^{-l} - c(v)|q+k|) \\
&\times \Big[\Theta(\Lambda_f e^{-l} - vc(v)|k+q+p|)\Theta(\Lambda_f e^{-l} - vc(v)|p+2(q+k)|) \\
&+\Theta(\Lambda_f e^{-l} - v|p-q-k|)\Theta(\Lambda_f e^{-l} - vc(v)|p-2(q+k)|)\Big] - \frac{3\mathscr{J}_1}{4z(l)}\frac{v^2}{c(v)} \\
&\times \Theta(\Lambda_f e^{-l} - v|p|)\Theta(\Lambda_f e^{-l} - 2vc(v)|k|)\Theta(\Lambda_f e^{-l} - vc(v)|3k+q|)\Theta(\Lambda_f e^{-l} - c(v)|k+q|).
\end{aligned}
$$

Here, $\Theta(x)$ denotes the Heaviside function and the notation $\Theta(x-y)$ implicitly enforces the condition $x \gg y$ for $x, y > 0$. Similarly, the beta function of $\alpha^{\mathsf{A}}_{1515}(k,q;p)$ takes the form

$$
\begin{aligned}
&\widehat{\beta}^{\mathsf{A}}_{1515}(k,q;p) = -\Delta_{1515}[k(l),q(l);p(l);l]\widehat{\alpha}^{\mathsf{A}}_{1515}(k,p;q) + \frac{w(v)}{16\pi z(l)}\left[2\alpha^{\mathsf{A}}_{1818} - \alpha^{\mathsf{S}}_{1818}\right] \\
&\times \Theta(\Lambda_f e^{-l} - v|k+q|)\left[\Theta(\Lambda_f e^{-l} - vc(v)|p+q-k|) + \Theta(\Lambda_f e^{-l} - vc(v)|k+p-q|)\right] \\
&- \frac{w(v)}{16\pi z(l)}\left[2\alpha^{\mathsf{A}}_{1845} + \alpha^{\mathsf{S}}_{1845}\right]\Big\{\Theta(\Lambda_f e^{-l} - v|k-q|)\Big[\Theta(\Lambda_f e^{-l} - vc(v)|k+q+p|)\log(c(v)\widehat{\Lambda}_b) \\
&\qquad +\Theta(vc(v)|k+q+p| - \Lambda_f e^{-l})\log\left(\frac{e^{-l}\Lambda_b}{v|k+p+q|}\right)\Big] \\
&+\Theta(\Lambda_f e^{-l} - |q-k|)\Big[\Theta(\Lambda_f e^{-l} - vc(v)|q+k-p|)\log(c(v)\widehat{\Lambda}_b) \\
&\qquad +\Theta(vc(v)|q+k-p| - \Lambda_f e^{-l})\log\left(\frac{e^{-l}\Lambda_b}{v|k+q-p|}\right)\Big]\Big\} \\
&+ \frac{w(v)}{16\pi z(l)}\alpha^{\mathsf{A}}_{1548}\Theta(\Lambda_f e^{-l} - |p|)\Big\{\Big[\Theta(\Lambda_f e^{-l} - 2vc(v)|k|) + \Theta(\Lambda_f e^{-l} - 2vc(v)|q|)\Big]\log(c(v)\widehat{\Lambda}_b) \quad \text{(P.17)} \\
&+\Theta(2vc(v)|k| - \Lambda_f e^{-l})\log\left(\frac{e^{-l}\Lambda_b}{2v|k|}\right) + \Theta(2vc(v)|q| - \Lambda_f e^{-l})\log\left(\frac{e^{-l}\Lambda_b}{2v|q|}\right)\Big\} \\
&- \frac{5\mathscr{J}_1}{24z(l)}\frac{v^2}{c(v)}\Theta(\Lambda_f e^{-l} - v|q-k|)\Theta(\Lambda_f e^{-l} - c(v)|q+k|) \\
&\times \Big[\Theta(\Lambda_f e^{-l} - vc(v)|k+q+p|)\Theta(\Lambda_f e^{-l} - vc(v)|p+2(q+k)|) \\
&+\Theta(\Lambda_f e^{-l} - v|p-q-k|)\Theta(\Lambda_f e^{-l} - vc(v)|p-2(q+k)|)\Big] + \frac{\mathscr{J}_1}{12z(l)}\frac{v^2}{c(v)} \\
&\times \Theta(\Lambda_f e^{-l} - v|p|)\Theta(\Lambda_f e^{-l} - 2vc(v)|k|)\Theta(\Lambda_f e^{-l} - vc(v)|3k+q|)\Theta(\Lambda_f e^{-l} - c(v)|k+q|).
\end{aligned}
$$

The beta function of $\alpha^{\mathsf{S}}_{1818}(k,q;p)$ is given by:

$$
\begin{aligned}
&\widehat{\beta}^{\mathsf{S}}_{1818}(k,q;p) = -\Delta_{1818}[k(l),q(l);p(l);l]\widehat{\alpha}^{\mathsf{S}}_{1818}(k,p;q) - \frac{3w(v)}{16\pi z(l)}\alpha^{\mathsf{A}}_{1515} \\
&\times \Theta(\Lambda_f e^{-l} - v|k+q|)\left[\Theta(\Lambda_f e^{-l} - vc(v)|p+q-k|) + \Theta(\Lambda_f e^{-l} - vc(v)|k+p-q|)\right] \\
&- \frac{\mathscr{J}_2}{8z(l)}\frac{v^2}{c(v)}\Theta(\Lambda_f e^{-l} - vc(v)|k-q|)\Big[\Theta(\min[v\Lambda_b,\Lambda_f]e^{-l} - v|k+p+q|) \quad \text{(P.18)} \\
&\qquad +\Theta(\min[v\Lambda_b,\Lambda_f]e^{-l} - v|k+q-p|)\Big]
\end{aligned}
$$

$$- \frac{3\mathscr{J}_2}{4z(l)}\frac{v^2}{c(v)}\Theta(\min[v\Lambda_b,\Lambda_f]e^{-l}-2v|k|)\Theta(\Lambda_f e^{-l}-vc(v)|p|).$$

Similarly the beta function of $\alpha^{\mathsf{A}}_{1818}(k,q;p)$ is given by:

$$\begin{aligned}\widehat{\beta}^{\mathsf{A}}_{1818}(k,q;p) &= -\Delta_{1818}[k(l),q(l);p(l);l]\widehat{\alpha}^{\mathsf{A}}_{1818}(k,p;q)+\frac{w(v)}{16\pi z(l)}[2\alpha^{\mathsf{A}}_{1515}-\alpha^{\mathsf{S}}_{1515}]\\ &\times\Theta(\Lambda_f e^{-l}-v|k+q|)\left[\Theta(\Lambda_f e^{-l}-vc(v)|p+q-k|)+\Theta(\Lambda_f e^{-l}-vc(v)|k+p-q|)\right]\\ &-\frac{5\mathscr{J}_2}{24z(l)}\Theta(\Lambda_f e^{-l}-vc(v)|k-q|)\left[\Theta(\min[v\Lambda_b,\Lambda_f]e^{-l}-v|k+p+q|)\right.\\ &\qquad\left.+\Theta(\min[v\Lambda_b,\Lambda_f]e^{-l}-v|k+q-p|)\right]\\ &+\frac{\mathscr{J}_2}{12z(l)}\frac{v^2}{c(v)}\Theta(\min[v\Lambda_b,\Lambda_f]e^{-l}-2v|k|)\Theta(\Lambda_f e^{-l}-vc(v)|p|).\end{aligned}\tag{P.19}$$

The beta function of $\alpha^{\mathsf{S}}_{1845}(k,q;p)$ reads

$$\begin{aligned}\widehat{\beta}^{\mathsf{S}}_{1845}(k,q;p) &= -\Delta_{1845}[k(l),q(l);p(l);l]\widehat{\alpha}^{\mathsf{S}}_{1845}(k,p;q)+\frac{3w(v)}{16\pi z(l)}\log\left(\frac{1}{w(v)}\right)\alpha^{\mathsf{A}}_{1548}\\ &\times\Theta(\Lambda_f-v^2|k+q|)\left[\Theta(\min[v\Lambda_b,\Lambda_f]-v|p+q-k|)+\Theta(\min[v\Lambda_b,\Lambda_f]-v|k+p-q|)\right]\\ &-\frac{3w(v)}{16\pi z(l)}\alpha^{\mathsf{A}}_{1515}\Theta(\Lambda_f e^{-l}-v|k-q|)\left[\Theta(\Lambda_f e^{-l}-vc(v)|k+p+q|)\log(c(v)\widehat{\Lambda}_b)\right.\\ &+\Theta(vc(v)|k+p+q|-\Lambda_f e^{-l})\log\left(\frac{e^{-l}\Lambda_b}{v|k+p+q|}\right)+\Theta(\Lambda_f e^{-l}-vc(v)|p-k-q|)\\ &\left.\times\log(c(v)\widehat{\Lambda}_b)+\Theta(vc(v)|p-k-q|-\Lambda_f e^{-l})\log\left(\frac{e^{-l}\Lambda_b}{v|p-k-q|}\right)\right].\end{aligned}\tag{P.20}$$

Similarly, the beta function of $\alpha^{\mathsf{A}}_{1845}(k,q;p)$ reads

$$\begin{aligned}\widehat{\beta}^{\mathsf{A}}_{1845}(k,q;p) &= -\Delta_{1845}[k(l),q(l);p(l);l]\widehat{\alpha}^{\mathsf{A}}_{1845}(k,p;q)-\frac{w(v)}{16\pi z(l)}\log\left(\frac{1}{w(v)}\right)[2\alpha^{\mathsf{A}}_{1548}-\alpha^{\mathsf{S}}_{1548}]\\ &\times\Theta(\Lambda_f-v^2|k+q|)\left[\Theta(\min[v\Lambda_b,\Lambda_f]-v|p+q-k|)+\Theta(\min[v\Lambda_b,\Lambda_f]-v|k+p-q|)\right]\\ &-\frac{w(v)}{16\pi z(l)}\left[2\alpha^{\mathsf{A}}_{1515}+\alpha^{\mathsf{S}}_{1515}\right]\Theta(\Lambda_f e^{-l}-v|k-q|)\left[\Theta(\Lambda_f e^{-l}-vc(v)|k+p+q|)\log(c(v)\widehat{\Lambda}_b)\right.\\ &+\Theta(vc(v)|k+p+q|-\Lambda_f e^{-l})\log\left(\frac{e^{-l}\Lambda_b}{v|k+p+q|}\right)+\Theta(\Lambda_f e^{-l}-vc(v)|p-k-q|)\\ &\left.\times\log(c(v)\widehat{\Lambda}_b)-\Theta(vc(v)|p-k-q|+\Lambda_f e^{-l})\log\left(\frac{e^{-l}\Lambda_b}{v|p-k-q|}\right)\right].\end{aligned}\tag{P.21}$$

The beta function of $\alpha^{\mathsf{S}}_{1548}(k,q;p)$ takes the form

$$\begin{aligned}\widehat{\beta}^{\mathsf{S}}_{1548}(k,q;p) &= -\Delta_{1548}[k(l),q(l);p(l);l]\widehat{\alpha}^{\mathsf{S}}_{1548}(k,p;q)\\ &+\frac{3w(v)}{16\pi z(l)}\log\left(\frac{1}{w(v)}\right)\alpha^{\mathsf{A}}_{1845}\Theta(\Lambda_f e^{-l}-v^2|k+q|)\left[\Theta(\min[v\Lambda_b,\Lambda_f]e^{-l}-v|k+p-q|)\right.\end{aligned}$$

$$+\Theta(\min[v\Lambda_b,\Lambda_f]e^{-l}-v|p+q-k|)\Big]-\frac{3w(v)}{16\pi z(l)}\alpha^{\mathsf{S}}_{1515}\Theta(\Lambda_f e^{-l}-v|p|) \tag{P.22}$$
$$\times\Big[\Theta(\Lambda_f e^{-l}-2vc(v)|k|)\log(c(v)\widehat{\Lambda}_b)+\Theta(\Lambda_f e^{-l}-2vc(v)|q|)\log(c(v)\widehat{\Lambda}_b)$$
$$+\Theta(2vc(v)|k|-\Lambda_f e^{-l})\log\left(\frac{e^{-l}\Lambda_b}{2v|k|}\right)+\Theta(2vc(v)|q|-\Lambda_f e^{-l})\log\left(\frac{e^{-l}\Lambda_b}{2v|q|}\right)\Big].$$

Finally, the beta function of $\alpha^{\mathsf{A}}_{1548}(k,q;p)$ is given by

$$\widehat{\beta}^{\mathsf{A}}_{1548}(k,q;p)=-\Delta_{1515}[k(l),q(l);p(l);l]\widehat{\alpha}^{\mathsf{A}}_{1548}(k,p;q)-\frac{w(v)}{16\pi z(l)}\log\left(\frac{1}{w(v)}\right)$$
$$\times\Big[2\alpha^{\mathsf{A}}_{1845}-\alpha^{\mathsf{S}}_{1845}\Big]\Theta(\Lambda_f e^{-l}-v^2|k+q|)\Big[\Theta(\min[v\Lambda_b,\Lambda_f]e^{-l}-v|k+p-q|)$$
$$+\Theta(\min[v\Lambda_b,\Lambda_f]e^{-l}-v|p+q-k|)\Big]+\frac{w(v)}{16\pi z(l)}\alpha^{\mathsf{A}}_{1515}\Theta(\Lambda_f e^{-l}-v|p|) \tag{P.23}$$
$$\times\Big[\Theta(\Lambda_f e^{-l}-2vc(v)|k|)\log(c(v)\widehat{\Lambda}_b)+\Theta(\Lambda_f e^{-l}-2vc(v)|q|)\log(c(v)\widehat{\Lambda}_b)$$
$$+\Theta(2vc(v)|k|-\Lambda_f e^{-l})\log\left(\frac{e^{-l}\Lambda_b}{2v|k|}\right)+\Theta(2vc(v)|q|-\Lambda_f e^{-l})\log\left(\frac{e^{-l}\widehat{\Lambda}_b}{2v|q|}\right)\Big].$$

In all of the above expressions for the beta functions, we have defined the scaling dimension of the four-fermion coupling functions as

$$\Delta_{N_1N_2N_3N_4}[k,q;p]\equiv\frac{1}{z(l)}\Big[2-z(l)+\widetilde{\eta}^{(\psi)}_{N_1}(-k+p/2)+\widetilde{\eta}^{(\psi)}_{N_2}(k+p/2)$$
$$+\widetilde{\eta}^{(\psi)}_{N_3}(q+p/2)+\widetilde{\eta}^{(\psi)}_{N_4}(-q+p/2)\Big]. \tag{P.24}$$

The solution to the momentum dependent beta functions requires the determination of the scale-dependent coupling functions at the hot spots. Therefore, we first solve the set of equations:

$$\frac{\mathrm{d}\alpha^{\mathsf{S}}_{1515}}{\mathrm{d}l}=-\Delta_{1515}[l]\alpha^{\mathsf{S}}_{1515}-\frac{3w(v)}{8\pi z(l)}\alpha^{\mathsf{A}}_{1818}-\frac{3w(v)}{8\pi z(l)}\alpha^{\mathsf{A}}_{1845}\log(c(v)\widehat{\Lambda}_b(l))$$
$$-\frac{3w(v)}{8\pi z(l)}\alpha^{\mathsf{S}}_{1548}\log(c(v)\widehat{\Lambda}_b(l))-\frac{\mathscr{J}_1}{z(l)}\frac{v^2}{zc(v)}, \tag{P.25}$$
$$\frac{\mathrm{d}\alpha^{\mathsf{A}}_{1515}}{\mathrm{d}l}=-\Delta_{1515}[l]\alpha^{\mathsf{A}}_{1515}+\frac{w(v)}{8\pi z(l)}\Big[2\alpha^{\mathsf{A}}_{1818}-\alpha^{\mathsf{S}}_{1818}\Big]+\frac{w(v)}{8\pi z(l)}\alpha^{\mathsf{A}}_{1548}\log(c(v)\widehat{\Lambda}_b(l))$$
$$-\frac{w(v)}{8\pi z(l)}\Big[2\alpha^{\mathsf{A}}_{1845}+\alpha^{\mathsf{S}}_{1845}\Big]\log(c(v)\widehat{\Lambda}_b(l))-\frac{\mathscr{J}_1}{3z(l)}\frac{v^2}{c(v)}, \tag{P.26}$$
$$\frac{\mathrm{d}\alpha^{\mathsf{S}}_{1818}}{\mathrm{d}l}=-\Delta_{1818}[l]\alpha^{\mathsf{S}}_{1818}-\frac{3w(v)}{8\pi z(l)}\alpha^{\mathsf{A}}_{1515}-\frac{\mathscr{J}_2}{z(l)}\frac{v^2}{c(v)}, \tag{P.27}$$
$$\frac{\mathrm{d}\alpha^{\mathsf{A}}_{1818}}{\mathrm{d}l}=-\Delta_{1818}[l]\alpha^{\mathsf{A}}_{1818}+\frac{w(v)}{8\pi z(l)}[2\alpha^{\mathsf{A}}_{1515}-\alpha^{\mathsf{S}}_{1515}]-\frac{\mathscr{J}_2}{3z(l)}\frac{v^2}{c(v)}, \tag{P.28}$$
$$\frac{\mathrm{d}\alpha^{\mathsf{S}}_{1845}}{\mathrm{d}l}=-\Delta_{1845}[l]\alpha^{\mathsf{S}}_{1845}+\frac{3w(v)}{8\pi z(l)}\log\left(\frac{1}{w(v)}\right)\alpha^{\mathsf{A}}_{1548}-\frac{3w(v)}{8\pi z(l)}\alpha^{\mathsf{A}}_{1515}\log(c(v)\widehat{\Lambda}_b), \tag{P.29}$$

$$\frac{\mathrm{d}\alpha^{\mathsf{A}}_{1845}}{\mathrm{d}l} = -\Delta_{1845}[l]\alpha^{\mathsf{A}}_{1845} - \frac{w(v)}{8\pi z(l)}\log\left(\frac{1}{w(v)}\right)[2\alpha^{\mathsf{A}}_{1548} - \alpha^{\mathsf{S}}_{1548}] - \frac{w(v)}{8\pi z(l)}\left[2\alpha^{\mathsf{A}}_{1515} + \alpha^{\mathsf{S}}_{1515}\right]\log(c(v)\widehat{\Lambda}_b), \tag{P.30}$$

$$\frac{\mathrm{d}\alpha^{\mathsf{S}}_{1548}}{\mathrm{d}l} = -\Delta_{1548}[l]\alpha^{\mathsf{S}}_{1548} + \frac{3w(v)}{8\pi z(l)}\log\left(\frac{1}{w(v)}\right)\alpha^{\mathsf{A}}_{1845} - \frac{3w(v)}{8\pi z(l)}\alpha^{\mathsf{S}}_{1515}\log(c(v)\widehat{\Lambda}_b), \tag{P.31}$$

$$\frac{\mathrm{d}\alpha^{\mathsf{A}}_{1548}}{\mathrm{d}l} = -\Delta_{1515}[l]\alpha^{\mathsf{A}}_{1548} - \frac{w(v)}{8\pi z(l)}\log\left(\frac{1}{w(v)}\right)\left[2\alpha^{\mathsf{A}}_{1845} - \alpha^{\mathsf{S}}_{1845}\right] + \frac{w(v)}{8\pi z(l)}\alpha^{\mathsf{A}}_{1515}\log(c(v)\widehat{\Lambda}_b), \tag{P.32}$$

where the length-scale dependent scaling dimension of the four-fermion couplings are given by the hot spot independent quantity:

$$\Delta_{N_1N_2N_3N_4}[l] = \frac{1}{z(l)}\left[2 - z(l) + 4\widetilde{\eta}^{(\psi)}\right]. \tag{P.33}$$

We are interested in the low-energy limit. This allows a further simplification rooted in the fact that $\widehat{\Lambda}_b(l) = \widehat{\Lambda}^{(0)}_b e^l$. Assuming that all four-fermion couplings are almost of the same order at a given energy scale, we can further approximate, to leading order in $l \gg 1$,

$$\frac{\mathrm{d}\alpha^{\mathsf{S}}_{1515}}{\mathrm{d}l} = -\alpha^{\mathsf{S}}_{1515} - \frac{3w(v)l}{8\pi}\alpha^{\mathsf{A}}_{1845} - \frac{3w(v)l}{8\pi}\alpha^{\mathsf{S}}_{1548} - \mathscr{J}_1\frac{v^2}{c(v)}, \tag{P.34}$$

$$\frac{\mathrm{d}\alpha^{\mathsf{A}}_{1515}}{\mathrm{d}l} = -\alpha^{\mathsf{A}}_{1515} + \frac{w(v)l}{8\pi}\alpha^{\mathsf{A}}_{1548} - \frac{w(v)l}{8\pi}\left[2\alpha^{\mathsf{A}}_{1845} + \alpha^{\mathsf{S}}_{1845}\right] - \frac{\mathscr{J}_1}{3}\frac{v^2}{c(v)}, \tag{P.35}$$

$$\frac{\mathrm{d}\alpha^{\mathsf{S}}_{1818}}{\mathrm{d}l} = -\alpha^{\mathsf{S}}_{1818} - \frac{3w(v)}{8\pi}\alpha^{\mathsf{A}}_{1515} - \mathscr{J}_2\frac{v^2}{c(v)}, \tag{P.36}$$

$$\frac{\mathrm{d}\alpha^{\mathsf{A}}_{1818}}{\mathrm{d}l} = -\alpha^{\mathsf{A}}_{1818} + \frac{w(v)}{8\pi}[2\alpha^{\mathsf{A}}_{1515} - \alpha^{\mathsf{S}}_{1515}] - \frac{\mathscr{J}_2}{3}\frac{v^2}{c(v)}, \tag{P.37}$$

$$\frac{\mathrm{d}\alpha^{\mathsf{S}}_{1845}}{\mathrm{d}l} = -\alpha^{\mathsf{S}}_{1845} - \frac{3w(v)l}{8\pi}\alpha^{\mathsf{A}}_{1515}, \tag{P.38}$$

$$\frac{\mathrm{d}\alpha^{\mathsf{A}}_{1845}}{\mathrm{d}l} = -\alpha^{\mathsf{A}}_{1845} - \frac{w(v)l}{8\pi}\left[2\alpha^{\mathsf{A}}_{1515} + \alpha^{\mathsf{S}}_{1515}\right], \tag{P.39}$$

$$\frac{\mathrm{d}\alpha^{\mathsf{S}}_{1548}}{\mathrm{d}l} = -\alpha^{\mathsf{S}}_{1548} - \frac{3w(v)l}{8\pi}\alpha^{\mathsf{S}}_{1515}, \tag{P.40}$$

$$\frac{\mathrm{d}\alpha^{\mathsf{A}}_{1548}}{\mathrm{d}l} = -\alpha^{\mathsf{A}}_{1548} + \frac{w(v)l}{8\pi}\alpha^{\mathsf{A}}_{1515}, \tag{P.41}$$

where we have dropped terms of order $\alpha^{\mathsf{S,A}}_{N_1N2N_3N_4}w(v)$ and $\alpha^{\mathsf{S,A}}_{N_1N2N_3N_4}w(v)\log(1/v)$ with respect to those terms of order $\alpha^{\mathsf{S,A}}_{N_1N2N_3N_4}w(v)l$ in the $l \gg 1$ and $w(v) \ll 1$ limits. Moreover, in the low-energy limit, $z(l) \approx 1$ and $\Delta_{N_1N_2N_3N_4}[l] \approx 1$.

A. Solution to the zero momentum beta functions

We proceed on solving the set of coupled beta functions in Eqs. (P.34) to (P.41). The first thing to notice is that the beta functions for $\alpha^{\mathsf{S}}_{1818}$ and $\alpha^{\mathsf{A}}_{1818}$ are determined solely by the

flow of $\alpha^{\mathsf{S}}_{1515}$ and $\alpha^{\mathsf{A}}_{1515}$ and these have no feedback on the flow of all other couplings. To simplify the discussion we adopt the following coupling redefinitions

$$x_1 \equiv e^l \alpha^{\mathsf{S}}_{1515}, \qquad x_2 \equiv e^l \alpha^{\mathsf{S}}_{1845}, \quad x_3 \equiv e^l \alpha^{\mathsf{S}}_{1548}, \tag{P.42}$$

$$x_4 \equiv e^l \alpha^{\mathsf{A}}_{1515}, \qquad x_5 \equiv e^l \alpha^{\mathsf{A}}_{1845}, \quad x_6 \equiv e^l \alpha^{\mathsf{A}}_{1548}. \tag{P.43}$$

With these definitions, Eqs. (P.34), (P.35) and (P.38) to (P.41) can be written in the matrix form:

$$\frac{\mathrm{d}}{\mathrm{d}l}\begin{pmatrix} x_1 \\ x_2 \\ x_3 \\ x_4 \\ x_5 \\ x_6 \end{pmatrix} = -\frac{w(v)l}{8\pi}\begin{pmatrix} 0 & 0 & 3 & 0 & 3 & 0 \\ 0 & 0 & 0 & 3 & 0 & 0 \\ 3 & 0 & 0 & 0 & 0 & 0 \\ 0 & 1 & 0 & 0 & 2 & -1 \\ 1 & 0 & 0 & 2 & 0 & 0 \\ 0 & 0 & 0 & -1 & 0 & 0 \end{pmatrix}\begin{pmatrix} x_1 \\ x_2 \\ x_3 \\ x_4 \\ x_5 \\ x_6 \end{pmatrix} - \frac{\mathscr{J}_1 v^2}{c(v)} e^l \begin{pmatrix} 1 \\ 0 \\ 0 \\ \frac{1}{3} \\ 0 \\ 0 \end{pmatrix}. \tag{P.44}$$

Denoting by $\boldsymbol{x}(l) = (x_1, x_2, x_3, x_4, x_5, x_6)^{\mathrm{T}}$, we solve this expression by imposing the boundary condition $\boldsymbol{x}(0) = (x_1^{(0)}, x_2^{(0)}, x_3^{(0)}, x_4^{(0)}, x_5^{(0)}, x_6^{(0)})^{\mathrm{T}}$. As it can be checked by direct differentiation, the solution to the system of coupled equations is given by

$$\boldsymbol{x}(l) = \sum_{j=1}^{6} \exp\left(-\frac{\lambda_j}{8\pi}\int_0^l \mathrm{d}\ell w(\ell)\ell\right)\left[b_j - \mathscr{J}_1 y_j \int_0^l \mathrm{d}\ell \frac{v(\ell)^2}{c(\ell)} \exp\left(\ell + \frac{\lambda_j}{8\pi}\int_0^\ell \mathrm{d}\ell' w(\ell')\ell'\right)\right]\boldsymbol{v}_j, \tag{P.45}$$

where $v(\ell), c(\ell)$ and $w(\ell)$ are given in Eqs. (4.98), (L.20) and (4.76), respectively. The λ_j's and $\boldsymbol{v}_j$'s correspond to the eigenvalues and eigenvectors of the matrix in Eq. (P.44), respectively. The eigenvalues of the associated matrix are given by

$$\lambda_1 = -\sqrt{14}, \quad \lambda_2 = \sqrt{14}, \quad \lambda_3 = -\sqrt{6}, \quad \lambda_4 = \sqrt{6}, \quad \lambda_5 = 0, \quad \& \quad \lambda_6 = 0. \tag{P.46}$$

and the corresponding eigenvectors by

$$\boldsymbol{v}_1 = \begin{pmatrix} 3\sqrt{14} \\ -3 \\ -9 \\ \sqrt{14} \\ -5 \\ 1 \end{pmatrix}, \quad \boldsymbol{v}_2 = \begin{pmatrix} -3\sqrt{14} \\ -3 \\ -9 \\ -\sqrt{14} \\ -5 \\ 1 \end{pmatrix}, \quad \boldsymbol{v}_3 = \begin{pmatrix} -\sqrt{6} \\ -3 \\ 3 \\ \sqrt{6} \\ -1 \\ 1 \end{pmatrix}, \quad \boldsymbol{v}_4 = \begin{pmatrix} \sqrt{6} \\ -3 \\ 3 \\ -\sqrt{6} \\ -1 \\ 1 \end{pmatrix},$$

$$\boldsymbol{v}_5 = \begin{pmatrix} 0 \\ 1 \\ 0 \\ 0 \\ 0 \\ 1 \end{pmatrix} \quad \& \quad \boldsymbol{v}_6 = \begin{pmatrix} 0 \\ -2 \\ -1 \\ 0 \\ 1 \\ 0 \end{pmatrix}. \tag{P.47}$$

Finally, b_j and y_j correspond to the expansion coefficients of $\boldsymbol{x}(0)$ and the source vector in Eq. (P.44), respectively, in the basis $\{\boldsymbol{v}_j\}_{\{j=1,\dots 6\}}$. These are given by

$$\boldsymbol{b} \equiv \begin{pmatrix} \frac{1}{112}(\sqrt{14}x_1^{(0)} - x_2^{(0)} - 3x_3^{(0)} + \sqrt{14}x_4^{(0)} - 5x_5^{(0)} + x_6^{(0)}) \\ \frac{1}{112}(-\sqrt{14}x_1^{(0)} - x_2^{(0)} - 3x_3^{(0)} - \sqrt{14}x_4^{(0)} - 5x_5^{(0)} + x_6^{(0)}) \\ \frac{1}{48}[-\sqrt{6}x_1^{(0)} + 3(-x_2^{(0)} + x_3^{(0)} + \sqrt{6}x_4^{(0)} - x_5^{(0)} + x_6^{(0)})] \\ \frac{1}{48}[\sqrt{6}x_1^{(0)} - 3(x_2^{(0)} - x_3^{(0)} + \sqrt{6}x_4^{(0)} + x_5^{(0)} - x_6^{(0)})] \\ \frac{1}{14}[2x_2^{(0)} - x_3^{(0)} + 3(x_5^{(0)} + 4x_6^{(0)})] \\ \frac{1}{14}(-3x_2^{(0)} - 2x_3^{(0)} + 6x_5^{(0)} + 3x_6^{(0)}) \end{pmatrix} \quad \& \quad \boldsymbol{y} \equiv \frac{1}{6\sqrt{14}} \begin{pmatrix} 1 \\ -1 \\ 0 \\ 0 \\ 0 \\ 0 \end{pmatrix}. \tag{P.48}$$

The solution in Eq. (P.45) clearly depends on the flow of $v(l)$. As discussed in Sec. 4.5-(*a*) the leading order beta functions and therefore their solutions are controlled provided that $w(l)l \ll 1$. This condition is achieved if and only if $1 \ll l \ll 1/w_0$, where $w_0 = w(v_0) \sim \sqrt{\ell_0}$, with v_0 denoting the bare value of the slope of the FS at the hot spots. Using this, the solution in Eq. (P.45) can be readily determined. In what follows we focus on the theory in which all the four-fermion couplings are set to zero at a the UV scale Λ_f. With this at hand, Eq. (P.45) takes the form

$$\begin{aligned} \boldsymbol{x}(l) = &-\frac{\mathscr{J}_1 v_0^2}{6\sqrt{14}c_0^2} \exp\left(\frac{\sqrt{14}w_0}{16\pi} l^2\right) \int_0^l \mathrm{d}\ell \exp\left(\ell - \frac{\sqrt{14}w_0}{16\pi}\ell^2\right) \boldsymbol{v}_1 \\ &+ \frac{\mathscr{J}_1 v_0^2}{6\sqrt{14}c_0} \exp\left(-\frac{\sqrt{14}w_0}{16\pi} l^2\right) \int_0^l \mathrm{d}\ell \exp\left(\ell + \frac{\sqrt{14}w_0}{16\pi}\ell^2\right) \boldsymbol{v}_2, \end{aligned} \tag{P.49}$$

A further integration over the length scale yields

$$\begin{aligned} \boldsymbol{x}(l) = &\frac{\mathscr{J}_1\sqrt{\pi}}{12\sqrt{14}} \frac{v_0^2}{c_0} \frac{e^{\frac{1}{4w_0 a}}}{\sqrt{aw_0}} \exp\left(aw_0 l^2\right) \left[\mathrm{Erf}\left(\frac{1-2aw_0 l}{2\sqrt{aw_0}}\right) - \mathrm{Erf}\left(\frac{1}{2\sqrt{aw_0}}\right)\right] \boldsymbol{v}_1 \\ &+ \frac{\mathscr{J}_1\sqrt{\pi}}{12\sqrt{14}} \frac{v_0^2}{c_0} \frac{e^{-\frac{1}{4w_0 a}}}{\sqrt{aw_0}} \exp\left(-aw_0 l^2\right) \left[\mathrm{Erfi}\left(\frac{1+2aw_0 l}{2\sqrt{aw_0}}\right) - \mathrm{Erfi}\left(\frac{1}{2\sqrt{aw_0}}\right)\right] \boldsymbol{v}_2. \end{aligned} \tag{P.50}$$

where for simplicity we have defined $a \equiv \sqrt{14}/16\pi < 1$. Here, $\mathrm{Erf}(x)$ [$\mathrm{Erfi}(x)$] is the (imaginary) error function. At this stage it is convenient to analyze the terms in each direction set by the eigenvectors $\boldsymbol{v}_1$ and $\boldsymbol{v}_2$. In both directions, the couplings $x_i(l)$ grow rapidly within the control window. In particular, the growth in the direction of $\boldsymbol{v}_1$ is much faster than that of $\boldsymbol{v}_2$ as we now argue. At the control energy scale $l_{\mathrm{con.}} \sim 1/w_0$, Eq. (P.50) is given, in the $w_0 \ll 1$ limit, by

$$\boldsymbol{x}(l_{\mathrm{con.}}) \sim \frac{\mathscr{J}_1}{6\sqrt{14}} \frac{v_0^2}{c_0} \left[\frac{e^{\frac{1}{w_0}}}{1-2a} - e^{\frac{a}{w_0}}\right] \boldsymbol{v}_1 + \frac{\mathscr{J}_1}{6\sqrt{14}(1+2a)} \frac{v_0^2}{c_0} e^{\frac{1}{w_0}} \boldsymbol{v}_2, \tag{P.51}$$

which suggests that, the couplings in that solve Eqs. (P.34) to (P.41) remain small at the boundary of the control window due to the exponential suppression arising from the tree-level

scaling dimension of the couplings. At a marginally larger scale, $\ell' \sim 1/(aw_0)$,

$$\boldsymbol{x}(l') \sim \frac{\mathscr{J}_1}{6\sqrt{14}}\frac{v_0^2}{c_0}\left[\frac{\sqrt{\pi}}{\sqrt{a}}\frac{e^{\frac{5}{4aw_0}}}{\sqrt{w_0}} - 2e^{\frac{1}{aw_0}}\right]\boldsymbol{v}_1 + \frac{\mathscr{J}_1}{18\sqrt{14}}\frac{v_0^2}{c_0}e^{\frac{1}{aw_0}}\boldsymbol{v}_2. \tag{P.52}$$

Since $5/4a > 1$, this implies that the the couplings in that solve Eqs. (P.34) to (P.41) become exponentially large in the $w_0 \ll 1$ limit. We further note that the coupling in the direction of $\boldsymbol{v}_1$ is always larger and grows faster than that in the direction of $\boldsymbol{v}_2$ at scales marginally larger than the control scale. Finally, note that at the scale $l^* \sim 1/\sqrt{w_0}$, Eq. (P.50) takes the leading order form in the $w_0 \ll 1$ limit:

$$\boldsymbol{x}(l^*) \sim \frac{\mathscr{J}_1}{6\sqrt{14}}\frac{v_0^2}{c_0}\left[e^{\frac{1}{\sqrt{w_0}}} - e^{a}\right]\boldsymbol{v}_1 + \frac{\mathscr{J}_1}{6\sqrt{14}}\frac{v_0^2}{c_0}\left[e^{\frac{1}{\sqrt{w_0}}} + e^{-a}\right]\boldsymbol{v}_2. \tag{P.53}$$

Although the $\boldsymbol{x}(l)$ couplings are exponentially large in the small w_0 limit, it follows that the couplings that solve Eqs. (P.34) to (P.41) are still exponentially small a this length scale as a consequence of the exponential suppression inherited from the tree-level scaling dimension of the couplings. Although up to the control scale $l_{\text{con.}} \sim 1/w_0$ the coupling in both directions is comparable in magnitude, we note that the fastest growing channel is that in the direction of $\boldsymbol{v}_1$. Therefore our primary focus lies on

$$\boldsymbol{x}(l) = \frac{\mathscr{J}_1\sqrt{\pi}}{12\sqrt{14}}\frac{v_0^2}{c_0}\frac{e^{\frac{1}{4w_0 a}}}{\sqrt{aw_0}}\exp\left(aw_0 l^2\right)\left[\text{Erf}\left(\frac{1-2aw_0 l}{2\sqrt{aw_0}}\right) - \text{Erf}\left(\frac{1}{2\sqrt{aw_0}}\right)\right]\boldsymbol{v}_1. \tag{P.54}$$

From this expression, the solution to Eqs. (P.36) and (P.37) can be readily obtained by direct integration.

P.2 Momentum-Dependent Beta Function at Quadratic Order

In Appendix Q we singled out the largest contribution to the beta function at quadratic order both in the WMDL, and beyond this approximation. The contribution to the beta function arises from the counterterm function in Eq. (Q.334) and which comes from zero momentum particle-particle processes. Using Eq. (P.8) in combination with the latter yields the largest quadratic order contribution to the beta functions:

$$\begin{aligned}\delta_2\widehat{\beta}^{\{j_i\}}_{\{N_i\};\{\sigma_i\}}(\{k_{i;N_i}\}) = &-\frac{e^l}{4\pi\Lambda_f}\sum_{l_1,l_2=1}^{N_f}\sum_{\rho_1,\rho_2=1}^{N_c}\sum_{M_1=1}^{8}\Theta\left(\Lambda_f e^{-l} - |e_{M_1}(\vec{k}_2^{\,*} + \vec{k}_1^{\,*}; v)|\right)\\ \times &\int_{-k_{\text{F}}e^{-l}}^{k_{\text{F}}e^{-l}}\frac{\mathrm{d}q_{M_1}}{(2\pi)}\widehat{\lambda}^{j_1 j_2 l_1 l_2}_{N_1 N_2 M_1[M_1+4]_8;\sigma_1\sigma_2\rho_1\rho_2}(k_{1;N_1}, k_{2;N_2}, [k_1+q]_{M_1}, [k_2-q]_{M_1})\\ \times &\,\widehat{\lambda}^{l_1 l_2 j_3 j_4}_{M_1[M_1+4]_8 N_3 N_4;\rho_1\rho_2\sigma_3\sigma_4}([k_1+q]_{M_1}, [k_2-q]_{M_1}, k_{3;N_3}, k_{4;N_4}),\end{aligned} \tag{P.55}$$

where $\widehat{\lambda}^{\{j_i\}}_{\{N_i\};\{\sigma_i\}}(\{k_{i,N_i}\})$ is defined in Eq. (4.45) and the extra exponential factor in the expression comes from making the transformation $q_{M_1} \to q_{M_1}(l)$ with $q_{M_1}(l)$ defined through

Eq. (4.41). Notice that, in the case where the coupling functions are momentum independent, the contribution becomes of order k_{F}/Λ_f which recovers the standard BCS result. Using the notation defined in Eq. (P.11), we can write the contribution in the pairing channel, as

$$\delta_2\widehat{\beta}^{\{j_i\}}_{\{N_i\};\{\sigma_i\}}(k,q;p) = -\frac{e^l}{4\pi\Lambda_f}\sum_{l_1,l_2=1}^{N_f}\sum_{\rho_1,\rho_2=1}^{N_c}\sum_{M_1=1}^{8}\Theta\left(\Lambda_f e^{-l}-|e_{M_1}(p^*;v)|\right) \times \int_{-k_{\mathrm{F}}e^{-l}}^{k_{\mathrm{F}}e^{-l}}\frac{\mathrm{d}x}{(2\pi)}\widehat{\alpha}^{j_1j_2l_1l_2}_{N_1N_2M_1[M_1+4]_8;\sigma_1\sigma_2\rho_1\rho_2}(k,k-x;p)\widehat{\alpha}^{l_1l_2j_3j_4}_{M_1[M_1+4]_8N_3N_4;\rho_1\rho_2\sigma_3\sigma_4}(k-x,q;p). \tag{P.56}$$

We now focus in the $N_c = 2$ and $N_f = 1$ case. Since $\alpha^{\mathsf{S}}_{1515}(k,q;p)$ is the fastest growing coupling, we focus on its beta function and the contribution at quadratic order sourced by itself. Using Eqs. (P.12), (P.13) and (P.14), the contribution we are interested on reads:

$$\delta_2\widehat{\beta}^{\mathsf{S}}_{1515}(k,q;p) = \frac{e^l}{2\pi\Lambda_f}\int_{-k_{\mathrm{F}}e^{-l}}^{k_{\mathrm{F}}e^{-l}}\frac{\mathrm{d}x}{(2\pi)}\widehat{\alpha}^{\mathsf{S}}_{1515}(k,k-x;p)\widehat{\alpha}^{\mathsf{S}}_{1515}(k-x,q;p). \tag{P.57}$$

To compare this expression with the leading order part of the beta function, we consider the case in which the momentum profile acquired by $\alpha^{\mathsf{S}}_{1515}(k,q;p)$ is the one obtained by solving the momentum-dependent beta function to linear order in the four-fermion couplings. Then, it is expected that $\alpha^{\mathsf{S}}_{1515}(k,q;p)$ is zero beyond some momentum scale much smaller than k_{F} as discussed in Sec. 4.5. Therefore, it follows that,

$$\begin{aligned}\delta_2\widehat{\beta}^{\mathsf{S}}_{1515}(k,q;p) &= \frac{e^l}{2\pi\Lambda_f}\int_{-k_{\mathrm{F}}e^{-l}}^{k_{\mathrm{F}}e^{-l}}\frac{\mathrm{d}x}{(2\pi)}\widehat{\alpha}^{\mathsf{S}}_{1515}(k,k-x;p)\widehat{\alpha}^{\mathsf{S}}_{1515}(k-x,q;p)\\ &\leq \frac{k_{\mathrm{F}}}{4\pi^2\Lambda_f}\left[\widehat{\alpha}^{\mathsf{S}}_{1515}\right]^2,\end{aligned} \tag{P.58}$$

where $\widehat{\alpha}^{\mathsf{S}}_{1515} \equiv \widehat{\alpha}^{\mathsf{S}}_{1515}(0,0;0)$ is the coupling evaluated at the hot spots. Notice that, here k_{F} is the dimensionful momentum which can be written as $k_{\mathrm{F}} = \Lambda_f\widehat{k}^{(0)}_{\mathrm{F}}e^l$, and thus

$$\delta_2\widehat{\beta}^{\mathsf{S}}_{1515}(k,q;p) \leq \frac{\widehat{k}^{(0)}_{\mathrm{F}}}{4\pi^2}e^l\left[\widehat{\alpha}^{\mathsf{S}}_{1515}\right]^2. \tag{P.59}$$

This inequality motivates the conservative control parameter for the expansion in the four-fermion coupling given in Eq. (4.85).

Appendix Q | One-Loop Quantum Corrections to the Four-Fermion Interaction

In this appendix we consider the one-loop quantum corrections to the four-fermion couplings up to quadratic order in the latter. We divide this appendix into two sections: We consider first the one-loop quantum corrections up to linear order in the four-fermion couplings in the weak-momentum dependence limit. Then, we estimate the largest contribution arising at quadratic order in the WMDL.

At the one-loop order, the diagrams in Figs. 4.7(a) to 4.7(h) and Figs. 4.10(a) and 4.10(b) give rise to the following correction to the quantum effective action

$$\begin{aligned}\delta\mathbf{\Gamma}^{(4,0)}_{1\mathrm{L}} = \frac{(2\pi)^3}{4}\sum_{\{\sigma_i=1\}}^{N_c}\sum_{\{j_i=1\}}^{N_f}\sum_{\{N_i=1\}}^{8}\int \mathrm{d}k_1\int \mathrm{d}k_2\int \mathrm{d}k_3\int \mathrm{d}k_4\; \mathit{\Gamma}^{\{j_i\}}_{\{N_i\};\{\sigma_i\}}(\{k_i\}) \\ \times \psi^{\dagger}_{N_1,\sigma_1,j_1}(k_1)\psi^{\dagger}_{N_2,\sigma_2,j_2}(k_2)\psi_{N_3,\sigma_3,j_3}(k_3)\psi_{N_4,\sigma_4,j_4}(k_4)\delta^{(3)}(k_1+k_2-k_3-k_4).\end{aligned} \tag{Q.1}$$

Here the four-point vertex function is denoted by $\mathit{\Gamma}^{\{j_i\}}_{\{N_i\};\{\sigma_i\}}(\{k_i\}) \equiv \mathit{\Gamma}^{j_1j_2j_3j_4}_{N_1N_2N_3N_4;\sigma_1\sigma_2\sigma_3\sigma_4}(k_1,k_2,k_3,k_4)$. In what follows we analyze separately the quantum corrections to the vertex function at linear and quadratic order in the four-fermion couplings.

Q.1 Quantum Corrections to Linear Order in $\lambda^{\{j_i\}}_{\{N_i\};\{\sigma_i\}}(\{k_{i;N_i}\})$

In the WMDL, the four-point vertex function is given, up to linear order in the four-fermion couplings, by

$$\begin{aligned}&\mathit{\Gamma}^{j_1j_2j_3j_4}_{N_1N_2N_3N_4;\sigma_1\sigma_2\sigma_3\sigma_4}(k_1,k_2,k_3,k_4) = \mu^{-1}\lambda^{j_1j_2j_3j_4}_{N_1N_2N_3N_4;\sigma_1\sigma_2\sigma_3\sigma_4} \\ &+\frac{\pi}{8\mu N_f}\sum_{\rho_1,\rho_2=1}^{N_c^2}\sum_{a=1}^{N_c^2-1}(\tau^a)_{\sigma_3\rho_1}(\tau^a)_{\rho_2\sigma_1}\lambda^{j_1j_2j_3j_4}_{\overline{N}_1N_2\overline{N}_3N_4;\rho_2\sigma_2\rho_1\sigma_4}\mathcal{H}_{N_1N_3}(k_1,k_3) \\ &+\frac{\pi}{8\mu N_f}\sum_{\rho_1,\rho_2=1}^{N_c^2}\sum_{a=1}^{N_c^2-1}(\tau^a)_{\sigma_3\rho_1}(\tau^a)_{\rho_2\sigma_2}\lambda^{j_1j_2j_3j_4}_{N_1\overline{N}_2\overline{N}_3N_4;\sigma_1\rho_2\rho_1\sigma_4}\mathcal{H}_{N_2N_3}(k_2,k_3) \\ &+\frac{\pi}{8\mu N_f}\sum_{\rho_1,\rho_2=1}^{N_c^2}\sum_{a=1}^{N_c^2-1}(\tau^a)_{\sigma_4\rho_1}(\tau^a)_{\rho_2\sigma_1}\lambda^{j_1j_2j_3j_4}_{\overline{N}_1N_2N_3\overline{N}_4;\rho_2\sigma_2\sigma_3\rho_1}\mathcal{H}_{N_1N_4}(k_1,k_4) \\ &+\frac{\pi}{8\mu N_f}\sum_{\rho_1,\rho_2=1}^{N_c^2}\sum_{a=1}^{N_c^2-1}(\tau^a)_{\sigma_4\rho_1}(\tau^a)_{\rho_2\sigma_2}\lambda^{j_1j_2j_3j_4}_{N_1\overline{N}_2N_3\overline{N}_4;\sigma_1\rho_2\sigma_3\rho_1}\mathcal{H}_{N_2N_4}(k_2,k_4)\end{aligned}$$

$$+\frac{\pi}{8\mu N_f}\sum_{\rho_1,\rho_2=1}^{N_c}\sum_{a=1}^{N_c^2-1}(\tau^a)_{\rho_1\sigma_2}(\tau^a)_{\rho_2\sigma_1}\lambda^{j_1j_2j_3j_4}_{\overline{N}_1\overline{N}_2N_3N_4;\rho_2\rho_1\sigma_3\sigma_4}\mathcal{P}_{N_1N_2}(k_1,k_2)$$

$$+\frac{\pi}{8\mu N_f}\sum_{\rho_1,\rho_2=1}^{N_c}\sum_{a=1}^{N_c^2-1}(\tau^a)_{\sigma_4\rho_1}(\tau^a)_{\sigma_3\rho_2}\lambda^{j_1j_2j_3j_4}_{N_1N_2\overline{N}_3\overline{N}_4;\sigma_1\sigma_2\rho_2\rho_1}\mathcal{P}_{N_3N_4}(k_3,k_4) \tag{Q.2}$$

$$+\frac{\pi^2}{12N_f^2\mu}\delta_{j_1j_3}\delta_{j_2j_4}\delta_{N_1N_3}\delta_{N_2N_4}\sum_{a,b=1}^{N_c^2-1}(\tau^a\tau^b)_{\sigma_1\sigma_3}(\tau^b\tau^a)_{\sigma_2\sigma_4}\left[\mathcal{S}_{N_1N_2}(k_3,k_2,k_2-k_4)+\mathcal{S}_{N_2N_1}(k_4,k_1,k_1-k_3)\right]$$

$$-\frac{\pi^2}{12N_f^2\mu}\delta_{j_2j_3}\delta_{j_1j_4}\delta_{N_2N_3}\delta_{N_1N_4}\sum_{a,b=1}^{N_c^2-1}(\tau^a\tau^b)_{\sigma_2\sigma_3}(\tau^b\tau^a)_{\sigma_1\sigma_4}\left[\mathcal{S}_{N_2N_1}(k_3,k_1,k_1-k_4)+\mathcal{S}_{N_1N_2}(k_4,k_2,k_2-k_3)\right]$$

$$+\frac{\pi^2}{12N_f^2\mu}\delta_{j_1j_3}\delta_{j_2j_4}\delta_{N_1N_3}\delta_{N_2N_4}\sum_{a,b=1}^{N_c^2-1}(\tau^a\tau^b)_{\sigma_1\sigma_3}(\tau^a\tau^b)_{\sigma_2\sigma_4}\left[\mathcal{R}_{N_1N_2}(k_1,k_2,k_2-k_4)+\mathcal{R}_{N_2N_1}(k_2,k_1,k_1-k_3)\right]$$

$$-\frac{\pi^2}{12N_f^2\mu}\delta_{j_2j_3}\delta_{j_1j_4}\delta_{N_2N_3}\delta_{N_1N_4}\sum_{a,b=1}^{N_c^2-1}(\tau^a\tau^b)_{\sigma_2\sigma_3}(\tau^a\tau^b)_{\sigma_1\sigma_4}\left[\mathcal{R}_{N_2N_1}(k_2,k_1,k_1-k_4)+\mathcal{R}_{N_1N_2}(k_1,k_2,k_2-k_3)\right].$$

Here $\lambda^{\{j_i\}}_{\{N_i\};\{\sigma_i\}}$ denote the dimensionless momentum-independent four-fermion couplings. In this expression we have defined the dimensionless the one-loop momentum integrations as

$$\mathcal{H}_{MN}(k,p)=v\int \mathrm{d}q\ D(q)G^{(0)}_{\overline{M}}(k+q;v)G^{(0)}_{\overline{N}}(p+q;v), \tag{Q.3}$$

$$\mathcal{P}_{MN}(k,p)\equiv v\int \mathrm{d}q\ D(q)G^{(0)}_{\overline{M}}(k+q;v)G^{(0)}_{\overline{N}}(p-q;v), \tag{Q.4}$$

$$\mathcal{S}_{MN}(k,p,l)=\mu v^2\int \mathrm{d}q\ D(q)D(l+q)G^{(0)}_{\overline{M}}(k+q;v)G^{(0)}_{\overline{N}}(p+q;v), \tag{Q.5}$$

$$\mathcal{R}_{MN}(k,p,l)\equiv \mu v^2\int \mathrm{d}q\ \ D(q)D(l-q)G^{(0)}_{\overline{M}}(k+q;v)G^{(0)}_{\overline{N}}(p-q;v). \tag{Q.6}$$

Here, $G^{(0)}_N(k;v)$ denotes the bare fermion propagator in Eq. (M.3) and $D(q)$ the propagator of the collective mode given in Eq. (2.6). The integrals $\mathcal{H}_{MN}(k,p)$ and $\mathcal{S}_{MN}(k,p,l)$ represent virtual processes in the particle-hole channel while the integrals $\mathcal{P}_{MN}(k,p)$ and $\mathcal{R}_{MN}(k,p,l)$ represent virtual processes in the particle-particle channel. In the rest of this appendix we consider the case in which the theory enjoys particle-hole symmetry. Therefore, we ignore the curvature of the FS in the analysis and only invoke it when its presence has significant physical consequences. In this case the particle-hole channel integrations can be read of from those in the particle-particle channel. This is because the bare fermion (self-consistent boson) propagator in Eq. (M.3) [Eq. (2.6)] is an odd (even) function of frequency and momentum. This guarantees that:

$$\begin{aligned}\mathcal{H}_{MN}(k,p)&=-\mathcal{P}_{MN}(k,-p),\\ \mathcal{S}_{MN}(k,p,l)&=-\mathcal{R}_{MN}(k,-p,-l).\end{aligned} \tag{Q.7}$$

In what follows we focus on the integrations in the particle-particle channel.

Q.2 Quantum Corrections in the Particle-Particle Channel

The integrals in the particle-particle channel in Eqs. (Q.4) and (Q.6) that appear in the quantum corrections to the four-point vertex function in Eq. (Q.2) can take any values of the hot spot indices for a fixed external momentum. In principle one has to consider all sixty-four cases separately for each integral. However, the symmetry properties of the integrals and the C_4 symmetry of the theory reduces considerably the number of cases to be addressed. Amongst all the possible choices of hot spot indices, the only independent ones that yield distinct integrals are those in which $M = 1$ and $N = 1, \ldots, 8$. The integrals for all other choices of hot spot indices can be obtained from these cases through an appropriate symmetry transformation. For the integral $\mathcal{P}_{MN}(k,p)$ this can be done through the identities:

$$\begin{aligned} \mathcal{P}_{NM}(k,p) &= \mathcal{P}_{MN}(p,k), \\ \mathcal{P}_{[1-M]_8[1-N]_8}(k,p) &= \mathcal{P}_{MN}\left(k^x, p^x\right), \\ \mathcal{P}_{[M+2]_8[N+2]_8}(k,p) &= \mathcal{P}_{MN}\left(k^{\frac{\pi}{2}}, p^{\frac{\pi}{2}}\right). \end{aligned} \tag{Q.8}$$

Similarly, for the integral $\mathcal{R}_{MN}(k,p,l)$ this can be done via the identities

$$\begin{aligned} \mathcal{R}_{NM}(k,p,l) &= \mathcal{R}_{MN}(p,k,-l), \\ \mathcal{R}_{[1-M]_8[1-N]_8}(k,p,l) &= \mathcal{P}_{MN}\left(k^x, p^x, l^x\right), \\ \mathcal{R}_{[M+2]_8[N+2]_8}(k,p,l) &= \mathcal{R}_{MN}\left(k^{\frac{\pi}{2}}, p^{\frac{\pi}{2}}, l^{\frac{\pi}{2}}\right). \end{aligned} \tag{Q.9}$$

In Eqs. (Q.8) and (Q.9), $[x]_8$ denotes the reminder of x divided by 8, $k^x = (k_0, -k_x, k_y)$ and $k^{\frac{\pi}{2}} = (k_0, -k_y, k_x)$. In what follows we separately analyze the $\mathcal{P}_{NM}(k,p)$ and $\mathcal{R}_{MN}(k,p,l)$ integrals for the cases in which $M = 1$ and $N = 1, \ldots, 8$.

Q.2-(a) The $\mathcal{P}_{MN}$ integrals

To simplify the discussion on the computation of the $\mathcal{P}_{MN}(k,p)$ integrals, we compute directly their contributions at the RG condition in Eq. (4.57). This effectively implies that we are evaluating the external spatial momenta at the local FS of hot spots M and N and at frequencies $k_0 = 3\mu/2$ and $p_0 = \mu/2$.

A. $\mathcal{P}_{11}(k,p)$

For $M = 1$ and $N = 1$, the integral in Eq. (Q.4) takes the following form at the RG condition in Eq. (4.57):

$$\begin{aligned} \mathcal{P}_{11}(k_x, p_x; \mu) \equiv v \int \mathrm{d}q \left[\frac{1}{|q_0| + c(v)(|q_x| + |q_y|)}\right] \left[\frac{1}{i\left(\frac{3\mu}{2} + q_0\right) + vq_x - q_y + 2vk_x}\right] \\ \times \left[\frac{1}{-i\left(\frac{\mu}{2} + q_0\right) - vq_x + q_y + 2vp_x}\right]. \end{aligned} \tag{Q.10}$$

Following the discussion in Sec. 4.2-(a) , this integration must be regularized by imposing an energy cutoff Λ_f on the electronic excitations. Furthermore, the $\vec{q}$ integration is also

confined to the momentum region where the propagator in Eq. (2.6) dominates over the bare one. Therefore, for a fixed external momenta k_x and p_x this integration is done over momenta $\vec{q}$ satisfying the constraints

$$|vq_x - q_y + 2vk_x| < \Lambda_f, \quad |vq_x - q_y - 2vp_x| < \Lambda_f, \quad |q_x| < \Lambda_b \quad \& \quad |q_y| < \Lambda_b, \tag{Q.11}$$

with $\Lambda_f \ll c(v)\Lambda_b$, and where we have set the cutoff along the FS to infinity. To make these UV cutoffs manifest in the integration we consider the change of variables into momentum away and along the local FS at hot spot $N = 4$:

$$X = q_x + vq_y \qquad \& \qquad Y = vq_x - q_y + v(k_x - p_x). \tag{Q.12}$$

Under this change of variables, the domain of integration in Eq. (Q.11) transforms to

$$\begin{gathered} |Y \pm v(k_x + p_x)| < \Lambda_f, \quad |X + vY + v^2(p_x - k_x)| < \Lambda_b, \qquad \& \\ |vX - Y + v(k_x - p_x)| < \Lambda_b. \end{gathered} \tag{Q.13}$$

If $v(k_x + p_x) \gg \Lambda_f$, then the integration over Y has no support and thus, the quantum correction vanishes. Therefore, in the limit in which $v|k_x + p_x| \ll \Lambda_f$, the Y integration is cutoff by Λ_f. Furthermore, for the X integration to have nonzero support, $|k_x - p_x| \ll \Lambda_b/v \sim \overline{k}_{\rm F}$, where $\overline{k}_{\rm F}$ is defined in Eq. (4.62). Notice that this offers no further constraint over the momenta than the one identified in Sec. 4.4-(*a*) . In this case the integration over X is effectively cutoff by Λ_b. Under this change of variables, and leaving the constraint on the external momentum implicit, the integration can be written, to the leading order in v

$$\begin{aligned} \mathcal{P}_{11}(k_x, p_x; \mu) = v \int\limits_{\mathbb{R}} \frac{\mathrm{d}q_0}{(2\pi)} \int\limits_{-\Lambda_b}^{\Lambda_b} \frac{\mathrm{d}X}{(2\pi)} \int\limits_{-\Lambda_f}^{\Lambda_f} \frac{\mathrm{d}Y}{(2\pi)} \left[\frac{1}{|q_0| + c(v)|X| + |c(v)Y + \Delta_r|}\right] \\ \times \left[\frac{1}{i\left(\frac{3\mu}{2} + q_0\right) + Y + \Delta_t}\right] \left[\frac{1}{-i\left(\frac{\mu}{2} + q_0\right) - Y + \Delta_t}\right]. \end{aligned} \tag{Q.14}$$

In arriving to this expression we have dropped terms of order $vc(v)X$ and $vc(v)Y$ with respect to those of order $c(v)X$ and $c(v)Y$ and a term of order $v\Delta_r$ with respect to the term of order Δ_r . Furthermore, $\Delta_t = v(k_x + p_x)$ and $\Delta_r = vc(v)(k_x - p_x)$ denote the minimum total and relative energy of the pair of virtual electrons taking part in the quantum correction, respectively. The term of order $c(v)Y$ inside the boson propagator only offers subleading corrections in the small $c(v)$ limit and dropping it has no effect in the convergence of the integral. Neglecting this term and integrating over X we obtain

$$\begin{aligned} \mathcal{P}_{11}(k_x, p_x; \mu) = \frac{w(v)}{\pi} \int\limits_{\mathbb{R}} \frac{\mathrm{d}q_0}{(2\pi)} \int\limits_{-\Lambda_f}^{\Lambda_f} \frac{\mathrm{d}Y}{(2\pi)} \log\left[1 + \frac{c(v)\Lambda_b}{|q_0| + |\Delta_r|}\right] \left[\frac{1}{i\left(\frac{3\mu}{2} + q_0\right) + Y + \Delta_t}\right] \\ \times \left[\frac{1}{-i\left(\frac{\mu}{2} + q_0\right) - Y + \Delta_t}\right]. \end{aligned} \tag{Q.15}$$

We analyze this expression in the following asymptotic limits: (*i*) $\mu \gg |\Delta_r|$ and $\mu \gg |\Delta_t|$, (*ii*) $|\Delta_t| \gg \mu$ and $|\Delta_r| \gg |\Delta_r|$, and (*iii*) $|\Delta_r| \gg \mu$ and $|\Delta_r| \gg |\Delta_t|$.

(*i*) For $\mu \gg |\Delta_t|$ and $\mu \gg |\Delta_r|$ we define the rescaled scales $\overline{\Lambda}_b = \Lambda_b/\mu$ and $\overline{\Lambda}_f = \Lambda_f/\mu$ after performing the scaling $(q_0, Y) \to \mu(q_0, Y)$. In the $|\Delta_t|/\mu \ll 1$ and $|\Delta_r|/\mu \ll 1$ limits Eq. (Q.15) takes the leading order form:

$$\mathcal{P}_{11}(k_x, p_x; \mu) = \frac{w(v)}{\pi} \int_{\mathbb{R}} \frac{\mathrm{d}q_0}{(2\pi)} \int_{-\overline{\Lambda}_f}^{\overline{\Lambda}_f} \frac{\mathrm{d}Y}{(2\pi)} \log\left[1 + \frac{c(v)\overline{\Lambda}_b}{|q_0|}\right] \times \left[\frac{1}{i\left(\frac{3}{2} + q_0\right) + Y}\right]\left[\frac{1}{-i\left(\frac{1}{2} + q_0\right) - Y}\right]. \tag{Q.16}$$

Integration over Y yields,

$$\mathcal{P}_{11}(k_x, p_x; \mu) = \frac{w(v)}{\pi^2} \int_{\mathbb{R}} \frac{\mathrm{d}q_0}{(2\pi)} \log\left[1 + \frac{c(v)\overline{\Lambda}_b}{|q_0|}\right] \times \left\{\arctan\left(\frac{2\overline{\Lambda}_f}{2q_0 + 1}\right) - \arctan\left(\frac{2\overline{\Lambda}_f}{3 + 2q_0}\right)\right\}. \tag{Q.17}$$

The integration over q_0 is performed by first symmetrizing in q_0 and dividing the integration into the $0 < q_0 < 1/2$ and $1/2 < q_0 < \infty$ regimes. In the $c(v)\overline{\Lambda}_b \gg \overline{\Lambda}_f \gg 1$ limit, the first regime yields a logarithmically divergent contribution in $c(v)\overline{\Lambda}_b$, while the second regime diverges as $\log(c(v)\overline{\Lambda}_b/\overline{\Lambda}_f)$. Taking both contributions into account we obtain

$$\mathcal{P}_{11}(k_x, p_x; \mu) = -\frac{w(v)}{2\pi^2} \log\left(c(v)\overline{\Lambda}_b\right) + \frac{w(v)}{2\pi^2} \log\left(\frac{c(v)\overline{\Lambda}_b}{\overline{\Lambda}_f}\right) = -\frac{w(v)}{2\pi^2} \log\left(\frac{\Lambda_f}{\mu}\right), \tag{Q.18}$$

where we used the definition for the rescaled cutoff.

(*ii*) For the case in which $|\Delta_t| \gg \mu$ and $|\Delta_t| \gg |\Delta_r|$ we assume, without loss of generality that $\Delta_t > 0$ and preform the scaling $(q_0, Y) \to \Delta_t(q_0, Y)$. Defining the rescaled scales $\overline{\Lambda}_b = \Lambda_b/\Delta_t$ and $\overline{\Lambda}_f = \Lambda_f/\Delta_t$, Eq. (Q.15) takes the leading order form

$$\mathcal{P}_{11}(k_x, p_x; \mu) = \frac{w(v)}{\pi} \int_{\mathbb{R}} \frac{\mathrm{d}q_0}{(2\pi)} \int_{-\overline{\Lambda}_f}^{\overline{\Lambda}_f} \frac{\mathrm{d}Y}{(2\pi)} \log\left[1 + \frac{c(v)\overline{\Lambda}_b}{|q_0| + \delta}\right] \times \left[\frac{1}{i\left(q_0 + \frac{3m}{2}\right) + Y + 1}\right]\left[\frac{1}{-i\left(\frac{m}{2} + q_0\right) - Y + 1}\right], \tag{Q.19}$$

where we have defined $\delta = |\Delta_r|/\Delta_t$ and $m = \mu/\Delta_t$. In the $\delta \ll 1$ and $m \ll 1$ limits one is tempted to set these two parameters to zero inside the integral. However, setting $m = 0$ in this expression yields a zero contribution in the large $\overline{\Lambda}_f$ limit. This is a symptom of the integration being proportional to m. In contrast, setting $\delta = 0$ is

legitimate and, upon integrating over Y we obtain, in the $\overline{\Lambda}_f \gg 1$ limit,

$$\mathcal{P}_{11}(k_x,p_x;\mu) = \frac{w(v)}{2\pi}\frac{1}{m-2i}\int\limits_{\mathbb{R}}\frac{\mathrm{d}q_0}{(2\pi)}\log\left[1+\frac{c(v)\overline{\Lambda}_b}{|q_0|}\right]\left\{\mathrm{sgn}\left(\frac{m}{2}+q_0\right)\right.$$
$$\left.-\mathrm{sgn}\left(\frac{3m}{2}+q_0\right)+\frac{1}{2\pi}\arctan\left(\frac{\frac{3m}{2}+q_0}{\overline{\Lambda}_f}\right)-\frac{1}{2\pi}\arctan\left(\frac{\frac{m}{2}+q_0}{\overline{\Lambda}_f}\right)\right\}. \tag{Q.20}$$

The integration over q_0 can be performed by symmetrizing the integrand in q_0 and further dividing the regime of integration into the regions $q_0 < 3m/2$ and $q_0 > 3m/2$. Integration in each region yields, in the $1 \ll \overline{\Lambda}_f \ll c(v)\overline{\Lambda}_b$ limit and to leading order in $m \ll 1$,

$$\mathcal{P}_{11}(k_x,p_x;\mu) \approx \frac{imw(v)}{8\pi^2}\log\left(\frac{c(v)\overline{\Lambda}_b}{\overline{\Lambda}_f}\right) = \frac{iw(v)}{8\pi^2}\frac{\mu}{\Delta_t}\log\left(\frac{c(v)\Lambda_b}{\Lambda_f}\right), \tag{Q.21}$$

where the last equality follows from the definition of the rescaled energy scales. We finally note that in the $\Delta_t < 0$ case we obtain the same result. In the limit under consideration, this is suppressed and its associated contribution to the beta function of the four-fermion couplings is negligible.

(*iii*) In the limit in which $|\Delta_r| \gg \mu$ and $|\Delta_r| \gg |\Delta_t|$ we assume that $\Delta_r > 0$ without loss of generality and perform the scaling $(q_0, Y) \to \Delta_r(q_0, Y)$. This way Eq. (Q.15) can be written as

$$\mathcal{P}_{11}(k_x,p_x;\mu) = \frac{w(v)}{\pi}\int\limits_{\mathbb{R}}\frac{\mathrm{d}q_0}{(2\pi)}\int\limits_{-\overline{\Lambda}_f}^{\overline{\Lambda}_f}\frac{\mathrm{d}Y}{(2\pi)}\log\left[1+\frac{c(v)\overline{\Lambda}_b}{|q_0|+1}\right]\left[\frac{1}{i\left(\frac{3m}{2}+q_0\right)+Y+\delta}\right]$$
$$\times\left[\frac{1}{-i\left(\frac{m}{2}+q_0\right)-Y+\delta}\right], \tag{Q.22}$$

where $\overline{\Lambda}_b = \Lambda_b/\Delta_r$, $\overline{\Lambda}_f = \Lambda_f/\Delta_r$, $\delta = \Delta_t/\Delta_r$ and $m = \mu/\Delta_r$. In the $\delta \ll 1$ and $m \ll 1$ limits we can set $\delta = 0$ inside the integrand, but we need to keep $m \neq 0$ because, as we shall see, setting $m = 0$ makes the integrand vanish, and at the same time, it introduces an IR divergence in the q_0 integration. Integration over Y yields,

$$\mathcal{P}_{11}(k_x,p_x;\mu) = \frac{w(v)}{m\pi^2}\int\limits_{\mathbb{R}}\frac{\mathrm{d}q_0}{(2\pi)}\log\left[1+\frac{c(v)\overline{\Lambda}_b}{|q_0|+1}\right]$$
$$\times\left\{\arctan\left(\frac{2\overline{\Lambda}_f}{m+2q_0}\right)-\arctan\left(\frac{2\overline{\Lambda}_f}{3m+2q_0}\right)\right\}. \tag{Q.23}$$

The q_0 integration can be performed by first symmetrizing the integrand and dividing the analysis into the $0 < q_0 < m/2$ and $m/2 < q_0 < \infty$ regimes. In the first regime, the integrand diverges logarithmically in $c(v)\overline{\Lambda}_b$ in the small m limit. In the second regime, setting $m = 0$ inside the integrand is legitimate. This one diverges as $\log(c(v)\overline{\Lambda}_b/\overline{\Lambda}_f)$

in the $c(v)\overline{\Lambda}_b \gg \overline{\Lambda}_f \gg 1$ limit. Collecting both results we obtain the leading order contribution

$$\mathcal{P}_{11}(k_x,p_x;\mu) = -\frac{w(v)}{2\pi^2}\log\left(c(v)\overline{\Lambda}_b\right) + \frac{w(v)}{2\pi^2}\log\left(\frac{c(v)\overline{\Lambda}_b}{\overline{\Lambda}_f}\right) = -\frac{w(v)}{2\pi^2}\log\left(\frac{\Lambda_f}{|\Delta_r|}\right). \quad \text{(Q.24)}$$

In the last equality we have used the definition of the rescaled UV cutoff and the fact that the case $\Delta_r < 0$ yields the same result.

Collecting the results from Eqs. (Q.18), (Q.21) and (Q.24), using the definitions $\Delta_r = vc(v)(k_x - p_x)$ and $\Delta_t = v(k_x + p_x)$, and bringing back the constraint on the external momentum, we can write Eq. (Q.15) as

$$\begin{aligned}\mathcal{P}_{11}(k_x,p_x;\mu) = &-\frac{w(v)}{2\pi^2}\Theta(\Lambda_f - v|k_x+p_x|) \\ &\times \mathscr{G}_{11}(\mu, v|k_x+p_x|, vc(v)|k_x-p_x|)\log\left(\frac{\Lambda_f}{\mathscr{F}_{11}\left(\mu, vc(v)|k_x-p_x|\right)}\right),\end{aligned} \quad \text{(Q.25)}$$

where the crossover function satisfies $\mathscr{F}_{11}(x,y) \approx \max(x,y)$. The overall function $\mathscr{G}_{11}(x,y)$ is given by

$$\mathscr{G}_{11}(x,y,z) = \begin{cases} 1 & x \gg y \quad \& \quad x \gg z, \\ 1 & z \gg y \quad \& \quad z \gg x, \\ -\frac{i}{4}\frac{x}{y}\log\left(\frac{c(v)\Lambda_b}{\Lambda_f}\right) & y \gg z \quad \& \quad y \gg x. \end{cases} \quad \text{(Q.26)}$$

B. $\mathcal{P}_{12}(k,p)$

For $M = 1$ and $N = 1$, the integral in Eq. (Q.4) takes the following form a the RG condition in Eq. (4.57):

$$\begin{aligned}\mathcal{P}_{12}(k_x,p_y;\mu) = -\int \mathrm{d}q \left[\frac{1}{|q_0| + c(v)(|q_x|+|q_y|)}\right]&\left[\frac{1}{i\left(\frac{3\mu}{2}+q_0\right) + vq_x - q_y + 2vk_x}\right] \\ &\times \left[\frac{1}{i\left(\frac{\mu}{2}+q_0\right) + q_x - vq_y + 2vp_y}\right].\end{aligned} \quad \text{(Q.27)}$$

Following the discussion in Sec. 4.2-(*a*) , this integration is regularized by imposing an energy cutoff Λ_f on the electronic excitations. The integration over $\vec{q}$ is also confined to the region where the propagator in Eq. (2.6) dominates over the the bare bosonic propagator. The integration over $\vec{q}$ must therefore be done over the region defined by

$$|vq_x - q_y + 2vk_x| < \Lambda_f, \quad |q_x - vq_y + 2vp_y| < \Lambda_f, \quad |q_x| < \Lambda_b, \quad |q_y| < \Lambda_b. \quad \text{(Q.28)}$$

To make Eq. (Q.27) depend explicitly on Λ_f and Λ_b we consider the following change of variables

$$X = q_x - vq_y + 2vp_y, \qquad \& \qquad Y = vq_x - q_y + 2vk_x. \quad \text{(Q.29)}$$

Under this transformation, the domain of integration transforms into

$$\begin{aligned} &|X|<\Lambda_f, \quad |Y|<\Lambda_f, \quad |X-vY+2v(k_x-vp_y)|<\Lambda_b, \quad \& \\ &\qquad\qquad |vX-Y-2v(p_y-vk_x)|<\Lambda_b. \end{aligned} \tag{Q.30}$$

It is clear that the integrations over X and Y are cutoff by Λ_f because $\Lambda_f \ll c(v)\Lambda_b \ll \Lambda_b$. According to the discussion in Sec. 4.4-(*a*) , the momenta p_y and k_x can be at most of order $\overline{k}_{\rm F} \sim \Lambda_b/v$. Since X and Y can be at most of order Λ_f, the last two conditions in this equation yield no further constraint on the external momentum.

In terms of the new variables and to the leading order in v, Eq. (Q.27) takes the leading order form

$$\begin{aligned} \mathcal{P}_{12}(k_x,p_y;\mu) = -v\int\limits_{\mathbb{R}}\frac{\mathrm{d}q_0}{(2\pi)}\int\limits_{-\Lambda_f}^{\Lambda_f}\frac{\mathrm{d}Y}{(2\pi)}\int\limits_{-\Lambda_f}^{\Lambda_f}\frac{\mathrm{d}X}{(2\pi)}\left[\frac{1}{i\left(\frac{\mu}{2}+q_0\right)+X}\right]\left[\frac{1}{i\left(\frac{3\mu}{2}+q_0\right)+Y}\right] \\ \times\left[\frac{1}{|q_0|+|c(v)X-vc(v)Y-\Delta_t|+|vc(v)X-c(v)Y+\Delta_r|}\right]. \end{aligned} \tag{Q.31}$$

where $\Delta_t = 2vc(v)(p_y - vk_x)$ and $\Delta_r = 2vc(v)(k_x - vp_y)$ denote the minimum total and relative energy of the virtual electron-electron pair involved in the quantum correction. We note that for this expression the natural cutoff for the boson plays no role because we are considering the limit in which $\Lambda_f \ll c(v)\Lambda_b$, and thus Λ_f cuts both the large X and Y integrations. In the small v limit, the terms of order vY and vX inside the boson propagator can be dropped with respect to those terms of order X and Y. This is because the former only give rise to subleading contributions in the small v limit. Therefore, in this limit we can write

$$\begin{aligned} \mathcal{P}_{12}(k_x,p_y;\mu) = -v\int\limits_{\mathbb{R}}\frac{\mathrm{d}q_0}{(2\pi)}\int\limits_{-\Lambda_f}^{\Lambda_f}\frac{\mathrm{d}Y}{(2\pi)}\int\limits_{-\Lambda_f}^{\Lambda_f}\frac{\mathrm{d}X}{(2\pi)}\left[\frac{1}{i\left(\frac{\mu}{2}+q_0\right)+X}\right] \\ \times\left[\frac{1}{i\left(\frac{3\mu}{2}+q_0\right)+Y}\right]\left[\frac{1}{|q_0|+|c(v)X-\Delta_t|+|c(v)Y-\Delta_r|}\right]. \end{aligned} \tag{Q.32}$$

We proceed on analyzing Eq. (Q.32) in the limits in which (*i*) $\mu \gg |\Delta_r|$ and $\mu \gg |\Delta_t|$, (*ii*) $|\Delta_r| \gg \mu$ and $|\Delta_r| \gg |\Delta_t|$, and (*iii*) $|\Delta_t| \gg |\Delta_r|$ and $|\Delta_t| \gg \mu$.

(*i*) For $\mu \gg |\Delta_r|$ and $\mu \gg |\Delta_t|$ we perform the scaling $(q_0, X, Y) \to \mu(q_0, X, Y)$ and take the small $|\Delta_r|/\mu$ and $|\Delta_t|/\mu$ limits. With this Eq. (Q.32) can be written as

$$\begin{aligned} \mathcal{P}_{12}(k_x,p_y;\mu) = -v\int\limits_{\mathbb{R}}\frac{\mathrm{d}q_0}{(2\pi)}\int\limits_{-\overline{\Lambda}_f}^{\overline{\Lambda}_f}\frac{\mathrm{d}Y}{(2\pi)}\int\limits_{-\overline{\Lambda}_f}^{\overline{\Lambda}_f}\frac{\mathrm{d}X}{(2\pi)}\left[\frac{1}{|q_0|+c(v)|X|+c(v)|Y|}\right] \\ \times\left[\frac{1}{i\left(\frac{3}{2}+q_0\right)+Y}\right]\left[\frac{1}{i\left(\frac{1}{2}+q_0\right)+X}\right], \end{aligned} \tag{Q.33}$$

where $\overline{\Lambda}_f = \Lambda_f/\mu$. One is tempted to set $c(v) = 0$ inside the integrand because the X and Y integrations are well-defined even in the large $\overline{\Lambda}_f$ limit. However, doing so introduces an IR divergence at $q_0 = 0$. We can, however, set $c(v)Y = 0$ inside the integral and integrate over Y after symmetrizing in both X and Y. Doing so we obtain

$$\mathcal{P}_{12}(k_x, p_y; \mu) = \frac{4v}{\pi} \int_{\mathbb{R}} \frac{\mathrm{d}q_0}{(2\pi)} \int_0^{\overline{\Lambda}_f} \frac{\mathrm{d}X}{(2\pi)} \left[\frac{1}{|q_0| + c(v)X}\right] \times \left[\frac{(1+2q_0)}{4X^2 + (1+2q_0)^2}\right] \arctan\left(\frac{2\overline{\Lambda}_f}{3+2q_0}\right). \tag{Q.34}$$

The integration over X can be performed as well, yielding

$$\mathcal{P}_{12}(k_x, p_y) = \frac{2v}{\pi^2} \int_{\mathbb{R}} \frac{\mathrm{d}q_0}{(2\pi)} \left\{ \frac{\arctan\left(\frac{2\overline{\Lambda}_f}{3+2q_0}\right)}{8q_0^2 + 2c(v)^2\,(1+2q_0)^2} \left(4|q_0| \arctan\left(\frac{2\overline{\Lambda}_f}{1+2q_0}\right) + c(v)\,[1+2q_0]\left[2\log\left(\frac{|1+2q_0|}{|q_0|}\right) + \log\left(\frac{[|q_0| + c(v)\overline{\Lambda}_f]^2}{(1+2q_0)^2 + 4\overline{\Lambda}_f^2}\right)\right]\right)\right\}. \tag{Q.35}$$

The final integration over q_0 can be done by first symmetrizing the integrand and by noticing that the leading order divergence comes from the regime in which $q_0 > 3/2$. The integration over q_0 yields, to leading order in $\overline{\Lambda}_f \gg 1$,

$$\mathcal{P}_{12}(k_x, p_y) = \frac{v}{4\pi} \log(\overline{\Lambda}_f) = \frac{v}{4\pi} \log\left(\frac{\Lambda_f}{\mu}\right). \tag{Q.36}$$

(*ii*) For $|\Delta_r| \gg \mu$ and $|\Delta_r| \gg |\Delta_t|$ we consider $\Delta_r > 0$ without loss of generality, perform the scaling $(q_0, X, Y) \to \Delta_r(q_0, X, Y)$ and write Eq. (Q.32) as

$$\mathcal{P}_{12}(k_x, p_y) = -v \int_{\mathbb{R}} \frac{\mathrm{d}q_0}{(2\pi)} \int_{-\overline{\Lambda}_f}^{\overline{\Lambda}_f} \frac{\mathrm{d}Y}{(2\pi)} \int_{-\overline{\Lambda}_f}^{\overline{\Lambda}_f} \frac{\mathrm{d}X}{(2\pi)} \left[\frac{1}{|q_0| + (|c(v)Y - 1| + c(v)|X|)}\right] \times \left[\frac{1}{iq_0 + Y}\right]\left[\frac{1}{iq_0 + X}\right], \tag{Q.37}$$

where $\overline{\Lambda}_f = \Lambda_f/\Delta_t$. Unlike the previous case we can set $c(v) = 0$ because the integration over Y and X are already well-defined in the large Y and X limits and setting $c(v) = 0$ introduces no IR divergence in the $q_0 = 0$ limit. The integration over X and Y yield

$$\mathcal{P}_{12}(k_x, p_y) = \frac{2v}{\pi^2} \int_{\mathbb{R}^+} \frac{\mathrm{d}q_0}{(2\pi)} \left[\frac{1}{q_0 + 1}\right] \arctan\left(\frac{\overline{\Lambda}_f}{q_0}\right)^2. \tag{Q.38}$$

In the $\overline{\Lambda}_f \gg 1$ limit the q_0 integration yields the leading order divergence

$$\mathcal{P}_{12}(k_x, p_y) = \frac{v}{4\pi} \log(\overline{\Lambda}_f) = \frac{v}{4\pi} \log\left(\frac{\Lambda_f}{|\Delta_r|}\right), \tag{Q.39}$$

where we have used the definition of the rescaled cutoff in the last equality. Furthermore, we have included the absolute value in the scale because the case $\Delta_r < 0$ yields the same contribution.

(*iii*) The case in which $|\Delta_t| \gg \mu$ and $|\Delta_t| \gg |\Delta_r|$ is the same as the previous case we analyzed upon exchanging Δ_t with Δ_r. It therefore follows that

$$\mathcal{P}_{12}(k_x, p_y) = \frac{v}{4\pi} \log\left(\frac{\Lambda_f}{|\Delta_t|}\right). \tag{Q.40}$$

Collecting the results from Eqs. (Q.36), (Q.39) and (Q.40) and using the definitions $\Delta_r = 2vc(v)(p_y + 2vk_x)$ and $\Delta_t = 2vc(v)(k_x - vp_y)$, we can write Eq. (Q.27) as

$$\mathcal{P}_{12}(k_x, p_y) = \frac{v}{4\pi} \log\left(\frac{\Lambda_f}{\mathscr{F}_{12}[\mu, 2vc(v)|vk_x - p_y|, 2vc(v)|k_x - vp_y|]}\right), \tag{Q.41}$$

where the crossover function satisfies $\mathscr{F}_{12}(x, y, z) \approx \max(x, y, z)$.

C. $\mathcal{P}_{13}(k, p)$

For $M = 1$ and $N = 3$, the integration in Eq. (Q.4) can be written, at the RG condition, as

$$\begin{aligned}\mathcal{P}_{13}(k_x, p_y; \mu) = v \int \mathrm{d}q \left[\frac{1}{|q_0| + c(v)(|q_x| + |q_y|)}\right] \left[\frac{1}{i\left(\frac{3\mu}{2} + q_0\right) + vq_x - q_y + 2vk_x}\right] \\ \times \left[\frac{1}{-i\left(\frac{\mu}{2} + q_0\right) - q_x - vq_y + 2vp_y}\right].\end{aligned} \tag{Q.42}$$

As suggested by the discussion in Sec. 4.2-(*a*) , the integration over the internal momentum is done over $\vec{q}$ satisfying the conditions

$$|vq_x - q_y + 2vk_x| < \Lambda_f, \quad |q_x + vq_y - 2vp_y| < \Lambda_f, \quad |q_x| < \Lambda_b, \quad \& \quad |q_y| < \Lambda_b \tag{Q.43}$$

To make Eq. (Q.42) depend explicitly on the cutoff scales we consider the change of variables:

$$Y = vq_x - q_y + 2vk_x, \qquad \& \qquad X = q_x + vq_y - 2vp_y. \tag{Q.44}$$

Under this change of variables and to leading order in v, the integration over X and Y is done over the region

$$\begin{aligned}|Y| < \Lambda_f, \quad |X| < \Lambda_f, \quad |X + vY + 2v(p_y - vk_x)| < \Lambda_b, \quad \& \\ |vX - Y + 2v(k_x + vp_y)| < \Lambda_b.\end{aligned} \tag{Q.45}$$

It is clear that the integration over X and Y are cutoff by Λ_f as a consequence of the inequality $\Lambda_f \ll c(v)\Lambda_b \ll \Lambda_b$. Furthermore, we note that the momenta k_x and p_y are, at most, of order $\bar{k}_{\rm F} \sim \Lambda_b/v$ as explained in Sec. 4.4-(*a*) . Therefore, Eq. (Q.45) offers no further constraint on the external momenta.

Under the change of variables, Eq.(Q.42) takes the form

$$\mathcal{P}_{13}(k_x,p_y;\mu) = v\int\limits_{\mathbb{R}}\frac{\mathrm{d}q_0}{(2\pi)}\int\limits_{-\Lambda_f}^{\Lambda_f}\frac{\mathrm{d}X}{(2\pi)}\int\limits_{-\Lambda_f}^{\Lambda_f}\frac{\mathrm{d}Y}{(2\pi)}\left[\frac{1}{i\left(\frac{3\mu}{2}+q_0\right)+Y}\right]\left[\frac{1}{-i\left(\frac{\mu}{2}+q_0\right)-X}\right] \times\left[\frac{1}{|q_0|+|c(v)X+vc(v)Y+\Delta_r|+|vc(v)X-c(v)Y+\Delta_t|}\right], \tag{Q.46}$$

to the leading order in v. Here, $\Delta_r = 2vc(v)(p_y - vk_x)$ and $\Delta_t = 2vc(v)(k_x + vp_y)$. In the small v limit the terms of order $vc(v)X$ and $vc(v)Y$ can be safely ignored inside the bosonic propagator. Doing so we arrive to the expression

$$\mathcal{P}_{13}(k_x,p_y;\mu) = v\int\limits_{\mathbb{R}}\frac{\mathrm{d}q_0}{(2\pi)}\int\limits_{-\Lambda_f}^{\Lambda_f}\frac{\mathrm{d}X}{(2\pi)}\int\limits_{-\Lambda_f}^{\Lambda_f}\frac{\mathrm{d}Y}{(2\pi)}\left[\frac{1}{i\left(\frac{3\mu}{2}+q_0\right)+Y}\right]\left[\frac{1}{-i\left(\frac{\mu}{2}+q_0\right)-X}\right] \times\left[\frac{1}{|q_0|+|c(v)X+\Delta_r|+|c(v)Y-\Delta_t|}\right]. \tag{Q.47}$$

The analysis of this expression follows the same steps as the one performed for Eq. (Q.32) because Eq. (Q.47) can be mapped into Eq. (Q.32). Therefore we conclude that

$$\mathcal{P}_{13}(k_x,p_y;\mu) = \frac{v}{4\pi}\log\left(\frac{\Lambda_f}{\mathscr{F}_{13}[\mu,2vc(v)|p_y-vk_x|,2vc(v)|k_x+vp_y|]}\right), \tag{Q.48}$$

where the crossover function satisfies $\mathscr{F}_{13}(x,y,z)\approx\max(x,y,z)$.

D. $\mathcal{P}_{14}(k,p)$

For $M=1$ and $N=4$, the integration in Eq. (Q.4) can be written, at the RG condition, as

$$\mathcal{P}_{14}(k_x,p_x;\mu) = v\int \mathrm{d}q\left[\frac{1}{|q_0|+c(v)(|q_x|+|q_y|)}\right]\left[\frac{1}{i\left(\frac{3\mu}{2}+q_0\right)+vq_x-q_y+2vk_x}\right] \times\left[\frac{1}{-i\left(\frac{\mu}{2}+q_0\right)-vq_x-q_y+2vp_x}\right]. \tag{Q.49}$$

According to the discussion in Sec. 4.2-(*a*) , the integration over $\vec{q}$ must be done over the region

$$|vq_x-q_y+2vk_x|<\Lambda_f,\quad |vq_x+q_y-2vp_x|<\Lambda_f,\quad |q_x|<\Lambda_b,\quad \&\quad |q_y|<\Lambda_b. \tag{Q.50}$$

To bring the explicit cutoff dependence into Eq. (Q.49) we consider the change of variables

$$Y = vq_x-q_y+2vk_x,\qquad X = q_x+vq_x+(1-v^2)k_x+(1+v^2)p_x\approx q_x+vq_x+k_x-p_x. \tag{Q.51}$$

With this change of variables, the integration region for X and Y is given, to leading order in $v \ll 1$, by

$$|Y| < \Lambda_f, \quad |Y - 2vX| < \Lambda_f, \quad |X + vY + p_x - k_x| < \Lambda_b, \quad \& \\ |vX - Y - v(k_x + p_x)| < \Lambda_b. \tag{Q.52}$$

The integration over Y is cutoff by Λ_f. There are two possible ways of cutting off the X integration in the UV for $\Lambda_f \ll c(v)\Lambda_b \ll \Lambda_b$. On the one hand, the condition $|Y - 2vX| < \Lambda_f$, requires that X is at most of order Λ_f/v. On the other hand, the condition $|X + vY + (p_x - k_x)| < \Lambda_b$ implies that the X integration has support provided that $|p_x - k_x| \ll \Lambda_b$, in which case the integration over X is cutoff by Λ_b. Therefore, the integration over X is cutoff in the UV by $\min(\Lambda_b, \Lambda_f/v)$. In either of these two cases, the integration in Eq. (Q.49) will be nonzero provided that $|p_x - k_x| \ll \Lambda_b$ and that $|p_x + k_x| \ll \Lambda_b/v \sim \overline{k}_{\rm F}$ with $\overline{k}_{\rm F}$ defined in Eq. (4.62). In the following we keep the constraint on the external momentum implicit.

Using the change of variables in Eq. (Q.51), we can write Eq. (Q.49), to leading order in $v \ll 1$, as

$$\mathcal{P}_{14}(k_x, p_x; \mu) = v \int\limits_{-\min(\Lambda_b, \Lambda_f/v)}^{\min(\Lambda_b, \Lambda_f/v)} \frac{\mathrm{d}X}{(2\pi)} \int\limits_{-\Lambda_f}^{\Lambda_f} \frac{\mathrm{d}Y}{(2\pi)} \int\limits_{\mathbb{R}} \frac{\mathrm{d}q_0}{(2\pi)} \left[\frac{1}{-i\left(\frac{\mu}{2} + q_0\right) + Y - 2vX}\right] \\ \times \left[\frac{1}{i\left(\frac{3\mu}{2} + q_0\right) + Y}\right] \left[\frac{1}{|q_0| + |c(v)X + vc(v)Y + \Delta_r| + |vc(v)X - c(v)Y + \Delta_t|)}\right]. \tag{Q.53}$$

Here, $\Delta_r = c(v)(p_x - k_x)$ and $\Delta_t = vc(v)(k_x + p_x)$. In the small v limit, one can safely neglect the terms of order $vc(v)Y$ and $vc(v)X$ inside the boson propagator. Furthermore, for finite v, the integration over X is convergent in the limit in which $\min(\Lambda_b, \Lambda_f/v)$ becomes larger than the intrinsic IR scale of the diagram. Since $\Lambda_f \ll \min(\Lambda_b, \Lambda_f/v)$ we can set the UV cutoff in the X direction to infinity. Doing so we obtain

$$\mathcal{P}_{14}(k_x, p_x; \mu) = v \int\limits_{\mathbb{R}} \frac{\mathrm{d}X}{(2\pi)} \int\limits_{-\Lambda_f}^{\Lambda_f} \frac{\mathrm{d}Y}{(2\pi)} \int\limits_{\mathbb{R}} \frac{\mathrm{d}q_0}{(2\pi)} \left[\frac{1}{-i\left(\frac{\mu}{2} + q_0\right) + Y - 2vX}\right] \\ \times \left[\frac{1}{i\left(\frac{3\mu}{2} + q_0\right) + Y}\right] \left[\frac{1}{|q_0| + |c(v)X + \Delta_r| + |c(v)Y - \Delta_t|)}\right]. \tag{Q.54}$$

Symmetrizing in X and assuming, without loss of generality that $\Delta_r > 0$, we can write

$$\mathcal{P}_{14}(k_x, p_x; \mu) = w(v) \int\limits_{-\Lambda_f}^{\Lambda_f} \frac{\mathrm{d}Y}{(2\pi)} \int\limits_{\mathbb{R}} \frac{\mathrm{d}q_0}{(2\pi)} \int\limits_{\Delta_r}^{\infty} \frac{\mathrm{d}X}{(2\pi)} \left[\frac{1}{i\left(\frac{3\mu}{2} + q_0\right) + Y}\right] \\ \times \left\{\left[\frac{1}{|q_0| + X + \Delta_r + |c(v)Y - \Delta_t|}\right] \left[\frac{Y - 2w(v)X + i\left(q_0 + \frac{\mu}{2}\right)}{\left(\frac{\mu}{2} + q_0\right)^2 + [Y - 2w(v)X]^2}\right]\right.$$

$$+\left[\frac{1}{|q_0|+X-\Delta_r+|c(v)Y-\Delta_t|}\right]\left[\frac{Y+2w(v)X+i\left(q_0+\frac{\mu}{2}\right)}{\left(\frac{\mu}{2}+q_0\right)^2+[Y+2w(v)X]^2}\right]\Bigg\}$$
$$+w(v)\int_{-\Lambda_f}^{\Lambda_f}\frac{\mathrm{d}Y}{(2\pi)}\int_{\mathbb{R}}\frac{\mathrm{d}q_0}{(2\pi)}\int_0^{\Delta_r}\frac{\mathrm{d}X}{(2\pi)}\left[\frac{1}{i\left(\frac{3\mu}{2}+q_0\right)+Y}\right] \tag{Q.55}$$
$$\times\Bigg\{\left[\frac{1}{|q_0|+X+\Delta_r+|c(v)Y-\Delta_t|}\right]\left[\frac{Y-2w(v)X+i\left(q_0+\frac{\mu}{2}\right)}{\left(\frac{\mu}{2}+q_0\right)^2+[Y-2w(v)X]^2}\right]$$
$$+\left[\frac{1}{|q_0|+\Delta_1-X+|c(v)Y-\Delta_t|}\right]\left[\frac{Y+2w(v)X+i\left(q_0+\frac{\mu}{2}\right)}{\left(\frac{\mu}{2}+q_0\right)^2+[Y+2w(v)X]^2}\right]\Bigg\}.$$

We analyze this expression in the following limits: (*i*) $\mu\gg\Delta_r$ and $\mu\gg|\Delta_t|$, (*ii*) $\Delta_r\gg\mu$ and $\Delta_r\gg|\Delta_t|$ and (*iii*) $|\Delta_t|\gg\mu$ and $|\Delta_t|\gg\Delta_r$.

(*i*) For $\mu\gg\Delta_r$ and $\mu\gg|\Delta_t|$ we perform the scaling $(q_0,X,Y)\to\mu(q_0,X,Y)$ and take the small $\Delta_r/\mu\ll1$ and $|\Delta_t|/\mu\ll1$ limits. Defining the rescaled cutoff $\overline{\Lambda}_f=\Lambda_f/\mu$, Eq. (Q.55) takes the form

$$\mathcal{P}_{14}(k_x,p_x;\mu)=w(v)\int_{-\overline{\Lambda}_f}^{\overline{\Lambda}_f}\frac{\mathrm{d}Y}{(2\pi)}\int_{\mathbb{R}}\frac{\mathrm{d}q_0}{(2\pi)}\int_{\mathbb{R}^+}\frac{\mathrm{d}X}{(2\pi)}\left[\frac{1}{i\left(\frac{3}{2}+q_0\right)+Y}\right]$$
$$\times\Bigg\{\left[\frac{1}{|q_0|+X+c(v)|Y|}\right]\left[\frac{Y-2w(v)X+i\left(q_0+\frac{1}{2}\right)}{\left(\frac{1}{2}+q_0\right)^2+[Y-2w(v)X]^2}\right] \tag{Q.56}$$
$$+\left[\frac{1}{|q_0|+X+c(v)|Y|}\right]\left[\frac{Y+2w(v)X+i\left(q_0+\frac{1}{2}\right)}{\left(\frac{1}{2}+q_0\right)^2+[Y+2w(v)X]^2}\right]\Bigg\}.$$

In the small v limit we can safely set $c(v)Y=0$ while keeping $w(v)$ nonzero. Integration over X yields to leading order in $w(v)$:

$$\mathcal{P}_{14}(k_x,p_x)=\frac{w(v)}{\pi}\log\left(\frac{1}{w(v)}\right)\int_{-\overline{\Lambda}_f}^{\overline{\Lambda}_f}\frac{\mathrm{d}Y}{(2\pi)}\int_{\mathbb{R}}\frac{\mathrm{d}q_0}{(2\pi)}\Bigg\{\left[\frac{1}{i\left(\frac{3}{2}+q_0\right)+Y}\right]$$
$$\times\frac{\left[i\left(\frac{1}{2}+q_0+iY\right)\right]}{4q_0^2w(v)^2+\left(iY+\frac{1}{2}+q_0\right)^2}\Bigg\}. \tag{Q.57}$$

To leading order in $w(v)\ll1$, the q_0 integration yields the leading order contribution in the $\overline{\Lambda}_f\gg1$ limit:

$$\mathcal{P}_{14}(k_x,p_x)=\frac{1}{2\pi^2}\log\left(\frac{1}{w(v)}\right)\log\left(\overline{\Lambda}_f\right)=\frac{1}{2\pi^2}\log\left(\frac{1}{w(v)}\right)\log\left(\frac{\Lambda_f}{\mu}\right), \tag{Q.58}$$

where we have used the definition of the rescaled UV cutoff.

(*ii*) For $\Delta_r \gg \mu$ and $\Delta_r \gg |\Delta_t|$ we consider the scaling transformation $(q_0, X, Y) \to \Delta_r(q_0, X, Y)$ and write Eq.(Q.49), in the small μ/Δ_r and $|\Delta_t|/\Delta_r$ limits, as

$$\begin{aligned}\mathcal{P}_{14}(k_x,p_x;\mu) = w(v)\int\limits_{-\overline{\Lambda}_f}^{\overline{\Lambda}_f}\frac{\mathrm{d}Y}{(2\pi)}\int\limits_{\mathbb{R}}\frac{\mathrm{d}q_0}{(2\pi)}\int\limits_{1}^{\infty}\frac{\mathrm{d}X}{(2\pi)}\left[\frac{1}{i+q_0+Y}\right]\left\{\left[\frac{1}{|q_0|+X+1+c(v)|Y|}\right]\right.\\ \times\left[\frac{Y-2w(v)X+iq_0}{q_0^2+[Y-2w(v)X]^2}\right]+\left[\frac{1}{|q_0|+X-1+c(v)|Y|}\right]\left.\left[\frac{Y+2w(v)X+iq_0}{q_0^2+[Y+2w(v)X]^2}\right]\right\}\\ +w(v)\int\limits_{-\overline{\Lambda}_f}^{\overline{\Lambda}_f}\frac{\mathrm{d}Y}{(2\pi)}\int\limits_{\mathbb{R}}\frac{\mathrm{d}q_0}{(2\pi)}\int\limits_{0}^{1}\frac{\mathrm{d}X}{(2\pi)}\left[\frac{1}{iq_0+Y}\right]\left\{\left[\frac{1}{|q_0|+X+1+c(v)|Y|}\right]\right.\\ \times\left[\frac{Y-2w(v)X+iq_0}{q_0^2+[Y-2w(v)X]^2}\right]+\left[\frac{1}{|q_0|+1-X+c(v)|Y|}\right]\left.\left[\frac{Y+2w(v)X+iq_0}{q_0^2+[Y+2w(v)X]^2}\right]\right\},\end{aligned} \tag{Q.59}$$

where $\overline{\Lambda}_f = \Lambda_f/\Delta_r$. In the small v limit, the term of order $c(v)|Y|$ can be safely neglected and an integration over X yields the leading order contribution in $v \ll 1$:

$$\begin{aligned}\mathcal{P}_{14}(k_x,p_x;\mu) = \frac{w(v)}{2\pi}\int\limits_{-\overline{\Lambda}_f}^{\overline{\Lambda}_f}\frac{\mathrm{d}Y}{(2\pi)}\int\limits_{\mathbb{R}}\frac{\mathrm{d}q_0}{(2\pi)}\left[\frac{1}{iq_0+Y}\right]\\ \times\left\{\frac{i(q_0+iY)\left[\operatorname{arcoth}(1+|q_0|)-2i\arctan\left(\frac{q_0}{Y}\right)+\log\left(\frac{q_0^2+Y^2}{4w(v)^2|q_0||q_0+2|}\right)\right]}{\{q_0+i[Y-2w(v)(|q_0|-1)]\}\{q_0+i[Y+2w(v)(1+|q_0|)]\}}\right\}.\end{aligned} \tag{Q.60}$$

At this stage we cannot simply set $w(v) = 0$ in the denominator because doing so introduces an IR divergence. We can, however, neglect the terms of order $w(v)|q_0|$ with respect to the terms of order q_0 in the denominator and integrate over q_0 in order to obtain

$$\begin{aligned}\mathcal{P}_{14}(k_x,p_x;\mu) = \frac{w(v)}{2\pi}\log\left(\frac{1}{w(v)}\right)\int\limits_{0}^{\overline{\Lambda}_f}\frac{\mathrm{d}Y}{(2\pi)}\frac{Y}{[w(v)+Y]^2}\\ +\frac{w(v)}{2\pi}\log\left(\frac{1}{w(v)}\right)\int\limits_{-\overline{\Lambda}_f}^{0}\frac{\mathrm{d}Y}{(2\pi)}\frac{\Theta(-Y-2w(v))Y}{[w(v)+Y]^2}.\end{aligned} \tag{Q.61}$$

Final integration over Y yields the leading order divergent term in the $\overline{\Lambda}_f \gg 1$ limit

$$\mathcal{P}_{14}(k_x,p_x;\mu) = \frac{w(v)}{2\pi^2}\log\left(\frac{1}{w(v)}\right)\log\left(\frac{\Lambda_f}{w(v)|\Delta_r|}\right), \tag{Q.62}$$

where we have used the definition $\overline{\Lambda}_f = \Lambda_f/\Delta_r$ and used the fact that the result remains unchanged when $\Delta_r < 0$. The extra factor of $w(v)$ in the IR scale implies that the actual momentum-dependent IR cutoff of the diagram is further suppressed by $w(v)$.

(*iii*) For $|\Delta_t| \gg \mu$ and $|\Delta_t| \gg \Delta_r$ we assume, without loss of generality, that $\Delta_t > 0$ and perform the scaling $(q_0, X, Y) \to \Delta_t(q_0, X, Y)$. Defining $\overline{\Lambda}_f = \Lambda_f/\Delta_t$, Eq. (Q.49) assumes the form

$$\mathcal{P}_{14}(k_x, p_x; \mu) = w(v) \int_{-\Lambda_f}^{\Lambda_f} \frac{\mathrm{d}Y}{(2\pi)} \int_{\mathbb{R}} \frac{\mathrm{d}q_0}{(2\pi)} \int_0^{\infty} \frac{\mathrm{d}X}{(2\pi)} \left[\frac{1}{iq_0 + Y}\right] \left\{ \left[\frac{1}{|q_0| + X + |c(v)Y - 1|}\right] \right. \\ \left. \times \left[\frac{Y - 2w(v)X + iq_0}{q_0^2 + (Y - 2w(v)X)^2}\right] + \left[\frac{1}{|q_0| + X + |c(v)Y - 1|}\right] \left[\frac{Y + 2w(v)X + iq_0}{q_0^2 + [Y + 2w(v)X]^2}\right] \right\}. \tag{Q.63}$$

In the small $c(v)$ limit we ignore the term of order $c(v)Y$, but we keep the $w(v)X$ terms nonzero. Integration over X yields, after keeping the leading order in $w(v)$ terms in the numerator,

$$\mathcal{P}_{14}(k_x, p_x; \mu) = \frac{w(v)}{\pi} \log\left(\frac{1}{w(v)}\right) \int_{-\overline{\Lambda}_f}^{\overline{\Lambda}_f} \frac{\mathrm{d}Y}{(2\pi)} \int_{\mathbb{R}} \frac{\mathrm{d}q_0}{(2\pi)} \left\{ \left[\frac{1}{iq_0 + Y}\right] \right. \\ \left. \times \frac{(iq_0 - Y)}{4(q_0 + 1)^2 w(v)^2 + (iY + q_0)^2} \right\}. \tag{Q.64}$$

In the denominator we can neglect the terms of order $w(v)q_0$ with respect to those of order q_0 and integrate over the latter in order to obtain

$$\mathcal{P}_{14}(k_x, p_x; \mu) = \frac{w(v)}{\pi} \log\left(\frac{1}{w(v)}\right) \int_0^{\overline{\Lambda}_f} \frac{\mathrm{d}Y}{(2\pi)} \Theta(Y) \\ \times \left[\frac{\mathrm{sgn}\,[Y - 2w(v)]}{8[Y^2 - w(v)^2]} \left[w(v) + Y - \mathrm{sgn}[Y - 2w(v)][w(v) - 3Y]\right]\right] \\ + \frac{w(v)}{\pi} \log\left(\frac{1}{w(v)}\right) \int_{-\overline{\Lambda}_f}^{0} \frac{\mathrm{d}Y}{(2\pi)} \left[\frac{\Theta[2w(v) + Y]}{4[w(v) - Y]} + \frac{\Theta[-Y - 2w(v)]Y}{2[w(v)^2 - Y^2]}\right]. \tag{Q.65}$$

Integrating over Y yields the logarithmically divergent contribution:

$$\mathcal{P}_{14}(k_x, p_x; \mu) = \frac{w(v)}{2\pi^2} \log\left(\frac{1}{w(v)}\right) \log\left(\frac{\Lambda_f}{w(v)|\Delta_t|}\right), \tag{Q.66}$$

where we have used the definition $\overline{\Lambda}_f = \Lambda_f/\Delta_t$ and the fact that the result is the same for $\Delta_t < 0$. The extra factor of $w(v)$ in the logarithm implies that the actual IR energy scale in the limit under consideration is $w(v)|\Delta_t|$.

Collecting the results from Eqs. (Q.58), (Q.62) and (Q.66), using the definitions $\Delta_t = vc(v)(k_x + p_x)$ and $\Delta_r = c(v)(p_x - k_x)$, and bringing back the constraint on the external momentum, we write

$$\mathcal{P}_{14}(k_x, p_x; \mu) = \frac{w(v)}{2\pi^2} \Theta(\Lambda_b - |p_x - k_x|) \log\left(\frac{1}{w(v)}\right) \\ \times \log\left(\frac{\Lambda_f}{\mathscr{F}_{14}(\mu, v|p_x - k_x|, v^2|k_x + p_x|)}\right), \tag{Q.67}$$

where the crossover function satisfies $\mathscr{F}_{14}(x,y,z) \approx \max(x,y,z)$.

E. $\mathcal{P}_{15}(k,p)$

For $M=1$ and $N=5$, the integration in Eq. (Q.4) can be written, at the RG condition, as

$$\mathcal{P}_{15}(k_x,p_x;\mu) = v\int \mathrm{d}q \left[\frac{1}{|q_0|+c(v)(|q_x|+|q_y|)}\right]\left[\frac{1}{i\left(\frac{3\mu}{2}+q_0\right)+vq_x-q_y+2vk_x}\right] \times\left[\frac{1}{-i\left(\frac{\mu}{2}+q_0\right)+vq_x-q_y-2vp_x}\right]. \tag{Q.68}$$

The integration over $\vec{q}$ is done, according to the discussion in Sec. 4.2-(*a*) , over the space defined by the conditions

$$|vq_x-q_y+2vk_x|<\Lambda_f, \quad |vq_x-q_y-2vp_x|<\Lambda_f, \quad |q_x|<\Lambda_b, \quad \& \quad |q_y|<\Lambda_b. \tag{Q.69}$$

To make the integration in Eq. (Q.68) depend explicitly on the cutoff scales we consider the change of variables

$$Y = vq_x-q_y+v(k_x-p_x), \qquad \& \qquad X = q_x+vq_y. \tag{Q.70}$$

This change of variables transform the integration regime to

$$\begin{aligned} |Y-v(p_x+k_x)|<\Lambda_f, \quad |Y+v(p_x+k_x)|<\Lambda_f,\\ |X+vY+v^2(p_x-k_x)|<\Lambda_b, \quad \& \quad |Y-vX+v(p_x-k_x)|<\Lambda_b. \end{aligned} \tag{Q.71}$$

For the Y integration to have nonzero support, we require that $|p_x+k_x| \ll \Lambda_f/v$, in which case the Y integration is cutoff by Λ_f in the UV. With this at hand, and in the $\Lambda_f \ll c(v)\Lambda_b \ll \Lambda_b$ limit we require that $|p_x-k_x| \ll \Lambda_b/v \sim \overline{k}_{\mathrm{F}}$ for the X integration to have nonzero support, in which case the X integration is cutoff by Λ_b. Here, $\overline{k}_{\mathrm{F}}$ is defined in Eq. (4.62). In what follows we keep the constraints on the external momentum implicit. With the aforementioned change of variables, Eq. (Q.68) is given, to leading order in v, by

$$\mathcal{P}_{15}(k_x,p_x;\mu) = v\int_{\mathbb{R}}\frac{\mathrm{d}q_0}{(2\pi)}\int_{-\Lambda_b}^{\Lambda_b}\frac{\mathrm{d}X}{(2\pi)}\int_{-\Lambda_f}^{\Lambda_f}\frac{\mathrm{d}Y}{(2\pi)}\left[\frac{1}{i\left(\frac{3\mu}{2}+q_0\right)+Y+\Delta_t}\right] \times\left[\frac{1}{-i\left(\frac{\mu}{2}+q_0\right)+Y-\Delta_t}\right]\left[\frac{1}{|q_0|+c(v)|X+vY|+|c(v)Y-vc(v)X+\Delta_r|}\right]. \tag{Q.72}$$

Here, $\Delta_r = vc(v)(p_x-k_x)$ and $\Delta_t = v(p_x+k_x)$ denote the relative and total energy of the pair of electrons involved in the loop. In arriving to this expression we have neglected the term of order $v\Delta_r$ with respect to Δ_r in the boson propagator to leading order in v. This is because both contributions effectively either add up or subtract upon integrating over X and Y. The integration over Ycan be done in the small $c(v)$ limit by neglecting the terms of order $vc(v)Y$ and $c(v)Y$ in the boson propagator. Likewise, the X integration can be

performed by safely neglecting the term of order $vc(v)X$ in the boson propagator. After integrating over X and Y we have

$$\mathcal{P}_{15}(k_x,p_x;\mu)=\frac{w(v)}{2\pi^2}\int\limits_{\mathbb{R}}\frac{\mathrm{d}q_0}{(2\pi)}\log\left[1+\frac{c(v)\Lambda_b}{|q_0|+|\Delta_r|}\right]\frac{1}{\mu+q_0-i\Delta_t}\\ \times\left\{\left[\arctan\left(\frac{\Lambda_f}{\frac{3\mu}{2}+q_0}\right)+\arctan\left(\frac{\Lambda_f}{\frac{\mu}{2}+q_0}\right)\right]\right\}. \tag{Q.73}$$

We proceed on analyzing this integration when (*i*) $\mu\gg|\Delta_r|$ and $\mu\gg|\Delta_t|$, (*ii*) $|\Delta_t|\gg|\Delta_r|$ and $|\Delta_t|\gg\mu$, and (*iii*) $|\Delta_r|\gg|\Delta_t|$ and $|\Delta_r|\gg\mu$.

(*i*) For $\mu\gg|\Delta_r|$ and $\mu\gg|\Delta_t|$ we consider the scaling $q_0\to q_0\mu$ and define, $\overline{\Delta}_t=|\Delta_t|/\mu$, $\overline{\Delta}_r=|\Delta_r|/\mu$, $\overline{\Lambda}_f=\Lambda/\mu$ and $\overline{\Lambda}_b=\Lambda_b/\mu$. In terms of these parameters Eq. (Q.73) takes the form

$$\mathcal{P}_{15}(k_x,p_x;\mu)=\frac{w(v)}{2\pi^2}\int\limits_{\mathbb{R}}\frac{\mathrm{d}q_0}{(2\pi)}\log\left[1+\frac{c(v)\overline{\Lambda}_b}{|q_0|+\overline{\Delta}_r}\right]\frac{1}{1+q_0-i\overline{\Delta}_t}\\ \times\left\{\left[\arctan\left(\frac{\overline{\Lambda}_f}{\frac{3}{2}+q_0}\right)+\arctan\left(\frac{\overline{\Lambda}_f}{\frac{1}{2}+q_0}\right)\right]\right\}. \tag{Q.74}$$

In the small $\overline{\Delta}_r$ and $\overline{\Delta}_t$ limits, these parameters can be set to zero without danger of introducing IR divergences in the integral. The final integration can be done by first symmetrizing the integrand in q_0 and then by considering the regimes where $q_0>\overline{\Lambda}_f$ and $q_0<\overline{\Lambda}_f$. The leading order divergent term in the $1\ll\overline{\Lambda}_f\ll c(v)\overline{\Lambda}_b$ limit comes from the latter regime and it is given, to leading order in these limits, by

$$\mathcal{P}_{15}(k_x,p_x;\mu)=\frac{w(v)}{2\pi^2}\left[\log\left(\frac{c(v)\Lambda_b}{\mu}\right)\log\left(\frac{\Lambda_f}{\mu}\right)-\frac{1}{2}\log\left(\frac{\Lambda_f}{\mu}\right)^2\right], \tag{Q.75}$$

where we have used the definitions $\overline{\Lambda}_f=\Lambda_f/\mu$ and $\overline{\Lambda}_b=\Lambda_b/\mu$.

(*ii*) For $|\Delta_t|\gg|\Delta_r|$ and $|\Delta_t|\gg\mu$, we assume, without loss of generality, that $\Delta_t>0$ and perform the scaling $q_0\to\Delta_t q_0$. In the small μ/Δ_t and $|\Delta_r|/\Delta_t$ limits, Eq. (Q.73) assumes the form

$$\mathcal{P}_{15}(k_x,p_x;\mu)=\frac{2w(v)}{\pi^2}\int\limits_{\mathbb{R}^+}\frac{\mathrm{d}q_0}{(2\pi)}\log\left[1+\frac{c(v)\overline{\Lambda}_b}{q_0}\right]\frac{q_0}{1+q_0^2}\arctan\left(\frac{\overline{\Lambda}_f}{q_0}\right). \tag{Q.76}$$

Here, $\overline{\Lambda}_b=\Lambda_b/\Delta_t$ and $\overline{\Lambda}_f=\Lambda_f/\Delta_t$. As in the previous case we can divide this integration into two regimes: $q_0>\overline{\Lambda}_f$ and $q_0<\overline{\Lambda}_f$. As before, the leading order divergent term in the $1\ll\overline{\Lambda}_f\ll c(v)\overline{\Lambda}_b$ limit comes from the latter regime and it has the double logarithm form:

$$\mathcal{P}_{15}(k_x,p_x;\mu)=\frac{w(v)}{2\pi^2}\left[\log\left(\frac{c(v)\Lambda_b}{|\Delta_t|}\right)\log\left(\frac{\Lambda_f}{|\Delta_t|}\right)-\frac{1}{2}\log\left(\frac{\Lambda_f}{|\Delta_t|}\right)^2\right]. \tag{Q.77}$$

In arriving to this expression we have used the definition of the rescaled cutoff scales and the fact that the result remains the same when $\Delta_t<0$.

(*iii*) For $|\Delta_r| \gg \mu$ and $|\Delta_r| \gg |\Delta_t|$, we assume, without loss of generality, that $\Delta_r > 0$ and perform the scaling $q_0 \to \Delta_r q_0$. Defining $\overline{\Lambda}_b = \Lambda_b/\Delta_r$, $\overline{\Lambda}_f = \Lambda_f/\Delta_r$, $\delta = |\Delta_t|/\Delta_r$ and $m = \mu/\Delta_r$, we can write Eq. (Q.73) as

$$\mathcal{P}_{15}(k_x, p_x; \mu) = \frac{w(v)}{2\pi^2} \int_{\mathbb{R}} \frac{\mathrm{d}q_0}{(2\pi)} \log\left[1 + \frac{c(v)\overline{\Lambda}_b}{|q_0|+1}\right] \frac{1}{m + q_0 - i\delta} \times \left\{\left[\arctan\left(\frac{\overline{\Lambda}_f}{\frac{3m}{2} + q_0}\right) + \arctan\left(\frac{\overline{\Lambda}_f}{\frac{m}{2} + q_0}\right)\right]\right\}. \tag{Q.78}$$

Setting both m and δ to zero introduces an IR divergence in the q_0 integration. For nonzero $m \ll 1$ and $\delta \ll 1$ we consider the cases in which (*a*) $\delta \gg m$ and (*b*) $m \gg \delta$.

(*a*) For $\delta \gg m$ we perform the scaling $q_0 \to \delta q_0$ and set $m/\delta = 0$ inside the integration. In this limit, Eq. (Q.78) reads

$$\mathcal{P}_{15}(k_x, p_x; \mu) = \frac{2w(v)}{\pi^2} \int_0^{\infty} \frac{\mathrm{d}q_0}{(2\pi)} \log\left[1 + \frac{c(v)\overline{\Lambda}_b}{\delta q_0 + 1}\right] \frac{q_0}{q_0^2 + 1} \arctan\left(\frac{\widehat{\Lambda}_f}{q_0}\right), \tag{Q.79}$$

where $\widehat{\Lambda}_f = \overline{\Lambda}_f/\delta$. The integration over q_0 is done prior to taking the $\delta \ll 1$ limit. This is done by dividing the q_0 integration into the $0 < q_0 < 1/\delta$ and $1/\delta < q_0 < \infty$. For $1 \ll \overline{\Lambda}_f \ll c(v)\overline{\Lambda}_b$ and $\delta \ll 1$, the first regime gives rise to a divergence of the form $\log[c(v)\overline{\Lambda}_b]\log(\delta)$ while the second one gives a double logarithmic divergence similar to the one found in the case where either μ or $|\Delta_t|$ are the largest energy scales in the integrand. The combination of the two contributions yields

$$\mathcal{P}_{15}(k_x, p_x; \mu) = \frac{w(v)}{2\pi^2}\left[\log\left(\frac{c(v)\Lambda_b}{|\Delta_r|}\right)\log\left(\frac{\Lambda_f}{\Delta_t}\right) - \frac{1}{2}\log\left(\frac{\Lambda_f}{|\Delta_r|}\right)^2\right]. \tag{Q.80}$$

In arriving to this expression we have used the definitions of the rescaled cutoff scales. Furthermore, the results remains the same for $\Delta_r < 0$, owing to the appearance of the absolute values in this expression.

(*b*) For $m \gg \delta$ we proceed as before by first scaling out m through the transformation $q_0 \to m q_0$. Defining $\widehat{\Lambda}_f = \overline{\Lambda}_f/m$, we write

$$\mathcal{P}_{15}(k_x, p_x; \mu) = \frac{w(v)}{2\pi^2} \int_{\mathbb{R}} \frac{\mathrm{d}q_0}{(2\pi)} \log\left[1 + \frac{c(v)\overline{\Lambda}_b}{m|q_0|+1}\right] \frac{1}{1+q_0} \times \left\{\left[\arctan\left(\frac{\widehat{\Lambda}_f}{\frac{3}{2} + q_0}\right) + \arctan\left(\frac{\widehat{\Lambda}_f}{\frac{1}{2} + q_0}\right)\right]\right\}. \tag{Q.81}$$

The integration over q_0 is done by first symmetrizing the integrand in q_0 and then by dividing the regime of integration into the $q_0 \gg 1/m$ and $q_0 \ll 1/m$ regions. In the $m \ll 1$ and $1 \ll \overline{\Lambda}_f \ll c(v)\overline{\Lambda}_b$ limits, the first regime yields a

double logarithmic divergence similar to the one found in the cases where either μ or $|\Delta_t|$ is the largest IR scale. The second regime, on the other hand, yields a divergence of the form $\log[c(v)\overline{\Lambda}_b]\log(m)$. Combining the two contributions together one obtains in these limits:

$$\mathcal{P}_{15}(k_x,p_x;\mu)=\frac{w(v)}{2\pi^2}\left[\log\left(\frac{\Lambda_b}{|\Delta_r|}\right)\log\left(\frac{\Lambda_f}{\mu}\right)-\frac{1}{2}\log\left(\frac{\Lambda_f}{|\Delta_r|}\right)^2\right]. \tag{Q.82}$$

In arriving to this final expression we have used the definition of the rescaled cutoffs and the fact that we obtain the exact same result for $\Delta_r<0$.

Collecting the results from Eqs. (Q.75), (Q.77), (Q.80) and (Q.82), using the definitions $\Delta_r=vc(v)(p_x-k_x)$ and $\Delta_t=v(p_x+k_x)$, and bringing back the extra constraint on the external momentum, we have

$$\begin{aligned}\mathcal{P}_{15}(k_x,p_x;\mu)=\frac{w(v)}{2\pi^2}\Theta\left(\Lambda_f-v|k_x+p_x|\right)\left[\log\left(\frac{c(v)\Lambda_b}{\mathscr{F}_{15}[\mu,vc(v)|p_x-k_x|,v|p_x+k_x|]}\right)\right. \\ \left.\times\log\left(\frac{\Lambda_f}{\mathscr{F}_{15}[\mu,v|p_x+k_x|]^2}\right)-\frac{1}{2}\log\left(\frac{\Lambda_f}{\mathscr{F}_{15}[\mu,vc(v)|p_x-k_x|,v|p_x+k_x|]}\right)^2\right].\end{aligned} \tag{Q.83}$$

Here, the crossover functions satisfy $\mathscr{F}_{15}(x,y,z)\approx\max(x,y,z)$.

F. $\mathcal{P}_{16}(k,p)$

For $M=1$ and $N=6$, the integration in Eq. (Q.4) can be written, at the RG condition, as

$$\begin{aligned}\mathcal{P}_{16}(k_x,p_y)=v\int\mathrm{d}q\left[\frac{1}{|q_0|+c(v)(|q_x|+|q_y|)}\right]\left[\frac{1}{i\left(\frac{3\mu}{2}+q_0\right)+vq_x-q_y+2vk_x}\right] \\ \times\left[\frac{1}{-i\left(\frac{\mu}{2}+q_0\right)+q_x-vq_y+2vp_y}\right].\end{aligned} \tag{Q.84}$$

As described in Sec. 4.2-(*a*) , the integration over $\vec{q}$ is done over the region defined by

$$|vq_x-q_y+2vk_x|<\Lambda_f,\quad |q_x-vq_y+2vp_y|<\Lambda_f,\quad |q_x|<\Lambda_b,\quad \&\quad |q_y|<\Lambda_b. \tag{Q.85}$$

To make Eq. (Q.84) depend explicitly on the cutoff scales we consider the change of variables

$$Y=vq_x-q_y+2vk_x\qquad\&\qquad X=q_x-vq_y+2vp_y. \tag{Q.86}$$

Under this change of variables the region of integration for both X and Y is now given by

$$\begin{aligned}|Y|<\Lambda_f,\quad |X|<\Lambda_f,\quad |X-vY+2v(vk_x-p_y)|<\Lambda_b,\quad \& \\ |vX-Y+2v(k_x-vp_y)|<\Lambda_b.\end{aligned} \tag{Q.87}$$

Both X and Y integrations are cutoff by Λ_f as a consequence of these two representing momenta that are perpendicular to each other. We further note that these two integrations

have nonzero support within the regime of validity of the theory exposed in Sec. 4.4-(a) and therefore there is no further constraint in the external momentum. Under the aforementioned change of variables we write Eq. (Q.84) as

$$\mathcal{P}_{16}(k_x,p_y;\mu)=v\int\limits_{\mathbb{R}}\frac{\mathrm{d}X}{(2\pi)}\int\limits_{-\Lambda_f}^{\Lambda_f}\frac{\mathrm{d}Y}{(2\pi)}\int\limits_{-\Lambda_f}^{\Lambda_f}\frac{\mathrm{d}q_0}{(2\pi)}\left[\frac{1}{i\left(\frac{3\mu}{2}+q_0\right)+Y}\right]\left[\frac{1}{-i\left(\frac{\mu}{2}+q_0\right)+X}\right]\times\left[\frac{1}{|q_0|+|c(v)X-vc(v)Y+\Delta_t|+|vc(v)X-c(v)Y+\Delta_r|}\right]. \tag{Q.88}$$

Here we have defined $\Delta_t=2vc(v)(vk_x-p_y)$ and $\Delta_r=2vc(v)(k_x-vp_y)$. In the small v limit, the terms of order $vc(v)Y$ and $vc(v)X$ in the boson propagator can be ignored. Doing so and comparing this expression to Eq. (Q.32) it follows immediately that

$$\mathcal{P}_{16}(k_x,p_y;\mu)=\frac{v}{4\pi}\log\left(\frac{\Lambda_f}{\mathscr{F}_{16}[\mu,2vc(v)|k_x-vp_y|,2vc(v)|vk_x-p_y|]}\right), \tag{Q.89}$$

where the crossover function satisfies $\mathscr{F}_{16}(x,y,z)\approx\max(x,y,z)$.

G. $\mathcal{P}_{17}(k,p)$

For $M=1$ and $N=7$, the integration in Eq. (Q.4) can be written, at the RG condition, as

$$\mathcal{P}_{17}(k_x,p_y;\mu)=v\int\mathrm{d}q\left[\frac{1}{|q_0|+c(v)(|q_x|+|q_y|)}\right]\left[\frac{1}{i\left(\frac{3\mu}{2}+q_0\right)+vq_x-q_y+2vk_x}\right]\times\left[\frac{1}{-i\left(\frac{\mu}{2}+q_0\right)+q_x+vq_y-2vp_y}\right]. \tag{Q.90}$$

As explained in Sec. 4.2-(a) , the integration over $\vec{q}$ is done over the region defined by the conditions

$$|vq_x-q_y+2vk_x|<\Lambda_f,\quad |q_x+vq_y-2vp_y|<\Lambda_f,\quad |q_x|<\Lambda_b,\quad \&\quad |q_y|<\Lambda_b. \tag{Q.91}$$

In order to make Eq. (Q.90) depend on the cutoff scales explicitly, we consider the change of variables,

$$X=q_x+vq_y-2vp_y,\qquad \&\qquad Y=vq_x-q_y+2vk_x. \tag{Q.92}$$

The integration over X and Y is restricted to the region

$$|Y|<\Lambda_f,\quad |X|<\Lambda_f,\quad |X+vY-2v(p_y-vk_x)|<\Lambda_b,\quad \&\quad |vX-Y+2v(k_x+vp_y)|<\Lambda_b. \tag{Q.93}$$

The integrations over X and Y are cutoff by Λ_f and they have nonzero support provided that both $k_x\ll\overline{k}_{\mathrm{F}}$ and $p_y\ll\overline{k}_{\mathrm{F}}$, with $\overline{k}_{\mathrm{F}}$ defined in Eq. (4.62). Therefore, there are no further constraints on the external momentum besides the one described in Sec. 4.4-(a)

regarding the validity of the low-energy theory in the momentum space. In terms of the new variables, Eq. (Q.90) takes the form

$$\mathcal{P}_{17}(k_x,p_y;\mu)=v\int\limits_{\mathbb{R}}\frac{\mathrm{d}q_0}{(2\pi)}\int\limits_{-\Lambda_f}^{\Lambda_f}\frac{\mathrm{d}X}{(2\pi)}\int\limits_{-\Lambda_f}^{\Lambda_f}\frac{\mathrm{d}Y}{(2\pi)}\left[\frac{1}{i\left(\frac{3\mu}{2}+q_0\right)+Y}\right]\left[\frac{1}{-i\left(\frac{\mu}{2}+q_0\right)+X}\right]\times\left[\frac{1}{|q_0|+|c(v)X+vc(v)Y+\Delta_t|+|vc(v)X-c(v)Y+\Delta_r|}\right]. \tag{Q.94}$$

where $\Delta_t=vc(v)(p_y-vk_x)$ and $\Delta_r=2vc(v)(k_x+vp_y)$. In the $v\ll 1$ limit, the terms of order $vc(v)Y$ and $vc(v)X$ can be safely dropped inside the boson propagator. In doing so one arrives to an expression analogous to that in Eq. (Q.42). We therefore conclude that,

$$\mathcal{P}_{17}(k_x,p_y;\mu)=\frac{v}{4\pi}\log\left(\frac{\Lambda_f}{\mathscr{F}_{17}[\mu,2vc(v)|p_y-vk_x|,2vc(v)|k_x+vp_y|]}\right), \tag{Q.95}$$

where the crossover function satisfies $\mathscr{F}_{17}(x,y,z)\approx\max(x,y,z)$.

H. $\mathcal{P}_{18}(k,p)$

For $M=1$ and $N=8$, the integration in Eq. (Q.4) can be written, at the RG condition, as

$$\mathcal{P}_{18}(k_x,p_x;\mu)=v\int\mathrm{d}q\left[\frac{1}{|q_0|+c(v)(|q_x|+|q_y|)}\right]\left[\frac{1}{i\left(\frac{3\mu}{2}+q_0\right)+vq_x-q_y+2vk_x}\right]\times\left[\frac{1}{-i\left(\frac{\mu}{2}+q_0\right)+vq_x+q_y-2vp_x}\right]. \tag{Q.96}$$

As discussed in Sec. 4.2-(*a*) , the integration over $\vec{q}$ is done on the region defined by

$$|vq_x-q_y+2vk_x|<\Lambda_f,\quad |vq_x+q_y-2vp_x|<\Lambda_f,\quad |q_x|<\Lambda_b,\quad \&\quad |q_y|<\Lambda_b. \tag{Q.97}$$

Eq. (Q.96) becomes explicitly dependent on the cutoff scales through the change of variables

$$\begin{aligned}Y&=vq_x-q_y+2vk_x,\quad \&\\ X&=vq_x+q_y-(1+v^2)p_x+(1-v^2)k_x\approx vq_x+q_y+(k_x-q_x).\end{aligned} \tag{Q.98}$$

Under the change of variables, the integration regime for X and Y corresponds to the region

$$\begin{aligned}&|Y|<\Lambda_f,\quad |Y-2vX|<\Lambda_f,\quad |X+vY+p_x-k_x|<\Lambda_b,\quad \&\\ &|Y-vX-v(k_x+p_x)|<\Lambda_b.\end{aligned} \tag{Q.99}$$

For the Y integration to have nonzero support, we require that $|X|\ll\Lambda_f/v$. On the other hand, when $\Lambda_f\ll c(v)\Lambda_b\ll\Lambda_b$, the X integration has nonzero support provided that $|p_x-k_x|\ll\Lambda_b$ and $|X|\ll\Lambda_b$. Of course, the relative magnitude between the two possible cutoff scales for the X integration is important. However, as we proceed to show,

Eq. (Q.96) is independent of the cutoff scales. We do this by setting all scales to infinity in the integration limits. However, the external momentum must satisfy $|p_x - k_x| \ll \Lambda_b$. Keeping this constraint implicit, we write Eq. (Q.96) in the new variables as

$$\mathcal{P}_{18}(k_x,p_x;\mu) = v\int_{\mathbb{R}}\frac{\mathrm{d}q_0}{(2\pi)}\int_{\mathbb{R}}\frac{\mathrm{d}X}{(2\pi)}\int_{\mathbb{R}}\frac{\mathrm{d}Y}{(2\pi)}\left[\frac{1}{i\left(\frac{3\mu}{2}+q_0\right)+Y}\right]\left[\frac{1}{-i\left(\frac{\mu}{2}+q_0\right)+2vX-Y}\right] \times\left[\frac{1}{|q_0|+(|c(v)X+w(v)^{-1}\Delta_r|+|c(v)Y-w(v)^{-1}\Delta_t|)}\right]. \tag{Q.100}$$

where $\Delta_r = v(p_x - k_x)$ and $\Delta_t = v^2(k_x + p_x)$. This integration is similar to that of the case in which $M = 1$ and $N = 4$ because in the small v limit, the hot spots $M = 1$ and $N = 8$ become nested. Thus, we expect that the naive momentum-dependent IR scales of the diagram will come with an extra factor of $w(v) = v/c(v)$ as it happened in the former case. This is the reason behind the $w(v)$ dependence appearing in the boson propagator. In what follows we consider this expression in the limits in which (*i*) $\mu \gg |\Delta_r|$ and $\mu \gg |\Delta_t|$, (*ii*) $|\Delta_r| \gg \mu$ and $|\Delta_r| \gg |\Delta_t|$, and (*iii*) $|\Delta_t| \gg \mu$ and $|\Delta_t| \gg |\Delta_r|$.

(*i*) For $\mu \gg |\Delta_t|$ and $\mu \gg |\Delta_r|$ we consider the scaling $(q_0, X, Y) \to \mu(q_0, X/c(v), Y)$ in Eq. (Q.100) and take the small $|\Delta_t|/\mu$ and $|\Delta_r|/\mu$ limits. Using the definition $w(v) = v/c(v)$, this yields

$$\mathcal{P}_{18}(k_x,p_x;\mu) = w(v)\int_{\mathbb{R}}\frac{\mathrm{d}q_0}{(2\pi)}\int_{\mathbb{R}}\frac{\mathrm{d}X}{(2\pi)}\int_{\mathbb{R}}\frac{\mathrm{d}Y}{(2\pi)}\left[\frac{1}{i\left(\frac{3}{2}+q_0\right)+Y}\right] \times\left[\frac{1}{|q_0|+|X|+c(v)|Y|}\right]\left[\frac{1}{-i\left(\frac{1}{2}+q_0\right)+2w(v)X-Y}\right]. \tag{Q.101}$$

For $v \ll 1$, the term of order $c(v)Y$ can be discarded without altering the convergence of the Y integration. On the other hand, setting $w(v) = 0$ introduces a UV divergence. Therefore, setting $c(v)Y = 0$ inside the boson propagator while keeping $w(v)$ nonzero yields,

$$\mathcal{P}_{18}(k_x,p_x;\mu) = w(v)\int_{\mathbb{R}}\frac{\mathrm{d}q_0}{(2\pi)}\int_{\mathbb{R}}\frac{\mathrm{d}X}{(2\pi)}\left[\frac{1}{|q_0|+|X|}\right]\frac{\Theta\left(\frac{3}{2}+q_0\right)-\Theta\left(\frac{1}{2}+q_0\right)}{2iw(v)X-1}. \tag{Q.102}$$

Integration over q_0 and X yields, to the leading order in $w(v)$,

$$\mathcal{P}_{18}(k_x,p_x;\mu) = -\frac{w(v)}{2\pi^2}\log\left(\frac{1}{w(v)}\right). \tag{Q.103}$$

(*ii*) For $|\Delta_r| \gg \mu$ and $|\Delta_r| \gg |\Delta_t|$, we consider, without loss of generality, that $\Delta_r > 0$ and perform the scaling $(q_0, X, Y) \to \Delta_r(q_0, X/c(v), Y)$ in Eq. (Q.100):

$$\mathcal{P}_{18}(k_x,p_x;\mu) = w(v)\int_{\mathbb{R}}\frac{\mathrm{d}q_0}{(2\pi)}\int_{\mathbb{R}}\frac{\mathrm{d}X}{(2\pi)}\int_{\mathbb{R}}\frac{\mathrm{d}Y}{(2\pi)}\left[\frac{1}{-i\left(\frac{m}{2}+q_0\right)+2w(v)X-Y}\right] \times\left[\frac{1}{i\left(\frac{3m}{2}+q_0\right)+Y}\right]\left[\frac{1}{|q_0|+(|X+w(v)^{-1}|+|c(v)Y-w(v)^{-1}\delta|)}\right], \tag{Q.104}$$

where $\delta = \Delta_t/\Delta_r$ and $m = \mu/\Delta_r$. In the small v limit, the integration over Y can be done by safely ignoring the term of order $c(v)Y$. Doing so we have

$$\mathcal{P}_{18}(k_x,p_x;\mu) = w(v)\int\limits_{\mathbb{R}}\frac{\mathrm{d}q_0}{(2\pi)}\int\limits_{\mathbb{R}}\frac{\mathrm{d}X}{(2\pi)}\left[\frac{1}{|q_0|+|X+w(v)^{-1}|+w(v)^{-1}|\delta|}\right] \times\left[\frac{\Theta\left(\frac{3m}{2}+q_0\right)-\Theta\left(\frac{m}{2}+q_0\right)}{2iw(v)X-m}\right]. \tag{Q.105}$$

We are interested in this integration in the $\delta \ll 1$ and $m \ll 1$ limits. Setting $\delta = 0$ inside the integrand is not a problem, but setting $m = 0$ introduces an IR divergence in the X integration. After symmetrizing in q_0 and scaling out $w(v)$ from the integrand we can write

$$\mathcal{P}_{18}(k_x,p_x;\mu) = -\int\limits_{\mathbb{R}}\frac{\mathrm{d}X}{(2\pi)}\int\limits_{\frac{w(v)m}{2}}^{\frac{3mw(v)}{2}}\frac{\mathrm{d}q_0}{(2\pi)}\left[\frac{1}{q_0+|X+1|}\right]\frac{(m+2iX)}{4X^2+m^2}. \tag{Q.106}$$

Integrating over X and then over q_0 yields, to the leading order in $m \ll 1$, the finite contribution

$$\mathcal{P}_{18}(k_x,p_x;\mu) = -\frac{w(v)}{8\pi}m = -\frac{w(v)}{8\pi}\frac{\mu}{|\Delta_r|}, \tag{Q.107}$$

where in the last equality we have used the fact that the same result is obtained in the case that $\Delta_r < 0$.

(*iii*) For $|\Delta_t| \gg \mu$ and $|\Delta_t| \gg |\Delta_r|$, we assume, without loss of generality, that $\Delta_t > 0$ and we perform the scaling $(q_0, X, Y) \to \Delta_t(q_0, X/c(v), Y)$ in Eq. (Q.100). Defining $m = \mu/\Delta_t$ and $\delta = \Delta_r/\Delta_t$ the latter assumes the form

$$\mathcal{P}_{18}(k_x,p_x;\mu) = w(v)\int\limits_{\mathbb{R}}\frac{\mathrm{d}q_0}{(2\pi)}\int\limits_{\mathbb{R}}\frac{\mathrm{d}X}{(2\pi)}\int\limits_{\mathbb{R}}\frac{\mathrm{d}Y}{(2\pi)}\left[\frac{1}{-i\left(\frac{m}{2}+q_0\right)+2w(v)X-Y}\right] \times\left[\frac{1}{i\left(\frac{3m}{2}+q_0\right)+Y}\right]\left[\frac{1}{|q_0|+(|X+w(v)^{-1}\delta|+|c(v)Y-w(v)^{-1}|)}\right]. \tag{Q.108}$$

We are interested in the $m \ll 1$ and $\delta \ll 1$ limits. We can set $\delta = 0$ inside the integration with no harm, but one needs to keep $m \neq 0$ in order to avoid spurious IR divergences. The integration over Y proceeds as before by ignoring the term of order $c(v)Y$ in the $v \ll 1$ limit. This integration results in

$$\mathcal{P}_{18}(k_x,p_x;\mu) = -2mw(v)\int\limits_{\frac{m}{2}}^{\frac{3m}{2}}\frac{\mathrm{d}q_0}{(2\pi)}\int\limits_{\mathbb{R}^+}\frac{\mathrm{d}X}{(2\pi)}\left[\frac{1}{q_0+X+w(v)^{-1}}\right]\frac{1}{m^2+4w(v)^2X^2}, \tag{Q.109}$$

where we have further symmetrized the resulting integrand in X. The integration over X and q_0 can be done in the small m and $w(v)$ limits, yielding the leading order finite contribution:

$$\mathcal{P}_{18}(k_x, p_x; \mu) = -\frac{w(v)}{8\pi}\frac{\mu}{|\Delta_t|}, \tag{Q.110}$$

where in the last equality we have used the fact that the same result is obtained in the case that $\Delta_t < 0$.

Collecting the results from Eqs. (Q.103), (Q.107) and (Q.110), using the definitions $\Delta_r = v(p_x - k_x)$ and $\Delta_t = v^2(p_x + k_x)$, and bringing back the constraint on the external momentum we can write

$$\mathcal{P}_{18}(k_x, p_x; \mu) = -\frac{1}{2\pi^2}\Theta(\Lambda_b - |p_x - k_x|)\frac{w(v)}{\mathscr{F}_{18}(\mu, v|k_x - p_x|, v^2|p_x + k_x|)}, \tag{Q.111}$$

where the crossover function is given by

$$\mathscr{F}_{18}(x, y, z)^{-1} = \begin{cases} \log\left(\frac{1}{w(v)}\right) & x \gg y, \quad \& \quad x \gg z, \\ \frac{\pi x}{4y} & y \gg x, \quad \& \quad y \gg z, \\ \frac{\pi x}{4z} & z \gg x, \quad \& \quad z \gg y. \end{cases} \tag{Q.112}$$

Q.2-(*b*) The $\mathcal{R}_{MN}$ integrals

We now consider the integrations defined in Eq. (Q.6). To simplify the discussion, we compute these directly at the RG condition given in Eq. (4.57). That is, we evaluate the integration at external momentum on the local FS of hot spots M and N and at frequencies $k_0 = 3\mu/2$, $p_0 = -\mu/2$ and $l_0 = -\mu$, with $\mu > 0$. The RG condition in Eq. (4.57) imposes an extra constraint on the external momentum due to the fact that in Eq. (Q.2), the corrections to the quantum effective action involving the $\mathcal{R}_{MN}$ integrals survive only if $N_3 = M$ and $N_4 = N$ or $N_3 = N$ and $N_4 = M$. The RG condition therefore requires that

$$e_M(\vec{k}; v) = e_N(\vec{p}; v) = e_M(\vec{k} + \vec{l}; v) = e_N(\vec{p} - \vec{l}; v) = 0. \tag{Q.113}$$

This implies that $e_N(\vec{l}) = -e_M(\vec{l}) = 0$. Thus, if $M \neq N$ and $M \neq [N+4]_8$, the RG condition fixes $\vec{l} = \vec{0}$. In the case where the hot spots M and N are the same or antipodal to each other, there is no further constraint on the momentum $\vec{l}$. We shall use this fact to simplify the following computations. Finally, we note that Eq. (Q.6) is finite by power counting and therefore we set all UV cutoffs to arbitrary large values. However, these cutoff scales are responsible for constraining the range of the external momentum in which the quantum corrections have nonzero support.

A. $\mathcal{R}_{11}(k, p, l)$

For $M = 1$ and $N = 1$, the integration in Eq. (Q.6) evaluated at the RG condition reads

$$\mathcal{R}_{11}(k_x, p_x, l_x; \mu) = \mu v^2 \int \mathrm{d}q \left[\frac{1}{|q_0| + c(v)(|q_x| + |q_y|)}\right]\left[\frac{1}{|q_0 + \mu| + c(v)(|l_x - q_x| + |v l_x + q_y|)}\right]$$

$$\times \left[\frac{1}{i\left(q_0+\frac{3\mu}{2}\right)+vq_x-q_y+2vk_x}\right]\left[\frac{1}{-i\left(q_0+\frac{\mu}{2}\right)-vq_x+q_y+2vp_x}\right]. \quad \text{(Q.114)}$$

From the discussion in Sec. 4.2-(*a*) , the integration over $\vec{q}$ is done over the momentum region determined by the conditions

$$\begin{gathered}|vq_x-q_y+2vk_x|<\Lambda_f, \quad |vq_x-q_y-2vp_y|<\Lambda_f, \qquad |q_x|<\Lambda_b,\\ |q_x-l_x|<\Lambda_b, \quad |q_y|<\Lambda_b, \quad \& \quad |q_y+vl_x|<\Lambda_b.\end{gathered} \quad \text{(Q.115)}$$

Although the integration in Eq. (Q.114) is finite by power counting, if the external momentum is too large, then the integration over q_x and q_y loose support. To analyze the regime of external momentum in which the integration has nonzero support, it is convenient to perform the shift $q_y \to q_y + vq_x + v(k_x - p_x)$ under which the domain of integration takes the form

$$\begin{gathered}|q_y-v(k_x+p_x)|<\Lambda_f, \quad |q_y+v(k_x+p_x)|<\Lambda_f, \quad |q_x|<\Lambda_b, \quad |q_x-l_x|<\Lambda_b,\\ |q_y+vq_x+v(k_x-p_x)|<\Lambda_b, \quad |q_y+vq_x+v(k_x-p_x+l_x)|<\Lambda_b.\end{gathered} \quad \text{(Q.116)}$$

Apart from the constraint on the momenta offered by the discussion in Sec. 4.4-(*a*) , the only constraints arising from this analysis correspond to $|k_x + p_x| \ll \Lambda_f/v$ and $|l_x| \ll \Lambda_b$ in order for the integrations to have nonzero support in the $\Lambda_f \ll c(v)\Lambda_b \ll \Lambda_b$ limit. Having this extra constraint implicit in the following discussion, we proceed by writing Eq. (Q.114) after the shift in the momentum:

$$\begin{aligned}\mathcal{R}_{11}(k_x,p_x,l_x;\mu) = \mu v^2 \int \mathrm{d}q \ &\left[\frac{1}{i\left(q_0+\frac{3\mu}{2}\right)-q_y+\frac{\Delta_1}{2}}\right]\left[\frac{1}{-i\left(q_0+\frac{\mu}{2}\right)+q_y+\frac{\Delta_1}{2}}\right]\\ \times &\left[\frac{1}{|q_0|+c(v)|q_x|+|c(v)q_y+\Delta_2|}\right]\left[\frac{1}{|q_0+\mu|+|\Delta_4-c(v)q_x|+|c(v)q_y+\Delta_3|)}\right].\end{aligned} \quad \text{(Q.117)}$$

where we have defined the momentum scales $\Delta_1 = 2v(k_x + p_x)$, $\Delta_2 = c(v)v(k_x - p_x)$, $\Delta_3 = vc(v)(k_x - p_x + l_x)$ and $\Delta_4 = c(v)l_x$. In this expression we have neglected the terms of order $v(c)q_x$ in the bosonic propagators. The integration over q_y is convergent in the absence of the terms of order $c(v)q_y$. Therefore, in the small v limit, this integration yields

$$\begin{aligned}\mathcal{R}_{11}(k_x,p_x,l_x;\mu) = -\frac{v^2}{c(v)}\frac{\mu}{\mu-i\Delta_1}\int_{-\frac{3\mu}{2}}^{-\frac{\mu}{2}}\frac{\mathrm{d}q_0}{(2\pi)}\int\frac{\mathrm{d}q_x}{(2\pi)}&\left[\frac{1}{|q_0|+|q_x|+|\Delta_2|}\right]\\ \times &\left[\frac{1}{|q_0+\mu|+|\Delta_4-q_x|+|\Delta_3|}\right],\end{aligned} \quad \text{(Q.118)}$$

where we have further performed the scaling $q_x \to q_x/c(v)$. In what follows we analyze this expression in the limit in which (*i*) $\mu \gg |\Delta_i|$ for $i = 1, 2, 3, 4$, (*ii*) $|\Delta_1| \gg \mu$ and $|\Delta_1| \gg |\Delta_i|$ for $i = 2, 3, 4$, (*iii*) $|\Delta_2| \gg \mu$ and $|\Delta_2| \gg |\Delta_i|$ for $i = 1, 3, 4$, (*iv*) $|\Delta_3| \gg \mu$ and $|\Delta_3| \gg |\Delta_i|$ for $i = 1, 2, 4$, and (*v*) $|\Delta_4| \gg \mu$ and $|\Delta_4| \gg |\Delta_i|$ for $i = 1, 2, 3$.

(*i*) For $\mu \gg |\Delta_i|$ with $i = 1,2,3,4$ we perform the scaling $(q_0, q_x) \to \mu(q_0, q_x)$ and take the $|\Delta_i|/\mu \ll 1$ limits for $i = 1,2,3,4$. This allows us to write Eq. (Q.118) as

$$\mathcal{R}_{11}(k_x, p_x, l_x; \mu) = -\frac{v^2}{c(v)} \int_{-\frac{3}{2}}^{-\frac{1}{2}} \frac{\mathrm{d}q_0}{(2\pi)} \int_{\mathbb{R}} \frac{\mathrm{d}q_x}{(2\pi)} \left[\frac{1}{|q_0| + q_x}\right] \left[\frac{1}{|q_0+1| + |q_x|}\right]. \tag{Q.119}$$

The integration over q_x is straightforward, and a further integration over q_0 yields the finite contribution

$$\mathcal{R}_{11}(k_x, p_x, l_x; \mu) = -\frac{v^2}{16\pi^2 c(v)} \left[\pi^2 + 4\log\left(\frac{27}{4}\right)\right]. \tag{Q.120}$$

(*ii*) For $|\Delta_1| \gg |\Delta_i|$ with $i = 2,3,4$ and $|\Delta_1| \gg \mu$ we note that Δ_1 appears in the overall multiplicative factor in Eq. (Q.118). Therefore, this scale will not be responsible for cutting off the integration in the IR completely. After the rescaling $(q_0, q_x) \to \Delta_1(q_0, q_x)$, Eq. (Q.118) can be written as

$$\begin{aligned}\mathcal{R}_{11}(k_x, p_x, l_x; \mu) = -\frac{\mu v^2}{c(v)\Delta_1} \frac{1}{m-i} \int_{-\frac{3m}{2}}^{-\frac{m}{2}} \frac{\mathrm{d}q_0}{(2\pi)} \int \frac{\mathrm{d}q_x}{(2\pi)} \left[\frac{1}{|q_0| + |q_x| + |\delta_2|}\right] \\ \times \left[\frac{1}{|q_0+m| + |\delta_4 - q_x| + |\delta_3|}\right],\end{aligned} \tag{Q.121}$$

where $m = \mu/\Delta_1$ and $\delta_i = \Delta_i/\Delta_1$ for $i = 2,3,4$. The IR structure of the integral will depend in the relative magnitude of the of these four scales. We therefore consider the limits in which (*a*) $|m| \gg |\delta_i|$, for $i = 2,3,4$, (*b*) $|\delta_2| \gg |m|$ and $|\delta_2| \gg |\delta_i|$ for $i = 3,4$, (*c*) $|\delta_3| \gg |m|$ and $|\delta_3| \gg |\delta_i|$ for $i = 2,4$, and (*d*) $|\delta_4| \gg |m|$ and $|\delta_4| \gg |\delta_i|$ for $i = 2,3$.

(*a*) For $|m| \gg |\delta_i|$ with $i = 2,3,4$ we can proceed by scaling out m out of the integral through the transformation $(q_0, q_x) \to m(q_0, q_x)$ and then proceed on taking the $|\delta_i|/m \ll 1$ limit. This allows us to write Eq. (Q.121) as

$$\mathcal{R}_{11}(k_x, p_x, l_x; \mu) = -\frac{v^2}{c(v)\Delta_1} \frac{\mu}{m-i} \int_{-\frac{3}{2}}^{-\frac{1}{2}} \frac{\mathrm{d}q_0}{(2\pi)} \int \frac{\mathrm{d}q_x}{(2\pi)} \left[\frac{1}{|q_0| + |q_x|}\right] \left[\frac{1}{|q_0+1| + |q_x|}\right]. \tag{Q.122}$$

Integration over q_x and q_0 is straightforward, yielding, in the $|m| \ll 1$ limit,

$$\mathcal{R}_{11}(k_x, p_x, l_x; \mu) = -\frac{iv^2}{16\pi^2 c(v)} \frac{\mu}{\Delta_1} \left[\pi^2 + 4\log\left(\frac{27}{4}\right)\right]. \tag{Q.123}$$

(*b*) For $|\delta_2| \gg |m|$ and $|\delta_2| \gg |\delta_i|$ with $i = 3,4$ we consider the scaling $(q_0, q_x) \to |\delta_2|(q_0, q_x)$ and take the $|m|/|\delta_2| \ll 1$ and $|\delta_i|/|\delta_2| \ll 1$ limits. This allows us to write Eq. (Q.121) as

$$\mathcal{R}_{11}(k_x, p_x, l_x; \mu) = -\frac{v^2}{c(v)\Delta_1} \frac{\mu}{m-i} \int_{-\frac{3\overline{m}}{2}}^{-\frac{\overline{m}}{2}} \frac{\mathrm{d}q_0}{(2\pi)} \int \frac{\mathrm{d}q_x}{(2\pi)} \left[\frac{1}{|q_0| + |q_x| + 1}\right] \left[\frac{1}{|q_0| + |q_x|}\right], \tag{Q.124}$$

where $\overline{m} = m/|\delta_2| = \mu/|\Delta_2| \ll 1$. We note that setting $\overline{m} = 0$ makes the integration vanish and therefore we have kept it nonzero to capture the leading order nonvanishing contribution from this expression. Integration over q_x yields

$$\mathcal{R}_{11}(k_x, p_x, l_x; \mu) = -\frac{v^2}{\pi c(v)\Delta_1}\frac{\mu}{m-i}\int\limits_{-\frac{3\overline{m}}{2}}^{-\frac{\overline{m}}{2}}\frac{\mathrm{d}q_0}{(2\pi)}\log\left(1+\frac{1}{|q_0|}\right). \tag{Q.125}$$

The integration over q_0 is straightforward and yields, in the $|m| \ll 1$ and $|\overline{m}| \ll 1$ limits

$$\mathcal{R}_{11}(k_x, p_x, l_x; \mu) = \frac{i\mu^2}{2\pi^2 c(v)\Delta_1|\Delta_2|}\log\left(\frac{\mu}{|\Delta_2|}\right), \tag{Q.126}$$

where we have neglected order one numbers with respect to the logarithmic IR divergence.

(*c*) For $|\delta_3| \gg |m|$ and $|\delta_3| \gg |\delta_i|$ with $i = 2, 4$ we consider the scaling $(q_0, q_x) \to |\delta_3|(q_0, q_x)$ and take the $|m|/|\delta_3| \ll 1$ and $|\delta_i|/|\delta_3| \ll 1$ limits. This allows us to write Eq. (Q.121) as

$$\mathcal{R}_{11}(k_x, p_x, l_x; \mu) = -\frac{\mu v^2}{c(v)\Delta_1}\frac{1}{m-i}\int\limits_{-\frac{3\overline{m}}{2}}^{-\frac{\overline{m}}{2}}\frac{\mathrm{d}q_0}{(2\pi)}\int\frac{\mathrm{d}q_x}{(2\pi)}\left[\frac{1}{|q_0|+|q_x|}\right]\left[\frac{1}{|q_0|+|q_x|+1}\right], \tag{Q.127}$$

where $\overline{m} = m/|\delta_3| = \mu/|\Delta_3|$. This is the same integration we performed in the previous case. Therefore we immediately conclude that, in the limit under consideration,

$$\mathcal{R}_{11}(k_x, p_x, l_x; \mu) = \frac{i\mu^2}{2\pi^2 c(v)\Delta_1|\Delta_3|}\log\left(\frac{\mu}{|\Delta_3|}\right). \tag{Q.128}$$

(*d*) For $|\delta_4| \gg |m|$ and $|\delta_4| \gg |\delta_i|$ with $i = 2, 3$ we assume, without loss of generality, that $\delta_4 > 0$ and consider the scaling $(q_0, q_x) \to \delta_4(q_0, q_x)$ and take the $|m|/|\delta_4| \ll 1$ and $|\delta_i|/|\delta_4| \ll 1$ limits. This allows us to write Eq. (Q.121) as

$$\mathcal{R}_{11}(k_x, p_x, l_x; \mu) = -\frac{\mu v^2}{c(v)\Delta_1}\frac{1}{m-i}\int\limits_{-\frac{3\overline{m}}{2}}^{-\frac{\overline{m}}{2}}\frac{\mathrm{d}q_0}{(2\pi)}\int\frac{\mathrm{d}q_x}{(2\pi)}\left[\frac{1}{|q_0|+|q_x|}\right]\left[\frac{1}{|q_0|+|1-q_x|}\right], \tag{Q.129}$$

where $\overline{m} = m/\delta_4 = \mu/\Delta_4 \ll 1$. Integration over q_0, followed by the integration over q_x yields, in the $|m| \ll 1$ and $|\overline{m}| \ll 1$ limits

$$\mathcal{R}_{11}(k_x, p_x, l_x; \mu) = \frac{i\mu^2}{\pi^2 c(v)\Delta_1|\Delta_4|}\log\left(\frac{\mu}{|\Delta_4|}\right). \tag{Q.130}$$

In here we have restored the absolute value in the scale Δ_4 since we obtain the same result for the $\delta_4 < 0$ case.

(*iii*) For $|\Delta_2| \gg |\Delta_i|$ with $i = 1, 3, 4$ and $|\Delta_2| \gg \mu$ we perform the scaling $(q_0, q_x) \to |\Delta_2|(q_0, q_x)$ in Eq. (Q.118) and proceed by taking the $|\Delta_i|/|\Delta_2| \ll 1$ and $\mu/|\Delta_2| \ll 1$ limits. This allows us to write

$$\mathcal{R}_{11}(k_x, p_x, l_x; \mu) = -\frac{v^2}{c(v)} \frac{\mu}{\mu - i\Delta_1} \int_{-\frac{3m}{2}}^{-\frac{m}{2}} \frac{\mathrm{d}q_0}{(2\pi)} \int \frac{\mathrm{d}q_x}{(2\pi)} \left[\frac{1}{|q_0| + |q_x| + 1}\right] \left[\frac{1}{|q_0| + |q_x|}\right], \tag{Q.131}$$

where $m = \mu/|\Delta_2| \ll 1$. Here we cannot set $m = 0$ in the integration limits because this makes the integration vanish. We have already computed this integration, and thus we readily obtain in the $m \ll 1$ limit:

$$\mathcal{R}_{11}(k_x, p_x, l_x; \mu) = \frac{v^2}{2\pi^2 c(v)|\Delta_2|} \frac{\mu^2}{\mu - i\Delta_1} \log\left(\frac{\mu}{|\Delta_2|}\right). \tag{Q.132}$$

We can further approximate this expression in the $\mu \gg |\Delta_1|$ and $\mu \ll |\Delta_1|$ limits as

$$\mathcal{R}_{11}(k_x, p_x, l_x; \mu) \overset{\mu \gg |\Delta_1|}{=} \frac{v^2 \mu}{2\pi^2 c(v)|\Delta_2|} \log\left(\frac{\mu}{|\Delta_2|}\right), \tag{Q.133}$$

$$\mathcal{R}_{11}(k_x, p_x, l_x; \mu) \overset{\mu \ll |\Delta_1|}{=} \frac{i\mu^2 v^2}{2\pi^2 c(v)\Delta_1|\Delta_2|} \log\left(\frac{\mu}{|\Delta_2|}\right). \tag{Q.134}$$

(*iv*) For $|\Delta_3| \gg |\Delta_i|$ with $i = 1, 2, 4$ and $|\Delta_3| \gg \mu$ we perform the scaling $(q_0, q_x) \to |\Delta_3|(q_0, q_x)$ in Eq. (Q.118) and take the $|\Delta_i|/|\Delta_3| \ll 1$ and $\mu/|\Delta_3| \ll 1$ limits. This renders the same integration we computed in the previous case. It follows immediately that,

$$\mathcal{R}_{11}(k_x, p_x, l_x; \mu) \overset{\mu \gg |\Delta_1|}{=} \frac{v^2 \mu}{2\pi^2 c(v)|\Delta_3|} \log\left(\frac{\mu}{|\Delta_3|}\right), \tag{Q.135}$$

$$\mathcal{R}_{11}(k_x, p_x, l_x; \mu) \overset{\mu \ll |\Delta_1|}{=} \frac{i\mu^2 v^2}{2\pi^2 c(v)\Delta_1|\Delta_3|} \log\left(\frac{\mu}{|\Delta_3|}\right). \tag{Q.136}$$

(*v*) For $|\Delta_4| \gg |\Delta_i|$ with $i = 1, 2, 3$ and $|\Delta_4| \gg \mu$ we assume without loss of generality that $\Delta_4 > 0$ and scale it out from the integration in Eq. (Q.118) through the transformation $(q_0, q_x) \to \Delta_4(q_0, q_x)$. In the $|\Delta_i|/\Delta_4 \ll 1$ and $\mu/\Delta_4 \ll 1$ limits we write Eq. (Q.118) as

$$\mathcal{R}_{11}(k_x, p_x, l_x; \mu) = -\frac{\mu v^2}{c(v)} \frac{1}{\mu - i\Delta_1} \int_{-\frac{3m}{2}}^{-\frac{m}{2}} \frac{\mathrm{d}q_0}{(2\pi)} \int \frac{\mathrm{d}q_x}{(2\pi)} \left[\frac{1}{|q_0| + |q_x|}\right] \left[\frac{1}{|q_0| + |1 - q_x|}\right], \tag{Q.137}$$

where $m = \mu/\Delta_4 \ll 1$. We have already performed this integration, and thus we obtain

$$\mathcal{R}_{11}(k_x, p_x, l_x; \mu) = \frac{\mu^2 v^2}{\pi^2 c(v)|\Delta_4|} \frac{1}{\mu - i\Delta_1} \log\left(\frac{\mu}{|\Delta_4|}\right), \tag{Q.138}$$

where the absolute value comes from the fact that we obtain the same result in the case where $\Delta_4 < 0$. Once again, we can further approximate this expression depending on the relative magnitude between μ and Δ_1. We therefore write

$$\mathcal{R}_{11}(k_x, p_x, l_x; \mu) \overset{\mu \gg |\Delta_1|}{=} \frac{\mu v^2}{\pi^2 c(v) |\Delta_4|} \log\left(\frac{\mu}{|\Delta_4|}\right), \tag{Q.139}$$

$$\mathcal{R}_{11}(k_x, p_x, l_x; \mu) \overset{\mu \ll |\Delta_1|}{=} \frac{i\mu^2 v^2}{\pi^2 c(v) \Delta_1 |\Delta_4|} \log\left(\frac{\mu}{|\Delta_4|}\right). \tag{Q.140}$$

Collecting the results from Eqs. (Q.120), (Q.123), (Q.126), (Q.128), (Q.130), (Q.133), (Q.134), (Q.135), (Q.136), (Q.139) and (Q.140), and bringing back the constraint on the external momentum, we can write Eq. (Q.114) as

$$\begin{aligned}\mathcal{R}_{11}(k_x, p_x, l_x; \mu) = &\frac{v^2 \Theta\left(\Lambda_f - v|p_x + k_x|\right) \Theta(\Lambda_b - |l_x|)}{4\pi^2 c(v)} \\ &\times \frac{\mathcal{U}_{11}[\mu, 2v(k_x + p_x), vc(v)(k_x - p_x), vc(v)(k_x - p_x + l_x), c(v) l_x]}{\mathcal{R}_{11}[\mu, 2v(k_x + p_x), vc(v)(k_x - p_x), vc(v)(k_x - p_x + l_x), c(v) l_x]},\end{aligned} \tag{Q.141}$$

where the crossover function $\mathcal{R}_{11}(x, y, z, v, w)$ is given by

$$\mathcal{R}_{11}(x, y, z, v, w) = \begin{cases} |x|, & |x| \gg |y|, |z|, |v|, |w|, \\ y, & |y| \gg |x|, |z|, |v|, |w|, \\ |z|, & |z| \gg |y|, |x|, |v|, |w|, \\ |v|, & |v| \gg |y|, |z|, |x|, |w|, \\ |w|, & |w| \gg |y|, |z|, |v|, |x|. \end{cases} \tag{Q.142}$$

$\mathcal{R}_{11}(x, y, z, v, w) \approx \max(x, y, z, v, w)$ and the crossover function $\mathcal{U}_{11}(x, y, z, u, w)$ is given by

$$\mathcal{U}_{11}(x, y, z, u, w) = \begin{cases} -|x| \left[\frac{\pi^2}{4} + \log\left(\frac{27}{4}\right)\right], & |x| \gg |y|, |z|, |u|, |w|, \\ -i|x| \left[\frac{\pi^2}{4} + \log\left(\frac{27}{4}\right)\right], & |y| \gg |x|, |z|, |u|, |w| \quad \& \quad |x| \gg |z|, |w|, |u|, \\ \frac{2ix^2}{|z|} \log\left(\frac{|x|}{|z|}\right), & |y| \gg |x|, |z|, |u|, |w| \quad \& \quad |z| \gg |x|, |u|, |w|, \\ \frac{2ix^2}{|u|} \log\left(\frac{x}{u}\right), & |y| \gg |x|, |z|, |u|, |w| \quad \& \quad |u| \gg |x|, |z|, |w|, \\ \frac{4ix^2}{|w|} \log\left(\frac{x}{w}\right), & |y| \gg |x|, |z|, |u|, |w| \quad \& \quad |w| \gg |x|, |z|, |u|, \\ 2|x| \log\left(\frac{|x|}{|z|}\right), & |z| \gg |x|, |y|, |u|, |w| \quad \& \quad |x| \gg |y|, \\ \frac{2ix^2}{y} \log\left(\frac{x}{z}\right), & |z| \gg |x|, |y|, |u|, |w| \quad \& \quad |y| \gg |x|, \\ 2|x| \log\left(\frac{|x|}{|u|}\right), & |u| \gg |x|, |y|, |z|, |w| \quad \& \quad |x| \gg |y|, \\ \frac{2ix^2}{y} \log\left(\frac{|x|}{|u|}\right), & |u| \gg |x|, |y|, |z|, |w| \quad \& \quad |y| \gg |x|, \\ 4|x| \log\left(\frac{|x|}{|w|}\right), & |w| \gg |x|, |y|, |u|, |z| \quad \& \quad |x| \gg |y|, \\ \frac{4ix^2}{y} \log\left(\frac{|x|}{|w|}\right), & |w| \gg |x|, |y|, |u|, |z| \quad \& \quad |y| \gg |x|. \end{cases} \tag{Q.143}$$

B. $\mathcal{R}_{12}(k,p,l)$

For $M=1$ and $N=2$, the integration in Eq. (Q.6) evaluated at the RG condition reads:

$$\mathcal{R}_{12}(k_x,p_y;\mu)=\mu v^2\int \mathrm{d}q\left[\frac{1}{|q_0|+c(v)(|q_x|+|q_y|)}\right]\left[\frac{1}{|q_0+\mu|+c(v)(|q_x|+|q_y|)}\right]$$
$$\times\left[\frac{1}{i\left(q_0+\frac{3\mu}{2}\right)+vq_x-q_y+2vk_x}\right]\left[\frac{1}{-i\left(q_0+\frac{\mu}{2}\right)+q_x-vq_y+2vp_y}\right]. \tag{Q.144}$$

We note that the structure of the integration is similar to that of Eq. (Q.27). In particular, the momentum integration is done over the same region defined by Eq. (Q.28). Furthermore, the external momentum receives no further constraint than the one discussed in Sec. 4.4-(*a*) . Setting all cutoffs to arbitrary large values, we proceed on integrating by performing the change of variables

$$X=q_x-vq_y+2vp_y,\qquad \&\qquad Y=vq_x-q_y+2vk_x, \tag{Q.145}$$

which renders Eq. (Q.144) as

$$\mathcal{R}_{12}(k_x,p_y;\mu)=\mu v^2\int_{\mathbb{R}}\frac{\mathrm{d}q_0}{(2\pi)}\int_{\mathbb{R}}\frac{\mathrm{d}X}{(2\pi)}\int_{\mathbb{R}}\frac{\mathrm{d}Y}{(2\pi)}\left[\frac{1}{|q_0|+|c(v)X+\Delta_1|+|c(v)Y+\Delta_2|}\right]$$
$$\times\left[\frac{1}{|q_0+\mu|+|c(v)X+\Delta_1|+|c(v)Y+\Delta_2|}\right]\left[\frac{1}{i\left(q_0+\frac{3\mu}{2}\right)+Y}\right]\left[\frac{1}{-i\left(q_0+\frac{\mu}{2}\right)+X}\right]. \tag{Q.146}$$

to the leading order in v. Similarly as we did in the treatment of Eq. (Q.27) we have neglected the terms of order $vc(v)Y$ and $vc(v)X$ in the boson propagator because these do not alter the convergence of the integral. We have further defined $\Delta_1=2vc(v)(vk_x-p_y)$ and $\Delta_2=2vc(v)(vp_y-k_x)$. We analyze this expression in the following limits: (*i*) $\mu\gg|\Delta_1|$ and $\mu\gg|\Delta_2|$, (*ii*) $|\Delta_1|\gg\mu$ and $|\Delta_1|\gg|\Delta_2|$, and (*iii*) $|\Delta_2|\gg\mu$ and $|\Delta_2|\gg|\Delta_1|$.

(*i*) For $\mu\gg|\Delta_1|$ and $\mu\gg|\Delta_2|$ we perform the scaling $(q_0,X,Y)\to\mu(q_0,X,Y)$ and take the $|\Delta_1|/\mu\ll 1$ and $|\Delta_2|/\mu\ll 1$ limits in Eq. (Q.146). This yields:

$$\mathcal{R}_{12}(k_x,p_y;\mu)=v^2\int_{\mathbb{R}}\frac{\mathrm{d}q_0}{(2\pi)}\int_{\mathbb{R}}\frac{\mathrm{d}X}{(2\pi)}\int_{\mathbb{R}}\frac{\mathrm{d}Y}{(2\pi)}\left[\frac{1}{|q_0|+c(v)|X|+c(v)|Y|}\right]$$
$$\times\left[\frac{1}{|q_0+1|+c(v)|X|+c(v)|Y|}\right]\left[\frac{1}{i\left(q_0+\frac{3}{2}\right)+Y}\right]\left[\frac{1}{-i\left(q_0+\frac{1}{2}\right)+X}\right]. \tag{Q.147}$$

For convenience we consider the shift $q_0\to q_0-1/2$ and write

$$\mathcal{R}_{12}(k_x,p_y;\mu)=v^2\int_{\mathbb{R}}\frac{\mathrm{d}q_0}{(2\pi)}\int_{\mathbb{R}}\frac{\mathrm{d}X}{(2\pi)}\int_{\mathbb{R}}\frac{\mathrm{d}Y}{(2\pi)}\left[\frac{1}{|q_0-1/2|+c(v)|X|+c(v)|Y|}\right]$$
$$\times\left[\frac{1}{|q_0+1/2|+c(v)|X|+c(v)|Y|}\right]\left[\frac{1}{i\left(q_0+1\right)+Y}\right]\left[\frac{1}{-iq_0+X}\right]. \tag{Q.148}$$

The integration over Y and X can be done in the small v limit by neglecting the terms of order $c(v)|Y|$ and $c(v)|X|$ inside the boson propagator. As we show by explicit computation, doing this introduces no IR divergences in the q_0 integration. After integrating over X and Y we obtain to leading order in $v \ll 1$:

$$\mathcal{R}_{12}(k_x, p_y; \mu) = \frac{1}{4} v^2 \int_{\mathbb{R}} \frac{\mathrm{d}q_0}{(2\pi)} \frac{\mathrm{sgn}\,(1+q_0)\,\mathrm{sign}(q_0)}{\left|q_0^2 - \frac{1}{4}\right|}. \tag{Q.149}$$

Although the integration seems to be divergent at $q_0 = 1/2$ this is not the case. This can be seen by symmetrizing in q_0, where it becomes clear that the integration is nonzero only for $q_0 > 1$. Integration over q_0 yields

$$\mathcal{R}_{12}(k_x, p_y; \mu) = \frac{v^2}{4\pi} \log(3). \tag{Q.150}$$

(*ii*) For $|\Delta_1| \gg \mu$ and $|\Delta_1| \gg |\Delta_2|$, we consider, without loss of generality the case in which $\Delta_1 > 0$ and perform the scaling $(q_0, X, Y) \to \Delta_1(q_0, X, Y)$ in Eq. (Q.146). In the small μ/Δ_1 and $|\Delta_2|/\Delta_1$ limits, Eq. (Q.146) takes the form

$$\begin{aligned}\mathcal{R}_{12}(k_x, p_y; \mu) = \frac{\mu}{\Delta_1} v^2 \int_{\mathbb{R}} \frac{\mathrm{d}q_0}{(2\pi)} \int_{\mathbb{R}} \frac{\mathrm{d}X}{(2\pi)} \int_{\mathbb{R}} \frac{\mathrm{d}Y}{(2\pi)} \left[\frac{1}{|q_0| + |c(v)X + 1| + c(v)|Y|}\right]^2 \\ \times \left[\frac{1}{iq_0 + Y}\right] \left[\frac{1}{-iq_0 + X}\right].\end{aligned} \tag{Q.151}$$

The integrations over X and Y are straightforward in the small v limit because setting $c(v)X$ and $c(v)Y$ inside the integrand is legitimate. After integrating over these two variables we obtain

$$\mathcal{R}_{12}(k_x, p_y; \mu) = \frac{1}{4} \frac{\mu}{\Delta_1} v^2 \int_{\mathbb{R}} \frac{\mathrm{d}q_0}{(2\pi)} \frac{1}{(|q_0| + 1)^2}. \tag{Q.152}$$

The final integration yields

$$\mathcal{R}_{12}(k_x, p_y; \mu) = \frac{v^2}{4\pi} \frac{\mu}{|\Delta_1|}. \tag{Q.153}$$

In here the absolute value comes from the fact that we obtain the same result in the $\Delta_1 < 0$ case.

(*iii*) For $|\Delta_2| \gg \mu$ and $|\Delta_2| \gg |\Delta_1|$ we consider the transformation $(q_0, X, Y) \to \Delta_2(q_0, X, Y)$ with either $\Delta_2 > 0$ or $\Delta_2 < 0$. After such a transformation and in the $|\Delta_1|/|\Delta_2| \ll 1$ and $\mu/|\Delta_2| \ll 1$ limits, Eq. (Q.146) takes the same form as in Eq. (Q.151), but with Δ_1 being replaced by Δ_2. It therefore follows that

$$\mathcal{R}_{12}(k_x, p_y; \mu) = \frac{v^2}{4\pi} \frac{\mu}{|\Delta_2|}. \tag{Q.154}$$

Collecting the results from Eqs. (Q.150), (Q.153) and (Q.154), and using the definitions $\Delta_1 = 2vc(v)(vk_x - p_y)$ and $\Delta_2 = 2vc(v)(vp_y - k_x)$ we can write Eq. (Q.144) as

$$\mathcal{R}_{12}(k_x, p_y; \mu) = \frac{v^2}{4\pi} \frac{\mathcal{U}_{12}[\mu, 2vc(v)|vk_x - p_y|, 2vc(v)|vp_y - k_x|]}{\mathcal{R}_{12}[\mu, 2vc(v)|vk_x - p_y|, 2vc(v)|vp_y - k_x|]}, \tag{Q.155}$$

where $\mathcal{R}_{12}(x, y, z) \approx \max(x, y, z)$ and the crossover function $\mathcal{U}_{12}(x, y, z)$ is given by

$$\mathcal{U}_{12}(x, y, z) = \begin{cases} \log(3), & x \gg y, z, \\ x, & y \gg x, z \quad \& \quad z \gg x, y. \end{cases} \tag{Q.156}$$

C. $\mathcal{R}_{13}(k, p, l)$

For $M = 1$ and $N = 3$, the integration in Eq. (Q.6) evaluated at the RG condition reads:

$$\begin{aligned} \mathcal{R}_{13}(k_x, p_y; \mu) = \mu v^2 \int \mathrm{d}q \left[\frac{1}{|q_0| + c(v)(|q_x| + |q_y|)}\right] \left[\frac{1}{|q_0 + \mu| + c(v)(|q_x| + |q_y|)}\right] \\ \times \left[\frac{1}{i\left(q_0 + \frac{3\mu}{2}\right) + vq_x - q_y + 2vk_x}\right] \left[\frac{1}{-i\left(q_0 + \frac{\mu}{2}\right) - q_x - vq_y + 2vp_y}\right]. \end{aligned} \tag{Q.157}$$

The integration over the loop momenta follows the same logic as the one used in the computation of Eq. (Q.42). In particular, this implies that the external momentum has no further constraints than the one discussed in Sec. 4.4-(*a*) . Because the integration is finite by power counting we set all cutoff scales to arbitrary large values and proceed on integrating by first performing the change of variables

$$Y = vq_x - q_y + 2vk_x, \qquad \& \qquad X = -q_x - vq_y + 2vp_y. \tag{Q.158}$$

Under this change of variables, Eq. (Q.157) takes the following form:

$$\begin{aligned} \mathcal{R}_{13}(k_x, p_y; \mu) = \mu v^2 \int_{\mathbb{R}} \frac{\mathrm{d}q_0}{(2\pi)} \int_{\mathbb{R}} \frac{\mathrm{d}X}{(2\pi)} \int_{\mathbb{R}} \frac{\mathrm{d}Y}{(2\pi)} \left[\frac{1}{|q_0| + |c(v)X + \Delta_1| + |c(v)Y - \Delta_2|}\right] \\ \times \left[\frac{1}{|q_0 + \mu| + |c(v)X + \Delta_1| + |c(v)Y - \Delta_2|}\right] \left[\frac{1}{i\left(q_0 + \frac{3\mu}{2}\right) + Y}\right] \left[\frac{1}{-i\left(q_0 + \frac{\mu}{2}\right) + X}\right], \end{aligned} \tag{Q.159}$$

where, to leading order in v, we have neglected the terms of order $vc(v)Y$ and $vc(v)X$ since these only offer subleading contributions upon integrating over X and Y. Here, we have defined the scales $\Delta_1 = 2vc(v)(vk_x - p_y)$ and $\Delta_2 = 2vc(v)(vp_y + k_x)$. The structure of this integration is identical to that of Eq. (Q.146). It follows immediately that this integration is given by

$$\mathcal{R}_{13}(k_x, p_y; \mu) = \frac{v^2}{4\pi} \frac{\mathcal{U}_{13}[\mu, 2vc(v)|vp_y + k_x|, 2vc(v)|vk_x - p_y|]}{\mathcal{R}_{13}[\mu, 2vc(v)|vp_y + k_x|, 2vc(v)|vk_x - p_y|]}, \tag{Q.160}$$

where $\mathcal{R}_{13}(x, y, z) \approx \max(x, y, z)$ and the crossover function $\mathcal{U}_{13}(x, y, z)$ is given by

$$\mathcal{U}_{13}(x, y, z) = \begin{cases} \log(3), & x \gg y, z, \\ x, & y \gg x, z \quad \& \quad z \gg x, y. \end{cases} \tag{Q.161}$$

D. $\mathcal{R}_{14}(k,p,l)$

For $M=1$ and $N=4$, the integration in Eq. (Q.6) evaluated at the RG condition reads:

$$\mathcal{R}_{14}(k_x,p_x;\mu)=\mu v^2\int \mathrm{d}q\ \left[\frac{1}{|q_0|+c(v)(|q_x|+|q_y|)}\right]\left[\frac{1}{|q_0+\mu|+c(v)(|q_x|+|q_y|)}\right]$$
$$\times\left[\frac{1}{i\left(q_0+\frac{3\mu}{2}\right)+vq_x-q_y+2vk_x}\right]\left[\frac{1}{-i\left(q_0+\frac{\mu}{2}\right)-vq_x-q_y+2vp_x}\right]. \tag{Q.162}$$

The integration over the loop momentum in this expression follows the same structure as the one considered in Eq. (Q.49). Because at the RG condition $\vec{l}=\vec{0}$, this implies that, apart from the constraint on the external momentum discussed in Sec. 4.4-(*a*) , we also require that $|p_x-k_x|\ll\Lambda_b$ in order for the integration over the momenta to have nonzero support. Keeping this constraint implicit in the discussion we proceed by performing the change of variables $q_x\to q_x-k_x+p_x$ and $q_y\to q_y+v(k_x+p_x)$, followed by the scaling $q_x\to q_x/c(v)$. With this, Eq. (Q.162) can be cast as

$$\mathcal{R}_{14}(k_x,p_x;\mu)=-\frac{\mu v^2}{c(v)}\int \mathrm{d}q\ \left[\frac{1}{|q_0|+|q_x+\Delta_2|+|c(v)q_y+\Delta_1|}\right]$$
$$\times\left[\frac{1}{|q_0+\mu|+|\Delta_2+q_x|+|\Delta_1+c(v)q_y|)}\right]$$
$$\times\left[\frac{1}{i\left(q_0+\frac{3\mu}{2}\right)+w(v)q_x-q_y}\right]\left[\frac{1}{i\left(q_0+\frac{\mu}{2}\right)+w(v)q_x+q_y}\right]. \tag{Q.163}$$

Here we have defined the scales $\Delta_1=vc(v)(k_x+p_x)$ and $\Delta_2=c(v)(p_x-k_x)$ and used the definition $w(v)=v/c(v)$. In the small v limit, the integration over q_y is done by setting $c(v)q_y=0$ inside the boson propagator. This yields

$$\mathcal{R}_{14}(k_x,p_x;\mu)=\frac{\mu v^2}{2c(v)}\int_{\mathbb{R}}\frac{\mathrm{d}q_0}{(2\pi)}\int_{\mathbb{R}}\frac{\mathrm{d}q_x}{(2\pi)}\ \left[\frac{1}{|q_0|+|q_x+\Delta_2|+|\Delta_1|}\right]$$
$$\times\left[\frac{1}{|q_0+\mu|+|\Delta_2+q_x|+|\Delta_1|}\right]\left[\frac{\Theta\left(\frac{\mu}{2}+q_0\right)-\Theta\left(-\frac{3\mu}{2}-q_0\right)}{q_0+\mu-iw(v)q_x}\right]. \tag{Q.164}$$

As it will become clear in what follows, we shift $q_x\to q_x-\Delta_2$ and define $\overline{\Delta}_2=w(v)\Delta_2$ because $\overline{\Delta}_2$ plays the role of the IR cutoff in the limit in which μ and Δ_1 are zero. With this shift we write

$$\mathcal{R}_{14}(k_x,p_x,\mu)=\frac{\mu v^2}{2c(v)}\int_{\mathbb{R}}\frac{\mathrm{d}q_0}{(2\pi)}\int_{\mathbb{R}}\frac{\mathrm{d}q_x}{(2\pi)}\ \left[\frac{1}{|q_0|+|q_x|+|\Delta_1|}\right]$$
$$\times\left[\frac{1}{|q_0+\mu|+|q_x|+|\Delta_1|}\right]\left[\frac{\Theta\left(\frac{\mu}{2}+q_0\right)-\Theta\left(-\frac{3\mu}{2}-q_0\right)}{q_0+\mu-iw(v)q_x-i\overline{\Delta}_2}\right]. \tag{Q.165}$$

We proceed by analyzing this expression in the limits: (*i*) $\mu\gg|\Delta_1|$ and $\mu\gg|\overline{\Delta}_2|$, (*ii*) $|\Delta_2|\gg\mu$ and $|\Delta_2|\gg|\overline{\Delta}_1|$, and (*iii*) $|\Delta_1|\gg\mu$ and $|\Delta_1|\gg|\overline{\Delta}_2|$.

(*i*) For $\mu \gg |\Delta_1|$ and $\mu \gg |\overline{\Delta}_2|$ we perform the transformation $(q_0, q_x) \to \mu(q_0, q_x)$ and take the $\mu/|\Delta_1| \ll 1$ and $|\overline{\Delta}_2|/|\Delta_1| \ll 1$ limits in Eq. (Q.165):

$$\mathcal{R}_{14}(k_x, p_x, l_x; \mu) = \frac{v^2}{2c(v)} \int_{\mathbb{R}} \frac{\mathrm{d}q_0}{(2\pi)} \int_{\mathbb{R}} \frac{\mathrm{d}q_x}{(2\pi)} \left[\frac{1}{|q_0| + |q_x|}\right] \left[\frac{1}{|q_0 + 1| + |q_x|}\right] \times \left[\frac{\Theta\left(\frac{1}{2} + q_0\right) - \Theta\left(-\frac{3}{2} - q_0\right)}{q_0 + 1 - iw(v)q_x}\right]. \tag{Q.166}$$

In the $v \ll 1$ limit we can set $w(v) = 0$ inside the integrand. Although the integrand seems to be IR divergent at $q_0 = -1$, this is spurious since the Heaviside functions cut off this divergence. Integration over q_x followed by an integration over q_0 yields,

$$\mathcal{R}_{14}(k_x, p_x; \mu) = \frac{v^2}{48\pi^2 c(v)} \left[5\pi^2 + 12\log(2)^2 + 6\mathrm{Li}_2(1/4)\right], \tag{Q.167}$$

where $\mathrm{Li}_2(x)$ is the dilogarithm function.

(*ii*) For $|\overline{\Delta}_2| \gg \mu$ and $|\overline{\Delta}_2| \gg |\Delta_1|$ we consider, without loss of generality, $\overline{\Delta}_2 > 0$ and perform the scaling $(q_0, q_x) \to \overline{\Delta}_2(q_0, q_x)$ in Eq. (Q.165). Taking the $\mu/\overline{\Delta}_2 \ll 1$ and $|\Delta_1|/\overline{\Delta}_2 \ll 1$ limits allows Eq. (Q.165) to be written as

$$\mathcal{R}_{14}(k_x, p_x; \mu) = \frac{\mu v^2}{2c(v)\overline{\Delta}_2} \int_{\mathbb{R}} \frac{\mathrm{d}q_0}{(2\pi)} \int_{\mathbb{R}} \frac{\mathrm{d}q_x}{(2\pi)} \left[\frac{1}{|q_0| + |q_x|}\right]^2 \left[\frac{\mathrm{sgn}(q_0)}{q_0 - iw(v)q_x - i}\right]. \tag{Q.168}$$

Setting $w(v) = 0$ in this expression is harmless in the small v limit. Further integration over q_0 and q_x is straightforward, yielding

$$\mathcal{R}_{14}(k_x, p_x; \mu) = \frac{\mu v^2}{4\pi c(v)|\overline{\Delta}_2|}, \tag{Q.169}$$

where the absolute value comes from the fact that the $\overline{\Delta}_2 < 0$ case yields the same result.

(*iii*) For $|\Delta_1| \gg \mu$ and $|\Delta_1| \gg |\overline{\Delta_2}|$ we perform the scaling $(q_0, q_x) \to |\Delta_1|(q_0, q_x)$ in Eq. (Q.165). This allows us to write

$$\mathcal{R}_{14}(k_x, p_x; \mu) = \frac{\mu v^2}{2c(v)|\Delta_1|} \int_{\mathbb{R}} \frac{\mathrm{d}q_0}{(2\pi)} \int_{\mathbb{R}} \frac{\mathrm{d}q_x}{(2\pi)} \left[\frac{1}{|q_0| + |q_x| + 1}\right] \times \left[\frac{1}{|q_0 + m| + |q_x| + 1}\right] \left[\frac{\Theta\left(\frac{m}{2} + q_0\right) - \Theta\left(-\frac{3m}{2} - q_0\right)}{q_0 + m - iw(v)q_x + i\delta}\right]. \tag{Q.170}$$

where $m = \mu/|\Delta_1|$ and $\delta = \overline{\Delta}_2/|\Delta_1|$. Setting both m and δ to zero in this expression makes the integration IR divergent. Setting $w(v)q_x = 0$, however, is legitimate. In the small v limit we set $w(v) = 0$ and integrate over q_x to obtain

$$\mathcal{R}_{14}(k_x, p_x; \mu) = \frac{mv^2}{2\pi c(v)} \int_{\mathbb{R}} \frac{\mathrm{d}q_0}{(2\pi)} \left\{ \left[\frac{\Theta\left(\frac{m}{2} + q_0\right) - \Theta\left(-\frac{3m}{2} - q_0\right)}{q_0 + m + i\delta}\right] \frac{\log\left[\frac{1+|q_0|}{1+|q_0+m|}\right]}{|q_0| - |q_0 + m|} \right\}. \tag{Q.171}$$

We analyze this expression for (*a*) $m \gg |\delta|$ and (*b*) $|\delta| \gg m$.

(*a*) For $m \gg |\delta|$ we can scale out m from the q_0 integration through the transformation $q_0 \to m q_0$. This allows us to write Eq. (Q.171), in the $m \gg |\delta|$ limit, as

$$\mathcal{R}_{14}(k_x, p_x; \mu) = \frac{v^2}{2\pi c(v)} \int_{\mathbb{R}} \frac{\mathrm{d}q_0}{(2\pi)} \left\{ \left[\frac{\Theta\left(\frac{1}{2} + q_0\right) - \Theta\left(-\frac{3}{2} - q_0\right)}{q_0 + 1} \right] \frac{\log\left[\frac{1+m|q_0|}{1+m|q_0+1|}\right]}{|q_0| - |q_0+1|} \right\}. \tag{Q.172}$$

Setting $m = 0$ in this expression makes the q_0 integration logarithmically divergent in the UV. This is a symptom of the integration being logarithmically divergent in $m \ll 1$. Upon integrating over q_0 for nonzero m, we obtain, to leading order in $m \ll 1$,

$$\mathcal{R}_{14}(k_x, p_x; \mu) = -\frac{v^2}{2\pi^2 c(v)} \frac{\mu}{|\Delta_1|} \log\left(\frac{\mu}{|\Delta_1|}\right). \tag{Q.173}$$

(*b*) For $|\delta| \gg m$ we assume, without loss of generality, that $\delta > 0$ and perform the scaling $q_0 \to q_0 \delta$ in Eq. (Q.171). Taking the $m/\delta \ll 1$ limit reduces Eq. (Q.171) to

$$\mathcal{R}_{14}(k_x, p_x; \mu) = \frac{v^2 \mu}{2\pi c(v)|\Delta_1|} \int_{\mathbb{R}^+} \frac{\mathrm{d}q_0}{(2\pi)} \left[\frac{q_0}{(q_0^2+1)(1+\delta q_0)} \right]. \tag{Q.174}$$

The integration over q_0 yields, in the $\delta \ll 1$ limit

$$\mathcal{R}_{14}(k_x, p_x; \mu) = \frac{v^2 \mu}{2\pi^2 c(v)|\Delta_1|} \log\left(\frac{|\Delta_1|}{|\overline{\Delta}_2|}\right), \tag{Q.175}$$

where the last equality follows from the definition of $\delta = \overline{\Delta}_2/|\Delta_1|$ and the fact that we obtain the same result for $\overline{\Delta}_2 < 0$.

Collecting the results from Eqs. (Q.167), (Q.169), (Q.173) and (Q.175), using the definitions $\Delta_1 = vc(v)(p_x + k_x)$ and $\overline{\Delta}_2 = v(p_x - k_x)$, and bringing back the constraint on the external momentum we obtain

$$\mathcal{R}_{14}(k_x, p_x, l_x; \mu) = \frac{v^2}{2\pi^2 c(v)} \Theta(\Lambda_b - |p_x - k_x|) \frac{\mathscr{U}_{14}[\mu, vc(v)|p_x + k_x|, v|p_x - k_x|]}{\mathscr{R}_{14}[\mu, vc(v)|p_x + k_x|, v|k_x - p_x|]}, \tag{Q.176}$$

where $\mathscr{R}_{14}(x, y, z) \approx \max(x, y, z)$ and

$$\mathscr{U}_{14}(x, y, z) = \begin{cases} \frac{1}{24}\left[5\pi^2 + 12\log(2)^2 + 6\mathrm{Li}_2(1/4)\right], & x \gg y, z, \\ \frac{\pi}{2}, & z \gg x, y, \\ x \log\left(\frac{y}{x}\right), & y \gg x, z \quad \& \quad x \gg z, \\ x \log\left(\frac{y}{z}\right), & y \gg x, z \quad \& \quad z \gg x. \end{cases} \tag{Q.177}$$

E. $\mathcal{R}_{15}(k,p,l)$

For $M=1$ and $N=5$, the integration in Eq. (Q.6) evaluated at the RG condition reads

$$\mathcal{R}_{15}(k_x,p_x,l_x;\mu)=\mu v^2\int \mathrm{d}q\ \left[\frac{1}{|q_0|+c(v)(|q_x|+|q_y|)}\right]\left[\frac{1}{|q_0+\mu|+c(v)(|l_x-q_x|+|vl_x-q_y|)}\right]\times\left[\frac{1}{i\left(q_0+\frac{3\mu}{2}\right)+vq_x-q_y+2vk_x}\right]\left[\frac{1}{-i\left(q_0+\frac{\mu}{2}\right)+vq_x-q_y-2vp_x}\right]. \tag{Q.178}$$

The RG condition offers no further constraint on l_x. However, according to the discussion in Sec. 4.2-(*a*) , the integration over the loop momentum must be done over the region defined by

$$\begin{aligned}&|vq_x-q_y+2vk_x|<\Lambda_f,\quad |vq_x-q_y-2vp_x|<\Lambda_f,\quad |q_x-l_x|<\Lambda_b,\\ &\quad |vl_x-q_y|<\Lambda_b,\quad |q_x|<\Lambda_b,\quad \&\quad |q_y|<\Lambda_b.\end{aligned} \tag{Q.179}$$

It is convenient at this stage to make the change of variables $q_y\to q_y+vq_x+v(k_x-p_x)$, under which the region of integration is transformed to

$$\begin{aligned}&|q_y-v(p_x+k_x)|<\Lambda_f,\quad |q_y+v(k_x+p_x)|<\Lambda_f,\quad |q_x-l_x|<\Lambda_b,\quad |q_x|<\Lambda_b,\\ &\quad |q_y+vq_x-v(l_x+k_x-p_x)|<\Lambda_b,\quad \&\quad |q_y+vq_x+v(k_x-p_x)|<\Lambda_b.\end{aligned} \tag{Q.180}$$

Apart from the constraints on the external momenta that the discussion in Sec. 4.4-(*a*) implies, we require that $|k_x+p_x|\ll\Lambda_f/v$ and $|l_x|\ll\Lambda_b$ for the integrations over q_x and q_y to have nonzero support. In what follows we keep these constraints implicit. Under the same change of variables Eq. (Q.178) adopts the form

$$\mathcal{R}_{15}(k_x,p_x,l_x;\mu)=\frac{\mu v^2}{c(v)}\int \mathrm{d}q\ \left[\frac{1}{i\left(q_0+\frac{3\mu}{2}\right)-q_y+\frac{\Delta_1}{2}}\right]\left[\frac{1}{-i\left(q_0+\frac{\mu}{2}\right)-q_y-\frac{\Delta_1}{2}}\right]\times\left[\frac{1}{|q_0|+(|q_x|+|c(v)q_y+vq_x+\Delta_2|)}\right]\left[\frac{1}{|q_0+\mu|+(|\Delta_4-q_x|+|\Delta_3-c(v)q_y-vq_x|)}\right], \tag{Q.181}$$

where we have further performed the rescaling $q_x\to q_x/c(v)$ and defined $\Delta_1=v(k_x+p_x)$, $\Delta_2=vc(v)(k_x-p_x)$, $\Delta_3=vc(v)(l_x-k_x+p_x)$ and $\Delta_4=c(v)l_x$. Since the integration is convergent by power counting we set the cutoff scales to arbitrary large values and set $vq_x=0$ inside the boson propagator since this does not alter the convergence of the q_x integration in the small v limit. Furthermore, in this same limit, the terms of order $c(v)q_y$ can be set to zero as well because the integration over q_y is convergent in the absence of this terms. Integration over q_y yields

$$\mathcal{R}_{15}(k_x,p_x,l_x;\mu)=\frac{\mu v^2}{c(v)}\int_{\mathbb{R}}\frac{\mathrm{d}q_0}{(2\pi)}\int_{\mathbb{R}}\frac{\mathrm{d}q_x}{(2\pi)}\left[\frac{\Theta\left(\frac{3\mu}{2}+q_0\right)-\Theta\left(-\frac{\mu}{2}-q_0\right)}{2(q_0+\mu)-i\Delta_1}\right]\times\left[\frac{1}{|q_0|+|q_x|+|\Delta_2|}\right]\left[\frac{1}{|q_0+\mu|+|q_x-\Delta_4|+|\Delta_3|}\right]. \tag{Q.182}$$

We analyze this expression in the following limits: (*i*) $\mu \gg |\Delta_i|$ for $i = 1,2,3,4$, (*ii*) $|\Delta_1| \gg \mu$ and $|\Delta_1| \gg |\Delta_i|$ for $i = 2,3,4$, (*ii*) $|\Delta_2| \gg \mu$ and $|\Delta_2| \gg |\Delta_i|$ for $i = 1,3,4$, (*iv*) $|\Delta_3| \gg \mu$ and $|\Delta_3| \gg |\Delta_i|$ for $i = 1,2,4$, and (*v*) $|\Delta_4| \gg \mu$ and $|\Delta_4| \gg |\Delta_i|$ for $i = 1,2,3$.

(*i*) For $\mu \gg |\Delta_i|$ with $i = 1,2,3,4$ we perform the scaling $(q_0, q_x) \to \mu(q_0, q_x)$ in Eq. (Q.182) and take the $|\Delta_i|/\mu \ll 1$ limits. Integrating over q_x in this limits we obtain

$$\mathcal{R}_{15}(k_x, p_x, l_x; \mu) = \frac{v^2}{2\pi c(v)} \int_{\mathbb{R}} \frac{\mathrm{d}q_0}{(2\pi)} \int_{\mathbb{R}} \frac{\mathrm{d}q_x}{(2\pi)} \left[\frac{\Theta\left(\frac{3}{2} + q_0\right) - \Theta\left(-\frac{1}{2} - q_0\right)}{[|q_0| - |q_0 + 1|](q_0 + 1)} \right] \log\left(\frac{|q_0 + 1|}{|q_0|} \right). \quad \text{(Q.183)}$$

Final integration over q_0 yields

$$\mathcal{R}_{15}(k_x, p_x, l_x; \mu) = \frac{v^2}{8\pi^2 c(v)} \left[\pi^2 + \log(2)^2 + 2\mathrm{Li}_2(-1/2) \right], \quad \text{(Q.184)}$$

where $\mathrm{Li}_2(x)$ is the dilogarithm function.

(*ii*) For $|\Delta_1| \gg \mu$ and $|\Delta_1| \gg |\Delta_i|$ with $i = 2,3,4$, we assume, without any loss of generality, that $\Delta_1 > 0$ and perform the scaling $(q_0, q_x) \to \Delta_1(q_0, q_x)$ in Eq. (Q.182). In the $\mu/\Delta_1 \ll 1$ and $|\Delta_i|/\Delta_1 \ll 1$ limits, Eq. (Q.182) takes the form

$$\mathcal{R}_{15}(k_x, p_x, l_x; \mu) = \frac{\mu v^2}{c(v)\Delta_1} \int_{\mathbb{R}} \frac{\mathrm{d}q_0}{(2\pi)} \int_{\mathbb{R}} \frac{\mathrm{d}q_x}{(2\pi)} \left[\frac{\mathrm{sgn}(q_0)}{2q_0 - i} \right] \left[\frac{1}{|q_0| + |q_x|} \right]^2. \quad \text{(Q.185)}$$

The integration over q_x and q_0 yields

$$\mathcal{R}_{15}(k_x, p_x, l_x; \mu) = \frac{\mu v^2}{2\pi c(v)|\Delta_1|}, \quad \text{(Q.186)}$$

where we have used the fact that we obtain the same result for $\Delta_1 < 0$.

(*iii*) For $|\Delta_2| \gg \mu$ and $|\Delta_2| \gg |\Delta_i|$ with $i = 1,3,4$ we assume, without loss of generality, that $\Delta_2 > 0$ and perform the scaling $(q_0, q_x) \to \Delta_2(q_0, q_x)$ in Eq. (Q.182). Defining $m = \mu/\Delta_2$ and $\delta_i = \Delta_i/\Delta_2$, we can write Eq. (Q.182) as

$$\begin{aligned} \mathcal{R}_{15}(k_x, p_x, l_x; \mu) = \frac{\mu v^2}{c(v)\Delta_2} \int_{\mathbb{R}} \frac{\mathrm{d}q_0}{(2\pi)} \int_{\mathbb{R}} \frac{\mathrm{d}q_x}{(2\pi)} \left[\frac{\Theta\left(\frac{3m}{2} + q_0\right) - \Theta\left(-\frac{m}{2} - q_0\right)}{2(q_0 + m) - i\delta_1} \right] \\ \times \left[\frac{1}{|q_0| + |q_x| + 1} \right] \left[\frac{1}{|q_0 + m| + |q_x - \delta_4| + |\delta_3|} \right]. \end{aligned} \quad \text{(Q.187)}$$

Setting all $\delta_i = 0$ and $m = 0$ inside the integration makes the q_0 integration vanish. This is a consequence of setting $m = 0$ and $\delta_1 = 0$ simultaneously. In contrast, setting $\delta_3 = \delta_4 = 0$ in the integrand is harmless and the integration takes the form

$$\begin{aligned} \mathcal{R}_{15}(k_x, p_x, l_x; \mu) = \frac{\mu v^2}{c(v)\Delta_2} \int_{\mathbb{R}} \frac{\mathrm{d}q_0}{(2\pi)} \int_{\mathbb{R}} \frac{\mathrm{d}q_x}{(2\pi)} \left[\frac{\Theta\left(\frac{3m}{2} + q_0\right) - \Theta\left(-\frac{m}{2} - q_0\right)}{2(q_0 + m) - i\delta_1} \right] \\ \times \left[\frac{1}{|q_0| + |q_x| + 1} \right] \left[\frac{1}{|q_0 + m| + |q_x|} \right]. \end{aligned} \quad \text{(Q.188)}$$

We take a look at this expression in the cases in which (*a*) $|\delta_1| \gg m$ and (*b*) $m \gg |\delta_1|$.

(*a*) For $|\delta_1| \gg m$, we assume without loss of generality that $\delta_1 > 0$, perform the scaling $(q_0, q_x) \to \delta_1(q_0, q_x)$ and take the $m/\delta_1 \ll 1$ limit. Doing so allows us to write Eq. (Q.188) as

$$\mathcal{R}_{15}(k_x, p_x, l_x; \mu) = \frac{8\mu v^2}{c(v)\Delta_2} \int\limits_{\mathbb{R}^+} \frac{\mathrm{d}q_0}{(2\pi)} \int\limits_{\mathbb{R}^+} \frac{\mathrm{d}q_x}{(2\pi)} \frac{q_0}{1+4q_0^2} \left[\frac{1}{\delta_1(q_0+q_x)+1}\right] \left[\frac{1}{q_0+q_x}\right]. \tag{Q.189}$$

The integration over q_x is straightforward, yielding

$$\mathcal{R}_{15}(k_x, p_x, l_x; \mu) = \frac{4\mu v^2}{\pi c(v)\Delta_2} \int\limits_{\mathbb{R}^+} \frac{\mathrm{d}q_0}{(2\pi)} \frac{q_0}{1+4q_0^2} \log\left(1+\frac{1}{q_0\delta_1}\right). \tag{Q.190}$$

In the $\delta_1 \ll 1$ limit, the leading order contribution from the q_0 integration is given by

$$\mathcal{R}_{15}(k_x, p_x, l_x; \mu) = \frac{\mu v^2}{4\pi^2 c(v)|\Delta_2|} \log\left(\frac{2|\Delta_2|}{|\Delta_1|}\right)^2, \tag{Q.191}$$

where we have used the fact that the same result is obtained in the cases that $\Delta_2 < 0$ and $\Delta_1 > 0$, $\Delta_2 > 0$ and $\Delta_1 < 0$, and $\Delta_2 < 0$ and $\Delta_1 < 0$.

(*b*) For $m \gg |\delta_1|$ we consider the scaling $(q_0, q_x) \to m(q_0, q_x)$ in Eq. (Q.188) and take the $|\delta_1|/\mu \ll 1$ limit to write the integration as

$$\begin{aligned}\mathcal{R}_{15}(k_x, p_x, l_x; \mu) = \frac{\mu v^2}{c(v)\Delta_2} \int\limits_{\mathbb{R}} \frac{\mathrm{d}q_0}{(2\pi)} \int\limits_{\mathbb{R}} \frac{\mathrm{d}q_x}{(2\pi)} \left[\frac{\Theta\left(\frac{3}{2}+q_0\right)-\Theta\left(-\frac{1}{2}-q_0\right)}{2(q_0+1)}\right] \\ \times \left[\frac{1}{m(|q_0|+|q_x|)+1}\right] \left[\frac{1}{|q_0+1|+|q_x|}\right].\end{aligned} \tag{Q.192}$$

Integration over q_x is straightforward

$$\mathcal{R}_{15}(k_x, p_x, l_x; \mu) = \frac{\mu v^2}{2\pi c(v)\Delta_2} \int\limits_{\mathbb{R}} \frac{\mathrm{d}q_0}{(2\pi)} \left[\frac{\Theta\left(\frac{3}{2}+q_0\right)-\Theta\left(-\frac{1}{2}-q_0\right)}{(q_0+1)[m(|q_0+1|-|q_0|)-1]}\right] \log\left(\frac{m|1+q_0|}{1+m|q_0|}\right). \tag{Q.193}$$

Integration over q_0 is done for finite m and, in the $m \ll 1$ limit we obtain the leading order contribution

$$\mathcal{R}_{15}(k_x, p_x, l_x; \mu) = \frac{\mu v^2}{4\pi^2 c(v)|\Delta_2|} \log\left(\frac{\mu}{2|\Delta_2|}\right)^2, \tag{Q.194}$$

where we have also used the fact that the integration yields the same result for the case $\Delta_2 < 0$.

(*iv*) For $|\Delta_3| \gg \mu$ and $|\Delta_3| \gg |\Delta_i|$ for $i = 1, 2, 4$ we note that, under the exchange $\Delta_2 \leftrightarrow \Delta_3$ and $\mu \leftrightarrow -\mu$ in Eq. (Q.182), followed by the change of variables $q_0 \to -q_0$

and $q_x \to q_x + \Delta_4$, this limit reduces to the one we computed previously. It therefore follows that

$$\begin{aligned}\mathcal{R}_{15}(k_x,p_x,l_x;\mu) &= \frac{\mu v^2}{4\pi^2 c(v)|\Delta_3|}\log\left(\frac{\mu}{2|\Delta_3|}\right)^2, \qquad \mu \gg |\Delta_1|,\\ \mathcal{R}_{15}(k_x,p_x,l_x;\mu) &= \frac{\mu v^2}{4\pi^2 c(v)|\Delta_3|}\log\left(\frac{2|\Delta_3|}{|\Delta_1|}\right)^2, \qquad |\Delta_1| \gg \mu.\end{aligned} \tag{Q.195}$$

(*v*) For $|\Delta_4| \gg \mu$ and $|\Delta_4| \gg |\Delta_i|$ with $i = 1,2,3$ we assume, without loss of generality, that $\Delta_4 > 0$ and perform the scaling $(q_0, q_x) \to \Delta_4(q_0, q_x)$ in Eq. (Q.182). Defining the ratios $m = \mu/\Delta_4$ and $\delta_i = \Delta_i/\Delta_4$ for $i = 1,2,3$, Eq. (Q.182) assumes the form

$$\begin{aligned}\mathcal{R}_{15}(k_x,p_x,l_x;\mu) = \frac{\mu v^2}{c(v)\Delta_4}\int_{\mathbb{R}}\frac{\mathrm{d}q_0}{(2\pi)}\int_{\mathbb{R}}\frac{\mathrm{d}q_x}{(2\pi)}\left[\frac{\Theta\left(\frac{3m}{2}+q_0\right)-\Theta\left(-\frac{m}{2}-q_0\right)}{2(q_0+m)-i\delta_1}\right]\\ \times\left[\frac{1}{|q_0|+|q_x|+|\delta_2|}\right]\left[\frac{1}{|q_0+m|+|q_x-1|+|\delta_3|}\right].\end{aligned} \tag{Q.196}$$

As in the previous cases, setting $\delta_1 = 0$ and $m = 0$ simultaneously make the integration vanish. Therefore we keep these two parameters nonzero. In contrast, setting $\delta_2 = \delta_3 = 0$ in this expression is harmless. In what follows we analyze Eq. (Q.196) in the (*a*) $|\delta_1| \gg m$ and (*b*) $m \gg |\delta_1|$ limits by setting $\delta_3 = \delta_2 = 0$.

(*a*) For $|\delta_1| \gg m$ we consider, without loss of generality, that $\delta_1 > 0$ and perform the scaling $(q_0, q_x) \to \delta_1(q_0, q_x)$ in Eq. (Q.196). In the $m/\delta_1 \ll 1$ limit, the integration takes the form

$$\begin{aligned}\mathcal{R}_{15}(k_x,p_x,l_x;\mu) = \frac{4\mu v^2}{c(v)\Delta_4}\int_{\mathbb{R}^+}\frac{\mathrm{d}q_0}{(2\pi)}\int_{\mathbb{R}}\frac{\mathrm{d}q_x}{(2\pi)}\left[\frac{q_0}{4q_0^2+1}\right]\left[\frac{1}{q_0+|q_x|}\right]\\ \times\left[\frac{1}{\delta_1 q_0+|\delta_1 q_x-1|}\right].\end{aligned} \tag{Q.197}$$

Integration over q_x yields

$$\mathcal{R}_{15}(k_x,p_x,l_x;\mu) = \frac{8\mu v^2}{\pi c(v)\Delta_4}\int_{\mathbb{R}^+}\frac{\mathrm{d}q_0}{(2\pi)}\frac{(1+q_0\delta_1)\log\left[\frac{q_0\delta_1}{1+q_0\delta_1}\right]}{1+2\delta_1 q_0}\frac{q_0}{4q_0^2+1}. \tag{Q.198}$$

The integration over q_0 is done for nonzero δ_1. In the $\delta_1 \ll 1$ limit, the leading order contribution is given by

$$\mathcal{R}_{15}(k_x,p_x,l_x;\mu) = \frac{\mu v^2}{2\pi^2 c(v)|\Delta_4|}\log\left(\frac{|\Delta_1|}{2|\Delta_4|}\right)^2, \tag{Q.199}$$

where we have used the fact that we obtain the same result regardless of the sign of both Δ_1 and Δ_4.

(*b*) For $m \gg |\delta_1|$ we scale out m from the integration in Eq. (Q.196) through the transformation $(q_0, q_x) \to m(q_0, q_x)$ and take the $|\delta_1|/m \ll 1$ limit. This yields

$$\mathcal{R}_{15}(k_x, p_x, l_x; \mu) = \frac{\mu v^2}{2c(v)\Delta_4} \int_{\mathbb{R}} \frac{\mathrm{d}q_0}{(2\pi)} \int_{\mathbb{R}} \frac{\mathrm{d}q_x}{(2\pi)} \left[\frac{\Theta\left(\frac{3}{2} + q_0\right) - \Theta\left(-\frac{1}{2} - q_0\right)}{q_0} \right] \times \left[\frac{1}{|q_0| + |q_x|} \right] \left[\frac{1}{m|q_0 + 1| + |mq_x - 1|} \right]. \tag{Q.200}$$

Setting $m = 0$ in the integrand introduces spurious divergences in both the q_0 and q_x integrations. For a nonzero m, the integration over q_0 and q_x can be carried in order to yield the leading order contribution in the $m = \mu/\Delta_4 \ll 1$ limit

$$\mathcal{R}_{15}(k_x, p_x, l_x; \mu) = \frac{\mu v^2}{2\pi^2 c(v)|\Delta_4|} \log\left(\frac{\mu}{2|\Delta_4|}\right)^2. \tag{Q.201}$$

In here we used the fact that the same result is obtained for $\Delta_4 < 0$.

Collecting the results from Eqs. (Q.184), (Q.186), (Q.191), (Q.194), (Q.195) , (Q.199) and (Q.201), using the definitions $\Delta_1 = v(k_x + p_x)$, $\Delta_2 = vc(v)(k_x - p_x)$, $\Delta_3 = vc(v)(l_x - k_x + p_x)$ and $\Delta_4 = c(v)l_x$, and bringing back the constraint on the external momentum we can write Eq. (Q.178) as

$$\mathcal{R}_{15}(k_x, p_x, l_x; \mu) = \frac{v^2}{4\pi^2 c(v)} \Theta(\Lambda_b - |l_x|)\Theta(\Lambda_f - v|k_x + p_x|) \times \frac{\mathscr{U}_{15}[\mu, v|k_x + p_x|, vc(v)|k_x - p_x|, vc(v)|l_x - k_x + p_x|, c(v)|l_x|]}{\mathscr{R}_{15}[\mu, v|k_x + p_x|, vc(v)|k_x - p_x|, vc(v)|l_x - k_x + p_x|, c(v)|l_x|]}, \tag{Q.202}$$

where $\mathcal{R}_{15}(x, y, z, u, w) \sim \max(x, y, z, y, w)$ and the crossover function $\mathscr{U}_{15}(x, y, z, u, w)$ is defined as

$$\mathscr{U}_{15}(x, y, z, u, w) = \begin{cases} \frac{x}{2}\left[\pi^2 + \log(2)^2 + 2\mathrm{Li}_2(-1/2)\right], & x \gg y, z, u, w, \\ \frac{\pi x}{2} & y \gg x, z, u, w, \\ x \log\left(\frac{x}{2z}\right)^2, & z \gg x, y, u, w \quad \& \quad x \gg y, \\ x \log\left(\frac{y}{2z}\right)^2, & z \gg x, y, u, w \quad \& \quad y \gg x, \\ x \log\left(\frac{x}{2u}\right)^2, & u \gg x, y, z, w \quad \& \quad x \gg y, \\ x \log\left(\frac{y}{2u}\right)^2, & u \gg x, y, z, w \quad \& \quad y \gg x, \\ x \log\left(\frac{x}{2w}\right)^2, & w \gg x, y, z, u \quad \& \quad x \gg y, \\ x \log\left(\frac{y}{2w}\right)^2, & w \gg x, y, z, u \quad \& \quad y \gg x. \end{cases} \tag{Q.203}$$

F. $\mathcal{R}_{16}(k, p, l)$

For $M = 1$ and $N = 6$, the integration in Eq. (Q.6) evaluated at the RG condition reads:

$$\mathcal{R}_{16}(k_x, p_y; \mu) = \mu v^2 \int \mathrm{d}q \left[\frac{1}{|q_0| + c(v)(|q_x| + |q_y|)} \right] \left[\frac{1}{|q_0 + \mu| + c(v)(|q_x| + |q_y|)} \right] \times \left[\frac{1}{i\left(q_0 + \frac{3\mu}{2}\right) + vq_x - q_y + 2vk_x} \right] \left[\frac{1}{-i\left(q_0 + \frac{\mu}{2}\right) + q_x - vq_y + 2vp_y} \right]. \tag{Q.204}$$

The integration over the loop momenta follows the same logic as the one used in the computation of Eq. (Q.84). In particular, this implies that the external momentum has no further constraints than the one discussed in Sec. 4.4-(*a*) . Because the integration is finite by power counting we set all cutoff scales to arbitrary large values and proceed on integrating by first performing the change of variables

$$Y = vq_x - q_y + 2vk_x, \qquad \& \qquad X = q_x - vq_y + 2vp_y. \tag{Q.205}$$

Under this change of variables, Eq. (Q.204) takes the following form

$$\begin{aligned}\mathcal{R}_{16}(k_x,p_y;\mu) = \mu v^2 \int\limits_{\mathbb{R}} \frac{\mathrm{d}q_0}{(2\pi)} \int\limits_{\mathbb{R}} \frac{\mathrm{d}X}{(2\pi)} \int\limits_{\mathbb{R}} \frac{\mathrm{d}Y}{(2\pi)} \left[\frac{1}{|q_0| + |c(v)X + \Delta_1| + |c(v)Y - \Delta_2|}\right] \\ \times \left[\frac{1}{|q_0+\mu| + |c(v)X + \Delta_1| + |c(v)Y - \Delta_2|}\right] \left[\frac{1}{i\left(q_0 + \frac{3\mu}{2}\right) + Y}\right] \left[\frac{1}{-i\left(q_0 + \frac{\mu}{2}\right) + X}\right],\end{aligned} \tag{Q.206}$$

where to leading order in v we have neglected the terms of order $vc(v)Y$ and $vc(v)X$ since these only offer subleading contributions upon integrating over X and Y. Here, we have defined the scales $\Delta_1 = 2vc(v)(vk_x - p_y)$ and $\Delta_2 = 2vc(v)(k_x - vp_y)$. The structure of this integration is identical to that of Eq. (Q.157). It follows immediately that this integration is given by

$$\mathcal{R}_{16}(k_x,p_y;\mu) = \frac{v^2}{4\pi} \frac{\mathcal{U}_{16}[\mu, 2vc(v)|vk_x - p_y|, 2vc(v)|k_x - vp_y|]}{\mathcal{R}_{16}[\mu, 2vc(v)|vk_x - p_y|, 2vc(v)|k_x - vp_y|]}, \tag{Q.207}$$

where $\mathcal{R}_{16}(x,y,z) \approx \max(x,y,z)$ and the crossover function $\mathcal{U}_{16}(x,y,z)$ is given by

$$\mathcal{U}_{16}(x,y,z) = \begin{cases} \log(3), & x \gg y,z, \\ x, & y \gg x,z \quad \& \quad z \gg x,y. \end{cases} \tag{Q.208}$$

G. $\mathcal{R}_{17}(k,p,l)$

For $M = 1$ and $N = 7$, the integration in Eq. (Q.6) evaluated at the RG condition reads:

$$\begin{aligned}\mathcal{R}_{17}(k_x,p_y;\mu) = \mu v^2 \int \mathrm{d}q \left[\frac{1}{|q_0| + c(v)(|q_x| + |q_y|)}\right] \left[\frac{1}{|q_0+\mu| + c(v)(|q_x| + |q_y|)}\right] \\ \times \left[\frac{1}{i\left(q_0 + \frac{3\mu}{2}\right) + vq_x - q_y + 2vk_x}\right] \left[\frac{1}{-i\left(q_0 + \frac{\mu}{2}\right) + q_x + vq_y - 2vp_y}\right].\end{aligned} \tag{Q.209}$$

The integration over the loop momenta follows the same logic as the one used in the computation of Eq. (Q.90). In particular, this implies that the external momentum has no further constraints than the one discussed in Sec. 4.4-(*a*) . Because the integration is finite by power counting we set all cutoff scales to arbitrary large values and proceed on integrating by first performing the change of variables

$$Y = vq_x - q_y + 2vk_x, \qquad \& \qquad X = q_x + vq_y - 2vp_y. \tag{Q.210}$$

Under this change of variables, Eq. (Q.209) takes the following form

$$\mathcal{R}_{17}(k_x,p_y;\mu)=\mu v^2\int_{\mathbb{R}}\frac{\mathrm{d}q_0}{(2\pi)}\int_{\mathbb{R}}\frac{\mathrm{d}X}{(2\pi)}\int_{\mathbb{R}}\frac{\mathrm{d}Y}{(2\pi)}\left[\frac{1}{|q_0|+|c(v)X+\Delta_1|+|c(v)Y-\Delta_2|}\right]$$
$$\times\left[\frac{1}{|q_0+\mu|+|c(v)X+\Delta_1|+|c(v)Y-\Delta_2|}\right]\left[\frac{1}{i\left(q_0+\frac{3\mu}{2}\right)+Y}\right]\left[\frac{1}{-i\left(q_0+\frac{\mu}{2}\right)+X}\right], \tag{Q.211}$$

where to leading order in v we have neglected the terms of order $vc(v)Y$ and $vc(v)X$ since these only offer subleading contributions upon integrating over X and Y. Here, we have defined the scales $\Delta_1=2vc(v)(p_y-vk_x)$ and $\Delta_2=2vc(v)(vp_y+k_x)$. The structure of this integration is identical to that of Eq. (Q.146). It follows immediately that this integration is given by

$$\mathcal{R}_{17}(k_x,p_y;\mu)=\frac{v^2}{4\pi}\frac{\mathcal{U}_{17}[\mu,2vc(v)|vp_y+k_x|,2vc(v)|p_y-vk_x|]}{\mathcal{R}_{17}[\mu,2vc(v)|vp_y+k_x|,2vc(v)|p_y-vk_x|]}, \tag{Q.212}$$

where $\mathcal{R}_{17}(x,y,z)\approx\max(x,y,z)$ and the crossover function $\mathcal{U}_{17}(x,y,z)$ is given by

$$\mathcal{U}_{17}(x,y,z)=\begin{cases}\log(3), & x\gg y,z,\\ x, & y\gg x,z \quad \& \quad z\gg x,y.\end{cases} \tag{Q.213}$$

H. $\mathcal{R}_{18}(k,p,l)$

For $M=1$ and $N=8$, the integration in Eq. (Q.6) evaluated at the RG condition reads:

$$\mathcal{R}_{18}(k_x,p_x,l_x;\mu)=\mu v^2\int\mathrm{d}q\ \left[\frac{1}{|q_0|+c(v)(|q_x|+|q_y|)}\right]\left[\frac{1}{|q_0+\mu|+c(v)(|q_x|+|q_y|)}\right]$$
$$\times\left[\frac{1}{i\left(q_0+\frac{3\mu}{2}\right)+vq_x-q_y+2vk_x}\right]\left[\frac{1}{-i\left(q_0+\frac{\mu}{2}\right)+vq_x+q_y-2vp_x}\right]. \tag{Q.214}$$

The integration over the spatial momentum $\vec{q}$ is the same as the one for Eq. (Q.49). Therefore, it follows that the external momentum receives the extra constraint $|p_x-k_x|\ll\Lambda_b$. Keeping this constraint implicit, we note that the integration in Eq. (Q.214) is convergent by power counting and thus we set all cutoff scales to arbitrary large values. After the change of variables $q_x\to q_x-k_x+p_x$ and $q_y\to q_y+v(k_x+p_x)$, followed by the scaling $q_x\to q_x/c(v)$, Eq. (Q.214) can be written as

$$\mathcal{R}_{18}(k_x,p_x,l_x;\mu)=\frac{\mu v^2}{c(v)}\int\mathrm{d}q\ \left[\frac{1}{|q_0|+|q_x+\Delta_1|+|c(v)q_y+\Delta_2|}\right]\left[\frac{1}{-i\left(q_0+\frac{\mu}{2}\right)+vq_x+q_y}\right]$$
$$\times\left[\frac{1}{|q_0+\mu|+|\Delta_1+q_x|+|c(v)q_y+\Delta_2|}\right]\left[\frac{1}{i\left(q_0+\frac{3\mu}{2}\right)+vq_x-q_y}\right]. \tag{Q.215}$$

Here, we have defined the momentum-dependent scales $\Delta_1 = c(v)(p_x - k_x)$ and $\Delta_2 = vc(v)(k_x + p_x)$. Integration over q_y can be done in the small v limit by neglecting those terms of order $c(v)q_y$:

$$\mathcal{R}_{18}(k_x,p_x,l_x;\mu) = \frac{i\mu v^2}{c(v)}\int\limits_{\mathbb{R}}\frac{\mathrm{d}q_0}{(2\pi)}\int\limits_{\mathbb{R}}\frac{\mathrm{d}q_x}{(2\pi)}\left[\frac{\Theta\left(\frac{\mu}{2}+q_0\right)-\Theta\left(\frac{3\mu}{2}+q_0\right)}{2w(v)q_x+i\mu}\right] \times\left[\frac{1}{|q_0|+|q_x+\Delta_1|+|\Delta_2|}\right]\left[\frac{1}{|q_0+\mu|+|\Delta_1+q_x|+|\Delta_2|}\right]. \tag{Q.216}$$

Similarly, as in the case in which $M = 1$ and $N = 4$, we note that setting $w(v) = 0$ is harmless as far as the integration over q_x is concerned. However, this sets to zero one of the important IR scales of the diagram. We therefore make the shift $q_x \to q_x - \Delta_1$ and redefine $\overline{\Delta}_1 = w(v)\Delta_1$. Doing so

$$\mathcal{R}_{18}(k_x,p_x,l_x;\mu) = \frac{i\mu v^2}{c(v)}\int\limits_{\mathbb{R}}\frac{\mathrm{d}q_0}{(2\pi)}\int\limits_{\mathbb{R}}\frac{\mathrm{d}q_x}{(2\pi)}\left[\frac{\Theta\left(\frac{\mu}{2}+q_0\right)-\Theta\left(\frac{3\mu}{2}+q_0\right)}{2w(v)q_x+2\overline{\Delta}_1+i\mu}\right] \times\left[\frac{1}{|q_0|+|q_x|+|\Delta_2|}\right]\left[\frac{1}{|q_0+\mu|+|q_x|+|\Delta_2|}\right]. \tag{Q.217}$$

The integration over q_x is convergent in the absence of the term of order $w(v)q_x$. Neglecting this term and integrating over q_x we obtain

$$\mathcal{R}_{18}(k_x,p_x,l_x;\mu) = \frac{i\mu v^2}{\pi c(v)}\frac{1}{2\overline{\Delta}_1+i\mu}\int\limits_{-\frac{3\mu}{2}}^{-\frac{\mu}{2}}\frac{\mathrm{d}q_0}{(2\pi)}\left[\frac{\log\left(\frac{|q_0|+|\Delta_2|}{|q_0+\mu|+|\Delta_2|}\right)}{|q_0|-|q_0+\mu|}\right]. \tag{Q.218}$$

In here it becomes clear that $\overline{\Delta}_1$ plays no role in the integration at all. We therefore analyze the (*i*) $\mu \gg |\Delta_2|$ and (*ii*) $|\Delta_2| \gg \mu$ limits.

(*i*) For $\mu \gg |\Delta_2|$, we perform the scaling $q_0 \to \mu q_0$ in Eq. (Q.218) and take the $|\Delta_2|/\mu \ll 1$ limit to obtain:

$$\mathcal{R}_{18}(k_x,p_x,l_x;\mu) = \frac{i\mu v^2}{\pi c(v)}\frac{1}{2\overline{\Delta}_1+i\mu}\int\limits_{-\frac{3}{2}}^{-\frac{1}{2}}\frac{\mathrm{d}q_0}{(2\pi)}\left[\frac{\log\left(\frac{|q_0|}{|q_0+1|}\right)}{|q_0|-|q_0+1|}\right]. \tag{Q.219}$$

The integration is straightforward and yields

$$\mathcal{R}_{18}(k_x,p_x,l_x;\mu) = \frac{i\mu v^2}{16\pi^2 c(v)}\frac{1}{2\overline{\Delta}_1+i\mu}\left[\pi^2+4\log\left(\frac{27}{4}\right)\right]. \tag{Q.220}$$

As it is customary we note that we can further approximate this expression depending on the relative magnitude of $\overline{\Delta}_1$ and μ:

$$\begin{aligned}\mathcal{R}_{18}(k_x,p_x,l_x;\mu) &\overset{\mu\gg|\overline{\Delta}_1|}{=} \frac{v^2}{16\pi^2 c(v)}\left[\pi^2+4\log\left(\frac{27}{4}\right)\right],\\ \mathcal{R}_{18}(k_x,p_x,l_x;\mu) &\overset{\mu\ll|\overline{\Delta}_1|}{=} \frac{i\mu v^2}{32\pi^2 c(v)\overline{\Delta}_1}\left[\pi^2+4\log\left(\frac{27}{4}\right)\right].\end{aligned} \tag{Q.221}$$

(*ii*) For $|\Delta_2| \gg \mu$ we assume, without loss of generality, that $\Delta_2 > 0$ and perform the scaling $q_0 \to \Delta_2 q_0$ in Eq. (Q.218). To leading order in $m = \mu/\Delta_2 \ll 1$ this expression reads

$$\mathcal{R}_{18}(k_x, p_x, l_x; \mu) = \frac{i\mu v^2}{\pi c(v)} \frac{1}{2\overline{\Delta}_1 + i\mu} \int_{-\frac{3m}{2}}^{-\frac{m}{2}} \frac{\mathrm{d}q_0}{(2\pi)} \frac{1}{1 + |q_0|}. \tag{Q.222}$$

To leading order in $m \ll 1$ we obtain

$$\mathcal{R}_{18}(k_x, p_x, l_x; \mu) = \frac{i\mu v^2}{2\pi^2 c(v)} \frac{1}{2\overline{\Delta}_1 + i\mu} \frac{\mu}{|\Delta_2|}, \tag{Q.223}$$

where we have used the fact that the same result is obtained in the case that $\Delta_2 < 0$. As we did before, we approximate this expression depending on the relative magnitude amongst μ and $\overline{\Delta}_1$. Doing this yields

$$\begin{aligned} \mathcal{R}_{18}(k_x, p_x, l_x; \mu) &\overset{\mu \gg |\overline{\Delta}_1|}{=} \frac{v^2}{2\pi^2 c(v)} \frac{\mu}{|\Delta_2|}, \\ \mathcal{R}_{18}(k_x, p_x, l_x; \mu) &\overset{\mu \ll |\overline{\Delta}_1|}{=} \frac{iv^2}{4\pi^2 c(v)} \frac{\mu^2}{\overline{\Delta}_1 |\Delta_2|}. \end{aligned} \tag{Q.224}$$

Collecting the results in Eqs. (Q.220), (Q.221) and (Q.224), using the definitions $\overline{\Delta}_1 = v(p_x - k_x)$ and $\Delta_2 = vc(v)(k_x + p_x)$, and bringing back the constraint on the external momentum we can write Eq. (Q.214) as

$$\mathcal{R}_{18}(k_x, p_x, l_x; \mu) = \frac{v^2}{4\pi^2 c(v)} \Theta(\Lambda_b - |p_x - k_x|) \frac{\mathscr{U}_{18}[\mu, v(p_x - k_x), vc(v)(k_x + p_x)]}{\mathscr{R}_{18}[\mu, v(p_x - k_x), vc(v)(k_x + p_x)]}, \tag{Q.225}$$

where $\mathscr{R}_{18}(x, y, z)$ is defined as

$$\mathscr{R}_{18}(x, y, z) = \begin{cases} |x|, & |x| \gg |y|, |z|, \\ y, & |y| \gg |x|, |z|, \\ |z|, & |z| \gg |y|, |x|. \end{cases} \tag{Q.226}$$

and the crossover function $\mathscr{U}_{18}(x, y, z)$ is given by

$$\mathscr{U}_{18}(x, y, z) = \begin{cases} \frac{|x|}{4}\left[\pi^2 + \log\left(\frac{27}{4}\right)\right], & |x| \gg |y|, |z|, \\ \frac{i|x|}{8}\left[\pi^2 + \log\left(\frac{27}{4}\right)\right], & |y| \gg |x|, |z| \quad \& \quad |x| \gg |z|, \\ 2|x|, & |z| \gg |x|, |y| \quad \& \quad |x| \gg |y|, \\ \frac{ix^2}{y}, & |z| \gg |x|, |y| \quad \& \quad |y| \gg |x|. \end{cases} \tag{Q.227}$$

Q.3 One-loop Counterterm Functions to linear order in $\lambda^{\{j_i\}}_{\{N_i\};\{\sigma_i\}}(\{k_{i;N_i}\})$

Having computed the integrations appearing in the leading-order quantum effective action in Eq. (Q.2) we proceed on determining the counterterm functions that make physical

	$\mathcal{R}_x$	$\mathcal{R}_y$	$\mathcal{R}_{\frac{\pi}{2}}$	$\mathcal{R}_{\pi}$	$\mathcal{R}_{\frac{3\pi}{2}}$	$\mathcal{R}_x \circ \mathcal{R}_{\frac{\pi}{2}}$	$\mathcal{R}_y \circ \mathcal{R}_{\frac{\pi}{2}}$	Related
λ_{1111}	λ_{8888}	λ_{4444}	λ_{3333}	λ_{5555}	λ_{7777}	λ_{6666}	λ_{2222}	
λ_{1144}	λ_{8855}	λ_{4411}	λ_{3366}	λ_{5588}	λ_{7722}	λ_{6633}	λ_{2277}	
λ_{1212}	λ_{8787}	λ_{4343}	λ_{3434}	λ_{5656}	λ_{7878}	λ_{6565}	λ_{2121}	
λ_{1247}	λ_{8752}	λ_{4316}	λ_{3461}	λ_{5683}	λ_{7825}	λ_{6538}	λ_{2174}	
λ_{1313}	λ_{8686}	λ_{4242}	λ_{3535}	λ_{5757}	λ_{7171}	λ_{6464}	λ_{2828}	♣
λ_{1346}	λ_{8653}	λ_{4217}	λ_{3568}	λ_{5782}	λ_{7124}	λ_{6431}	λ_{2875}	♡
λ_{1414}	λ_{8585}	λ_{4141}	λ_{3636}	λ_{5858}	λ_{7272}	λ_{6363}	λ_{2727}	
λ_{1515}	λ_{8484}	λ_{4848}	λ_{3737}	λ_{5151}	λ_{7373}	λ_{6262}	λ_{2626}	
λ_{1526}	λ_{8473}	λ_{4837}	λ_{3748}	λ_{5162}	λ_{7384}	λ_{6251}	λ_{2615}	
λ_{1537}	λ_{8462}	λ_{4826}	λ_{3751}	λ_{5173}	λ_{7315}	λ_{6248}	λ_{2684}	
λ_{1548}	λ_{8451}	λ_{4815}	λ_{3762}	λ_{5184}	λ_{7326}	λ_{6237}	λ_{2673}	
λ_{1616}	λ_{8383}	λ_{4747}	λ_{3838}	λ_{5252}	λ_{7474}	λ_{6161}	λ_{2525}	
λ_{1634}	λ_{8365}	λ_{4721}	λ_{3856}	λ_{5278}	λ_{7412}	λ_{6143}	λ_{2587}	
λ_{1717}	λ_{8282}	λ_{4646}	λ_{3131}	λ_{5353}	λ_{7575}	λ_{6868}	λ_{2424}	♣
λ_{1724}	λ_{8275}	λ_{4631}	λ_{3146}	λ_{5368}	λ_{7582}	λ_{6853}	λ_{2417}	♡
λ_{1818}	λ_{8181}	λ_{4545}	λ_{3232}	λ_{5454}	λ_{7676}	λ_{6767}	λ_{2323}	
λ_{1823}	λ_{8176}	λ_{4532}	λ_{3245}	λ_{5467}	λ_{7681}	λ_{6754}	λ_{2318}	
λ_{1845}	λ_{8154}	λ_{4518}	λ_{3267}	λ_{5481}	λ_{7623}	λ_{6732}	λ_{2376}	

Table Q.1: Symmetry relations between the four-fermion coupling functions in terms of the hot spot indices only arising from Eq. (4.4) and up to exchange of the first two and last two indices. Here we have used the simplified notation $\lambda_{\{N_i\}} = \lambda^{\{\sigma_i\}}_{\{N_i\}}(\{k_{i;N_i}\})$ and the corresponding transformation in the momentum is left implicit. The rows marked with ♣ and ♡ are further related by the property in Eq. (4.3).

observables independent of the UV scale Λ_f to leading order in the four-fermion coupling functions. For this purpose we focus only on those coupling functions that are independent from each other with respect to the C_4 symmetry of the theory. In Table Q.1 we show the relation amongst different allowed coupling-functions as a consequence of the C_4 symmetry of the theory and up to the relation offered by Eq. (4.3). We focus only on those coupling in the first column of Table Q.1.

To linear order in the four-fermion coupling functions, there are four groups closed under the RG. These are given in Table. 4.1. Amongst the four groups, we focus on Group 1, because, in the absence of momentum dependence, these involve the zero momentum pairing channel couplings and are the only couplings sourced by the spin fluctuations in the case where all four-fermion couplings are set to zero in the UV.

Q.3-(a) Group 1

Here, we build the counterterm functions for the independent coupling functions belonging to Group 1 in Table 4.1. The coupling functions in this group correspond to $\lambda^{\{j_i\}}_{1515;\{\sigma_i\}}(\{k_{i;N_i}\})$, $\lambda^{\{j_i\}}_{1818;\{\sigma_i\}}(\{k_{i;N_i}\})$, $\lambda^{\{j_i\}}_{1845;\{\sigma_i\}}(\{k_{i;N_i}\})$ and $\lambda^{\{j_i\}}_{1548;\{\sigma_i\}}(\{k_{i;N_i}\})$.

A. *Counterterm Function for* $\lambda^{\{j_i\}}_{1515;\{\sigma_i\}}(\{k_{i;N_i}\})$

In the following we use Eq. (Q.2), the properties in Eqs. (Q.7) to (Q.9), the relations amongst couplings shown in Table Q.1 and the RG conditions in Eq. (4.57) to build the counterterm function $Z^{\{j_i\}}_{1515;\{\sigma_i\}}(\{k_{i;N_i}\})$. This one is given by

$$
\begin{aligned}
Z^{j_1j_2j_3j_4}_{1515;\sigma_1\sigma_2\sigma_3\sigma_4}(k_1^x,k_2^x,k_3^x,k_4^x) = 1 + \lambda^{j_1j_2j_3j_4}_{1515;\sigma_1\sigma_2\sigma_3\sigma_4}(k_1^x,k_2^x,k_3^x,k_4^x)^{-1}\Bigg[\\
+\frac{\pi}{8N_f}\sum_{\rho_1,\rho_2=1}^{N_c^2}\sum_{a=1}^{N_c^2-1}(\tau^a)_{\sigma_3\rho_1}(\tau^a)_{\rho_2\sigma_1}\lambda^{j_1j_2j_3j_4}_{1818;\rho_2\sigma_2\rho_1\sigma_4}\mathcal{P}_{11}(k_1^x,-k_3^x;\mu) \\
+\frac{\pi}{8N_f}\sum_{\rho_1,\rho_2=1}^{N_c^2}\sum_{a=1}^{N_c^2-1}(\tau^a)_{\sigma_3\rho_1}(\tau^a)_{\rho_2\sigma_2}\lambda^{j_1j_2j_3j_4}_{1845;\sigma_1\rho_2\rho_1\sigma_4}\mathcal{P}_{15}(k_3^x,-k_2^x;\mu) \\
+\frac{\pi}{8N_f}\sum_{\rho_1,\rho_2=1}^{N_c^2}\sum_{a=1}^{N_c^2-1}(\tau^a)_{\sigma_4\rho_1}(\tau^a)_{\rho_2\sigma_1}\lambda^{j_1j_2j_3j_4}_{1845;\rho_2\sigma_2\sigma_3\rho_1}\mathcal{P}_{15}(k_1^x,-k_4^x;\mu) \\
+\frac{\pi}{8N_f}\sum_{\rho_1,\rho_2=1}^{N_c^2}\sum_{a=1}^{N_c^2-1}(\tau^a)_{\sigma_4\rho_1}(\tau^a)_{\rho_2\sigma_2}\lambda^{j_1j_2j_3j_4}_{1818;\sigma_1\rho_2\sigma_3\rho_1}\mathcal{P}_{11}(-k_2^x,k_4^x;\mu) \\
-\frac{\pi}{8N_f}\sum_{\rho_1,\rho_2=1}^{N_c}\sum_{a=1}^{N_c^2-1}(\tau^a)_{\rho_1\sigma_2}(\tau^a)_{\rho_2\sigma_1}\lambda^{j_1j_2j_3j_4}_{1548;\rho_2\rho_1\sigma_3\sigma_4}\mathcal{P}_{15}(k_1^x,k_2^x;\mu) \\
-\frac{\pi}{8N_f}\sum_{\rho_1,\rho_2=1}^{N_c}\sum_{a=1}^{N_c^2-1}(\tau^a)_{\sigma_4\rho_1}(\tau^a)_{\sigma_3\rho_2}\lambda^{j_1j_2j_3j_4}_{1548;\sigma_1\sigma_2\rho_2\rho_1}\mathcal{P}_{15}(k_3^x,k_4^x;\mu) \\
+\frac{\pi^2}{12N_f^2}\delta_{j_1j_3}\delta_{j_2j_4}\sum_{a,b=1}^{N_c^2-1}(\tau^a\tau^b)_{\sigma_1\sigma_3}(\tau^b\tau^a)_{\sigma_2\sigma_4}\left[\mathcal{R}_{15}(k_3^x,-k_2^x,k_4^x-k_2^x;\mu)+\mathcal{R}_{15}(-k_1^x,k_4^x,k_1^x-k_3^x;\mu)\right] \\
-\frac{\pi^2}{12N_f^2}\delta_{j_1j_3}\delta_{j_2j_4}\sum_{a,b=1}^{N_c^2-1}(\tau^a\tau^b)_{\sigma_1\sigma_3}(\tau^a\tau^b)_{\sigma_2\sigma_4}\left[\mathcal{R}_{15}(k_1^x,k_2^x,k_2^x-k_4^x;\mu)+\mathcal{R}_{15}(k_1^x,k_2^x,k_3^x-k_1^x;\mu)\right].
\end{aligned}
\tag{Q.228}
$$

Here, $\mathcal{P}_{11},\mathcal{P}_{15}$ and $\mathcal{R}_{15}$ are given in Eqs. (Q.25), (Q.83) and (Q.202), respectively. As it will prove useful for determining the contribution of this counterterm function to the beta functions of the four-fermion coupling functions, let us define the differential operator

$$
\begin{aligned}
\mathsf{D} \equiv{}& \mu\frac{\partial}{\partial\mu} - \widehat{k}_{\mathrm{F}}\frac{\partial}{\partial\widehat{k}_{\mathrm{F}}} - \widehat{\Lambda}_b\frac{\partial}{\partial\widehat{\Lambda}_b} - z\widehat{\beta}_v\frac{\partial}{\partial\widehat{v}} \\
&+\sum_{\{M_i=1\}}^{8}\sum_{\{\sigma_i=1\}}^{N_c}\sum_{\{j_i=1\}}^{N_f}\left[\prod_{i=1}^{4}\int \mathrm{d}x_i\right]\widehat{\lambda}^{\{j_i\}}_{\{N_i\};\{\sigma_i\}}(\{x_i\})\frac{\delta}{\delta\widehat{\lambda}^{\{j_i\}}_{\{N_i\};\{\sigma_i\}}(\{x_i\})}.
\end{aligned}
\tag{Q.229}
$$

We now consider the following expressions:

$$
\mathsf{C}_1 = \mathsf{D}\left[\frac{\lambda^{\{j_i\}}_{\{N_i\};\{\sigma_i\}}}{\lambda^{\{l_i\}}_{\{M_i\};\{\rho_i\}}(\{x_i\})}\mathcal{P}_{11}(x,y;\mu)\right]\Bigg|_{\mu=\Lambda_f},
\tag{Q.230}
$$

$$\mathsf{C}_2 = \mathsf{D}\left[\frac{\lambda^{\{j_i\}}_{\{N_i\};\{\sigma_i\}}}{\lambda^{\{l_i\}}_{\{M_i\};\{\rho_i\}}(\{x_i\})}\mathcal{P}_{15}(x,y;\mu)\right]\Bigg|_{\mu=\Lambda_f}, \tag{Q.231}$$

$$\mathsf{C}_3 = \mathsf{D}\left[\frac{1}{\lambda^{\{l_i\}}_{\{M_i\};\{\rho_i\}}(\{x_i\})}\mathcal{R}_{15}(x,y,z;\mu)\right]\Bigg|_{\mu=\Lambda_f}. \tag{Q.232}$$

Here we have left implicit the dependence of the C_i's on the momentum, spin, flavor and hot spot indices. Using Eqs. (Q.25), (Q.83) and (Q.202) it is straightforward to see that, to leading order in $v \ll 1$,

$$\mathsf{C}_1 = \frac{w(v)}{2\pi^2}\frac{\lambda^{\{j_i\}}_{\{N_i\};\{\sigma_i\}}}{\lambda^{\{l_i\}}_{\{M_i\};\{\rho_i\}}(\{x_i\})}\Theta(\Lambda_f - v|x+y|)\Theta(\Lambda_f - vc(v)|x-y|), \tag{Q.233}$$

$$\begin{aligned}\mathsf{C}_2 = -\frac{w(v)}{2\pi^2}\frac{\lambda^{\{j_i\}}_{\{N_i\};\{\sigma_i\}}}{\lambda^{\{l_i\}}_{\{M_i\};\{\rho_i\}}(\{x_i\})}\Theta(\Lambda_f - v|x+y|)\Big\{&\Theta(\Lambda_f - vc(v)|x-y|)\log\left(c(v)\widehat{\Lambda}_b\right)\\ +\Theta(vc(v)|x-y| - \Lambda_f)\log&\left(\frac{\Lambda_b}{v|x-y|}\right)\Big\}.\end{aligned} \tag{Q.234}$$

$$\begin{aligned}\mathsf{C}_3 = -\frac{v^2}{c(v)}\frac{\Theta(\Lambda_b - |z|)\Theta(\Lambda_f - v|x+y|)}{\lambda^{\{l_i\}}_{\{M_i\};\{\rho_i\}}(\{x_i\})}\Bigg\{&\frac{\mathscr{J}_1}{\pi^2}\Theta(\Lambda_f - vc(v)|x-y|)\\ &\times\Theta(\Lambda_f - vc(v)|z-x+y|)\Theta(\Lambda_f - c(v)|z|)\\ -\frac{1}{2\pi^2}&\left(\frac{\Lambda_f}{vc(v)|z-x+y|}\right)\log\left(\frac{\Lambda_f}{vc(v)|z-x+y|}\right)\Theta(vc(v)|z-x+y| - \Lambda_f)\\ \times\Theta(c(v)|z-x+y| - |x+y|)&\Theta(|z-x+y| - |x-y|)\Theta(v|z-x+y| - |z|)\\ -\frac{1}{2\pi^2}&\left(\frac{\Lambda_f}{c(v)|z|}\right)\log\left(\frac{\Lambda_f}{c(v)|z|}\right)\Theta(c(v)|z| - \Lambda_f)\Theta(c(v)|z| - v|x+y|)\\ &\times\Theta(|z| - v|x-y|)\Theta(|z| - v|z-x+y|)\Bigg\},\end{aligned} \tag{Q.235}$$

where we have defined

$$\mathscr{J}_1 = \frac{1}{8}\left[\pi^2 + \log(2)^2 + 2\mathrm{Li}_2\left(-\frac{1}{2}\right)\right]. \tag{Q.236}$$

In Eqs. (Q.233) to (Q.235), the Heaviside functions $\Theta(x-y)$ are to be understood as enforcing the conditions $x \gg y$. Therefore, terms of the form $(y/x)\log(y/x)\Theta(x-y)$ in Eq. (Q.235) offer only negligible contributions in the range implied by the Heaviside functions. With this at hand we have that, to leading order we approximate C_3 as

$$\begin{aligned}\mathsf{C}_3 \approx -\frac{\mathscr{J}_1 v^2}{\pi^2 c(v)}\frac{1}{\lambda^{\{l_i\}}_{\{M_i\};\{\rho_i\}}(\{x_i\})}&\Theta(\Lambda_f - v|x+y|)\Theta(\Lambda_f - vc(v)|x-y|)\\ &\times\Theta(\Lambda_f - vc(v)|z-x+y|)\Theta(\Lambda_f - c(v)|z|).\end{aligned} \tag{Q.237}$$

In this expression we have also used the fact that, in the limit of interest, $\Lambda_b \gg \Lambda_f$. Therefore, $\Theta(\Lambda_b - |z|)\Theta(\Lambda_f - c(v)|z|) = \Theta(\Lambda_f - c(v)|z|)$.

B. *Counterterm Function for* $\lambda^{\{j_i\}}_{1818;\{\sigma_i\}}(\{k_{i;N_i}\})$

In the following we use Eq. (Q.2), the properties in Eqs. (Q.7) to (Q.9), the relations amongst couplings shown in Table Q.1 and the RG conditions in Eq. (4.57) to build the counterterm function $Z^{\{j_i\}}_{1818;\{\sigma_i\}}(\{k_{i;N_i}\})$. This one is given by

$$
\begin{aligned}
Z^{j_1j_2j_3j_4}_{1818;\sigma_1\sigma_2\sigma_3\sigma_4}(k_1^x,k_2^x,k_3^x,k_4^x) &= 1+\lambda^{j_1j_2j_3j_4}_{1818;\sigma_1\sigma_2\sigma_3\sigma_4}(k_1^x,k_2^x,k_3^x,k_4^x)^{-1}\Bigg[\\
&+\frac{\pi}{8N_f}\sum_{\rho_1,\rho_2=1}^{N_c^2}\sum_{a=1}^{N_c^2-1}(\tau^a)_{\sigma_3\rho_1}(\tau^a)_{\rho_2\sigma_1}\lambda^{j_1j_2j_3j_4}_{1515;\rho_2\sigma_2\rho_1\sigma_4}\mathcal{P}_{11}(k_1^x,-k_3^x;\mu)\\
&+\frac{\pi}{8N_f}\sum_{\rho_1,\rho_2=1}^{N_c^2}\sum_{a=1}^{N_c^2-1}(\tau^a)_{\sigma_3\rho_1}(\tau^a)_{\rho_2\sigma_2}\lambda^{j_1j_2j_3j_4}_{1548;\sigma_1\rho_2\rho_1\sigma_4}\mathcal{P}_{18}(-k_3^x,k_2^x;\mu)\\
&+\frac{\pi}{8N_f}\sum_{\rho_1,\rho_2=1}^{N_c^2}\sum_{a=1}^{N_c^2-1}(\tau^a)_{\sigma_4\rho_1}(\tau^a)_{\rho_2\sigma_1}\lambda^{j_1j_2j_3j_4}_{1548;\rho_2\sigma_2\sigma_3\rho_1}\mathcal{P}_{18}(k_1^x,-k_4^x;\mu)\\
&+\frac{\pi}{8N_f}\sum_{\rho_1,\rho_2=1}^{N_c^2}\sum_{a=1}^{N_c^2-1}(\tau^a)_{\sigma_4\rho_1}(\tau^a)_{\rho_2\sigma_2}\lambda^{j_1j_2j_3j_4}_{1515;\sigma_1\rho_2\sigma_3\rho_1}\mathcal{P}_{11}(-k_2^x,k_4^x;\mu) \qquad \text{(Q.238)}\\
&-\frac{\pi}{8N_f}\sum_{\rho_1,\rho_2=1}^{N_c}\sum_{a=1}^{N_c^2-1}(\tau^a)_{\rho_1\sigma_2}(\tau^a)_{\rho_2\sigma_1}\lambda^{j_1j_2j_3j_4}_{1845;\rho_2\rho_1\sigma_3\sigma_4}\mathcal{P}_{18}(k_1^x,k_2^x;\mu)\\
&-\frac{\pi}{8N_f}\sum_{\rho_1,\rho_2=1}^{N_c}\sum_{a=1}^{N_c^2-1}(\tau^a)_{\sigma_4\rho_1}(\tau^a)_{\sigma_3\rho_2}\lambda^{j_1j_2j_3j_4}_{1845;\sigma_1\sigma_2\rho_2\rho_1}\mathcal{P}_{18}(k_3^x,k_4^x;\mu)\\
&+\frac{\pi^2}{12N_f^2}\delta_{j_1j_3}\delta_{j_2j_4}\sum_{a,b=1}^{N_c^2-1}(\tau^a\tau^b)_{\sigma_1\sigma_3}(\tau^b\tau^a)_{\sigma_2\sigma_4}\left[\mathcal{R}_{18}(k_3^x,-k_2^x,k_4^x-k_2^x;\mu)+\mathcal{R}_{18}(-k_1^x,k_4^x,k_1^x-k_3^x;\mu)\right]\\
&-\frac{\pi^2}{12N_f^2}\delta_{j_1j_3}\delta_{j_2j_4}\sum_{a,b=1}^{N_c^2-1}(\tau^a\tau^b)_{\sigma_1\sigma_3}(\tau^a\tau^b)_{\sigma_2\sigma_4}\left[\mathcal{R}_{18}(k_1^x,k_2^x,k_2^x-k_4^x;\mu)+\mathcal{R}_{18}(k_1^x,k_2^x,k_3^x-k_1^x;\mu)\right].
\end{aligned}
$$

Here, $\mathcal{P}_{11},\mathcal{P}_{18}$ and $\mathcal{R}_{18}$ are given in Eqs. (Q.25), (Q.111) and (Q.225), respectively. As it will turn out to be convenient, we define the following quantities

$$
\mathsf{C}_4=\mathsf{D}\left[\frac{\lambda^{\{j_i\}}_{\{N_i\};\{\sigma_i\}}}{\lambda^{\{l_i\}}_{\{M_i\};\{\rho_i\}}(\{x_i\})}\mathcal{P}_{18}(x,y;\mu)\right]\Bigg|_{\mu=\Lambda_f}, \qquad \text{(Q.239)}
$$

$$
\mathsf{C}_5=\mathsf{D}\left[\frac{1}{\lambda^{\{l_i\}}_{\{M_i\};\{\rho_i\}}(\{x_i\})}\mathcal{R}_{18}(x,y,z;\mu)\right]\Bigg|_{\mu=\Lambda_f}, \qquad \text{(Q.240)}
$$

where D is defined in Eq. (Q.229). Here we have left implicit the dependence of the C_i's on the momentum, spin, flavor and hot spot indices. Using Eqs. (Q.25), (Q.111) and (Q.225)

we obtain

$$\mathsf{C}_4 = -\frac{w(v)}{8\pi}\Theta(\Lambda_b - |x-y|)\left\{\left(\frac{\Lambda_f}{v|x-y|}\right)\Theta(v|x-y|-\Lambda_f)\Theta(|x-y|-v|x+y|)\right.$$
$$\left. + \left(\frac{\Lambda_f}{v^2|x+y|}\right)\Theta(v|x+y|-|x-y|)\Theta(v^2|x+y|-\Lambda_f)\right\}\frac{\lambda^{\{j_i\}}_{\{N_i\};\{\sigma_i\}}}{\lambda^{\{l_i\}}_{\{M_i\};\{\rho_i\}}(\{x_i\})}, \tag{Q.241}$$

$$\mathsf{C}_5 = -\frac{\mathscr{J}_2 v^2}{\pi^2 c(v)}\frac{1}{\lambda^{\{l_i\}}_{\{M_i\};\{\rho_i\}}(\{x_i\})}\Theta(\Lambda_b-|x-y|)\Theta(\Lambda_f - vc(v)|x+y|)\Theta(\Lambda_f - v|x-y|), \tag{Q.242}$$

where we have defined

$$\mathscr{J}_2 = \frac{1}{16}\left[\pi^2 + \log\left(\frac{27}{4}\right)\right]. \tag{Q.243}$$

Because the Heaviside functions $\Theta(x-y)$ enforce the condition that $x \gg y$, those terms of the form $(y/x)\Theta(x-y)$ offer only subleading contributions in momentum. Therefore, to be consistent with the approximations we have done in computing the quantum corrections, we further approximate C_4 and C_5 as

$$\mathsf{C}_4 \approx 0 \tag{Q.244}$$

$$\mathsf{C}_5 \approx -\frac{\mathscr{J}_2 v^2}{c(v)}\frac{1}{\lambda^{\{l_i\}}_{\{M_i\};\{\rho_i\}}(\{x_i\})}\Theta(\min[v\Lambda_b,\Lambda_f]-v|x-y|)\Theta(\Lambda_f - vc(v)|x+y|). \tag{Q.245}$$

Notice that for C_5 we have used the fact that $\Theta(\Lambda_b-|x-y|)\Theta(\Lambda_f-v|x-y|) = \Theta(\min[v\Lambda_b,\Lambda_f]-v|x-y|)$.

C. *Counterterm Function for* $\lambda^{\{j_i\}}_{1845;\{\sigma_i\}}(\{k_{i;N_i}\})$

In the following we use Eq. (Q.2), the properties in Eqs. (Q.7) to (Q.9), the relations amongst couplings shown in Table Q.1 and the RG conditions in Eq. (4.57) to build the counterterm function $Z^{\{j_i\}}_{1845;\{\sigma_i\}}(\{k_{i;N_i}\})$. This one is given by

$$Z^{j_1j_2j_3j_4}_{1845;\sigma_1\sigma_2\sigma_3\sigma_4}(k^x_1,k^x_2,k^x_3,k^x_4) = 1 + \lambda^{j_1j_2j_3j_4}_{1845;\sigma_1\sigma_2\sigma_3\sigma_4}(k^x_1,k^x_2,k^x_3,k^4_x)^{-1}\Bigg[$$
$$+\frac{\pi}{8N_f}\sum_{\rho_1,\rho_2=1}^{N_c^2}\sum_{a=1}^{N_c^2-1}(\tau^a)_{\sigma_3\rho_1}(\tau^a)_{\rho_2\sigma_1}\lambda^{j_1j_2j_3j_4}_{1548;\rho_2\sigma_2\rho_1\sigma_4}\mathcal{P}_{14}(k^x_1,-k^x_3)$$
$$+\frac{\pi}{8N_f}\sum_{\rho_1,\rho_2=1}^{N_c^2}\sum_{a=1}^{N_c^2-1}(\tau^a)_{\sigma_3\rho_1}(\tau^a)_{\rho_2\sigma_2}\lambda^{j_1j_2j_3j_4}_{1515;\sigma_1\rho_2\rho_1\sigma_4}\mathcal{P}_{15}(-k^x_2,k^x_3)$$
$$+\frac{\pi}{8N_f}\sum_{\rho_1,\rho_2=1}^{N_c^2}\sum_{a=1}^{N_c^2-1}(\tau^a)_{\sigma_4\rho_1}(\tau^a)_{\rho_2\sigma_1}\lambda^{j_1j_2j_3j_4}_{1515;\rho_2\sigma_2\sigma_3\rho_1}\mathcal{P}_{15}(k^x_1,-k^x_4) \tag{Q.246}$$
$$+\frac{\pi}{8N_f}\sum_{\rho_1,\rho_2=1}^{N_c^2}\sum_{a=1}^{N_c^2-1}(\tau^a)_{\sigma_4\rho_1}(\tau^a)_{\rho_2\sigma_2}\lambda^{j_1j_2j_3j_4}_{1548;\sigma_1\rho_2\sigma_3\rho_1}\mathcal{P}_{14}(-k^x_2,k^x_4)$$

$$
\begin{aligned}
&- \frac{\pi}{8N_f} \sum_{\rho_1,\rho_2=1}^{N_c} \sum_{a=1}^{N_c^2-1} (\tau^a)_{\rho_1\sigma_2} (\tau^a)_{\rho_2\sigma_1} \lambda^{j_1 j_2 j_3 j_4}_{1818;\rho_2\rho_1\sigma_3\sigma_4} \mathcal{P}_{18}(k_1^x, k_2^x) \\
&- \frac{\pi}{8N_f} \sum_{\rho_1,\rho_2=1}^{N_c} \sum_{a=1}^{N_c^2-1} (\tau^a)_{\sigma_4\rho_1} (\tau^a)_{\sigma_3\rho_2} \lambda^{j_1 j_2 j_3 j_4}_{1818;\sigma_1\sigma_2\rho_2\rho_1} \mathcal{P}_{18}(-k_4^x, -k_3^x).
\end{aligned}
$$

Here, $\mathcal{P}_{14}$, $\mathcal{P}_{15}$ and $\mathcal{P}_{18}$ are given in Eqs. (Q.67), (Q.83) and (Q.111), respectively. At this stage it is convenient to define

$$
\mathsf{C}_6 = \mathsf{D} \left[\frac{\lambda^{\{j_i\}}_{\{N_i\};\{\sigma_i\}}}{\lambda^{\{l_i\}}_{\{M_i\};\{\rho_i\}}(\{x_i\})} \mathcal{P}_{14}(x, y; \mu) \right] \Big|_{\mu=\Lambda_f}, \tag{Q.247}
$$

where D is defined in Eq. (Q.229). Here we have left implicit the dependence of the C_6 on the momentum, spin, flavor and hot spot indices. Making use of Eq. (Q.67) it is straightforward to obtain:

$$
\mathsf{C}_6 = -\frac{w(v)}{2\pi^2} \frac{\lambda^{\{j_i\}}_{\{N_i\};\{\sigma_i\}}}{\lambda^{\{l_i\}}_{\{M_i\};\{\rho_i\}}(\{x_i\})} \log\left(\frac{1}{w(v)}\right) \Theta(\min[v\Lambda_b, \Lambda_f] - v|x-y|)\Theta(\Lambda_f - v^2|x+y|). \tag{Q.248}
$$

In arriving to this expression we have used the fact that $\Theta(\Lambda_b - |x-y|)\Theta(\Lambda_f - v|x-y|) = \Theta(\min[v\Lambda_b, \Lambda_f] - v|x-y|)$.

D. *Counterterm Function for* $\lambda^{\{j_i\}}_{1548;\{\sigma_i\}}(\{k_{i;N_i}\})$

In the following we use Eq. (Q.2), the properties in Eqs. (Q.7) to (Q.9), the relations amongst couplings shown in Table Q.1 and the RG conditions in Eq. (4.57) to build the counterterm function $Z^{\{j_i\}}_{1548;\{\sigma_i\}}(\{k_{i;N_i}\})$. This on is given by

$$
\begin{aligned}
Z^{j_1 j_2 j_3 j_4}_{1548;\sigma_1\sigma_2\sigma_3\sigma_4}(k_1,k_2,k_3,k_4) &= 1 + \lambda^{j_1 j_2 j_3 j_4}_{1548;\sigma_1\sigma_2\sigma_3\sigma_4}(k_1^x, k_2^x, k_x^3, k_4^x)^{-1} \Bigg[\\
&+ \frac{\pi}{8N_f} \sum_{\rho_1,\rho_2=1}^{N_c^2} \sum_{a=1}^{N_c^2-1} (\tau^a)_{\sigma_3\rho_1} (\tau^a)_{\rho_2\sigma_1} \lambda^{j_1 j_2 j_3 j_4}_{1845;\rho_2\sigma_2\rho_1\sigma_4} \mathcal{P}_{14}(k_1^x, -k_3^x) \\
&+ \frac{\pi}{8N_f} \sum_{\rho_1,\rho_2=1}^{N_c^2} \sum_{a=1}^{N_c^2-1} (\tau^a)_{\sigma_3\rho_1} (\tau^a)_{\rho_2\sigma_2} \lambda^{j_1 j_2 j_3 j_4}_{1818;\sigma_1\rho_2\rho_1\sigma_4} \mathcal{P}_{18}(-k_2^x, k_3^x) \\
&+ \frac{\pi}{8N_f} \sum_{\rho_1,\rho_2=1}^{N_c^2} \sum_{a=1}^{N_c^2-1} (\tau^a)_{\sigma_4\rho_1} (\tau^a)_{\rho_2\sigma_1} \lambda^{j_1 j_2 j_3 j_4}_{1818;\rho_2\sigma_2\sigma_3\rho_1} \mathcal{P}_{18}(k_1^x, -k_4^x) \\
&+ \frac{\pi}{8N_f} \sum_{\rho_1,\rho_2=1}^{N_c^2} \sum_{a=1}^{N_c^2-1} (\tau^a)_{\sigma_4\rho_1} (\tau^a)_{\rho_2\sigma_2} \lambda^{j_1 j_2 j_3 j_4}_{1845;\sigma_1\rho_2\sigma_3\rho_1} \mathcal{P}_{14}(k_4^x, -k_2^x) \\
&- \frac{\pi}{8N_f} \sum_{\rho_1,\rho_2=1}^{N_c} \sum_{a=1}^{N_c^2-1} (\tau^a)_{\rho_1\sigma_2} (\tau^a)_{\rho_2\sigma_1} \lambda^{j_1 j_2 j_3 j_4}_{1515;\rho_2\rho_1\sigma_3\sigma_4} \mathcal{P}_{15}(k_1^x, k_2^x)
\end{aligned} \tag{Q.249}
$$

$$-\frac{\pi}{8N_f}\sum_{\rho_1,\rho_2=1}^{N_c}\sum_{a=1}^{N_c^2-1}(\tau^a)_{\sigma_4\rho_1}(\tau^a)_{\sigma_3\rho_2}\lambda^{j_1j_2j_3j_4}_{1515;\sigma_1\sigma_2\rho_2\rho_1}\mathcal{P}_{15}(-k_4^x,-k_3^x).$$

Here, $\mathcal{P}_{14}$, $\mathcal{P}_{15}$ and $\mathcal{P}_{18}$ are given in Eqs. (Q.67), (Q.83) and (Q.111), respectively.

Q.3-(*b*) Quantum Corrections to Quadratic Order in $\lambda^{\{j_i\}}_{\{N_i\};\{\sigma_i\}}(\{k_{i;N_i}\})$

We turn our attention to the corrections of the quantum effective action at quadratic order in the four-fermion couplings and focus only on the four-point vertex function. In the presence of momentum dependence in the coupling functions, this one reads,

$$\begin{aligned}
&{}_2\Gamma^{j_1j_2j_3j_4}_{N_1N_2N_3N_4;\sigma_1\sigma_2\sigma_3\sigma_4}(k_1,k_2,k_3,k_4)= \qquad (Q.250)\\
&-\frac{1}{2\mu^2}\sum_{l_1,l_2=1}^{N_f}\sum_{\rho_1,\rho_2=1}^{N_c}\sum_{M_1,M_2=1}^{8}\int \mathrm{d}q\lambda^{j_1l_1j_3l_2}_{N_1M_1N_3M_2;\sigma_1\rho_1\sigma_3\rho_2}(k_{1;N_1},[q-k_1]_{M_1},k_{3;N_3},[q-k_3]_{M_2})\\
&\times\lambda^{l_2j_2l_1j_4}_{M_2N_2M_1N_4;\rho_2\sigma_2\rho_1\sigma_4}([q-k_3]_{M_2},k_{2;N_2},[q-k_1]_{M_1},k_{4;N_4})G_{M_1}(q-k_1)G_{M_2}(q-k_3)\\
&+\frac{1}{2\mu^2}\sum_{l_1,l_2=1}^{N_f}\sum_{\rho_1,\rho_2=1}^{N_c}\sum_{M_1,M_2=1}^{8}\int \mathrm{d}q\lambda^{l_1j_2j_3l_2}_{M_1N_2N_3M_2;\rho_1\sigma_2\sigma_3\rho_2}([q-k_2]_{M_1},k_{2;N_2},k_{3;N_3},[q-k_3]_{M_2})\\
&\times\lambda^{j_1l_2l_1j_4}_{N_1M_2M_1N_4;\sigma_1\rho_2\rho_1\sigma_4}(k_{2;N_1},[q-k_3]_{N_2},[q-k_2]_{N_3},k_{4;N_4})G_{M_1}(q-k_2)G_{M_2}(q-k_3)\\
&+\frac{1}{2\mu^2}\sum_{l_1,l_2=1}^{N_f}\sum_{\rho_1,\rho_2=1}^{N_c}\sum_{M_1,M_2=1}^{8}\int \mathrm{d}q\lambda^{j_1l_1l_2j_4}_{N_1M_1M_2N_4;\sigma_1\rho_1\rho_2\sigma_4}(k_{1;N_1},[q-k_1]_{M_1},[q-k_4]_{M_2},k_{4;N_4})\\
&\times\lambda^{l_2j_2j_3l_1}_{M_2N_2N_3M_1;\rho_2\sigma_2\sigma_3\rho_1}([q-k_4]_{M_2},k_{2;N_2},k_{3;N_3},[q-k_1]_{M_1})G_{M_1}(q-k_1)G_{M_2}(q-k_4)\\
&-\frac{1}{2\mu^2}\sum_{l_1,l_2=1}^{N_f}\sum_{\rho_1,\rho_2=1}^{N_c}\sum_{M_1,M_2=1}^{8}\int \mathrm{d}q\lambda^{l_1j_2l_2j_4}_{M_1N_2M_2N_4;\rho_1\sigma_2\rho_2\sigma_4}([q-k_2]_{M_1},k_{2;N_2},[q-k_4]_{M_2},k_{4;N_4})\\
&\times\lambda^{j_1l_2j_3l_1}_{N_1M_2N_3M_1;\sigma_1\rho_2\sigma_3\rho_1}(k_{1;N_1},[q-k_4]_{M_2},k_{3;N_3},[q-k_2]_{M_1})G_{M_1}(q-k_2)G_{M_2}(q-k_4)\\
&+\frac{1}{2\mu^2}\sum_{l_1,l_2=1}^{N_f}\sum_{\rho_1,\rho_2=1}^{N_c}\sum_{M_1,M_2=1}^{8}\int \mathrm{d}q\lambda^{j_1j_2l_1l_2}_{N_1N_2M_1M_2;\sigma_1\sigma_2\rho_1\rho_2}(k_{1;N_1},k_{2;N_2},[k_1+q]_{M_1},[k_2-q]_{M_2})\\
&\times\lambda^{l_1l_2j_3j_4}_{M_1M_2N_3N_4;\rho_1\rho_2\sigma_3\sigma_4}([k_1+q]_{M_1},[k_2-q]_{M_2},k_{3;N_3},k_{4;N_4})G_{M_1}(q+k_1)G_{M_2}(k_2-q).
\end{aligned}$$

To a first approximation in the WMDL, one can ignore the momentum dependence in the coupling functions. In doing so, Eq. (Q.250) takes the simpler form

$$\begin{aligned}
&{}_2\Gamma^{j_1j_2j_3j_4}_{N_1N_2N_3N_4;\sigma_1\sigma_2\sigma_3\sigma_4}(k_1,k_2,k_3,k_4)= \qquad (Q.251)\\
&-\frac{1}{2\mu}\sum_{l_1,l_2=1}^{N_f}\sum_{\rho_1,\rho_2=1}^{N_c}\sum_{M_1,M_2=1}^{8}\lambda^{j_1l_1j_3l_2}_{N_1M_1N_3M_2;\sigma_1\rho_1\sigma_3\rho_2}\lambda^{l_2j_2l_1j_4}_{M_2N_2M_1N_4;\rho_2\sigma_2\rho_1\sigma_4}\mathcal{O}_{M_1M_2}(k_1,k_3)\\
&+\frac{1}{2\mu}\sum_{l_1,l_2=1}^{N_f}\sum_{\rho_1,\rho_2=1}^{N_c}\sum_{M_1,M_2=1}^{8}\lambda^{l_1j_2j_3l_2}_{M_1N_2N_3M_2;\rho_1\sigma_2\sigma_3\rho_2}\lambda^{j_1l_2l_1j_4}_{N_1M_2M_1N_4;\sigma_1\rho_2\rho_1\sigma_4}\mathcal{O}_{M_1M_2}(k_2,k_3)
\end{aligned}$$

$$+\frac{1}{2\mu}\sum_{l_1,l_2=1}^{N_f}\sum_{\rho_1,\rho_2=1}^{N_c}\sum_{M_1,M_2=1}^{8}\lambda^{j_1 l_1 l_2 j_4}_{N_1 M_1 M_2 N_4;\sigma_1\rho_1\rho_2\sigma_4}\lambda^{l_2 j_2 j_3 l_1}_{M_2 N_2 N_3 M_1;\rho_2\sigma_2\sigma_3\rho_1}\mathcal{O}_{M_1 M_2}(k_1,k_4)$$
$$-\frac{1}{2\mu}\sum_{l_1,l_2=1}^{N_f}\sum_{\rho_1,\rho_2=1}^{N_c}\sum_{M_1,M_2=1}^{8}\lambda^{l_1 j_2 l_2 j_4}_{M_1 N_2 M_2 N_4;\rho_1\sigma_2\rho_2\sigma_4}\lambda^{j_1 l_2 j_3 l_1}_{N_1 M_2 N_3 M_1;\sigma_1\rho_2\sigma_3\rho_1}\mathcal{O}_{M_1 M_2}(k_2,k_4)$$
$$+\frac{1}{2\mu}\sum_{l_1,l_2=1}^{N_f}\sum_{\rho_1,\rho_2=1}^{N_c}\sum_{M_1,M_2=1}^{8}\lambda^{j_1 j_2 l_1 l_2}_{N_1 N_2 M_1 M_2;\sigma_1\sigma_2\rho_1\rho_2}\lambda^{l_1 l_2 j_3 j_4}_{M_1 M_2 N_3 N_4;\rho_1\rho_2\sigma_3\sigma_4}\mathcal{Q}_{M_1 M_2}(k_1,k_2),$$

where we have defined the integrations

$$\mathcal{O}_{MN}(k,p)=\mu^{-1}\int \mathrm{d}q G_M(q-k)G_N(q-p), \tag{Q.252}$$
$$\mathcal{Q}_{MN}(k,p)=\mu^{-1}\int \mathrm{d}q G_M(q+k)G_N(p-q). \tag{Q.253}$$

In the absence of the curvature of the FS, these two integrations are related due to the particle-hole symmetry of the theory:

$$\mathcal{O}_{MN}(k,p)=-\mathcal{Q}_{MN}(-k,p). \tag{Q.254}$$

There are, in principle, sixty-four different integrations of the form given in Eq. (Q.253). However, this expression satisfies the following symmetry properties inherited from the C_4 symmetry of the theory and the freedom of relabeling the loop momenta:

$$\begin{aligned}\mathcal{Q}_{MN}(k,p)&=\mathcal{Q}_{NM}(p,k),\\ \mathcal{Q}_{[1-M]_8[1-N]_8}(k,p)&=\mathcal{Q}_{MN}(k^x,p^x),\\ \mathcal{Q}_{[M+2]_8[N+2]_8}(k,p)&=\mathcal{Q}_{MN}\left(k^{\frac{\pi}{2}},p^{\frac{\pi}{2}}\right),\end{aligned} \tag{Q.255}$$

where $[x]_8$ denotes the reminder of x divided by 8, $k^x=(k_0,-k_x,k_y)$ and $k^{\frac{\pi}{2}}=(k_0,-k_y,k_x)$. In what follows we analyze $\mathcal{Q}_{MN}(k,p)$ for the cases $M=1$ and $N=1,\ldots,8$. All other choices of hot spot indices can be obtained from these ones through the symmetry properties in Eq. (Q.255).

Q.3-(c) The $\mathcal{Q}_{MN}$ Integrals

To simplify the computation of the $\mathcal{Q}_{MN}$ integrations we consider them at the RG condition in Eq. (4.57).

A. $\mathcal{Q}_{11}(k,p)$

At the RG condition in Eq. (4.57) and at zero external momentum, the integration in Eq. (Q.253) for $M=1$ and $N=1$ reads

$$\mathcal{Q}_{11}(\mu)=\mu^{-1}\int \mathrm{d}q\left[\frac{1}{i\left(\frac{3\mu}{2}+q_0\right)+vq_x+q_y}\right]\left[\frac{1}{-i\left(\frac{\mu}{2}+q_0\right)-vq_x-q_y}\right]. \tag{Q.256}$$

According to the discussion in Sec. 4.2-(*a*) , the integration over q_y and q_x is done over the momentum range:

$$|vq_x + q_y| < \Lambda_f \quad \& \quad |q_x - vq_y| < k_{\rm F}. \tag{Q.257}$$

To make this cutoff structure explicit, we change variables to momentum away and along the local FS at hot spot $N = 1$:

$$Y = vq_x - q_y, \qquad X = q_x - vq_y. \tag{Q.258}$$

With this change of variables, Eq. (Q.256) takes the following form

$$\mathcal{Q}_{11}(\mu) = \mu^{-1} \int\limits_{\mathbb{R}} \frac{\mathrm{d}q_0}{(2\pi)} \int\limits_{-k_{\rm F}}^{k_{\rm F}} \frac{\mathrm{d}X}{(2\pi)} \int\limits_{-\Lambda_f}^{\Lambda_f} \frac{\mathrm{d}Y}{(2\pi)} \left[\frac{1}{i\left(\frac{3\mu}{2} + q_0\right) + Y} \right] \left[\frac{1}{-i\left(\frac{\mu}{2} + q_0\right) - Y} \right]. \tag{Q.259}$$

Clearly, the integration over X decouples and yields an enhancement in the size of the patch of the FS. The integration over Y is finite in the $\Lambda_f/\mu \gg 1$ limit. Therefore, integrating over Y and q_0 yields the finite contribution

$$\mathcal{Q}_{11}(\mu) = -\frac{k_{\rm F}}{4\pi^2 \mu}. \tag{Q.260}$$

It is not difficult to see that this offers no contribution to the beta functions of the four-fermion couplings. Therefore, we do not consider Eq. (Q.256) in the presence of nonzero external momentum.

B. $\mathcal{Q}_{12}(k, p)$

At the RG condition in Eq. (4.57) and at zero external momentum, the integration in Eq. (Q.253) for $M = 1$ and $N = 2$ reads

$$\mathcal{Q}_{12}(\mu) = \mu^{-1} \int \mathrm{d}q \left[\frac{1}{i\left(\frac{3\mu}{2} + q_0\right) + vq_x + q_y} \right] \left[\frac{1}{-i\left(\frac{\mu}{2} + q_0\right) + q_x + vq_y} \right]. \tag{Q.261}$$

According to the discussion in Sec. 4.2-(*a*) , the integration over q_y and q_x is done over the momentum range:

$$|vq_x + q_y| < \Lambda_f \quad \& \quad |q_x - vq_y| < k_{\rm F}. \tag{Q.262}$$

To make this cutoff structure explicit, we change variables to momentum away and along the local FS at hot spot $N = 1$:

$$Y = vq_x - q_y, \qquad X = q_x + vq_y. \tag{Q.263}$$

Under this change of variables, the integration domain changes to

$$|Y| < \Lambda_f, \quad \& \quad |Y - 2vX| < k_{\rm F}. \tag{Q.264}$$

Since $\Lambda_f \ll k_{\rm F}$ it becomes clear that the X integration is cutoff by $k_{\rm F}/v$. With this at hand, we can write Eq. (Q.261) in terms of the new variables as

$$\mathcal{Q}_{12}(\mu) = \mu^{-1} \int_{\mathbb{R}} \frac{\mathrm{d}q_0}{(2\pi)} \int_{-\Lambda_f}^{\Lambda_f} \frac{\mathrm{d}Y}{(2\pi)} \int_{-\frac{k_{\rm F}}{v}}^{\frac{k_{\rm F}}{v}} \frac{\mathrm{d}X}{(2\pi)} \left[\frac{1}{i\left(\frac{3\mu}{2}+q_0\right)+Y}\right] \left[\frac{1}{-i\left(\frac{\mu}{2}+q_0\right)+X}\right]. \quad \text{(Q.265)}$$

Integration over q_0 yields

$$\mathcal{Q}_{12}(\mu) = \mu^{-1} \int_{-\Lambda_f}^{\Lambda_f} \frac{\mathrm{d}Y}{(2\pi)} \int_{-\frac{k_{\rm F}}{v}}^{\frac{k_{\rm F}}{v}} \frac{\mathrm{d}X}{(2\pi)} \left[\frac{\Theta(X)-\Theta(-Y)}{X+Y+i\mu}\right]. \quad \text{(Q.266)}$$

To proceed on integrating we note that, upon the shift $X \to X - Y$, the integration takes the form

$$\mathcal{Q}_{12}(\mu) = \mu^{-1} \int_{-\Lambda_f}^{\Lambda_f} \frac{\mathrm{d}Y}{(2\pi)} \int_{-\frac{k_{\rm F}}{v}}^{\frac{k_{\rm F}}{v}} \frac{\mathrm{d}X}{(2\pi)} \left[\frac{\Theta(X-Y)-\Theta(-Y)}{X+i\mu}\right]. \quad \text{(Q.267)}$$

In here, we have neglected the shift in the cutoff of the X integration because Y is at most of order $\Lambda_f \ll k_{\rm F}/v$. Symmetrizing in both X and Y yields

$$\mathcal{Q}_{12}(\mu) = \mu^{-1} \int_{0}^{\Lambda_f} \frac{\mathrm{d}Y}{(2\pi)} \int_{Y}^{\frac{k_{\rm F}}{v}} \frac{\mathrm{d}X}{(2\pi)} \frac{2X}{X^2+\mu^2}. \quad \text{(Q.268)}$$

In the $k_{\rm F} \gg \Lambda_f \gg \mu$ limits, we obtain the leading order power-law divergent term

$$\mathcal{Q}_{12}(\mu) = \frac{1}{2\pi^2}\left(\frac{\Lambda_f}{\mu}\right)\log\left(\frac{k_{\rm F}}{v\Lambda_f}\right). \quad \text{(Q.269)}$$

Despite the logarithmic divergent coefficient in the $k_{\rm F} \gg \Lambda_f$ limit, this expression offers no contribution to the beta functions of the four-fermion couplings. For nonzero external momentum, this fact remains unchanged.

C. $\mathcal{Q}_{13}(k,p)$

At the RG condition in Eq. (4.57) and at zero external momentum, the integration in Eq. (Q.253) for $M=1$ and $N=3$ reads

$$\mathcal{Q}_{13}(\mu) = \mu^{-1} \int \mathrm{d}q \left[\frac{1}{i\left(\frac{3\mu}{2}+q_0\right)+vq_x+q_y}\right] \left[\frac{1}{-i\left(\frac{\mu}{2}+q_0\right)-q_x+vq_y}\right]. \quad \text{(Q.270)}$$

According to the discussion in Sec. 4.2-(*a*) , the integration over q_y and q_x is done over the momentum range:

$$|vq_x + q_y| < \Lambda_f \quad \& \quad |q_x - vq_y| < k_{\rm F}. \tag{Q.271}$$

To make this cutoff structure explicit, we change variables to momentum away and along the local FS at hot spot $N = 1$:

$$Y = vq_x - q_y, \qquad X = q_x - vq_y. \tag{Q.272}$$

Under this change of variables, Eq. (Q.270) takes the same form as Eq. (Q.265) except for the fact that the X integration is cutoff by $k_{\rm F}$ only. It is straightforward to see that

$$\mathcal{Q}_{13}(\mu) = \frac{1}{2\pi^2}\left(\frac{\Lambda_f}{\mu}\right)\log\left(\frac{k_{\rm F}}{\Lambda_f}\right), \tag{Q.273}$$

in the $k_{\rm F} \gg \Lambda_f$ limit. Once again, this expression will offer no contribution to the beta functions of the four-fermion couplings and therefore, it is not necessary to take a look at the nonzero external momentum case.

D. $\mathcal{Q}_{14}(k,p)$

At the RG condition in Eq. (4.57) and at zero external momentum, the integration in Eq. (Q.253) for $M = 1$ and $N = 4$ reads

$$\mathcal{Q}_{14}(\mu) = \mu^{-1}\int {\rm d}q \left[\frac{1}{i\left(\frac{3\mu}{2} + q_0\right) + vq_x + q_y}\right]\left[\frac{1}{-i\left(\frac{\mu}{2} + q_0\right) - vq_x + q_y}\right]. \tag{Q.274}$$

According to the discussion in Sec. 4.2-(*a*) , the integration over q_y and q_x is done over the momentum range:

$$|vq_x + q_y| < \Lambda_f \quad \& \quad |q_x - vq_y| < k_{\rm F}. \tag{Q.275}$$

It is convenient to change variables to

$$Y = vq_x + q_y, \qquad Y = q_x - vq_y. \tag{Q.276}$$

Under this change of variables Eq. (Q.274) can be written, to leading order in $v \ll 1$, as

$$\mathcal{Q}_{14}(\mu) = \mu^{-1}\int\limits_{\mathbb{R}}\frac{{\rm d}q_0}{(2\pi)}\int\limits_{-\Lambda_f}^{\Lambda_f}\frac{{\rm d}Y}{(2\pi)}\int\limits_{-k_{\rm F}}^{k_{\rm F}}\frac{{\rm d}X}{(2\pi)}\left[\frac{1}{i\left(\frac{3\mu}{2} + q_0\right) + Y}\right]\left[\frac{1}{-i\left(\frac{\mu}{2} + q_0\right) + Y - 2vX}\right]. \tag{Q.277}$$

We note that if one sets $v = 0$, the integration diverges linearly in the large $k_{\rm F}$ limit. For nonzero v, the integration is convergent for $k_{\rm F} \gg \mu$. Scaling $X \to X/v$ allows us to write

$$\mathcal{Q}_{14}(\mu) = \frac{1}{v\mu}\int\limits_{\mathbb{R}}\frac{{\rm d}q_0}{(2\pi)}\int\limits_{-\Lambda_f}^{\Lambda_f}\frac{{\rm d}Y}{(2\pi)}\int\limits_{-vk_{\rm F}}^{vk_{\rm F}}\frac{{\rm d}X}{(2\pi)}\left[\frac{1}{i\left(\frac{3\mu}{2} + q_0\right) + Y}\right]\left[\frac{1}{-i\left(\frac{\mu}{2} + q_0\right) + Y - 2X}\right]. \tag{Q.278}$$

Integrating over q_0 yields

$$\mathcal{Q}_{14}(\mu) = \frac{1}{v\mu}\int_{-\Lambda_f}^{\Lambda_f}\frac{\mathrm{d}Y}{(2\pi)}\int_{-vk_{\mathrm{F}}}^{vk_{\mathrm{F}}}\frac{\mathrm{d}X}{(2\pi)}\left[\frac{\Theta(Y-2X)-\Theta(-Y)}{i\mu+2(Y-X)}\right]. \tag{Q.279}$$

We consider this integral in two main cases: when (*i*) $\Lambda_f \gg vk_{\mathrm{F}}$ and (*ii*) $\Lambda_f \gg vk_{\mathrm{F}}$.

(*i*) In the case that $\Lambda_f \gg vk_{\mathrm{F}}$, we can make the shift $Y \to Y + X$ and write Eq. (Q.279) as

$$\mathcal{Q}_{14}(\mu) = \frac{1}{v\mu}\int_{-\Lambda_f}^{\Lambda_f}\frac{\mathrm{d}Y}{(2\pi)}\int_{-vk_{\mathrm{F}}}^{vk_{\mathrm{F}}}\frac{\mathrm{d}X}{(2\pi)}\left[\frac{\Theta(Y-X)-\Theta(-Y-X)}{i\mu+2Y}\right]. \tag{Q.280}$$

The shift in the cutoff of the Y integration has been neglected because X is at most of order $vk_{\mathrm{F}} \ll \Lambda_f$. Symmetrizing in both X and Y we obtain

$$\mathcal{Q}_{14}(\mu) = \frac{1}{v\mu}\int_{0}^{vk_{\mathrm{F}}}\frac{\mathrm{d}X}{(2\pi)}\int_{X}^{\Lambda_f}\frac{\mathrm{d}Y}{(2\pi)}\frac{8Y}{4Y^2+\mu^2}. \tag{Q.281}$$

The integration over Y followed by the integration over X yields, in the $\Lambda_f \gg vk_{\mathrm{F}} \gg \mu$ limit

$$\mathcal{Q}_{14}(\mu) = \frac{k_{\mathrm{F}}}{2\pi^2\mu}\log\left(\frac{\Lambda_f}{vk_{\mathrm{F}}}\right). \tag{Q.282}$$

Similarly as in previous cases, this provides no contribution to the beta function for the four-fermion couplings.

(*ii*) When $\Lambda_f \ll vk_{\mathrm{F}}$ we can perform the shift $X \to X + Y$ and write Eq. (Q.279) as

$$\mathcal{Q}_{14}(\mu) = \frac{1}{v\mu}\int_{-\Lambda_f}^{\Lambda_f}\frac{\mathrm{d}Y}{(2\pi)}\int_{-vk_{\mathrm{F}}}^{vk_{\mathrm{F}}}\frac{\mathrm{d}X}{(2\pi)}\left[\frac{\Theta(-Y-2X)-\Theta(-Y)}{i\mu-2X}\right]. \tag{Q.283}$$

Once again, the cutoff in the X integration has been left untouched because Y is at most of order $\Lambda_f \ll vk_{\mathrm{F}}$. After symmetrizing in X and Y we can write

$$\mathcal{Q}_{14}(\mu) = \frac{1}{v\mu}\int_{0}^{\Lambda_f}\frac{\mathrm{d}Y}{(2\pi)}\int_{Y/2}^{vk_{\mathrm{F}}}\frac{\mathrm{d}X}{(2\pi)}\frac{4X}{4X^2+\mu^2}. \tag{Q.284}$$

The integration over X and Y yield the divergent contribution in the $vk_{\mathrm{F}} \gg \Lambda_f$ limits:

$$\mathcal{Q}_{14}(\mu) = \frac{\Lambda_f}{4\pi v\mu}\log\left(\frac{vk_{\mathrm{F}}}{\Lambda_f}\right). \tag{Q.285}$$

In contrast to the limit in which Λ_f is the largest scale, this term has an enhancement in $1/v$. This yields a significant contribution to the beta functions of the four-fermion couplings due to the flow of v. However, as we are about to see, the enhancement is rather minimal compared to that of the case in which $N = 1$ and $M = 5$. Furthermore, Eq. (Q.274) yields the same result in the presence of nonzero momentum as a consequence of the integral being IR in the $\mu = 0$ limit.

E. $\mathcal{Q}_{15}(k, p)$

For $M = 1$ and $N = 5$, the integral in Eq. (Q.253) evaluated at the frequencies implied by the RG condition in Eq. (4.57), reads

$$\mathcal{Q}_{15}(\vec{k},\vec{p};\mu) = \mu^{-1}\int \mathrm{d}q \left[\frac{1}{i\left(\frac{3\mu}{2}+q_0\right)+vq_x+q_y+e_1(\vec{k};v)}\right] \times\left[\frac{1}{-i\left(\frac{\mu}{2}+q_0\right)+vq_x+q_y+e_5(\vec{p};v)}\right]. \tag{Q.286}$$

According to the discussion in Sec. 4.2-(*a*) , the integration over the momenta is limited to the region:

$$|vq_x+q_y+e_1(\vec{k};v)|<\Lambda_f \quad |vq_x+q_y+e_5(\vec{k};v)|<\Lambda_f, \quad \& \quad |q_y-vq_x|<k_{\mathrm{F}}. \tag{Q.287}$$

To make the integration depend explicitly on the UV cutoff we consider the change of variables

$$Y = vq_x+q_y, \qquad \& \qquad X = q_x - vq_y. \tag{Q.288}$$

With this change of variables, the integration domain is transformed to

$$|Y+e_1(\vec{k};v)|<\Lambda_f \quad \& \quad |Y+e_5(\vec{k};v)|<\Lambda_f, \quad \& \quad |X|<k_{\mathrm{F}}. \tag{Q.289}$$

which requires the energy of the electrons to be constrained as $|e_1(\vec{k};v)| \ll \Lambda_f$ and $|e_5(\vec{k};v)| \ll \Lambda_f$ so that the integration over Y has nonzero support. In the case that $|e_1(\vec{k};v)| \ll \Lambda_f$ and $|e_5(\vec{k};v)| \ll \Lambda_f$, the integration over Y is cutoff by Λ_f. Keeping this constraint implicit, and noting that the X integration decouples, we can write Eq. (Q.290) as

$$\mathcal{Q}_{15}(\vec{k},\vec{p};\mu) = \frac{k_{\mathrm{F}}}{2\pi\mu}\int_{\mathbb{R}}\frac{\mathrm{d}q_0}{(2\pi)}\int_{-\Lambda_f}^{\Lambda_f}\frac{\mathrm{d}Y}{(2\pi)}\left[\frac{1}{i\left(\frac{3\mu}{2}+q_0\right)+Y+e_1(\vec{k};v)}\right] \times\left[\frac{1}{-i\left(\frac{\mu}{2}+q_0\right)+Y+e_5(\vec{p};v)}\right]. \tag{Q.290}$$

Integration over the frequency yields

$$\mathcal{Q}_{15}(\vec{k},\vec{p};\mu) = \frac{k_{\mathrm{F}}}{2\pi\mu}\int_{-\Lambda_f}^{\Lambda_f}\frac{\mathrm{d}Y}{(2\pi)}\left[\frac{\Theta[Y+e_1(\vec{k};v)]-\Theta[-Y-e_5(\vec{p};v)]}{i\mu+2Y+e_1(\vec{k};v)+e_5(\vec{p};v)}\right]. \tag{Q.291}$$

We continue on analyzing this expression by making the shift $Y \to Y - e_1(\vec{k}; v)$, under which we obtain

$$\mathcal{Q}_{15}(\vec{k}, \vec{p}; \mu) = \frac{k_{\rm F}}{2\pi\mu} \int_{-\Lambda_f}^{\Lambda_f} \frac{{\rm d}Y}{(2\pi)} \left[\frac{\Theta(Y) - \Theta(-Y - \Delta)}{i\mu + 2Y + \Delta} \right]. \tag{Q.292}$$

Here we have defined $\Delta \equiv e_5(\vec{p}; v) - e_1(\vec{k}; v) = -e_1(\vec{p} + \vec{k}; v)$, where the last equality follows from the fact that $e_1(\vec{p}; v) = -e_5(\vec{p}; v)$ and that the electronic dispersions are linear functions of momentum in the absence of the curvature of the FS. We have further neglected the shift in the UV cutoff because we are considering the limit in which $\Lambda_f \gg |e_1(\vec{k}; v)|$. We continue analyzing this expression in the limits in which (*i*) $\mu \gg |\Delta|$ and (*ii*) $\mu \ll |\Delta|$.

(*i*) For $\mu \gg |\Delta|$ we consider the scaling $Y \to \mu Y$ and take the $|\Delta|/\mu \ll 1$ limit. Defining $\overline{\Lambda}_f = \Lambda_f/\mu$, Eq. (Q.292) takes the form

$$\mathcal{Q}_{15}(\vec{k}, \vec{p}; \mu) = \frac{k_{\rm F}}{2\pi\mu} \int_{-\overline{\Lambda}_f}^{\overline{\Lambda}_f} \frac{{\rm d}Y}{(2\pi)} \left[\frac{\Theta(Y) - \Theta(-Y)}{i + 2Y} \right]. \tag{Q.293}$$

Integration over Y yields the logarithmically divergent contribution

$$\mathcal{Q}_{15}(k, p; \mu) = \frac{k_{\rm F}}{4\pi^2\mu} \log\left(\frac{\Lambda_f}{\mu} \right). \tag{Q.294}$$

(*ii*) For $|\Delta| \gg \mu$ we assume that $\Delta > 0$ without loss of generality and consider the scaling $Y \to \Delta Y$ and take the $\mu/\Delta \ll 1$ limit. Defining $\overline{\Lambda}_f = \Lambda_f/\Delta$, Eq. (Q.292) takes the form

$$\mathcal{Q}_{15}(\vec{k}, \vec{p}; \mu) = \int_{-\overline{\Lambda}_f}^{\overline{\Lambda}_f} \frac{{\rm d}Y}{(2\pi)} \left[\frac{\Theta(Y) - \Theta(-Y - 1)}{2Y + 1} \right]. \tag{Q.295}$$

Integration over Y yields the logarithmically divergent contribution

$$\mathcal{Q}_{15}(k, p; \mu) = \frac{k_{\rm F}}{4\pi^2\mu} \log\left(\frac{\Lambda_f}{|\Delta|} \right), \tag{Q.296}$$

where we have used the fact that the $\Delta < 0$ case yields the exact same contribution.

Collecting the two results, it follows that Eq. (Q.286) can be written as

$$\mathcal{Q}_{15}(\vec{k}, \vec{p}; \mu) = \frac{k_{\rm F}}{4\pi^2\mu} \log\left(\frac{\Lambda_f}{\mathscr{I}_{15}(\mu, |e_1(\vec{k} + \vec{p}; v)|)} \right), \tag{Q.297}$$

where $\mathscr{I}_{15}(x, y) \sim \max(x, y)$. The logarithmic divergence combined with the enhancement by $k_{\rm F}$ yields a significant contribution to the beta functions of the four-fermion couplings. In fact, this is much larger than that of the case in which $M = 1$ and $N = 4$, where the effective enhancement appearing in the beta functions is at most of order $\log(1/v)$.

F. $\mathcal{Q}_{16}(k,p)$

At the RG condition in Eq. (4.57) and at zero external momentum, the integration in Eq. (Q.253) for $M=1$ and $N=6$ reads

$$\mathcal{Q}_{16}(\mu)=\mu^{-1}\int \mathrm{d}q\left[\frac{1}{i\left(\frac{3\mu}{2}+q_0\right)+vq_x+q_y}\right]\left[\frac{1}{-i\left(\frac{\mu}{2}+q_0\right)-q_x-vq_y}\right]. \tag{Q.298}$$

According to the discussion in Sec. 4.2-(*a*) , the integration over q_y and q_x is done over the momentum range:

$$|vq_x+q_y|<\Lambda_f \quad \& \quad |q_x-vq_y|<k_{\mathrm{F}}. \tag{Q.299}$$

To make this cutoff structure explicit, we change variables to momentum away and along the local FS at hot spot $N=1$:

$$Y=vq_x-q_y, \qquad X=-q_x-vq_y. \tag{Q.300}$$

Under this change of variables, Eq. (Q.298) takes the same form as Eq. (Q.265). Therefore we obtain

$$\mathcal{Q}_{16}(\mu)=\frac{1}{2\pi^2}\left(\frac{\Lambda_f}{\mu}\right)\log\left(\frac{k_{\mathrm{F}}}{v\Lambda_f}\right), \tag{Q.301}$$

in the $k_{\mathrm{F}}/v\gg\Lambda_f$ limit. This expression will offer no contribution to the beta functions of the four-fermion couplings and therefore, it is not necessary to take a look at the nonzero external momentum case.

G. $\mathcal{Q}_{17}(k,p)$

At the RG condition in Eq. (4.57) and at zero external momentum, the integration in Eq. (Q.253) for $M=1$ and $N=7$ reads

$$\mathcal{Q}_{17}(\mu)=\mu^{-1}\int \mathrm{d}q\left[\frac{1}{i\left(\frac{3\mu}{2}+q_0\right)+vq_x+q_y}\right]\left[\frac{1}{-i\left(\frac{\mu}{2}+q_0\right)-q_x+vq_y}\right]. \tag{Q.302}$$

According to the discussion in Sec. 4.2-(*a*) , the integration over q_y and q_x is done over the momentum range:

$$|vq_x+q_y|<\Lambda_f \quad \& \quad |q_x-vq_y|<k_{\mathrm{F}}. \tag{Q.303}$$

To make this cutoff structure explicit, we change variables to momentum away and along the local FS at hot spot $N=1$:

$$Y=vq_x-q_y, \qquad X=-q_x+vq_y. \tag{Q.304}$$

Under this change of variables, Eq. (Q.302) takes the same form as Eq. (Q.265) except for the fact that the X integration is cutoff by k_{F} only. It is straightforward to see that

$$\mathcal{Q}_{17}(\mu)=\frac{1}{2\pi^2}\left(\frac{\Lambda_f}{\mu}\right)\log\left(\frac{k_{\mathrm{F}}}{\Lambda_f}\right), \tag{Q.305}$$

in the $k_{\mathrm{F}}\gg\Lambda_f$ limit. This expression will offer no contribution to the beta functions of the four-fermion couplings and therefore, we do not to take a look at the nonzero external momentum case.

H. $\mathcal{Q}_{18}(k,p)$

At the RG condition in Eq. (4.57) and at zero external momentum, the integration in Eq. (Q.253) for $M=1$ and $N=8$ reads

$$\mathcal{Q}_{18}(\mu)=\mu^{-1}\int \mathrm{d}q\left[\frac{1}{i\left(\frac{3\mu}{2}+q_0\right)+vq_x+q_y}\right]\left[\frac{1}{-i\left(\frac{\mu}{2}+q_0\right)+vq_x-q_y}\right]. \tag{Q.306}$$

According to the discussion in Sec. 4.2-(*a*) , the integration over q_y and q_x is done over the momentum range:

$$|vq_x+q_y|<\Lambda_f \quad \& \quad |q_x-vq_y|<k_{\mathrm{F}}. \tag{Q.307}$$

It is convenient to change variables to

$$Y=vq_x+q_y, \qquad X=q_x-vq_y. \tag{Q.308}$$

Under this change of variables Eq. (Q.274) can be written, to leading order in $v\ll 1$, as

$$\mathcal{Q}_{18}(\mu)=\mu^{-1}\int_{\mathbb{R}}\frac{\mathrm{d}q_0}{(2\pi)}\int_{-\Lambda_f}^{\Lambda_f}\frac{\mathrm{d}Y}{(2\pi)}\int_{-k_{\mathrm{F}}}^{k_{\mathrm{F}}}\frac{\mathrm{d}X}{(2\pi)}\left[\frac{1}{i\left(\frac{3\mu}{2}+q_0\right)+Y}\right]\left[\frac{1}{-i\left(\frac{\mu}{2}+q_0\right)-Y+2vX}\right]. \tag{Q.309}$$

We note that if one sets $v=0$, the integration diverges linearly in the large k_{F} limit. For nonzero v, the integration is convergent for $k_{\mathrm{F}}\gg\mu$. Scaling $X\to X/v$ allows us to write

$$\mathcal{Q}_{18}(\mu)=\frac{1}{v\mu}\int_{\mathbb{R}}\frac{\mathrm{d}q_0}{(2\pi)}\int_{-\Lambda_f}^{\Lambda_f}\frac{\mathrm{d}Y}{(2\pi)}\int_{-vk_{\mathrm{F}}}^{vk_{\mathrm{F}}}\frac{\mathrm{d}X}{(2\pi)}\left[\frac{1}{i\left(\frac{3\mu}{2}+q_0\right)+Y}\right]\left[\frac{1}{-i\left(\frac{\mu}{2}+q_0\right)-Y+2X}\right]. \tag{Q.310}$$

Integrating over q_0 yields

$$\mathcal{Q}_{14}(\mu)=\frac{1}{v\mu}\int_{-\Lambda_f}^{\Lambda_f}\frac{\mathrm{d}Y}{(2\pi)}\int_{-vk_{\mathrm{F}}}^{vk_{\mathrm{F}}}\frac{\mathrm{d}X}{(2\pi)}\left[\frac{\Theta(2X-Y)-\Theta(-Y)}{i\mu+2X}\right]. \tag{Q.311}$$

Upon symmetrizing over X and Y we obtain

$$\mathcal{Q}_{14}(\mu)=\frac{1}{v\mu}\int_{0}^{\Lambda_f}\frac{\mathrm{d}Y}{(2\pi)}\int_{0}^{vk_{\mathrm{F}}}\frac{\mathrm{d}X}{(2\pi)}\frac{4X\Theta(2X-Y)}{4X^2+\mu^2}. \tag{Q.312}$$

We consider this integral in two main cases: (*i*) $\Lambda_f\gg vk_{\mathrm{F}}$ and (*ii*) $\Lambda_f\ll vk_{\mathrm{F}}$.

(*i*) In the case that $\Lambda_f\gg vk_{\mathrm{F}}$, Eq. (Q.312) can be written as

$$\mathcal{Q}_{18}(\mu)=\frac{1}{v\mu}\int_{0}^{vk_{\mathrm{F}}}\frac{\mathrm{d}X}{(2\pi)}\int_{2X}^{\Lambda_f}\frac{\mathrm{d}Y}{(2\pi)}\frac{4X}{4X^2+\mu^2}. \tag{Q.313}$$

The final integration yields, in the $\Lambda_f \gg v k_{\rm F}$ limit:

$$\mathcal{Q}_{18}(\mu) = \frac{1}{4\pi}\left(\frac{\Lambda_f}{\mu}\right)\log\left(\frac{v k_{\rm F}}{\mu}\right). \tag{Q.314}$$

Due to the logarithmic divergence in $k_{\rm F}/\mu = \widehat{k}_{\rm F}$, this expression introduces an order one contribution to the beta functions of the four-fermion couplings. This is still subleading with respect to the case in which $M = 1$ and $N = 5$. Therefore, we omit including the momentum dependence in this quantum correction.

(*ii*) For the opposite limit, when $\Lambda_f \ll v k_{\rm F}$ we can perform the shift $X \to X + Y$ and write Eq. (Q.312) as

$$\mathcal{Q}_{18}(\mu) = \frac{1}{v\mu}\int_0^{\Lambda_f}\frac{{\rm d}Y}{(2\pi)}\int_{Y/2}^{v k_{\rm F}}\frac{{\rm d}X}{(2\pi)}\frac{4X\Theta(2X-Y)}{4X^2+\mu^2}. \tag{Q.315}$$

Final integration over the remaining variables yields

$$\mathcal{Q}_{18}(\mu) = \frac{1}{2\pi^2 v}\left(\frac{\Lambda_f}{\mu}\right)\log\left(\frac{v k_{\rm F}}{\Lambda_f}\right). \tag{Q.316}$$

This is a similar situation as the one encountered in the $M = 1$ and $N = 4$ case. This expression gives rise to a significant contribution to the beta function for the four-fermion couplings. However, this one is negligible with respect to the case with $M = 1$ and $N = 5$ where the enhancement is given by $k_{\rm F}$, rather than Λ_f/v.

Q.3-(*d*) The $\mathcal{Q}_{15}(k,p)$ and $\mathcal{O}_{15}(k,p)$ integrals in the presence of curvature of the FS

In the previous section we showed that the largest contribution to the beta function for the four-fermion couplings comes from the processes that involve antipodal electrons in intermediate states due to the enhancement provided by the nonzero density of states at the Fermi level. These two contributions come from the integrals $\mathcal{Q}_{MN}(k,p)$ in Eq. (Q.253) (particle-particle) and $\mathcal{O}_{MN}(k,p)$ in Eq. (Q.252) (particle-hole) with $M = 1$ and $N = 5$. In the absence of curvature of the FS, these two are related to each other. Here we show that, upon the inclusion of the curvature of the FS, only the particle-particle integral yields a nonzero contribution to the beta function of the four-fermion couplings. For simplicity we evaluate these expressions at the RG conditions in Eq. (4.57) and further set the external momentum to zero. In the presence of nonzero external momentum, the computations follow the same logic.

In the presence of curvature of the FS, the dispersion relations at hot spots $M = 1$ and $N = 5$ are modified to

$$e_1(\vec{k};v;\eta) = v k_x + k_y - \eta k_x^2, \quad \& \quad e_5(\vec{k};v;\eta) = -v k_x - k_y - \eta k_x^2, \tag{Q.317}$$

where η is the dimensionful curvature of the FS. At the RG condition in Eq. (4.57) and zero external momentum, the integrations in Eqs. (Q.252) and (Q.253) adopt the following form

$$\mathcal{O}_{15}(\mu) = \mu^{-1} \int \mathrm{d}q \left[\frac{1}{i\left(q_0 - \frac{3\mu}{2}\right) + vq_x + q_y - \eta q_x^2}\right] \left[\frac{1}{i\left(q_0 - \frac{\mu}{2}\right) - vq_x - q_y - \eta q_x^2}\right], \tag{Q.318}$$

$$\mathcal{Q}_{15}(\mu) = \mu^{-1} \int \mathrm{d}q \left[\frac{1}{i\left(q_0 + \frac{3\mu}{2}\right) + vq_x - q_y - \eta q_x^2}\right] \left[\frac{1}{-i\left(q_0 + \frac{\mu}{2}\right) + vq_x + q_y - \eta q_x^2}\right]. \tag{Q.319}$$

Let us consider each integration independently.

$\underline{\mathcal{O}_{15}(\mu)}$: The integration over the momentum in Eq. (Q.318) is done, according to the discussion in Sec. 4.2-(*a*) , over the momentum range

$$|vq_x + q_y - \eta q_x^2| < \Lambda_f, \quad \& \quad |vq_x + q_y + \eta q_x^2| < \Lambda_f. \tag{Q.320}$$

This comes just from requiring that the particle-hole pair in the intermediate state is within the shell of thickness Λ_f around the FS. Now, the momentum along the FS, is bounded by k_{F}. In the small v limit, this corresponds to the q_x integration. In this limit, it is convenient to define the new variables

$$X = q_x, \qquad \& \qquad Y = vq_x + q_y - \eta q_x^2. \tag{Q.321}$$

Under this change of variables, the range of integration is now of the form

$$|Y| < \Lambda_f, \quad |Y + 2\eta X^2| < \Lambda_f, \quad \& \quad |X| < k_{\mathrm{F}}. \tag{Q.322}$$

This implies that X is bounded by $\min(\sqrt{\Lambda_f}/\sqrt{\eta}, k_{\mathrm{F}})$ as a consequence of Y being at most of order Λ_f. Since k_{F} represents the size of the patch on the FS where it can be regarded as a straight line, it follows that $\eta \sim 1/k_{\mathrm{F}}$ and thus, $\min(\sqrt{\Lambda_f}/\sqrt{\eta}, k_{\mathrm{F}}) = \sqrt{\Lambda_f k_{\mathrm{F}}}$ in the $k_{\mathrm{F}} \gg \Lambda_f$ limit. With this new change of variables we can write Eq. (Q.318) as

$$\begin{aligned}\mathcal{O}_{15}(\mu) = \mu^{-1} \int_{\mathbb{R}} \frac{\mathrm{d}q_0}{(2\pi)} \int_{-\Lambda_f}^{\Lambda_f} \frac{\mathrm{d}Y}{(2\pi)} \int_{-\sqrt{\Lambda_f k_{\mathrm{F}}}}^{\sqrt{\Lambda_f k_{\mathrm{F}}}} \frac{\mathrm{d}X}{(2\pi)} \left[\frac{1}{i\left(q_0 - \frac{3\mu}{2}\right) + Y}\right] \\ \times \left[\frac{1}{i\left(q_0 - \frac{\mu}{2}\right) - Y - 2\eta X^2}\right].\end{aligned} \tag{Q.323}$$

We can scale out η via $X \to X/\sqrt{\eta} \sim \sqrt{k_{\mathrm{F}}} X$ and write

$$\begin{aligned}\mathcal{O}_{15}(\mu) = \sqrt{k_{\mathrm{F}}}\mu^{-1} \int_{\mathbb{R}} \frac{\mathrm{d}q_0}{(2\pi)} \int_{-\Lambda_f}^{\Lambda_f} \frac{\mathrm{d}Y}{(2\pi)} \int_{-\sqrt{\Lambda_f}}^{\sqrt{\Lambda_f}} \frac{\mathrm{d}X}{(2\pi)} \left[\frac{1}{i\left(q_0 - \frac{3\mu}{2}\right) + Y}\right] \\ \times \left[\frac{1}{i\left(q_0 - \frac{\mu}{2}\right) - Y - 2X^2}\right].\end{aligned} \tag{Q.324}$$

Integration over q_0 yields

$$\mathcal{O}_{15}(\mu) = 2\sqrt{k_{\rm F}}\mu^{-1}\int\limits_{-\Lambda_f}^{\Lambda_f}\frac{{\rm d}Y}{(2\pi)}\int\limits_{0}^{\sqrt{\Lambda_f}}\frac{{\rm d}X}{(2\pi)}\left[\frac{\Theta(Y+2X^2)-\Theta(-Y)}{2X^2+2Y-i\mu}\right]. \tag{Q.325}$$

In this expression we can make the following scaling $X \to \sqrt{\Lambda_f}$ and $Y \to \Lambda_f Y$. Doing so, and defining $m = \mu/\Lambda_f \ll 1$, we obtain

$$\mathcal{O}_{15}(\mu) = 2\sqrt{k_{\rm F}\Lambda_f}\mu^{-1}\int\limits_{-1}^{1}\frac{{\rm d}Y}{(2\pi)}\int\limits_{0}^{1}\frac{{\rm d}X}{(2\pi)}\left[\frac{\Theta(Y+2X^2)-\Theta(-Y)}{2X^2+2Y-im}\right]. \tag{Q.326}$$

The remaining integration is regular in the $m = 0$ limit and thus we conclude that

$$\mathcal{O}_{15}(\mu) \sim \frac{\sqrt{k_{\rm F}\Lambda_f}}{\mu}. \tag{Q.327}$$

This expression has no contribution to the beta function as a consequence of the power-law dependence in both μ and $k_{\rm F}$.

$\underline{\mathcal{Q}_{15}(\mu)}$: The integration over the momentum in Eq. (Q.319) is done, according to the discussion in Sec. 4.2-(*a*) , over the momentum range

$$|vq_x + q_y - \eta q_x^2| < \Lambda_f, \quad \& \quad |q_x| < k_{\rm F}, \tag{Q.328}$$

in the small v limit. Here we have chosen q_x to be the momentum along the FS in a first approximation in the small v limit. As we shall see, this should not modify the logic we are about to present. What is important in here is that we can now perform the following change of variables

$$X = q_x, \qquad \& \qquad Y = vq_x + q_y - \eta q_x^2. \tag{Q.329}$$

Under this change of variables it is easy to see that Eq. (Q.319) takes the following form

$$\mathcal{Q}_{15}(\mu) = \mu^{-1}\int\limits_{\mathbb{R}}\frac{{\rm d}q_0}{(2\pi)}\int\limits_{-\Lambda_f}^{\Lambda_f}\frac{{\rm d}Y}{(2\pi)}\int\limits_{-k_{\rm F}}^{k_{\rm F}}\frac{{\rm d}X}{(2\pi)}\left[\frac{1}{i\left(q_0+\frac{3\mu}{2}\right)+Y}\right]\left[\frac{1}{-i\left(q_0+\frac{\mu}{2}\right)+Y}\right]. \tag{Q.330}$$

This is nothing else than the zero external momentum version of Eq. (Q.290). Therefore, this reduces to the same computation we did in the absence of curvature. In the presence of external momentum, the same discussion applies, and the computation reduces to the case in which the curvature of the internal electrons is ignored.

With this discussion at hand, it becomes clear that the only dominant contribution to the beta function of the four-fermion couplings will come from either the particle-particle or particle-hole diagrams that involve antipodal electrons if one ignores the curvature of the

FS. In the presence of curvature of the FS, only the former becomes important. Therefore, in the WMDL, the largest contribution to the beta function comes from the counterterm functions in the zero momentum particle-particle channel:

$$
\begin{aligned}
{}_2A^{j_1j_2j_3j_4}_{N_1N_2N_3N_4;\sigma_1\sigma_2\sigma_3\sigma_4}(\{k_{i;N_i}\}) = -\frac{k_{\mathrm{F}}}{8\pi^2\mu}\lambda^{j_1j_2j_3j_4}_{N_1N_2N_3N_4;\sigma_1\sigma_2\sigma_3\sigma_4}(\{k_{i;N_i}\})^{-1}\sum_{l_1,l_2=1}^{N_f}\sum_{\rho_1,\rho_2=1}^{N_c}\sum_{M_1=1}^{8} \\
\times \lambda^{j_1j_2l_1l_2}_{N_1N_2M_1[M_1+4]_8;\sigma_1\sigma_2\rho_1\rho_2}\lambda^{l_1l_2j_3j_4}_{M_1[M_1+4]_8N_3N_4;\rho_1\rho_2\sigma_3\sigma_4}\log\left(\frac{\Lambda_f}{\mathscr{J}_{15}(\mu,|e_{M_1}(\vec{k}_1^{\,*}+\vec{k}_2^{\,*};v)|)}\right),
\end{aligned}
\tag{Q.331}
$$

where $\vec{k}_i^{\,*}$ denotes the momentum evaluated at the RG condition in Eq. (4.57) and which depends on the choices of N_1, N_2, N_3 and N_4.

Q.3-(e) Quadratic Corrections Beyond the WMDL

So far we have considered the contributions to the beta functions at quadratic order in the four-fermion couplings within the WMDL. In this approximation, the four-fermion couplings are assumed to be nonzero along the FS. However, for a theory in which the four-fermion couplings are tuned to zero in the UV, the spin fluctuations source an interaction that is nonzero only in a confined region close to the hot spots. This is because electrons far away from the hot spots decouple from the spin fluctuations at sufficiently low-energies. Because of this, it is important to go beyond the WMDL in the computation of the contributions to the beta function at quadratic order by incorporating the momentum profile generated by the spin fluctuations to leading order in $\lambda^{\{j_i\}}_{\{N_i\};\{\sigma_i\}}(\{k_{i;N_i}\})$.

We are interested in the largest contribution to the beta function at quadratic order in the four-fermion couplings. In the absence of momentum dependence, we showed that this corresponds to the particle-particle diagrams that involve virtual electrons that lie on antipodal points on the FS. In the presence of momentum dependence, we expect this to be the case as well. This is because this are the only processes in which the virtual electrons can explore an extended region of the FS without energy cost. Hence, in the presence of momentum dependence, the largest contribution will arise from the quantum correction:

$$
\begin{aligned}
{}_2\Gamma^{j_1j_2j_3j_4}_{N_1N_2N_3N_4;\sigma_1\sigma_2\sigma_3\sigma_4}(k_1,k_2,k_3,k_4) \approx \frac{1}{2\mu^2}\sum_{l_1,l_2=1}^{N_f}\sum_{\rho_1,\rho_2=1}^{N_c}\sum_{M_1=1}^{8}\int \mathrm{d}q\; G_{M_1}(q+k_1) \\
\times G_{[M_1+4]_8}(k_2-q)\lambda^{j_1j_2l_1l_2}_{N_1N_2M_1[M_1+4]_8;\sigma_1\sigma_2\rho_1\rho_2}(k_{1;N_1},k_{2;N_2},[k_1+q]_{M_1},[k_2-q]_{[M_1+4]_8}) \\
\times \lambda^{l_1l_2j_3j_4}_{M_1[M_1+4]_8N_3N_4;\rho_1\rho_2\sigma_3\sigma_4}([k_1+q]_{M_1},[k_2-q]_{[M_1+4]_8},k_{3;N_3},k_{4;N_4}).
\end{aligned}
\tag{Q.332}
$$

In here we can consider this expression to leading order in v_0, which allows us to ignore the momentum dependence of the coupling functions inside the fermion propagators while keeping the momentum dependence in the four-fermion couplings. The integrations over the frequency and momentum away from the FS follows the same logic as in the computation of Eq. (Q.286). Because the four-fermion couplings depend only on the momentum along the FS, the integration over the momentum away from the FS and the frequency can be done

to obtain the quantum correction at the RG condition in Eq. (4.57)

$$
\begin{aligned}
{}_2\Gamma^{j_1j_2j_3j_4}_{N_1N_2N_3N_4;\sigma_1\sigma_2\sigma_3\sigma_4}(\{k_{i;N_i}\}) \approx \frac{1}{4\pi\mu^2}\sum_{l_1,l_2=1}^{N_f}\sum_{\rho_1,\rho_2=1}^{N_c}\sum_{M_1=1}^{8}\int_{-k_{\mathrm{F}}}^{k_{\mathrm{F}}}\frac{\mathrm{d}q_{M_1}}{(2\pi)} \\
\times \lambda^{j_1j_2l_1l_2}_{N_1N_2M_1[M_1+4]_8;\sigma_1\sigma_2\rho_1\rho_2}(k_{1;N_1},k_{2;N_2},[k_1+q]_{M_1},[k_2-q]_{M_1}) \\
\times \lambda^{l_1l_2j_3j_4}_{M_1[M_1+4]_8N_3N_4;\rho_1\rho_2\sigma_3\sigma_4}([k_1+q]_{M_1},[k_2-q]_{M_1},k_{3;N_3},k_{4;N_4}) \\
\times \log\left(\frac{\Lambda_f}{\mathscr{I}_{M_1[M_1+4]_8}(\mu,|e_{M_1}(\vec{k}_2^{\,*}+\vec{k}_1^{\,*};v)|)}\right).
\end{aligned}
\tag{Q.333}
$$

In here we have further used the fact that $q_{M_1}=q_{M_2}$ since $M_1=[M_2+4]_8$, and we have cut off the integration over the momentum along the FS by the Fermi momentum. The local counterterm function we need to add to the bare action to eliminate the Λ_f dependence in the physical observables has the following structure

$$
\begin{aligned}
{}_2A^{j_1j_2j_3j_4}_{N_1N_2N_3N_4;\sigma_1\sigma_2\sigma_3\sigma_4}(\{k_{i;N_i}\}) = -\frac{\lambda^{j_1j_2j_3j_4}_{N_1N_2N_3N_4;\sigma_1\sigma_2\sigma_3\sigma_4}(\{k_{i;N_i}\})^{-1}}{4\pi\mu}\sum_{l_1,l_2=1}^{N_f}\sum_{\rho_1,\rho_2=1}^{N_c} \\
\times\sum_{M_1=1}^{8}\int_{-k_{\mathrm{F}}}^{k_{\mathrm{F}}}\frac{\mathrm{d}q_{M_1}}{(2\pi)}\lambda^{j_1j_2l_1l_2}_{N_1N_2M_1[M_1+4]_8;\sigma_1\sigma_2\rho_1\rho_2}(k_{1;N_1},k_{2;N_2},[k_1+q]_{M_1},[k_2-q]_{M_1}) \\
\times \lambda^{l_1l_2j_3j_4}_{M_1[M_1+4]_8N_3N_4;\rho_1\rho_2\sigma_3\sigma_4}([k_1+q]_{M_1},[k_2-q]_{M_1},k_{3;N_3},k_{4;N_4}) \\
\times \log\left(\frac{\Lambda_f}{\mathscr{I}_{M_1[M_1+4]_8}(\mu,|e_{M_1}(\vec{k}_2^{\,*}+\vec{k}_1^{\,*};v)|)}\right).
\end{aligned}
\tag{Q.334}
$$

References

[1] Raj K. Pathria and Paul D. Beale. Statistical Mechanics. Elsevier Science, 1996. ISBN 9780080541716. URL https://books.google.ca/books?id=PIk9sF9j2oUC.

[2] Jean Zinn-Justin. Quantum Field Theory and Critical Phenomena. Oxford University Press, 4th edition, 2002. doi: 10.1093/acprof:oso/9780198509233.001.0001. URL http://www.oxfordscholarship.com/view/10.1093/acprof:oso/9780198509233.001.0001/acprof-9780198509233.

[3] Xiao-Gang. Wen. Quantum Field Theory of Many-Body Systems: From the Origin of Sound to an Origin of Light and Electrons: From the Origin of Sound to an Origin of Light and Electrons. Oxford Graduate Texts. OUP Oxford, 2004. ISBN 9780198530947. URL https://books.google.ca/books?id=llnlrfdR4YgC.

[4] Daniel J. Amit and Victor Martin-Mayor. Field Theory, the Renormalization Group, and Critical Phenomena. World Scientific, 3rd edition, 2005. doi: 10.1142/5715. URL https://www.worldscientific.com/doi/abs/10.1142/5715.

[5] Giuseppe Mussardo. Statistical field theory: an introduction to exactly solved models in statistical physics. Oxford Graduate Texts. Oxford Univ. Press, New York, NY, 2010. URL https://cds.cern.ch/record/1281256.

[6] Subir Sachdev. Quantum Phase Transitions. Cambridge University Press, 2 edition, 2011. doi: 10.1017/CBO9780511973765.

[7] Uwe C. Täuber. Critical Dynamics: A Field Theory Approach to Equilibrium and Non-Equilibrium Scaling Behavior. Cambridge University Press, 2014. doi: 10.1017/CBO9781139046213. URL https://doi.org/10.1017/CBO9781139046213.

[8] Hagen Kleinert and Verena Schulte-Frohlinde. Critical Properties of ϕ^4-Theories. WORLD SCIENTIFIC, 2001. doi: 10.1142/4733. URL https://www.worldscientific.com/doi/abs/10.1142/4733.

[9] Lin Fei, Simone Giombi, and Igor R. Klebanov. Critical O(N) models in $6-\epsilon$ dimensions. Phys. Rev. D, 90:025018, Jul 2014. doi: 10.1103/PhysRevD.90.025018. URL https://link.aps.org/doi/10.1103/PhysRevD.90.025018.

[10] Lev Landau. Zur Theorie der Phasenumwandlungen I. Sov. Phys. JETP, 7(19), 1937.

[11] Lev Landau. Zur Theorie der Phasenumwandlungen II. Phys. Z. Sowjetunion, 11 (26-35), 1937.

[12] Arkady. P. Levanyuk. Sov. Phys. JETP, 36(571), 1959.

[13] Vitaly L. Ginzburg. Sov. Phys. Sol. State, 2(1824), 1960.

[14] Alexander Altland and Ben D. Simons. Condensed Matter Field Theory. Cambridge University Press, 2 edition, 2010. doi: 10.1017/CBO9780511789984.

[15] T. Senthil, Ashvin Vishwanath, Leon Balents, Subir Sachdev, and Matthew P. A. Fisher. Deconfined quantum critical points. Science, 303(5663):1490–1494, Mar 2004. ISSN 0036-8075. doi: 10.1126/science.1091806. URL http://science.sciencemag.org/content/303/5663/1490.

[16] Leo P. Kadanoff. Scaling laws for Ising models near T_c. Physics Physique Fizika, 2: 263–272, Jun 1966. doi: 10.1103/PhysicsPhysiqueFizika.2.263. URL https://link.aps.org/doi/10.1103/PhysicsPhysiqueFizika.2.263.

[17] Kenneth G. Wilson. Renormalization group and critical phenomena. I. Renormalization group and the Kadanoff scaling picture. Phys. Rev. B, 4:3174–3183, Nov 1971. doi: 10.1103/PhysRevB.4.3174. URL https://link.aps.org/doi/10.1103/PhysRevB.4.3174.

[18] Kenneth G. Wilson. Renormalization group and critical phenomena. II. Phase-space cell analysis of critical behavior. Phys. Rev. B, 4:3184–3205, Nov 1971. doi: 10.1103/PhysRevB.4.3184. URL https://link.aps.org/doi/10.1103/PhysRevB.4.3184.

[19] Philippe Di Francesco, Pierre Mathieu, and David Sénéchal. Conformal field theory. Graduate texts in contemporary physics. Springer, New York, NY, 1997. URL https://cds.cern.ch/record/639405.

[20] Eduardo Fradkin. Field Theories of Condensed Matter Physics. Cambridge University Press, 2 edition, 2013. doi: 10.1017/CBO9781139015509.

[21] Nathan Seiberg. Naturalness versus supersymmetric non-renormalization theorems. Physics Letters B, 318(3):469 – 475, Dec 1993. ISSN 0370-2693. doi: 10.1016/0370-2693(93)91541-T. URL https://www.sciencedirect.com/science/article/pii/037026939391541T.

[22] Riccardo Rattazzi, Vyacheslav S. Rychkov, Erik Tonni, and Alessandro Vichi. Bounding scalar operator dimensions in 4d CFT. Journal of High Energy Physics, 2008(12): 031, Dec 2008. URL http://stacks.iop.org/1126-6708/2008/i=12/a=031.

[23] Sheer El-Showk, Miguel F. Paulos, David Poland, Slava Rychkov, David Simmons-Duffin, and Alessandro Vichi. Solving the 3d Ising model with the conformal bootstrap II. c-Minimization and precise critical exponents. Journal of Statistical Physics, 157 (4):869–914, Dec 2014. ISSN 1572-9613. doi: 10.1007/s10955-014-1042-7. URL https://doi.org/10.1007/s10955-014-1042-7.

[24] Grigory Tarnopolsky, Lin Fei, Simone Giombi, and Igor R. Klebanov. Yukawa conformal field theories and emergent supersymmetry. Progress of Theoretical and

Experimental Physics, 2016(12), Nov 2016. ISSN 2050-3911. doi: 10.1093/ptep/ptw120. URL https://dx.doi.org/10.1093/ptep/ptw120.

[25] Kenneth G. Wilson and Michael E. Fisher. Critical exponents in 3.99 dimensions. Phys. Rev. Lett., 28:240–243, Jan 1972. doi: 10.1103/PhysRevLett.28.240. URL https://link.aps.org/doi/10.1103/PhysRevLett.28.240.

[26] Kenneth G. Wilson. Quantum field theory models in less than 4 dimensions. Phys. Rev. D, 7:2911–2926, May 1973. doi: 10.1103/PhysRevD.7.2911. URL https://link.aps.org/doi/10.1103/PhysRevD.7.2911.

[27] G.'t Hooft. A planar diagram theory for strong interactions. Nuclear Physics B, 72(3):461 – 473, Apr 1974. ISSN 0550-3213. doi: https://doi.org/10.1016/0550-3213(74)90154-0. URL http://www.sciencedirect.com/science/article/pii/0550321374901540.

[28] A. J. Schofield. Non-Fermi liquids. Contemporary Physics, 40(2):95–115, Nov 1999. doi: 10.1080/001075199181602. URL https://doi.org/10.1080/001075199181602.

[29] R. J. Cava, B. Batlogg, R. B. van Dover, D. W. Murphy, S. Sunshine, T. Siegrist, J. P. Remeika, E. A. Rietman, S. Zahurak, and G. P. Espinosa. Bulk superconductivity at 91 K in single-phase oxygen-deficient perovskite $Ba_2YCu_3O_{9-\delta}$. Phys. Rev. Lett., 58:1676–1679, Apr 1987. doi: 10.1103/PhysRevLett.58.1676. URL https://link.aps.org/doi/10.1103/PhysRevLett.58.1676.

[30] M. Gurvitch and A. T. Fiory. Resistivity of $La_{1.825}Sr_{0.175}CuO_4$ and $YBa_2Cu_3O_7$ to 1100 K: Absence of saturation and its implications. Phys. Rev. Lett., 59:1337–1340, Sep 1987. doi: 10.1103/PhysRevLett.59.1337. URL https://link.aps.org/doi/10.1103/PhysRevLett.59.1337.

[31] N. P. Armitage, D. H. Lu, C. Kim, A. Damascelli, K. M. Shen, F. Ronning, D. L. Feng, P. Bogdanov, Z.-X. Shen, Y. Onose, Y. Taguchi, Y. Tokura, P. K. Mang, N. Kaneko, and M. Greven. Anomalous electronic structure and pseudogap effects in $Nd_{1.85}Ce_{0.15}CuO_4$. Phys. Rev. Lett., 87:147003, Sep 2001. doi: 10.1103/PhysRevLett.87.147003. URL https://link.aps.org/doi/10.1103/PhysRevLett.87.147003.

[32] Stephen D. Wilson, Pengcheng Dai, Shiliang Li, Songxue Chi, H. J. Kang, and J. W. Lynn. Resonance in the electron-doped high-transition-temperature superconductor $Pr_{0.88}LaCe_{0.12}CuO_{4-\delta}$. Nature, 442:59 EP –, Jul 2006. URL https://doi.org/10.1038/nature04857.

[33] E. M. Motoyama, G. Yu, I. M. Vishik, O. P. Vajk, P. K. Mang, and M. Greven. Spin correlations in the electron-doped high-transition-temperature superconductor $Nd_{2-x}Ce_xCuO_{4\pm\delta}$. Nature, 445:186 EP –, Jan 2007. URL https://doi.org/10.1038/nature05437.

[34] F. Schmitt, W. S. Lee, D.-H. Lu, W. Meevasana, E. Motoyama, M. Greven, and Z.-X. Shen. Analysis of the spectral function of $Nd_{1.85}Ce_{0.15}CuO_4$ obtained by angle-resolved photoemission spectroscopy. Phys. Rev. B, 78:100505, Sep 2008. doi: 10.

1103/PhysRevB.78.100505. URL https://link.aps.org/doi/10.1103/PhysRevB.78.100505.

[35] T. Helm, M. V. Kartsovnik, I. Sheikin, M. Bartkowiak, F. Wolff-Fabris, N. Bittner, W. Biberacher, M. Lambacher, A. Erb, J. Wosnitza, and R. Gross. Magnetic breakdown in the electron-doped cuprate superconductor $Nd_{2-x}Ce_xCuO_4$: The reconstructed Fermi surface survives in the strongly overdoped regime. Phys. Rev. Lett., 105:247002, Dec 2010. doi: 10.1103/PhysRevLett.105.247002. URL http://link.aps.org/doi/10.1103/PhysRevLett.105.247002.

[36] K. Hashimoto, K. Cho, T. Shibauchi, S. Kasahara, Y. Mizukami, R. Katsumata, Y. Tsuruhara, T. Terashima, H. Ikeda, M. A. Tanatar, H. Kitano, N. Salovich, R. W. Giannetta, P. Walmsley, A. Carrington, R. Prozorov, and Y. Matsuda. A sharp peak of the zero-temperature penetration depth at optimal composition in $BaFe_2(As_{1-x}P_x)_2$. Science, 336:1554, Jun 2012. doi: 10.1126/science.1219821. URL http://science.sciencemag.org/content/336/6088/1554.

[37] H. v. Löhneysen, T. Pietrus, G. Portisch, H. G. Schlager, A. Schröder, M. Sieck, and T. Trappmann. Non-Fermi-liquid behavior in a heavy-fermion alloy at a magnetic instability. Phys. Rev. Lett., 72:3262–3265, May 1994. doi: 10.1103/PhysRevLett.72.3262. URL https://link.aps.org/doi/10.1103/PhysRevLett.72.3262.

[38] N. D. Mathur, F. M. Grosche, S. R. Julian, I. R. Walker, D. M. Freye, R. K. W. Haselwimmer, and G. G. Lonzarich. Magnetically mediated superconductivity in heavy fermion compounds. Nature, 394:39 EP –, Jul 1998. URL https://doi.org/10.1038/27838.

[39] J. Custers, P. Gegenwart, H. Wilhelm, K. Neumaier, Y. Tokiwa, O. Trovarelli, C. Geibel, F. Steglich, C. Pépin, and P. Coleman. The break-up of heavy electrons at a quantum critical point. Nature, 424:524 EP –, Jul 2003. URL https://doi.org/10.1038/nature01774.

[40] T. Park, F. Ronning, H. Yuan, M. Salamon, R. Movshovich, J. Sarrao, and J. Thompson. Hidden magnetism and quantum criticality in the heavy fermion superconductor $CeRhIn_5$. Nature, 440:65, Mar 2006. doi: 10.1038/nature04571. URL http://www.nature.com/nature/journal/v440/n7080/full/nature04571.html.

[41] Yoichi Kamihara, Takumi Watanabe, Masahiro Hirano, and Hideo Hosono. Iron-based layered superconductor $La[O_{1-x}F_x]FeAs$ ($x = 0.050.12$) with $T_c = 26$ K. Journal of the American Chemical Society, 130(11):3296–3297, Mar 2008. doi: 10.1021/ja800073m. URL https://doi.org/10.1021/ja800073m.

[42] Zhi-An Ren, Jie Yang, Wei Lu, Wei Yi, Xiao-Li Shen, Zheng-Cai Li, Guang-Can Che, Xiao-Li Dong, Li-Ling Sun, Fang Zhou, and Zhong-Xian Zhao. Superconductivity in the iron-based F-doped layered quaternary compound $Nd[O_{1-x}F_x]FeAs$. EPL (Europhysics Letters), 82(5):57002, May 2008. doi: 10.1209/0295-5075/82/57002. URL https://doi.org/10.1209%2F0295-5075%2F82%2F57002.

[43] X. H. Chen, T. Wu, G. Wu, R. H. Liu, H. Chen, and D. F. Fang. Superconductivity at 43 K in $SmFeAsO_{1-x}F_x$. Nature, 453:761 EP –, Jun 2008. URL https://doi.org/10.1038/nature07045.

[44] Clarina de la Cruz, Q. Huang, J. W. Lynn, Jiying Li, W. Ratcliff II, J. L. Zarestky, H. A. Mook, G. F. Chen, J. L. Luo, N. L. Wang, and Pengcheng Dai. Magnetic order close to superconductivity in the iron-based layered $LaO_{1-x}F_xFeAs$ systems. Nature, 453:899 EP –, Jun 2008. URL https://doi.org/10.1038/nature07057.

[45] G. F. Chen, Z. Li, D. Wu, G. Li, W. Z. Hu, J. Dong, P. Zheng, J. L. Luo, and N. L. Wang. Superconductivity at 41 K and its competition with spin-density-wave instability in layered $CeO_{1-x}F_xFeAs$. Phys. Rev. Lett., 100:247002, Jun 2008. doi: 10.1103/PhysRevLett.100.247002. URL https://link.aps.org/doi/10.1103/PhysRevLett.100.247002.

[46] Marianne Rotter, Marcus Tegel, Dirk Johrendt, Inga Schellenberg, Wilfried Hermes, and Rainer Pöttgen. Spin-density-wave anomaly at 140 K in the ternary iron arsenide $BaFe_2As_2$. Phys. Rev. B, 78:020503, Jul 2008. doi: 10.1103/PhysRevB.78.020503. URL https://link.aps.org/doi/10.1103/PhysRevB.78.020503.

[47] R. H. Liu, G. Wu, T. Wu, D. F. Fang, H. Chen, S. Y. Li, K. Liu, Y. L. Xie, X. F. Wang, R. L. Yang, L. Ding, C. He, D. L. Feng, and X. H. Chen. Anomalous transport properties and phase diagram of the FeAs-based $SmFeAsO_{1-x}F_x$ superconductors. Phys. Rev. Lett., 101:087001, Aug 2008. doi: 10.1103/PhysRevLett.101.087001. URL https://link.aps.org/doi/10.1103/PhysRevLett.101.087001.

[48] N.W. Ashcroft and N.D. Mermin. Solid State Physics. Cengage Learning, 2011. ISBN 9788131500521. URL https://books.google.ca/books?id=x_s_YAAACAAJ.

[49] J.D. Jackson. Classical electrodynamics. Wiley, 1975. ISBN 9780471431329. URL https://books.google.ca/books?id=_7rvAAAAMAAJ.

[50] L. Landau. The theory of a Fermi liquid. Sov. Phys. JETP, 3:920, Jan 1957. URL http://www.jetp.ac.ru/cgi-bin/dn/e_003_06_0920.pdf.

[51] L. Landau. Oscillations in a Fermi liquid. Sov. Phys. JETP, 5:101, Aug 1957. URL http://www.jetp.ac.ru/cgi-bin/dn/e_005_01_0101.pdf.

[52] I. Ia. Pomeranchuk. On the stability of a Fermi liquid. Sov. Phys. JETP, 8:361, May 1959. URL http://www.jetp.ac.ru/cgi-bin/dn/e_008_02_0361.pdf.

[53] J. M. Luttinger. Fermi surface and some simple equilibrium properties of a system of interacting fermions. Phys. Rev., 119:1153–1163, Aug 1960. doi: 10.1103/PhysRev.119.1153. URL https://link.aps.org/doi/10.1103/PhysRev.119.1153.

[54] J. Polchinski. Effective Field Theory and the Fermi Surface. ArXiv High Energy Physics - Theory e-prints, Jun 1992. URL https://arxiv.org/pdf/hep-th/9210046.pdf.

[55] R. Shankar. Renormalization-group approach to interacting fermions. Rev. Mod. Phys., 66:129–192, Jan 1994. doi: 10.1103/RevModPhys.66.129. URL http://link.aps.org/doi/10.1103/RevModPhys.66.129.

[56] Gennady Y. Chitov and David Sénéchal. Renormalization-group study of interacting electrons. Phys. Rev. B, 52:13487–13496, Nov 1995. doi: 10.1103/PhysRevB.52.13487. URL https://link.aps.org/doi/10.1103/PhysRevB.52.13487.

[57] Gennady Y. Chitov and David Sénéchal. Fermi liquid as a renormalization-group fixed point: The role of interference in the Landau channel. Phys. Rev. B, 57:1444–1456, Jan 1998. doi: 10.1103/PhysRevB.57.1444. URL https://link.aps.org/doi/10.1103/PhysRevB.57.1444.

[58] Gennady Y. Chitov and Andrew J. Millis. Leading temperature corrections to Fermi-liquid theory in two dimensions. Phys. Rev. Lett., 86:5337–5340, Jun 2001. doi: 10.1103/PhysRevLett.86.5337. URL https://link.aps.org/doi/10.1103/PhysRevLett.86.5337.

[59] J. Bardeen, L. N. Cooper, and J. R. Schrieffer. Microscopic theory of superconductivity. Phys. Rev., 106:162–164, Apr 1957. doi: 10.1103/PhysRev.106.162. URL https://link.aps.org/doi/10.1103/PhysRev.106.162.

[60] J. Bardeen, L. N. Cooper, and J. R. Schrieffer. Theory of superconductivity. Phys. Rev., 108:1175–1204, Dec 1957. doi: 10.1103/PhysRev.108.1175. URL https://link.aps.org/doi/10.1103/PhysRev.108.1175.

[61] Henrik Bruus and Karsten Flensberg. Many-body quantum theory in condensed matter physics - an introduction. Oxford University Press, United States, 2004. URL https://books.google.ca/books?id=v5vhg1tYLC8C.

[62] Sin-itiro Tomonaga. Remarks on Bloch's Method of Sound Waves applied to Many-fermion Problems. Progress of Theoretical Physics, 5(4):544–569, Jul 1950. ISSN 0033-068X. doi: 10.1143/ptp/5.4.544. URL https://dx.doi.org/10.1143/ptp/5.4.544.

[63] J. M. Luttinger and J. C. Ward. Ground-state energy of a many-fermion system. II. Phys. Rev., 118:1417–1427, Jun 1960. doi: 10.1103/PhysRev.118.1417. URL https://link.aps.org/doi/10.1103/PhysRev.118.1417.

[64] Daniel C. Mattis and Elliott H. Lieb. Exact solution of a many-fermion system and its associated boson field. Journal of Mathematical Physics, 6(2):304–312, Jul 1965. doi: 10.1063/1.1704281. URL https://doi.org/10.1063/1.1704281.

[65] F D M Haldane. Luttinger liquid theory of one-dimensional quantum fluids. I. properties of the Luttinger model and their extension to the general $1d$ interacting spinless Fermi gas. Journal of Physics C: Solid State Physics, 14(19):2585–2609, Jul 1981. doi: 10.1088/0022-3719/14/19/010. URL https://doi.org/10.1088%2F0022-3719%2F14%2F19%2F010.

[66] J Voit. One-dimensional Fermi liquids. Reports on Progress in Physics, 58(9):977–1116, Sep 1995. doi: 10.1088/0034-4885/58/9/002. URL https://doi.org/10.1088%2F0034-4885%2F58%2F9%2F002.

[67] R. B. Laughlin. Anomalous quantum hall effect: An incompressible quantum fluid with fractionally charged excitations. Phys. Rev. Lett., 50:1395–1398, May 1983. doi: 10.1103/PhysRevLett.50.1395. URL https://link.aps.org/doi/10.1103/PhysRevLett.50.1395.

[68] B. I. Halperin, Patrick A. Lee, and Nicholas Read. Theory of the half-filled Landau level. Phys. Rev. B, 47:7312–7343, Mar 1993. doi: 10.1103/PhysRevB.47.7312. URL https://link.aps.org/doi/10.1103/PhysRevB.47.7312.

[69] V. J. Goldman and B. Su. Resonant tunneling in the quantum Hall regime: Measurement of fractional charge. Science, 267(5200):1010–1012, Feb 1995. ISSN 0036-8075. doi: 10.1126/science.267.5200.1010. URL http://science.sciencemag.org/content/267/5200/1010.

[70] R. de Picciotto, M. Reznikov, M. Heiblum, V. Umansky, G. Bunin, and D. Mahalu. Direct observation of a fractional charge. Nature, 389:162 EP –, Sep 1997. URL https://doi.org/10.1038/38241.

[71] L. Saminadayar, D. C. Glattli, Y. Jin, and B. Etienne. Observation of the $e/3$ fractionally charged Laughlin quasiparticle. Phys. Rev. Lett., 79:2526–2529, Sep 1997. doi: 10.1103/PhysRevLett.79.2526. URL https://link.aps.org/doi/10.1103/PhysRevLett.79.2526.

[72] T. Senthil. Quantum matters: Physics beyond Landau's paradigms, 2004. URL https://arxiv.org/abs/cond-mat/0411275.

[73] T. Holstein, R. E. Norton, and P. Pincus. de Haas-van Alphen effect and the specific heat of an electron gas. Phys. Rev. B, 8:2649–2656, Sep 1973. doi: 10.1103/PhysRevB.8.2649. URL https://link.aps.org/doi/10.1103/PhysRevB.8.2649.

[74] M. Yu. Reizer. Relativistic effects in the electron density of states, specific heat, and the electron spectrum of normal metals. Phys. Rev. B, 40:11571–11575, Dec 1989. doi: 10.1103/PhysRevB.40.11571. URL http://link.aps.org/doi/10.1103/PhysRevB.40.11571.

[75] Patrick A. Lee and Naoto Nagaosa. Gauge theory of the normal state of high-T_c superconductors. Phys. Rev. B, 46:5621–5639, Sep 1992. doi: 10.1103/PhysRevB.46.5621. URL http://link.aps.org/doi/10.1103/PhysRevB.46.5621.

[76] Joseph Polchinski. Low-energy dynamics of the spinon-gauge system. Nuclear Physics B, 422(3):617–633, Jul 1994. doi: 10.1016/0550-3213(94)90449-9. URL https://www.sciencedirect.com/science/article/pii/0550321394904499?via%3Dihub.

[77] Chetan Nayak and Frank Wilczek. Renormalization group approach to low temperature properties of a non-Fermi liquid metal. Nuclear Physics B, 430(3):534 – 562,

Nov 1994. ISSN 0550-3213. doi: https://doi.org/10.1016/0550-3213(94)90158-9. URL http://www.sciencedirect.com/science/article/pii/0550321394901589.

[78] B. L. Altshuler, L. B. Ioffe, and A. J. Millis. Low-energy properties of fermions with singular interactions. Phys. Rev. B, 50:14048–14064, Nov 1994. doi: 10.1103/PhysRevB.50.14048. URL http://link.aps.org/doi/10.1103/PhysRevB.50.14048.

[79] Patrick A. Lee, Naoto Nagaosa, and Xiao-Gang Wen. Doping a Mott insulator: Physics of high-temperature superconductivity. Rev. Mod. Phys., 78:17–85, Jan 2006. doi: 10.1103/RevModPhys.78.17. URL https://link.aps.org/doi/10.1103/RevModPhys.78.17.

[80] Sung-Sik Lee, Patrick A. Lee, and T. Senthil. Amperean pairing instability in the U(1) spin liquid state with Fermi surface and application to $\kappa-(\mathrm{BEDT-TTF})_2\mathrm{cu}_2(\mathrm{CN})_3$. Phys. Rev. Lett., 98:067006, Feb 2007. doi: 10.1103/PhysRevLett.98.067006. URL https://link.aps.org/doi/10.1103/PhysRevLett.98.067006.

[81] Sung-Sik Lee. Low-energy effective theory of Fermi surface coupled with U(1) gauge field in $2+1$ dimensions. Phys. Rev. B, 80:165102, Oct 2009. doi: 10.1103/PhysRevB.80.165102. URL http://link.aps.org/doi/10.1103/PhysRevB.80.165102.

[82] Tobias Holder and Walter Metzner. Anomalous dynamical scaling from nematic and U(1) gauge field fluctuations in two-dimensional metals. Phys. Rev. B, 92:041112, Jul 2015. doi: 10.1103/PhysRevB.92.041112. URL http://link.aps.org/doi/10.1103/PhysRevB.92.041112.

[83] Haruki Watanabe and Ashvin Vishwanath. Criterion for stability of Goldstone modes and Fermi liquid behavior in a metal with broken symmetry. 111(46):16314–16318, Oct 2014. doi: 10.1073/pnas.1415592111.

[84] Ribhu K. Kaul, Alexei Kolezhuk, Michael Levin, Subir Sachdev, and T. Senthil. Hole dynamics in an antiferromagnet across a deconfined quantum critical point. Phys. Rev. B, 75:235122, Jun 2007. doi: 10.1103/PhysRevB.75.235122. URL https://link.aps.org/doi/10.1103/PhysRevB.75.235122.

[85] T. Senthil. Critical Fermi surfaces and non-Fermi liquid metals. Phys. Rev. B, 78:035103, Jul 2008. doi: 10.1103/PhysRevB.78.035103. URL http://link.aps.org/doi/10.1103/PhysRevB.78.035103.

[86] Yoichi Ando, Kouji Segawa, Seiki Komiya, and A. N. Lavrov. Electrical resistivity anisotropy from self-organized one dimensionality in high-temperature superconductors. Phys. Rev. Lett., 88:137005, Mar 2002. doi: 10.1103/PhysRevLett.88.137005. URL https://link.aps.org/doi/10.1103/PhysRevLett.88.137005.

[87] V. Hinkov, D. Haug, B. Fauqué, P. Bourges, Y. Sidis, A. Ivanov, C. Bernhard, C. T. Lin, and B. Keimer. Electronic liquid crystal state in the high-temperature superconductor $YBa_2Cu_3O_{6.45}$. Science, 319(5863):597–600, Feb 2008. ISSN 0036-8075. doi: 10.1126/science.1152309. URL http://science.sciencemag.org/content/319/5863/597.

[88] Jiun-Haw Chu, James G. Analytis, Chris Kucharczyk, and Ian R. Fisher. Determination of the phase diagram of the electron-doped superconductor $Ba(Fe_{1-x}Co_x)_2As_2$. Phys. Rev. B, 79:014506, Jan 2009. doi: 10.1103/PhysRevB.79.014506. URL https://link.aps.org/doi/10.1103/PhysRevB.79.014506.

[89] T.-M. Chuang, M. P. Allan, Jinho Lee, Yang Xie, Ni Ni, S. L. Bud'ko, G. S. Boebinger, P. C. Canfield, and J. C. Davis. Nematic electronic structure in the "parent" state of the Iron-based superconductor $Ca(Fe_{1-x}Co_x)_2As_2$. Science, 327(5962):181–184, Jan 2010. ISSN 0036-8075. doi: 10.1126/science.1181083. URL http://science.sciencemag.org/content/327/5962/181.

[90] M. J. Lawler, K. Fujita, Jhinhwan Lee, A. R. Schmidt, Y. Kohsaka, Chung Koo Kim, H. Eisaki, S. Uchida, J. C. Davis, J. P. Sethna, and Eun-Ah Kim. Intra-unit-cell electronic nematicity of the high-T_c copper-oxide pseudogap states. Nature, 466:347 EP –, Jul 2010. URL https://doi.org/10.1038/nature09169.

[91] Jiun-Haw Chu, James G. Analytis, Kristiaan De Greve, Peter L. McMahon, Zahirul Islam, Yoshihisa Yamamoto, and Ian R. Fisher. In-plane resistivity anisotropy in an underdoped Iron Arsenide superconductor. Science, 329(5993):824–826, Aug 2010. ISSN 0036-8075. doi: 10.1126/science.1190482. URL http://science.sciencemag.org/content/329/5993/824.

[92] Jörg Fink, Victor Soltwisch, Jochen Geck, Enrico Schierle, Eugen Weschke, and Bernd Büchner. Phase diagram of charge order in $La_{1.8-x}$ $Eu_{0.2}Sr_xCuO_4$ from resonant soft X-ray diffraction. Phys. Rev. B, 83:092503, Mar 2011. doi: 10.1103/PhysRevB.83.092503. URL https://link.aps.org/doi/10.1103/PhysRevB.83.092503.

[93] S. Kasahara, H. J. Shi, K. Hashimoto, S. Tonegawa, Y. Mizukami, T. Shibauchi, K. Sugimoto, T. Fukuda, T. Terashima, Andriy H. Nevidomskyy, and Y. Matsuda. Electronic nematicity above the structural and superconducting transition in $BaFe_2(As_{1-x}P_x)_2$. Nature, 486:382 EP –, Jun 2012. URL https://doi.org/10.1038/nature11178.

[94] R. Zhou, Z. Li, J. Yang, D. L. Sun, C. T. Lin, and Guo-qing Zheng. Quantum criticality in electron-doped $BaFe_{2-x}Ni_xAs_2$. Nature Communications, 4:2265 EP –, Aug 2013. URL https://doi.org/10.1038/ncomms3265.

[95] Xingye Lu, J. T. Park, Rui Zhang, Huiqian Luo, Andriy H. Nevidomskyy, Qimiao Si, and Pengcheng Dai. Nematic spin correlations in the tetragonal state of uniaxial-strained $BaFe_{2-x}Ni_xAs_2$. Science, 345(6197):657–660, Aug 2014. ISSN 0036-8075. doi: 10.1126/science.1251853. URL http://science.sciencemag.org/content/345/6197/657.

[96] Sung-Sik Lee. Recent developments in non-Fermi liquid theory. Annu. Rev. of Condens. Matter Phys., 9(1):227–244, Dec 2018. doi: 10.1146/annurev-conmatphys-031016-025531. URL https://doi.org/10.1146/annurev-conmatphys-031016-025531.

[97] Hiroyuki Yamase and Hiroshi Kohno. Instability toward formation of quasi-one-dimensional Fermi surface in two-dimensional $t - J$ model. Journal of the Physical Society of Japan, 69(7):2151–2157, Feb 2000. doi: 10.1143/JPSJ.69.2151. URL https://doi.org/10.1143/JPSJ.69.2151.

[98] Christoph J. Halboth and Walter Metzner. d-wave superconductivity and Pomeranchuk instability in the two-dimensional Hubbard model. Phys. Rev. Lett., 85:5162–5165, Dec 2000. doi: 10.1103/PhysRevLett.85.5162. URL https://link.aps.org/doi/10.1103/PhysRevLett.85.5162.

[99] Vadim Oganesyan, Steven A. Kivelson, and Eduardo Fradkin. Quantum theory of a nematic Fermi fluid. Phys. Rev. B, 64:195109, Oct 2001. doi: 10.1103/PhysRevB.64.195109. URL https://link.aps.org/doi/10.1103/PhysRevB.64.195109.

[100] W. Metzner, D. Rohe, and S. Andergassen. Soft Fermi surfaces and breakdown of Fermi-liquid behavior. Phys. Rev. Lett., 91:066402, Aug 2003. doi: 10.1103/PhysRevLett.91.066402. URL https://link.aps.org/doi/10.1103/PhysRevLett.91.066402.

[101] Hae-Young Kee, Eugene H. Kim, and Chung-Hou Chung. Signatures of an electronic nematic phase at the isotropic-nematic phase transition. Phys. Rev. B, 68:245109, Dec 2003. doi: 10.1103/PhysRevB.68.245109. URL https://link.aps.org/doi/10.1103/PhysRevB.68.245109.

[102] Hiroyuki Yamase, Vadim Oganesyan, and Walter Metzner. Mean-field theory for symmetry-breaking Fermi surface deformations on a square lattice. Phys. Rev. B, 72:035114, Jul 2005. doi: 10.1103/PhysRevB.72.035114. URL https://link.aps.org/doi/10.1103/PhysRevB.72.035114.

[103] Luca Dell'Anna and Walter Metzner. Fermi surface fluctuations and single electron excitations near Pomeranchuk instability in two dimensions. Phys. Rev. B, 73:045127, Jan 2006. doi: 10.1103/PhysRevB.73.045127. URL https://link.aps.org/doi/10.1103/PhysRevB.73.045127.

[104] Michael J. Lawler, Daniel G. Barci, Victoria Fernández, Eduardo Fradkin, and Luis Oxman. Nonperturbative behavior of the quantum phase transition to a nematic Fermi fluid. Phys. Rev. B, 73:085101, Feb 2006. doi: 10.1103/PhysRevB.73.085101. URL https://link.aps.org/doi/10.1103/PhysRevB.73.085101.

[105] J. Quintanilla and A. J. Schofield. Pomeranchuk and topological Fermi surface instabilities from central interactions. Phys. Rev. B, 74:115126, Sep 2006. doi: 10.1103/PhysRevB.74.115126. URL https://link.aps.org/doi/10.1103/PhysRevB.74.115126.

[106] Michael J. Lawler and Eduardo Fradkin. Local quantum criticality at the nematic quantum phase transition. Phys. Rev. B, 75:033304, Jan 2007. doi: 10.1103/PhysRevB.75.033304. URL https://link.aps.org/doi/10.1103/PhysRevB.75.033304.

[107] Luca Dell'Anna and Walter Metzner. Electrical resistivity near Pomeranchuk instability in two dimensions. Phys. Rev. Lett., 98:136402, Mar 2007. doi: 10.1103/PhysRevLett.98.136402. URL https://link.aps.org/doi/10.1103/PhysRevLett.98.136402.

[108] P Wölfle and A. Rosch. Fermi liquid near a quantum critical point. J. Low Temp Phys., 147:165–177, May 2007. doi: 10.1007/s10909-007-9308-y. URL https://link.springer.com/article/10.1007%2Fs10909-007-9308-y#citeas.

[109] Eun-Ah Kim, Michael J. Lawler, Paul Oreto, Subir Sachdev, Eduardo Fradkin, and Steven A. Kivelson. Theory of the nodal nematic quantum phase transition in superconductors. Phys. Rev. B, 77:184514, May 2008. doi: 10.1103/PhysRevB.77.184514. URL https://link.aps.org/doi/10.1103/PhysRevB.77.184514.

[110] Yejin Huh and Subir Sachdev. Renormalization group theory of nematic ordering in d-wave superconductors. Phys. Rev. B, 78:064512, Aug 2008. doi: 10.1103/PhysRevB.78.064512. URL https://link.aps.org/doi/10.1103/PhysRevB.78.064512.

[111] Mario Zacharias, Peter Wölfle, and Markus Garst. Multiscale quantum criticality: Pomeranchuk instability in isotropic metals. Phys. Rev. B, 80:165116, Oct 2009. doi: 10.1103/PhysRevB.80.165116. URL https://link.aps.org/doi/10.1103/PhysRevB.80.165116.

[112] Dmitrii L. Maslov and Andrey V. Chubukov. Fermi liquid near Pomeranchuk quantum criticality. Phys. Rev. B, 81:045110, Jan 2010. doi: 10.1103/PhysRevB.81.045110. URL https://link.aps.org/doi/10.1103/PhysRevB.81.045110.

[113] Max A. Metlitski and Subir Sachdev. Quantum phase transitions of metals in two spatial dimensions. I. Ising-nematic order. Phys. Rev. B, 82:075127, Aug 2010. doi: 10.1103/PhysRevB.82.075127. URL https://link.aps.org/doi/10.1103/PhysRevB.82.075127.

[114] Denis Dalidovich and Sung-Sik Lee. Perturbative non-Fermi liquids from dimensional regularization. Phys. Rev. B, 88:245106, Dec 2013. doi: 10.1103/PhysRevB.88.245106. URL http://link.aps.org/doi/10.1103/PhysRevB.88.245106.

[115] S. Lederer, Y. Schattner, E. Berg, and S. A. Kivelson. Enhancement of superconductivity near a nematic quantum critical point. Phys. Rev. Lett., 114:097001, Mar 2015. doi: 10.1103/PhysRevLett.114.097001. URL https://link.aps.org/doi/10.1103/PhysRevLett.114.097001.

[116] Yoni Schattner, Samuel Lederer, Steven A. Kivelson, and Erez Berg. Ising nematic quantum critical point in a metal: A Monte Carlo study. Phys. Rev. X, 6:031028, Aug 2016. doi: 10.1103/PhysRevX.6.031028. URL http://link.aps.org/doi/10.1103/PhysRevX.6.031028.

[117] Wenliang Zhang, J. T. Park, Xingye Lu, Yuan Wei, Xiaoyan Ma, Lijie Hao, Pengcheng Dai, Zi Yang Meng, Yi-feng Yang, Huiqian Luo, and Shiliang Li. Effect of nematic order on the low-energy spin fluctuations in detwinned $BaFe_{1.935}Ni_{0.065}As_2$. Phys. Rev.

Lett., 117:227003, Nov 2016. doi: 10.1103/PhysRevLett.117.227003. URL https://link.aps.org/doi/10.1103/PhysRevLett.117.227003.

[118] Zhaoyu Liu, Yanhong Gu, Wei Zhang, Dongliang Gong, Wenliang Zhang, Tao Xie, Xingye Lu, Xiaoyan Ma, Xiaotian Zhang, Rui Zhang, Jun Zhu, Cong Ren, Lei Shan, Xianggang Qiu, Pengcheng Dai, Yi-feng Yang, Huiqian Luo, and Shiliang Li. Nematic quantum critical fluctuations in $BaFe_{2-x}Ni_xAs_2$. Phys. Rev. Lett., 117:157002, Oct 2016. doi: 10.1103/PhysRevLett.117.157002. URL https://link.aps.org/doi/10.1103/PhysRevLett.117.157002.

[119] Samuel Lederer, Yoni Schattner, Erez Berg, and Steven A. Kivelson. Superconductivity and non-Fermi liquid behavior near a nematic quantum critical point. Proceedings of the National Academy of Sciences, 114(19):4905–4910, Apr 2017. ISSN 0027-8424. doi: 10.1073/pnas.1620651114. URL https://www.pnas.org/content/114/19/4905.

[120] P. Jakubczyk and A. Eberlein. Thermodynamics of the two-dimensional XY model from functional renormalization. Phys. Rev. E, 93:062145, Jun 2016. doi: 10.1103/PhysRevE.93.062145. URL https://link.aps.org/doi/10.1103/PhysRevE.93.062145.

[121] T. R. Kirkpatrick and D. Belitz. Nature of the quantum phase transition in clean itinerant Heisenberg ferromagnets. Phys. Rev. B, 67:024419, Jan 2003. doi: 10.1103/PhysRevB.67.024419. URL https://link.aps.org/doi/10.1103/PhysRevB.67.024419.

[122] Andrey V. Chubukov, Catherine Pépin, and Jerome Rech. Instability of the quantum-critical point of itinerant ferromagnets. Phys. Rev. Lett., 92:147003, Apr 2004. doi: 10.1103/PhysRevLett.92.147003. URL https://link.aps.org/doi/10.1103/PhysRevLett.92.147003.

[123] Jérôme Rech, Catherine Pépin, and Andrey V. Chubukov. Quantum critical behavior in itinerant electron systems: Eliashberg theory and instability of a ferromagnetic quantum critical point. Phys. Rev. B, 74:195126, Nov 2006. doi: 10.1103/PhysRevB.74.195126. URL https://link.aps.org/doi/10.1103/PhysRevB.74.195126.

[124] Alexander Steppke, Robert Küchler, Stefan Lausberg, Edit Lengyel, Lucia Steinke, Robert Borth, Thomas Lühmann, Cornelius Krellner, Michael Nicklas, Christoph Geibel, Frank Steglich, and Manuel Brando. Ferromagnetic quantum critical point in the heavy-fermion metal $YbNi_4(P_{1-x}As_x)_2$. Science, 339(6122):933–936, Feb 2013. ISSN 0036-8075. doi: 10.1126/science.1230583. URL http://science.sciencemag.org/content/339/6122/933.

[125] Yi Li, Elliott H. Lieb, and Congjun Wu. Exact results for itinerant ferromagnetism in multiorbital systems on square and cubic lattices. Phys. Rev. Lett., 112:217201, May 2014. doi: 10.1103/PhysRevLett.112.217201. URL https://link.aps.org/doi/10.1103/PhysRevLett.112.217201.

[126] T. Okano, S. Kitao, M. Seto, T. Atou, M. Itoh, M. Matoba, and Y. Kamihara. A ferromagnetic quantum critical point in heavy-fermion iron oxypnictide $CeFe_{1-x}Cr_xPO$.

Journal of Applied Physics, 117(17):17E123, Apr 2015. doi: 10.1063/1.4916808. URL https://doi.org/10.1063/1.4916808.

[127] Shenglong Xu, Yi Li, and Congjun Wu. Sign-problem-free quantum Monte Carlo study on thermodynamic properties and magnetic phase transitions in orbital-active itinerant ferromagnets. Phys. Rev. X, 5:021032, Jun 2015. doi: 10.1103/PhysRevX.5.021032. URL https://link.aps.org/doi/10.1103/PhysRevX.5.021032.

[128] M. Brando, D. Belitz, F. M. Grosche, and T. R. Kirkpatrick. Metallic quantum ferromagnets. Rev. Mod. Phys., 88:025006, May 2016. doi: 10.1103/RevModPhys.88.025006. URL https://link.aps.org/doi/10.1103/RevModPhys.88.025006.

[129] Xiao Yan Xu, Kai Sun, Yoni Schattner, Erez Berg, and Zi Yang Meng. Non-Fermi liquid at $(2+1)$D ferromagnetic quantum critical point. Phys. Rev. X, 7:031058, Sep 2017. doi: 10.1103/PhysRevX.7.031058. URL https://link.aps.org/doi/10.1103/PhysRevX.7.031058.

[130] S. A. Kivelson, E. Fradkin, and V. J. Emery. Electronic liquid-crystal phases of a doped Mott insulator. Nature, 393:550 EP –, Jun 1998. URL https://doi.org/10.1038/31177.

[131] Ar. Abanov and Andrey V. Chubukov. Spin-fermion model near the quantum critical point: One-loop renormalization group results. Phys. Rev. Lett., 84:5608–5611, Jun 2000. doi: 10.1103/PhysRevLett.84.5608. URL http://link.aps.org/doi/10.1103/PhysRevLett.84.5608.

[132] Ar. Abanov, Andrey V. Chubukov, and J. Schmalian. Quantum-critical theory of the spin-fermion model and its application to cuprates: Normal state analysis. Adv. Phys., 52(3):119–218, Jul 2003. doi: 10.1080/0001873021000057123. URL http://dx.doi.org/10.1080/0001873021000057123.

[133] Ar. Abanov and A. Chubukov. Anomalous scaling at the quantum critical point in itinerant antiferromagnets. Phys. Rev. Lett., 93:255702, Dec 2004. doi: 10.1103/PhysRevLett.93.255702. URL http://link.aps.org/doi/10.1103/PhysRevLett.93.255702.

[134] Max A. Metlitski and Subir Sachdev. Quantum phase transitions of metals in two spatial dimensions. II. Spin density wave order. Phys. Rev. B, 82:075128, Aug 2010. doi: 10.1103/PhysRevB.82.075128. URL http://link.aps.org/doi/10.1103/PhysRevB.82.075128.

[135] Sean A. Hartnoll, Diego M. Hofman, Max A. Metlitski, and Subir Sachdev. Quantum critical response at the onset of spin-density-wave order in two-dimensional metals. Phys. Rev. B, 84:125115, Sep 2011. doi: 10.1103/PhysRevB.84.125115. URL http://link.aps.org/doi/10.1103/PhysRevB.84.125115.

[136] Nicolas Doiron-Leyraud and Louis Taillefer. Quantum critical point for stripe order: An organizing principle of cuprate superconductivity. Physica C: Superconductivity, 481:161 – 167, Nov 2012. ISSN 0921-4534. doi: https://doi.org/10.1016/j.

physc.2012.04.040. URL http://www.sciencedirect.com/science/article/pii/S0921453412002560. Stripes and Electronic Liquid Crystals in Strongly Correlated Materials.

[137] E. Berg, M. Metlitski, and S. Sachdev. Sign-problem-free quantum Monte Carlo of the onset of antiferromagnetism in metals. Science, 338:1606, Dec 2012. doi: 10.1126/science.1227769. URL http://science.sciencemag.org/content/338/6114/1606.

[138] Junhyun Lee, Philipp Strack, and Subir Sachdev. Quantum criticality of reconstructing Fermi surfaces in antiferromagnetic metals. Phys. Rev. B, 87:045104, Jan 2013. doi: 10.1103/PhysRevB.87.045104. URL http://link.aps.org/doi/10.1103/PhysRevB.87.045104.

[139] Vanuildo S. de Carvalho and Hermann Freire. Breakdown of Fermi liquid behavior near the hot spots in a two-dimensional model: A two-loop renormalization group analysis. Nuclear Physics B, 875(3):738 – 756, Oct 2013. ISSN 0550-3213. doi: 10.1016/j.nuclphysb.2013.07.016. URL http://www.sciencedirect.com/science/article/pii/S0550321313003829.

[140] Max H. Gerlach, Yoni Schattner, Erez Berg, and Simon Trebst. Quantum critical properties of a metallic spin-density-wave transition. Phys. Rev. B, 95:035124, Jan 2017. doi: 10.1103/PhysRevB.95.035124. URL http://link.aps.org/doi/10.1103/PhysRevB.95.035124.

[141] Vanuildo S. de Carvalho and Hermann Freire. Evidence of a short-range incommensurate d-wave charge order from a fermionic two-loop renormalization group calculation of a $2d$ model with hot spots. Annals of Physics, 348:32 – 49, Sep 2014. ISSN 0003-4916. doi: 10.1016/j.aop.2014.05.009. URL http://www.sciencedirect.com/science/article/pii/S0003491614001171.

[142] Shouvik Sur and Sung-Sik Lee. Quasilocal strange metal. Phys. Rev. B, 91:125136, Mar 2015. doi: 10.1103/PhysRevB.91.125136. URL http://link.aps.org/doi/10.1103/PhysRevB.91.125136.

[143] Aavishkar A. Patel, Philipp Strack, and Subir Sachdev. Hyperscaling at the spin density wave quantum critical point in two-dimensional metals. Phys. Rev. B, 92:165105, Oct 2015. doi: 10.1103/PhysRevB.92.165105. URL http://link.aps.org/doi/10.1103/PhysRevB.92.165105.

[144] Stefan A. Maier and Philipp Strack. Universality in antiferromagnetic strange metals. Phys. Rev. B, 93:165114, Apr 2016. doi: 10.1103/PhysRevB.93.165114. URL http://link.aps.org/doi/10.1103/PhysRevB.93.165114.

[145] Yoni Schattner, Max H. Gerlach, Simon Trebst, and Erez Berg. Competing orders in a nearly antiferromagnetic metal. Phys. Rev. Lett., 117:097002, Aug 2016. doi: 10.1103/PhysRevLett.117.097002. URL http://link.aps.org/doi/10.1103/PhysRevLett.117.097002.

[146] Shouvik Sur and Sung-Sik Lee. Anisotropic non-Fermi liquids. Phys. Rev. B, 94: 195135, Nov 2016. doi: 10.1103/PhysRevB.94.195135. URL http://link.aps.org/doi/10.1103/PhysRevB.94.195135.

[147] Zi-Xiang Li, Fa Wang, Hong Yao, and Dung-Hai Lee. Nature of the effective interaction in electron-doped cuprate superconductors: A sign-problem-free quantum Monte Carlo study. Phys. Rev. B, 95:214505, Jun 2017. doi: 10.1103/PhysRevB.95.214505. URL https://link.aps.org/doi/10.1103/PhysRevB.95.214505.

[148] Peter Lunts, Andres Schlief, and Sung-Sik Lee. Emergence of a control parameter for the antiferromagnetic quantum critical metal. Phys. Rev. B, 95:245109, Jun 2017. doi: 10.1103/PhysRevB.95.245109. URL https://link.aps.org/doi/10.1103/PhysRevB.95.245109.

[149] Zi-Xiang Li, Fa Wang, Hong Yao, and Dung-Hai Lee. What makes the T_c of monolayer FeSe on $SrTiO_3$ so high: a sign-problem-free quantum Monte Carlo study. Science Bulletin, 61(12):925 – 930, Jun 2016. ISSN 2095-9273. doi: 10.1007/s11434-016-1087-x. URL http://www.sciencedirect.com/science/article/pii/S2095927316300962.

[150] B. L. Altshuler, L. B. Ioffe, and A. J. Millis. Critical behavior of the $T = 0$ $2k_F$ density-wave phase transition in a two-dimensional Fermi liquid. Phys. Rev. B, 52:5563–5572, Aug 1995. doi: 10.1103/PhysRevB.52.5563. URL https://link.aps.org/doi/10.1103/PhysRevB.52.5563.

[151] Dominic Bergeron, Debanjan Chowdhury, Matthias Punk, Subir Sachdev, and A.-M. S. Tremblay. Breakdown of Fermi liquid behavior at the $(\pi, \pi) = 2k_F$ spin-density wave quantum-critical point: The case of electron-doped cuprates. Phys. Rev. B, 86:155123, Oct 2012. doi: 10.1103/PhysRevB.86.155123. URL https://link.aps.org/doi/10.1103/PhysRevB.86.155123.

[152] Clément Sire, Chandra M. Varma, Andrei E. Ruckenstein, and Thierry Giamarchi. Theory of the marginal-Fermi-liquid spectrum and pairing in a local copper oxide model. Phys. Rev. Lett., 72:2478–2481, Apr 1994. doi: 10.1103/PhysRevLett.72.2478. URL https://link.aps.org/doi/10.1103/PhysRevLett.72.2478.

[153] C. M. Varma, P. B. Littlewood, S. Schmitt-Rink, E. Abrahams, and A. E. Ruckenstein. Phenomenology of the normal state of CuO high-temperature superconductors. Phys. Rev. Lett., 63:1996–1999, Oct 1989. doi: 10.1103/PhysRevLett.63.1996. URL https://link.aps.org/doi/10.1103/PhysRevLett.63.1996.

[154] Chandra M. Varma, Nussinov M, and Wim van Saarloos. Singular or non-Fermi liquids. Physics Reports, 361:267–417, May 2002. doi: 10.1016/S0370-1573(01)00060-6. URL http://www.sciencedirect.com/science/article/pii/S0370157301000606.

[155] Dietrich Roscher, Emilio Torres, and Philipp Strack. Dual QED_3 at "$N_f = 1/2$' is an interacting CFT in the infrared. Journal of High Energy Physics, 2016(11):17, Nov 2016. ISSN 1029-8479. doi: 10.1007/JHEP11(2016)017. URL https://doi.org/10.1007/JHEP11(2016)017.

[156] Sung-Sik Lee. Emergence of supersymmetry at a critical point of a lattice model. Phys. Rev. B, 76:075103, Aug 2007. doi: 10.1103/PhysRevB.76.075103. URL https://link.aps.org/doi/10.1103/PhysRevB.76.075103.

[157] Hidenori Sonoda. Phase Structure of a Three-Dimensional Yukawa Model. Progress of Theoretical Physics, 126(1):57–80, Jul 2011. ISSN 0033-068X. doi: 10.1143/PTP.126.57. URL https://dx.doi.org/10.1143/PTP.126.57.

[158] Tarun Grover, D. N. Sheng, and Ashvin Vishwanath. Emergent space-time supersymmetry at the boundary of a topological phase. Science, 344(6181):280–283, Apr 2014. ISSN 0036-8075. doi: 10.1126/science.1248253. URL http://science.sciencemag.org/content/344/6181/280.

[159] Nikolai Zerf, Chien-Hung Lin, and Joseph Maciejko. Superconducting quantum criticality of topological surface states at three loops. Phys. Rev. B, 94:205106, Nov 2016. doi: 10.1103/PhysRevB.94.205106. URL https://link.aps.org/doi/10.1103/PhysRevB.94.205106.

[160] John A. Hertz. Quantum critical phenomena. Phys. Rev. B, 14:1165–1184, Aug 1976. doi: 10.1103/PhysRevB.14.1165. URL http://link.aps.org/doi/10.1103/PhysRevB.14.1165.

[161] A. J. Millis. Effect of a nonzero temperature on quantum critical points in itinerant fermion systems. Phys. Rev. B, 48:7183–7196, Sep 1993. doi: 10.1103/PhysRevB.48.7183. URL http://link.aps.org/doi/10.1103/PhysRevB.48.7183.

[162] Yong Baek Kim, Akira Furusaki, Xiao-Gang Wen, and Patrick A. Lee. Gauge-invariant response functions of fermions coupled to a gauge field. Phys. Rev. B, 50:17917–17932, Dec 1994. doi: 10.1103/PhysRevB.50.17917. URL http://link.aps.org/doi/10.1103/PhysRevB.50.17917.

[163] Balazs Meszena, Petter Säterskog, Andrey Bagrov, and Koenraad Schalm. Nonperturbative emergence of non-Fermi-liquid behavior in $d = 2$ quantum critical metals. Phys. Rev. B, 94:115134, Sep 2016. doi: 10.1103/PhysRevB.94.115134. URL https://link.aps.org/doi/10.1103/PhysRevB.94.115134.

[164] Petter Säterskog, Balazs Meszena, and Koenraad Schalm. Two-point function of a $d = 2$ quantum critical metal in the limit $k_F \to \infty$, $N_f \to 0$ with $N_f k_F$ fixed. Phys. Rev. B, 96:155125, Oct 2017. doi: 10.1103/PhysRevB.96.155125. URL https://link.aps.org/doi/10.1103/PhysRevB.96.155125.

[165] Petter Säterskog. A framework for studying a quantum critical metal in the limit $N_f \to 0$. SciPost Phys., 4:15, Mar 2018. doi: 10.21468/SciPostPhys.4.3.015. URL https://scipost.org/10.21468/SciPostPhys.4.3.015.

[166] Chetan Nayak and Frank Wilczek. Non-Fermi liquid fixed point in 2 + 1 dimensions. Nuclear Physics B, 417(3):359 – 373, Apr 1994. ISSN 0550-3213. doi: 10.1016/0550-3213(94)90477-4. URL http://www.sciencedirect.com/science/article/pii/0550321394904774.

[167] Luminita N. Mihaila, Nikolai Zerf, Bernhard Ihrig, Igor F. Herbut, and Michael M. Scherer. Gross-Neveu-Yukawa model at three loops and Ising critical behavior of Dirac systems. Phys. Rev. B, 96:165133, Oct 2017. doi: 10.1103/PhysRevB.96.165133. URL https://link.aps.org/doi/10.1103/PhysRevB.96.165133.

[168] Nikolai Zerf, Luminita N. Mihaila, Peter Marquard, Igor F. Herbut, and Michael M. Scherer. Four-loop critical exponents for the Gross-Neveu-Yukawa models. Phys. Rev. D, 96:096010, Nov 2017. doi: 10.1103/PhysRevD.96.096010. URL https://link.aps.org/doi/10.1103/PhysRevD.96.096010.

[169] Lorenzo Di Pietro and Emmanuel Stamou. Scaling dimensions in QED_3 from the ϵ-expansion. Journal of High Energy Physics, 2017(12):54, Dec 2017. ISSN 1029-8479. doi: 10.1007/JHEP12(2017)054. URL https://doi.org/10.1007/JHEP12(2017)054.

[170] Lorenzo Di Pietro, Zohar Komargodski, Itamar Shamir, and Emmanuel Stamou. Quantum electrodynamics in $d = 3$ from the ϵ-expansion. Phys. Rev. Lett., 116:131601, Apr 2016. doi: 10.1103/PhysRevLett.116.131601. URL https://link.aps.org/doi/10.1103/PhysRevLett.116.131601.

[171] Lorenzo Di Pietro and Emmanuel Stamou. Operator mixing in the ϵ-expansion: Scheme and evanescent-operator independence. Phys. Rev. D, 97:065007, Mar 2018. doi: 10.1103/PhysRevD.97.065007. URL https://link.aps.org/doi/10.1103/PhysRevD.97.065007.

[172] Sudip Chakravarty, Richard E. Norton, and Olav F. Syljuåsen. Transverse gauge interactions and the vanquished Fermi liquid. Phys. Rev. Lett., 74:1423–1426, Feb 1995. doi: 10.1103/PhysRevLett.74.1423. URL https://link.aps.org/doi/10.1103/PhysRevLett.74.1423.

[173] A. Liam Fitzpatrick, Shamit Kachru, Jared Kaplan, and S. Raghu. Non-Fermi-liquid fixed point in a Wilsonian theory of quantum critical metals. Phys. Rev. B, 88:125116, Sep 2013. doi: 10.1103/PhysRevB.88.125116. URL http://link.aps.org/doi/10.1103/PhysRevB.88.125116.

[174] Ipsita Mandal and Sung-Sik Lee. Ultraviolet/infrared mixing in non-Fermi liquids. Phys. Rev. B, 92:035141, Jul 2015. doi: 10.1103/PhysRevB.92.035141. URL http://link.aps.org/doi/10.1103/PhysRevB.92.035141.

[175] Ipsita Mandal. Superconducting instability in non-Fermi liquids. Phys. Rev. B, 94:115138, Sep 2016. doi: 10.1103/PhysRevB.94.115138. URL https://link.aps.org/doi/10.1103/PhysRevB.94.115138.

[176] T. Senthil and R. Shankar. Fermi surfaces in general codimension and a new controlled nontrivial fixed point. Phys. Rev. Lett., 102:046406, Jan 2009. doi: 10.1103/PhysRevLett.102.046406. URL https://link.aps.org/doi/10.1103/PhysRevLett.102.046406.

[177] Shouvik Sur and Sung-Sik Lee. Chiral non-Fermi liquids. Phys. Rev. B, 90:045121, Jul 2014. doi: 10.1103/PhysRevB.90.045121. URL http://link.aps.org/doi/10.1103/PhysRevB.90.045121.

[178] A. Bhattacharyya, D. D. Khalyavin, F. Krüger, D. T. Adroja, A. M. Strydom, W. A. Kockelmann, and A. D. Hillier. Incommensurate spin-density-wave antiferromagnetism in $CeRu_2Al_2B$. Phys. Rev. B, 93:060410, Feb 2016. doi: 10.1103/PhysRevB.93.060410. URL https://link.aps.org/doi/10.1103/PhysRevB.93.060410.

[179] Jáchym Sýkora, Tobias Holder, and Walter Metzner. Fluctuation effects at the onset of the $2k_F$ density wave order with one pair of hot spots in two-dimensional metals. Phys. Rev. B, 97:155159, Apr 2018. doi: 10.1103/PhysRevB.97.155159. URL https://link.aps.org/doi/10.1103/PhysRevB.97.155159.

[180] Joseph Polchinski. Renormalization and effective Lagrangians. Nuclear Physics B, 231 (2):269 – 295, Jan 1984. ISSN 0550-3213. doi: 10.1016/0550-3213(84)90287-6. URL http://www.sciencedirect.com/science/article/pii/0550321384902876.

[181] Christof Wetterich. Exact evolution equation for the effective potential. Physics Letters B, 301(1):90 – 94, Feb 1993. ISSN 0370-2693. doi: 10.1016/0370-2693(93)90726-X. URL http://www.sciencedirect.com/science/article/pii/037026939390726X.

[182] K. Miyake, S. Schmitt-Rink, and C. M. Varma. Spin-fluctuation-mediated even-parity pairing in heavy-fermion superconductors. Phys. Rev. B, 34:6554–6556, Nov 1986. doi: 10.1103/PhysRevB.34.6554. URL https://link.aps.org/doi/10.1103/PhysRevB.34.6554.

[183] D. J. Scalapino, E. Loh, and J. E. Hirsch. d-wave pairing near a spin-density-wave instability. Phys. Rev. B, 34:8190–8192, Dec 1986. doi: 10.1103/PhysRevB.34.8190. URL https://link.aps.org/doi/10.1103/PhysRevB.34.8190.

[184] Tôru Moriya, Yoshinori Takahashi, and Kazuo Ueda. Antiferromagnetic spin fluctuations and superconductivity in two-dimensional metals -a possible model for high T_c oxides. Journal of the Physical Society of Japan, 59(8):2905–2915, Apr 1990. doi: 10.1143/JPSJ.59.2905. URL https://doi.org/10.1143/JPSJ.59.2905.

[185] Zi-Xiang Li, Fa Wang, Hong Yao, and Dung-Hai Lee. Nature of the effective interaction in electron-doped cuprate superconductors: A sign-problem-free quantum Monte Carlo study. Phys. Rev. B, 95:214505, Jun 2017. doi: 10.1103/PhysRevB.95.214505. URL https://link.aps.org/doi/10.1103/PhysRevB.95.214505.

[186] Stefan A. Maier and Philipp Strack. Universality in antiferromagnetic strange metals. Phys. Rev. B, 93:165114, Apr 2016. doi: 10.1103/PhysRevB.93.165114. URL http://link.aps.org/doi/10.1103/PhysRevB.93.165114.

[187] Jared Kaplan Steve A. Kivelson A. Liam Fitzpatrick, Shamit Kachru and Srinivas Raghu. Slow fermions in quantum critical metals, 2014. URL https://arxiv.org/abs/1402.5413.

[188] C. M. Varma. Quantum criticality in quasi-two-dimensional itinerant antiferromagnets. Phys. Rev. Lett., 115:186405, Oct 2015. doi: 10.1103/PhysRevLett.115.186405. URL http://link.aps.org/doi/10.1103/PhysRevLett.115.186405.

[189] P. Monthoux, A. V. Balatsky, and D. Pines. Weak-coupling theory of high-temperature superconductivity in the antiferromagnetically correlated copper oxides. Phys. Rev. B, 46:14803–14817, Dec 1992. doi: 10.1103/PhysRevB.46.14803. URL https://link.aps.org/doi/10.1103/PhysRevB.46.14803.

[190] D. T. Son. Superconductivity by long-range color magnetic interaction in high-density quark matter. Phys. Rev. D, 59:094019, Apr 1999. doi: 10.1103/PhysRevD.59.094019. URL https://link.aps.org/doi/10.1103/PhysRevD.59.094019.

[191] Andrey V. Chubukov and Jörg Schmalian. Superconductivity due to massless boson exchange in the strong-coupling limit. Phys. Rev. B, 72:174520, Nov 2005. doi: 10.1103/PhysRevB.72.174520. URL https://link.aps.org/doi/10.1103/PhysRevB.72.174520.

[192] Max A. Metlitski, David F. Mross, Subir Sachdev, and T. Senthil. Cooper pairing in non-Fermi liquids. Phys. Rev. B, 91:115111, Mar 2015. doi: 10.1103/PhysRevB.91.115111. URL https://link.aps.org/doi/10.1103/PhysRevB.91.115111.

[193] M. Horio, T. Adachi, Y. Mori, A. Takahashi, T. Yoshida, H. Suzuki, L. C. C. Ambolode II, K. Okazaki, K. Ono, H. Kumigashira, H. Anzai, M. Arita, H. Namatame, M. Taniguchi, D. Ootsuki, K. Sawada, M. Takahashi, T. Mizokawa, Y. Koike, and A. Fujimori. Suppression of the antiferromagnetic pseudogap in the electron-doped high-temperature superconductor by protect annealing. Nature Communications, 7:10567 EP –, Feb 2016. URL https://doi.org/10.1038/ncomms10567.

[194] L. Rosa, P. Vitale, and C. Wetterich. Critical exponents of the Gross-Neveu model from the effective average action. Phys. Rev. Lett., 86:958–961, Feb 2001. doi: 10.1103/PhysRevLett.86.958. URL https://link.aps.org/doi/10.1103/PhysRevLett.86.958.

[195] F. Höfling, C. Nowak, and C. Wetterich. Phase transition and critical behavior of the $d = 3$ Gross-Neveu model. Phys. Rev. B, 66:205111, Nov 2002. doi: 10.1103/PhysRevB.66.205111. URL https://link.aps.org/doi/10.1103/PhysRevB.66.205111.

[196] Carsten Honerkamp. Density waves and cooper pairing on the honeycomb lattice. Phys. Rev. Lett., 100:146404, Apr 2008. doi: 10.1103/PhysRevLett.100.146404. URL https://link.aps.org/doi/10.1103/PhysRevLett.100.146404.

[197] Holger Gies, Lukas Janssen, Stefan Rechenberger, and Michael M. Scherer. Phase transition and critical behavior of $d = 3$ chiral fermion models with left-right asymmetry. Phys. Rev. D, 81:025009, Jan 2010. doi: 10.1103/PhysRevD.81.025009. URL https://link.aps.org/doi/10.1103/PhysRevD.81.025009.

[198] Holger Gies and Lukas Janssen. UV fixed-point structure of the three-dimensional Thirring model. Phys. Rev. D, 82:085018, Oct 2010. doi: 10.1103/PhysRevD.82.085018. URL https://link.aps.org/doi/10.1103/PhysRevD.82.085018.

[199] Jens Braun, Holger Gies, and Daniel D. Scherer. Asymptotic safety: A simple example. Phys. Rev. D, 83:085012, Apr 2011. doi: 10.1103/PhysRevD.83.085012. URL https://link.aps.org/doi/10.1103/PhysRevD.83.085012.

[200] Walter Metzner, Manfred Salmhofer, Carsten Honerkamp, Volker Meden, and Kurt Schönhammer. Functional renormalization group approach to correlated fermion systems. Rev. Mod. Phys., 84:299–352, Mar 2012. doi: 10.1103/RevModPhys.84.299. URL https://link.aps.org/doi/10.1103/RevModPhys.84.299.

[201] Michael M. Scherer, Stefan Uebelacker, and Carsten Honerkamp. Instabilities of interacting electrons on the honeycomb bilayer. Phys. Rev. B, 85:235408, Jun 2012. doi: 10.1103/PhysRevB.85.235408. URL https://link.aps.org/doi/10.1103/PhysRevB.85.235408.

[202] Lukas Janssen and Holger Gies. Critical behavior of the $(2+1)$-dimensional Thirring model. Phys. Rev. D, 86:105007, Nov 2012. doi: 10.1103/PhysRevD.86.105007. URL https://link.aps.org/doi/10.1103/PhysRevD.86.105007.

[203] D. Mesterházy, J. Berges, and L. von Smekal. Effect of short-range interactions on the quantum critical behavior of spinless fermions on the honeycomb lattice. Phys. Rev. B, 86:245431, Dec 2012. doi: 10.1103/PhysRevB.86.245431. URL https://link.aps.org/doi/10.1103/PhysRevB.86.245431.

[204] Andreas Eberlein and Walter Metzner. Effective interactions and fluctuation effects in spin-singlet superfluids. Phys. Rev. B, 87:174523, May 2013. doi: 10.1103/PhysRevB.87.174523. URL https://link.aps.org/doi/10.1103/PhysRevB.87.174523.

[205] C. Platt, W. Hanke, and R. Thomale. Functional renormalization group for multi-orbital Fermi surface instabilities. Advances in Physics, 62(4-6):453–562, Jan 2014. doi: 10.1080/00018732.2013.862020. URL https://www.tandfonline.com/doi/abs/10.1080/00018732.2013.862020.

[206] Jing Wang, Andreas Eberlein, and Walter Metzner. Competing order in correlated electron systems made simple: Consistent fusion of functional renormalization and mean-field theory. Phys. Rev. B, 89:121116, Mar 2014. doi: 10.1103/PhysRevB.89.121116. URL https://link.aps.org/doi/10.1103/PhysRevB.89.121116.

[207] Lukas Janssen and Igor F. Herbut. Antiferromagnetic critical point on graphene's honeycomb lattice: A functional renormalization group approach. Phys. Rev. B, 89:205403, May 2014. doi: 10.1103/PhysRevB.89.205403. URL https://link.aps.org/doi/10.1103/PhysRevB.89.205403.

[208] Stefan A. Maier, Andreas Eberlein, and Carsten Honerkamp. Functional renormalization group for commensurate antiferromagnets: Beyond the mean-field picture. Phys. Rev. B, 90:035140, Jul 2014. doi: 10.1103/PhysRevB.90.035140. URL https://link.aps.org/doi/10.1103/PhysRevB.90.035140.

[209] Andreas Eberlein. fermionic two-loop functional renormalization group for correlated fermions: Method and application to the attractive Hubbard model. Phys. Rev. B, 90:

115125, Sep 2014. doi: 10.1103/PhysRevB.90.115125. URL https://link.aps.org/doi/10.1103/PhysRevB.90.115125.

[210] Andreas Eberlein. Self-energy effects in functional renormalization group flows of the two-dimensional $t-t'$ Hubbard model away from van Hove filling. Phys. Rev. B, 92: 235146, Dec 2015. doi: 10.1103/PhysRevB.92.235146. URL https://link.aps.org/doi/10.1103/PhysRevB.92.235146.

[211] Emilio Torres, Laura Classen, Igor F. Herbut, and Michael M. Scherer. fermion-induced quantum criticality with two length scales in Dirac systems. Phys. Rev. B, 97:125137, Mar 2018. doi: 10.1103/PhysRevB.97.125137. URL https://link.aps.org/doi/10.1103/PhysRevB.97.125137.

[212] Tim R. Morris. The exact renormalization group and approximate solutions. Int. J. Mod. Phys. A., 9(14):2411 – 2449, Jun 1994. doi: 10.1142/S0217751X94000972. URL https://www.worldscientific.com/doi/abs/10.1142/S0217751X94000972.

[213] M. Reuter. Nonperturbative evolution equation for quantum gravity. Phys. Rev. D, 57:971–985, Jan 1998. doi: 10.1103/PhysRevD.57.971. URL https://link.aps.org/doi/10.1103/PhysRevD.57.971.

[214] N Dupuis. Fermi liquid theory: a renormalization group point of view, Apr 1996. URL https://arxiv.org/abs/cond-mat/9604189.

[215] Elihu Abrahams and Peter Wölfe. Critical quasiparticle theory applied to heavy fermion metals near an antiferromagnetic quantum phase transition. Proc. Natl. Acad. Sci., 109:3238, Jan 2012. doi: 10.1073/pnas.1200346109. URL http://www.pnas.org/content/109/9/3238.abstract.